Durham University

Durham E-Theses

Characterising fracture systems within upfaulted basement highs in the Hebridean Islands: an onshore analogue for the Clair Field

BENJAMIN SAMUEL GARRICK FRANKLIN

How to cite:

FRANKLIN, BENJAMIN SAMUEL GARRICK (2013) Characterising fracture systems within upfaulted basement highs in the Hebridean Islands: an onshore analogue for the Clair Field. Doctoral thesis, Durham University.

Use policy

The full-text may be used and/or reproduced, and given to third parties in any format or medium, without prior permission or charge, for personal research or study, educational, or not-for-profit purposes provided that:

- a full bibliographic reference is made to the original source
- a https://etheses.durham.ac.uk/id/eprint/7765/ is made to the metadata record in Durham E-Theses
- the full-text is not changed in any way

The full-text must not be sold in any format or medium without the formal permission of the copyright holders.

Please consult the full Durham E-Theses policy for further details.

Academic Support Office, The Palatine Centre, Durham University, Stockton Road, Durham, DH1 3LE
e-mail: e-theses.admin@durham.ac.uk Tel: +44 0191 334 6107
https://etheses.durham.ac.uk

DEPARTMENT OF EARTH SCIENCES, DURHAM UNIVERSITY

Characterising fracture systems within upfaulted basement highs in the Hebridean Islands: an onshore analogue for the Clair Field

Benjamin Samuel Garrick Franklin

2013

This thesis is submitted in accordance with the regulations
for the degree of Doctor of Philosophy in the University of Durham,
Department of Earth Sciences, 2013

Abstract

The Outer Hebrides are a structurally complex area, comprised predominantly of crystalline basement rocks of the Lewisian Gneiss Complex with the multiply reactivated Outer Hebrides Fault Zone following eastern portions of the islands for over 200 km along strike. In Eastern Lewis, the Permo-Triassic Stornoway Formation unconformably overlies Lewisian basement rocks of the OHFZ in a half-graben. This structural setting is analogous to the major offshore Clair oil field, where oil is found within Devonian-Carboniferous red beds of the Clair Group directly overlying Lewisian Gneiss Complex rocks of the Rona Ridge, which was upfaulted in the Mesozoic. Oil connection and flow has been proven in the basement rocks at Clair, however, little is known about the nature of fracturing and faulting within the basement and how these faults link to the cover sequence. Here, the cover and basement rocks of the Outer Hebridean Islands of Lewis and Harris are studied as an analogue.

Faults, fault rocks and deformation are characterised within the Stornoway Formation, and at the basement-cover interface, allowing recognition of Mesozoic and younger faults within the Lewisian and their separation from older structures. Three fault sets are distinguished within the Stornoway Formation: a NNW-SSE striking normal fault set (Set 1); a N-S and E-W quadrimodal normal fault set (Set 2); and a less numerous late E-W strike-slip set (Set 3). Tertiary dolerite dyke intrusion occurred along Set 1 and Set 2 faults prior to the formation of Set 3. Palaeostress analyses reveal that Set 1 and 2 result from E-W and ENE-WSW directed extension vectors, followed by E-W directed contraction associated with Set 3. These orientations are interpreted to be representative of Mesozoic extension related to the opening of the Atlantic, followed by Cenozoic contraction. Faults in the Stornoway Formation are accompanied by development of authigenic clay-bearing gouges and cataclasites, ± calcite cement and late zeolite. Zeolite is often associated with secondary porosity, produced through dissolution of calcite. Mesozoic and younger faults are readily identified in Lewisian Gneiss rocks of the Stornoway region based on fault rock characterisation, and these faults also display an ENE-WSW directed extension vector. The major bounding faults of the Stornoway Formation are sub-parallel with the local foliation and the reactivation of the basement foliation by Mesozoic faults is proven. Fault trends identified within the Stornoway Formation are also sub-parallel with the local foliation. Conjugate faulting apparent in the Stornoway Formation is not present within the Lewisian, possibly indicating a degree of structural detachment between faulting in the basement and faulting in the cover, probably linked to the development of low-angle faults within the Stornoway Formation within metres of and parallel with the basement-cover unconformity. The basement-cover interface displays abundant evidence of fluid overpressure, potentially linked with dewatering during lithification and local fault movements.

Mesozoic and younger-age brittle fault rocks post-date pre-existing extensive ductile and brittle deformation that are most intense within the OHFZ. Brittle fault rocks of pre-Mesozoic age are associated with pseudotachylites, fine grained cataclasites, epidote-bearing cataclasites and pumpellyite-bearing cataclasites. Mesozoic fault rocks contain authigenic clay-bearing gouges and cataclasites often associated with zeolite and adularia mineralisation that often accompanies the development of secondary porosity within the fault rocks. This chronological fault rock assemblage represents the continued exhumation of the islands after the successively lower temperature and pressures conditions experienced since the initial development of the basement gneiss complex. Across Lewis, fault rock characterisation allows identification of major Mesozoic and younger structures that cross the islands, with a km-scale offset postulated across the major Seaforth Fault that may link the major NE-SW striking Minch Fault to a NE-SW striking fault lying offshore western Lewis/Harris. On Lewis, the predominant orientation of Mesozoic structures is NNW-SSE, becoming NW-SE on Harris, south of the Seaforth Fault and where foliation becomes pervasively NW-SE. It seems highly likely that, as identified in the Stornoway Region, the foliation orientation plays a significant role in the development of later structures.

At Clair, fault rock development within the Devonian-Carboniferous Clair Group is dependent on the host lithology, with gouges formed in mudstones, and granulation seams found in porous, oil-bearing sandstones. Calcite-cemented breccias are present in zones of calcite cemented host rock. Pyrite and calcite vein mineralisation are associated with oil influx, and a late phase of dissolution was accompanied by faulting that produced uncemented brittle fault rocks (gouge). In the basement, oil is seen along open fractures and in vug-like secondary porosity associated with adularia mineralisation, of which two forms are present. Euhedral adularia is often altered to green clay and partially to wholly infills tensile fractures that may predate the emplacement of the Clair Group. Later adularia occurs as 'speckled' veins, with haematite, clay, calcite, pyrite, minor zeolite and oil, and appears to be contemporaneous with calcite-pyrite veining (i.e. Mesozoic in age). Porosity in both adularia-bearing fractures is associated with oil staining. The basement displays little evidence of extensive mylonites or phyllonites that are obvious in the OHFZ of the Outer Hebrides.

Scalability studies show that it is difficult to assign power-law spacing distributions to fractures within the basement rocks of the Hebrides. Fractures parallel with Mesozoic structures do however tend to display a greater degree of organisation with more clustering of fractures as the faults are approached. Mesozoic fault-perpendicular fracture sets display more strongly random fracture spacing distributions consistent with a jointing origin. At Clair, fracture spacing studies in the cover show a low fracture density compared to basement, with fracture spacing that is clustered and may be well represented by power-laws. Dissolution has locally produced a randomly spaced fracture network. Although fracture spacings in the Hebridean Lewisian are generally random, fracture apertures define a clear power law relationship over ~5 orders of magnitude. Similarly, results from the Clair group also display equivalent power law relationships.

Declaration

No part of this thesis has previously been submitted for a degree at this or any other university. The work described in this thesis is entirely that of the author, except where reference is made to previously published or unpublished work.

Signed:

Date:

Benjamin S. G. Franklin

University of Durham

Department of Earth Sciences

April 2013

Copyright © by Benjamin S. G. Franklin
The copyright of this thesis rests with the author. No quotation or data from it should be published without the author's prior written consent and any information derived from it should be acknowledged.

Acknowledgements

This PhD was funded by the Clair Joint Venture Group – my thanks go to them for generously making this work possible, in particular Andy Conway at ConocoPhillips. In addition, I would like to thank the AAPG Grants-in-Aid scheme, which has enabled me to carry extensive microscopy analysis. This PhD has given me some fantastic opportunities, experiences and knowledge.

Firstly my thanks go to my supervisors Bob Holdsworth and Ken McCaffrey and equally Richard Walker. I have enjoyed fieldwork with Bob and Rich, highlights have included being pinned to a fence by the wind on top of a cliff, and enjoying the weather in the lovely Seaforth Valley. Thank you for receiving my anti-line transect emails, Bob and Ken. Bob has allowed me to attend AGU in San Francisco in addition to many other conferences, as well as the EGU Basement Geology Summer School in the Italian Alps and the structural course at Aachen. I met great people and learned a great deal during these events.

Next my thanks go to the fieldwork assistants that have helped me – Simon and Viv. They kept me company and helped me get through the line transect data collection. Simon in particular kept me company tramping over peat bogs, and whilst sampling the delights of the insect wildlife in the Seaforth Valley and those slippy phyllosilicate-bearing shear zones. Viv helped me immensely by keeping up to date with various news topics from 'The Week' magazine. Both helped me collect an immense amount of data. In the Hebrides I would also really like to thank Pat, Henry, Rosie and Blaine for letting me live very comfortably in their home.

I would also like to thank the other structural geology students at Durham for great discussions over the years, most importantly Jen Pless who helped me with many things. In addition thanks to Dave A, Rich W, Max W, Dave S, Anna-Marie D, Bansri R, Rachael B. Thanks also to Joel and GRL for collection of the laser scanning data in terrible conditions. Max, Bansri and Anna I thank in particular for being my neighbouring desk buddies.

Sharing a good place to call home with Viv has been a highlight of my time at Durham - I wouldn't even be here if it wasn't for meeting Viv in the first place. Thanks also to Rich for having me to live with him during my internship at SRK. I would like to thank the Durham gang for some really great times – Iona M, Sarah P, Izzy Y, Dave A, Ian B, Suzie Q, Niamh M, BJ and Amy C and all the others. I hope there are more to come, and Durham icebreaker 'wine tasting' wouldn't have been the same without you all!

My parents have been a constant source of encouragement and support, thank you for everything. Thank you to all of my Oxford and Kenilworth friends. Namely: Rich, Ben, Jo, Dave, Holly, Krysia, Annie, Hannah, Ellie, Jack, Katie and Paola.

I would most like to thank Simon out of everybody. He has constantly supported me through the whole writing up process as well as some truly tough line transects. I would not be quite so well-fed without his help.

Table of Contents

Chapter 1: Introduction and Regional Review 1

1.1 Project Aims 2

1.2 Structure of this thesis 3

1.3 Lewisian Complex Regional Geology 4

1.3.1 Geological background 4

1.3.2 Outer Hebridean Geology and Tectonic History 8

1.3.2.1 Tectonic History of Faulting in the Northern Zone of the Outer Hebrides Fault Zone 12

1.3.2.1.1 Stornoway Formation 13

1.3.2.2 Tectonic History of Faulting in the Southern Zone of the Outer Hebrides Fault Zone 14

1.3.3 Shear Zones and Linkage across the Minch 14

1.4 Faroe-Shetland Basin 16

1.5 A note on the fracture characteristics of the Lewisian Gneiss of the Scottish mainland **.... 23**

1.6 Concluding remarks 23

Chapter 2: Methods 25

2.1 Lineaments 25

2.2 Fieldwork 28

2.2.1 Definitions 29

2.2.1.1 Foliation 29

2.2.1.2 Fractures, joints and faults 29

2.2.1.2.1 The Coulomb-Navier Criterion 30

2.2.1.2.2 Reactivation of faults 33

2.2.1.3 Fault structure 34

2.2.1.4 Fault rocks 35

2.2.1.4.1 Cataclastic Fault Rocks 38

2.2.1.4.2 Pseudotachylite 39

2.2.1.4.3 Ductile fault rocks 39

2.2.1.5 Kinematic (shear sense) indicators 39

2.2.1.5.1 Subsidiary fractures arrays 40

2.2.1.5.2 Slickenfibres and slickenlines 40

2.2.1.6 Recognition of Reactivation 43

2.2.1.7 Fluid flow in the crust 43
2.2.2 Palaeostress 44
2.2.3 Tangent-lineation plots 45
2.2.3.1 Simple Shear Tensor Average Stress Inversion Method (Sperner et al., 1993) 46
2.3 Fracture attribute analysis - 1D Line transects 47
2.3.1 Spacing and aperture 47
2.3.2 Fracture attribute data distribution types 48
2.3.2.1 Power-law distribution 50
2.3.2.2 Negative exponential distribution 50
2.3.2.3 Log-normal distribution 51
2.3.2.4 Factors affecting data distribution 51
2.3.3 Bulk attributes 53
2.3.3.1 Fracture density 53
2.3.3.2 Coefficient of Variation 53
2.4 Thin Section Work 54
2.4.1 Scanning Electron Microscopy 55
2.4.1.1 Energy dispersive x-ray spectroscopy 56
Chapter 3: Brittle faulting and fracturing in the Stornoway Region of Lewis, and the relationship between the basement and the Stornoway Formation 57
3.1 Introduction 57
3.1.1 Rationale and Objectives 57
3.2 Geological Setting 58
3.2.1 Regional Geology 58
3.2.2 Local Geology of the Stornoway Region 59
3.2.2.1 Lewisian Gneiss 60
3.2.2.2 Stornoway Formation 60
3.2.3 Study sites and methods 62
3.3 Stornoway Formation 63
3.3.1 Stornoway Formation Lineaments: 63
3.3.2 Field observations within the Stornoway Formation 65
3.3.2.1 Fault characterisation 66
3.3.2.2 Inferred faulting sequence within the Stornoway Formation 68

3.3.2.3 Bounding Faults 75
3.3.3 Stornoway Formation Fault Rock Microstructure Characterisation 75
3.3.3.1 Country Rock Microstructures 75
3.3.3.2 Sequence of Fault Formation 76
3.3.3.3 Deformation Processes 80
3.3.3.4 Clay Development 85
3.3.3.5 Fluid Flow and mineralisation 87
3.4 Lewisian Gneiss of the Stornoway Region 93
3.4.1 Lewisian Gneiss Lineaments 93
3.4.2 Field observations: Lewisian-hosted Faults 96
3.4.2.1 Eye Peninsula 98
3.4.2.1.1 Garrabost 98
3.4.2.1.2 Pabail South 100
3.4.2.1.3 Pabail North 102
3.4.2.1.4 Seisiadar South 104
3.4.2.1.5 Seisiadar North 107
3.4.2.1.6 Port Mholair 109
3.4.2.1.7 Suardail 111
3.4.2.2 Tob Leireabhaigh and the Memorial Cairn 111
3.4.2.3 Tolstadh Beach and Gleann Tolstadh 116
3.4.2.4 Arnish 118
3.4.3 Summary of Stornoway Region Lewisian Fieldwork 120
3.4.4 Basement-hosted fault rock characterisation 121
3.4.4.1 Fault rock types 123
3.4.4.2 Fault rock discussion 141
3.4.5 Fieldwork Fault Orientation Results – splitting using fault rock analysis 144
3.4.6 Effect of Foliation 145
3.5 Basement cover interface 147
3.5.1 Basement cover interface field localities 148
3.5.1.1 Garrabost 148
3.5.1.2 Dun Mor 150
3.5.1.3 Suardail 153
3.5.1.4 Earabhig 156
3.5.2 Summary of faulting at the basement-cover contact 159

3.5.3 Basement-cover interface microstructures 160
3.6 Synthesis of Results 163
3.6.1 Lineaments 163
3.6.2 Fieldwork 163
3.6.3 Microscope Results 167
3.6.4 Synthesis 168
3.6.5 Conclusions 172
Chapter 4: Brittle faulting and fracturing within Lewis 174
4.1 Introduction 174
4.1.1 Objectives 174
4.2 Geological background 174
4.2.1 Regional Geology 175
4.2.1.1 OHFZ 175
4.2.1.2 Post-Caledonian Faulting 175
4.2.2 Study Sites and methods 175
4.3 Lineament analysis 177
4.4 Fieldwork Results – West Lewis and North Lewis 180
4.4.1 North Lewis: Cunndal/Port Stoth E-W faulting 180
4.4.1.1 Cunndal 182
4.4.1.2 Port Stoth 184
4.4.1.3 Port Ness 186
4.4.1.4 Summary of N Lewis 188
4.4.2 West Lewis and Bernera: NNW and ENE trending lineaments 188
4.4.2.1 Mealabost, Siadar and Bragar 189
4.4.2.2 Dail Beag and Dail Mhor 191
4.4.2.3 Garenin 195
4.4.2.4 Carloway and Breascleit 199
4.4.2.5 Bernera 202
4.4.2.6 W Lewis summary 206
4.4.3 Seaforth Lineament and related outcrops 207
4.4.3.1 Cliobh and road cuttings 207
4.4.3.2 Seaforth Valley 211
4.4.3.3 Rhenigidale 216

4.4.3.4 Seaforth Lineament Summary 219
4.5 Fieldwork Results from eastern Lewis 219
4.5.1 Tolstadh Gob Thais 220
4.5.2 Parc District, East Lewis 224
4.5.2.1 Cearsiadar Road and Cearsiadar Quarry 225
4.5.2.2 Marbhig 228
4.5.2.3 Orasaigh Quarry 231
4.5.3 Summary of fieldwork results 235
4.6 Fault rock characterisation 237
4.6.1 E-W dip-slip faults: North Lewis 237
4.6.2 NNW-SSE trending structures – Rhenigidale and Seaforth 239
4.6.3 E-W structures, strike-slip - Orasaigh 243
4.6.4 Summary of rock microstructures 246
4.6.4.1 Conditions of faulting 246
4.7 Discussion 247
4.7.1 Lineament analysis 247
4.7.2 Fieldwork: Faulting Synthesis 247
4.7.3 Basement structural controls on faulting 250
4.7.4 Brittle fault rocks: conditions of formation 251
4.7.5 Differences between east and west Lewis 251
4.7.6 Seaforth Lineament 252
4.7.7 Synthesis 253
4.8 Conclusions 258
Chapter 5: Brittle faulting and fracturing within Harris and Scalpay 260
5.1 Introduction 260
5.1.1 Objectives 260
5.2 Geology 261
5.2.1 Regional Geology 261
5.2.1.1 Outer Hebrides Fault Zone 261
5.2.1.2 South Harris Shear Zones (SHSZ) 261
5.2.1.3 Post-Caledonian Faulting 262
5.2.2 Study Sites and methods 262

5.3 Lineament analysis....264
5.4 Fieldwork results outside the OHFZ....268
5.4.1 Beitearsaig and Hushinish Road, NW Harris....269
5.4.2 Luskentyre, Luskentyre Old Road and Grose Bay....273
5.4.3 Borve and Scarasta....278
5.4.4 Northton....281
5.4.5 Summary of fieldwork outside the OHFZ....283
5.5 Fieldwork results within the OHFZ....284
5.5.1 Rubha Vallerip....284
5.5.2 Scalpay....288
5.5.3 Summary of Fieldwork inside OHFZ....292
5.6 Fieldwork results synthesis....293
5.6.1 Pre-Mesozoic structures....293
5.6.2 Mesozoic and younger structures....294
5.7 Fault rock characterisation....296
5.7.1 NW-SE striking faults with soft gouge – Scalpay and Beitearsaig....296
5.7.1.1 Scalpay....296
5.7.1.1.1 Conditions of faulting at Scalpay....298
5.7.1.2 Beitearsaig....299
5.7.1.2.1 Conditions of faulting at Beitearsaig....302
5.7.1.3 Summary and comparison of fault rocks from Beitearsaig and Scalpay....302
5.7.2 NW-SE striking faults with basement inheritance from mylonite – Grose Bay....303
5.7.2.1 Conditions of faulting at Grose Bay....304
5.7.3 NNE-SSW striking faults with zeolite mineralisation – SW Harris....305
5.7.3.1 Fault rocks from the meta-sediments....305
5.7.3.2 Fault rocks from the metanorite....307
5.7.3.2.1 Conditions of faulting at Northton....310
5.7.4 Summary of microscopy observations....310
5.8 Discussion....311
5.8.1 Lineament analysis....311
5.8.2 Fieldwork: Faulting synthesis for Harris....311
5.8.3 Basement structural controls on faulting....319

5.8.4 Brittle fault rocks: conditions of formation 319
5.8.5 Synthesis 321
5.9 Conclusions 324
Chapter 6: Brittle faulting and fracturing in the Clair core 326
6.1 Introduction 326
6.1.1 Rationale and Objectives 328
6.2 Geology and Previous Work 329
6.2.1 Regional Geology 329
6.2.1.1 Basement Geology 330
6.2.1.2 Clair Group Geology 331
6.2.1.3 Fractures in the Clair Field 332
6.2.1.3.1 Fracturing in the Basement 332
6.2.1.3.2 Fracturing in the Cover (Clair Group) 332
6.2.1.3.3 Fracture fills 335
6.2.1.4 Oil at Clair 336
6.2.2 The Clair Cores and Study Locations 336
6.3 Macroscopic Core Observations 337
6.3.1 Clair Group 337
6.3.2 Basal Conglomerate and Basement-Cover Interface 341
6.3.2.1 Basal conglomerate 341
6.3.2.2 Basement-cover interface 344
6.3.3 Summary of findings from the cover 345
6.3.4 Basement 346
6.3.5 Summary of findings from macroscopic observations of the core 351
6.4 Microscopy 351
6.4.1 Clair Group microscopic observations 351
6.4.1.1 Well 206/8-10z 352
6.4.1.2 Well 206/8-8 353
6.4.2 Basement microscopic observations 355
6.4.2.1 Well 206/7a-2 355
6.4.2.2 Well 206/8-2 360
6.4.2.3 Well 206/8-8 363
6.4.2.4 Conditions of fracture and faulting in the Clair Field 364

6.4.2.5 Summary of basement microscopy findings 365
6.5 Discussion 368
6.5.1 Basement porosity 369
6.5.2 Comparison to the Hebrides 370
6.5.2.1 Cover 371
6.5.2.2 Basement 372
6.5.2.3 Basement – Cover Interface 372
6.6 Conclusions 373
Chapter 7: Quantification of Fracture Characteristics 375
7.1 Introduction 375
7.1.1 Rationale and Objectives 375
7.1.2 Methodology - a note on attribute vs. cumulative frequency plot interpretation 375
7.2 Spacing - lineament transect data 377
7.2.1 Methods – lineament transects 377
7.2.2 Results 378
7.2.2.1 Summary and discussion 382
7.3 Spacing – Lewis and Harris fieldwork transect data 382
7.3.1 Methods – fieldwork transects 382
7.3.1.1 Study sites for transect data collection 384
7.3.2 Results 385
7.3.2.1 Background fracturing 387
7.3.2.1.1 Summary and discussion 390
7.3.2.2 Mesozoic faulting 390
7.3.2.2.1 Summary and discussion 402
7.3.2.3 Cenozoic E-W striking faulting 403
7.3.2.3.1 Summary and discussion 406
7.3.2.4 Lithological effects 407
7.3.2.4.1 Massive vs. banded gneiss 407
7.3.2.4.1.1 Summary and discussion 414
7.3.2.4.2 Fracturing within the SHSZ 415
7.3.2.4.2.1 Summary and discussion 419
7.3.3 Spacing data from Lewis and Harris Summary 420
7.4 Spacing data from Clair 421

7.4.1 Methods – core transects 421
7.4.1.1 Study sites for transect data collection 421
7.4.2 Clair A to E (Clair Group) spacing results 422
7.4.2.1 Clair A to E (Clair Group) spacing summary and discussion 426
7.4.3 Clair F (basal conglomerate and basement) spacing results 427
7.4.3.1 Clair F (basement) spacing summary and discussion 429
7.5 Aperture - Lewis and Harris fieldwork transect data 430
7.5.1 Preliminary aperture mechanics investigation 431
7.6 Aperture data from Clair 436
7.6.1 Clair A to E aperture results 436
7.6.1.1 Clair A to E aperture summary and discussion 438
7.6.2 Clair F (basement) and onshore aperture results 438
7.6.2.1 Clair F (basement) and onshore aperture summary and discussion 441
7.7 Discussion 441
7.7.1 Lineament transect spacing 441
7.7.2 Fieldwork transect spacing and aperture 442
7.7.3 Clair Field spacing and aperture 444
7.8 Conclusions 445
Chapter 8: Discussion and Conclusions 448
8.1 Introduction 448
8.2 Synthesis 448
8.2.1 Stornoway Formation and surrounding basement faulting 448
8.2.2 Faulting on Lewis and Harris 451
8.2.3 Clair Field 454
8.2.4 Comparison between the mainland, Outer Hebrides and Clair 456
8.2.5 Thin section work 460
8.2.5.1 Thin section work – cover 460
8.2.5.2 Thin section work – basement 461
8.2.5.3 Porosity at Clair 461
8.2.5.4 Tectonic synthesis 462
8.2.6 Scalability of fractures 466
8.3 Impact 467

8.3.1 Applications 470
8.4 Conclusions 471
8.5 Future Work 473
References 475
Appendices 486

List of Figures

Figure 1.1: Map of the lithology of the Lewisian Gneiss Complex of the Outer Hebrides. Ages of the components of the Outer Hebrides.....5
Figure 1.2: Map showing trend of foliation, digitised from the BGS maps of Lewis and Harris.....11
Figure 1.3: Linkage of shear zones across the Minch as postulated by Dearnley (1962).....15
Figure 1.4: Orientations of fractures and foliation from inclined well 205/21a-4z in the Lancaster Prospect (from Slightam, 2012).....18
Figure 1.5: Structural map offshore northern Scotland......19
Figure 2.1: Lidar data from the northern tip of Great Bernera at 1:25,000 scale......26
Figure 2.2: Foliation trend in blue digitised from BGS structural maps......28
Figure 2.3: Types of fractures.....29
Figure 2.4: Fault classes based on relative displacements across the fault.....30
Figure 2.5: Mohr circle representation of stress at failure for 2D example.....32
Figure 2.6: (**A**) Andersonian Theory of Faulting. (**B**) Conjugate faulting. **C**) 3D modification.....33
Figure 2.7: Fault zone terminology (Caine et al., 1996).....35
Figure 2.8: Breccia classification (Woodcock and Mort, 2008).....37
Figure 2.9: Widely cited conceptual model of fault rock variation with temperature/pressure conditions (depth).....38
Figure 2.10: Subsidiary fractures that can be used to determine kinematics of a fault.....40
Figure 2.11: Slickenfibre development on a fault surface.....41
Figure 2.12: Slickenline formation on fault surfaces.....42
Figure 2.13: Examples of fault shear sense criteria on brittle fault surfaces.....42
Figure 2.14: Construction and interpretation of tangent lineation diagrams.....45
Figure 2.15: Palaeostress analysis results from the Simple Shear Tensor method.....46
Figure 2.16: Showing measurements obtained for aperture and spacing along a 1D line transect.....48
Figure 2.17: Aperture vs Average Spacing/Normalised cumulative frequency.....48
Figure 2.18: Fault parameter distribution types, presented with logged and linear axes.....49
Figure 2.19: Borve 2 spacing plot with logarithmic x and y axes.....52
Figure 2.20: Method for obtaining oriented samples form outcrop.....54
Figure 2.21: SEM images of cataclasite from the Stornoway Formation.....55
Figure 2.22: Spectrum obtained from scanning a selected mineral.....56
Figure 3.1: The location and cross section of the Stornoway Formation.....59
Figure 3.2: From Steel and Wilson (1975), showing the three unit model and changing active fault scarps through time in the Stornoway Formation.....61
Figure 3.3: Histogram of fault dips measured in the Stornoway Formation.....62

Figure 3.4: Map showing the lineament analysis within the Stornoway Formation and results (**A**) compared to fieldwork results (**B**) 64
Figure 3.5: Stornoway Formation lineaments by area. 65
Figure 3.6: Map showing localities visited within the Stornoway Formation and surrounding Lewisian Gneiss. 66
Figure 3.7: Field images 67
Figure 3.8: Top: Stratigraphic log from Steel and Wilson (1975), showing the three units of the Stornoway Formation. Bottom: Tangent lineation plots of fieldwork results split by units. 70
Figure 3.9: Type localities for each fault set in the Stornoway Formation.....73
Figure 3.10: Chronological sequence of fault sets and Tertiary dyke intrusion with stress inversions carried out on fieldwork data collected from faults within the Stornoway Formation 74
Figure 3.11: Development of fault rock within the Stornoway Formation 80
Figure 3.12: Deformation characteristics from Stornoway Formation fault rocks.....83
Figure 3.13: Kinematic indicators in Stornoway Formation fault rocks. 84
Figure 3.14 (next page): Clay developed within fault rocks of the Stornoway Formation 86
Figure 3.15: Evidence for fluid flow interaction within fault gouges and cataclasites of the Stornoway Formation 90
Figure 3.16: Fluid flow evidence from SEM analysis, all from localities at Garrabost/Aignish 92
Figure 3.17: Lineament analysis results from within the Lewisian performed on Nextmap lidar images at multiple scales 94
Figure 3.18: Foliation in the Lewisian Gneiss as digitesed from the BGS 1:100,000 scale Lewis and Harris structure maps 95
Figure 3.19: Lineament azimuth (degrees) vs lineament length (m) for Eastern Lewis. 96
Figure 3.20: Field localities in the Lewisian Gneiss of the Stornoway region.....97
Figure 3.21: Outcrop photos and interpretation from Garrabost 99
Figure 3.22: Stereonet of data collected from Garrabost 100
Figure 3.23: Outcrops at Pabail South 101
Figure 3.24: All measurements from Pabail South 102
Figure 3.25: Pabail North Outcrops. 103
Figure 3.26: Stereonet of data collected from Pabail North. 104
Figure 3.27: Seisiadar South outcrop images 107
Figure 3.28: Stereonet of data collected from Seisiadar South.....107
Figure 3.29: Seisiadar North outcrop images 108
Figure 3.30: Seisiadar North stereonet.....109
Figure 3.31: Port Mholair exposures 110
Figure 3.32: Stereonet of data collected at Port Mholair.....110
Figure 3.33: Stereonet of data collected at Suardail in the Lewisian. 111

Figure 3.34: Tob Leireabhaigh outcrop images. 113
Figure 3.35: Exposure at Memorial Cairn. 114
Figure 3.36: Principal faults at Memorial Cairn locality....115
Figure 3.37: Stereonet of data collected from Tob Learabhaigh and Memorial Cairn localities ...115
Figure 3.38: Outcrop images of the area around Tosltadh Beach....117
Figure 3.39: Stereonet of data collected at Tolstadh 118
Figure 3.40: Outcrops in the Lewisian at Arnish.....119
Figure 3.41: Stereonet of data collected from Arnish. 120
Figure 3.42 : Setting of Mesozoic fault at Suardail.
Figure 3.43: Group 1 fault rocks, all from Pabail South.....126
Figure 3.44: Epidote-cemented fault rocks (Group 2 faults).....129
Figure 3.45: Pumpellyite/clinozoisite-bearing fault rock (Group 3 fault rock).....130
Figure 3.46: Zeolite bearing faults, lacking adularia and albite (Group 4 fault rocks) 133
Figure 3.47: Adularia – zeolite – authigenic clay faults (Group 4 fault rocks).....134
Figure 3.48: Adularia, zeolite, and authigenic clay, porous fault rocks under SEM (Group 4 fault rocks).....135
Figure 3.49: Clay-bearing gouge and cataclasite developed along the major SE dipping fault at Seisiadar South (Group 5 fault rock).....138
Figure 3.50: Characteristics of faults with clay-bearing gouges (Group 5 fault rocks).....140
Figure 3.51: Map showing localities found with oil staining. 141
Figure 3.52: Fieldwork orientation results, showing foliation; faults are identified as pre-Mesozoic, and Mesozoic-Cenozoic age.....145
Figure 3.53: Graphs showing fault C value vs foliation C value (top), and fault K value vs foliation K value (bottom), with a linear regression line fitted to all of the data. 147
Figure 3.54: Contact at Garrabost. 149
Figure 3.55: Stereonet of data collected from the Garrabost contact.....150
Figure 3.56: Outcrop of Stornoway Formation 'cake' at Dun Mor.....153
Figure 3.57: Stereonet of data collected at Dun Mor.....153
Figure 3.58: Clastic and carbonate veins measured at Dun Mor. 153
Figure 3.59: Suardail outcrop images. 155
Figure 3.60: Data collected at Suardail within the Stornoway Formation and Lewisian Gneiss. ..156
Figure 3.61: Fault orientation data collected from Earabhig. 157
Figure 3.62: Earabhig basement-cover interface images. 158
Figure 3.63: Stereonets of data collected from Dun Mor, Earabhig and Suardail 159
Figure 3.64: Photomicrographs from the basement-cover interface. 162
Figure 3.65: Interpreted lineaments and fault orientations, based on fieldwork results. 168
Figure 3.66: Terrestrial laser scan data from Suardail.....170

Figure 3.67: Conceptual model of faulting in the Stornoway Region with accompanying fault rock images 172
Figure 4.1: Showing geology of Lewis and Harris underlain by digital surface model (DSM) processed from Nextmap ® data.. 176
Figure 4.2: Digitised Foliation trend from Lewis and Harris (left, in blue) and lineaments picked from DSM (right, in green).. 177
Figure 4.3: Western Lewis lineament analysis and fieldwork results comparison. 178
Figure 4.4: Eastern Lewis lineament analysis and fieldwork results comparison 179
Figure 4.5: Variation in lineament orientation overlying foliation trend 180
Figure 4.6: Geological map of N Lewis 181
Figure 4.7: Outcrop at Cunndal. 183
Figure 4.8: Stereonet of data collected at Cunndal 184
Figure 4.9: Outcrop at Port Stoth 185
Figure 4.10: Orientation data collected from Port Stoth 186
Figure 4.11: Outcrop at Port Ness 187
Figure 4.12: Structural data collected from Port Ness 188
Figure 4.13: Field localities in western Lewis and northwest Harris 189
Figure 4.14: Outcrop at Siadar 190
Figure 4.15: Orientation data collected from Siadar and Mealabost 190
Figure 4.16: Location of Dail Beag and Dail Mhor localities. 193
Figure 4.17: Outcrops at Dail Beag and Dail Mhor. 194
Figure 4.18: Orientation data collected from Dail Beag and Dail Mhor 195
Figure 4.19: Map of field localities at Garenin. 197
Figure 4.20: Outcrop at Garenin 198
Figure 4.21: Orientation data collected from Garenin 199
Figure 4.22: Carloway and Breascleit field localities 200
Figure 4.23: Field localities at Carloway 201
Figure 4.24: Orientation data collected from the Carloway and Breascleit outcrops 202
Figure 4.25: Field localities at Bernera. 204
Figure 4.26: Outcrop at Bernera 205
Figure 4.27: Orientation data collected from Bernera and nearby road cuts 206
Figure 4.28: Field localities at Cliobh 209
Figure 4.29: Outcrop at Cliobh 210
Figure 4.30: Orientation data collected from Cliobh. 211
Figure 4.31: Field Localities on the Seaforth Lineament 213
Figure 4.32: Main field localities in the Seaforth Valley 215
Figure 4.33: Structural log collected across the Seaforth Valley fault 215

Figure 4.34: Orientation data collected from the Seaforth Valley 216
Figure 4.35: Localities at Rhenigidale and Scalpay. 217
Figure 4.36: Field outcrops at Rhenigidale. 218
Figure 4.37: Orientation data collected from Rhenigidale 218
Figure 4.38: Field localities of east Lewis. 220
Figure 4.39: Map of localities at Gob Thais 222
Figure 4.40: Field localities at Gob Thais within the OHFZ 223
Figure 4.41: Orientation data collected from Gob Thais 223
Figure 4.42: Field localities in the Parc District. Lineaments indicated. 225
Figure 4.43 Field outcrops along road to Cearsiadar and at Cearsiadar Quarry. 228
Figure 4.44: Orientation data collected from Cearsiadar Road and Quarry 228
Figure 4.45: Field localities at Marbhig.....230
Figure 4.46: Orientation data collected from Marbhig 231
Figure 4.47: Field locality at Orasaigh Quarry 233
Figure 4.48: Orasaigh structural log taken perpendicular to the main fault surface at Orasaigh. .234
Figure 4.49: Orientation data collected from Orasaigh.....235
Figure 4.50: Photomicrographs of faults at Cunndal and Port Stoth, northern region of Lewis....238
Figure 4.51: Photomicrographs from Seaforth and Rhenigidale 241
Figure 4.52: BSEM images from Seaforth 242
Figure 4.53: BSEM images from Seaforth 243
Figure 4.54: Photomicrographs of fault rocks collected from Orasaigh Quarry. 245
Figure 4.55: Lineament analysis results from west Lewis 254
Figure 4.56: Conceptual structural model of faulting in Lewis with accompanying fault rock sections where available. 256
Figure 4.57: The Seaforth Fault and digitised major offshore structures.....257
Figure 5.1: Showing geology of Lewis and Harris underlain by digital surface model (DSM) processed from Nextmap ® data.. 263
Figure 5.2: Digitised foliation trend on Lewis and Harris based on BGS data 265
Figure 5.3: South Harris lineament analysis data 266
Figure 5.4: Variation of lineament orientation overlying foliation trend. 267
Figure 5.5: Lineament azimuth vs lineament length for lineaments picked on Harris. 268
Figure 5.6: Field localities at Beitearsaig and along Hushinish Road with interpreted lineaments. 271
Figure 5.7: Outcrop at Beitearsaig. 272
Figure 5.8: Orientation data collected from Beitearsaig and Hushinish Road. 273
Figure 5.9: Field Localities at Grose Bay and Luskentyre.....276
Figure 5.10: Outcrops at Luskentyre and Grose Bay 277

Figure 5.11: Orientation data collected from Luskentyre, Luskentyre Old Road and Grose Bay...278
Figure 5.12: Outcrops at Borve and Scarasta 280
Figure 5.13: Orientation data from Borve and Scarasta.....280
Figure 5.14: Outcrop at Northton.....282
Figure 5.15: Orientation data from Northton.....283
Figure 5.16 : Outcrop at Rubha Vallerip 288
Figure 5.17: Orientation data collected from Rubha Vallerip 288
Figure 5.18: Map of field localities at Scalpay 290
Figure 5.19: Field localities on Scalpay 291
Figure 5.20: Orientation data collected from Scalpay.....291
Figure 5.21: Photomicrographs of foliated fault gouge from Scalpay North Harbour Fault.....298
Figure 5.22: Photomicrographs of sample collected from Beitearsaig foliated fault rock.....302
Figure 5.23: Photomicrographs of fault samples from Grose Bay.....304
Figure 5.24: Photomicrographs of cataclasite and vein samples from Northton 308
Figure 5.25: Photomicrographs of gouge collected from fault at Northton. 309
Figure 5.26: From Evans et al. (1991), showing postulated Oligocene Basin immediately offshore SE Harris. 315
Figure 5.27: (**A**) Digitised major structures on Lewis and Harris. (**B**) Sinistral dominantly strike-slip displacements on faults indicated 318
Figure 5.28: Lineament analysis results and fieldwork results from Harris. 322
Figure 5.29: Conceptual block model of fault in Harris with accompanying fault rock sections where available.....323
Figure 6.1: Map of basement highs and related Mesozoic faults, showing outline of Scotland. Moine Thrust also shown.....327
Figure 6.2: Clair Field phase 1 development area 328
Figure 6.3: Stratigraphic details of the Clair Group 331
Figure 6.4: Lineaments picked from the cover sequence (top) and basement (bottom) from 3D seismic horizon analysis in the Clair Field.....334
Figure 6.5: From Barr et al. (2007). (**A**) Open fracture strike from well data with number of open fractures seen in each well. (**B**) Open and closed fractures from well 206/8-8. 335
Figure 6.6: Observations from cores of the Lower Clair Group.....341
Figure 6.7: Observations from the basal conglomerate, Lower Clair Group.....344
Figure 6.8: Observations from the basement-cover interface of the basal conglomerate (Lower Clair Group) and Lewisian basement 345
Figure 6.9: Clair basement well logs.....349
Figure 6.10: Observations of the Clair basement cores. 351
Figure 6.11: Photomicrographs of vuggy porosity within Unit V of the Lower Clair Group.....353

Figure 6.12: Photomicrographs of fine interstitial sandstone collected from the basal conglomerate.....354
Figure 6.13: Photo micrographs from core 206/7a-2.....360
Figure 6.14: Photomicrographs from 206/8-2.....363
Figure 6.15: Photomicrographs from basement fault zone at 2490.3 m in well 206/8-8.....364
Figure 7.1: Geological map of Lewis and Harris, showing lineament transects and localities of transect data collected on fieldwork.....378
Figure 7.2: Rose diagrams of lineament orientations intersected by each transect.....380
Figure 7.3: Lineament transects results, showing spacing (m) vs. cumulative frequency/transect line length.....381
Figure 7.4: Orientation data collected from transects listed in Table 7.5.....387
Figure 7.5: Distribution of spacing data collected from joint dominated localities.....389
Figure 7.6: Map showing location of Seaforth, Memorial Cairn and Seisiadar transects and stereonets.....392
Figure 7.7: Map showing location of Garrabost, Pabail and Port Stoth transects and stereonets.....393
Figure 7.8: Graphs of fault perpendicular spacing data collected from transects at Mesozoic fault dominated localities.....396
Figure 7.9: Graphs of fault parallel spacing data collected from transects at Mesozoic fault dominated localities.....397
Figure 7.10: Plots of data collected at Pabail.....399
Figure 7.11: Distribution of spacing data collected from Port Stoth.....400
Figure 7.12: Distribution of spacing data collected from Garrabost.....401
Figure 7.13: Distribution of spacing data collected from Orasaigh.....405
Figure 7.14: Orientation data collected from the transects at Orasaigh.....406
Figure 7.15: Map showing location of transects at Borve.....408
Figure 7.16: Graph of fractures per metre, showing fracture frequency along the Borve transects.....410
Figure 7.17: Distribution of spacing data collected from Borve.....412
Figure 7.18: Distribution of spacing data collected from Borve 1.....413
Figure 7.19: Distribution of spacing data collected from the SHSZ.....417
Figure 7.20: Orientation data collected from the transects on the SHSZ.....419
Figure 7.21: Graphs of spacing data collected from transects Clair transects A to E.....425
Figure 7.22: Graphs of spacing data collected from Clair transect F.....428
Figure 7.23: Aperture data collected from Lewis and Harris.....430
Figure 7.24: From Gudmundsson (2011), showing fracture dip dimension (R) and strike dimension (L).....431

Figure 7.25: Log/log plots of aperture vs cumulative frequency/transect length for Mode 1 and Mode 2 fracture recorded from the Memorial Cairn fault-perpendicular transect. 433
Figure 7.26: Distribution of fracture length data from the Memorial Cairn perpendicular transect locality split between mode 1 and mode 2 fractures. 434
Figure 7.27: Relationship between fracture aperture and fracture length, Memorial Cairn fault-perpendicular transect.....435
Figure 7.28: Graphs of aperture data collected from Clair transects A-E. 437
Figure 7.29: Graph of aperture vs cumulative frequency/average spacing. 440
Figure 8.1: 3D block diagram of faulting in the Stornoway Formation 450
Figure 8.2: Map of Lewis and Harris showing major faults 454
Figure 8.3: Comparison of lineament orientations across the Lewisian Gneiss Complex.....458
Figure 8.4: Map showing foliation trend of Harris with South Harris Shear Zones and terrane names marked. 459
Figure 8.5: Fault development model for faults parallel with foliation strike but not dip.....462

List of Tables

Table 1.1: Summary for of tectonic phases identified at Clair (the Faroe Shetland Basin) and in the Outer Hebrides.....20
Table 1.2: Fault classification, after Sibson (1977) and Woodcock and Mort, 2008). For breccia types see Figure 2.8. 36
Table 3.1: Fault and dyke set orientations and chronologies inferred across the Stornoway Formation on the basis of cross cutting relationships. See Figure 3.6 for locations. 68
Table 7.1: Results for lineament transects across the Lewisian Complex. 379
Table 7.2: Table of number of data-points excluded from each plot type (and percentage of total data). 382
Table 7.3: Transect localities from Lewis and Harris. Transects marked parallel and perpendicular were taken parallel and perpendicular to Mesozoic dominated fracture sets. 384
Table 7.4: Line transect results. 385
Table 7.5: Results for background fracturing 387
Table 7.6: Table of number of data-points excluded from each plot type (and percentage of total data). 390
Table 7.7: Details of transects taken at localities dominated by Mesozoic age faults. 394
Table 7.8: Table of number of data-points excluded from each plot type (and percentage of total data). 398
Table 7.9: Line transects undertaken at Orasaigh Quarry. 403
Table 7.10: Showing no of excluded data points.....406
Table 7.11: Results from Transects undertaken at Borve. 409
Table 7.12: Table of number of data-points excluded from each plot type (and percentage of total data). 414
Table 7.13: Results from Transects undertaken at the SHSZ.....415
Table 7.14: Table of number of data-points excluded from each plot type (and percentage of total data). 418
Table 7.15: Transect localities from the Clair cores. 422
Table 7.16: Results from transects Clair A to E. 423
Table 7.17: Fracture fills encountered in the Clair core transects. 423
Table 7.18: Table of number of data-points excluded from each plot type (and percentage of total data). 426
Table 7.19: Results from transect F. 427
Table 7.20: Table of number of data-points excluded from each plot type (and percentage of total data). 429
Table 7.21: Clair A-E aperture data. 436

Table 7.22: Table of number of data-points excluded from each plot type (and percentage of total data). 438
Table 7.23: Aperture data from basement rocks. 439
Table 7.24: Fractures sampled by each transect. 439
Table 7.25: Table of number of data-points excluded from each plot type (and percentage of total data) for Clair F. 441
Table 8.1: Deformation, mineralisation synthesis for Lewis, Harris and Clair. ?? Denotes likely presence, although not proven in the field. 464

Chapter 1: Introduction and Regional Review

The Clair Field is the largest remaining oil field in the UK continental shelf, and is situated in the last frontier oil exploration region, west of the Shetland Islands. The field is of national importance and is likely to be active until at least 2050, with a recent multi-billion pound investment announced by the operators of the field. At Clair, oil is produced from Devonian-Carboniferous Clair Group rocks that overlie Lewisian-like basement rocks of the Rona Ridge (e.g. Allen and Mange-Rajetzky, 1992). The basement of the Rona Ridge lies above the oil-water contact (e.g. Baron et al., 2008), well tests demonstrate that linkage occurs across the field within the basement, and significant production has occurred in tests directly from the basement rocks (Falt et al., 1992; Coney et al., 1993). Production from basement rocks is governed by the existence of fractures (Falt et al., 1992) and production from fractured media is dependent on a number of factors including fracture size, orientation and density (Jolly and Cosgrove, 2003), in addition to fracture mineralisation/fill. Calcite and pyrite filled factures are associated with contemporaneous oil influx, and are often at least partially open (e.g. Finlay et al., 2011; Pless, 2011). Pyrite and oil in these fractures has been dated as Mesozoic in age (Finlay et al., 2011). As the Clair Field basement is poorly sampled from well data and cores, it is important to study analogues for the field in order to better understand fracturing and faulting characteristics and factors influencing fracture development within the basement rocks. In this thesis, fracture systems exposed on the Outer Hebridean islands of Lewis and Harris are studied for this purpose. Study of the fracture systems onshore will also yield better understanding of the history of faulting and fracturing within the Lewisian and may have implications for the geological history of NW Scotland.

Analysis of Lewisian Gneiss rocks in outcrop as an analogue for those offshore is important for the understanding of fracturing in and prediction of reservoir properties (e.g. Pless, 2011; Slightam, 2012). With this in mind, characterisation of faults and fractures in the Hebrides has been undertaken using several techniques, including regional lineament analysis, extensive fieldwork, fault rock analysis, and collection of quantitative 1D line transect data in specific contexts in order to understand particular aspects of fracturing in the Hebrides and at Clair. Together, the techniques used encompass multiple scales and have been used to produce a comprehensive fracture characterisation in the Outer Hebrides and comparison to Clair, contributing to an increased understanding of fractures in these regions.

1.1 Project Aims

This project was initiated in order to meet four specific aims that were originally set out in agreement with the Clair Joint Venture Group:

1. *A detailed characterisation of the fracture patterns and attributes in the onshore Lewisian Complex in the Hebridean Islands*.

   Regional mapping, analysis and microstructural studies are used to group brittle faults into fracture sets using parameters such as orientation, movement direction, nature of infill and relative ages obtained from cross-cutting relationships. This is combined with quantitative studies of the fracture spacing and aperture attributes in particular contexts in order to investigate whether these attributes are generally scale-invariant across the islands, or whether they exhibit more scale-limited domainal patterns.

2. *An assessment of the controls on fracture patterns.*

   In addition to characterisation of fractures, the studies mentioned above are also used to constrain controls on fracture development, such as the presence of foliation and pre-existing structures within the OHFZ. These results can be compared to Clair and the Scottish Mainland fracture study of Pless (2011).

3. *Use mapping and structural analyses to compare and contrast fracture system attributes in adjacent units of basement and cove*r.

   This is achieved through direct comparison of faults between the Lewisian basement and Permo-Triassic Stornoway Formation cover, and within the Clair Field basement and overlying Devonian-Carboniferous Clair Group. This allows identification of Mesozoic faulting within the Lewisian Gneiss of the Hebrides, and gives valuable insights into the nature of deformation processes at the basement/cover interface. At Clair and in the Hebrides, porosity within the basement and cover rocks is examined and compared.

4. *Place further constraints on the geological affinities of the Clair basement*

   An in depth fracture and fracture-fill characterisation on the both the Hebrides and within the Clair Field allows direct comparison of the deformation and mineralisation experienced by the two regions.

These aims are addressed collectively in the following chapters where individual research questions are introduced.

1.2 Structure of this thesis

The chapters present in this thesis are briefly described below. Each chapter contains specific research questions addressed by introduction, background, discussions and conclusions. Due to the general much lower number of structural studies undertaken on the Outer Hebrides when compared to the Scottish mainland, the first three chapters build a framework for the study of brittle fracturing, particularly of Mesozoic and younger ages, within the rocks of Lewis and Harris. This is followed by a comparison study carried out on the Clair core, and finally by a quantitative analysis of specific fracture characteristics.

Chapter 1 – *Introduction and regional review*

This chapter introduces the motivation for and research issues addressed by this work, in addition to providing a regional geological review.

Chapter 2 – *Methodology*

This chapter covers the methods used in this thesis during lineament analysis, fieldwork, and 1D line transect data collection and analysis. Further methods are presented where necessary in each chapter.

Chapter 3 - *Brittle faulting and fracturing in the Stornoway Region of Lewis, and the relationship between the basement and the Stornoway Formation*

This chapter is a study of the faulting and fracturing in the Stornoway Region of Lewis with a main objective of identification of Mesozoic and younger faults, known to be important at Clair, within the Lewisian. This is achieved through use of remote sensing data, field mapping and microscopy.

Chapter 4 – *Chapter 4: Brittle faulting and fracturing within Lewis*

This chapter studies faulting and fracturing more widely on Lewis north and east of the Seaforth Fault, using and building on the fault rock characterisation of Chapter 3 in order to identify further Mesozoic and younger structures within the Lewisian across the island.

Chapter 5 - *Brittle faulting and fracturing within Harris and Scalpay*

This chapter studies faulting and fracturing south and west of the Seaforth Fault, where orientations are notably different to those found elsewhere in Lewis. Mesozoic structures are identified and examined.

Chapter 6 - *Brittle faulting and fracturing in the Clair core*

This chapter studies fracturing within the Lewisian-like basement and Clair Group cover rocks of the Clair Field. Controls on fault rock development and fracture infill are investigated and compared to the onshore findings, alongside the origins of the important porosity occurring in the Clair Field.

Chapter 7 - *Quantification and scalability of fracture characteristics*

This chapter studies the quantification of spacing and aperture data collected from 1D line transect data across fractures and faults in specific contexts in the Clair Field and the Outer Hebrides.

Chapter 8 – *Discussion and Conclusions*

This chapter builds on the discussions present in the previous chapters in order to summarise the results of the work undertaken in this thesis.

1.3 Lewisian Complex Regional Geology

1.3.1 Geological background

The Lewisian Gneiss Complex (LGC) is part of an ancient cratonic area found on both sides of the Atlantic (Krabbendam et al., 2009). The LGC was, throughout the Precambrian, part of three supercontinents, Kenorland, Columbia, Rodinia (Pesonen et al., 2003), subsequently being incorporated into Laurentia (Krabbendam et al., 2009). The region then lay near the margin of Laurentia until the breakup of Pangaea and the formation of the Atlantic (Macdonald and Fettes, 2007). As such, the Lewisian Gneiss Complex is related to the terranes of Canada and Greenland, and is particularly correlated with the Nagssugtoqidian gneisses of Eastern Greenland (Myers, 1987; Mason and Brewer, 2004). Originally, the LGC was interpreted as one contiguous block with different areas having undergone different levels and stages of metamorphism. Recent

geochemical dating has since been used to produce a terrane-based hypothesis for the LGC (Kinny et al., 2005, Figure 1.1), with the Lewisian Gneiss Complex formed from the coalescence of different blocks/terranes, each containing a different tectono-metamorphic Archaean and Proterozoic history.

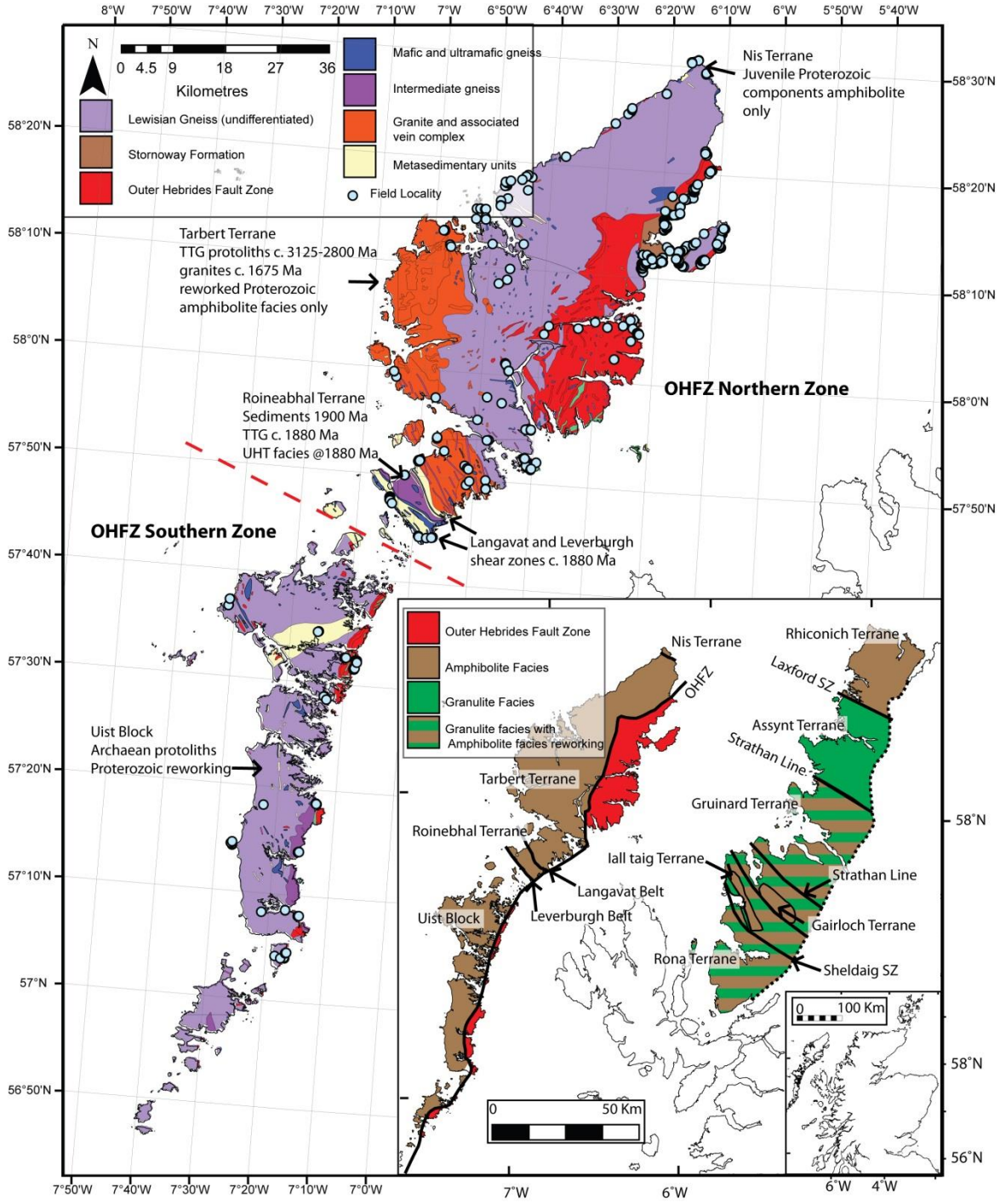

Figure 1.1: Map of the lithology of the Lewisian Gneiss Complex of the Outer Hebrides. Ages of the components of the Outer Hebrides are indicated. Inset shows the positions of the proposed component terranes and ages of the basement rocks. Inset shows the location of the Complex in NW Scotland. ST, Sole Thrust of the Moine Thrust Zone; MT, Moine Thrust; OHFZ, Outer Hebrides Fault Zone; SZ, shear zone. Modified from Kinny et al. (2005) and BGS maps of the area.

In general, the gneisses of the LGC are typically grey in colour with a well-defined foliation, however metasediments and mafic rock units are also present incorporated into the LGC. The earliest gneiss formation is believed to have begun around 3000 Ma during the late Archaean, with intrusion of TTG (Tonalite-Trondhjemite-Granodiorite) plutonic material into the crust (Krabbendam et al., 2009). Significant later magmatism, intrusive dyking, and deformational events have since affected the LGC (e.g. Trewin, 2004; Goodenough et al., 2009).

Following emplacement of TTG rocks, several broad stages of metamorphism have been recorded from the LGC, described below:

1. Badcallian granulite facies metamorphism in the late Archaean/early Palaeoproterozoic. This phase of metamorphism affected parts of the LGC. Two high grade events have been recognised at 2730 Ma (Gruinard terrane) and 2490 Ma (Assynt terrane) (Krabbendam et al., 2009).
2. Inverian amphibolite facies events, occurring between 2490 - 2400 Ma affecting the Assynt and Gruinard terranes (Krabbendam et al., 2009), pre-dating the Scourie Dyke Suite. The Inverian event is linked to the development of the NW-SE trending shear zones that often separate terranes (e.g. Goodenough et al., 2010).
3. Intrusion of Scourie Dykes, that have been correlated with the 'Younger Basic' dykes of the Outer Hebrides, occurring between 2400 – 2000 Ma (Krabbendam et al., 2009).
4. Granulite facies metamorphism of the South Harris Igneous Complex occurred at 1870-1830 Ma (Krabbendam et al., 2009). Some authors attribute this to the Laxfordian event (below) (Kinny et al., 2005).
5. Laxfordian amphibolite to greenschist facies event, occurred at 1740 Ma, with gneisses on the Hebrides undergoing migmatisation and granite intrusion at 1675 Ma (Krabbendam et al., 2009).

In addition to these metamorphic events, various supracrustal and arc-related rocks are present within the LGC. The main examples of supracrustal rocks are found in the Rhoinebhal terrane, Nis terrane, and within the Loch Maree Group (e.g. Trewin, 2004). However other bands of metasediments and probably related mafic igneous units are not uncommon throughout the Lewisian of the Outer Hebrides e.g. in pods and lenses throughout the Eye Peninsula.

Work done on the mainland has found that the LGC may be divided into units separated by NW trending shear zones, across which tectonic histories, metamorphic grade, and lithology can vary significantly. These NW trending shear zones have recently been reinterpreted as fundamental terrane boundaries within the Lewisian (Figure 1.1) (Kinny and Friend, 1997; Friend et al., 2001; Kinny et al., 2005), a hypothesis that is being debated (e.g. Whitehouse and Bridgwater, 2001; Park et al., 2005; Mason and Brewer, 2005). Overall however, the LGC is composed of gneisses

with Archaean protoliths (with exceptions) that have undergone areally-constrained granulite and amphibolite facies metamorphism. The following terranes have been identified within the LGC (Figure 1.1, from Kinny et al., 2005):

- Rhiconich Terrane: Palaeoproterozoic protoliths unaffected by granulite facies metamorphism of the Badcallian and Inverian events. Scourie Dykes cut amphibolite facies structures. Laxfordian event affecting the whole area.
- Assynt Terrane: Archaean protoliths, have been metamorphosed to granulite facies during the Badcallian, with localised retrogression in the later Inverian and Laxfordian events.
- Gruinard Terrane: Protoliths of Archaean age, in addition to supracrustal rock correlated with the Loch Maree Group of the Gairloch terrane. Granulite and ex-granulite facies TTG gneisses.
- Gairloch Terrane: Palaeoproterozoic volcanic and metasedimentary rocks of the Loch Maree Group. Amphibolite facies metamorphism occurred in the Palaeoproterozoic.
- Ialltaig Terrane: Palaeoproterozoic protoliths of TTG granulite and ex-granulite facies gneisses. Granulite facies metamorphism occurred in the Palaeoproterozoic.
- Rona Terrane: Archean age protoliths, with amphibolite facies gneisses formed during the Archaean.
- Nis Terrane: Palaeoproterozoic rocks, dominantly plutonic but with metasedimentary material. Amphibolite facies conditions recorded, highly deformed.
- Tarbert Terrane: Archaean protoliths, TTG gneisses have undergone amphibolite facies metamorphism prior to intrusion by Scourie Dykes (Younger Basics). Extensive granite intrusion and veining on West Lewis and Harris during (Laxfordian) amphibolite facies metamorphism at 1675 Ma.
- Roineabhal Terrane: Palaeoproterozoic South Harris Igneous Complex surrounded by metasedimentary belts, between the Tarbert terrane and Uist block that may be contiguous beneath this terrane (Park, 2005). Evidence of granulite facies metamorphism at 1870 Ma that has been attributed by some authors to the Laxfordian event (Wheeler et al., 2010).

- Uist/Barra Block: Mostly undifferentiated Archaean gneisses at amphibolite facies grade. Granulites exist in the footwall of the Outer Hebrides Fault Zone (OHFZ, see section 1.3.2) on Barra and South Uist.

1.3.2 Outer Hebridean Geology and Tectonic History

As described above, the Outer Hebrides are comprised of three 'terranes' or blocks according to the terrane hypothesis (Kinny et al., 2005). However, as discussed by Park (2005), the Tarbert terrane and the Uist block may be one contiguous unit that underlies the more-or-less isoclinal synform occupied by the South Harris Igneous Complex, bounded by steep NW-SE striking shear zones. Multiple deformation events are known to have affected the gneisses of the Outer Hebrides and have produced a complex overprinted pattern of deformation (Fettes et al., 1992). The main tectonic feature of the Outer Hebrides is the Outer Hebrides Fault Zone (OHFZ) (Sibson, 1977), with a long history of deformation possibly initiated during the Laxfordian event (Fettes et al., 1992). Most of the gneisses within the Outer Hebrides consist of similar TTG gneisses to the mainland with a larger proportion of supracrustal rocks (Whitehouse and Bridgwater, 2001). Owing to the segmented and arcuate nature of the OHFZ, it is often split into a northern (Lewis and Harris) and southern zone (North Uist, Benbecula, South Uist and islands to the south) (e.g. Butler et al., 1995; Butler, 1995; Imber, 1998; Imber et al., 2001; Imber et al., 2002).

In the north of the Outer Hebrides, gneiss formation on Harris occurred at around 2700 - 2800 Ma from U-Pb zircon dating of an amphibole-biotite quartzo-feldspathic gneiss and Pb-Pb dating of a tonalite, respectively (Pidgeon and Aftalion, 1972; Friend et al., 2001). A date of 3125 Ma obtained from a metatexite in northwest Harris is also assumed to represent protolith formation (Friend et al., 2001). The formation of these gneisses has been attributed to the Scourian metamorphic event (Mendum, 2009), and these earliest gneisses have been termed the 'Scourian Gneisses' by Trewin (2004). However, metasediments and associated basic rocks that are enclosed within these gneisses seem to represent the oldest rocks of the complex (Fettes and Mendum, 1987; Fettes et al., 1992). Grey gneisses of the Hebrides are typically amphibole-biotite quartzo-feldspathic gneisses. Pyroxene-bearing gneisses are localised to Barra and South Uist within granulite facies rocks (Coward, 1973) lying in the hangingwall of the Outer Hebrides Fault Zone. This structural relationship may represent the exhumation of these granulite facies units from depth during thrusting (Fettes et al., 1992). However, there is evidence of granulite facies metamorphism also recorded in the footwall rocks of the Outer Hebrides and this spatial distribution of amphibolite and granulite facies rocks may represent an original prograde transition (Fettes and Mendum, 1987; Whitehouse and Bridgwater, 2001). Emplacement of late Scourian granite bodies and microdiorite intrusions (Fettes et al., 1992) are suggested to be related to the breakup of Kenorland (Macdonald and Fettes, 2007).

The Inverian event, occurring after Scourian metamorphism and prior to the intrusion of the Scourie Dykes (aka Younger Basics), is recorded in the Outer Hebrides by NNE-SSW trending folds and NW-SE trending shear zones that often contain Younger Basic dykes (Fettes et al., 1992). On

Lewis, a NE-SW shear zone has been hypothesised due to the rotation of foliation found in NW Lewis (Watson, 1969). The shear zone is believed to lie offshore between Bernera and the Butt of Lewis and also predates the emplacement of the Younger Basic dyke suite (Fettes et al., 1992). A Younger Basic dyke on Lewis has yielded an age of 2400 Ma (Lambert et al., 1970), and these dykes have been widely stated as being equivalent to the mainland Scourie Dyke Swarm and equivalent to the Nagssugtoqidian dykes of Greenland (Mason and Brewer, 2004).

Following intrusion of the Younger Basic suite of dykes, the South Harris Igneous Complex (SHIC) and the Ness belt of north Lewis represent the products of a tectonically active volcanic arc environment (Mendum, 2009). The SHIC is composed of a Palaeoproterozoic andesitic arc-type assemblage metamorphosed to granulite facies, flanked by the Langavat belt to the north and enclosing the Leverburgh belt in the south (Graham, 1980), with both belts being comprised of Palaeoproterozoic metasediments (Whitehouse and Bridgwater, 2001; Trewin, 2004). The granulite metamorphism associated with the area has been attributed to the Laxfordian metamorphic event recognised elsewhere as amphibolite facies grade (Whitehouse and Bridgwater, 2001). Mendum (2009) suggests that the sediments of the Langavat and Leverburgh Belts were deposited in a volcanic arc environment around 1890 – 1880 Ma, followed by subduction and intrusion of the SHIC. The SHIC is composed of four meta-igneous lithologies: metagabbro, meta-anorthosite, metanorite and metadiorite (Mendum, 2009). During the Laxfordian, the Langavat and Leverburgh Belts were active as shear zones (Coward and Park, 1987). Coward and Park (1987) suggest that the Langavat shear zone acted as a low angle structure into which the granulite facies rocks of the igneous complex were intruded. The Langavat Belt has been postulated to be a terrane boundary (Friend et al., 2001; Trewin, 2004). The amphibolite grade Leverburgh Belt lies in the same structural setting as the Langavat Belt at the base of the South Harris Complex and is also sheared (Fettes et al., 1992; Park, 2010). As these belts are sheared they are also referred to as the South Harris Shear Zones (e.g. Trewin, 2004) and they have been equated to the NW-SE trending basement hosted shear zones within the Lewisian of the Scottish mainland such as the Canisp Shear Zone (e.g. Dearnley, 1962; Park, 2010; Whitehouse and Bridgwater, 2001). However, other authors suggest that the mainland shear zones detach along the OHFZ (e.g. Lailey et al., 1989).

Laxfordian reworking was pervasive in the Outer Hebrides with the exception of localised areas of eastern Barra, the Uists and Benbecula. It produced a folding style characterised by broad hinge zones and narrow attenuated limbs (Fettes et al., 1992). The Laxfordian is thought to have occurred during continental collision as part of the process of the growth of Columbia (Macdonald and Fettes, 2007). On the Outer Hebrides, Laxfordian reworking was widespread with only small pods of Scourian fabrics preserved (Coward, 1990).The Laxfordian occurred under amphibolite

facies conditions (Mendum, 2009), with, perhaps, the exception of the SHIC and metasedimentary belts at granulite facies grade (Whitehouse and Bridgwater, 2001). Archaean ('Scourian') gneisses were reworked with development of a foliation and lineation (Fettes and Mendum, 1987; Fettes et al., 1992; Mendum, 2009). In water deficient granulitic units and large Younger Basic bodies Laxfordian metamorphism is limited to local shear zone development. Pseudotachylites from Lewis dated to 1900 Ma may record early Laxfordian deformation (Sherlock et al., 2009).

Migmatisation, granite emplacement and pegmatitic veining are associated with the Laxfordian event, particularly in northwest Harris and southwest Lewis, forming the Uig Hills - South Harris Granite Vein Complex, around 1400 Ma (Fettes et al., 1992). These intrusions have been subjected to thrusting that intensifies towards the Outer Hebrides Fault Zone whilst the bodies were apparently still cooling (Fettes et al., 1992). The multiple tectonic events described above have led to complex foliation patterns across the islands (Figure 1.2, Fettes et al., 1992).

Laxfordian and post-Laxfordian uplift is recorded in Ar-Ar ages of biotite that give cooling ages of around 1440 Ma (Kelley et al., 1994). Data from Rb-Sr dating gave a range of biotite closure ages from 1655-954 Ma (Cliff and Rex, 1989). This uplift is believed to be related to the Grenville orogeny and assembly of Rodinia (Cliff and Rex, 1989), and may possibly have produced dextral oblique shear on the supracrustal belts in South Harris (aka the South Harris Shear Zones) (Butler, 1995) that may have offset the Southern Zone of the OHFZ (Imber et al., 2002). In addition, the uplift of the Lewis/Harris area may have created the source area of the Torridonian sandstones of mainland Scotland (Cliff and Rex, 1989).

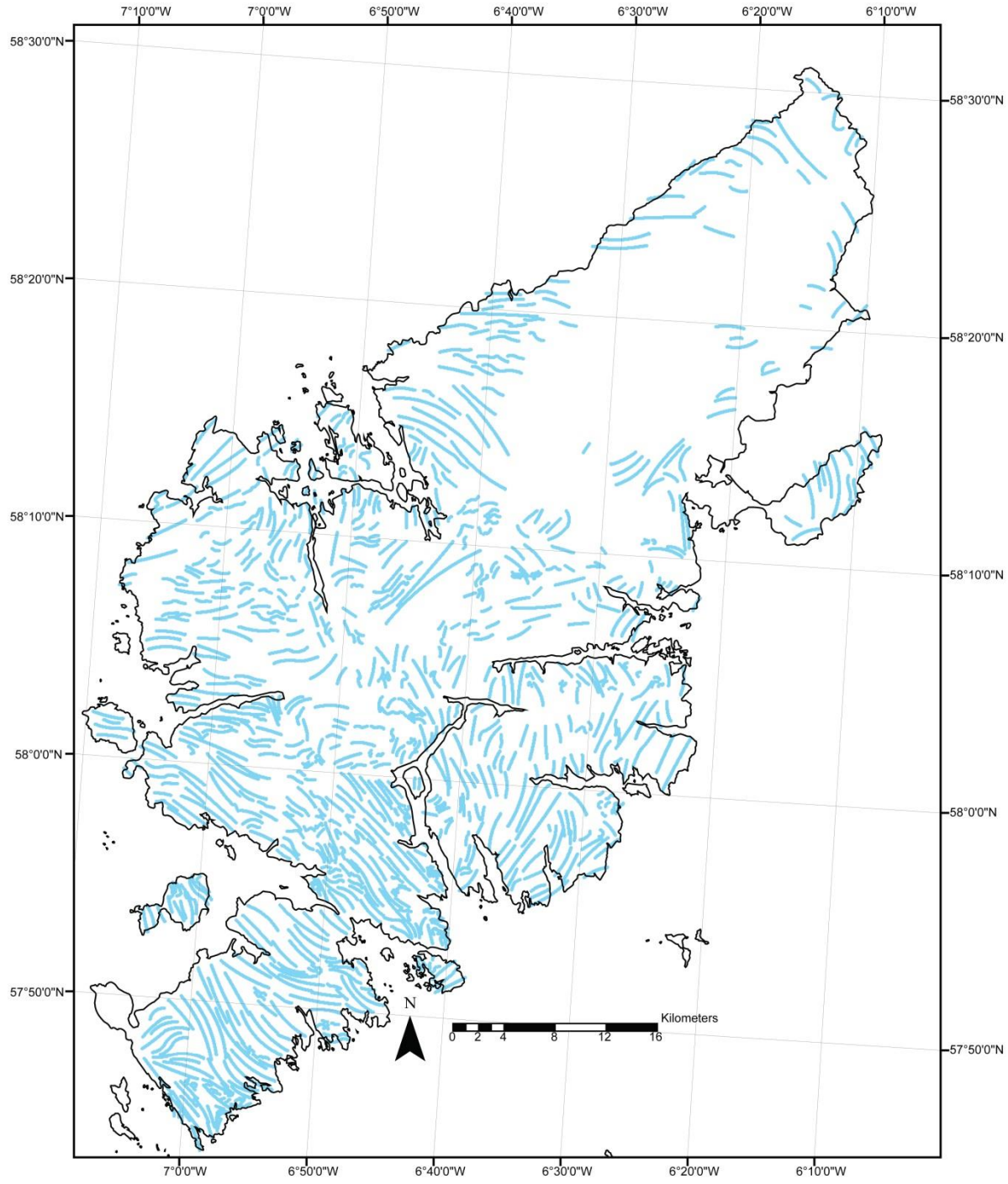

Figure 1.2: Map showing trend of foliation, digitised from the BGS maps of Lewis and Harris.

Later deformation in the Outer Hebrides is associated with initiation, displacement and alteration along the Outer Hebrides Fault Zone (OHFZ) on the eastern side of the islands (e.g. Imber et al., 2002), in addition to later (Mesozoic and younger) faulting across the islands that is discussed in this thesis. Across the OHFZ, the Lewisian Gneiss Complex may be split into western (footwall) and eastern (hangingwall) components. In addition, the OHFZ may be split into two sub-zones on the basis of geography and deformation – the northern and southern zones (e.g. Butler, 1995; Imber, 1998; Imber et al., 2002; Fettes et al., 1992). The northern and southern zones have undergone a

complex deformation history, with multiple brittle tectonic events and reactivations that have created a complex fracture network.

1.3.2.1 Tectonic History of Faulting in the Northern Zone of the Outer Hebrides Fault Zone

Stages of evolution of the OHFZ have been determined in previous studies. The main stages of evolution of the northern zone OHFZ are given here:

1. The Outer Hebrides Fault Zone was initiated between 1700 - 1100 Ma as part of the terrane amalgamation process, most likely during or before Grenville time (Imber et al., 2002; Park, 2005). This age is constrained by the fact that late Laxfordian pegmatites are reworked in mylonite zones (Imber et al., 2002). However, in Harris the late Laxfordian granites are believed to have been affected (Fettes et al., 1992). The earliest phase of shearing in the Northern Zone includes development of the 'pervasive mylonites' of Scalpay and southeast Lewis (e.g. Imber et al., 2001). This phase of faulting is lacking in the Southern Zone (Imber et al., 2001).
2. Dextral oblique shear along the SHSZ is believed to have followed this initial phase of thrusting (Imber et al., 2001). This movement is associated with uplift the north of the SHSZ around 1100 Ma (Cliff and Rex, 1989).
3. Extensional movements on the OHFZ at around 1000 Ma allowed deposition of the Torridonian around this time in the Minch Basin (Brewer and Smythe, 1984; Fyfe et al., 1993; Mendum et al., 2009).
4. Caledonian reactivation of the Outer Hebrides Fault Zone included periods of thrusting, in addition to possible late Caledonian sinistral strike slip along phyllonite belts (Lisle, 1993; Butler et al., 1995; Imber et al., 2001; Mendum et al., 2009). Earlier Laxfordian fabrics were reactivated (Coward, 1990). Pseudotachylite fault rocks have been found with ages of 430 Ma, corresponding to Caledonian deformation (Kelley et al., 1994). Pseudotachylite and ultracataclasites are associated with Caledonian top-to-the NW thrusting. Extensional fabrics found along the phyllonites may be associated with post-Caledonian fault movements (Imber, 1998).
5. The Minch and Sea of Hebrides Basins are half-grabens developed along the Minch Fault in the hangingwall of the OHFZ and are believed to have reactivated the OHFZ at depth after the Caledonian (Stein, 1988; Stein and Blundell, 1990). Mendum (2009) suggests that steep faulting related to uplift and basin formation may have occurred in the Devonian and Carboniferous. Carboniferous sediments up to 2 km thick have been

interpreted within the Minch and Sea of Hebrides basins (Stein, 1992), but this was refined to a maximum of 250 m in seismic data by O'Neill and England (1994).

6. Permo-Triassic sediments unconformably overlie Carboniferous sediments in the Minch, and are clearly associated with normal faulting in the Stornoway Formation (Steel and Wilson, 1975; Storetvedt and Steel, 1977). 0.5 – 1 km of Permo-Triassic rocks are thought to exist in the Minch/Sea of Hebrides Basin (O'Neill and England, 1994).
7. Jurassic rocks have been interpreted within the Minch/Sea of Hebrides basin and are found outcropping on islands of the Inner Hebrides (e.g. Hesselbo et al., 1998). However, the Jurassic strata identified on seismic lines do not appear to thicken towards the Minch Fault. This lack of thickening may point to these sediments being lain down in a post-rift thermal sag setting after the cessation of tectonism (O'Neill and England, 1994). Up to 2 km of Jurassic strata may exist in the basin (O'Neill and England, 1994).
8. Some degree of Cretaceous inversion is believed to have occurred (O'Neill and England, 1994; Stein, 1988), with uplift concentrated along the Mid-Minch High (east of the Eye Peninsula) and possibly the Outer Hebrides (Stein, 1988). Cretaceous faulting is suggested to have occurred on the islands by Slightam (2012), but no evidence is presented for it.
9. Oligocene sediments have also been found in the Minch/Sea of the Hebrides Basin (Evans et al., 1979; Evans et al., 1991; Smythe and Kenolty, 1975). The presence of these deposits in one basin adjacent to the Minch Fault is highly suggestive that these were deposited before or during faulting (Evans et al., 1991), although the size of the suggested basin is approximately 5km in length.

Faulting timing and levels of sedimentation within the Minch/Sea of the Hebrides is not homogeneous along the length of the basin (e.g. Evans et al., 1991, Fyfe et al., 1993). However, reactivation is seen along the entire length of the OHFZ at various stages. Extensional reactivation postdating thrusting has been observed on Barra (Macinnes et al., 2000), South Uist (Osinski et al., 2001), and further north on North Uist, Lewis and Harris (e.g. Imber, 1998).

1.3.2.1.1 Stornoway Formation

Mesozoic faulting resulted in the deposition of the Stornoway Formation in a westerly dipping half-graben sequence of alluvial fan deposits (Steel and Wilson, 1975; Storetvedt and Steel, 1977) occurring over the Outer Hebrides Fault Zone (Figure 1.1). The Stornoway Formation has been described as undeformed (Butler et al., 1995), relative to the surrounding OHFZ. On inspection, the Stornoway Formation is found to be riddled with many minor and intermediate scale faults (see Chapter 3).

1.3.2.2 Tectonic History of Faulting in the Southern Zone of the Outer Hebrides Fault Zone

Similar to the Northern Zone, the Southern Zone has a long and complex history of reactivation. However, heterogeneity exists along the OHFZ and there are some significant differences between rocks observed along the Southern Zone. Primary differences in the southern zone when compared to the northern zone include:

1. The presence of granulite facies rocks (the leucocratic granulite Corodale Gneiss and also eastern Barra) in the hangingwall of the OHFZ (e.g. Coward, 1972; Whitehouse, 1993 Mendum, 2009). These are of a higher grade than rocks in the footwall to the west (Whitehouse and Bridgwater, 2001).
2. There is a lack of the earliest phase amphibolite and greenschist facies ductile thrusting (mylonites) in the southern zone (Imber, 1998; Imber et al., 2002).

1.3.3 Shear Zones and Linkage across the Minch

The NW-SE trending structures that are a feature of the LGC often separate the individual basement blocks identified above (see Figure 1.1), and are frequently interpreted to be Inverian in age (e.g. Attfield, 1987; Goodenough et al., 2010). The suggestion that these shear zones may have been linked across the Minch has been investigated (Dearnley, 1962). Dearnley (1962) suggests 77 km sinistral strike-slip offset along the Minch Fault would enable linkage of shear zones of the Outer Hebrides with those on the mainland (Figure 1.3).

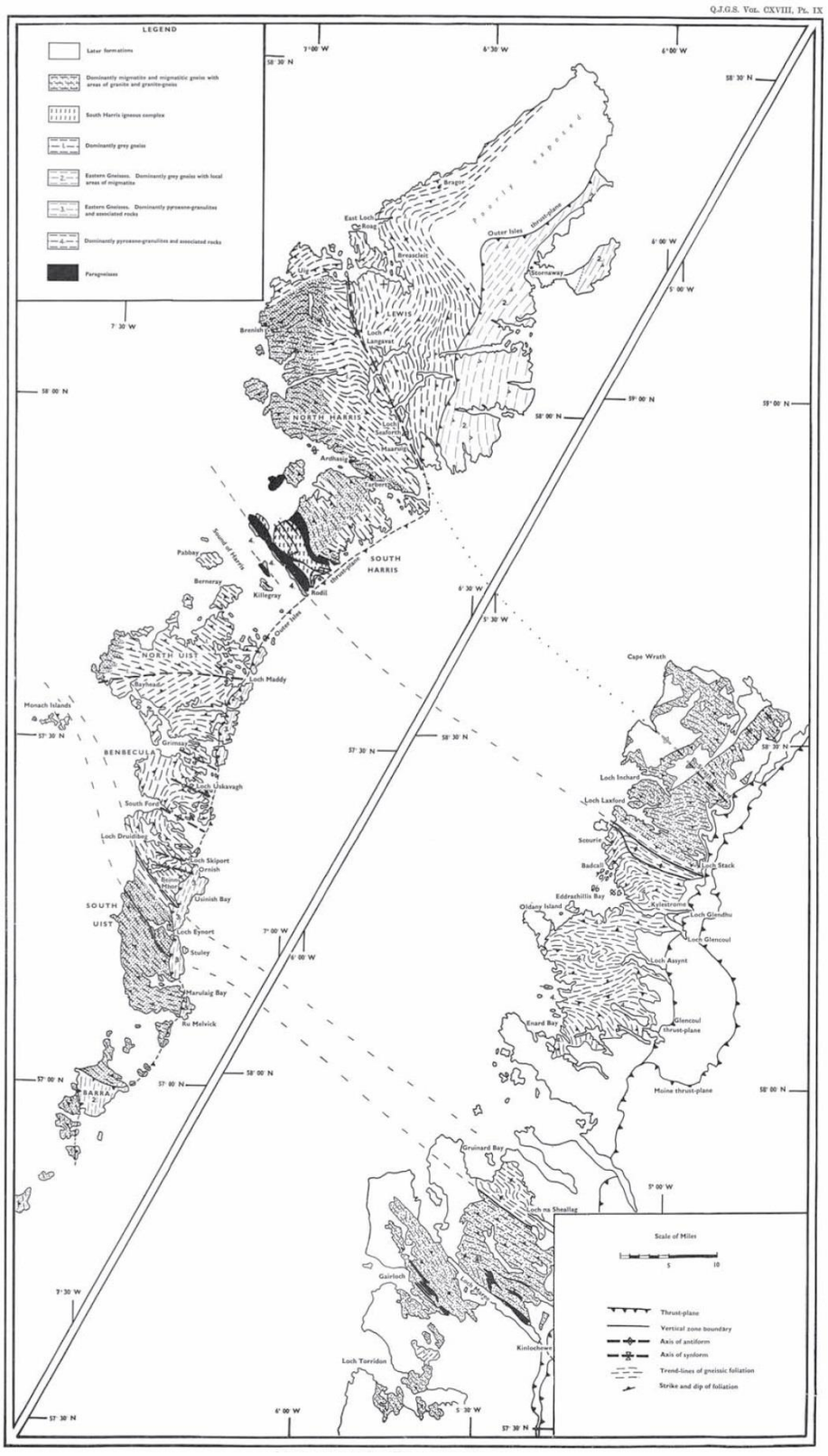

Figure 1.3: Linkage of shear zones across the Minch as postulated by Dearnley (1962).

In their ramp and flat shear zone model, Coward and Park (1987) say that there can be no precise match of shear zones across the Minch since the major displacements can be transferred from the ramps to the flats, where the ramps are the exposed NW-SE shear zones and most of the LGC is a shear zone flat. Coward and Park (1987) do however suggest that the South Harris Shear Zones

may be linked with the Laxford Shear Zone, and they dismiss Dearnley's (1962) hypothesis of significant strike slip displacement across the Minch causing a link with the Gairloch Shear Zone. However, strike-slip motion across the Minch has since been shown to have occurred (e.g. Butler, 1995; Butler et al., 1995; Imber, 1998). Linkage of the Gairloch and South Harris Shear Zones has also been suggested more recently (Park, 2010) on the basis of lithological similarities and this possible sinistral strike-slip motion.

The Ness transfer zone may offset the OHFZ (Stein, 1988). As mentioned in chapter 2, the rocks at Ness contain supracrustal assemblages that include metasediments and anorthositic remnants (Watson, 1969). These rocks comprise an assemblage very similar to the Langavat belt of South Harris (Coward et al., 1969) and dating of them has yielded an age of 1860 ± 240 Ma (Whitehouse, 1990). This age is similar to the minimum age of the SHIC determined from anorthosite by Cliff et al., 1983) (Whitehouse, 1990). The agreement in ages between the SHSZ and Ness Shear Zone has been used to suggest a temporal link between the two (Whitehouse and Bridgwater, 2001).

Basement structures formed in the early Proterozoic have controlled basin development in the area during phases of extension, with the system of NW-SE trending shear zones enabling en-echelon basin development (Stein, 1988). NW-SE shear zones may detach onto the OHFZ (Whitehouse and Bridgwater, 2001).

1.4 Faroe-Shetland Basin

The Clair Field lies approximately seventy kilometres west of the Shetland Islands (Figure 1.5) and is located in the east of the Faroe-Shetland Basin (FSB). The FSB is comprised of a series of NE-SW trending basins separated by upfaulted footwall blocks with basement in their cores that may be viewed as the along-strike continuation of the Moinian and Lewisian belts of the Scottish Caledonides (Dean et al., 1999). Whole rock Rb-Sr dating performed on basement rocks from wells in the FSB gave an age of 2527 ± 73 Ma, (Ritchie and Darbyshire, 1984), and this is believed to indicate that the basement is at least partly of Scourian affinities and related to the onshore Lewisian complex of northwest Scotland (e.g. Duindam and Van Hoorn, 1987). In addition, seismic wave velocities within the basement are similar to those seen within the Lewisian of the mainland (Smith and Bott, 1975). A minimum age of 2300 Ma was obtained from K-Ar dating of a dolerite in the basement of the Rona Ridge 80 km SW of Clair (Slightam, 2012). Corresponding lithological observations suggest the continuation of Lewisian Gneiss along the length of the Rona Ridge and along structural trend from the Isles of Lewis and Harris.

Sub-basins were formed in the FSB during repeated phases of rifting in the Devonian-Carboniferous, Permo-Triassic, Cretaceous and Palaeocene rifting, leading to deposition in rift-bound depocentres during those periods (Moy and Imber, 2009). The oldest known sedimentary rocks preserved in the basin are the Clair Group, a fluviatile red-bed sequence deposited in an endorheic (closed drainage basin) setting during the Devonian. The Clair Group thickens towards the Shetland Spine Fault SW of Clair (Figure 1.5), suggesting that the fault was active during deposition (McKie and Garden, 1996; Pless, 2011). Permo-Triassic red beds were deposited in the basins following renewed extension on NW dipping faults, towards which the sediments thicken (Dean et al., 1999; Sørensen, 2003). Marine conditions became established in the late Triassic, with transgressions recognised in the area (Sørensen, 2003). From the Jurassic onwards, the area is dominated by the effects of the central Atlantic opening (Roberts et al., 1999). In the Jurassic, tectonic activity decreased (Stoker et al., 1993) and marine sediments were deposited diachronously in the basins. During this time the FSB may have acted as an epi-continental seaway (Stoker et al., 1993). Uplift and erosion began in the latest Jurassic and may have marked the onset of Cretaceous rifting, with the activation of eastward dipping faults (Stoker et al., 1993). Three rifting phases have been identified from sediment thickness variations by Dean (1999); early Cretaceous, the early late Cretaceous, and late Cretaceous. Central parts of the FSB formed deep depocentres with up to 3000 m of sediment (Sørensen, 2003). These sediments are often truncated against NW-SE lineaments that span the basin (Dore et al., 1997; Sørensen, 2003) that may have reactivated shear zones within the underlying basement at depth (Dore et al., 1997). Prior to the final continental break-up in the Early Eocene, renewed rifting occurred during the Palaeocene (Sørensen, 2003). Final break-up was associated with intense volcanism and formation of extensive lavas that occurred between 62 and 58 Ma (Sørensen, 2003).

An estimated four billion bbl of oil resides in fractured reservoirs of Devonian-Carboniferous rocks that overlie the crystalline basement high of the Rona Ridge (Coney et al., 1993). Connection of the reservoir is known to exist through the basement (Coney et al., 1993) with oil found within fractures of Mesozoic age (Finlay et al., 2011). The Clair Group is split into Upper and Lower Units, separated by a Visean unconformity. Inversion followed the Clair Group Deposition (Roberts et al., 1999). The lateral continuation of the OHFZ has been postulated to exist within the basement of the Rona Ridge (e.g. Dean et al., 1999). The Clair Group is truncated against the base Cretaceous unconformity and covered by Cretaceous shallow marine sandstones and deep water mudstones of the Shetland Group (Barr et al., 2007). A comparison between the tectonic histories of the Clair and Outer Hebrides regions is shown in Table 1.1. For further details of the geology of the Clair Field the reader is directed to Chapter 6.

The basement rocks at Clair are comprised of amphibolite facies granodioritic, granitic and basic gneisses with cross-cutting pegmatite veins (Pless, 2011), with very similar rocks also seen 80 km SW of Clair on the continuation of the Rona Ridge that closely resemble the lithologies present on Lewis (Slightam, 2012). The study of Lewis and Harris as an analogue for the Rona Ridge can also be justified by its existence along trend from the Clair Field in a similar structural setting (Slightam, 2012). Pless (2011) found the foliation to be weakly defined and trending N-S to NNW-SSE in the gneisses of Clair well 206/7a-2, and at the Lancaster Prospect (Figure 1.5), foliation was found to trend strongly NE-SW and dip steeply (Slightam, 2012). The variation in foliation orientation may be expected as across Lewis and Harris the foliation changes from a prominent NW-SE trend to NE-SW trend over distances of kilometres or less (Figure 1.2). Data presented by Slightam (2012) also shows similarities in the orientation of the foliation and fractures – i.e. fractures appear to be parallel and sub-parallel with the foliation (Figure 1.4).

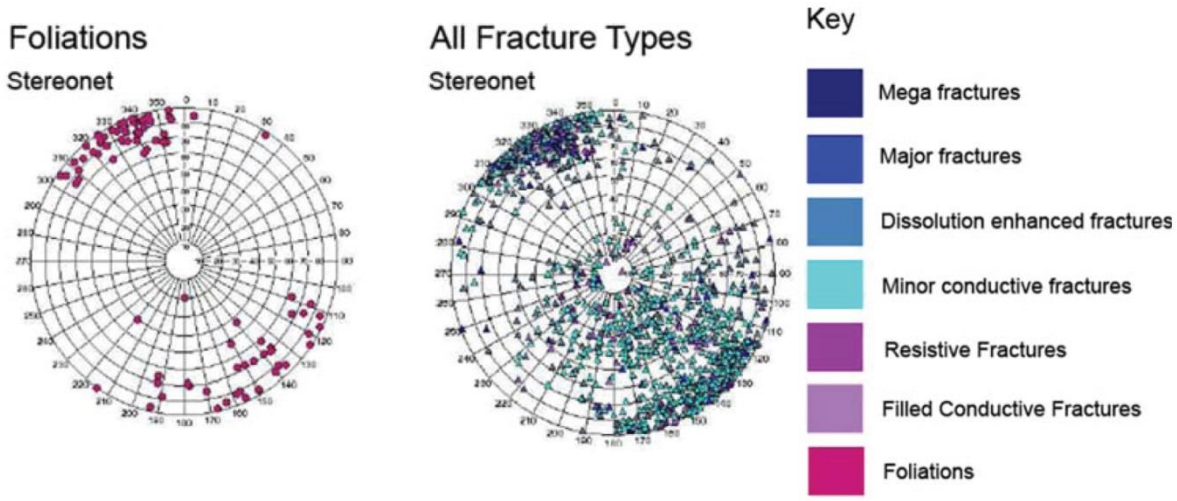

Figure 1.4: Orientations of fractures and foliation from inclined well 205/21a-4z in the Lancaster Prospect (from Slightam, 2012).

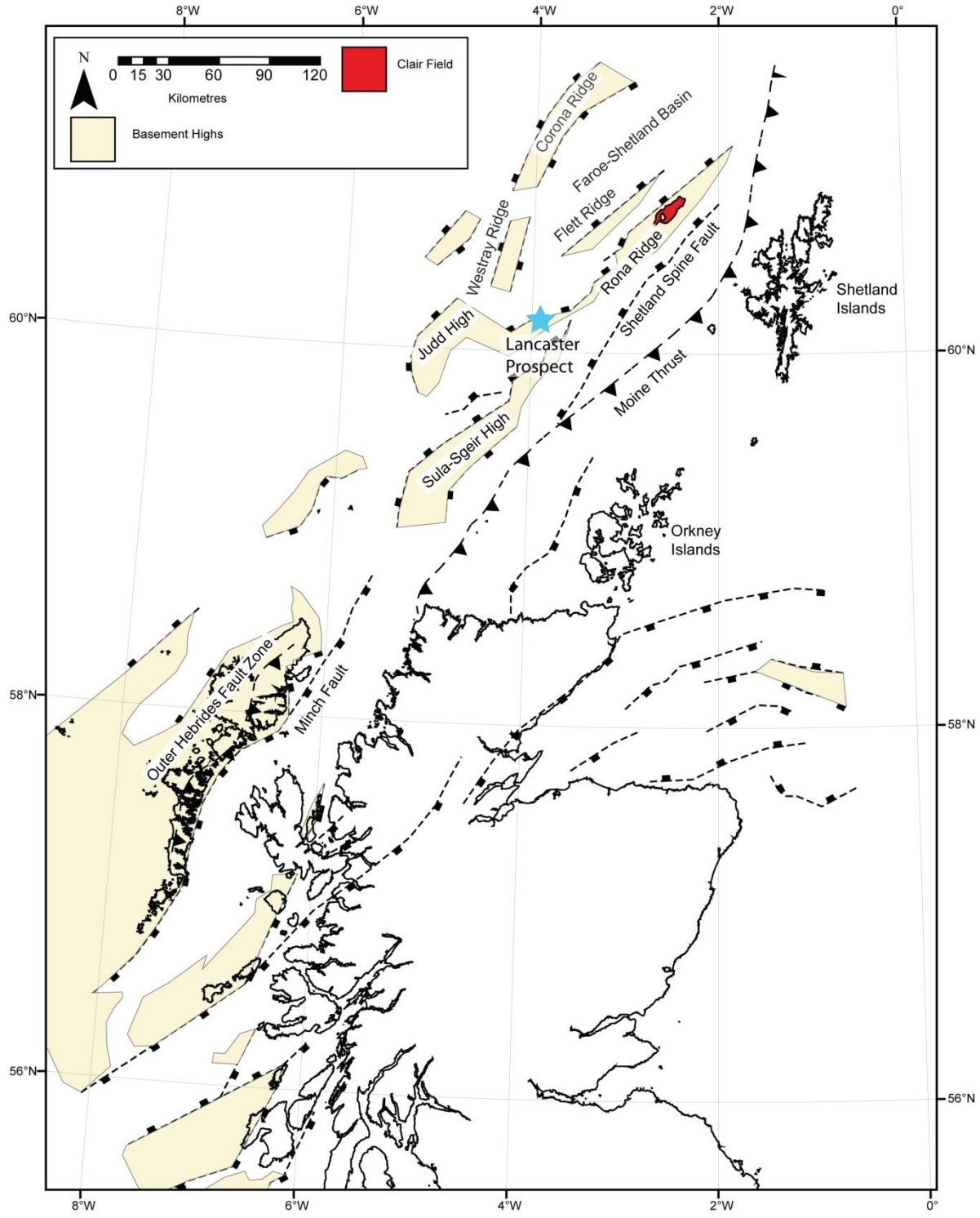

Figure 1.5: Structural map offshore northern Scotland. Basement highs from Sørensen (1993) and Roberts and Holdsworth (1997). Note position of Lancaster Prospect and Clair Field along strike from the Outer Hebrides.

Table 1.1: Summary for of tectonic phases identified at Clair (the Faroe Shetland Basin) and in the Outer Hebrides.

Time/Event	**Faroe Shetland Basin area**	**Outer Hebrides**
Gneiss protoliths	Acidic and basic intrusives, minor sedimentary rocks	Sedimentary and igneous units intruded by acidic bodies and 'Older Basics' intruded (Mendum et al., 2009).
Main Scourian 3.1Ga – 2.5Ga	Gneiss formation. The gneiss includes pyroxene granulites, acidic and basic gneisses and metasedimentary rocks. (Ritchie & Darbyshire, 1984)	Gneiss formation - migmatisation, amphibolite and granulite facies metamorphism. Formation of 'grey gneiss' and strong foliation (Mendum et al., 2009).
Late Scourian c. 2.6-2.0 Ga	Affected Clair similar to Outer Hebrides? Possible basement thrusts (Stoker et al., 1993)	Range of intrusions cutting earlier foliations (Mendum et al., 2009). Overall NNE-SSW foliation trend. Younger Basics intruded at 2.4Ga are generally thought to be equivalent to Scourie Dykes, but possibly separate on the grounds of geochemistry (Mason & Brewer, 2004).
Laxfordian 1.6-1.8Ga		Accretion of the South Harris Complex and amphibolite facies metamorphism (granulite within the South Harris Igneous Complex) – folding, planar and linear fabrics and migmatisation (e.g. Cliff et al., 1983; Whitehouse and Bridgwater, 2001) followed by intrusion of the Uig Hills – Harris granite complex (e.g. van Breemen et al., 1971). Maximum age of the initiation of the OHFZ (Fettes et al., 1992; Imber et al., 2002).
Grenvillian 1.1Ga		Dextral oblique offset and uplift of the Lewis/Harris block across the SHSZ (Cliff and Rex, 1989). Thrusting recognised on the northern OHFZ around 1100 Ma (Imber et al., 2002). Extension may have followed and allowed formation of Minch Basin and Torridonian group deposition around 1000Ma (Stein, 1988).

Time/Event	Faroe Shetland Basin area	Outer Hebrides
Caledonian 430Ma	Reactivated basement thrusts from the Caledonian are believed to have been reactivated as post-Caledonian normal faults (Stoker et al., 1993).	Series of thrust movements along the OHFZ marking the Caledonian Orogeny - Scandian event at 430 Ma, Grampian at 470 Ma (Macdonald and Fettes, 2007).
Devonian-Carboniferous	Deposition of the Clair Group in an extensional intermontane setting (Allen and Mange-Rajetzky, 1992), possibly following extensional collapse (Bartholomew et al., 1993; Knott et al., 1993; Hinz et al., 1993).	Possible post-orogenic extension and collapse along NNE-SSW phyllonitic shear zones (Imber, 1998; Imber et al., 2001).
Carboniferous	Compressional inversion post-Clair Group deposition (Roberts et al., 1999).	No manifestation of inversion?
Permo-Triassic	Relatively minor rifting. NE-SW faulting (Dean et al., 1999).	Up to 3000m thick sequence of synrift deposits in the Minch (Stoker et al., 1993) represented onshore by the syn-sedimentary Stornoway Formation.
Jurassic	Minor rifting. NNE-SSW faults seen on Corona Ridge (Figure 1.5; Dean et al., 1999).	2500 m thick sequence in the Minch north of Lewis that thickens towards basin bounding faults (Stoker, 1993). However offshore South Harris, Jurassic sediments are believed to be post-rift with no evidence of synrift deposition, i.e., Jurassic normal faulting did not occur on the Minch fault
Cretaceous – Palaeocene.	Major NE-SW striking rifting in Early Cretaceous, early Late Cretaceous, Late Cretaceous and the Palaeocene (e.g. Dean et al., 1999). Late Cretaceous inversion structures are present (Roberts et al., 1999.	No deposits present, however inversion events may have affected the region with the formation of the Mid-Minch High (Stein, 1988).

Time/Event	Faroe Shetland Basin area	Outer Hebrides
Palaeogene	Series of inversion events affecting the region interrupting subsidence. Produced mainly NE-SW trending folds in the FSB (Ritchie et al., 2008).	Faulting offshore South Harris during the Oligocene (O'Neill and England, 1994).

1.5 A note on the fracture characteristics of the Lewisian Gneiss of the Scottish mainland

This project follows on from work undertaken by Pless (2011). Pless (2011) concentrated on understanding the fracture characteristics within the Lewisian of the mainland of NW Scotland, with particular focus on fracture spacing, as an analogue for the Clair Field. Analogue studies are required at Clair as connection through the field is believed to occur through fractures within basement rocks that have so far not been exploited or investigated. The main findings from Pless (2011) are:

- Basement rocks at Clair are lithologically comparable to the mainland Lewisian Gneiss Complex of the Rhiconich Terrane, containing Laxfordian granites and pegmatites.
- Fracture orientations within the Clair Field are similar to those of the mainland Lewisian.
- The majority of fractures within the Lewisian Gneiss Complex of the mainland formed during the Proterozoic, whilst at Clair numerous Mesozoic and Cenozoic age fractures are present.
- Consistent power law (i.e. scale invariant) relationships were interpreted from both mainland and Clair fracture spacing data.
- Increased fracture density in shear zones was attributed to the effect of penetrative foliation. Differences in fracture density and spacing were also noted in differing lithologies.

In general, consistent power law relationships were found for fault spacing of individual fracture sets at the regional and fieldwork scale, indicating that fractures on the mainland were scalable. However, whilst Precambrian faulting and fracturing in the mainland Lewisian is common, Mesozoic and younger faulting that is important in the Clair Field (see above) is rather poorly represented (Pless, 2011). The Outer Hebrides represent a better analogue to the Clair Field in this respect, having been upfaulted in the Mesozoic (Roberts and Holdsworth, 1999). Hence fracture characteristics on the Hebrides may be expected to be similar to those at Clair.

This study builds on that of Pless (2011) in order to add further geological constraints to the affinities of the Clair basement with a rigorous study of qualitative and quantitative fracture characteristics from the Hebridean Islands.

1.6 Concluding remarks

The presence of similar basement and an overlying sedimentary sequence, in a similar structural setting, make the Isles of Lewis and Harris an appropriate analogue for the study of fracturing and faulting in the Clair Field basement rocks and overlying Clair Group. The poorly studied Mesozoic

faulting and deformation on Lewis and Harris is of particular interest as Mesozoic deformation is very important in the Faroe-Shetland Basin and not been widely preserved onshore mainland Scotland (Pless, 2011). The identification and characterisation of Mesozoic faulting in the Hebrides is a central part of this thesis.

Chapter 2: Methods

Analysis in this thesis is performed at three primary scales: regional lineament analysis, local fieldwork, and microstructure and mineralogical analysis using optical and scanning electron microscopy (SEM). These methods are introduced below and further specific methodological details are presented in each chapter as necessary.

2.1 Lineaments

'A lineament is a mappable, simple or composite linear feature of a surface, whose parts are aligned in a rectilinear or slightly curvilinear relationship and which differs distinctly from the patterns of adjacent features and presumably reflects a subsurface phenomenon' (O'Leary et al., 1976).

Lineaments have often been used in order to identify and group tectonic trends (e.g. Ananaba and Ajakaiye, 1987; Dore et al., 1999). The process of extracting linear features from remotely sensed images is termed lineament analysis. Picking lineaments for the purpose of interpreting geological features must be undertaken with caution as it can be subjective and open to the interpretation of the picker. As such, '*guarded use of lineament analysis can be useful and will give the overall preferred lineament orientations, but should not be used in testing hypotheses - rather it is good for suggesting them*' – Parsons and Yearley, 1986.

Therefore lineament analysis is used in this thesis to give a background to the km- to hundreds of m-scale tectonic trends of the region and highlight areas of interest that have then been ground-truthed through fieldwork. Picking of lineaments was undertaken manually in order to avoid the selection of non-geological linear features such as roads and field boundaries, and using the geological knowledge of the interpreter (e.g. Suzen and Toprak, 1998). However, lineament analysis remains an imprecise science due to the dependence on the person performing the picking. In order to make the lineament analysis as accurate as possible, the procedure used a systematic approach and was performed four times independently, at 1:25,000, 1:50,000 and 1:100,000 scales. Lineament picking was performed at 1:1,000 scale in the Stornoway Formation and in the immediately adjacent areas of underlying Lewisian gneisses due to a lack of defined lineaments in the lidar data in the region. Lineaments already picked at the lowest resolution were not picked subsequently in the higher resolution analysis in order to compare the orientations of lineaments visible at each scale.

Nextmap® aerial lidar data was obtained from the BGS in Edinburgh and was analysed to produce hillshades, illuminated from 045°, 135°, 225° and 315° with multiple vertical exaggerations, in

addition to slope maps, break-in-slope maps and aspect maps (Figure 2.1). Multiple hillshades with varying illumination azimuths are produced in order to highlight lineaments with different orientations (e.g. Koopmans, 1986). The datasets produced were analysed collectively in ArcGIS for lineaments, which were then digitised. Lineament picking at 1:1,000 scale was performed on high resolution aerial photographs, also obtained from the BGS.

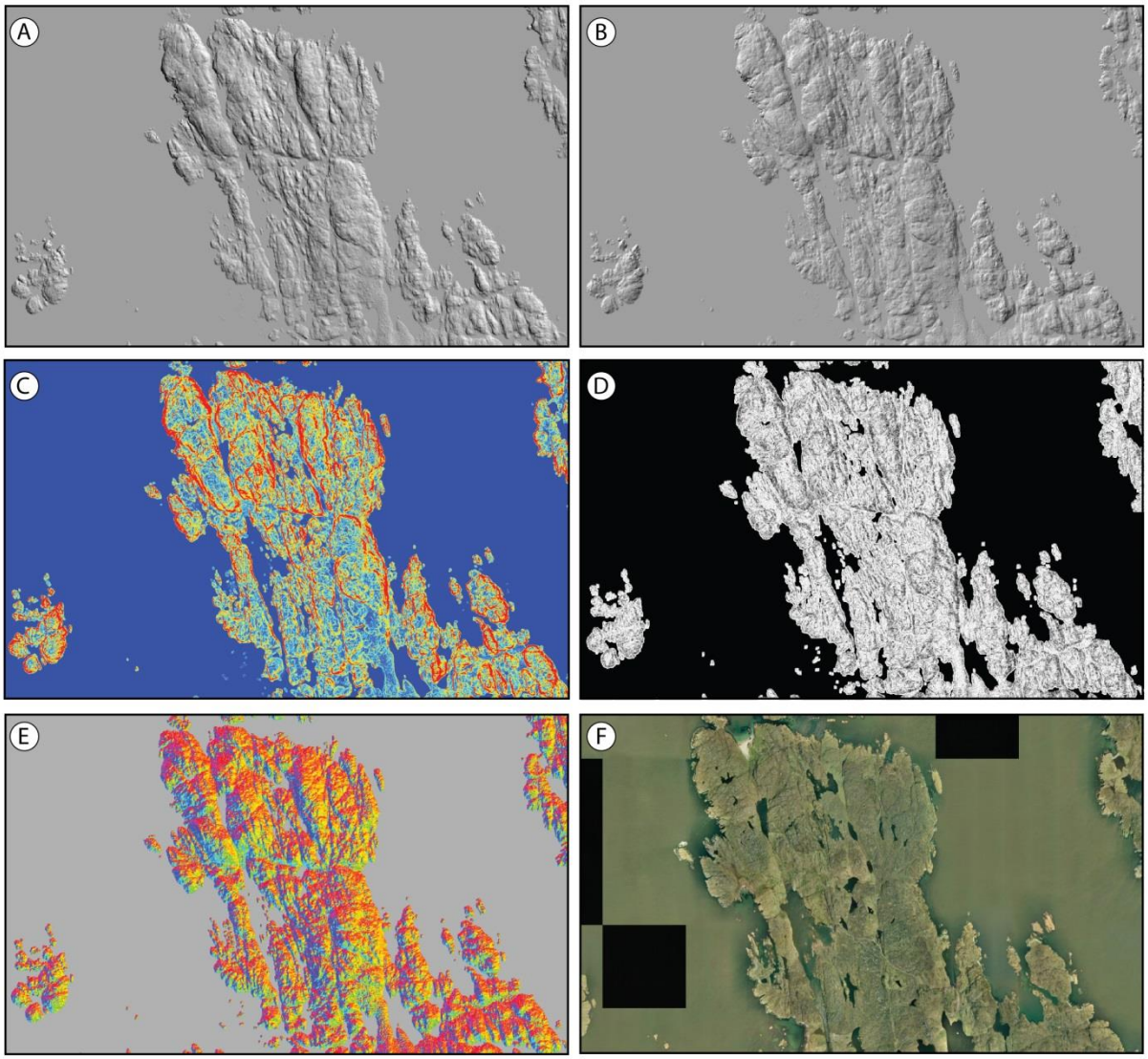

Figure 2.1: Lidar data from the northern tip of Great Bernera at 1:25,000 scale. Processed for (**A**) Hillshade, illuminated from 045**°**. (**B**) Hillshade, illuminated from 315**°.** (**C**) Slope – highlights areas with high topographic gradient. (**D**) Break in slope – highlights changes in topographic gradient. (**E**) Aspect – highlights slope facing direction. (**F**) Aerial imagery.

Results from the lineament picking may then be analysed in order to determine predominant orientations. In addition, lineament data can be analysed for spacing characteristics in ArcGIS. It is important to determine whether fractures are scalable and what scaling laws may be applied to the results, for instance whether the fractures are fractal in nature (e.g. Nicol et al., 1996; Odling, 1997; Berkowitz et al., 2000; Sleight, 2001; Gabrielsen et al., 2002) as this can be compared to field data and data collected on the mainland by Pless (2011).

As part of the lineament analysis within the Lewisian, the foliation in the basement gneisses was digitised from BGS maps in order to eliminate topographic trends caused directly by the foliation (Figure 2.2). During analysis, features lying parallel with the foliation trend were ignored as there was no objective way of differentiating foliation from fault lineaments (as per the definition given above). However, this approach creates a bias against fractures that lie parallel to the foliation trend. Nonetheless major lineaments (i.e. > 200 m in length) often cut through varying orientations of the foliation. This is useful as there is widespread variation in foliation strike over relatively short distances (i.e. 100s m) in the most of the Hebridean outcrop and this means that most moderate to large faults > 200 m in length are difficult to miss.

Lineament analysis is limited to identification of high angle (dips > 45 degrees) structures, as any lower angle structures wrap around topography, making them difficult to identify. Low-angle thrusts present in the OHFZ of Lewis and Harris fall into this category, with their orientations digitised from the BGS maps and shown in the rose diagram in Figure 2.2. These low angle structures are not identified in the lineament analyses of chapter 3-5. Even though thrusts in the Hebrides often form topographic features, it is not possible to distinguish them in the lidar data as linear features. Nonetheless, low angle structures will be identified and characterised in the fieldwork sections. This emphasises the importance of ground-truthing lineament data and not using it alone to test hypotheses.

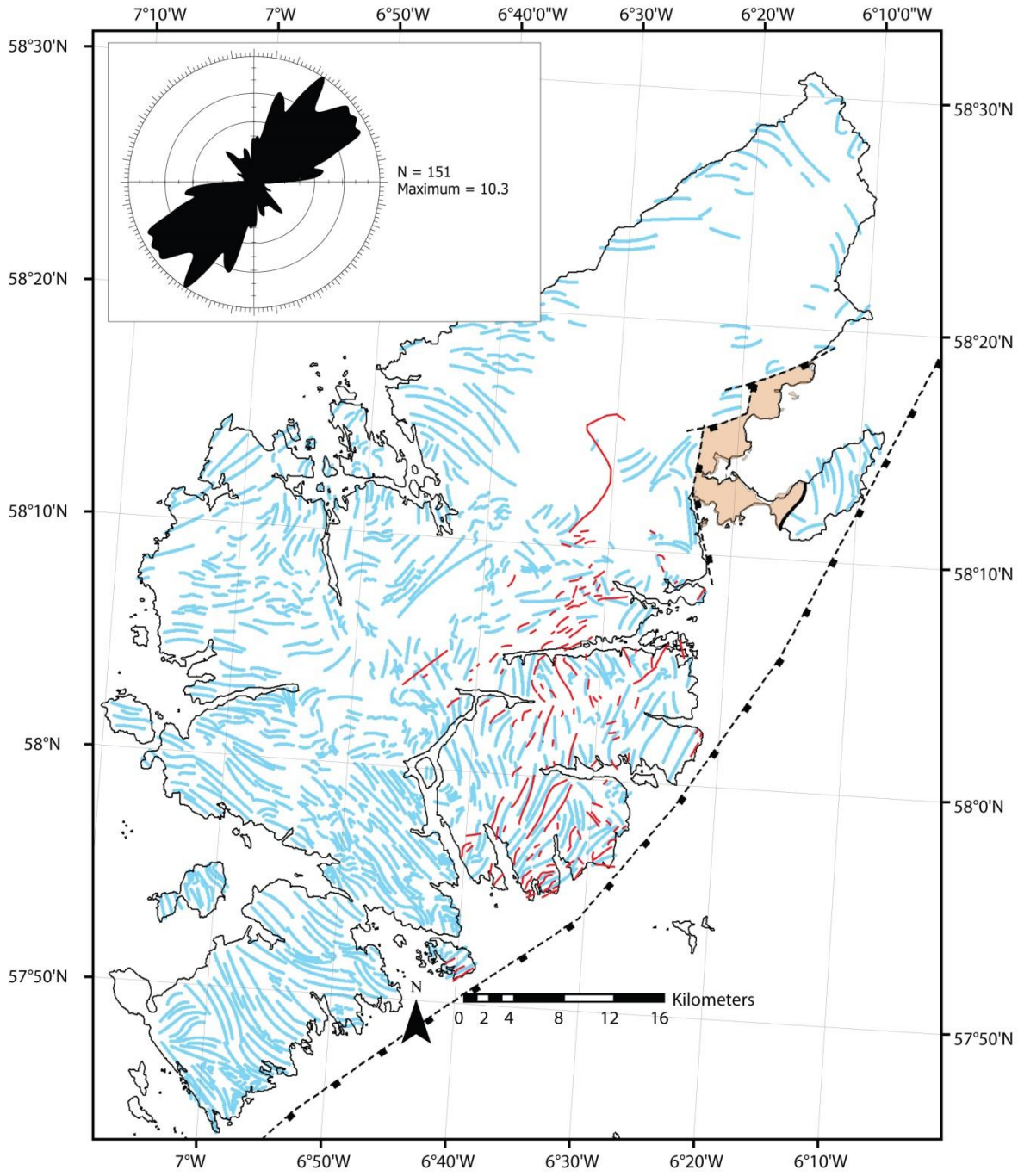

Figure 2.2: Foliation trend in blue digitised from BGS structural maps. Red lines are thrusts shown in the rose diagram, digitised from BGS maps.

2.2 Fieldwork

Eight hundred and forty-six localities were visited on the Isles of Lewis and Harris over the course of four and a half months of fieldwork from 2009-2011, in addition to industry and conference fieldtrips, and fieldtrips for collection of lidar data. Fieldwork was undertaken in order to: ground-truth lineaments recognised during the lineament analysis; identify and characterise fractures at the outcrop scale (not visible at lineament scale); and, collect samples for microscope-scale

fracture characterisation. From field and microscope data relevant geological observations such as fault kinematics, fault rock styles, and cross-cutting relationships (to allow relative dating of fractures) can be obtained. Areas were selected for mapping on the basis of good exposure as viewed from satellite data, combined with the presence of features of interest identified in the lineament analysis. In addition, a number of key localities were identified from previous studies, most notably the PhD theses of Sibson (1977b), Butler (1995) and Imber (1997). At different localities, general fault and fracture mapping was carried out to obtain an overall background of the fracturing occurring in an area, in addition to detailed studies of more major faults. Orientation data obtained from the field are plotted on equal area stereonets and linearly scaled rose plots constructed in Stereo32© v1.0.3 and Myfault™ v1.04.

2.2.1 Definitions

2.2.1.1 Foliation

A foliation is a homogeneously distributed planar structure in a rock (Twiss and Moores, 1992), and in this thesis it is used to describe the alignment of flattened aggregates/grains of quartz and feldspar and/or platy minerals such as biotite and amphibole within the grey gneisses of Lewis and Harris.

2.2.1.2 Fractures, joints and faults

A fracture is a surface along which rocks or minerals have broken and material has lost cohesion (Twiss and Moores, 1992). Fractures encompass mode I (extensional) and mode II and III (shear fractures) (Figure 2.3). Hybrid fractures exhibit both extension and shear.

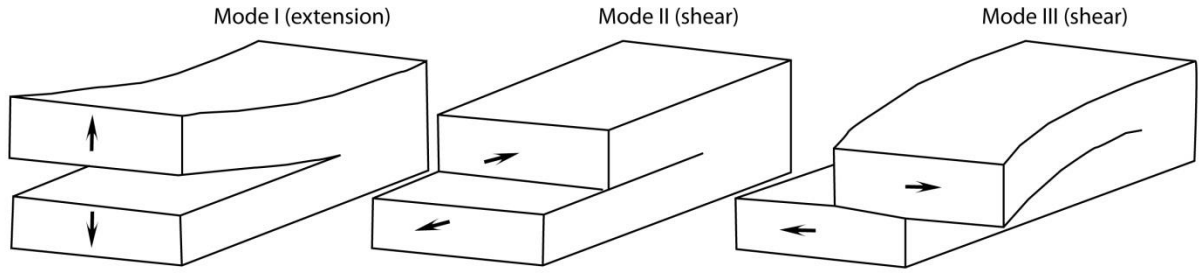

Figure 2.3: The distinctions among the types of fractures are based on the relative displacement of material across the fracture. (**A**) Mode I (extension) fracture. Relative displacement is perpendicular to the fracture. (**B**) Mode II (shear) fracture. Relative displacement is parallel to the fracture and perpendicular to the edge of the fracture. (**C**) Mode III (shear) fracture. Relative displacement is sliding parallel to the fracture and to the fracture edges redrawn from Twiss and Moores, 1992 Twiss and Moores (1992).

Fracture types are distinguished by offset and fill, falling into three broad categories:

- Joints – Fractures with very small displacement normal to their surfaces, and very little or no displacement parallel with their surfaces (Twiss and Moores, 1992). If there is no shear displacement, a joint is an extension fracture. Later shear displacement can accumulate along joints, i.e. they can be reactivated (Twiss and Moores, 1992).
- Veins – An extension (mode I) fracture filled with minerals, e.g. quartz, epidote, calcite, zeolite etc., either singly or together. Shear and hybrid fractures may form veins with slickenfibres. Some veins in the Lewisian gneisses are filled with pseudotachylite (friction melts), especially in the region of the OHFZ (e.g. Sibson, 1977a).
- Faults – A fault is a surface or narrow zone along which one side of the rock unit has moved relative to the other. Most faults are brittle shear fractures or zones of closely spaced shear fractures (Twiss and Moores, 1992). Faults types include dip-slip, strike-slip and oblique-slip (Figure 2.4).

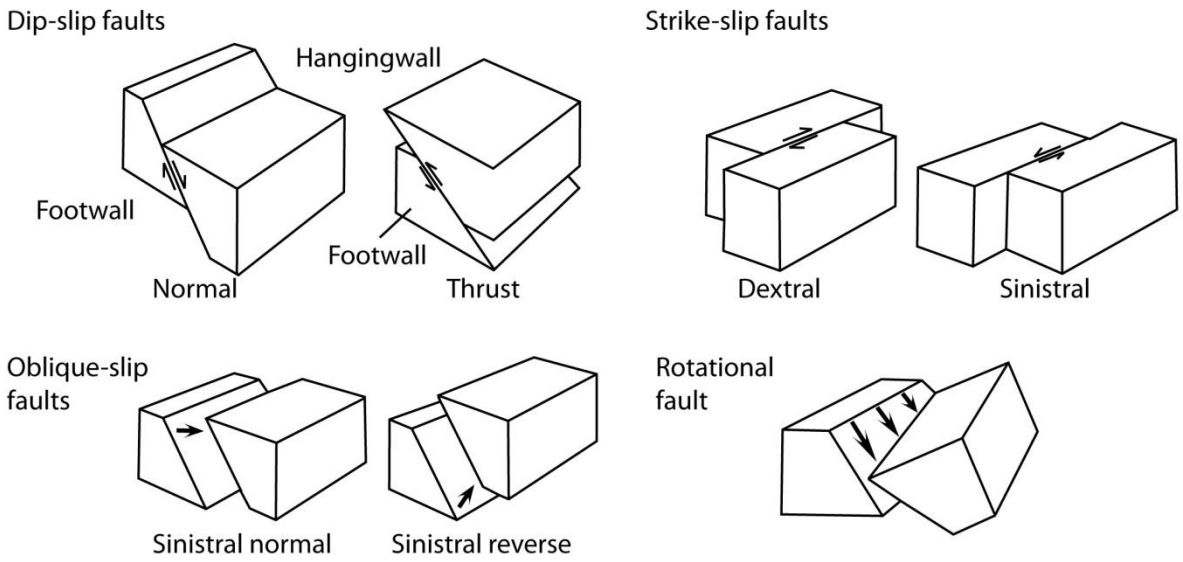

Figure 2.4: Fault classes based on relative displacements across the fault. Redrawn from Twiss and Moores (1992).

2.2.1.2.1 The Coulomb-Navier Criterion

The formation of the fault type is dependent on stress orientation and the presence of pre-existing structures. The Coulomb-Navier Criterion provides the basis for simple models of tectonic faulting, representing the yield point (point of brittle failure) for intact rocks (e.g. Yamaji, 2003). Any stress state in the Earth can be described by three orthogonal principal stresses (σ_1, σ_2, σ_3). If the orientation of a fracture plane relative to the maximum principal stress (σ_1) is known along

with confining pressure, the normal (σN) and shear stresses (σS) acting on the plane at failure can be calculated and a Mohr circle can be drawn (Figure 2.5). The fracture plane angle Θ is the angle between σ_1 and the fracture plane, and this is equal to the orientation perpendicular to the fracture plane from the σ_3 axis. Hence, the normal and shear stresses are indicated by the point on the Mohr circle that makes an angle of 2Θ from σ_1 (Yamaji, 2003, Figure 2.5). A series of these critical points describe the failure envelope, which is symmetric about the horizontal axis because the specimen and the applied stresses have axial symmetry (Yamaji, 2003). Failure occurs when the Mohr circle moves or expands when differential stress (σ_1 - σ_3) increases until the circle touches the envelope. Shear stress needed to produce failure of the rock increases as the confining pressure increases, and rocks cannot bear large tensile stresses. Hence, the envelope has a 'V' shape, touching the σN axis to the left of the σS axis. Tensile stresses are most commonly produced by increases in pore fluid pressure. Pore fluid pressure does not affect the shear stress but lowers the normal stresses acting across a plane, described by the following equation:

$$\sigma_e = \sigma_N - p_f$$

Where σ_e is the effective stress, σ_N is the normal stress, and p_f is the pore fluid pressure. Hence, increasing pore fluid pressure shifts the Mohr circle to the left. When the pore fluid pressure reaches the tensile strength of the rock, hydrofracturing occurs. These fractures will orientate themselves parallel with the maximum principle stress (σ_1) and open parallel with the minimum principal stress (σ_3).

The Coulomb-Navier criterion is described by the following equation:

$$|\sigma_S| = \tau_0 + \mu\sigma_N$$

Where $|\sigma S|$ (the brittle strength of the rock, i.e. the critical shear stress) is linearly related to the normal stress (σN), and μ is the coefficient of internal friction (Twiss and Moores, 1992). The Coulomb failure criterion predicts the critical state of stress needed to create a shear fracture. In a tensile regime (i.e. left of the Y axis in Figure 2.5) rock behaviour is better modelled by the Griffith Criterion, and combinations of failure criteria can be used to produce composite failure envelopes (Figure 2.5). Tensile failure in a rock occurs when the Mohr's circle touches the failure envelope left of the Y axis.

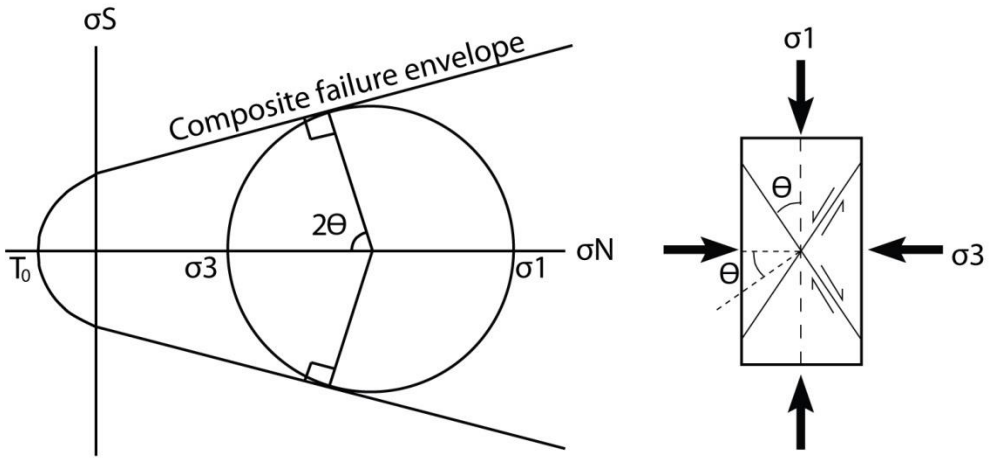

Figure 2.5: Mohr circle representation of stress at failure for 2D example shown. Redrawn from Twiss and Moores (1992).

Anderson's Theory (Anderson, 1951) of faulting uses the Coulomb-Navier criterion for fracturing to provide a theoretical explanation for the formation of the three principal fault types (normal, reverse, and strike-slip, Figure 2.6A). As the Earth's surface is a free surface, it can support no shear stress and therefore one of the three principal normal stresses must lie orthogonal to the surface (Twiss and Moores, 1992)(Figure 2.6A). The formation of the fault type is therefore dependent on which of the three principal stresses is perpendicular to the Earth's surface. However, Oertel (1965) observed the development of four fault plane families with orthorhombic symmetry ('quadrimodal' or 'polymodal' faulting), and Reches (1978) derives a model for the faulting of rocks in three dimensions, showing that quadrimodal faulting is required to accommodate 3D, non-plane strain deformation (Reches, 1978, Figure 2.6B-C). Reches (1978) shows that four sets of faults with orthorhombic symmetry develop in a three dimensional strain field in a rock containing many pre-existing faults, whereas two sets of faults with a conjugate pattern result from plane strain (Reches, 1978; Reches, 1983). Polymodal faulting has since been shown to develop in rocks without pre-existing fractures through microcrack interaction (Healy et al., 2006a; Healy et al., 2006b).

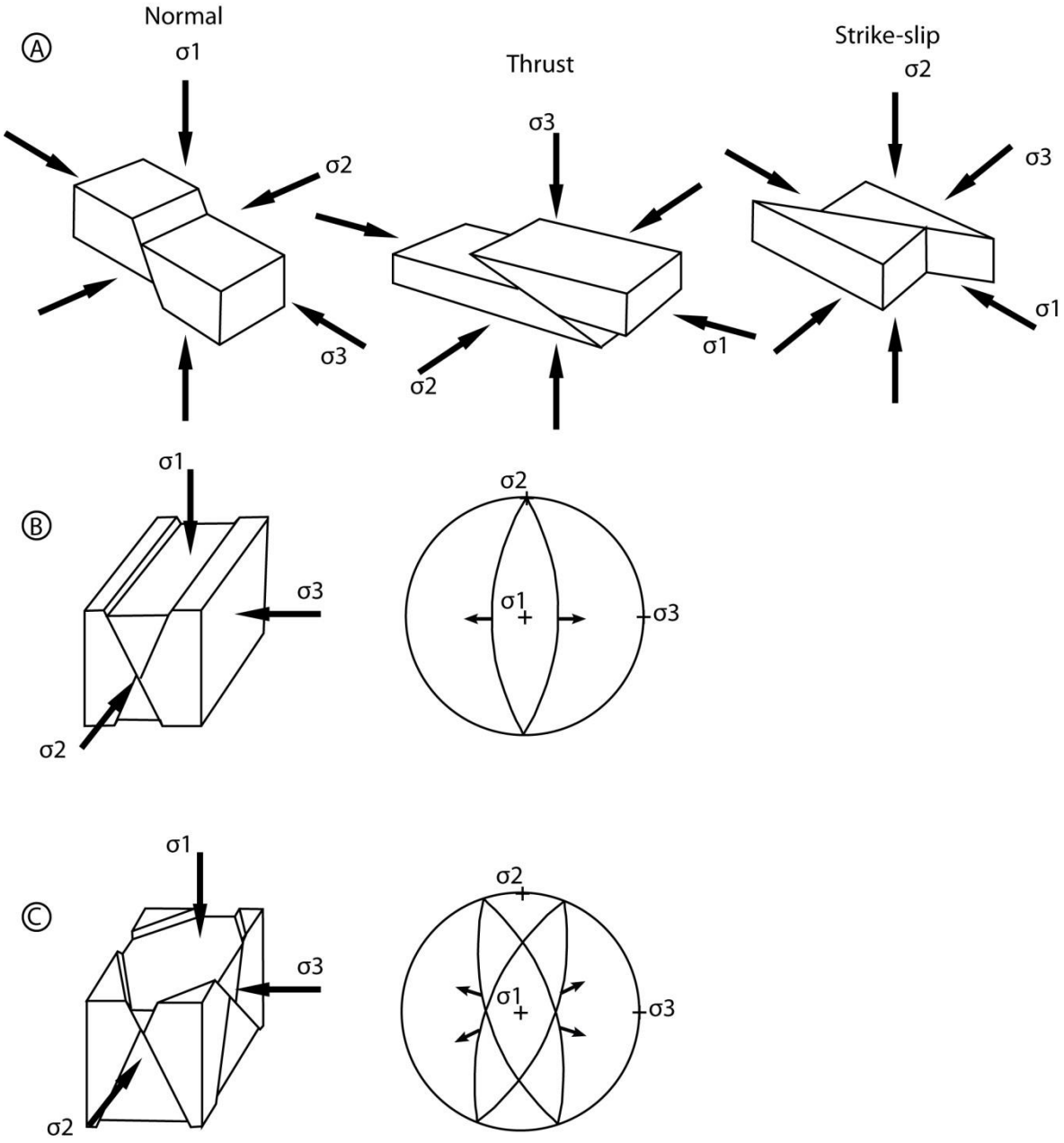

Figure 2.6: (**A**) Andersonian Theory of Faulting. (**B**) Conjugate faulting. **C**) 3D modification. Redrawn from Reches (1983)

2.2.1.2.2 Reactivation of faults

The frictional strength of a pre-existing fault is represented by Amonton's Law:

$\tau_f = \mu_f \sigma_N$

Where σ_N is the normal stress acting on the surface, and μ_f is the coefficient of sliding friction (Yamaji, 2003). When shear stress overcomes of the frictional strength of the rock, sliding occurs

on the surface. The shear stress needed to initiate shear on a pre-existing surface is usually less than that required to initiate a new fracture, unless the fault rock is well cemented (e.g. Yamaji, 2003). μ_f typically has a value of 0.6-0.85 for a very wide variety of rock types, a relationship informally known as Byerlee's Law (Byerlee, 1978) . Some materials, such as talc, serpentinite and smectite have anomalously low friction coefficients (in some cases as low as 0.2) and, if present along a fault will weaken it. Thus, reactivation depends on the frictional strength (expressed by the value of μ_f), the fluid pressure and the orientation of the local stress regime acting on the fault (e.g. Jolly and Sanderson, 1997). Continued reactivation of misorientated faults requires pore fluid pressure above hydrostatic values to prevent the formation of new faults (Sibson, 1990) or anomalously low friction fault rocks (e.g. Collettini et al., 2009). Pre-existing heterogeneities in the crust are often reactivated and strongly influence features such as fault-bounded basins (e.g. Butler et al., 1997). Phyllosilicate minerals such as clay, serpentine, and mica have lower coefficients of friction than other minerals and these minerals are often found along faults (e.g. Wintsch et al., 1995; Yamaji, 2003; Imber et al., 2008).

2.2.1.3 Fault structure

The fault structure terminology described by Caine et al. (1996) is widely accepted (Figure 2.7). Fault zones reside in country rock (the protolith) that often grades into a damage zone, surrounding a highly strained fault core where fault rocks are typically concentrated. Principal Slip Zones occur within the fault core, where the bulk of coseismic deformation is accommodated (Sibson, 2003). Varying degrees of damage zone and fault core development can occur. Fault zones may either be conduits or barriers to fluid flow, depending on the nature of the protolith, and the amount of fault core and fault damage zone development (Caine et al., 1996). For example, a fault with a well-developed fault rock in the fault core may act as a barrier to fluid flow. A fault with a well-developed damage zone may act as a conduit. In crystalline rocks, fault cores are often associated with fluid flow (e.g. Walker et al., 2013).

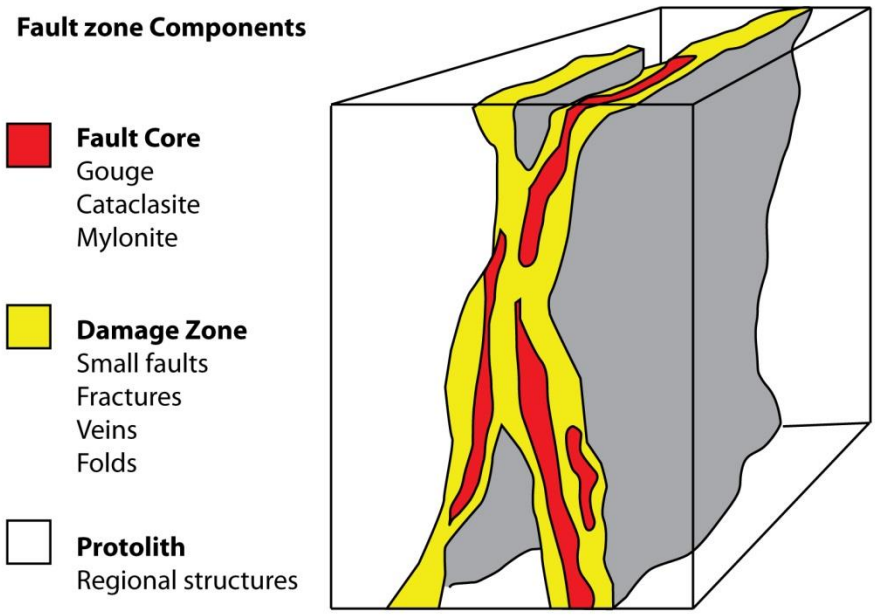

Figure 2.7: Fault zone terminology (Caine et al., 1996).

2.2.1.4 Fault rocks

The classification system for fault rocks used here corresponds to that presented by Sibson (1977a) and Woodcock and Mort (2008) (Table 2.2 and Figure 2.8). Two main categories of fault rock can be distinguished – brittle and ductile, occurring nearer the surface and at depth, respectively (Figure 2.9). Brittle fault rocks are the dominant types studied in this thesis, and have been augmented with the addition of foliated cataclasite and foliated ultracataclasite in Table 1.2 (e.g. Chester et al., 1985).

Table 2.2: Fault classification, after Sibson (1977) and Woodcock and Mort, 2008). For breccia types see Figure 2.8.

			Random Fabric		Foliated	
>30% large clasts >2 mm		75-100% large clasts (>2 mm)	FAULT BRECCIA	crackle breccia		
		60-75% large clasts (>2 mm)		mosaicbreccia		
		30-60% large clasts (>2 mm)		chaotic breccia		
		Incohesive	Fault Gouge (visible fragments <30% of rock mass)			
<30% large clasts >2 mm	COHESIVE	Glass/de-vitrified glass	Pseudotachylite			
		0-50% matrix (<0.1 mm)	Protocataclasite	Cataclasite Series	Protomylonite/phyllonite	Mylonite Series
		50-90% matrix (<0.1 mm)	Cataclasite Foliated ultracataclasite		Mylonite/phyllonite	
		90-100% matrix (<0.1 mm)	Ultracataclasite, Foliated ultracataclasite		Ultramylonite/phyllonite	
		Grain growth pronounced			Blastomylonite	

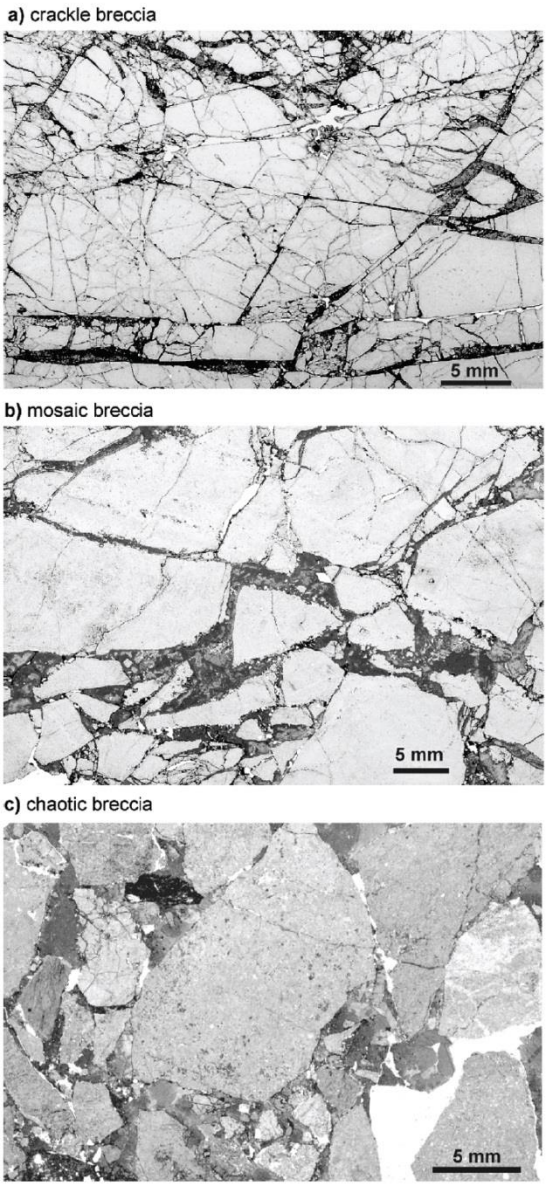

Figure 2.8: Breccia classification (Woodcock and Mort, 2008).

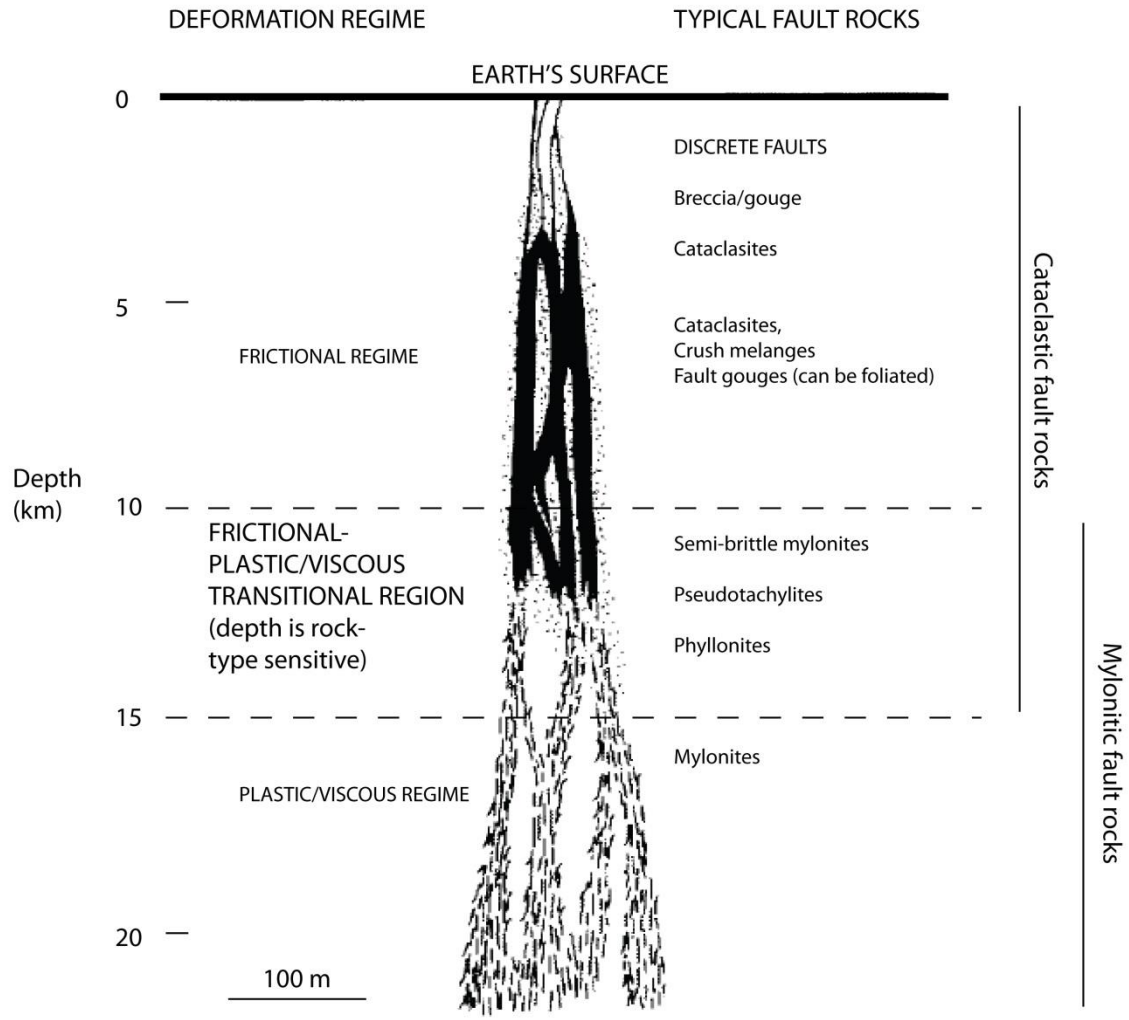

Figure 2.9: Widely cited conceptual model of fault rock variation with temperature/pressure conditions (depth) (Rutter et al., 2001 after Sibson, 1977a).

2.2.1.4.1 Cataclastic Fault Rocks

Brittle deformation along faults forms cataclastic fault rocks, comprised of rocks that have been fractured into clasts and ground into increasingly small fragments (Twiss and Moores, 1992). These are produced through cataclastic flow occurring during displacement along the fault, whereby brittle fragmentation of grains occurs with rotation of grain fragments accompanied by frictional grain boundary sliding and dilatancy (Sibson, 1977a). Cataclastic fabrics are characterised by sharp angular shapes of clasts and grains, transgranular fractures and a large grain size range. Cataclastic flow produces a progressive decrease in grain size and a progressive increase in the volume fraction of cataclastic material through continual fracturing and cataclasis of larger grains and incorporation of material from the wall rock protolith through abrasion (Twiss and Moores, 1992).

Brittle fault rocks formed in the upper few kilometres of the crust are generally incohesive gouges and breccias, which may be foliated. At greater depths, the higher confining pressures produce

highly indurated, cohesive cataclasites (Sibson, 1977a), which also may be foliated. In both cases, the foliation development usually reflects the presence of fluids and the onset of low temperature diffusive mass transfer processes such as pressure solution (Rutter et al., 2001). All brittle fault rocks are also frequently associated with contemporaneous mineralisation along fault zones reflecting the periodic development of high fluid pressures.

In general, as displacement increases fault rock thickness also increases, and there is a corresponding correlation between grain size and strain (Twiss and Moores, 1992). Slickenlines and other kinematic indicators in fault rocks can give an indication of the direction of shear (section 2.2.1.5).

2.2.1.4.2 Pseudotachylite

Pseudotachylites are typically unfoliated rocks of glass or devitrified glass, often associated with cataclasites, and occurring along fault zones (Twiss and Moores, 1992). Pseudotachylites are interpreted to be quenched melt formed during rapid frictional sliding, particularly in dry fault zones and at depth (e.g. Sibson, 1977a)(Figure 2.9). They can be recognised in the field by their sharp wall rock boundaries and injection veins. Under the microscope, they often display flow textures, rounded quartz clasts margins, devitrification textures, and lack of mica and amphibole within the matrix and corrosion of these minerals at the wall rock (Passchier and Trouw, 1996).

2.2.1.4.3 Ductile fault rocks

Cohesive fault rocks formed due to ductile deformation (e.g. crystal plasticity at depth) are termed mylonites (and phyllosilicate-rich phyllonites, Table 2.2). Mylonites are foliated and usually lineated, and produced through shear at high temperatures and pressures at depth usually exceeding 10 km in the crust (Figure 2.9). Polygonal and sutured grain boundaries with mylonites differ from the angular grains within cataclasites. Mylonites are found in ductile shear zones ranging from < 1 m to > 1 km in thickness (Twiss and Moores, 1992). Shear zones are generally regarded as the ductile expression of faults in the crust (Figure 2.9) and can similarly accommodate reverse, strike slip or normal relative displacements. Lineations in mylonites, alongside other kinematic indicators, can indicate the causal shear sense of the mylonite.

2.2.1.5 Kinematic (shear sense) indicators

Kinematics of fault (and shear) zones can be easily examined through observation of displaced markers (such as bedding). Where offset is not immediately apparent, kinematics can be

determined through observation of secondary fracture arrays and veins, and observations such as slickenlines (striæ) and slickenfibres on the fault surface (e.g. Figure 2.13). Movement direction can be accurately assessed through observations of slickenlines or ductile lineations, followed by determination of shear sense from other structures parallel to the linear features and normal to the fault/foliation plane.

2.2.1.5.1 Subsidiary fractures arrays

Asymmetric secondary fracture arrays can be used to determine shear sense along a fault. Minor R, R', P and T fractures can develop adjacent to the main fault plane (Figure 2.10). R shears are synthetic, having the same sense of shear as the imposed shear forming around 15° to it (Twiss and Moores, 1992). R' shears are antithetic, with an opposing sense of shear to that imposed, and orientated at 75-80° to it (Twiss and Moores, 1992). P fractures are synthetic and form at a small angle (10°) to the imposed shear (Twiss and Moores, 1992). T fractures are tension fractures and can form 30-90° to the fault surface.

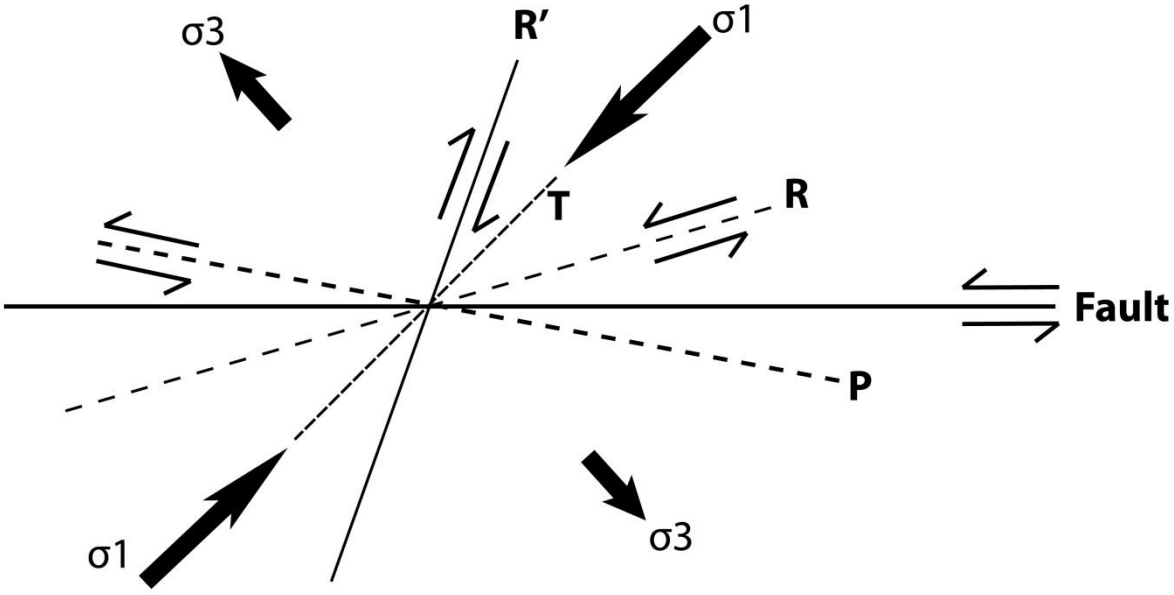

Figure 2.10: Subsidiary fractures that can be used to determine kinematics of a fault. From Twiss and Moores (1992).

2.2.1.5.2 Slickenfibres and slickenlines

Fault plane observations of slickenfibres (Figure 2.11) and slickenlines (Figure 2.12) can be used to determine shear sense. Slickenfibres are mineral fibre-lineations that occur on fault surfaces and in fibrous vein fillings. Continuity of mineral fibres across veins and shear surfaces imply that

mineral growth kept pace with gradual displacement across the fault surface (Twiss and Moores, 1992). Slickenlines are caused by small protrusions and irregularities on the fault surface, called asperities. These asperities produce lineations when the fault moves, and individual scratches/gouge marks end when the asperity breaks off the fault surface. Slickolites may be formed when there is a component of shortening across the fault (Twiss and Moores, 1992).

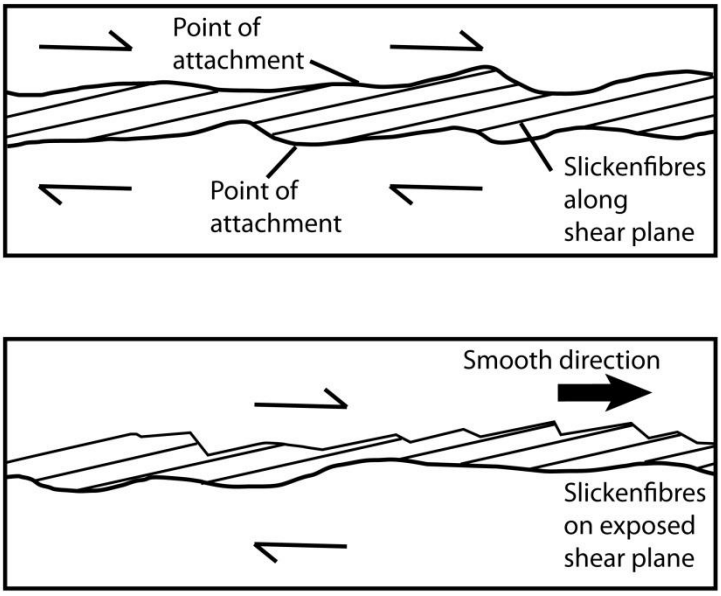

Figure 2.11: Slickenfibre development on a fault surface (from Twiss and Moores, 1992). (**A**) Arrows from the wall rock along the slickenfibre lengths point in the direction of movement of the opposite fault wall. (**B**) Smooth direction of slickenfibres defines the direction of relative slip of the block.

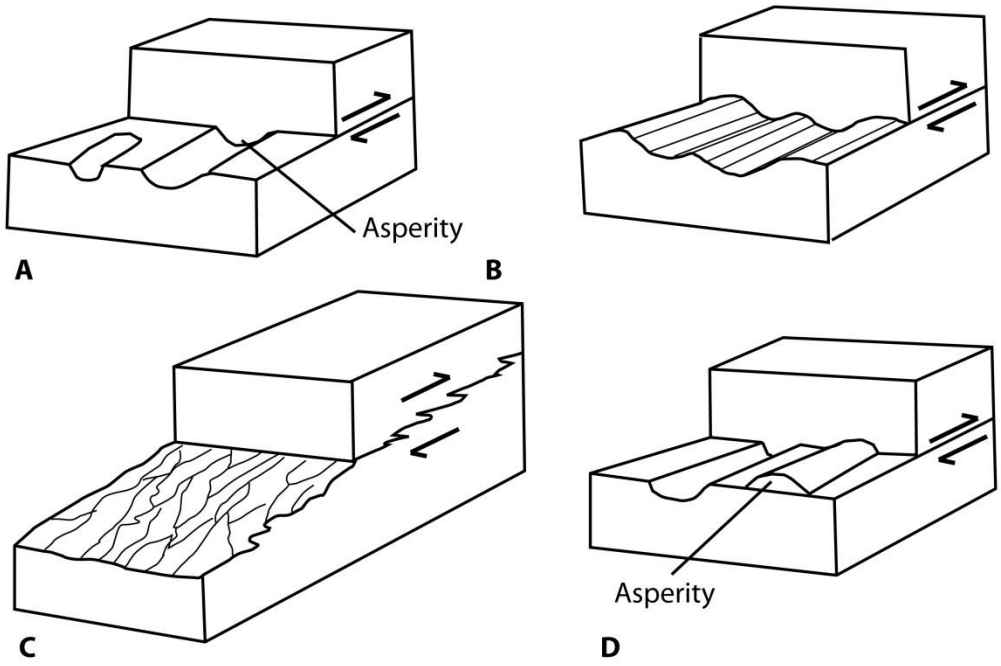

Figure 2.12: Slickenline formation on fault surfaces (from Twiss and Moores, 1992). (**A**) Slickenlines formed by gouging of one side of the fault surfaces by hard asperities on the other side. (**B**) Ridge-in-groove slickenlines, formed by linear irregularities in the fault surface that parallel the slip direction. (**C**) Spiked irregularities on a slickolite solution surface. (**D**) Mineral streak lineations from the wearing and smearing of mineral grains.

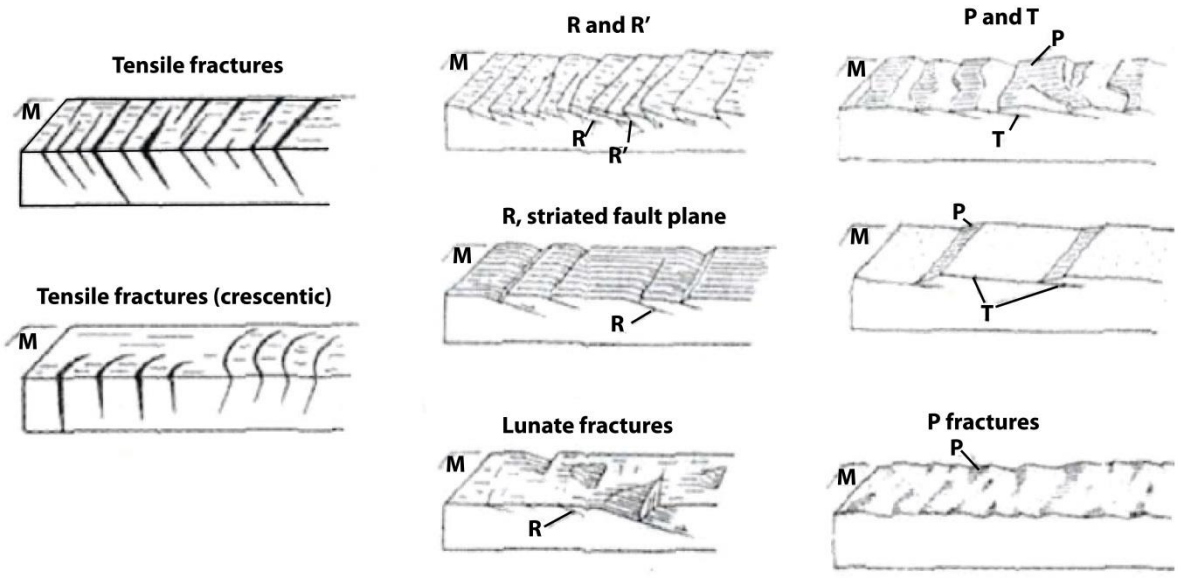

Figure 2.13: Examples of fault shear sense criteria on brittle fault surfaces Redrawn from Petit (1987).

2.2.1.6 Recognition of Reactivation

Reactivation of a fault is defined as '*the accommodation of geologically separable displacement events (intervals > 1Ma) along pre-existing structures*' (Holdsworth et al., 1997). Reactivation occurs when stress conditions are such that it is mechanically easier to reactivate a pre-existing fault instead of initiating a new one (e.g. Sibson, 1985). As such, in this thesis it is most often used to refer to faults where fault rock overprinting is present, e.g. zeolite and clay cataclasite/gouge brecciating epidote cataclasite along the same fault.

2.2.1.7 Fluid flow in the crust

The outer ~10 km of all crust contains abundant water in pores and fractures (Fyfe, 1985). Sources for crustal fluids include meteoric water, water derived from dehydration reactions, magmatic fluids, connate water and hydrocarbons (Sibson, 1994), and during burial and compaction of sediments large volumes of aqueous fluids are liberated (Best, 2003). Pore fluids have an important impact on effective stresses and faulting (section 2.2.1.2). Fluid pressure change with depth from hydrostatic to lithostatic (overpressured), depending on the depth of a seal (Sibson, 1990).

Faults and fractures formed in the crust produce fluid pathways parallel with the σ_2 axis (e.g. Sibson, 1994). Faults are usually observed to be associated with neomineralisation and retrogression of existing minerals in the surrounding wall rocks and within clasts incorporated into the faults (e.g. Imber et al., 1997), and growth of fracture networks during deformation play a major role in facilitating fluid flow through the crust (e.g. Cox, 2007). In crystalline rocks, fracture permeability depends on fracture density, orientation, and the hydraulic conductivity of the fractures present (Barton et al., 1995). Fluid flow has occurred through fractures within the Lewisian over the course of its history, with microcracks and joints acting as primary post-Laxfordian fluid conduits on the Scottish mainland (Hay et al., 1988).

Normal faults have been identified as both barriers and conduits for fluid flow (e.g. Caine et al., 1996; Sibson, 2000) and are of most interest in this study, forming the dominant Mesozoic and younger structures in the Outer Hebrides and at Clair (see later chapters). Textural observations from hydrothermal vein systems suggest that fluid flow in fracture systems occurs episodically, and in cases of faults, fluid influx and permeability are linked to the seismic cycle (Sibson, 1994). Mechanisms for fluid distribution include: Dilatancy during the fault loading cycle, formation of rupture irregularities and post-seismic fluid redistribution around them and post-seismic discharge of fluids from overpressured portions of the crust through fault-valve action when ruptures breach impermeable barriers (seals) (Sibson, 1994).

Fluids in the crust are dominated by H_2O and CO_2, with other minor constituents of volatiles such as N_2 (e.g. Andersen et al., 1993). Reactions and alterations are complexly governed by the chemical potential of these fluids, in addition to the presence of dissolved salts such as NaCl and KCl (e.g. Hay, 1978; Best, 2003). Secondary minerals formed during fracturing provide important information regarding the composition of the fluids and the environment of mineralisation (e.g. Weisenberger and Bucher, 2011). When basement rocks enter the brittle part of the crust fluids circulating in fracture porosity can result in the dissolution of high temperature minerals (like feldspar) and precipitation of lower temperature secondary minerals (like zeolite and adularia; Weisenberger and Bucher, 2010).

2.2.2 Palaeostress

The orientations of causative stress regimes can be determined through analysis of faults and fault slip data obtained from field observations. Palaeostress analysis has been performed on orientation data collected during fieldwork within the Stornoway Formation of Lewis and on selected (Mesozoic and younger) faults from the surrounding basement gneiss, with the analysis performed in the MyFault™ (v 1.04) software of Pangaea Scientific Ltd. This analysis has been undertaken to quantify stress orientations that can be qualitatively described from the observations collected in the field. Five inversion methods can be quickly analysed and compared within the MyFault™ software. The analysis used in this thesis is the Simple Shear Tensor Average, selected for its minimisation of the stress errors produced during recalculation. Low levels of strain within the generally minor Mesozoic structures of the Stornoway region make palaeostress analysis appropriate in this study. Myfault™ produces arrows that indicate the principal directions of stress in the horizontal plane. If the horizontal stress $\sigma_H \geq \sigma_{max}$ an inward pointing arrow is used. Otherwise, the arrows point outwards (as in this thesis).

Whilst palaeostress analysis has been undertaken on data collected from the Stornoway region, it has not been performed on the Lewisian basement hosted faults elsewhere. This is because in the Stornoway Region, the faults are found to be in 'upright' positions, with conjugate pairs symmetrical about a vertical plane, i.e. they have not been significantly rotated. Elsewhere across Lewis and Harris, Mesozoic and younger structures exist with potentially significant displacement of kilometres or more (e.g. the Seaforth and North Harbour Faults, see chapter 4 and 5), and the amount of rotational strain (i.e. any large-scale rotation/tilting across kilometres of Lewis and Harris) due to these faults and earlier events since the Archean cannot be accurately assessed. It would not be appropriate to perform palaeostress analysis where the amount of rotational strain is not known.

2.2.3 Tangent-lineation plots

Tangent lineation plots combine information about the shear plane orientation , the orientation of the slickenline in that plane, and the sense of shear on the plane (Twiss and Moores, 1992). The directions of maximum resolved shear stress on a set of planes uniformly distributed on the plotted hemisphere form regular patterns whose shapes depend on the ratio of the principal stress differences (Twiss and Moores, 1992):

$\Phi = (\sigma_2 - \sigma_3) / (\sigma_1 - \sigma_3)$

Tangent lineation plots are useful in discriminating between fault sets and checking whether faults that are grouped together are kinematically compatible – i.e. do they produce a realistic pattern on the tangent-lineation plots. Tangent lineation plots also allow stress conditions to be extracted through visual inspection (e.g. Figure 2.14).

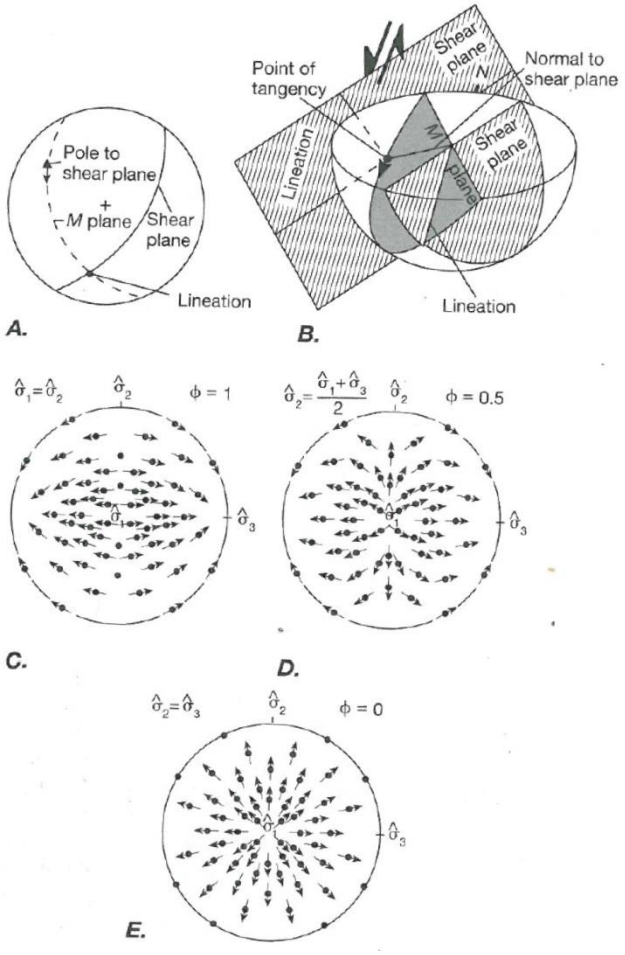

Figure 2.14: Construction and interpretation of tangent lineation diagrams (from Twiss and Moores, 1992). (**A** – **B**) The tangent lineations are plotted as arrows through the pole to the shear plane, tangent to the great circle that contains the shear plane pole and the lineation orientation in the shear plane. (**C** – **E**) Directions of maximum resolved shear stress on a set of planes having a uniform distribution of orientations over the plotted hemisphere, with different values of the stress difference ratio ϕ.

2.2.3.1 Simple Shear Tensor Average Stress Inversion Method (Sperner et al., 1993)

The Simple Shear Tensor Average calculates the simple shear stress state at each fault, with the intermediate principal stress lying in the fault plane perpendicular to the slip direction. The stress tensors from each fault are averaged together to give an estimate of the regional stress tensor. The angle between the maximum principal stress and the fault plane can be varied to search for the minimum deviation between the faults in the set; MyFault™ scans between 0 and 45°.

This method assumes that slip occurs in the same direction as when the fault was first formed (i.e. the fault is not reactivated), and it also does not allow for an estimate of the intermediate principal stress. The intermediate stress value will tend to lie close to 0.5, where maximum and minimum principal stresses are normalised to one and zero. Hence the stress ratio is equal to the intermediate stress.

MyFault™ recalculates the principal stress directions, at least the same number of times as there are samples, using bootstrap resampling methods, where the dataset is randomly resampled with the same number of data points as the original. This produces duplication of one or more of the original records, and MyFault™ recalculates the principal stress tensor. These results are plotted as 'stress errors' in the palaeostress analyses results (e.g. Figure 2.15). The Simple Shear Tensor Average method has been found to produce the smallest spread of stress errors with the data collected from fieldwork and hence is used in this thesis.

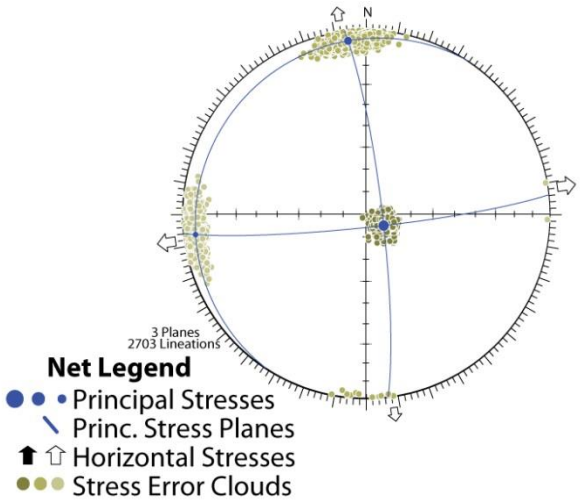

Figure 2.15: Palaeostress analysis results from the Simple Shear Tensor method.

2.3 Fracture attribute analysis - 1D Line transects

Fractures exist over a wide range of scales, from the largest faults to microfractures, and this range is responsible for scaling effects observed in fractured rock hydrology and mechanical properties (Barton, 1995). In order to accurately define fracture system geometry it is necessary to quantify specific fracture characteristics. Fracture system geometry comprises the detailed characteristics of fracture organisation, including fracture spacing, orientation, aperture and length (e.g. Hudson and Priest, 1979; Peacock and Sanderson, 1992; Bour et al., 2002; Olson, 2007). For this purpose, 1D line transects were performed across selected outcrops in the Hebrides. One-dimensional line transects have been shown to be an effective way of collecting data for statistical analysis of fracture attributes such as length, aperture and spacing (e.g. Gillespie et al., 1993; Pickering et al., 1995; Bonnet et al., 2001; Sleight, 2001; McCaffrey et al., 2003; Torabi and Berg, 2011; Pless, 2011), and can easily be collected from logs and boreholes during resource exploration.

1D line transects are performed simply by selecting the outcrops for study and laying out a tape measure along them, measuring the position, orientation and other attributes of each fracture encountered (e.g. Figure 2.16). Analysis is undertaken to determine the distribution type present and various other bulk parameters may also be calculated in order to quantify specific fracture attributes. Analysis is usually performed by plotting the variable studied against cumulative frequency (e.g. Gillespie et al., 1993) with the distribution type present being determined through visual inspection and subsequent regression analysis (e.g. Jolly and Cosgrove, 2003; McCaffrey et al., 2003). Relevant attributes can then be described quantitatively and findings compared between different geological contexts.

2.3.1 Spacing and aperture

Fracture spacing and aperture are studied in this thesis as this data can be directly compared back to the Clair cores. Fracture spacing along the line transect is calculated as the distance between the margins of adjacent transects (Figure 2.16). When the spacing distribution is power-law, the degree of clustering of the faults can be quantified and compared across multiple data sets using the slope of the power-law trend line that fits the distribution, i.e. the power-law exponent (Belfield, 1998). Aperture is simply the width of the fracture of interest (Figure 2.16). Plotting aperture against cumulative frequency normalised to transect length enables the density of fractures of a particular aperture to be ascertained (Ortega et al., 2006).

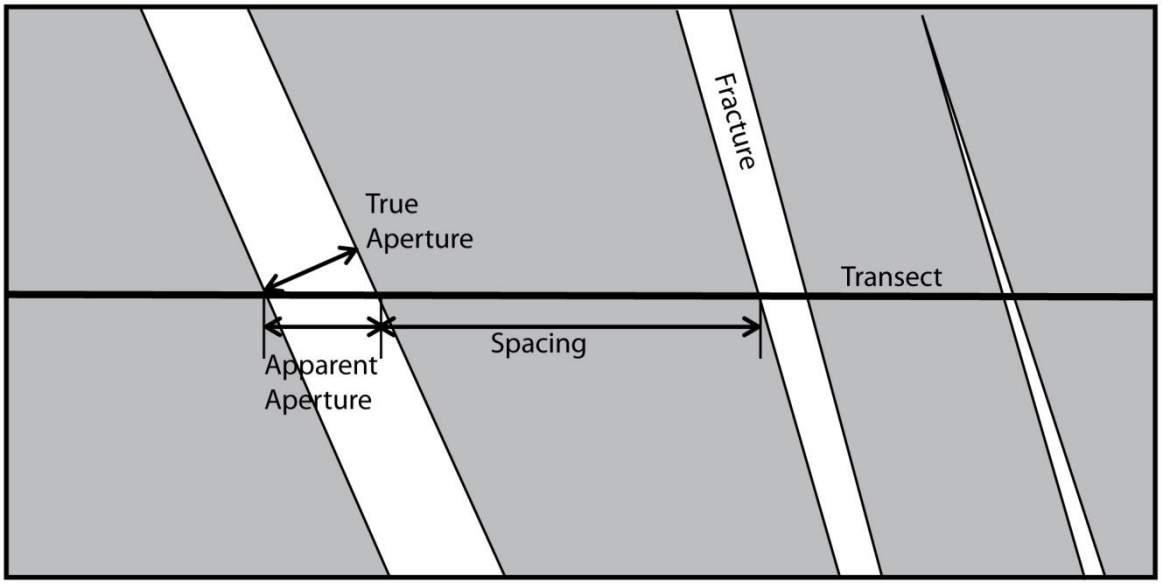

Figure 2.16: Showing measurements obtained for aperture and spacing along a 1D line transect. Redrawn from Gillespie et al. (1999).

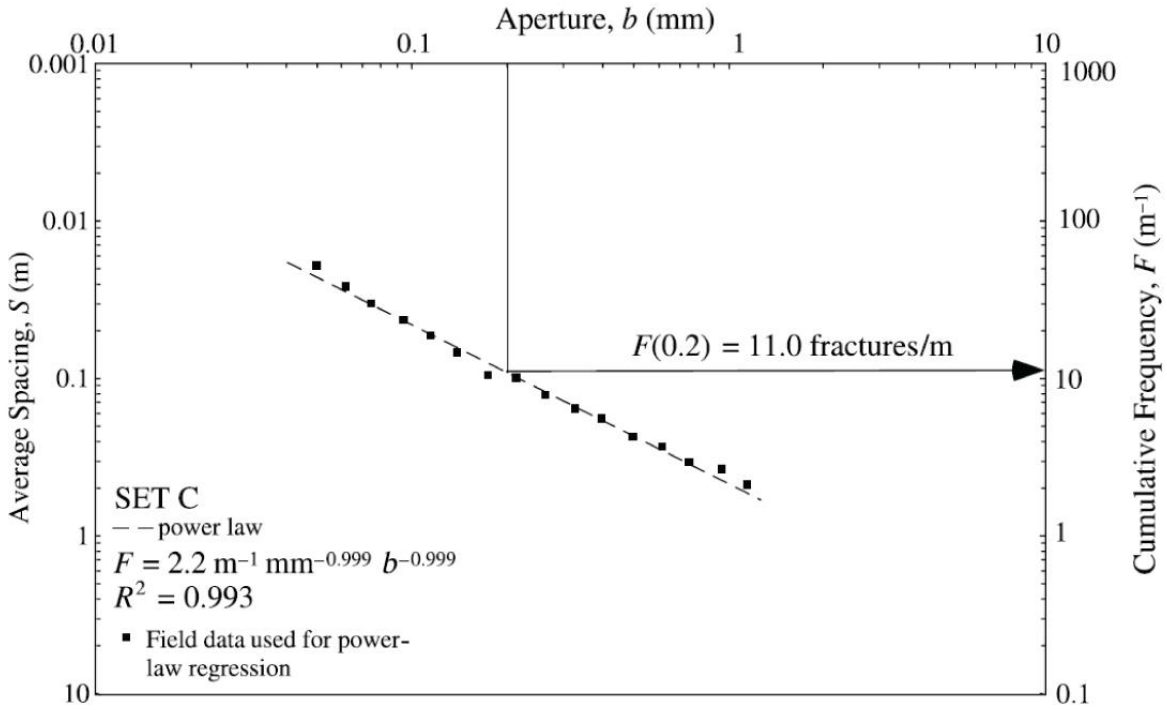

Figure 2.17: Aperture vs. Average Spacing/Normalised cumulative frequency. From Ortega et al. (2006).

2.3.2 Fracture attribute data distribution types

The common distribution types are shown in Figure 2.18. Fault attributes such as spacing, length, and aperture are often found to have skewed distributions such as log-normal, exponential and power-law distributions (e.g. McCaffrey et al., 2003). Most often, fracture attributes are

determined to be best represented by power-law distributions (e.g. Nicol et al., 1996; Peacock, 2002; Kim and Sanderson, 2005; Pless, 2011; Torabi and Berg, 2011; Kolyukhin and Torabi, 2012), although distribution types such as negative exponential and log-normal distributions have also been identified (e.g. Ackermann et al., 2001; Soliva and Schultz, 2008), and power-law spacing distributions may break down with fault development (Torabi and Berg, 2011; Kolyukhin and Torabi, 2012). The simplest method used to determine which distribution is appropriate for a dataset is to plot the data on a cumulative frequency/variable graph (e.g. McCaffrey et al., 2003 Torabi and Berg, 2011). In this thesis, plots have been constructed in Microsoft Excel by ordering the data from smallest to largest and plotting the attribute against cumulative frequency normalised to transect length to enable comparison between transects. Plotting these using combinations of logarithmic and linear axes enables the most common distributions to be distinguished, and appropriate regression curves may be fitted by a least-squares approach, allowing direct comparison between datasets.

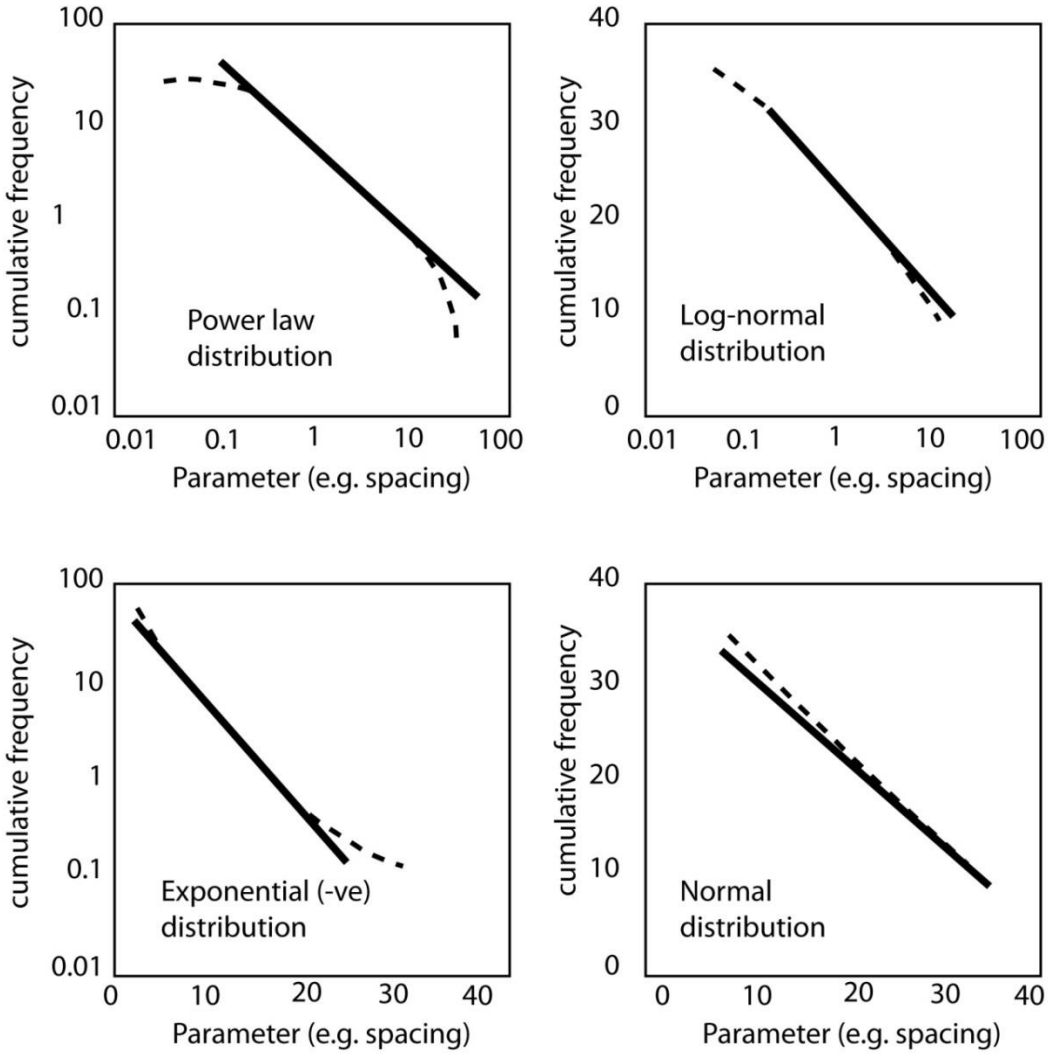

Figure 2.18: Fault parameter distribution types, presented with logged and linear axes. Redrawn from McCaffrey et al. (2003). Tails represent censoring and truncation effects.

2.3.2.1 Power-law distribution

Power-law distributions display straight lines on plots with logarithmic x and y axes, and power-laws have been extensively used to describe fracture characteristics such as spacing, aperture and length (e.g. Nicol et al., 1996; Torabi and Berg, 2011). Power-law distributions represent datasets that are self-similar over multiple orders of magnitude, i.e. they are fractal (e.g. Velde et al., 1991; Torabi and Berg, 2011). The most important feature of fractal geometry is the lack of any homogenisation scale or representative volume (Bonnet et al., 2001) (i.e. the scale of study does not alter the results). It is popular to assign power-law trend lines to fault and fracture data as it allows prediction of scale invariant fracture attributes at scales outside of that which it is possible to directly measure them at, such as below seismic resolution during hydrocarbon exploration. Power-law distributions are represented by the equation:

$$N = aS^{-C}$$

Where 'N' is the cumulative number, 'a' is related to the number of faults, 'S' is a measure of size and 'C' is the power-law exponent and gradient of the slope of the distribution (Pickering et al., 1995). The power-law exponent gives the ratio of the smallest faults to the largest faults (Ackermann and Schlische, 1997). Hence, in populations with larger power-law exponents (steeper slopes), smaller values (e.g. fault spacings/lengths/apertures) are relatively more important. Where the power-law exponent value for a spacing distribution is relatively high, it indicates greater clustering of faults (Gillespie et al., 1993). The power-law exponent can be directly compared between line samples obtained in different contexts. Ortega et al. (2006) show that for spacing to be scale-invariant, fracture size must be taken into account, as the number of fractures sampled of any given range varies with the scale of sampling. Using this method, plotting aperture along the x-axis and normalised cumulative frequency on the y-axis, it is possible to predict fracture densities for fractures of selected size (Figure 2.17).

2.3.2.2 Negative exponential distribution

Negative exponential distributions display as straight lines on a plot with logarithmic y-axis and linear x-axis. This distribution represents a random array of values. When applied to fracture spacing, a negative exponential distribution represents spacings associated with randomly positioned discontinuities along a line, i.e. the positions of the fractures are mutually independent (Priest and Hudson, 1976b; Hudson and Priest, 1979). The gradient of the cumulative distribution function is the exponent, and represents the relative importance of smaller or larger fracture values. A steeper gradient represents a greater preponderance of smaller values in the dataset (e.g. Sleight, 2001). Joints can display an exponential spacing distribution, particularly when

multiple sets are sampled (Gillespie et al., 1993). Exponential spacing distributions have also been recognised in some fault systems (e.g. Soliva and Schultz, 2008).

2.3.2.3 Log-normal distribution

Log-normal distributions plot as straight lines on plots with a linear y axis and a logarithmic x-axis. Log-normal distributions are so named as when y = log(x), the distribution plots as a bell shape on a histogram (i.e. normally) (Sleight, 2001). These distributions represent large numbers of small values, with decreasing numbers of larger values. Joints have been known to display a log-normal spacing distribution (Gillespie et al., 1993).

2.3.2.4 Factors affecting data distribution

It is important to consider whether samples obtained during this data collection are representative. The population is the total set of measurements that could theoretically be obtained from the rock being studied (Swan and Sandilands, 1995). The statistical sample obtained from the rock is a subset of the overall population and is taken to represent the properties of the overall population (Swan and Sandilands, 1995). Any bias introduced into the sample means that the sample may not be representative of the population as a whole.

There are multiple factors that affect the shape of any distributions obtained from line transects. The first and most obvious influence is that due to data quantity. A minimum number of at least 50 fractures is preferable during data analysis (e.g. Johnston et al., 1994), and Bonnet el al. (2001) suggest collection of at least 200 fractures per transect in order to adequately define the power-law length distribution. If too few fractures are sampled, it becomes more difficult to define straight line portions of a power-law distribution due to the proportionally greater effects of censoring and truncation bias. All observed fracture populations are affected by 'truncation' and 'censoring' effects that alter the appearance of the distribution (Bonnet et al., 2001). Small fractures are incompletely observed as the limit of resolution of the study is approached (truncation). This causes a shallowing of the distribution trend towards the smaller end of the scale (Bonnet et al., 2001). Larger fractures tend to be incompletely sampled because they pass outside of the observed resolution, causing a steepening of the slope of the distribution trend at the larger end of the scale range (Bonnet et al., 2001) (Figure 2.19). The effects of truncation and censoring cannot be fully statistically distinguished from the underlying distribution, and this work is not centred around the development of new statistical techniques. Hence, in this thesis (chapter 7), the three main potential distribution types (power-law, exponential or log-normal) for fracture data are presented for each transect.

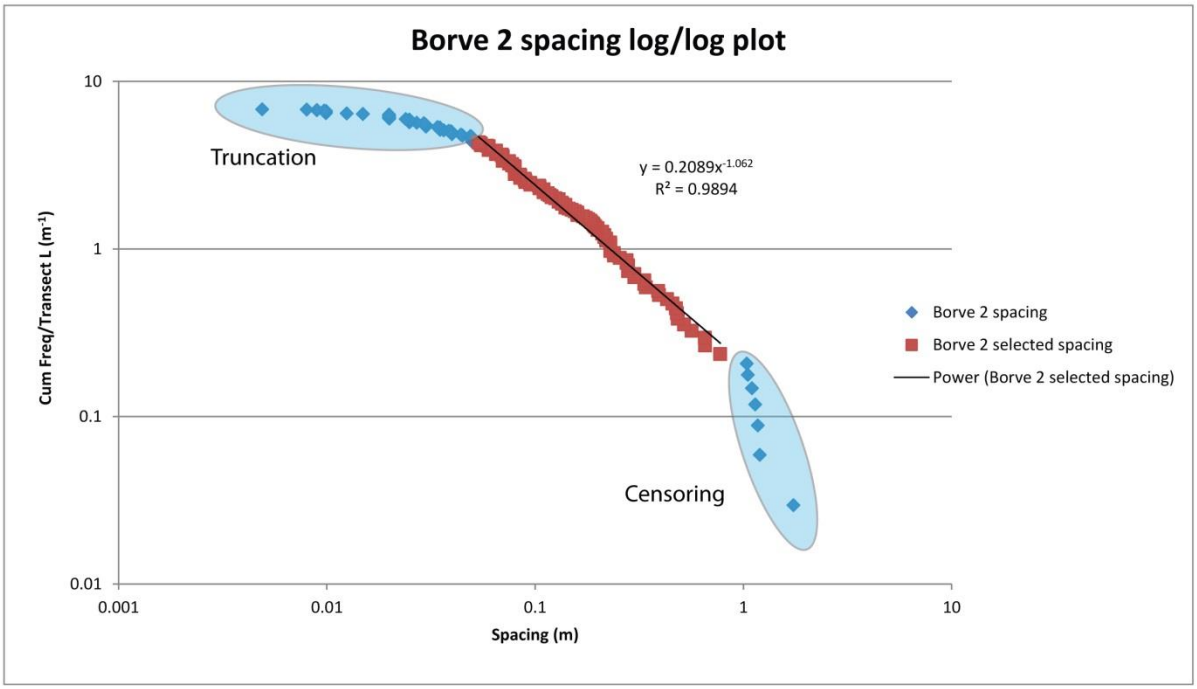

Figure 2.19: Borve 2 spacing plot with logarithmic x and y axes. Straight line section can be described by a power-law trend line (selected and indicated in red), with a D value of 1.062. Truncation and censoring indicated.

Other sources of variation in fault scaling data arise from:

- Combining data sets from multiple transects (multi-line sampling) can be undertaken in cases where the data is sparse. This however has obvious implications for interpretation of the resulting distribution, which will not be representative of a fracture sets measured in either line if the lines are not continuous along the same outcrop. Hence this technique is only used where line transects are continuous across the outcrop.
- Geological variables such as lithology and pre-existing structures (e.g. Knott et al., 1993; Wilkins and Gross, 2002; Kim and Sanderson, 2005).
- Maturity of the fracture and fault systems and development of fault linkage can also have a significant impact on fault scaling characteristics such as displacement (Wojtal, 1994; Wojtal, 1996).
- Reactivation of a fracture or fault system (Kim et al., 2001; Kim and Sanderson, 2005).
- Differences in spacing characteristics have also been identified where stratigraphy causes a level of detachment between faulting above and below weak horizons (e.g. Soliva and Schultz, 2008).
- Deformation may change with scale, affecting subsequent fracture distributions (Fossen and Hesthammer, 2000).

One dimensional line transects will also inherently display orientation bias. For this reason it is important to obtain transects at multiple orientations, where possible, in order to be able to

compare different fracture set characteristics. In this study, faults of particular age have been sampled with transects parallel and perpendicular to the master fault strike.

2.3.3 Bulk attributes

In order to provide a more complete measure of fracture spacing characteristics, several further attributes can be calculated from line transect data.

2.3.3.1 Fracture density

Fracture density (i.e. the number of fractures over the length of measurement) is the simplest measure of fracture spacing and provides an estimate of the number of fractures present, usually at macroscopic scale. A fundamental limitation of this measure is that it applies only to the scale that the analysis was conducted at, and is effectively meaningless at other scales (e.g. Ortega et al., 2006). For this reason, it is important to assess whether the fracture spacing is scalable (i.e. power-law), in which case, fracture density at other scales can then be determined. The relative fracture density can also be assessed visually from the population plots as each is normalised to line length. Steeper slopes indicate a relatively higher fracture density (McCaffrey et al., 2003).

2.3.3.2 Coefficient of Variation

The coefficient of variation (Cv) is defined as the ratio of the standard deviation to the mean:

$$\mathrm{Cv} = \frac{(\text{Standard deviation})}{(\text{mean spacing})}$$

Cv measures the degree of spatial clustering or anti-clustering in each data set (Gillespie et al., 1999; McCaffrey et al., 2003). For a random distribution, the mean and standard deviation are equal and Cv = 1 (McCaffrey et al., 2003). If the fractures are spatially clustered, Cv > 1, and if the veins are anticlustered (i.e. more regularly spaced) Cv < 1. For perfectly regularly spaced fractures, Cv = 0. Clustering of veins requires there to be a higher probability of each fracture forming close to other fractures. Conversely, anticlustering requires that each fracture has a higher probability of forming away from other fractures (McCaffrey et al., 2003). Thus the Cv value can be used to help distinguish between clustered spacing distributions (log-normal and power-law) and randomly spaced fracture sets (exponential distributions).

2.4 Thin Section Work

Three hundred and seventy-three orientated hand samples were obtained from multiple localities in order to investigate the micro-scale characteristics of fault rocks, veins and wall rocks such as mineralogy, kinematics, and evidence of fluid flow and mineralisation/alteration (Figure 2.20). From these samples, one hundred and sixty-one thin sections were produced. Fault rock thin sections display slices of rock that were cut perpendicular to the fault surface and with a long edge of the thin section orientated parallel with slickenlines, where present. This cutting orientation preserves the maximum amount of kinematic and deformation mechanism indicators that are obtainable from the fault rock.

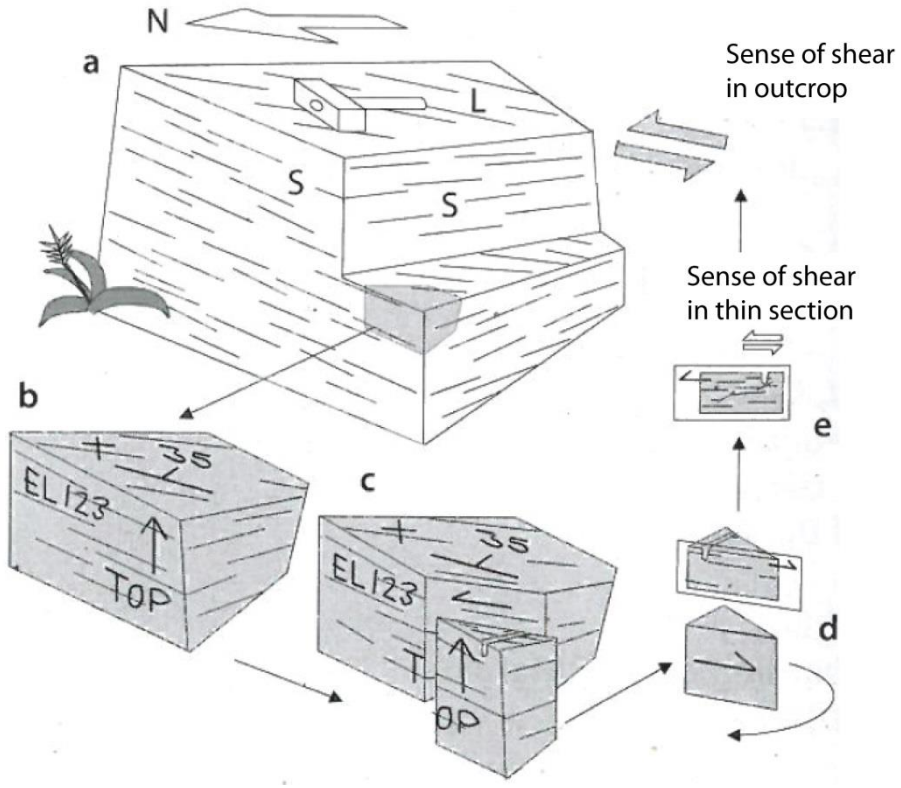

Figure 2.20: Method for obtaining oriented samples form outcrop, from Passchier and Trouw (1996).

Samples of soft incohesive clay gouge were obtained from outcrop and through non-rotational insertion of 15 cm length u-PVC tubes into the outcrop face. This is followed by gentle excavation, before being set in resin and thin-sectioned. This allows microscopic examination of rarely studied soft clay-bearing gouges. Thin sectioned samples were analysed under; optical microscopy using a petrographic microscope, and, using a scanning electron microscope (SEM) alongside an energy

dispersive x-ray spectroscope (EDX) in order to investigate micro-scale characteristics and mineralogy.

2.4.1 Scanning Electron Microscopy

Twelve thin sections and six polished blocks were produced for SEM analysis. SEM produces images of a sample by scanning it with electrons and displaying the return signal collected by an electron detector. Two primary detection modes exist: secondary electron images, and back-scattered electron images can be produced. It is possible to add an X-ray spectrometer to an SEM and mineral identification of the spectra can be undertaken (Reed, 1996). Magnification ranges from ~1,000 (1µm resolution) to 100,000 (10 nm resolution). Secondary electrons are emitted from near the surface of the sample during interaction with the scanning beam electrons. Secondary electron images are used primarily for topographic contrast (Figure 2.21B)(Reed, 1996). Back-scattered electrons originate from the high energy scanning beam and are reflected from the surface of interest. Heavier elements back-scatter electrons more effectively than lighter elements, and thus appear brighter in the subsequent image. Back scattered images can therefore be used to distinguish areas with different or similar compositions within a sample (Figure 2.21A) (Reed, 1996).

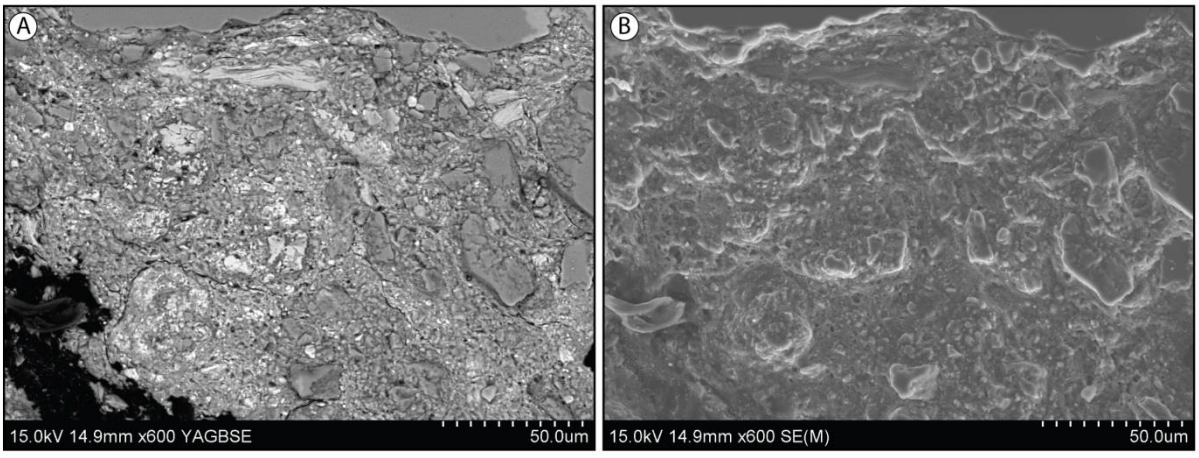

Figure 2.21: SEM images of cataclasite from the Stornoway Formation. (**A**) Back-scattered electron image, highlighting compositional variation. (**B**) Secondary electron image, highlighting topographical variation.

2.4.1.1 Energy dispersive x-ray spectroscopy

Characteristic x-rays are produced by electron transitions between energy levels in the inner electron shells of atoms during bombardment by the beam electrons in SEM. Energy dispersive x-ray spectrometers consist of an x-ray detector that produces electronic pulses in proportion to the size of the x-rays received. X-ray spectra are produced with lines or peaks that represent the characteristic elements present within the studied sample. These spectra can be compared to type samples and used to identify the minerals present (e.g. Figure 2.22) (Reed, 1996).

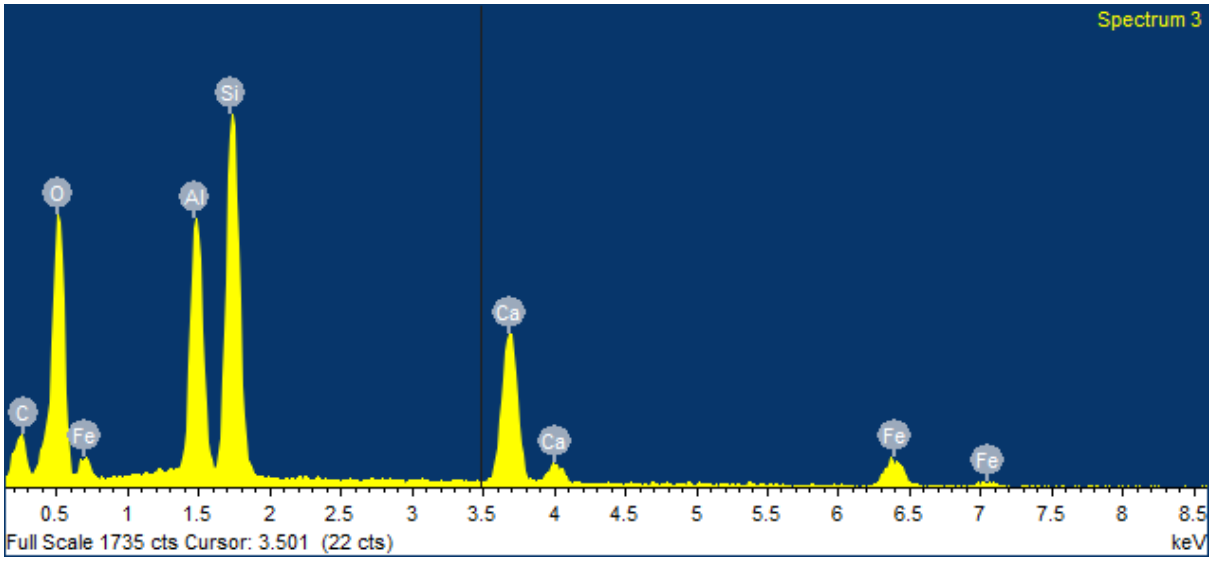

Figure 2.22: Spectrum obtained from scanning a selected mineral. Identification is possible through comparison of the relative peak heights and elements in the spectrum to type samples. The above spectrum indicates the mineral is epidote ($Ca_2Al_2O.(Al,Fe^{3+})OH[Si_3O_7][SiO_4]$, Deer et al., 1992).

Chapter 3: Brittle faulting and fracturing in the Stornoway Region of Lewis, and the relationship between the basement and the Stornoway Formation

3.1 Introduction

In many onshore regions, the nature of the basement-cover interface and structural relationships between basement and cover sequences are commonly poorly understood, and may be difficult to study because of limited exposure. The Hebridean islands contain the westernmost outcrops of Mesozoic-aged rocks in the British Isles: the Permo-Triassic Stornoway Formation (Steel and Wilson, 1975; Storetvedt and Steel, 1977). This formation directly overlies basement rocks of the Lewisian Gneiss, including parts of the Outer Hebrides Fault Zone (OHFZ), enabling direct comparison of faults and structures between the basement and cover.

The identification of Mesozoic faults and the recognition of fault geometries and kinematics is of particular interest along the European Atlantic continental margin as it allows for better constraints on hydrocarbon system timings, in addition to enhancing the understanding of continental breakup and the formation of the Atlantic. The relationship between faulting in the cover and faulting in the basement is surprisingly poorly understood, but is increasingly important economically because fractured basement rocks are becoming increasingly significant in the exploration of frontier hydrocarbon systems, particularly in the West of Shetland region. Understanding basement fault characteristics is important as these faults can control faulting in the cover (e.g. Butler et al., 1997; Holdsworth et al., 1997), and hence affect subsurface fluid flow. In most areas, the nature of the basement cover interface (e.g. whether it is faulted or not) is difficult to study, but the excellent exposures on Lewis allow for a detailed structural characterisation. In addition, the Stornoway Formation is cut by hundreds of faults that may be directly compared to those seen in the surrounding basement rocks, to understand the modes and processes of faulting as they cut through the basement-cover interface.

3.1.1 Rationale and Objectives

The Outer Hebrides represent an opportunity to study basement-cover faulting, which may be analogous to active hydrocarbon plays in the West of Shetland (e.g. the Clair Field). In the Clair Field, the oil-water contact within the Clair Group is known to be lower than the adjacent basement high of the Rona Ridge (e.g. Baron et al., 2008), and connection across the field through the basement high is known to occur, predominantly through fractures that must have been open during the Mesozoic (Finlay et al., 2011). Therefore, understanding the basement-cover interface

and faulting between basement and cover rocks is very important for constraining predictions about field behaviour in the sub-surface. Here faulting in the Stornoway Formation that overlies the Lewisian Complex Gneiss of the basement is examined, followed by faulting within the basement and at the basement-cover interface. The following questions are addressed:

- What are the characteristics of faulting within the cover sequence?
- Is faulting in the cover controlled by faulting within the basement?
- Is faulting of Mesozoic age distinguishable within the basement?
- What controls are there on faulting within the basement?
- What is the nature of the basement-cover interface?

3.2 Geological Setting

3.2.1 Regional Geology

The Outer Hebrides contain excellent exposures for the study of brittle and ductile shear zones, particularly within the OHFZ: a multiply reactivated fault system initiated in the Proterozoic (e.g. Imber et al., 2002; Mason and Brewer, 2004; Macdonald and Fettes, 2007), with a long, complex and varied history of compartmentalisation along its length (e.g. Macinnes et al., 2000; Imber et al., 2002; Osinski et al., 2001), including phases of faulting in the Mesozoic (e.g. Trewin, 2004). The OHFZ fault systems are abundantly exposed, providing a record of deformation events within the Lewisian Gneiss, since fault initiation in the Proterozoic (e.g. Butler, 1995; Imber, 1998; Imber et al., 2002; Mason and Brewer, 2004). Repeated reactivation of the OHFZ has produced multiple overprinting fabrics and faults, and a complex arcuate zone of deformation exposed for > 200 km, from Vatersay in the far south of the Outer Hebridean chain to eastern Lewis in the north (Figure 1.1). On Lewis, the OHFZ is well exposed along the east coast, allowing study of the various fault rock assemblages and respective cross-cutting and overprinting relationships (Butler, 1995; Imber, 1998). Deformation events are known to include initiation during ductile thrusting, followed by brittle thrusting, strike-slip movements, and normal faulting, with significant localisation along pre-existing structures (e.g. Imber et al., 2002). Most recently, the OHFZ is thought to have been reactivated at depth in the Mesozoic producing the Minch Basin (Stein, 1988; O'Neill and England, 1994; Trewin, 2004), with syn-rift Triassic and post-rift Jurassic sediment deposition in the fault hangingwall (O'Neill and England, 1994). The Permo-Triassic phase of extension and deposition is recorded onshore in the conglomeratic Stornoway Formation (Storetvedt and Steel, 1977). The Stornoway Formation is linked with development of the Minch Basin and was deposited in fault-controlled half-graben, with alluvial fans shedding material over the downthrown fault hangingwalls (Steel and Wilson, 1975).

3.2.2 Local Geology of the Stornoway Region

The Stornoway Formation is now exposed as a ~15 km strike length, conglomerate-filled half-graben system with bounding fault traces trending NNW-SSE, N-S, and ENE-WSW. These deposits are dominated by massive conglomeratic units. Steel and Wilson (1975) present a sedimentological analysis of the Stornoway Formation that is used to propose the development of a series of rotated fault-bound blocks within the underlying Lewisian (Figure 3.1 cross section). However, they did not study the faulting present in outcrop or the nature of the basal unconformity with the underlying basement rocks. This study encompasses faulting affecting both the Stornoway Formation and its counterparts in the surrounding Lewisian Gneiss (Figure 3.1).

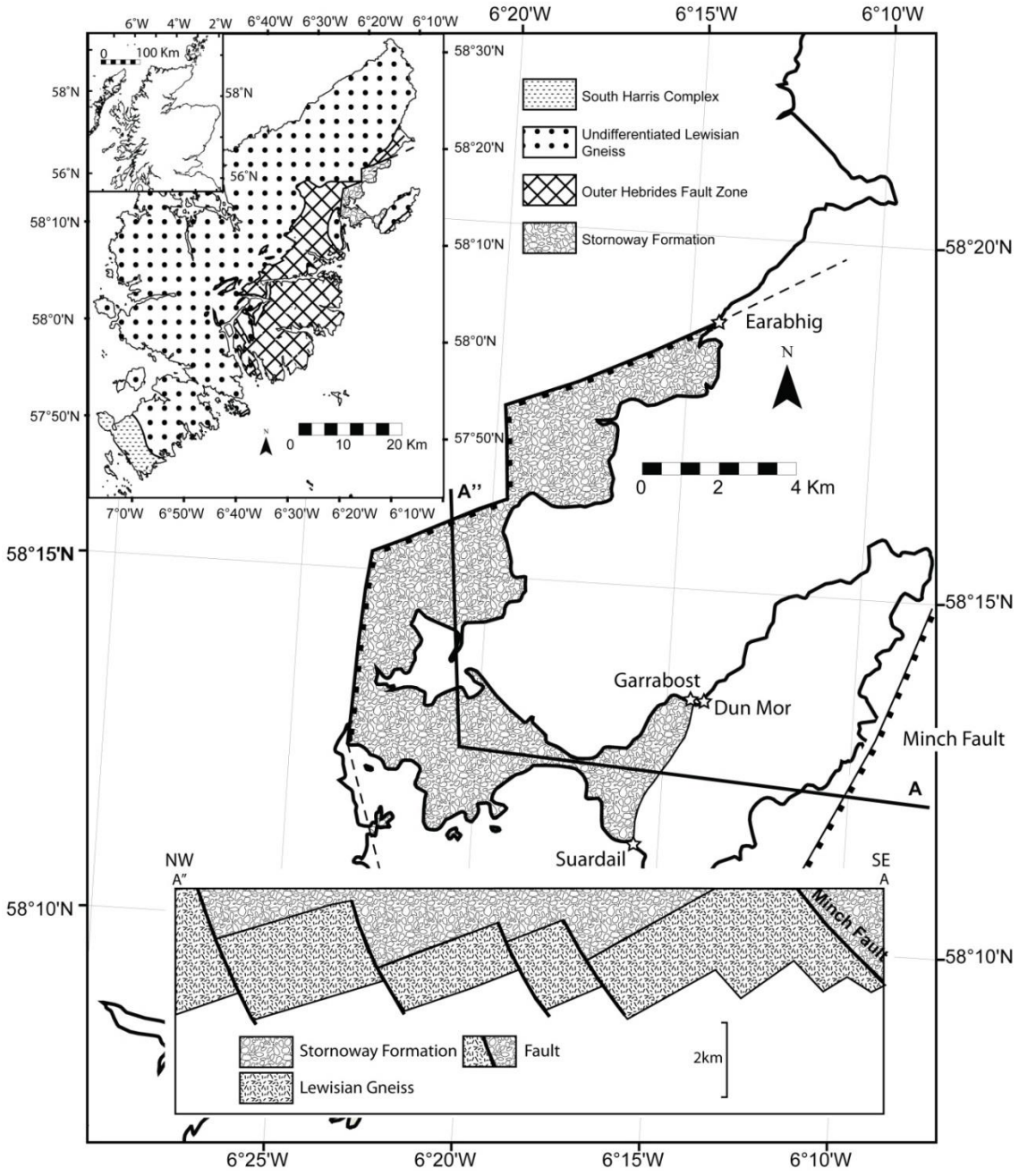

Figure 3.1: The location and cross section of the Stornoway Formation, modified from Steel and Wilson, 1975. Starred localities mark exposed basement-cover interface locations.

3.2.2.1 Lewisian Gneiss

Gneisses of the Outer Hebrides are amphibolite facies grade, having been retrogressed during the Laxfordian event, which reworked the gneisses to varying degrees across the Outer Hebrides (e.g. Fettes et al., 1992). Hornblende-biotite gneisses dominate in the Isle of Lewis (Fettes et al., 1992). This assemblage is interleaved with mafic units termed the *Older* and *Younger Basics*, which are cut by Laxfordian granites and pegmatite dykes (e.g. Fettes et al., 1992). In the region immediately adjacent to the Stornoway Formation rocks, the country rock is mostly composed of the heavily faulted OHFZ rocks (e.g. Figure 3.1) where ductile and brittle deformations have altered mainly hornblende-biotite gneisses to a range of mylonitic, phyllonitic and cataclastic rocks and hydrothermal alteration products (e.g. Imber et al., 2001; Imber et al., 2002; Sibson, 1977b).

3.2.2.2 Stornoway Formation

The Stornoway Formation is overwhelmingly composed of conglomerate with cobble-sized clasts derived directly from the surrounding Lewisian Gneiss and OHFZ (Stevens, 1914; Steel and Wilson, 1975). These are set in a light brown fine-grained sandy matrix containing smaller lithic clasts and limonite, siderite, and calcite cements. Porosity, which can be estimated from optical microscopy, varies from more than 20% to 0%. Clasts are mostly comprised of gneisses and cataclastic fault rocks derived directly from the Lewisian rocks in the OHFZ with sizes ranging from boulders (3 m across) near the bounding faults to mm scales, with a modal diameter of around 12 cm. The total thickness of the formation is estimated to be 4 km by Steel and Wilson (1975), but later authors attribute thicknesses of nearer to 1.2 km (Trewin, 2004). Bedding is generally massive, but sub-metre scale beds of coarse to fine sandstone exist particularly in the area between Cnoc and Holm in the centre of the Stornoway Formation to the east of Stornoway town (Figure 3.6**,** Steel and Wilson, 1975). Steel and Wilson (1975) suggest that the formation is comprised of six alluvial fan successions with floodplain deposits. Using their observations, they hypothesise the existence of three units within the succession, younging towards the west, each deposited in a separate rifting and alluvial fan building episode (Figure 3.2). Beds in the west of the formation are youngest and have therefore undergone less rotation. Bedding dips increase to the east from values of 12-15° near the bounding faults in the west to 45° seen at Suardail.

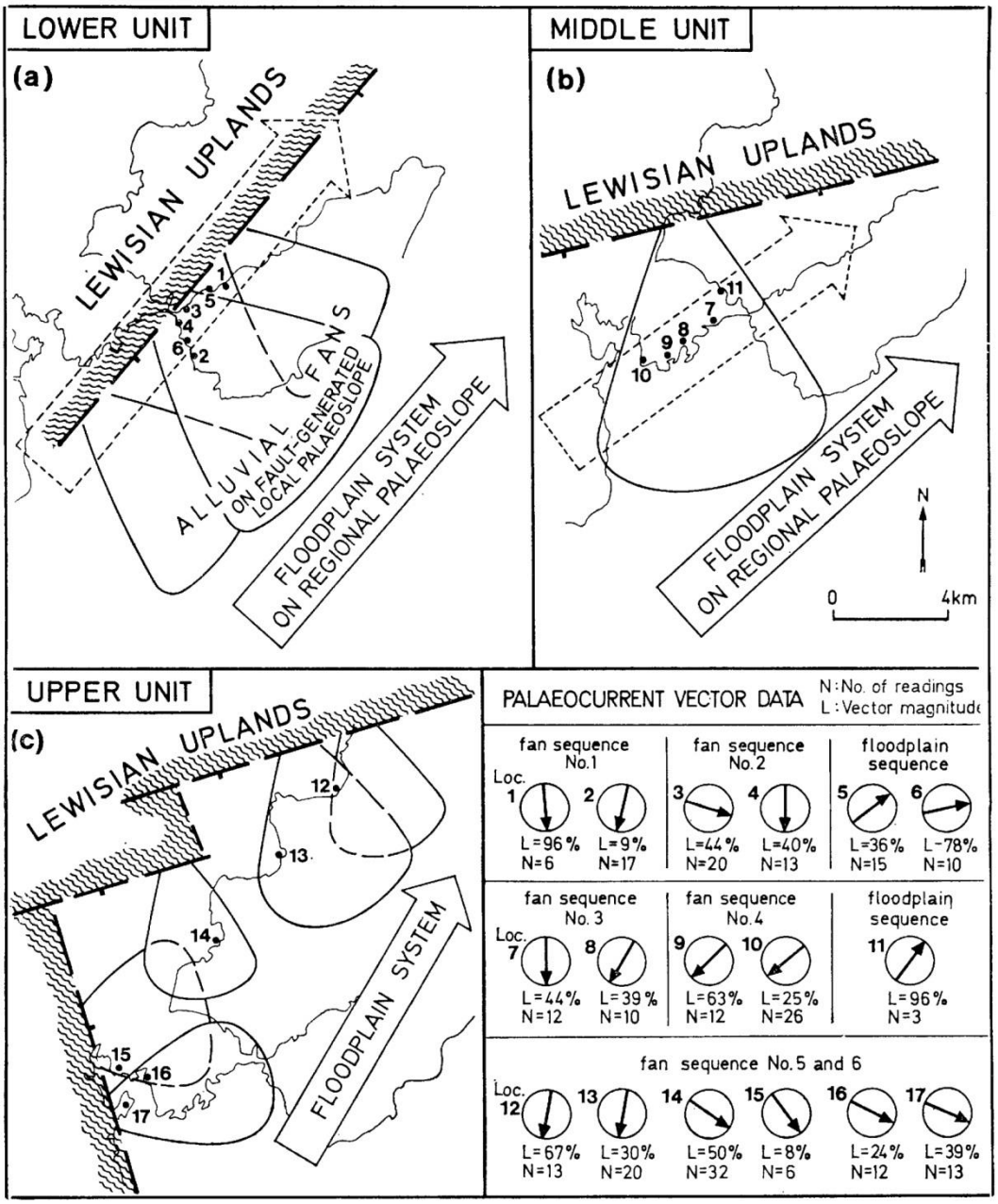

Figure 3.2: From Steel and Wilson (1975), showing the three unit model and changing active fault scarps through time. Orientations of alluvial fans and floodplain systems are based on interpretations of the palaeocurrent data.

The Stornoway Formation is cut by hundreds of variably-dipping brittle faults (Figure 3.3) that are easily identifiable on aerial imagery, enabling lineament analysis. Steeply-dipping to subvertical Palaeogene-age dykes (up to 6 m thick) trending NNW-SSE to N-S are also locally present in the Stornoway region, and these are often observed intruding along, and being cut by, faults. These relationships allow formulation of a relative chronology for fault movements and deformation, as discussed below.

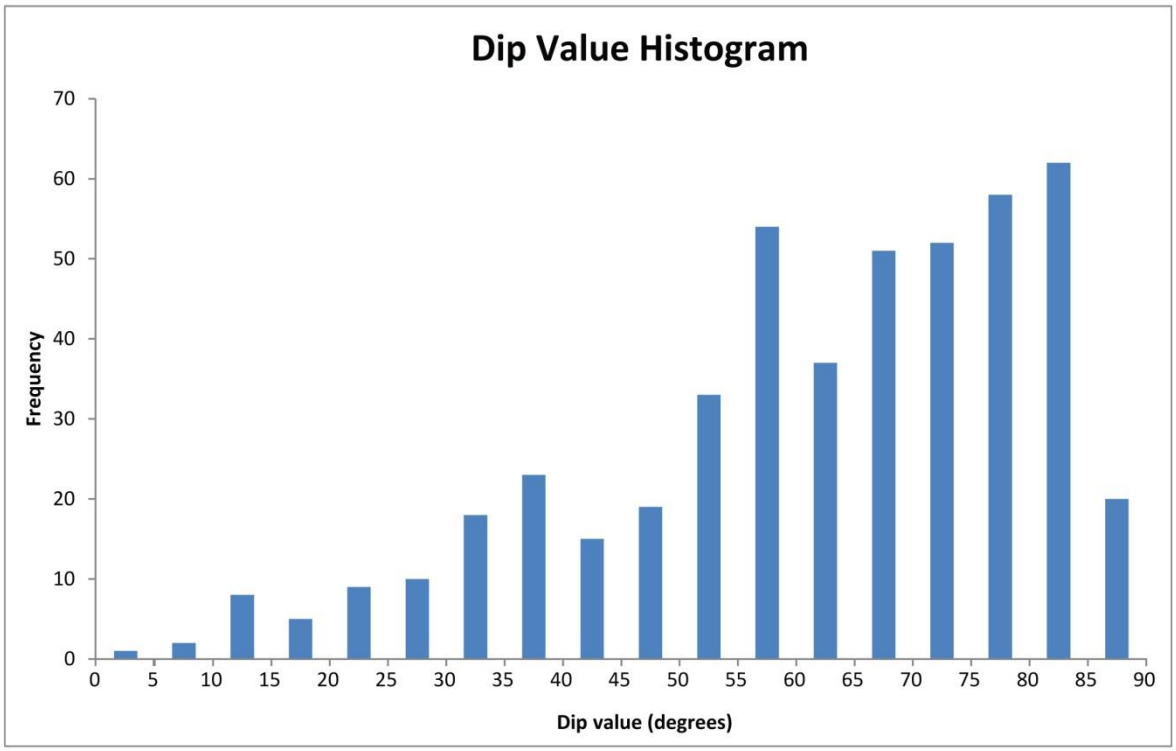

Figure 3.3: Histogram of fault dips measured in the Stornoway Formation during the present study.

3.2.3 Study sites and methods

The Stornoway Formation and Lewisian Gneisses of the OHFZ outcrop at the coast near Stornoway, with excellent exposures of minor/intermediate/major scale faulting within and outside the Formation, and the basement-cover interface visible at several localities. The position of the faulted Stornoway Formation immediately adjacent to and overlying the OHFZ (Figure 3.1) allows direct comparison of the faulting and deformation fabrics seen in these two rock units. This has been achieved using lineament analysis, fieldwork, and thin section study. Many outcrops in the Stornoway Formation are accessible only at low tide, and cliffs are usually sub-vertical and around 10-20 m high. In areas where cliff heights are greater, access is more limited (e.g. the north of the region east of Griais, Figure 3.6). Within the Stornoway Formation, every accessible location was visited and analysed for evidence of faulting. A total of 311 localities were recorded, each representing a fault or group of faults. Four localities were visited for exposures of the basement/cover interface.

In the surrounding Lewisian, cliff heights vary from two-to-three metres to in excess of 40 m in the north of the region. Localities visited here were selected for accessibility and exposure (see Figure 3.20 for localities). For example, the low cliffs at Pabail, Seisiadar, and Port Mholair allow access to excellent exposures near the major Mesozoic Minch Fault. On the north side of the

Peninsula Garrabost provides an excellent cross-section through deformed Lewisian Gneiss immediately adjacent to the unconformity at Garrabost and Dun Mor. In the south of the region cliff heights increase rapidly to the south of Tob Leireabhaigh with no accessible stretches. At Tolstadh the north of the beach is backed by cliffs over 40 m high; and the surrounding cliff-faces are inaccessible at this location. At Earabhig a cave with exposure of the basement-cover contact is inaccessible from land but is accessible via sea kayak. A total of 298 localities have been studied in the Lewisian Gneiss of the region surrounding the Stornoway Formation.

3.3 Stornoway Formation

3.3.1 Stornoway Formation Lineaments:

High-resolution aerial photographs were used to accurately digitise faults at 1:1000 scale within the Stornoway Formation (Figure 3.4) Although Nextmap® imagery is available for the region, it is not appropriate for digitising high resolution faulting within the Stornoway Formation, since faulting is minor and exposure is typically limited to the coastal strip. Distinctions can be made between dykes and faults using aerial imagery, and fieldwork was also used to confirm this. A total of 488 fault traces (lineaments) were identified, with obvious groups trending NNW-SSE, E-W and N-S. Comparison between rose plots of data gathered in the field and lineament data show a favourable agreement (Figure 3.4), with minor differences attributable to sampling of slightly different populations – for example, lineament analysis was performed in areas that are inaccessible such as offshore islets, and fieldwork reveals more faulting than is visible in the aerial imagery. Figure 3.5 shows the orientation of picked faults by area. NNW-SSE faults in particular are widespread across the Stornoway Formation region and can be found in every area. E-W faults also appear widespread with a particularly strong grouping in the south (pink and navy areas, Figure 3.5), and in the north (yellow and red areas, Figure 3.5).

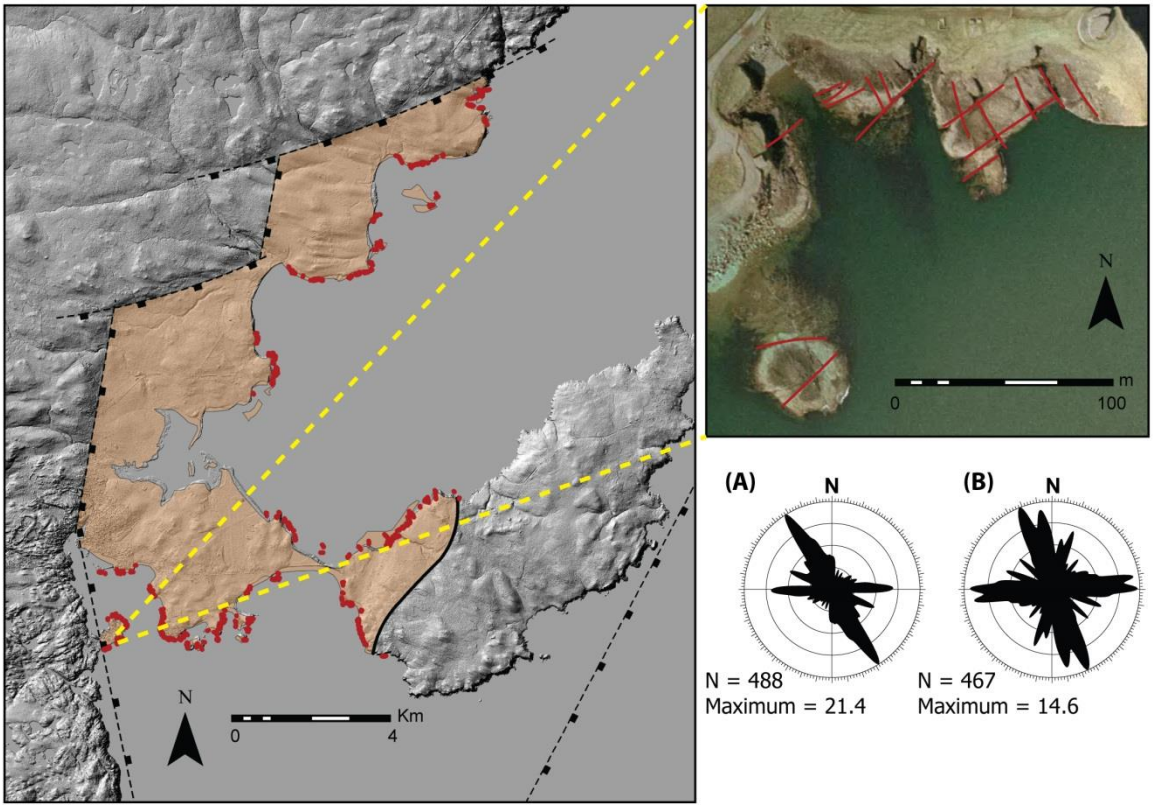

Figure 3.4: Map showing the lineament analysis within the Stornoway Formation and results (**A**) compared to fieldwork results (**B**). Image at left shows brown Stornoway Formation overlying a DEM with major faults indicated. Surrounding onshore rock is Lewisian Gneiss. Inset top right shows lineaments as they appear at 1:1,000 scale on aerial imagery. Red lines indicate picked lineaments, yellow dashed lines indicate position of aerial photograph on DEM

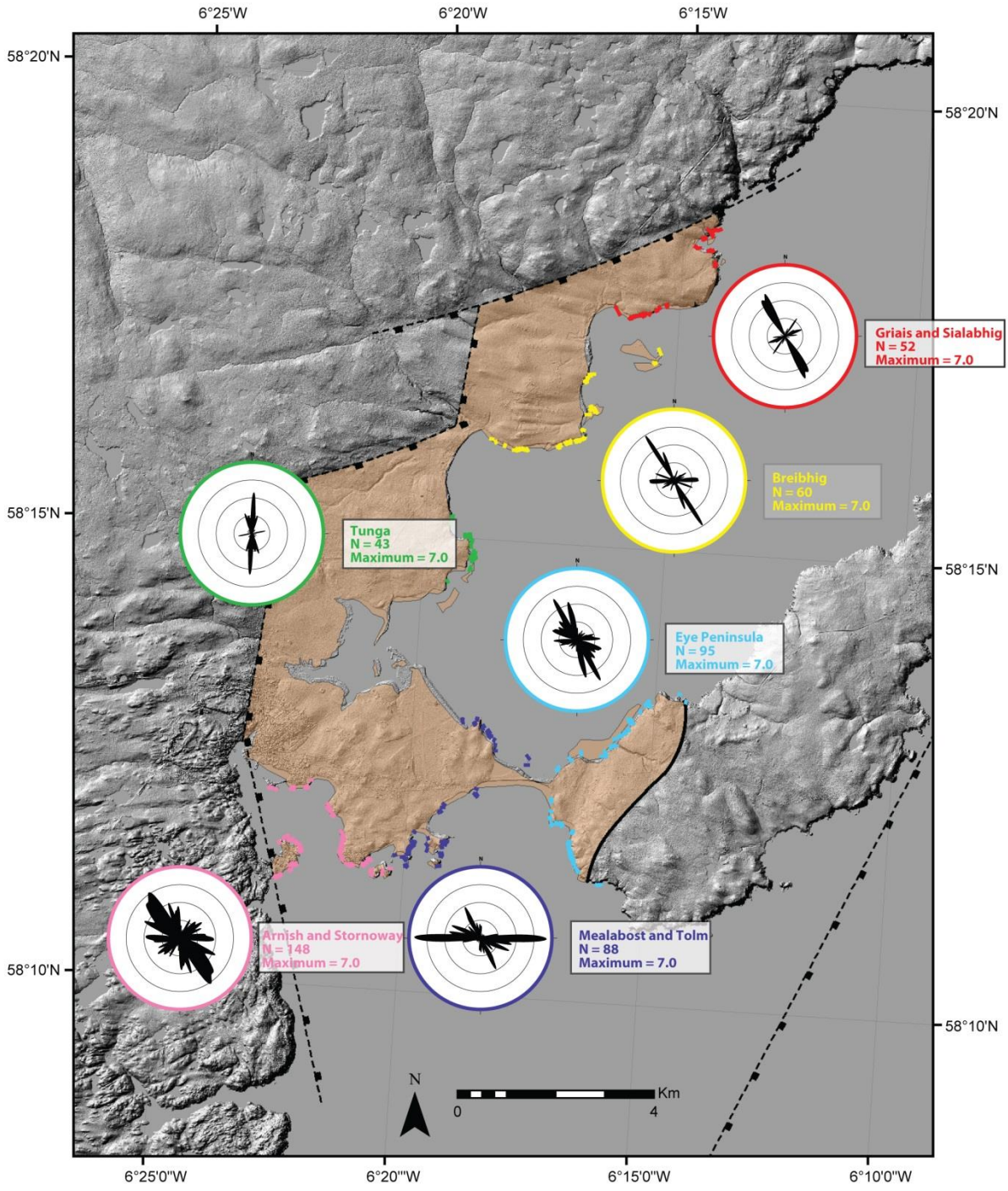

Figure 3.5: Stornoway Formation lineaments by area. Rose plot maxima are 7.

3.3.2 Field observations within the Stornoway Formation

Extensive fieldwork was undertaken in the Stornoway Formation and a total of 478 faults were visited and measured in the field (Figure 3.6), confirming the trends identified in the lineament analysis (Figure 3.4 and Figure 3.5).

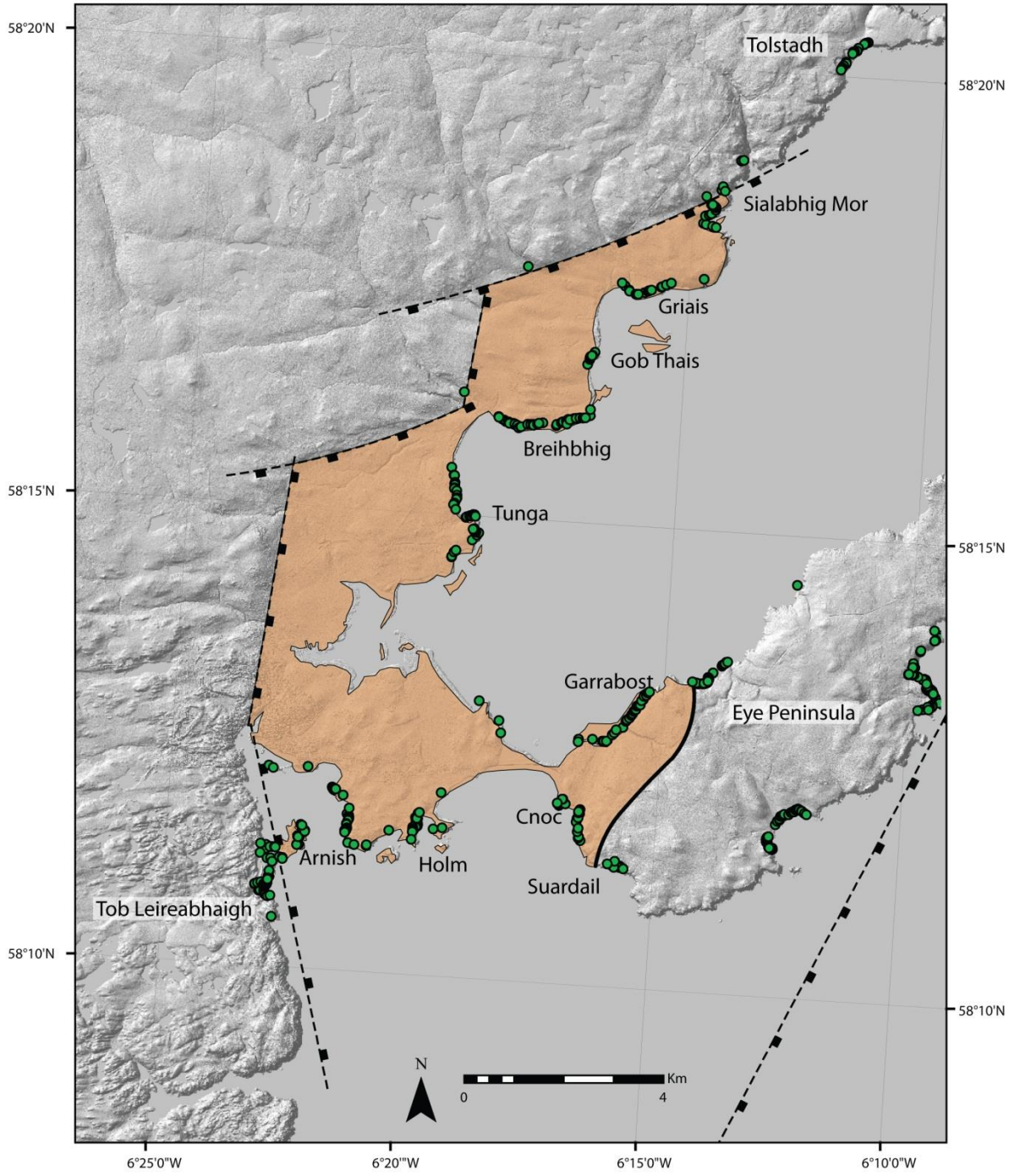

Figure 3.6: Map showing localities visited within the Stornoway Formation and surrounding Lewisian Gneiss.

3.3.2.1 Fault characterisation

Most faults cutting the Stornoway Formation are moderately to steeply-dipping features (Figure 3.3) with predominantly normal or normal-oblique offsets. Fault kinematics are evident from the widespread preservation of slickenlines on exposed fault planes and from offset local bedding surfaces (e.g. Figure 3.7A). The majority of faults show small- to intermediate-scale displacements

(decimetres to several metres), although this is usually difficult to quantify accurately due to the massive nature of the Stornoway Formation units. Conjugate pairs of normal faults are widely preserved in an upright position, suggesting that regional rotation around horizontal axes has had only a minor effect on the orientation of many faults.

The faults are typically lined with about 2-5 cm of microbreccia/cataclasite or gouge that is at times cemented with carbonate, and most faults analysed under the microscope also contain zeolite (section 3.3.3). Larger structures are observed, and have fault rock thicknesses up to 40 cm (Figure 3.7B), although these are rare. Fault breccias, where present, are chaotic with abrupt wall contacts. Clasts of breccia within the faults are composed of lithic clasts of Lewisian Gneiss that have been incorporated into the faults from the Stornoway Formation (Figure 3.7C). Faults and the adjacent wall-rocks often contain calcite cements (Figure 3.7C-D).

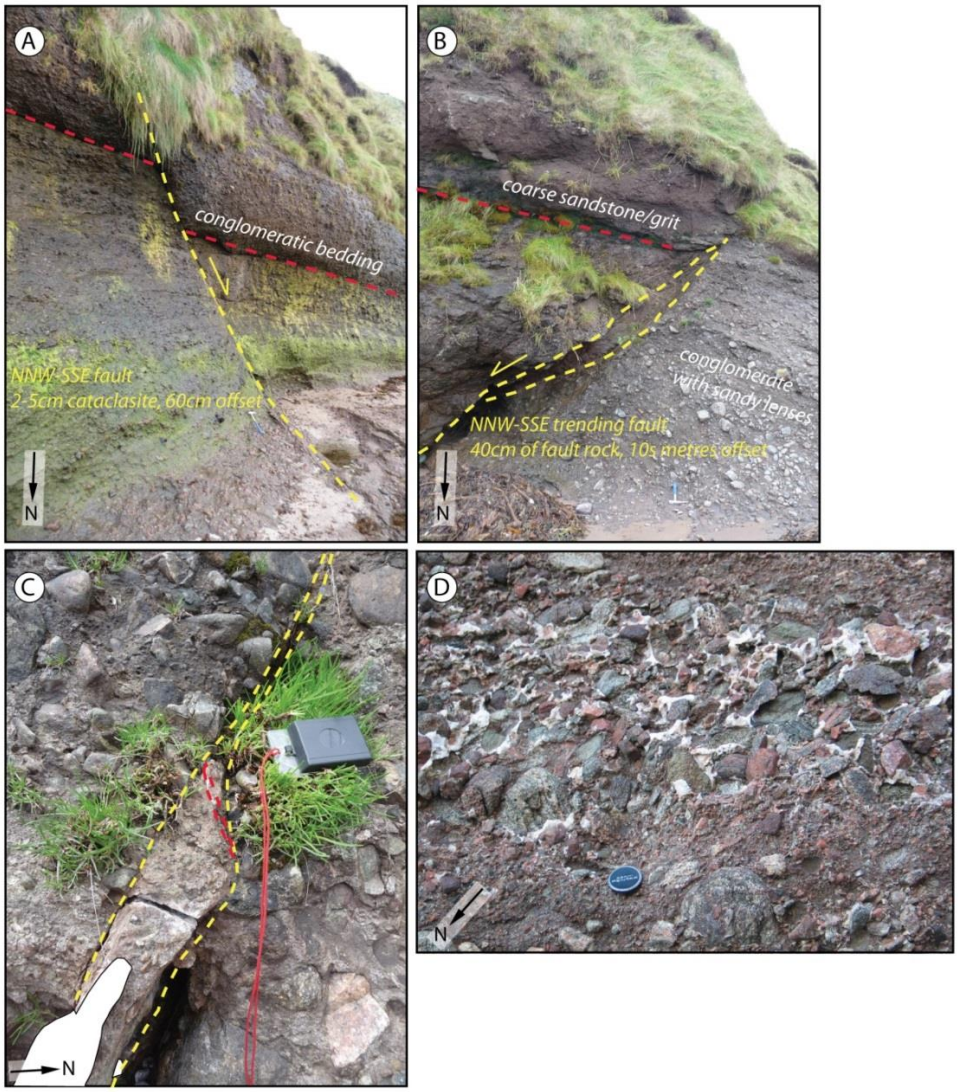

Figure 3.7: Field images. (**A**) Typical minor normal faulting within the Stornoway Formation. (**B**) Example of intermediate scale fault, with 40 cm thick fault rock. (**C**) Carbonate mineralisation associated faulting. (**D**) Carbonate mineralisation associated replacement of interstitial matrix.

3.3.2.2 Inferred faulting sequence within the Stornoway Formation

On the basis of cross cutting relationships seen in the field, faults within the Stornoway Formation may be grouped into sets and chronologically ordered. Table 3.1 shows fault sets identified in each area ordered chronologically (see Figure 3.6 for localities).

Table 3.1: Fault and dyke set orientations and chronologies inferred across the Stornoway Formation on the basis of cross cutting relationships. See Figure 3.6 for locations.

Age	Sialabhig Mor	Griais	Gob Thais	Breibhig	East of Breibhig	Tunga	Garrabost	Cnoc	Suardail	Holm	Arnish
OLDER	ENE-WSW, NW-SE	NNW-SSE, E-W	NNW-SSE, E-W	E-W and NE-SW	N-S and NNW-SSE	NNW-SSE	NNW-SSE	WNW-ESE	NE-SW/NNW-SE	NW-SE and E-W?	NNW-SSE
		N-S, NE-SW?		N-S		N-S and NE-SW	N-S	N-S	N-S, NW-SE/NE-SW?	N-S	N-S sinistral
		Dyke		**Dyke**		**Dyke**	**Dyke**				**Dyke**
						N-S?					
				E-W/NE-SW		E-W		E-W	E-W	E-W	E-W
YOUNGER						Low angle? N-S?				Low angle?	E-W low angle

The collected fault data are shown divided geographically to correspond with the three units of the formation identified by Steel and Wilson (1975), and excluding set 3 (later strike-slip) faults (Figure 3.8). The following observations and implications can be made:

1. Bedding increases in dip across the formation from NW to SE.

   Implication: Consistent with the suggestion that the bounding faults in the west represent the later stages of normal faulting.
2. NNW-SSE striking faulting is very obvious in unit 1 and 3 in the field, and is also present in unit 2 but in smaller numbers. This is confirmed by the lineament analysis (Figure 3.5).

   Implication: NNW-SSE striking faults are widespread. If Steel and Wilson model were strictly applied, early faulting from unit 1 would not be expected to be present in units 2 and 3. Indicates possible multiple NNW-SSE striking fault sets?
3. N-S striking faulting is most evident in unit 3 in the area around Tunga, close to the Unit 3 bounding fault (present day bounding faults).

   Implication: If the lineament analysis is accurate, this agrees with fieldwork observations of N-S faults cutting NNW-SSE structures, i.e. N-S faults locally post-date NNW-SSE trending faulting.
4. E-W dip-slip faulting of set 1 is localised in the north of the Stornoway Formation in unit 3.

   Implication: E-W dip-slip faulting represents the latest phase of faulting according to Steel and Wilson (1975), and as such E-W dip-slip faulting is likely to be grouped with N-S faulting.

5. A 10-15 cm wide brecciated dyke striking N-S is present at Tunga in poorly exposed outcrop.

   Implication: Faulting along dyke margins may have occurred following dyke intrusion into the Stornoway Formation.

The above observations alongside Table 3.1 suggest that N-S striking faults and E-W striking dip-slip faults represent a later stage of rift faulting. Within the oldest sedimentary unit (unit 1), NNW-SSE striking normal oblique dextral faulting is most prevalent, and this fault set is cross cut by N-S striking normal oblique sinistral faults in the field. Although NNW-SSE striking faults also exist in unit 3, they are most prevalent in unit 1 and are also cut by N-S faulting within unit 3.

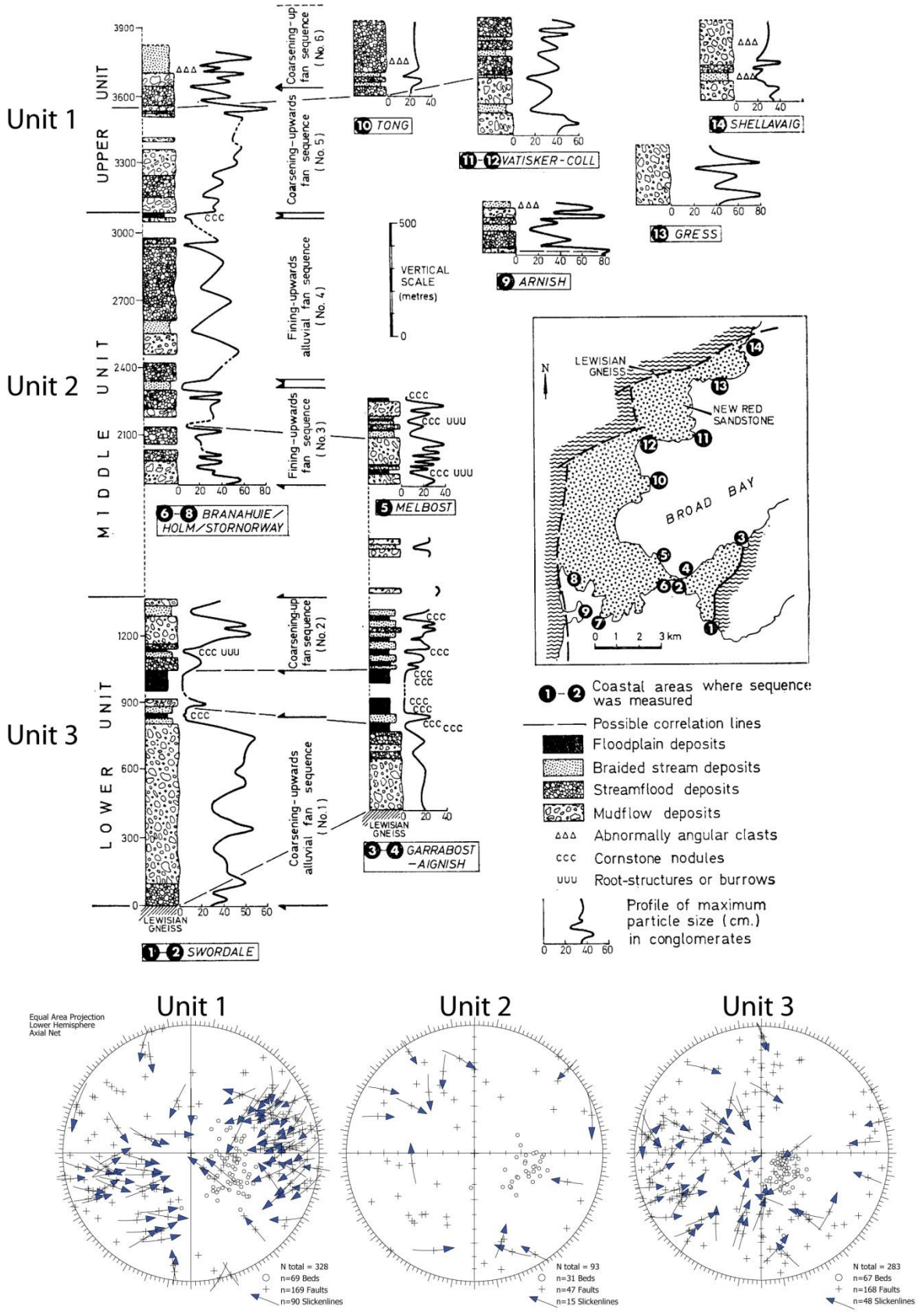

Figure 3.8: Top: Stratigraphic log from Steel and Wilson (1975), showing the three units of the Stornoway Formation. Bottom: Tangent lineation plots of fieldwork results split by units as defined by Steel and Wilson (1975).

On the basis of the above observations, cross-cutting relationships, spatial relationships and kinematics, the following structural sets are distinguishable, with type localities shown in Figure 3.9, and overall results in Figure 3.10, alongside palaeostress analysis:

- **Set 1**. A widespread set of dominantly NNW-SSE-striking normal oblique dextral conjugate faults, particularly intense in unit 1 of the Stornoway Formation. In some thin sections produced from fault cores, several overprinting fault movement phases are visible with slight differences in the fault rock clast vs. clay contents. This points to multiple slip events on individual faults. Overall, the fault movements identified give an E-W extension vector. NE-SW striking faults splay from NNW-SSE faults and are therefore assumed to be part this group (e.g. at Arnish).

  Associated fault rocks vary from incohesive gouges to well indurated foliated cataclasites.
- **Set 2**. A widespread set of N-S-striking normal-oblique sinistral motion conjugate faults, probably contemporaneous with conjugate E-W-striking normal dip-slip faulting localised in the north of the Stornoway Formation area, and most obvious at Sialabhig Mor, adjacent to the northern bounding fault. N-S oblique sinistral faults are consistently later than set 1, and have distinct kinematics. From Figure 3.5 in the central (green) area around Tunga, N-S oriented faulting is dominant and is probably associated with proximity to the bounding fault at this locality.

  Associated fault rocks include incohesive gouges and well-indurated foliated cataclasites. Both this set and set 1 pre-date emplacement of Palaeogene dykes, some of which intrude along NNW-SSE and N-S striking faults.
- **Set 3**. A set of steeply dipping E-W strike-slip faults. At one locality a conjugate pair is observed with dextral motion on an ENE-WSW striking fault, and sinistral motion on a more E-W striking fault (Figure 3.9). This set is restricted mainly to the south around Arnish, Holm and Cnoc (see Figure 3.6 for locations), and is visible offsetting Palaeogene dolerite dykes associated with the North Atlantic Igneous Province (Fettes et al., 1992).

  Associated fault rocks comprise gouge-breccias with calcite mineralisation, preserving examples of extension fractures (mode I), and fault jogs containing cemented fault breccias. Fault rocks do not include foliated cataclasites.

In general, the effects of faulting are minor in terms of finite displacement, with displacements across individual faults rarely exceeding a few tens of centimetres. Although bedding is tilted to a varying degree across the formation, pairs of conjugate faults in set 1 and 2 are symmetric about a vertical axis (visible in Figure 3.10 stereonets), indicating that only minor amounts of regional

rotation around a horizontal axis is possible. On this basis, stress inversions have been performed to produce a quantitative guide to the causative stress directions through the history of the Stornoway Formation. The data for these fault sets and stress inversion are shown in Figure 3.10. These stress inversions produce results similar to the orientations of extension described by various authors for the northwest Atlantic margin. For example, many authors suggest that Permo-Triassic extension was directed NW-SE, followed by E-W Jurassic extension (Dean et al., 1999; Dore et al., 1999). These extensional phases are thought to have been followed by regional compression and inversion in the Palaeocene and Eocene (Ritchie et al., 2008). Set 1 faults give a near E-W extension vector. This is followed by an ENE-WSW extension vector located approximately 15° anti-clockwise from the Set 1 extension vector, produced by Set 2. Set 3 faults indicate E-W directed contraction.

Although faulting appears to be upright with only minor rotations around a horizontal axis, back rotation of sets 1 and 2 was performed to look into the possible effects of domino fault block rotation and bed tilting on fault orientation (Figure 3.10, right-hand side). Each fault has been rotated back to the original local horizontal bedding and palaeostress analysis re-performed. The back rotated faults show the same general fault orientations, and the horizontal stresses are rotated 10-20° anticlockwise. The conjugate nature of the faults, clearly visible in the Set 1 and Set 2 original data (Figure 3.10, left-hand side), becomes less obvious after this rotation, suggesting that fault formation occurred mostly after bed rotation. Tangent lineation plots of this data are also show in Figure 3.10. When back rotated, these plots are also significantly altered and disrupted, and patterns are clearer in the original data. Both Set 1 and Set 2 tangent-lineation plots are most similar to Figure 2.14E, indicating that $\sigma_2 = \sigma_3$ and the stress difference ratio is close to zero (Twiss and Moores, 1992). The tangent-lineation plot for Set 3 faults displays fewer data points, however the stress regime is obviously different, with the tangent-lineations pointing around the outer radius of the stereonet. Thus the stress difference ratio is close ≥ 0.5 (Twiss and Moores, 1992).

Set 2 faults have been grouped to include N-S and E-W striking normal faults. E-W striking faults are particularly localised to the north of the Stornoway Formation area near the bounding fault, and N-S striking faults are particularly localised near the bounding fault in the west. Hence, both N-S striking faults and E-W striking faults are dominant in the youngest units (Unit 3) of the Stornoway Formation as identified by Steel and Wilson (1975), and are probably related to the orientation of the bounding faults in the west and north of the formation. It seems likely that these bounding faults were active contemporaneously (e.g. Steel and Wilson, 1975), hence E-W and N-S striking faults are grouped in the same set here.

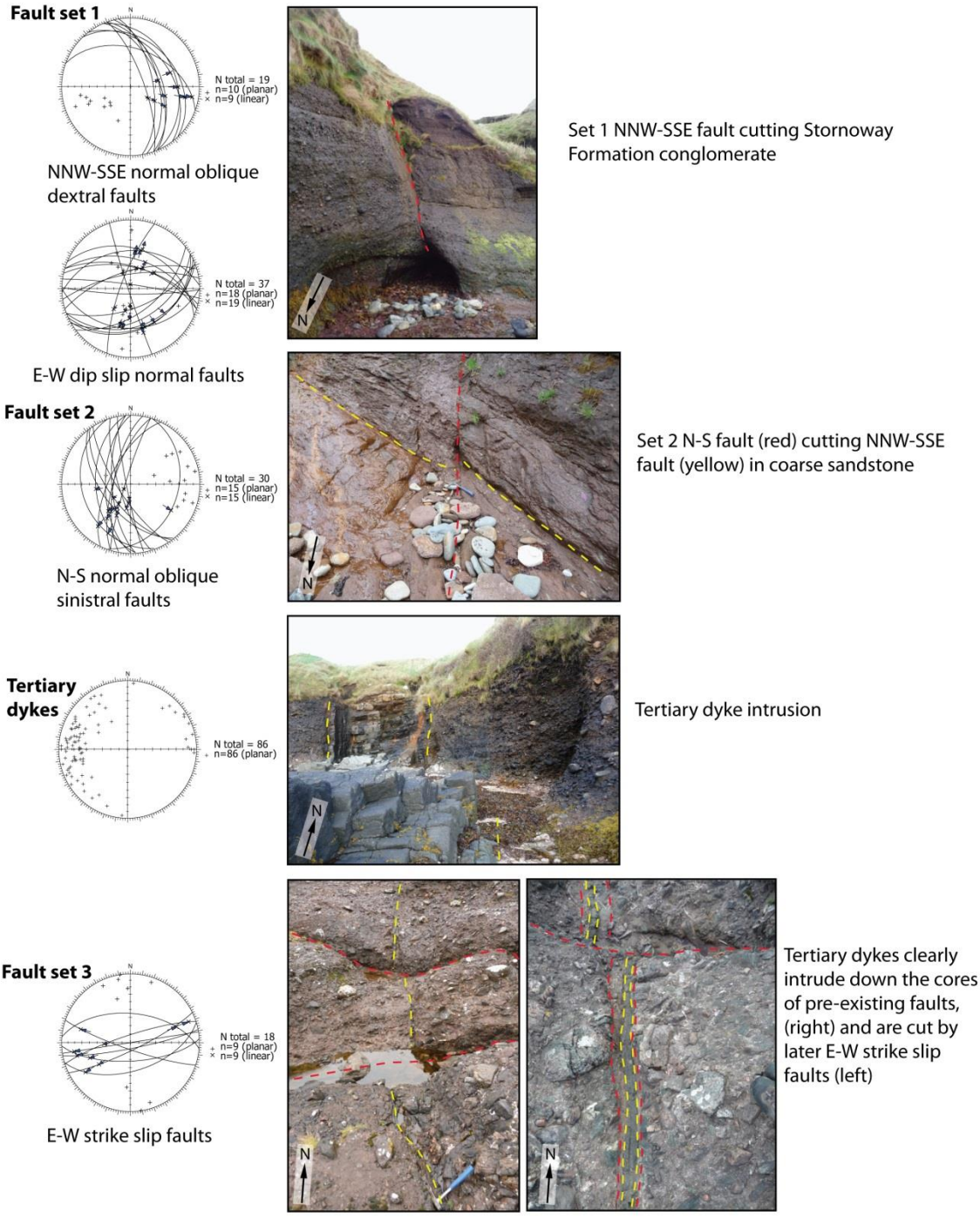

Figure 3.9: Type localities for each fault set. (Set 1) NNW-SSE trending normal oblique dextral motion faults. (Set 2) N-S trending normal oblique sinistral offset faults, occurring alongside E-W dip-slip faulting localised to the north. (Set 3) Late E-W strike-slip faulting localised to the south of the Stornoway Formation. (Dykes) Dolerite dykes that precede the formation of Set 3 faults.

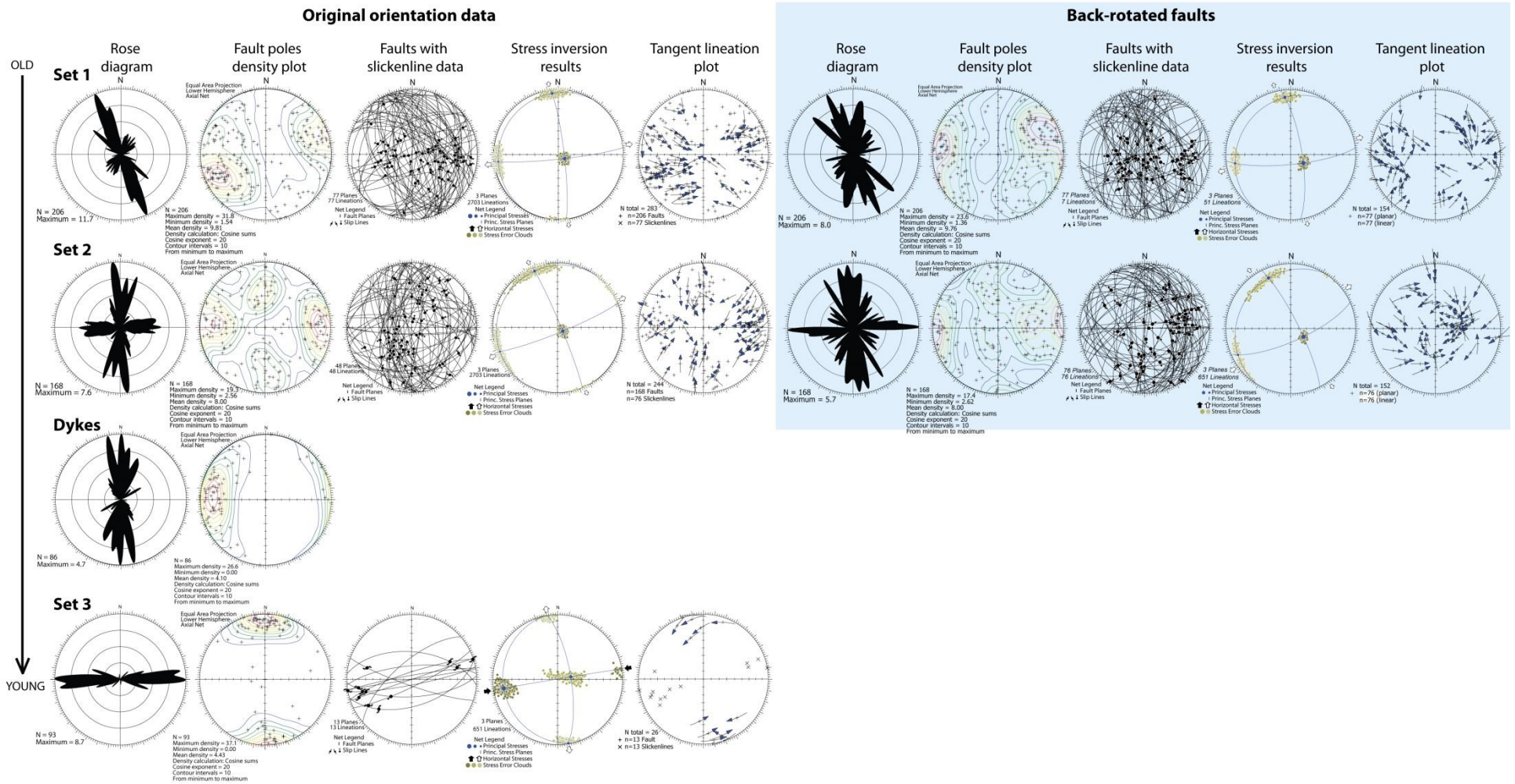

Figure 3.10: Chronological sequence of fault sets and Tertiary dyke intrusion with stress inversions carried out on fieldwork data collected from faults within the Stornoway Formation (for more details on the tangent lineation plot see Twiss and Moores, 1992, p206). Plots highlighted in blue show sets 1 and 2 back rotated to horizontal bedding at each fault locality. Note that tangent-lineation plot arrows show movement of the footwall.

3.3.2.3 Bounding Faults

The bounding faults of the Stornoway Formation are clearly important regional features with a significant displacement (likely hundreds of metres). The faults trend NNW-SSE in the Arnish Peninsula region, N-S in the central region, and ENE-WSW in the north of the Stornoway Formation (Figure 3.6).

At Arnish, a few metres east of the unexposed trace of the bounding fault, Stornoway Formation conglomerates are extremely coarse, containing boulders up to 3 m across. Such large clast sizes in an alluvial system require a very high energy environment for transport, with deposition proximal to the source; thus it is here inferred that the conglomerate is derived directly from the upthrown footwall scarp at this locality. At Earabhig, also adjacent to a major bounding fault of the Stornoway Formation, the conglomerate is noticeably finer grained compared to Arnish with clasts of around 8-10 cm across. This difference in clast size indicates a lower-energy provenance to the conglomerate exposed at Earabhig than at Arnish. It is possible that the Earabhig conglomerate is not derived from the immediate footwall of the bounding fault, but rather that the conglomerate is derived from the footwalls of faults that existed further to the north within the Lewisian (i.e. the bounding fault here may simply be one of several large scale faults). Alternatively, the fault here may not be the primary bounding fault of the Stornoway Formation and may have cut through an already pre-existing Stornoway Formation. This would again indicate the likely presence of further normal faults to the north within the Lewisian.

3.3.3 Stornoway Formation Fault Rock Microstructure Characterisation

Thirty-nine thin sections were obtained from a range of faults throughout the Stornoway Formation.

3.3.3.1 Country Rock Microstructures

About 10 % of the Stornoway Formation conglomerate is matrix material composed of limonite and fine sand-sized clasts. Minor amounts of chlorite and other phyllosilicate clasts (<5%) confirm the extreme textural immaturity of the rock and local provenance. Calcite is irregularly distributed throughout the formation, and is often present within the matrix. Locally the fine grained matrix and porosity is entirely replaced by undeformed crystalline calcite infill that completely surrounds clasts of conglomerate. This mineralisation is seen in bands and channels up to 4 m in length and 0.5 m across, distributed heterogeneously throughout the Stornoway Formation. However, areas also exist completely lacking calcite, and in areas where calcite is not present, clasts are often seen rimmed with iron oxides.

Lithic clasts are typically either hornblende-biotite grey gniesses or ductilely/cataclastically deformed gneisses from the OHFZ. In thin section, these clasts are easily identified by their gneissose, mylonitic, or epidote-cataclastic textures, alteration of feldspars, amphiboles and phyllosilicate minerals to secondary minerals, and recrystallization of quartz**.**

3.3.3.2 Sequence of Fault Formation

Using textural overprinting relationships seen in the field and thin sections of the fault rock samples, it is possible to construct a rock development model from faults within the Stornoway Formation, presented below. This model can be applied to all fault sets due to the similar styles of faulting within the Stornoway Formation observed, and the fact that fault rocks from different fault sets are generally indistinguishable under the microscope with the exception of set 3 that contains clasts of cataclastic zeolite (see section 3.3.3.5). Under the microscope fault rocks show a gradational increase in strain intensity accommodated by the rock as the fault core is approached. This strain intensity has been used as a proxy for time in order to describe the following deformation sequence during fault rock formation:

1. *Intragranular fracturing, with fractures initiating at clast contacts and propagating into clasts* (Figure 3.11B). Typical undeformed protolith is shown in Figure 3.11A. Intragranular fractures result in porosity increases. Microfractures have calcite infills, <0.1 mm thick. Clasts are generally >0.1 mm across.
   Implications: Increased stress causes initial fracturing and pore space production, Presence of calcite suggesting that fluids were present and that local hydrofracturing was associated with mineralisation.

2. *Fractures link, producing transgranular fractures, propagating from clast contacts* (also visible in Figure 3.11B). Non-ferroan calcite mineralisation occurs in microcracks within clasts and in the matrix. Most clasts < 1mm across.
   Implications: Porosity/permeability increases permit further fluid influx.

3. *Crushing and initial cataclastic flow produces microbreccias and cataclasites, mafic minerals and phyllosilicates alter* (Figure 3.11C and D). Brown matrix development occurs between clasts as clays form from the alteration of pre-existing epidote, phyllosilicates and mafic mineral clasts incorporated into the fault, whilst iron oxide forms from the alteration of ferrous opaques. Large clasts undergo cataclasis preferentially, and feldspars in particular are highly fractured. Most clasts within the fault rock are still identifiable as lithic fragments. Pore space production and calcite

mineralisation continue with grain fracturing. Elongate, brown, clay-rich bands begin to develop. Most clasts are < 0.5 mm across. Mafic minerals and phyllosilicates develop a rim of alteration or are completely altered to brown authigenic clay minerals (Figure 3.11E-F). The authigenic clay-bearing matrix is not associated with porosity.

Implications: Grain size decrease and clay development lower fault rock porosity. Proportion of mafic minerals decreases and potentially weak clay bands begin to develop. Limited evidence of strain localisation onto clay-rich layers.

4. *Alteration and pressure solution, operating alongside cataclastic flow, produces clay-rich cataclasites and microbreccias* (Figure 3.11G-H). With increasing strain, the proportion of matrix increases, and grain size decreases (Figure 3.11G-H), from up to 1 mm (Figure 3.11G) to less than 0.2 mm toward the fault core (Figure 3.11H). Authigenic clay-rich (up to 80%) bands develop (e.g. Figure 3.11H). In more developed cataclasites, non-uniformly-distributed clasts show long axis alignments parallel to the bounding fault plane. Non-ferroan carbonate is preserved as clasts. Original chlorites and other mafic minerals are absent or rare and highly altered. Lithic fragments up to several millimetres across are incorporated from the wall rocks, but most clasts of up to 1 mm across are composed of single minerals, of which most are feldspars. Crude banding is produced with brown clay-rich and white clay-poor lenses developed in the highest strain areas. Minor epidote and amphibole clasts are concentrated in brown clay bands (e.g. Figure 3.13B) and are very often partially altered to clays. These clays are visible under SEM altering from amphibole (e.g. Figure 3.14H), and with blades of clay aligning parallel with the fault slip surfaces and wrapping clasts within the fault rock (Figure 3.14E-J). Pore space is absent or infilled with calcite cement. Small discontinuous veinlets of calcite/stilbite around 0.2 mm across and 1 mm long are found within cataclasites, and commonly lie parallel to fault margins. In addition, areas of very fine-grained cataclasite are commonly cemented with very fine-grained zeolite. Most clasts are < 0.25 mm.

   Implications: Fluids allow species mobility and authigenic clay formation, at times within concentrated bands of much reduced porosity when compared to the wall rocks. Late stage fluid flow along the faults has produced intact zeolite veining.

5. *Continued alteration and cataclastic flow produce well foliated cataclasites* with clay-rich and clay-poor bands (Figure 3.11I-J). Sigma-shaped clasts comprised of rounded lithic clasts and feldspar crystals are evident, up to 1.5 mm across (Figure 3.11J). Very

fine-grained quartz-feldspar aggregates found within these foliated cataclasites (e.g. Figure 3.11J) have non-uniform crystal sizes, indicating that they are a cataclastic product (e.g. Figure 3.11G) (Passchier and Trouw, 1996). Porphyroclasts and very fine quartz-feldspar aggregates are often surrounded by a halo of dark clay- and iron-oxide rich material, indicating possible pressure solution. Porosity is absent or below the resolution of optical microscopy, and little to no carbonate visible. Foliated cataclasite is spatially associated with a darkening of the clayey bands, possibly due to the action of pressure solution, which may also explain the dearth of calcite found in these fault rocks.

Implications: Cataclasis can produce low porosity foliated fault rocks. The high strain concentrates clays into layers. Concentration of strain along clay bands may have caused further disaggregation and grain size reduction of quartz-feldspar masses when these masses are wrapped by high strain clay bands. Calcite is absent, possibly due to inhibition of fluid flow and mineralisation by porosity-filling authigenic clays and/or due to the effects of pressure solution. Most clasts are <0.1 mm.

6. *Zeolite and authigenic clay formation occurs through alteration of fine cataclastic material and carbonate*. Very fine-grained zeolite halos, up to 0.5 mm across, are seen surrounding porosity associated with irregular calcite grains (Figure 3.15E). Individual zeolite crystals reach a maximum size of 0.05 mm across, whilst modal size is below 0.01 mm. Crystal habit indicates that the zeolite may be stilbite (Figure 3.15D and F). The calcite found in the centre of these halos is patchy with serrated margins and parallel extinction, probably representing a dissolution texture. Calcite with this texture is also seen partially filling open fractures within some fault rocks, and displaying porosity development along cleavage planes within crystals of calcite. These open fractures may have been preserved through high pore fluid pressures. Calcite dissolution probably occurred synchronous with formation of the zeolite halo. In all cases, zeolites are associated with authigenic clays - probably smectitic - indicating temperatures of formation potentially lower than 100°C (Velde, 1985). In thin section, the zeolites are usually seen as discontinuous veins lying parallel and sub-parallel to wall rock margins, and as patches within the fault rock surrounding patchy calcite. Zeolite is also observed as a cement within the cataclasites with crystal sizes of generally less than 0.01 mm (Figure 3.15A). Under SEM, zeolite cemented cataclasites do not appear to be deformed (e.g. Figure 3.16A-B).

   Implications: Late-stage fluid migration post-dating faulting has created secondary porosity through the dissolution of calcite and precipitation of zeolite that must be

associated with fluid influx. Zeolite mineralisation may have dominantly occurred after faulting had ceased.

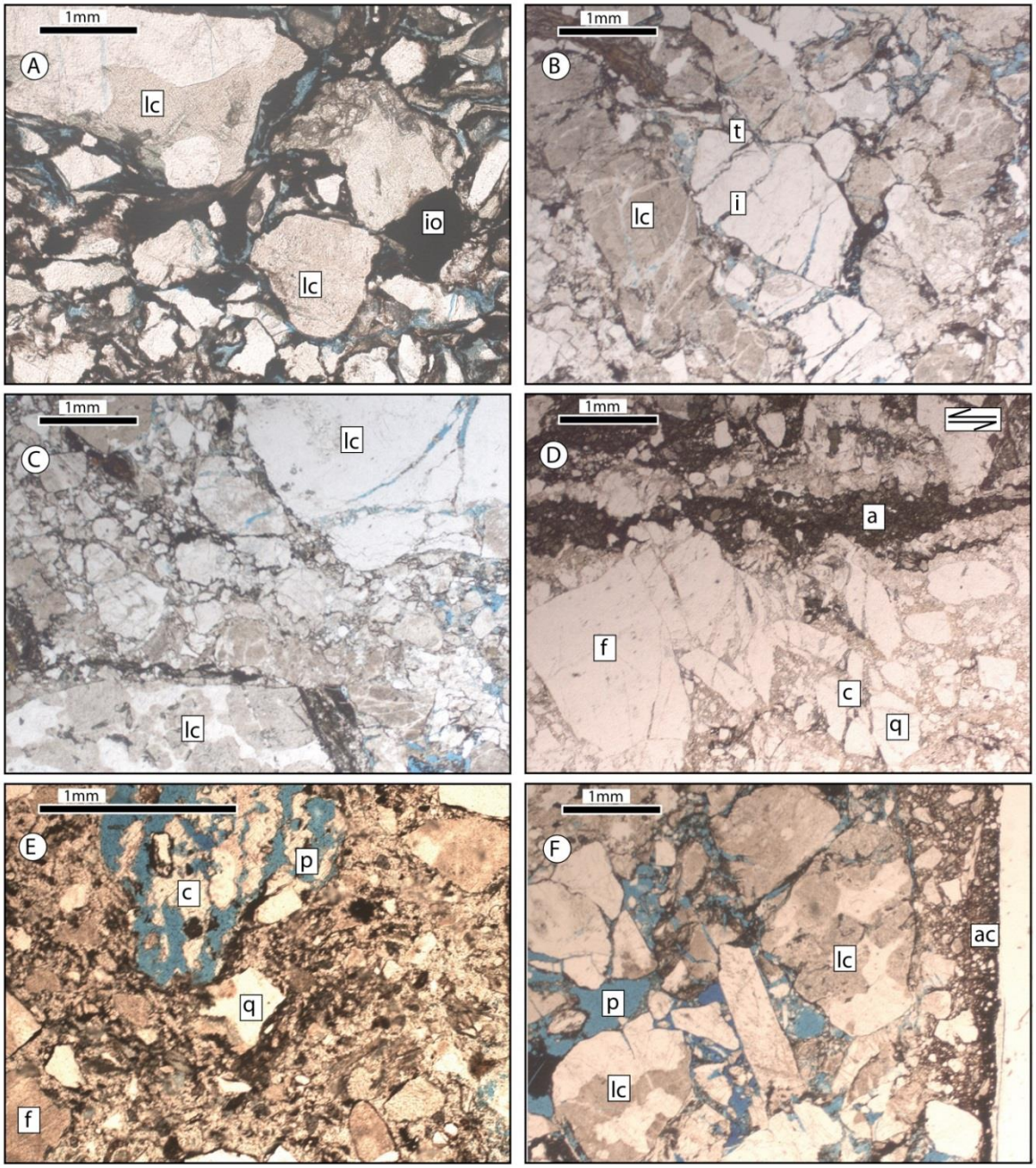

Figure 3.11 (continued next page): (**A**) (From Cnoc) PPL. Fresh country rock. Clast of sub angular Lewisian Gneiss (lc) cemented by iron oxide (io) and calcite. Pore space indicated in blue. (**B**) (From Cnoc) PPL. Initial intragranular fractures (i) propagate away from grain contacts within lithic clasts (lc). Increase in porosity at this stage is filled with calcite. Transgranular fractures form (t) (**C**) (From Cnoc) PPL. Grain-size reduction occurs through cataclasis of lithic clasts (lc). (**D**) (From Arnish) PPL. Early stage faulting forms shear plane with larger clasts at margins being incorporated into the fault (f) and undergoing cataclasis. Amphibole (a) appears fresh. Feldspar (f) and quartz (q) clasts contain calcite-filled microfractures (c). (**E**) (From Garrabost) PPL. Continued cataclasis, development of fine matrix with some alteration to brown clays. Carbonate (c) visible in larger pore spaces (p) with later dissolution and probable zeolite rim. Within the cataclasite clasts are monomineralic, dominated by quartz (q) and feldspar (f). (**F**) (From Cnoc) PPL. Fault development leads to core rich in authigenic smectitic clays (ac) altering from primary minerals. Porosity is low compared to country rock (left of image), showing unaltered lithic clasts (lc) and porosity (p).

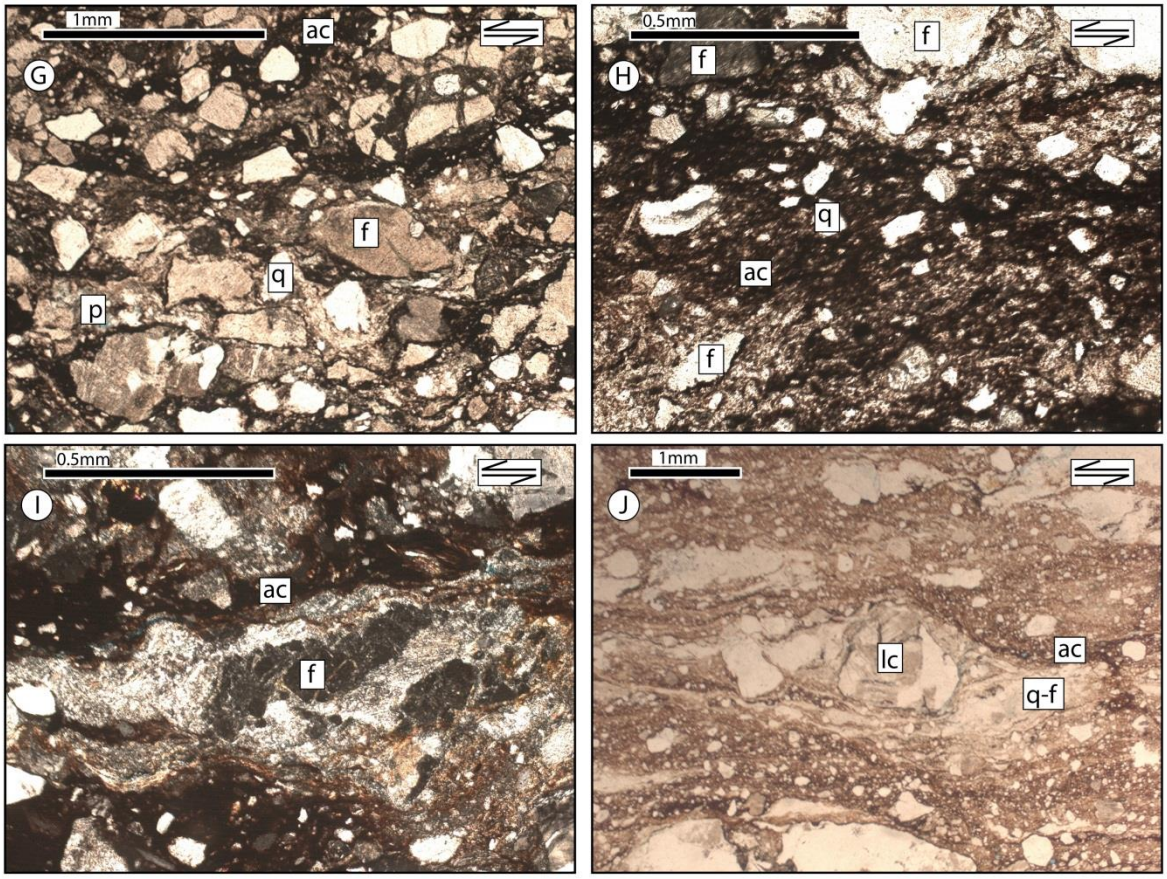

Figure 3.11 (continued): Development of fault rock within the Stornoway Formation (continued) (**G**) (From Garrabost/Aignish) PPL. Development of coarse banding with alteration of mafic minerals and phyllosilicates to smectitic clays (ac), minor amounts of pore space remaining (p). (**H**) (From Garrabost/Aignish) PPL. Grain size diminution, slight shape preferred orientation parallel with fault margins, increased proportion of rock composed of matrix, little/no porosity remaining. (**I**) (From Garrabost/Aignish) XPL. Fine foliation development and fine aggregates of quartz and feldspar (q-f) develop from lithic clasts (lc), wrapped with authigenic clay (ac). (**J**) (From Griais) PPL. Well foliated cataclasite, remaining lithic fragments develop mantles, very fine grained matrix, aggregates of quartz and feldspar (q-f) develop.

3.3.3.3 Deformation Processes

Cataclastic deformation processes are widely preserved in the Stornoway Formation fault rocks (e.g. Figure 3.12). Relatively large lithic clasts up to several centimetres across undergo cataclasis preferentially, with angular corners exhibiting preferential cataclasis. The fracturing of relatively large clasts produces porosity (e.g. Figure 3.12A, Figure 3.13C, Figure 3.13D, Figure 3.13E) that is commonly infilled with calcite. Porosity produced in the initial fracturing of clasts is commonly truncated against bands of higher strain that are typically indicated by the presence of widespread authigenic clays and smaller grain sizes (Figure 3.12B). It is clear that authigenic clays develop with strain and are syntectonic (see Figure 3.14); individual clay mineral grains are about 1 µm across. Extremely fine-grained cataclastic material is visible particularly at the boundaries between adjacent grains of quartz and feldspar (e.g. Figure 3.12D), and within the matrix. Clay wraps clasts as small as 1 µm across (e.g. Figure 3.14H-I). Rare phyllosilicate clasts within the fault

rocks are usually internally strained (e.g. exhibiting kinks: Figure 3.12H) and are at least partially altered.

There is only limited evidence for granular flow, in that the particularly fine areas of quartzo-feldspathic aggregate (e.g. Figure 3.12E-F) do not contain visible porosity under an optical microscope. Under SEM these aggregates are clearly composed of angular cataclastic grains of quartz or feldspar ranging from 1-20 μm (Figure 3.12G), with little evidence for dissolution and re-precipitation. Figure 3.13 shows various shear sense indicators visible within faults rocks of the Stornoway Formation. These include domino faulting, asymmetric microfolds within fault rock fabrics, offset clasts, porphyroclast 'eyes' and subsidiary fracture arrays. Images shown in Figure 3.13 are from fault sets 1-3 within the Stornoway Formation and observations have been used to confirm the kinematics identified within the field.

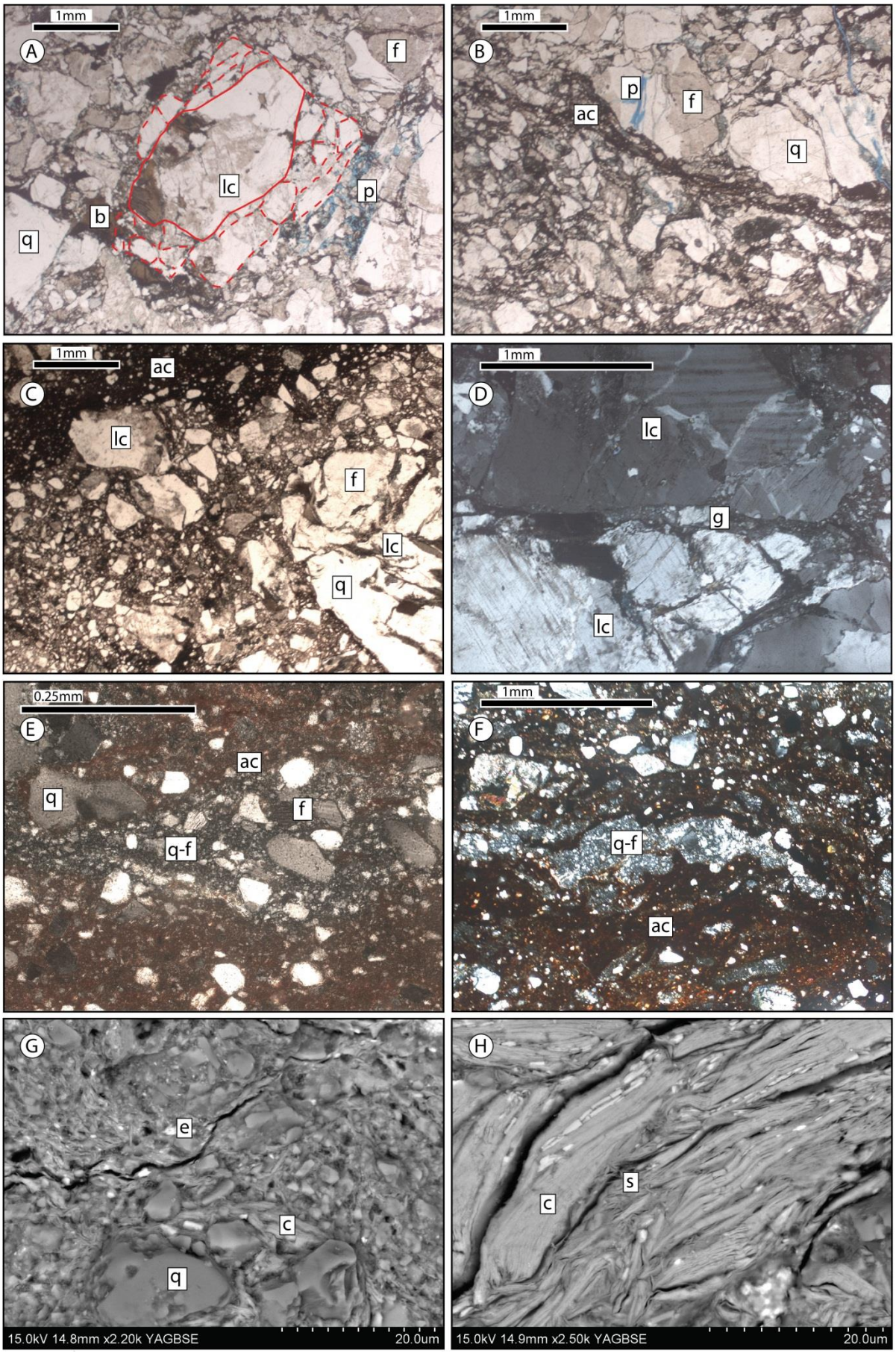
1mm
A
f
lc
p
b
q
1mm
B
p
ac
f
q
1mm
C
ac
lc
f
lc
q
1mm
D
lc
g
lc
0.25mm
E
ac
q
f
q-f
1mm
F
q-f
ac
G
e
c
q
15.0kV 14.8mm x2.20k YAGBSE
20.0um
H
s
c
15.0kV 14.9mm x2.50k YAGBSE
20.0um

Figure 3.12: (previous page) Deformation characteristics. (**A**) (From Cnoc) PPL. Disaggregated and brecciated lithic clast (lc) (marked by dashed red lines). Note association with pore space (p). Biotite (b), feldspar (f) and quartz (q). (**B**) (From Cnoc) PPL. Deformation band with authigenic clay and reduced porosity. (**C**) (From Holm) PPL. Lithic clast (lc) partially brecciated, with development of authigenic clay banding. (**D**) (From Griais) XPL. Cataclasis occurring between two lithic clasts (lc) producing a narrow band of very fine breccia (gouge). (**E**) (From Griais) XPL. Quartz-feldspar aggregate (q-f) surrounded by authigenic clay (ac). (**F**) (From Holm) XPL. Quartz-feldspar aggregate (q-f) banded with authigenic clay (ac). (**G**) (From Garrabost/Aignish). BSEM image of cataclastic fabric from fault core Clasts wrapped by clays – grain size reduction and usual random heterogeneous organisation, prior to foliation development. Quartz (q), epidote (e) and chlorite (c) shown. (**H**) (From Garrabost/Aignish). BSEM image of phyllosilicates such as biotite and chlorite (shown here, (c)) undergo kinking and alteration (here to smectite, (s)) within fault cores.

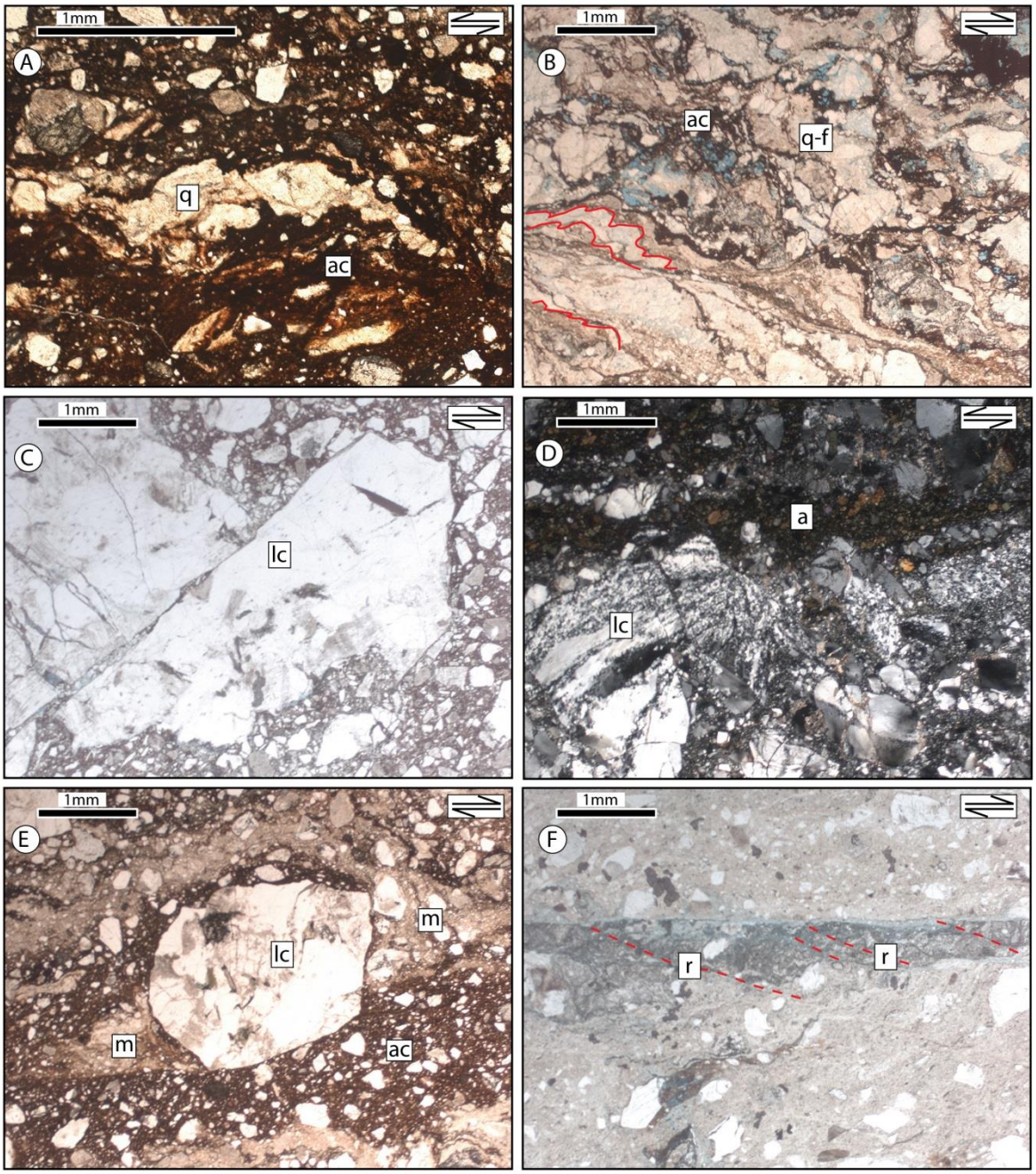

Figure 3.13: Kinematic indicators in Stornoway Formation Fault rocks. (**A**) (From Holm) PPL. Domino type faulting of a fine grained quartz aggregate (q) surrounded by authigenic clay (ac). (**B**) (From Breibhig) PPL. Verging folds within fault rock, highlighted in red and defined by authigenic clays (ac) and fine grained quartzo-feldspathic aggregates (q-f). (**C**) (From Breibhig) PPL. Domino-fragmented offset lithic remnant porphyroclast (lc).(**D**) (From Arnish) XPL. Fragmented lithic clast (lc) at wall rock margin. Fault core composed of cataclastic amphibole (a). (**E**) (From Garrabost/Aignish) PPL. Mantled porphyroclast (lc) surrounded by authigenic clay (ac) with mantle of material originating from the porphyroclast (m). (**F**) (From Garrabost/Aignish) PPL. Riedel shears (r) oblique to fault surface.

3.3.3.4 Clay Development

Authigenic clay develops primarily from the chemical breakdown of detrital grains of mafic minerals, epidote, and phyllosilicates (e.g. Figure 3.14H). Figure 3.14A shows the result of cataclasis in three different mineral types: unaltered quartz, heavily altered feldspar, and authigenic clays formed from phyllosilicates. In particular, it is widely observed that dark authigenic clays surround epidote clasts (Figure 3.14B) and chlorite (Figure 3.14C-D).

Clasts of altered and fresh feldspar are incorporated into the Stornoway Formation fault rocks. In some cases heavily altered, cloudy or sericitised feldspar clasts within fault cores preserve dark brown clay rims (e.g. Figure 3.14C, bottom of image), indicating probable authigenic clay development from feldspar alteration products as opposed to fresh feldspar. The clays are clearly syntectonic, wrapping cataclastic clasts, commonly with a preferred orientation (Figure 3.14E-H). This implies that rather than clay forming as a direct replacement product it is forming as new mineral overgrowths.

The composition of clays produced throughout the fault rocks are highly heterogeneous, as indicated in BSE images (Figure 3.14E -J) and associated EDX spectra. Bright clay minerals in the BSE images are iron rich, and there exists significant compositional heterogeneity of authigenic clays across distances of less than 10 µm (Figure 3.14I, sampling resolution is <1µm (Jones, 2012)). The composition of these clays is highly dependent on the mineral from which they are derived, as opposed to any general composition imposed by homogenous fluid flow and alteration. White clay minerals in the BSE images appear dark brown under optical microscopy and are commonly associated with cataclasis of epidote and chlorite grains and alteration (Figure 3.14B, Figure 3.14E-F, Figure 3.14J).

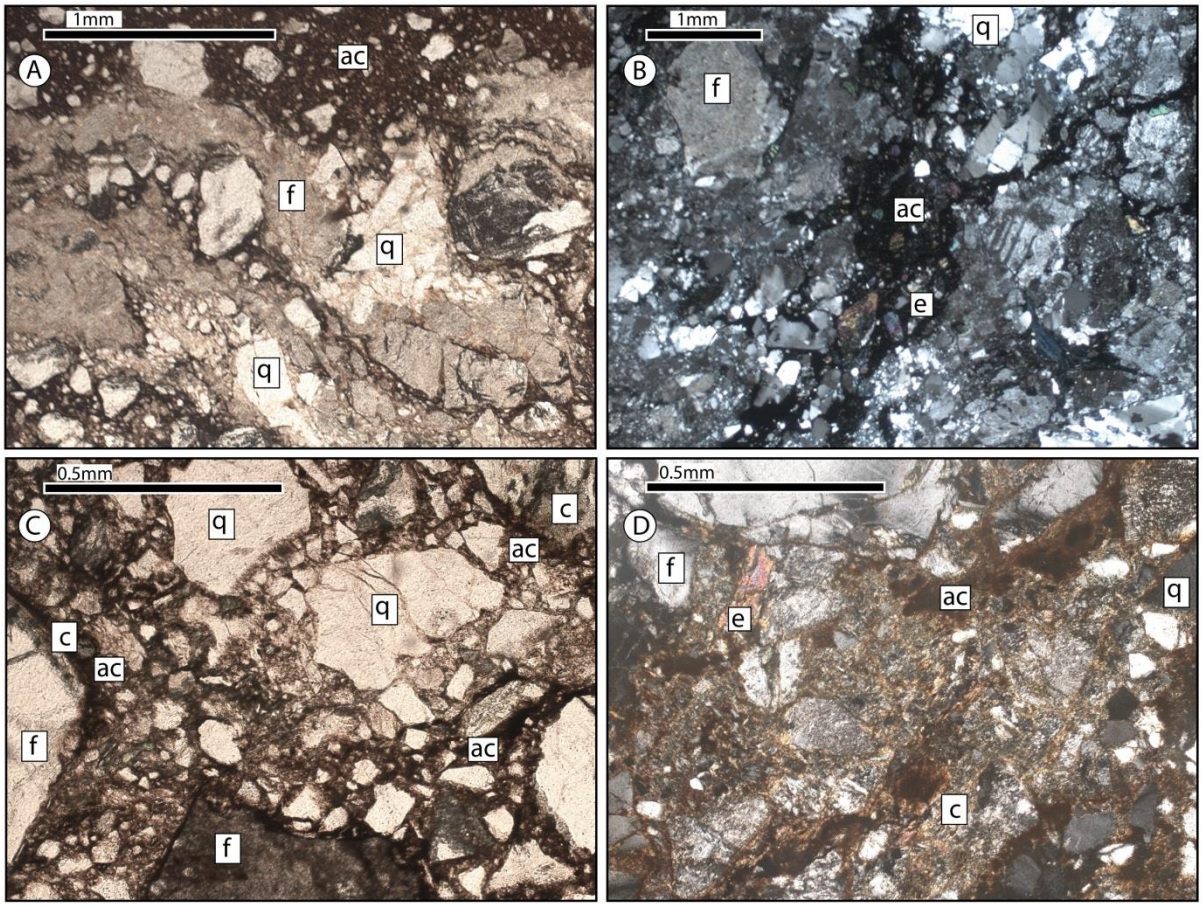

Figure 3.14 (continued next page): Clay developed within fault rocks of the Stornoway Formation. (**A**) (From Holm) PPL. Quartzo-feldspathic cataclasite, surrounded by brown authigenic clay (ac). Feldspar (f) displays an alteration rim and finer grained clast size than quartz clasts (q). (**B**) (From Griais) XPL. Epidote (e) is altered to brown authigenic clay (ac) amidst quartz-feldspar clasts (q and f). (**C**) (From Breibhig) PPL. Altered feldspar (f), and authigenic clay (ac) formed from chlorite (c) and feldspars. Feldspars and chlorites are surrounded by darker rims of clay. (**D**) (From Breibhig) XPL. Authigenic clay formed from chlorite (c) and epidote (e). Chlorite/clay alteration is heavily disaggregated between clasts of feldspar (f) and quartz (q).

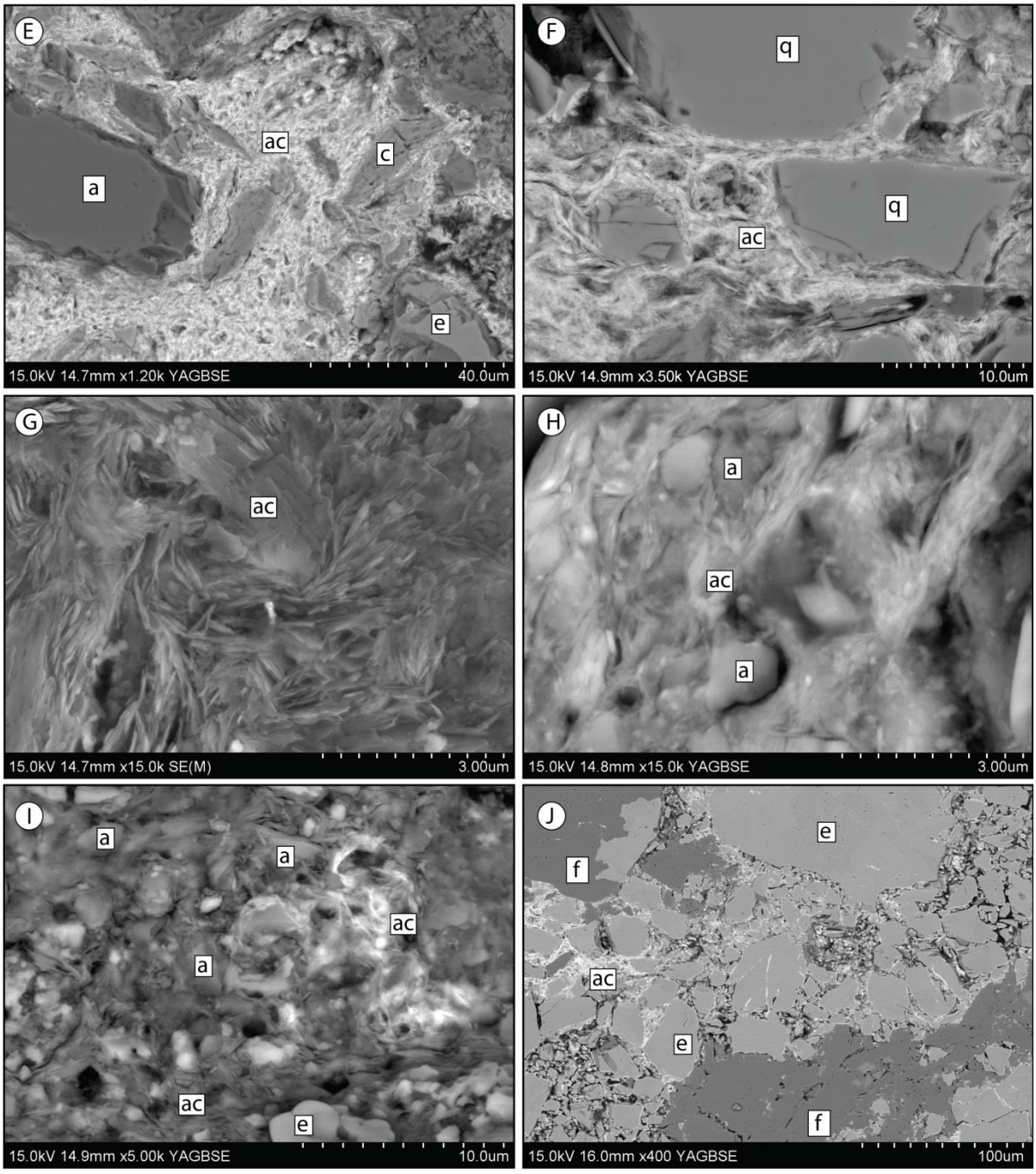

Figure 3.14 (continued): (**E**) (From Griais) BSEM image. Authigenic syntectonic clays wrapping albite (a), epidote (e), and chlorite (c) clasts. Clay is iron rich, probably altering from chlorite. (**F**) (From Griais) BSEM image. Offset quartz clast (q) separated by aligned iron rich authigenic clay needles. (**G**) (From Griais) SE (M) image. Authigenic clay is comprised of acicular needles. (**H**) (From Holm) BSEM image. Authigenic clay (ac) altering from amphibole clasts (a). (**I**) (From Garrabost/Aignish) BSEM image. Authigenic clay minerals of differing compositions (ac) forming from amphibole (a) and epidote (e). (**J**) (From Griais) BSEM image. Cataclastic epidote (e) undergoing alteration to iron rich authigenic clay (ac).

3.3.3.5 Fluid Flow and mineralisation

Alteration of host minerals, and new mineralisation along faults and fractures indicate that there have been several phases of fluid flow. Calcite is common as matrix cement, and as infill in

microcracks (Figure 3.15A). Calcite mineralisation is also incorporated into the faults as clasts and matrix material of cataclasites (Figure 3.15B). Calcite veining and mineralisation displays serrated margins, and individual calcite crystals enter extinction simultaneously in crossed polarized light, indicating a previously contiguous origin, and hence a degree of dissolution, producing porosity (Figure 3.15C-F). Figure 3.15D illustrates this well and euhedral crystals of zeolite (probably stilbite) are visible filling the resulting pore space. Calcite is observed also as a partially dissolved mass, set in the fine-grained authigenic clay-dominated cataclasite, associated with porosity and a light grey halo of probable zeolite (Figure 3.15E). From this observation it appears as though the fluids that caused dissolution of calcite were contemporaneous with or were followed by a fluid influx through the created porosity, which favoured the crystallisation of zeolite. Zeolites in crystalline rocks have been shown to be associated with secondary porosity (e.g. Weisenberger, 2009; Walker et al., 2013).

Porosity is also often seen within calcite crystals, developing pores along the planes of cleavage around 0.1 mm across. Although throughout fault rock development stages 1-5 given above (section 3.3.3.2) there is a general decrease in porosity of the rock, sparse vuggy porosity is still present with much of the fault rocks, with irregularly shaped pores less than 0.5 mm across. These pores may be preserved due to high pore fluid pressures during faulting, or potentially due to dissolution of calcite, as observed in stage 6. In one example within a moderately well-developed fault rock, an open fracture 0.5 mm across has been partially filled with calcite (slide 19I).

In an example of Set 1 faulting (Figure 3.15G and Figure 3.16C-F), discontinuous partially dissolved needle-like calcite occurs, partially or wholly replaced by zeolite. The origin of these forms is not clear, but they may be remnant calcite slickenfibres incorporated into the fault core, having undergone partial dissolution and replacement. Figure 3.15I-J exhibit clear zeolite masses within fault cores that do not appear to have undergone cataclasis, confirming the hypothesis that zeolite mineralisation has occurred post-faulting. Tertiary dykes are relatively common in the regions around Garrabost and Breibhig intruding pre-existing set 1 and 2 fault cores. Figure 3.15J shows a sample from immediately adjacent to a Tertiary dyke intruding along the fault. The dyke itself contains zeolite mineralisation within amygdales and the fault appears to have been a conduit for a murky yellow zeolite mineralisation that is not seen elsewhere. It is possible that fluids originating from the dyke have produced this mineralisation within the fault core, and this may also be the case with other faults that are proximal to Tertiary dykes. However, this does not necessarily mean that all zeolites are Tertiary in age. Most are associated with Mesozoic faults well away from any Tertiary dykes and zeolites are only found as fragments within post-Tertiary dyke (Set 3) faults.

Many fault core cataclasites are wholly cemented with very fine-grained, post-tectonic, crystalline zeolite (e.g. Figure 3.16A and B). Yet other fault cores (e.g. Figure 3.12G) show a complete lack of this late phase zeolite or porosity, possibly due to a lack of initial permeability needed to enable fluid flow and alteration. Hence the presence of zeolite mineralisation and cementation is neither consistent nor predictable throughout the Stornoway Formation faults.

The zeolite present has been identified as Na-Stilbite on the basis of crystal form and EDS spectra from 2 fault rock samples. Low levels of Mg found in two EDX spectra point to the possibility of minor Mg substitution, which has been recorded in Stilbite in basalts (Slaughter, 1970). Replacement of early-zeolites is common in many settings (e.g. Velde, 1985), but no evidence for this has been seen in the Stornoway samples. Zeolites and smectites have a high molar volume (e.g. Neuhoff et al., 1999). It is likely that the molar volume increase associated with zeolite formation contributes to the reduction of porosity in the fault rock itself, indicating that the pore space associated with zeolites is most likely due to the dissolution of calcite (e.g. Figure 3.11E). Hence, late carbonate-dissolving fluids are believed to have also precipitated secondary zeolite, explaining why zeolites are associated with pore spaces in many of the fault rocks.

Most faults within the Stornoway Formation are indistinguishable in terms of their patterns of development and fault rock textures/mineralogy, indicating formation under similar conditions. However, Set 3 faults do not develop foliated cataclasites, or porosity or associated zeolite mineralisation (stages 5 to 7 above). Indeed, clasts within the fault rocks of Group 3 contain zeolites, indicating that Group 3 faulting may post-date zeolite mineralisation. The presence of zeolites is indicative of temperatures of less than 200°C (Velde, 1985; Frey, 1987). In addition type 1 deformation twinning observed in calcite is indicative of temperatures less than 170°C (Passchier and Trouw, 1996).

Assuming a normal geothermal gradient in the area of 30°C per kilometre, the observations above indicate depths of less than 6 km. Underplating of igneous material beneath NW Scotland is thought to be responsible for significant denudation in the area since the beginning of the Tertiary (e.g. Brodie and White, 1994; Tiley et al., 2004), and on Lewis, is thought to be associated with a maximum of 3 km of erosion (Persano et al., 2007). Hence, it is likely that the faults studied here have been buried to a depth of around 3 km or less. Evidence of a significant fault scarp at Arnish, in the form of 4-5 m boulders adjacent to the bounding fault, indicates that faulting at least initially breached to the surface and formed local topography. This give a fault rock depth range of 0-3 km represented within outcrops of the Stornoway Formation.

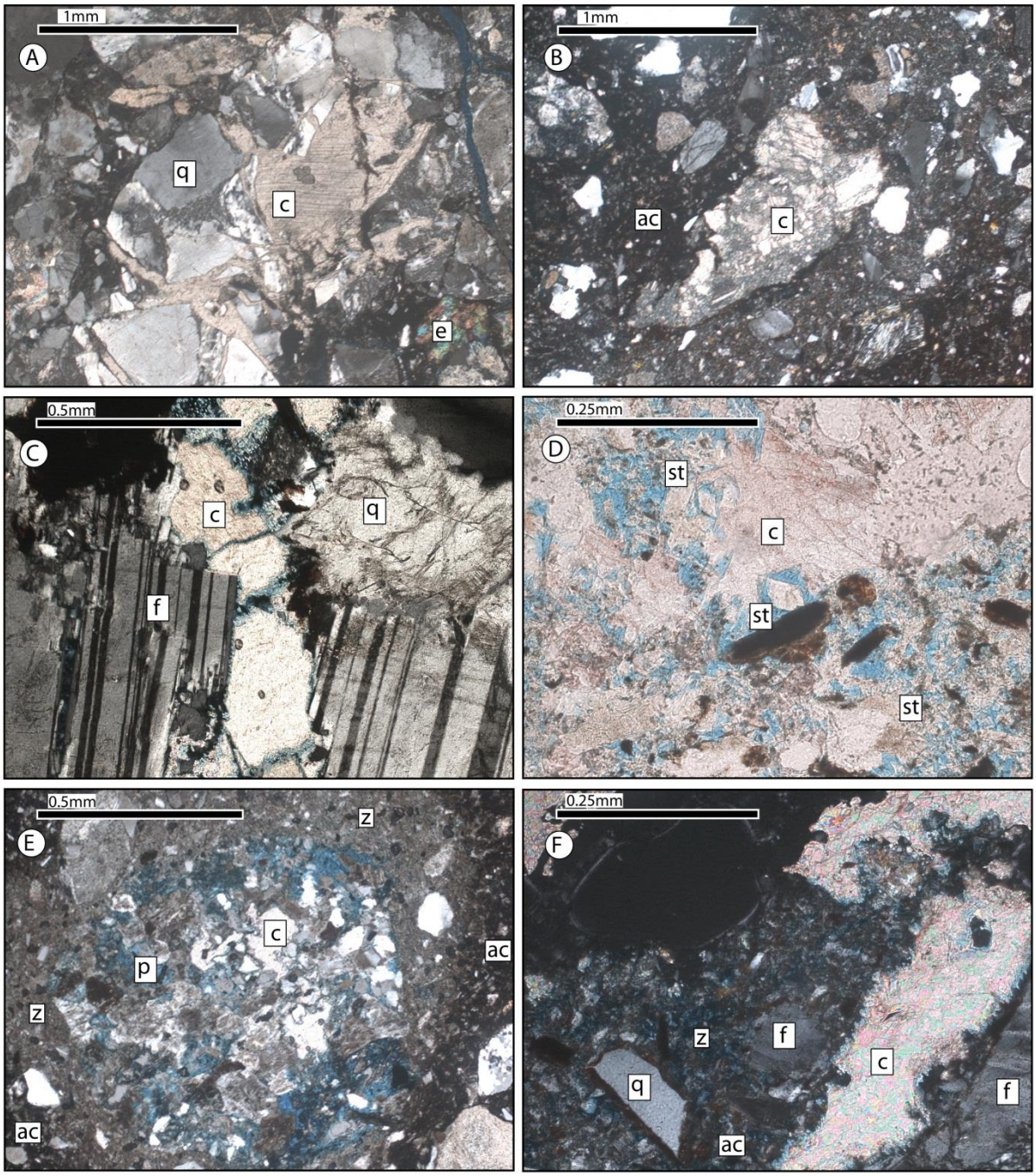

Figure 3.15 (continued next page): Evidence for fluid flow interaction within fault gouges and cataclasites of the Stornoway Formation. (**A**) (From Garrabost/Aignish) XPL. Calcite cement within microfractures, indicating fluid flow in early stages of fault development. (**B**) (From Garrabost/Aignish) XPL. Cataclastic calcite (c) and authigenic clay development (ac) indicating syn-faulting fluid flow. (**C**) (From Griais) XPL. Calcite vein (c) within a large fault clast composed of kinked feldspar (f) and quartz (q) filled with inclusion trails and fractures. Calcite is partially dissolved. Note pore space in blue (p). (**D**) (From Garrabost/Aignish) PPL. Patchy calcite (c) with uniform extinction indicates partial dissolution producing porosity (in blue). Euhedral stilbite crystals (st) fill pore space . (**E**) (From Breibhig) XPL. Patchy, partially dissolved calcite with uniform extinction (c), with pore space development (p), and grey halo of very fine zeolite (z) within authigenic clay (ac) rich matrix of the fault rock. (**F**) (From Garrabost/Aignish) XPL. Partially dissolved calcite associated with porosity (in blue), authigenic clay (ac), and zeolite (z) formation. Note euhedral crystal terminations of zeolites.

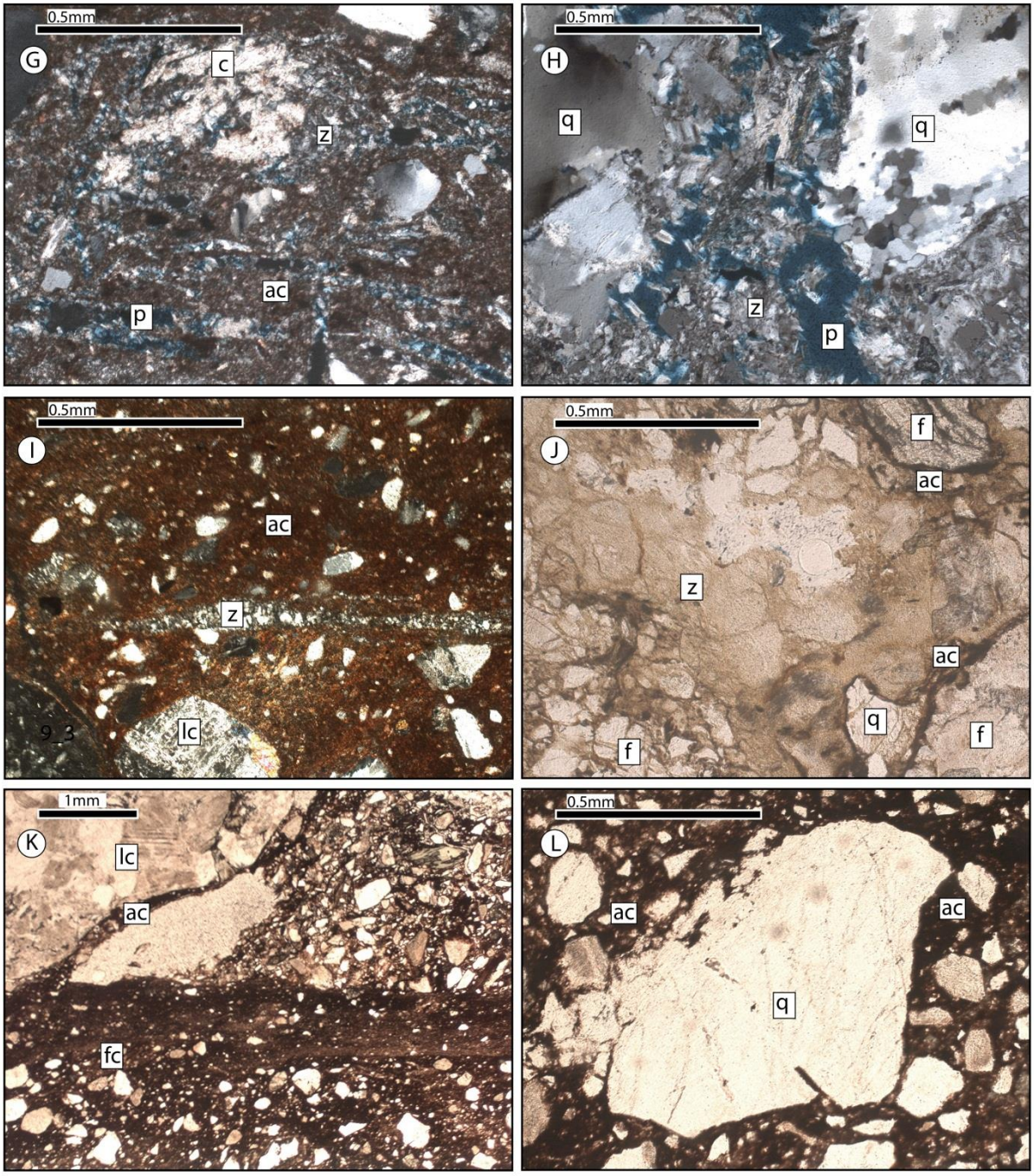

Figure 3.15 (fluid evidence and effects continued): (**G**) (From Garrabost/Aignish) XPL. 'Spicule'-like forms comprised of calcite (c) and zeolite (z), probably stilbite, surrounded by authigenic clay (ac) within fault cataclasite. Porosity shown with blue stain. (**H**) (From Garrabost/Aignish) XPL. Porosity in blue (p) associated with zeolite growth (z), possibly stilbite. (**I**) (From Garrabost/Aignish) XPL. Zeolite vein (z) with authigenic clay (ac) matrix of a fault gouge with lithic clasts (lc). (**J**) (Breibhig) PPL. Heavily altered feldspar clasts (f) with authigenic clay alteration haloes (ac) and zeolite (z). This fault is intruded by a Tertiary Dyke, 2 cm from this position, and these zeolites may be related to this. (**K**) (From Garrabost/Aignish) PPL. Authigenic clay gouge (ac) adjacent to lithic clast (lc) injecting into country rock from the fault core (fc). (**L**) (From Griais) PPL. Quartz clast in fault core, surrounded by dark halo of authigenic clay (ac), with gradational transition to lighter brown matrix.

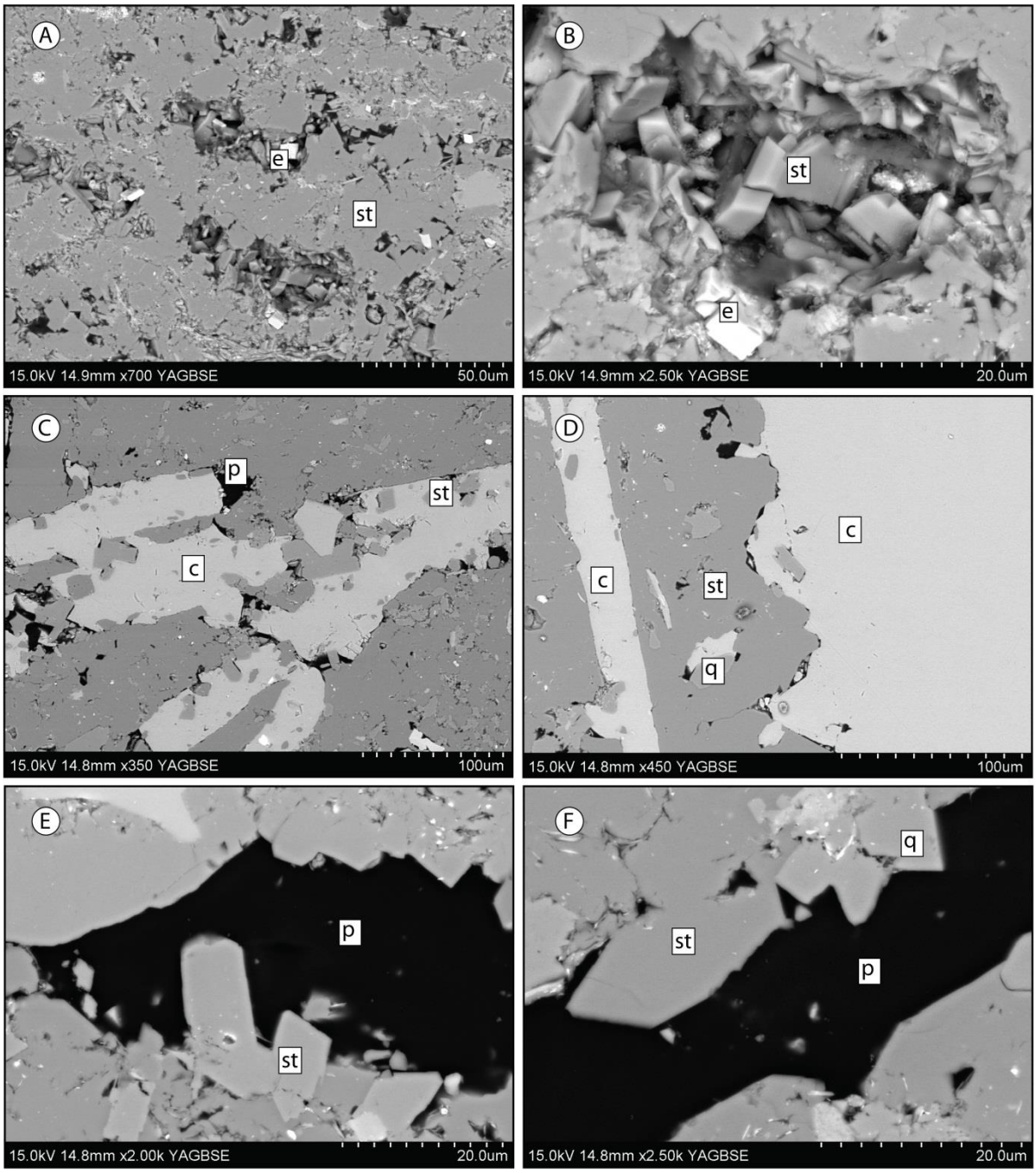

Figure 3.16: Fluid flow evidence from SEM analysis, all from localities at Garrabost/Aignish. BSEM images. (**A**) Fault gouge with pore space partially infilled with mineralisation – euhdral crystal terminations are visible. Bright white minerals are epidote (e), and groundmass is stilbite (st). (**B**) Higher resolution image of A**:** Pore space is infilled with euhedral minerals. When compared with typical cataclasite/gouges in figure 9G for example, you can clearly see there is a later mineralisation overprint here. Crystal shapes are indicative of stilbite (st), and EDX spectra containing low levels of Mg confirm this observation. (**C**) From fault gouge, calcite mineralisation occurring as elongated spicule-like forms (c), also shown in Figure 11G, alongside euhedral blocky stilbite crystals (st). (**D**) Calcite-stilbite mineralisation. (**E**) and (**F**) Stilbite (st) crystallising inside pore space (p).

3.4 Lewisian Gneiss of the Stornoway Region

3.4.1 Lewisian Gneiss Lineaments

A lineament analysis across eastern Lewis (Figure 3.17) has been performed to give an overview of fracture orientations and concentrations within the Lewisian within 5 km of the Stornoway Formation. This was done at multiple scales using high resolution Nextmap© lidar imagery with a resolution down to 2.5 m horizontally and 1 m vertically. Nextmap data were converted to hillshades and analysed for slope, break in slope, and aspect. Analysis was performed on the eastern side of Lewis at 1:100,000 (187 lineaments), 1:50,000 (1268 lineaments), 1:25,000 (481 lineaments), and locally at 1:1,000 (1141 lineaments). The lineaments digitised at lower resolutions were not re-picked at higher resolutions.

The spurious effect of weak foliation planes producing topographic relief was overcome through digitisation of the foliation trend from the BGS 1:100,000 Lewis and Harris (north) structure map (Figure 3.18), and discounting lineaments that lay parallel to this. Digitised lineaments are assumed to be faults and this was confirmed by ground-truthing during fieldwork. Although a swath of Tertiary dykes are known to cross the island in a NNW-SSE direction (Fettes et al., 1992), these were nearly always found to be intruded along earlier faults, and in some cases, to have reactivated faulted margins. In the region immediately surrounding the Stornoway Formation, lineaments were picked at a 1:1000 scale from aerial photography, excluding foliation, in order to compare these results to the faulting orientations recorded from fieldwork within the Stornoway Formation (see above).

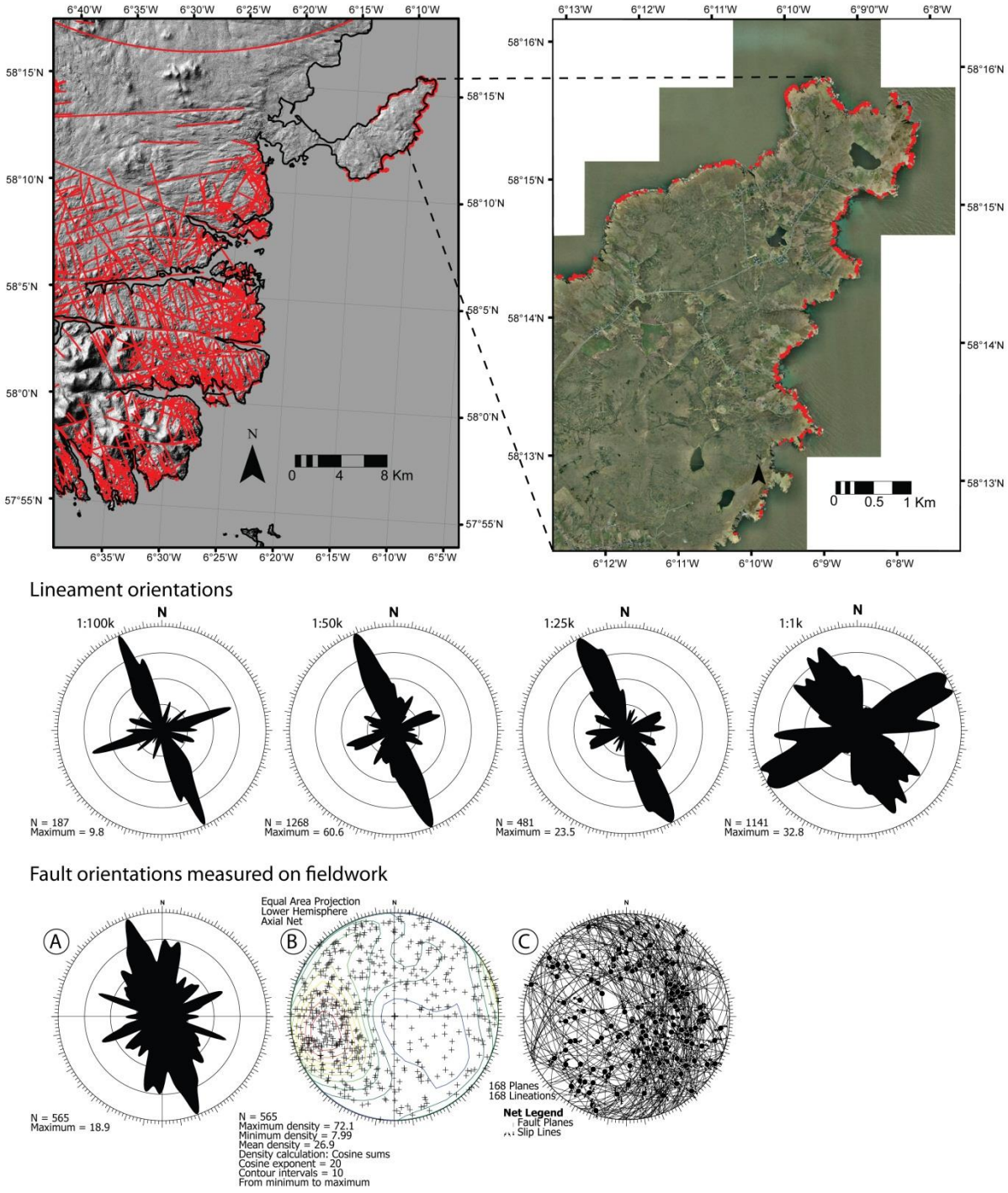

Figure 3.17: Lineament analysis results from within the Lewisian performed on Nextmap lidar images at multiple scales: rose diagrams are from Nextmap© data interpreted at 1:100k, 1:50k, 1:25k (top left map), and 1:1k scales performed on aerial photography (top right map). (**A** - **C**) show fieldwork results from the Stornoway region for comparison with lineament analysis. (**A**) Rose plot of faults measured in the field. (**B**) Stereonet of poles of all faults measured in the field with density contouring. (**C**) Faults with associated slip data only. Faults plot as great circles with slip data plotted on the corresponding great circle.

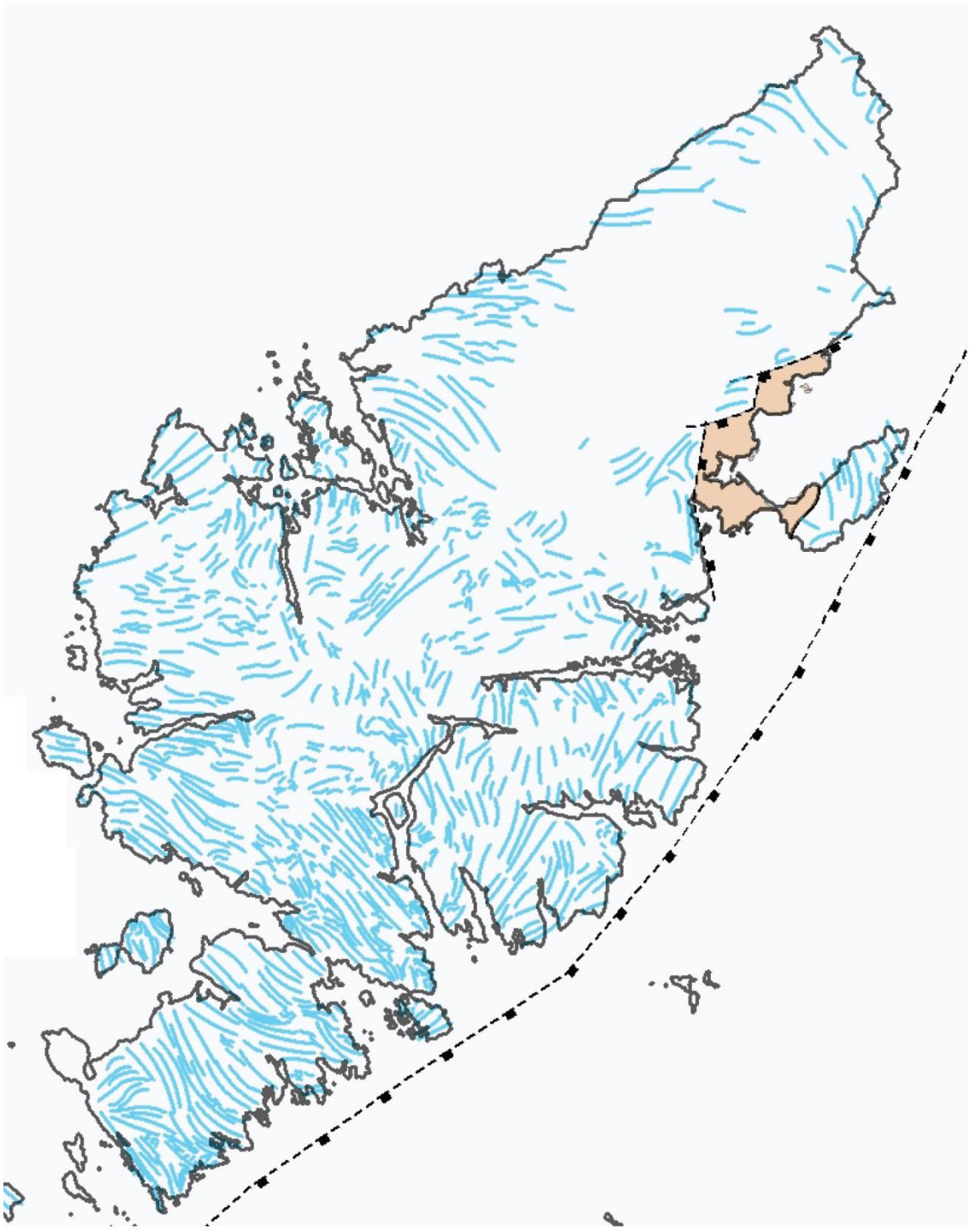

Figure 3.18: Foliation in the Lewisian Gneiss digitised from the BGS 1:100,000 scale Lewis and Harris structure maps, with the Stornoway Formation in brown, and major normal faults shown.

Dominant orientations determined from the lineament analysis are NNW-SSE and ENE-WSW, with the longest lineament orientations also corresponding to these orientations (Figure 3.19). At the 1:1,000 scale on the Eye Peninsula, the orientation of identified fractures is again very similar to that seen at 1:25,000 scale and above. Remotely sensed lineament trace orientation results are similar in orientation to faulting observed during fieldwork in the OHFZ (Figure 3.17).

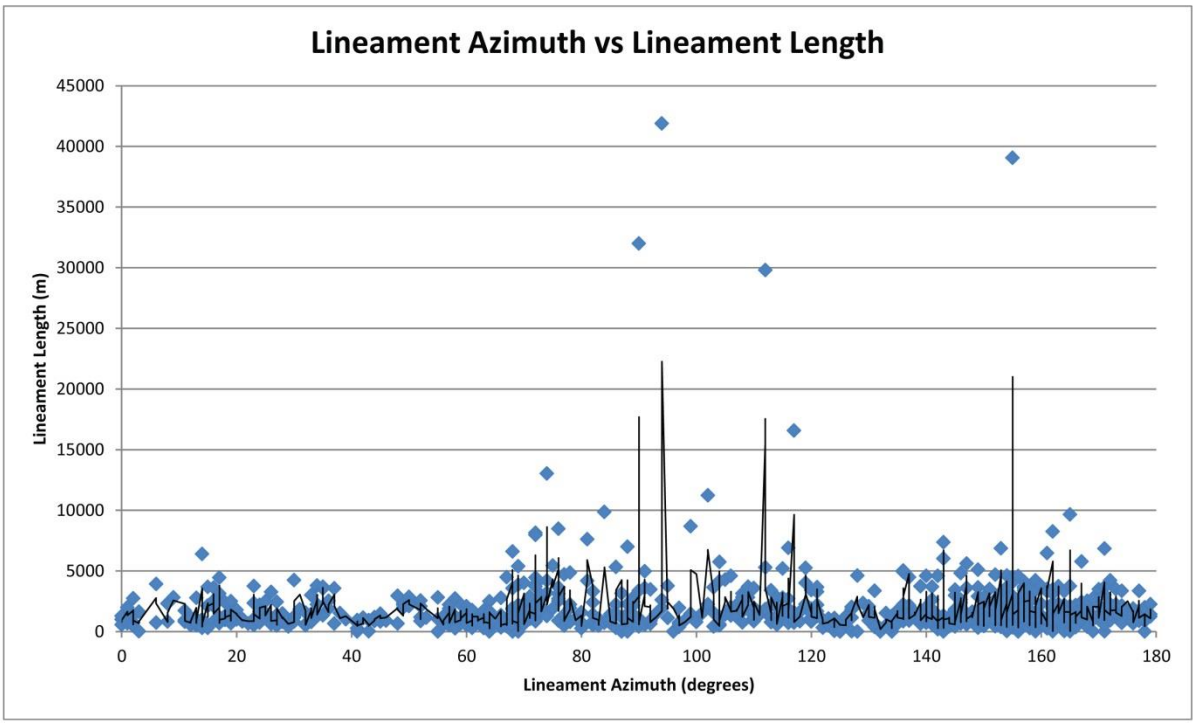

Figure 3.19: Lineament azimuth (degrees) vs. lineament length (m) for Eastern Lewis. Blue points represent individual lineaments, black line is a 5 point moving average. Notable peaks are at E-W, WNW-ESE and NNW-SSE.

3.4.2 Field observations: Lewisian-hosted Faults

The coastal exposures of Lewisian Gneiss, surrounding the Stornoway Formation, comprise the complex and repeatedly deformed rocks of the Outer Hebrides Fault Zone (e.g. Fettes et al., 1992; Butler, 1995; Imber, 1998; Imber et al., 2001; Imber et al., 2002). The present study was primarily concerned with the identification and characterisation of Mesozoic- and Cenozoic-age brittle faults in these basement rocks. These structures were identified in the Lewisian by direct comparison and correlation with Stornoway Formation-hosted faults, including detailed field and microstructural analysis, i.e. Mesozoic to Cenozoic faults cutting the Lewisian are identified on the basis that they carry fault rocks identical or similar to those seen cutting the Stornoway Formation (i.e. containing authigenic smectitic clay with zeolite and calcite, alongside the same deformation mechanisms seen within the Stornoway Formation). In addition faults are observed cutting both the basement and cover rocks at Suardail, and Mesozoic age faulting has been characterised at that locality (section 3.4.4). Eleven principal areas were visited in the Lewisian in the immediate vicinity of the Stornoway region (these are named in Figure 3.20).

Tob Leireabhaigh/Memorial Cairn and Tolstadh are the closest localities to the major bounding faults of the Stornoway Formation, and particularly at Tob Leireabhaigh there is easily accessible faulting striking parallel with the offshore Stornoway Formation bounding fault. On the Eye

peninsula, the Garrabost area is heavily faulted with multiple phases of deformation preserved immediately adjacent to the unconformity, with several outcrops of isolated and partially faulted Stornoway Formation present. However, the BGS interpretation that this area is outside the OHFZ as shown in Figure 3.20 is questionable. The Pabail and Seisiadar areas both contain expanses of outcrop interpreted to lie within the OHFZ and are correspondingly heavily faulted. Port Mholair and the northern portion of the Seisiadar localities (Seisiadar North) are noticeably fractured to a lesser extent than other localities on the Eye Peninsula, and this is in agreement with the interpretation that these areas lie outside the OHFZ. Each area is discussed in turn with regards to the geology and fault rock composition.

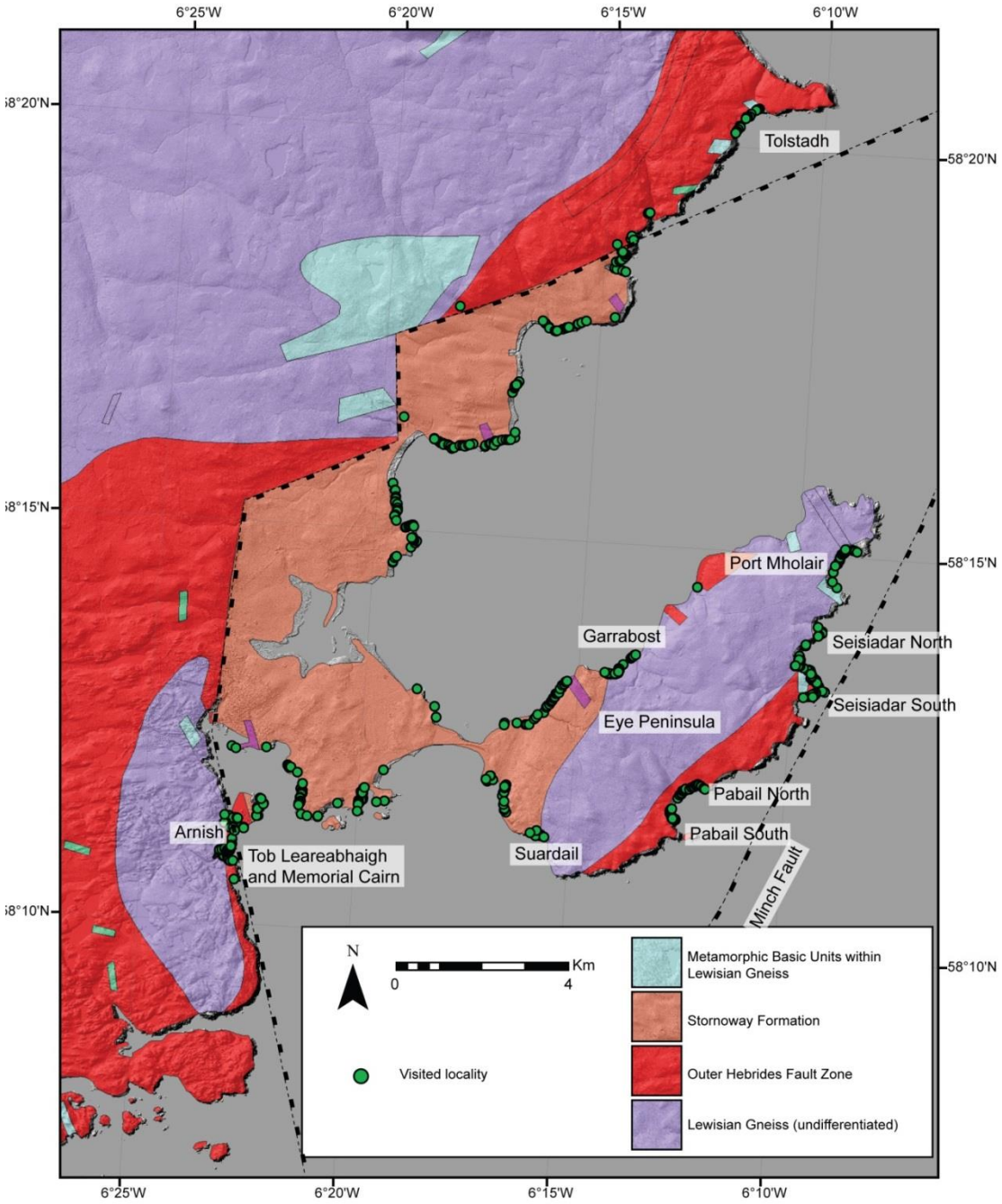

Figure 3.20: Field localities in the Lewisian Gneiss of the Stornoway region.

3.4.2.1 Eye Peninsula

3.4.2.1.1 Garrabost

The beach and cliffs at Garrabost (NB 5113 3380 to NB 5143 33890) provide excellent continuous exposure of Lewisian Gneiss immediately adjacent to the unconformable contact at the base of the Stornoway Formation (Figure 3.21 and Figure 3.22). The Lewisian here is composed of biotite gneisses interleaved with older and younger basic bodies, with pegmatite and possible silicic metasedimentary units. Foliation is pervasive, except in massive pegmatites and mafic (older and younger basic amphibolite) units. A large-scale west-verging fold is visible on the beach with a wavelength of 10 m and an amplitude of 2 -3 m (Figure 3.21B), but otherwise the foliation generally dips moderately to the ENE. The gneiss is heavily fractured and faulted with multiple fracture sets evident (e.g. Figure 3.21C), most notably including phases of epidote ultracataclasite-bearing faults, and later cross-cutting clay-rich cataclasites and gouges that reactivate at least 6 of the outcropping epidote-bearing faults. Within these reactivated faults, epidote ultracataclasite is reworked as a breccia in fault cores in a matrix of brown authigenic clays up to 15 cm thick, with clasts of epidote cataclasite up to several cm across. Epidote cataclasite faults display obvious pistachio-green colouration visible in the field, and are generally discrete structures around 1-2 cm thick.

Seventeen clay-dominated faults were observed in the field with no evidence of reactivation, which are either NNW-SSE-striking (normal oblique dextral) or E-W-striking dip-slip faults. These structures have the same kinematics as faults identified in Set 1 and Set 2 of the Stornoway Formation faults, with fault rocks up to 7 cm thick. These faults are minor discrete structures with no evidence of a significant damage zone. One example of a NE-SW striking clay-rich fault is observed reactivating an epidote cataclasite fault, which shows strike-slip kinematics. This fault cuts all other adjacent structures. It is possible this fault may be a part of Set 3 identified within the Stornoway Formation. Clay-rich faults commonly lie parallel to the foliation (e.g. Figure 3.21I-K). The ENE dip of the foliation (Figure 3.22) is coincident with both clay-rich and epidote cataclasite-bearing faults that also lie along the foliation plane. Epidote veins generally dipping moderately to the northwest may be subsidiary structures related to phases of normal motion on epidote cataclasite-bearing faults.

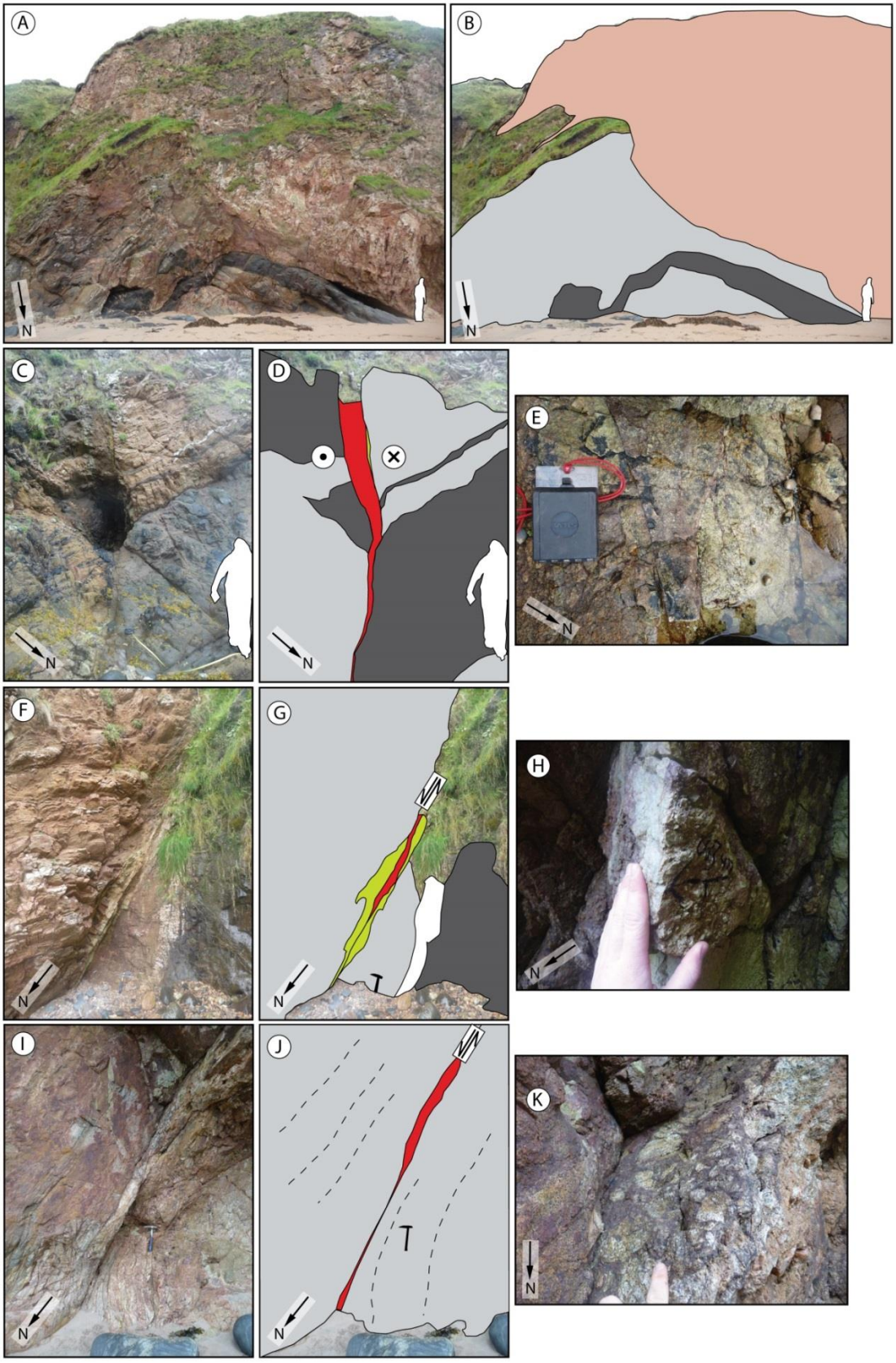

Figure 3.21: Outcrop photos and interpretation from Garrabost. Grey = grey gneiss, pink = pegmatitic gneiss, black = amphibolite, green = epidote ultracataclasite, red = clay-bearing reddy brown fault rock. (**A - B**) Folded ultramafic unit. (**C** - **E**) Late E-W strike-slip structure and fault rock. (**F** - **H**) NNW-SSE striking normal fault with clay-rich gouge cementing clasts of epidote ultracataclasite. (**I** - **K**) NNW-SSE striking normal fault, with clay-bearing breccia and cataclasite, parallel with the foliation.

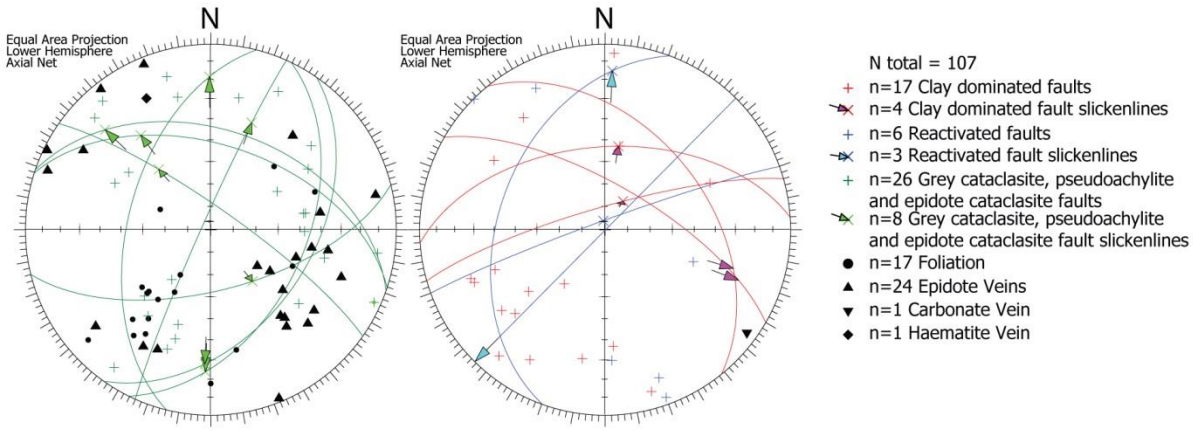

Figure 3.22: Stereonet of data collected from Garrabost. Late stage NW-SE and NE-SW striking faults are most common, usually associated with calcite and clay development. Late E-W strike-slip faulting is also evident. Faults with slip data recorded are shown with a great circle in addition to the pole.

3.4.2.1.2 Pabail South

Pabail South (NB 52720 30403 to NB 52898 310118) lies within the area indicated as the OHFZ in Figure 3.20. Foliation generally strikes ENE-WSW. Early ductile deformation includes a phase of ENE-WSW trending shear zones that are also visible at Seisiadar and Pabail North. Multiple phases of brittle deformation have produced overprinting fault rocks in the area, with pseudotachylite, grey 'peppery' cataclasites, epidote ultracataclasites, and clay-rich gouges and cataclasites (Figure 3.23, Figure 3.24). The pink colouration of some clay-bearing cataclasites is probably due to zeolites and adularia mineralisation (see fault rock characterisation below).

As can be seen in Figure 3.24, clay-bearing faults are nearly all NW-SE trending, with the exception of one northwards-dipping fault. These orientations correspond well with those identified in the Stornoway Formation. Structures reactivated by clay-bearing faults have more variable orientations, likely reflecting reactivation of non-optimally orientated structures. Figure 3.23A-C shows a multiply reactivated fault zone, with pseudotachylite, epidote cataclasite, and clay-bearing fault rocks. Pseudotachylite injection veins originate from a fault plane now composed of clay-bearing gouge and cataclasite, indicating reactivation of an earlier structure. Similarly Figure 3.23D-F shows a green epidote cataclasite fault rock that has been reactivated with pink-brown cataclasite, probably bearing zeolite and adularia fault rock. Other pseudotachylite- (Figure 3.23H - I), epidote- cataclasite- and grey cataclasite-bearing faults have broad variations in their orientations. The foliation generally dips towards the south-southeast, and, unlike Garrabost, there is no clear similarity in the trend of the foliation and late clay-bearing faults. Pink fractures that may be zeolitic or haematitic are associated with NNW-trending structures (Figure 3.23J-K).

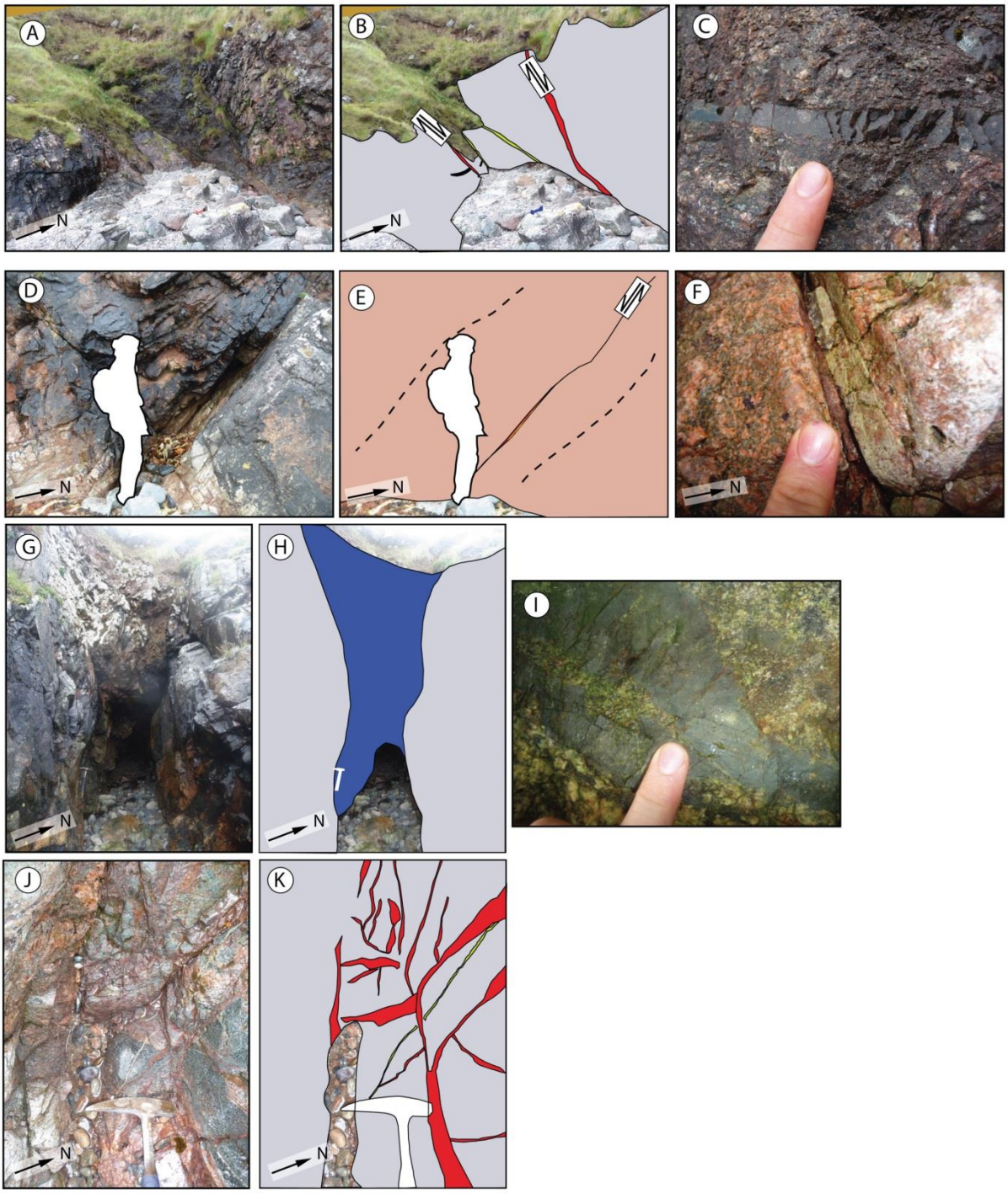

Figure 3.23: Outcrops at Pabail South. Grey = grey gneisses, pink = granitic gneiss, red = late clay- and haematite-rich fault rock, green = epidote ultracataclasite, blue = peppery grey cataclasite, black = pseudotachylite, and dashed lines show foliation. (**A** - **C**) Multiple fault rock assemblages. (**C**) Pseudotachylite veining. (**D** - **F**) E-W-striking epidote ultracataclasite reactivated with band of pink-brown cataclasite, probably containing fine-grained zeolites. (**G** - **I**) High angle NNE-SSW-striking fault associated with predominantly with peppery cataclasites (**I**) and minor epidote veining. (**J, K**) Haematite fractures related to a relatively late NNW-SSE-striking fault clearly cross-cutting an epidote vein.

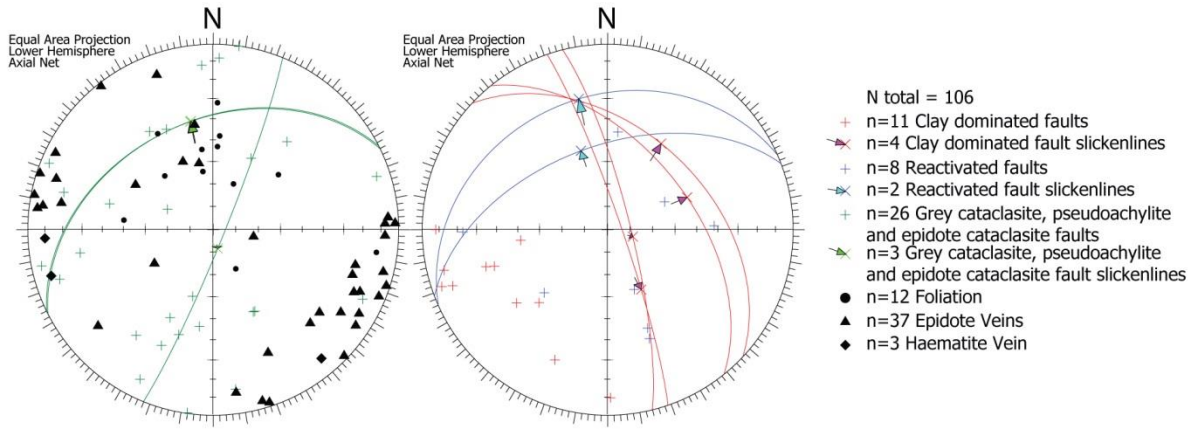

Figure 3.24: All measurements from Pabail South. Epidote veins strike NE-SW, mirroring the OHFZ trace. NE-dipping faults are most common, associated with calcite and clay development. Faults with slip data recorded are shown with a great circle in addition to the pole.

3.4.2.1.3 Pabail North

Pabail North (NB 52898 310118 to NB 53385 31223) lies within the area of the OHFZ, and is highly faulted with phases of ductile and brittle deformation. Strongly foliated grey gneisses carry lenses of amphibolite, usually of Older Basic origin. Foliation dips shallowly to the northeast and southwest. Ductile deformation is represented by phyllonites with top to the NW thrusting evident (Figure 3.25 A-C), and ENE-trending altered ductile shear zones.

Brittle deformation is represented by the presence of pseudotachylite, epidote cataclasites, and calcite-, haematite-, and clay-rich brittle faulting. Minor clay-dominated faults are observed (Figure 3.26), and are commonly associated with parallel calcite veins (Figure 3.25D-I, Figure 3.26). These faults are < 0.5 cm thick, strike NNW-SSE and offset a pre-existing low-angle pseudotachylite thrust plane (Figure 3.25J-L). These minor faults parallel a major NNW-SSE striking dip-slip normal fault, with 4-5 m of chaotic breccia and poorly indurated cataclasite, and may be a part of the footwall damage zone of that structure. These late clay-bearing faults also cut and offset epidote ultracataclasites and epidote veins that generally strike NE-SW. Epidote cataclasite faults and other non-clay-bearing faults have more variable strikes than the clay-bearing faults.

Shallowly southeast dipping phyllonites are spatially associated with and cross cut pseudotachylite. The phyllonites contain clay bearing discontinuities with dip-slip normal kinematics. The presence of clay suggests these faults may be relatively young, however they are also cut by the phase of NNW-SSE striking clay-bearing faults.

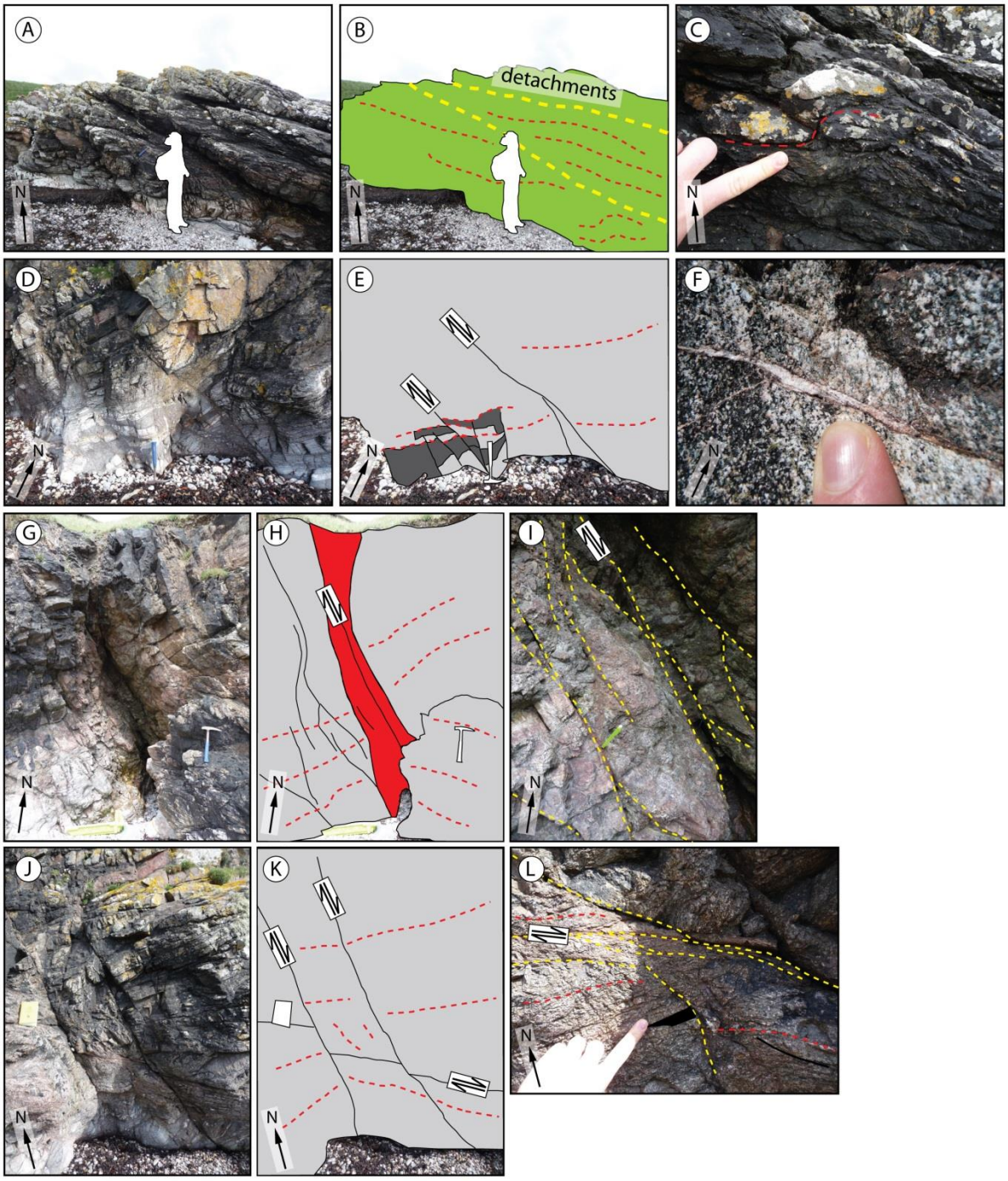

Figure 3.25 (previous page): Pabail North Outcrops. Green = phyllonite, grey = grey gneisses, dark grey = amphibolite, red = clay and calcite rich fault core, red dashed line = foliation, yellow dashed line = discrete fault surfaces. (**A** - **C**) Phyllonite with NW-verging up-dip folds, indicating thrust displacements, cut by discrete detachment surfaces parallel with the phyllonitic foliation. (**D** - **F**) NNW-SSE striking minor normal oblique dextral faulting associated with carbonate and red mineralisation (**F**). (**G** - **I**) Minor/intermediate scale N-S striking normal oblique dextral fault, with zone of brecciation, reddy brown clay, and carbonate mineralisation. Reddy-brown soft gouge (**I**) visible with pencil protruding. (**J** - **L**) NNW striking normal faults with up to 10 cm displacement, offsetting a lower angle normal detachment surface with up to 10-15 cm of brecciated protophyllonite (shown in **L**), cutting pseudotachylite (in black: **L**). The main detachment surface is a discrete area of brown gouge with Riedel shears indicating normal motion.

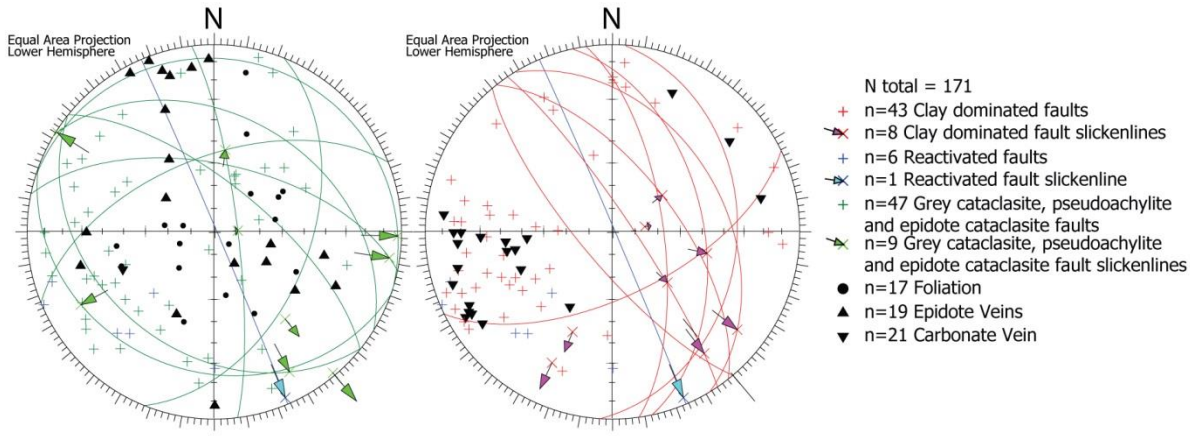

Figure 3.26: Stereonet of data collected from Pabail North. NE dipping faults are associated with late stage structures associated with calcite and clay development and normal oblique dextral offsets. Faults with slip data recorded are shown with a great circle in addition to the pole.

3.4.2.1.4 Seisiadar South

Seisiadar South (NB 55667 33215 to NB 55611 34082) lies within the area identified as the OHFZ and is highly fractured and faulted. Gneiss here is typical of that seen elsewhere, with lenses of older basic amphibolite, pegmatites and metasedimentary rocks, including a band of marble. Foliation generally dips to the east-northeast and pegmatite veins and basic bodies are generally concordant with the foliation. However, there is some evidence of NE-SW trending relict earlier foliation within a metadiorite body several tens of metres across.

Faults here preserve a similar record to that at Pabail North. Early ductile, near vertical, indurated NE-SW trending shear zones are common, with earlier brittle deformation including pseudotachylite faulting, epidote cataclasites/ultracataclasites, and later clay-rich brown gouges and breccias often associated with calcite mineralisation. Ductile phyllonites are present with evidence of NW-directed thrusting and clay-rich extensional (top-to-SE) detachments localising along them.

Epidote ultracataclasites are associated with highly fractured rock (Figure 3.27A-C), with 3 showing reactivation by clay-bearing light pink-brown faults (Figure 3.27D-F). The pink colouration observed in these faults is probably due to adularia and zeolites. Several phases of later slip are evident within the phyllonites, initially linked to epidote mineralisation and normal faulting, with epidote-rich surfaces detaching onto the phyllonite contact shown in Figure 3.27J-L. Following this, a further phase of faulting associated with clay development has brecciated the epidote fault rocks. Figure 3.28 shows that these epidote-bearing faults and pseudotachylites have a strongly defined trend with the majority dipping southeast. As seen at most other localities, normal kinematics are usually associated with epidote bearing faults.

Clay-bearing normal faults are observed, many of which are parallel with the foliation within the gneiss (Figure 25). Clay-bearing foliation-parallel, ENE-dipping faults are seen alongside a large-scale steeply SE dipping fault set (e.g. Figure 3.27G-I). The SE dipping fault in image

Figure 3.27G-I is comprised of a >2 m wide zone of chaotic brecciated, well-indurated gneiss with breccia clasts up to 50 cm across, and with clear dip-slip slickenlines in brown clay on a slip surface localised to the footwall. Seisiadar South is the closest location to the major SE dipping, km- scale, dip-slip normal displacement Minch fault that lies approximately 200 m offshore and forms the western bounding structure of the Mesozoic Minch Basin (Stein, 1988; Morton, 1992; O'Neill and England, 1994; Dore et al., 1999; Trewin, 2004). Analysis of the fault rock from the SE dipping trending faults (Figure 3.49A-D) shows that they contain features characteristic of other faults identified as Mesozoic in age that generally dip to the ENE, and it was not possible to identify the relative ages of the these two fault orientations. This may indicate that SE dipping faulting was contemporaneous with ENE dipping faulting, possibly as part of a polymodal fault set. Both fault orientations are associated with calcite mineralisation.

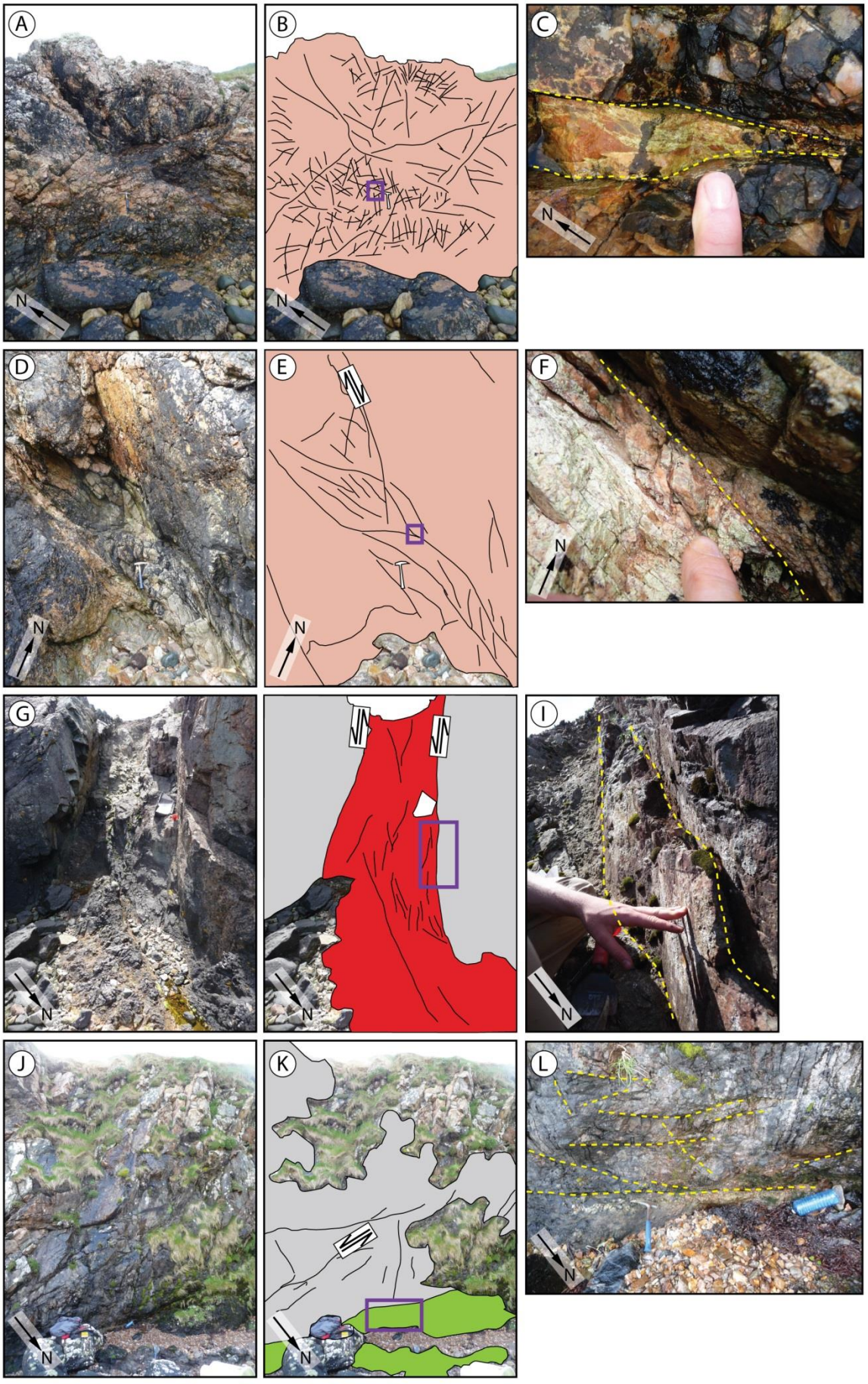
A
B
C
D
E
F
G
I
J
K
L
N

Figure 3.27 (previous page): Seisiadar South outcrop images. Pink = pegmatitic gneiss, grey = Grey gneiss, red = late clay-bearing fault rocks, green = phyllonite, yellow dashed lines = faults, red dashed lines = foliation. (**A** - **C**) Fractured and grain size-reduced pegmatitic gneiss cemented with epidote. (**D** - **F**) Pegmatitic gneiss, cut by a NNW-SSE trending normal oblique dextral fault, containing brecciated epidote in light brown clay-bearing cement, possibly containing zeolite. (**G** - **I**) A major NE-SW trending fault with dip-slip normal motion slickenlines, several hundred metres from the Minch Fault. A 1.5-2m wide zone of chaotic brecciated gneiss associated with clay mineralisation. (**J** - **L**) A phyllonite body truncated against grey gneiss by clay-rich fault containing brecciated epidote and carbonate. Minor epidote veneer fault surfaces detach onto the phyllonite surface with normal motion kinematic indicators.

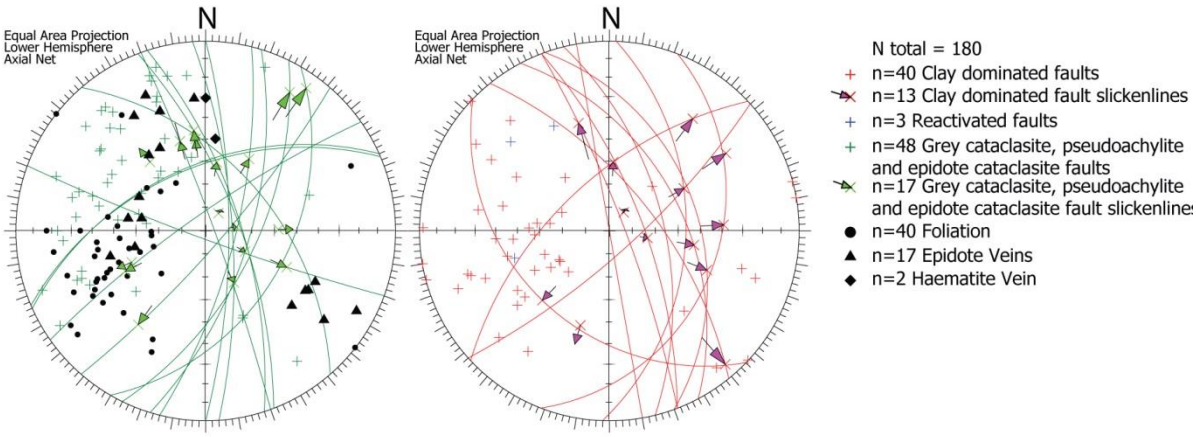

Figure 3.28: Stereonet of data collected from Seisiadar South. Faults with slip data recorded are shown with a great circle in addition to the pole.

3.4.2.1.5 Seisiadar North

Seisiadar North (NB 55611 34082 to NB 56011 34830) lies in the region identified by the BGS as being outside the OHFZ. Fracturing is less intense than regions to the south, however faults and fractures are still numerous. Prominent early ductile shear zones are very well exposed, trending ENE-WSW with a near vertical dip, and displaying sinistral kinematic indicators; these are also observed to the south in Seisiadar South and at Pabail. The large shear zone in Figure 3.29D-F is over 3 m thick and comprised of a sheared amphibolite, with clasts of grey gneiss also incorporated into the shear zone core. These ductile shear zones are cut by epidote bearing faults and hence are early. Their ENE-WSW trending orientations may reflect the NE-SW strike of the relict foliation observed at Seisiadar South. Given the shear zones incorporate grey gneiss blocks, the amphibolite is likely to be Younger Basic (Scourie Dyke) age. The foliation in this area generally trends NNW-SSE with some variability (Figure 3.30) that is probably attributable to local reorientation about these ENE-WSW ductile shear zones (e.g. Figure 3.29D-F).

Faulting is dominated by NE- and WNW-dipping epidote ultracataclasite faults and breccias. Epidote cataclasite faults are associated with both normal and thrust movements. Figure 3.29A-C

shows an early northeast-dipping thrust localising at the boundary between a younger basic body and granitic/pegmatitic gneiss. The fault rock is very well indurated with epidote. Similarly with those faults described above, epidote cataclasite bearing faults are discrete, and typically less than 1-2 cm thick. ENE-WSW trending early shear zones are clearly cut by epidote-veneered fault surfaces trending NNE-SSW with normal motion slickenline steps (Figure 3.29F). Clay-bearing faults were identified in the field, in addition to 2 clay-bearing reactivated faults (i.e. containing clasts of epidote cataclasite). These clay-rich faults are up to 2 cm thick.

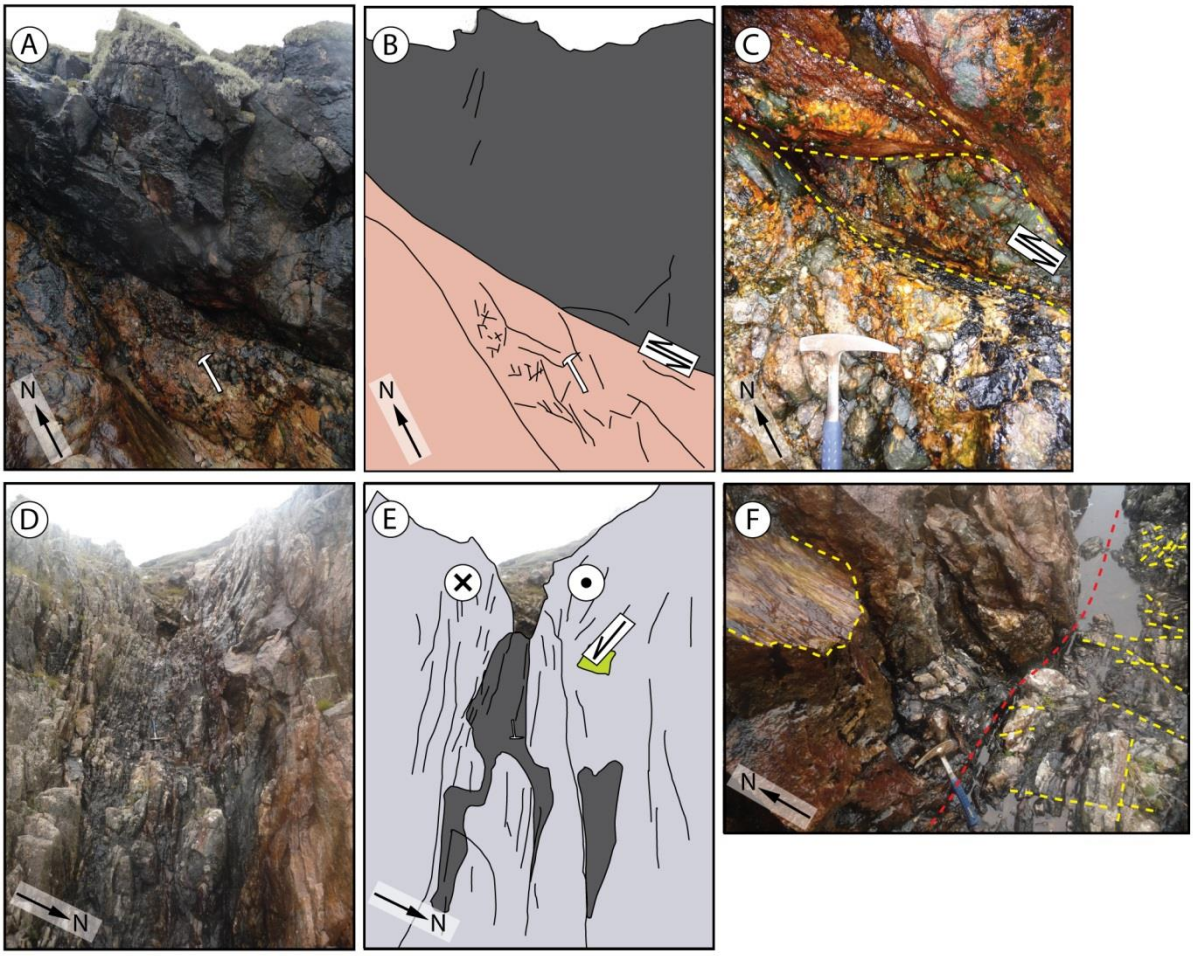

Figure 3.29: Seisiadar North outcrop images. Dark grey = amphibolite, pink = granitic gneiss, light grey = grey gneiss, green = epidote fault surface, yellow dashed line = faults, red dashed line = shear zone margin. (**A** - **C**) showing epidote cataclasite fault rock, very well indurated, along a minor thrust fault localising between a younger basic and granitic gneiss. (**D** - **E**) large ENE-WSW trending dextral shear zone, cut by an epidote fault surface with normal motion kinematic indicators (shown in **F**). This shear zone appears to be localising along an amphibolite and incorporates large clasts of wall rock.

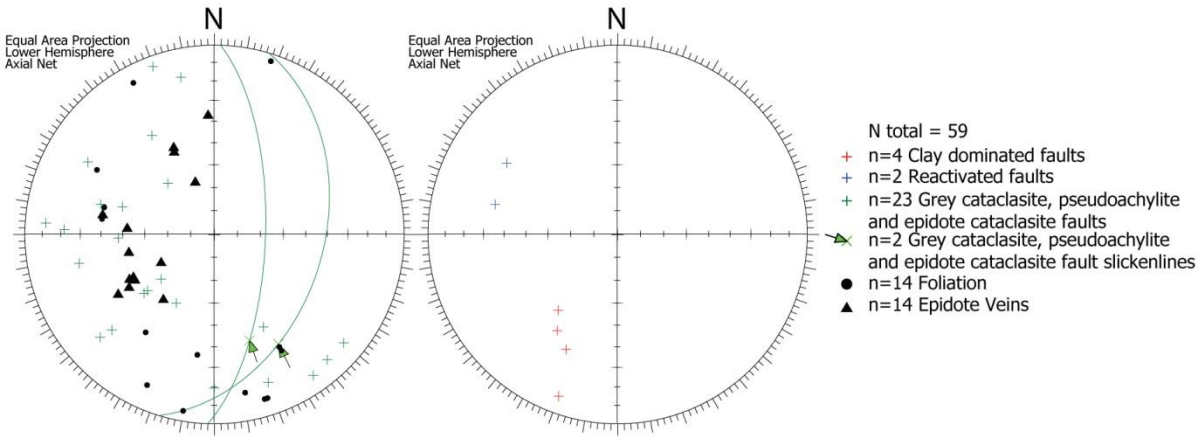

Figure 3.30: Seisiadar North stereonet. Note the spread of the foliation measurements. Dominant NW-SE faulting trend reflects late stage faults associated with clay and carbonate development. Faults with slip data recorded are shown with a great circle in addition to the pole.

3.4.2.1.6 Port Mholair

Port Mholair (NB 56440 35738 to NB 56908 36556) lies in the region identified by the BGS as lying outside the OHFZ (Figure 3.20). Fracturing here is of a lower intensity to that seen elsewhere on the Eye Peninsula and is dominated by jointing. No evidence for kinematic indicators (e.g. slickenlines) was found. The gneiss is composed of banded grey gneiss with bands of Younger Basics up to 20 m wide, and pink and orange gneiss that may be metasedimentary in origin. Foliation is consistently NNW-SSE striking and dips to the east-northeast. Faulting is rarer than elsewhere and is mostly composed of epidote cataclasite faults dipping steeply to the east and NW. However, there are five faults with red-brown clay gouge development and chaotic breccias that cross-cut older structures (Figure 3.31).

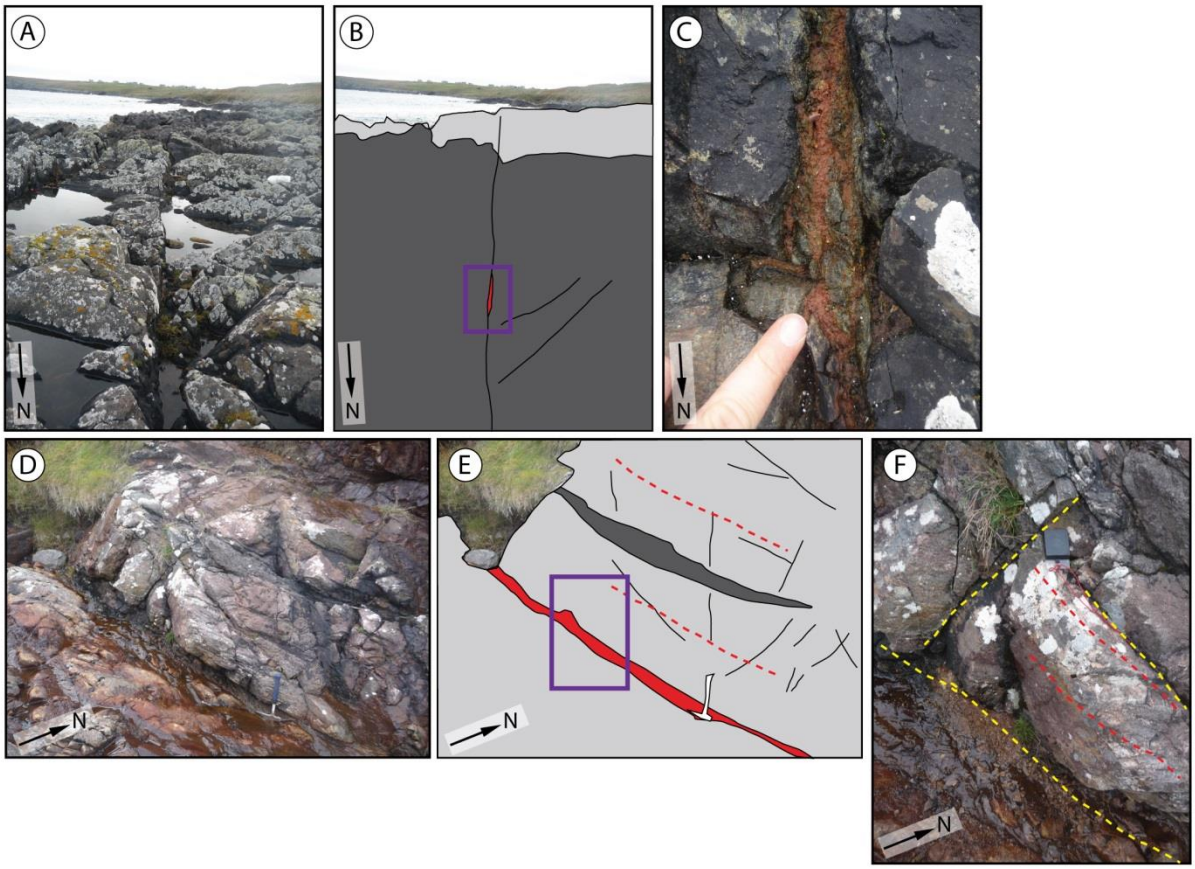

Figure 3.31: Port Mholair exposures. Dark grey = amphibolite, light grey = grey gneiss, red = clay-bearing fault rock, yellow dashed line = fault, red dashed line = foliation. (**A** - **C**) Fault cutting through Older Basic body, with reddy brown gouge and breccia up to 8 cm thick. Clasts of amphibolite within the fault core are altered (**C**). (**D** - **F**) Fault with clay-rich fault rock and breccia, sub-parallel to the foliation. Note presence of sheared Older Basic unit.

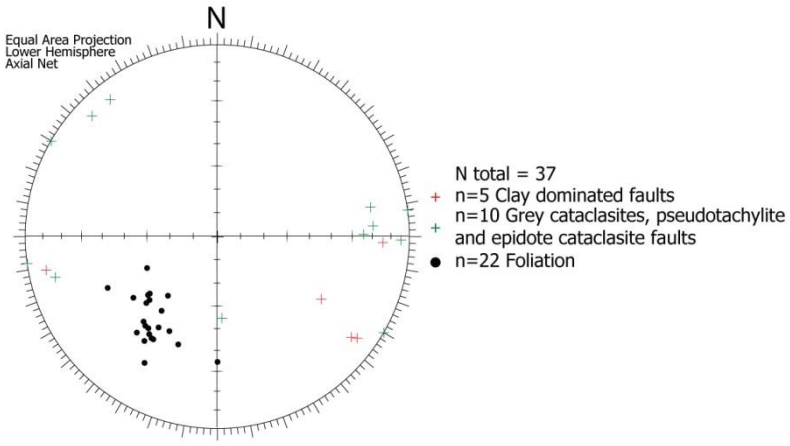

Figure 3.32: Stereonet of data collected at Port Mholair. NE-SW dominant faulting trend is attributable to epidote ultracataclasite faults.

3.4.2.1.7 Suardail

The locality within the Lewisian Gneiss at Suardail (NB 4958 3007) lies immediately adjacent to the basement-cover interface separating the Stornoway Formation and the Lewisian (see Figure 3.42A-C and Figure 3.59A-D). The basement rocks are pink granitic gneisses interleaved with older basic amphibolite units. The foliation generally dips towards the southeast, with clay-bearing faults at a similar orientation (Figure 3.33).

There are 11 faults exposed at Suardail with grey cataclasite and epidote cataclasite/ultracataclasite fault rocks, that show a dominantly NE-SW trend, dipping to the southeast. This is similar to orientations of epidote cataclasite bearing faults observed across the Eye Peninsula. Several faults cut the Stornoway Formation and Lewisian Gneiss. Those that do are dip-slip normal, and associated with brown clay-rich gouges and cataclasites. E-W, N-S and NW-SE trending faults were identified with clay-bearing gouge and cataclasites and normal motions, with up to 5-6 cm of fault rock. There are faults dipping towards the NNE that have very similar slickenline orientations to the main fault, and these are likely to be part of the main fault system.

E-W striking dip-slip faults and NNW-SSE striking normal oblique (dextral) faults (Figure 3.33) are probably related to Set 1 faulting identified within the Stornoway Formation, whilst N-S striking faults may be part of Set 2. Faulting at Suardail is further discussed in sections 3.4.4.1 and 3.5.1.3.

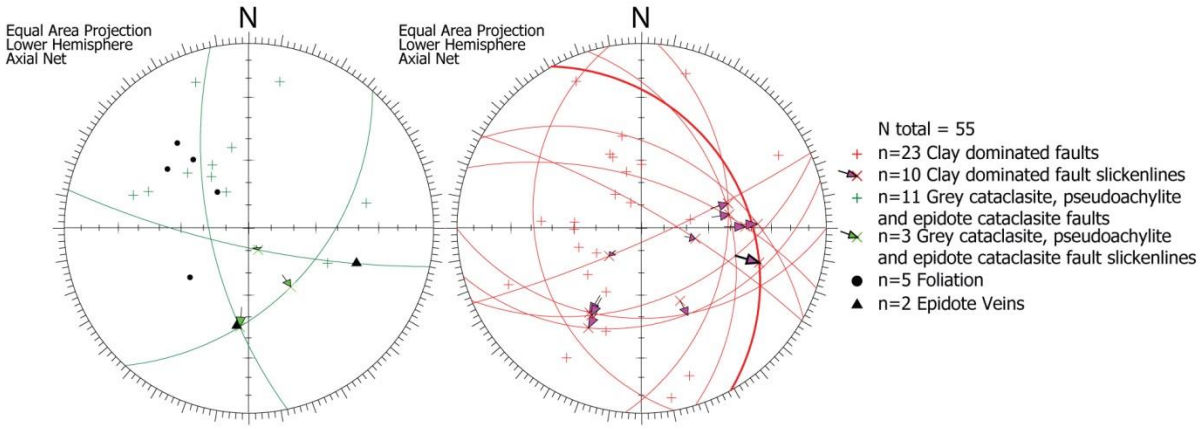

Figure 3.33: Stereonet of data collected at Suardail in the Lewisian. Bold Red great circle and slickenlines represent the orientation and kinematics on the main fault at Suardail that partly forms the Stornoway-Lewisian contact. Faults with slip data recorded are shown with a great circle in addition to the pole.

3.4.2.2 Tob Leireabhaigh and the Memorial Cairn

Tob Leireabhaigh (NB 4255 2999 to NB 4257 2948) and the Memorial Cairn (NB 4254 2988) lie in the region identified as the OHFZ by the BGS (Figure 3.20). Immediately offshore from the area is

the NNW-SSE trending, east-northeast dipping Mesozoic aged bounding fault of the Stornoway Formation, with several hundred metres offset, downthrowing to the east. The area is dominated by faults parallel to this trend and lying in the plane of the local foliation in the gneisses (Figure 3.37). At the Memorial Cairn locality, there are three primary NNW-SSE trending structures (Fault A, B, and C, Figure 3.35) dipping to the east with normal oblique dextral motion indicated by slickenlines and subsidiary fracture sets. There is a clear history of reactivation recorded at this locality, with ductile deformed gneiss cut by epidote ultracataclasite faults, overprinted with later zeolite and carbonate bearing faulting with clay gouge development. The thick zones of gouge and breccia on these faults indicate substantial offset (probably at least 10s of meters) that is localised along the contacts of foliation parallel amphibolite units (Figure 3.35 and Figure 3.36). Principal faults contain up to 5 cm of gouge immediately overlying a relatively unfractured footwall surface, with up to 1 m of chaotic breccia on the hangingwall side of the fault, followed by mosaic and crackle breccias. In addition to the east-dipping normal faults, there are also multiple near vertical faults with an apparent top to the east sense of motion. These may be rotated normal faults.

Fractures and faults are common in Tob Leireabhaigh. The gneiss is generally composed of grey gneisses with pegmatitic veins/granitic areas and rarer amphibolite units, invariably highly sheared and altered (e.g. Figure 3.34A-C). Structural data collected from the area (Figure 3.37) displays a strong dominantly NNW-SSE trending, ENE dipping group of faults with normal oblique dextral offsets, lying generally parallel with the foliation. Most of the faults (>90%) measured are dominated by fault rocks similar to those at the Memorial Cairn, with authigenic clay gouges, zeolite- and carbonate-rich cataclasites. About 10% of the faults display evidence of reactivation, with clasts of brecciated epidote cataclasite found within clay-bearing fault rock. One of these is Fault A, shown in Figure 3.35 and Figure 3.36A-C. Most clay-rich faults are sub-parallel to foliation in the area, localised along the foliation. Epidote cataclasite-bearing faults trend N-S, E-W and NNW-SSE, with the fault surface and fault rock of the fault shown in Figure 3.36A-C clearly containing epidote cataclasite.

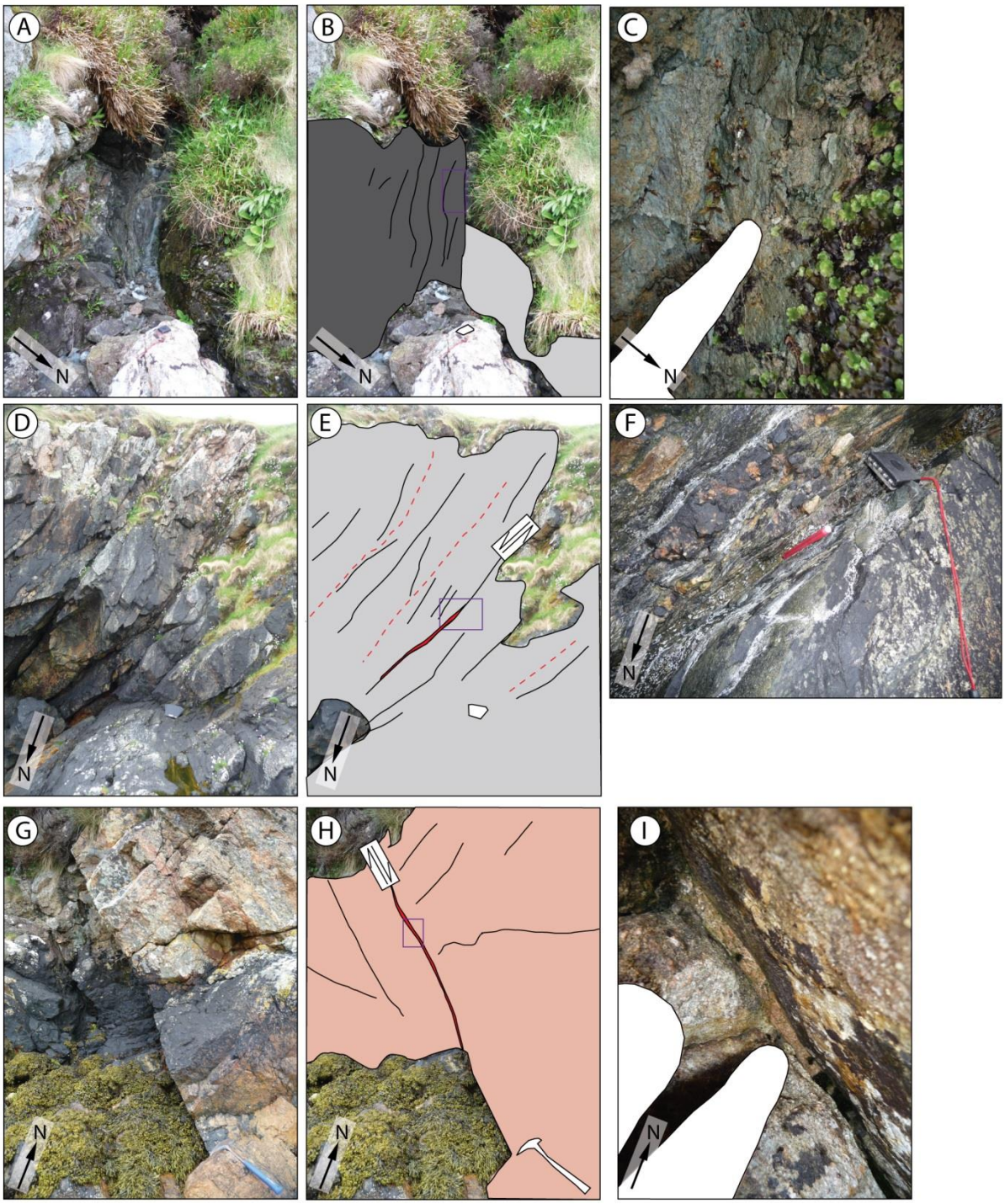

Figure 3.34: Tob Leireabhaigh outcrop images. Dark grey = amphibolite, pink = granitic gneiss, light grey = grey gneiss, red = clay-bearing fault rock, red dashed line = foliation, purple box = area of interest. (**A** - **C**) Very heavily altered amphibolite now comprised dominantly of clay in a zone approximately 60 cm thick; shearing is localised here along this body. (**D** - **F**) Clay-bearing faults localised in the foliation plane; pencil is within soft gouge ~5 cm thick. (**G** - **I**) Clay-bearing fault cuts granitic gneiss, and reactivates the epidote-bearing fault surface.

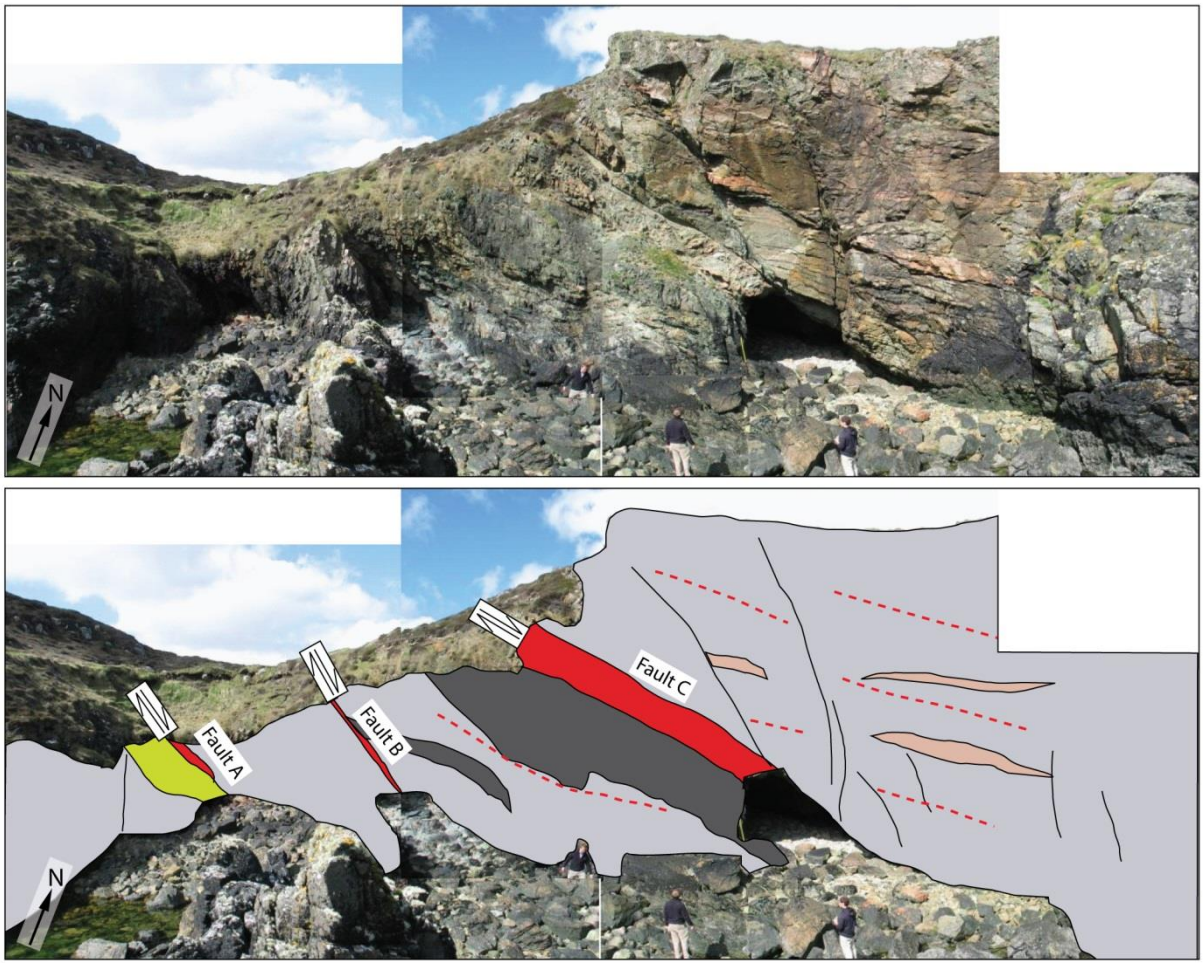

Figure 3.35: Exposure at Memorial Cairn; principal faults provide kinematic indicators (see Figure 3.36). Dark grey = amphibolite, pink = granitic gneiss, light grey = grey gneiss, red = clay-bearing fault rock – gouges and chaotic breccia, pale green = epidote-bearing fault rock, red dashed line = foliation. Note parallelism of foliation and the fault at this locality with the widest zone of fault rock (fault C). Fault A, B and C are shown in Figure 3.36.

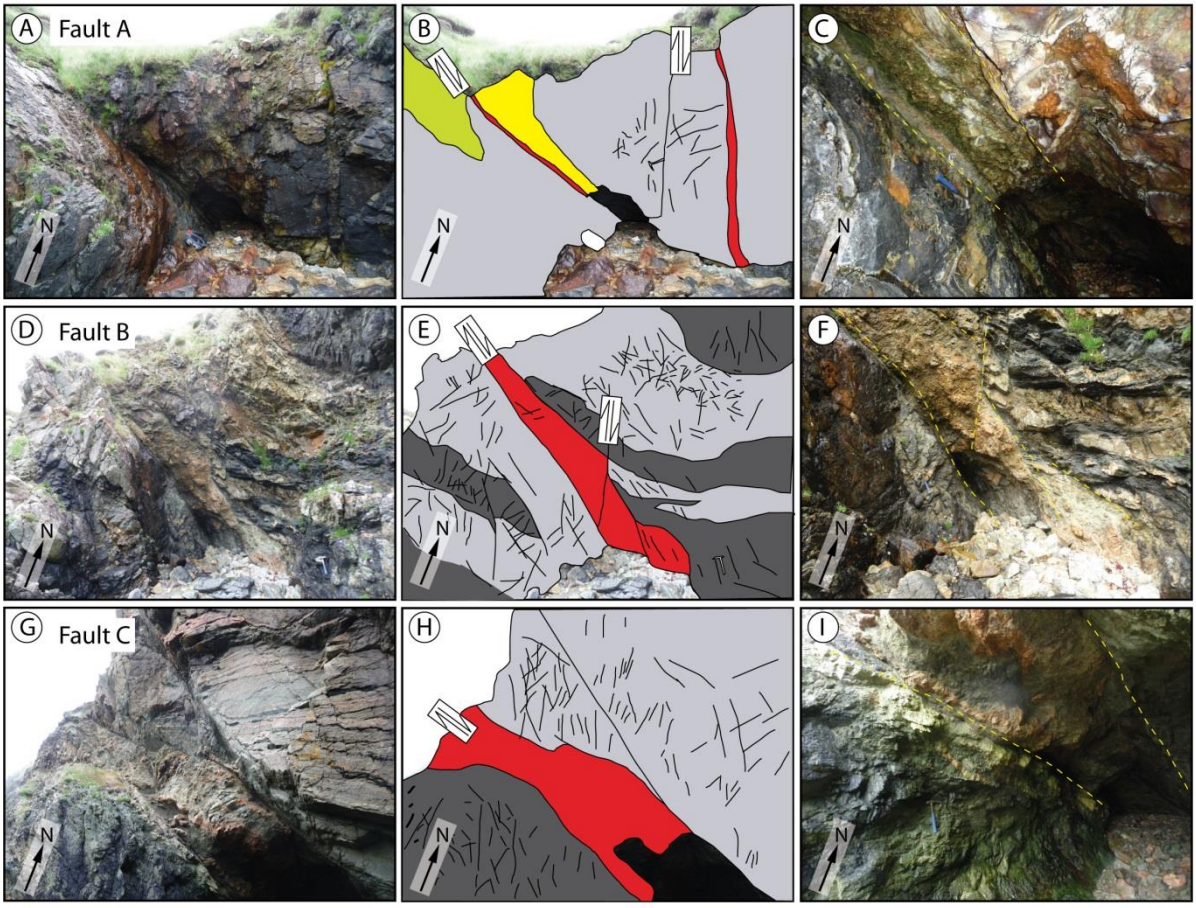

Figure 3.36: Principal faults at Memorial Cairn locality (see Figure 3.35 for locations). Dark grey = amphibolite, pink = granitic gneiss, light grey = grey gneiss, red = clay-bearing fault rock, line green = epidote fault rock, yellow = carbonate cemented breccia, yellow dashed lines = faults. (**A** - **C**) Fault A. (**D** - **F**) Fault B. (**G** - **I**) Fault C. All faults are localised to some extent along the foliation, particularly along weak altered mafic units. Surrounding rock is densely fractured. Note presence of reverse faults closely associated with fault cores of principal faults (e.g. **B** and **E**).

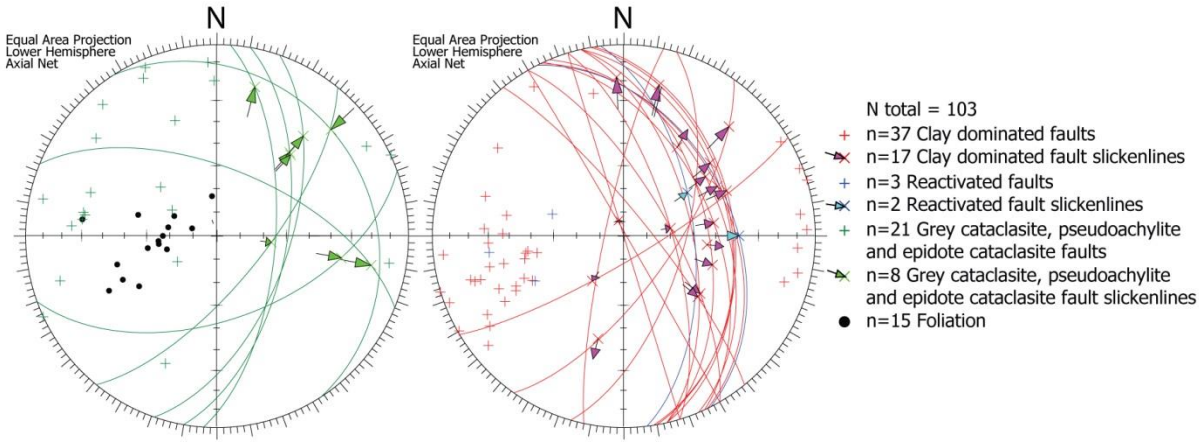

Figure 3.37: Stereonet of data collected from Tob Leareabhaigh and Memorial Cairn localities. Foliation and faults are commonly parallel. Predominant fault trend is NNW-SSE associated with clay development and calcite mineralisation. Faults with slip data recorded are shown with a great circle in addition to the pole.

3.4.2.3 Tolstadh Beach and Gleann Tolstadh

Tolstadh (Beach: NB 5412 4618 to NB 5467 4673, Gleann Tolstadh: NB 5222 4439) lies within the area identified as the OHFZ. The beach where data was gathered is believed to lie in the footwall of a major thrust (Fettes et al., 1992), and hence the gneiss is highly altered and very heavily fractured and faulted to the extent that it is described as 'mashed gneiss', with multiple phases of faulting visible. Thrusts dipping shallowly towards the SE were identified within the mashed gneiss with top-to-the NE motion, cut by clay bearing faults. Forty-seven clay-bearing faults were observed at Tolstadh (e.g. Figure 3.38E – F and G - I), comprised primarily of NNW-SSE trending minor faults associated with calcite mineralisation and brittle low-angle structures dipping to the northeast, southwest and northwest, which are cut by the higher angle NNW-SSE trending faults. These later faults have normal oblique dextral offsets associated with carbonate mineralisation and clay and haematite formation. Brittle low angle extensional structures lie parallel to (and reactivate) the local foliation in ductile-deformed gneisses (Figure 3.38A-C). Fractures reactivate the margins of sheared basic units within the gneiss that are probably altered younger basics (e.g. Figure 3.38D-F). Within the fault cores of these low-angle structures, chaotic breccias and clayey gouges incorporating the surrounding host rock are present, with thicknesses of around 5 cm. These clay bearing low-angle structures may be synchronous with those identified on the Eye Peninsula that often lie along the phyllonitic foliation. Normal kinematic indicators are evident across most clay-dominated faults, with a few low-angle structures displaying reverse kinematics on epidote cataclasite and phyllonite-related slip surfaces. Offsets on these faults are likely to be relatively small due to their relatively small thicknesses, but may be as much as several metres. Clay-rich normal faults probably represent the latest phase of faulting, particularly along NNW-SSE trending normal oblique dextral faults associated with carbonate and minor clay and haematite formation (Figure 3.38G-I), which post-dates earlier epidote veins and related faults (Figure 3.38J-K).

There is some spread in the orientation data (Figure 3.39), but in general most clay-bearing faults are NW-SE trending, dipping to the northeast and southwest, probably indicating a conjugate system related to Set 1 identified within the Stornoway Formation. Also, N-S striking normal-oblique sinistral faults and clay-bearing fault rocks outcrop, which possibly belong to Set 2 identified within the Stornoway Formation based on this orientation and kinematics. Carbonate veining at Tolstadh is quite widespread, again with a spread of orientation data, but one particularly intensely veined area has consistently orientated veins dipping steeply to the NW.

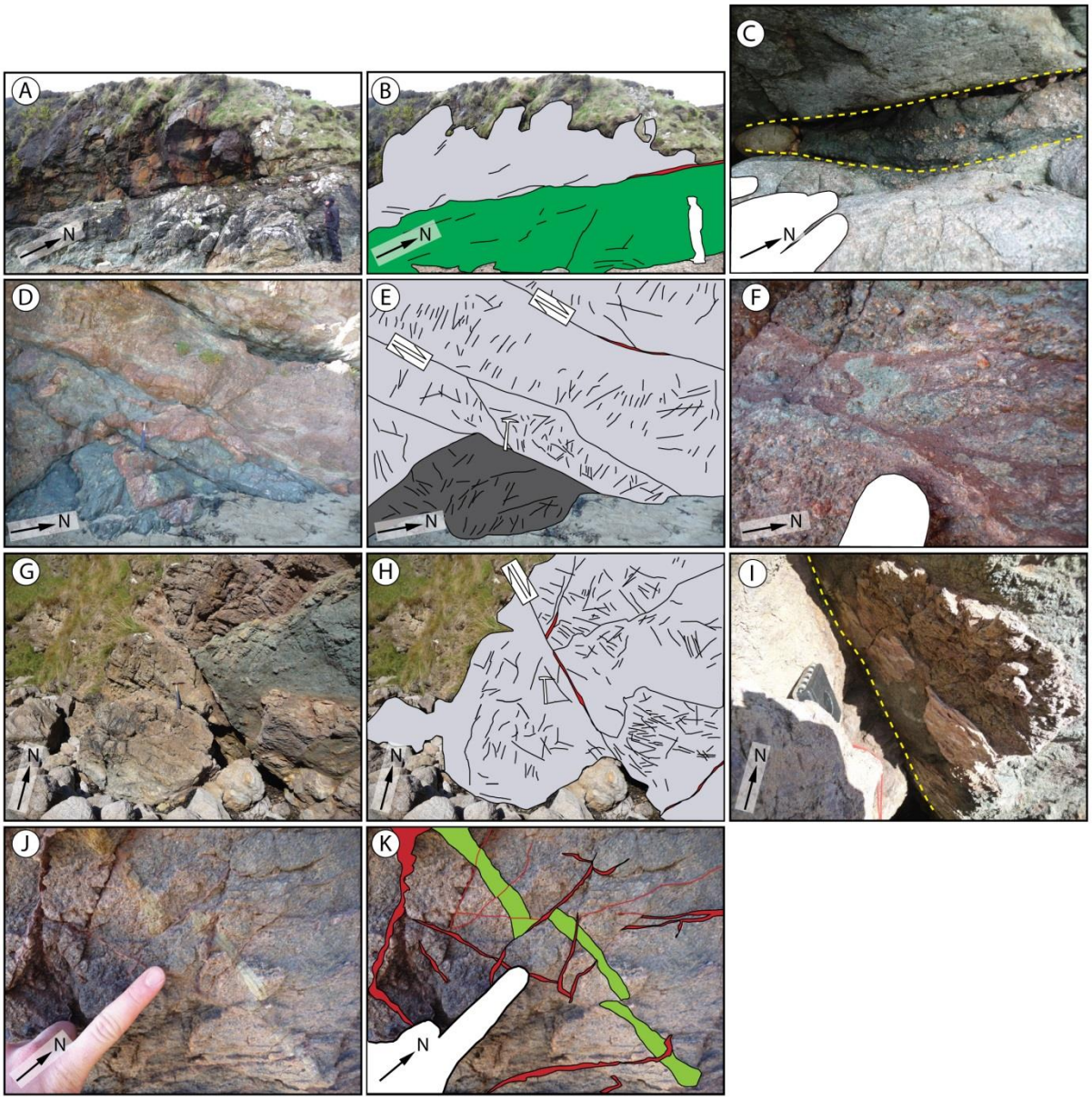

Figure 3.38: Outcrop images of the area around Tolstadh Beach. Dark grey = amphibolite, pink = granitic gneiss, light grey = grey gneiss, red = clay-bearing fault rock, pale green = epidote vein, dark red = haematite/carbonate veining, dark green = protophyllonitic gneiss, yellow dashed line = fault. (**A** - **C**) SW dipping shallow structure with clay-bearing cataclasite/breccia up to 5 cm across, localising along boundary between typical grey gneiss (hangingwall) and densely fractured phyllonitic tectonised gneiss (footwall). Hangingwall surface preserves evidence of earlier epidote faulting. (**D** - **F**) Northward dipping shallow normal faults localised along altered mafic unit boundaries. (**G** - **I**) NNW-SSE trending normal oblique dextral faulting associated with massive carbonate mineralisation (**I**) in the fault core and minor clay and haematite formation. This represents the latest phase of faulting at this locality. (**J** - **K**) Haematite-calcite veins and microfaults associated with late faulting post-date early epidote veining.

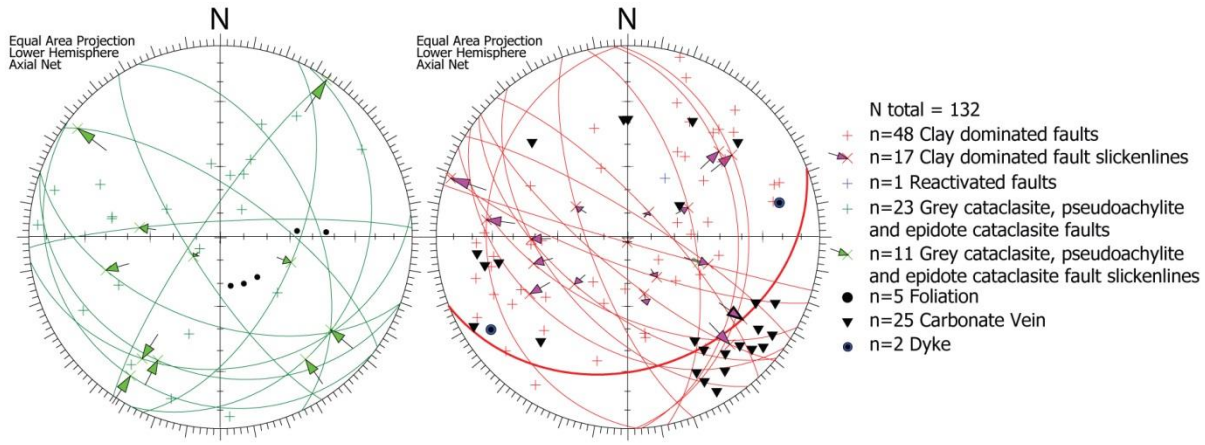

Figure 3.39: Stereonet of data collected at Tolstadh. Bold red great circle indicates the orientation of the bounding fault at Earabhig, with associated slip vector. Predominant fault orientation is NW-SE to NNW-SSE, associated with late stage normal faults (clay-bearing). Faults with slip data recorded are shown with a great circle in addition to the pole.

3.4.2.4 Arnish

The gneiss at Arnish (quarry and road cuttings at NB 4249 3044) is composed of strongly foliated grey gneiss with pods/lenses of pegmatitic/granitic and mafic gneiss, all parallel to the east-dipping foliation. Orientation data is shown in Figure 3.41. The fabric at Arnish is tectonic in origin, displaying W to NW verging folds of approximately 1 m wavelength (Figure 3.40A), which are related to a phase of ductile top-to-the-NW thrust motion that pre-dates brittle faulting. The foliation is concordant with phyllosilicate-rich thrust bands up to 20 cm thick and with remnant altered amphibolite clasts in their cores (Figure 3.40D-F), indicating that these thrusts probably localised along the Older or Younger Basic amphibolite units due to low mechanical strength, with alteration producing the phyllosilicates. Pseudotachylite is also found in bands parallel with the foliation and as high-angle injection veins. Cross-cutting relationships indicate that the pseudotachylite represents the earliest-recorded brittle deformation. Further to the northwest of the verging folds described above, east to southeast verging down-dip folds are superimposed over the foliation, associated with minor normal faulting that followed thrusting (Figure 3.40B-C). These small normal faults have epidote ultracataclasite cores with hangingwalls that are downthrown to the southeast (Figure 3.40G-H). The latest phase of deformation visible at Arnish is an ENE dipping set of normal faults associated with calcite mineralisation and clay development and dense fracturing (Imber, 1998, Figure 3.40I-K). This late phase of faulting could be continuous with some of the faulting described at the Memorial Cairn that lies ~400m SSE of this locality.

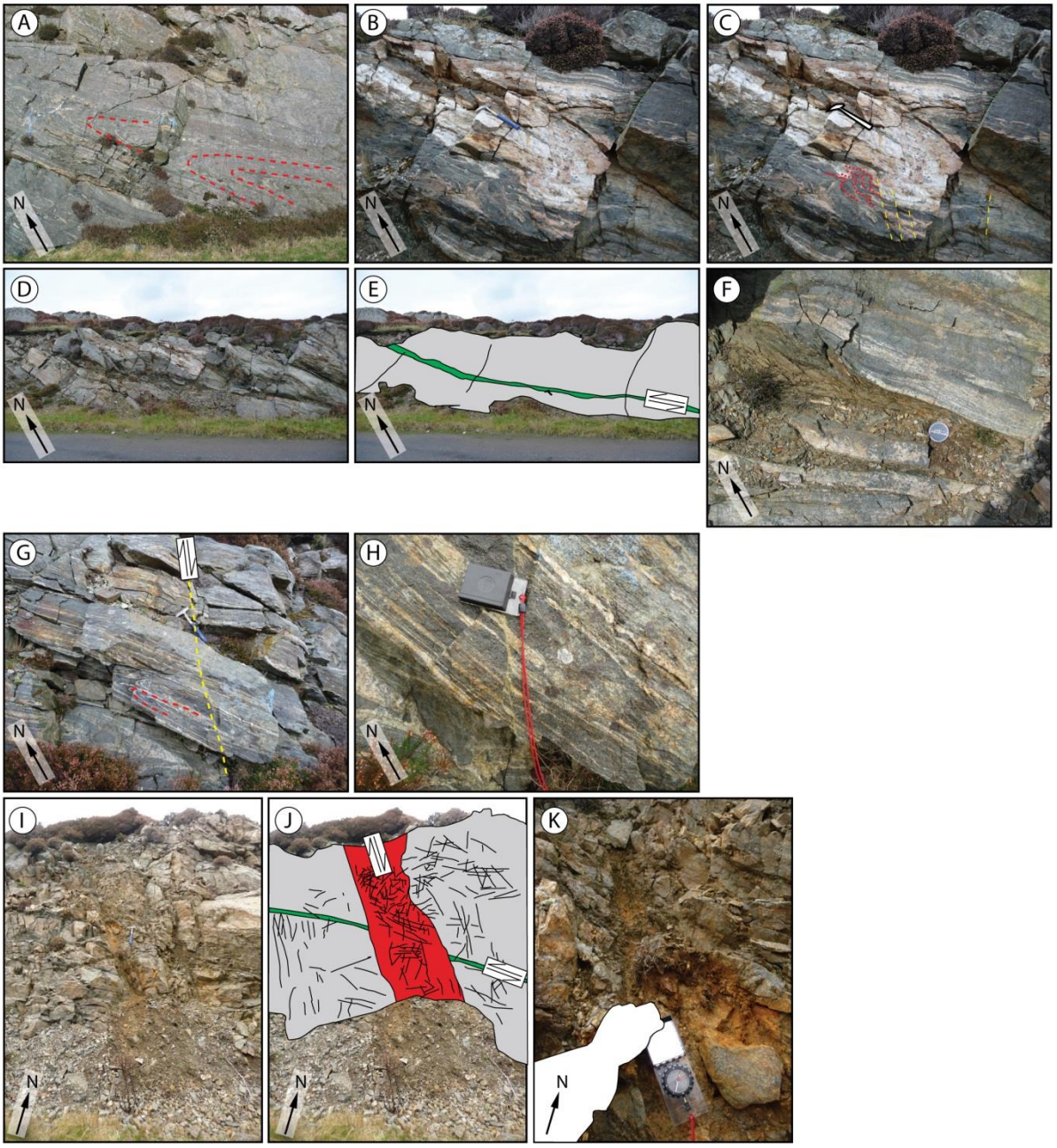

Figure 3.40: Outcrops in the Lewisian at Arnish. Light grey = grey gneiss, red = clay-bearing fault rock, green = phyllonitic gneiss with thrust kinematics, yellow dashed line = fault, red dashed line = foliation. (**A**) NW verging folds in the foliation are consistent with early ductile top to the NW thrusting. (**B** - **C**) Early thrust-related folds are overprinted by SE verging down-dip folds and associated normal epidote cataclasite faults (also **G** - **H**). (**D** - **F**) Low angle top to the northwest phyllonitic thrust parallel with the foliation. Within the thrust, relict clasts of amphibolite are visible surrounded by phyllosilicate material. (**G** -**H**) Epidote cataclasite normal faults: down to the SE. (**I** - **K**) Latest phase of faulting associated with clay development and calcite mineralisation, trending NNW-SSE and parallel with the Minch Fault offshore, and the Memorial Cairn locality faulting (previous section).

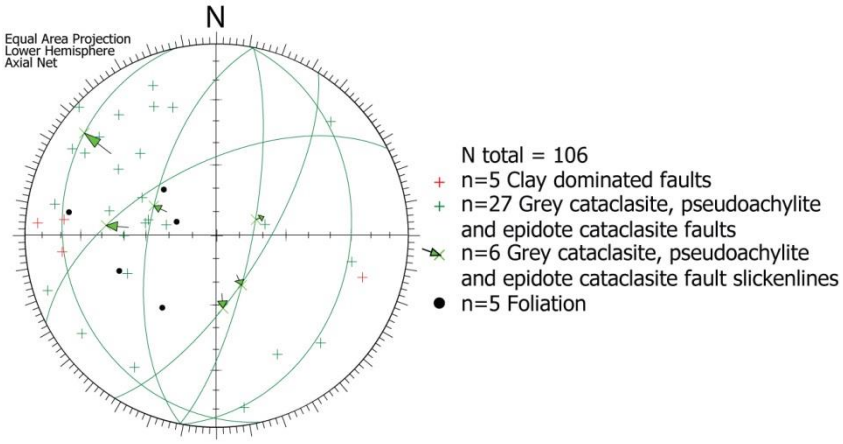

Figure 3.41: Stereonet of data collected from Arnish. Note overall SE dip of faults reflects normal faults with epidote ultracataclasites that post-date thrusting. Faults with slip data recorded are shown with a great circle in addition to the pole.

3.4.3 Summary of Stornoway Region Lewisian Fieldwork

Within the Stornoway region, multiple phases of deformation are evident within the Lewisian Gneiss. From the observations above these can be summarised as (oldest to latest based on cross-cutting relationships observed in the field):

1. Laxfordian shearing and amphibolite facies metamorphism, transposing the younger basics into parallelism with the foliation.
2. Late Laxfordian pegmatite intrusion, which in some locations remains discordant to the foliation.
3. Early widespread shear zones across the Eye Peninsula. Comprised of elongate clasts of country rock wrapped by a discrete interconnected network of phyllosilicates, up to 2 m metres across, and cut by later epidote cataclasite and pseudotachylite-bearing faults.
4. Ductile, top to the NW thrusting, with formation of mylonites.
5. Pseudotachylite formation commonly along the foliation planes, and associated epidote cataclasite faulting.
6. Development of phyllonites with at least one phase of thrust faulting, and associated epidote veins and faults.
7. Post-thrusting epidote cataclasite normal faulting, with down-throw to the SE. Also discrete green detachments surfaces within phyllonites.
8. Eastward dipping normal detachment faulting within and along existing phyllonite boundaries with soft clayey gouge, seen at Seisiadar, and at Pabail cross-cut by later calcite associated NNW-SSE striking faults.
9. Southeast and east -northeast dipping normal faulting associated with clay development and carbonate mineralisation, commonly localising along pre-existing planes of weakness.

May also be associated with conjugate pairs. North-south striking late faults are also observed.

10. Late E-W strike-slip faulting associated with clay development.

3.4.4 Basement-hosted fault rock characterisation

Sixty-eight thin sections were produced from samples obtained from the Lewisian Gneiss of the Stornoway Region with emphasis on identifying the nature and development of fault rocks associated with Mesozoic or younger faults. Fault rocks were characterized in order to compare results within the Lewisian Gneiss and between the Lewisian and Stornoway Formation fault rocks. One example of a fault cutting both Lewisian and Stornoway Formation rocks was examined at the Suardail basement-cover interface as a type locality for Mesozoic or later faulting within the Lewisian Gneiss (Figure 3.42). Epidote veins within the fault have undergone two phases of cataclasis, indicating reactivation of a pre-existing structure originally cemented with epidote and the later phase associated with brown authigenic clay development and zeolite. As this fault cuts the Stornoway Formation, the latest phase of faulting at this locality in the Lewisian is Mesozoic or younger, and so it follows that the faulting associated with brown authigenic clay development and zeolites is Mesozoic/Cenozoic age fault rock. This fault splays as a lateral ramp from the main contact at this locality (see 3.5.1.3).

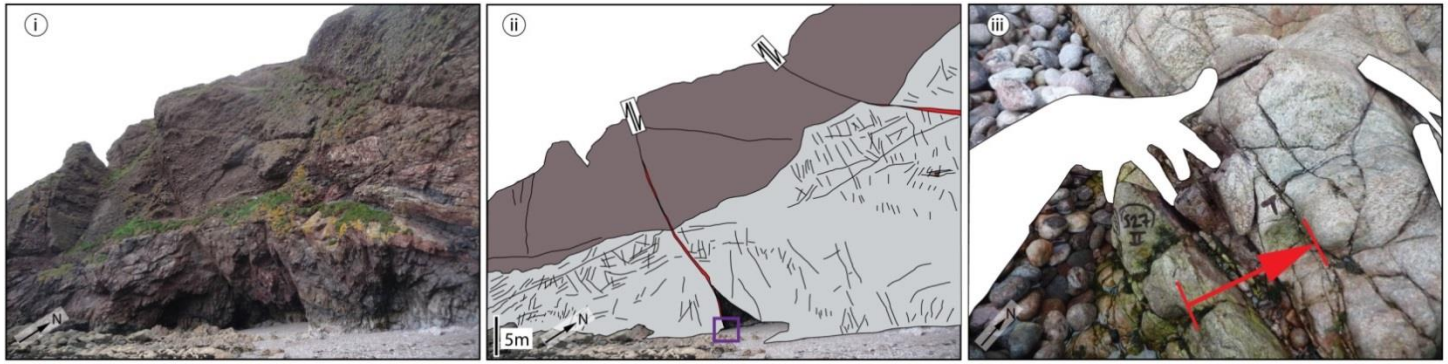
i
ii
iii
N
5m
N
N

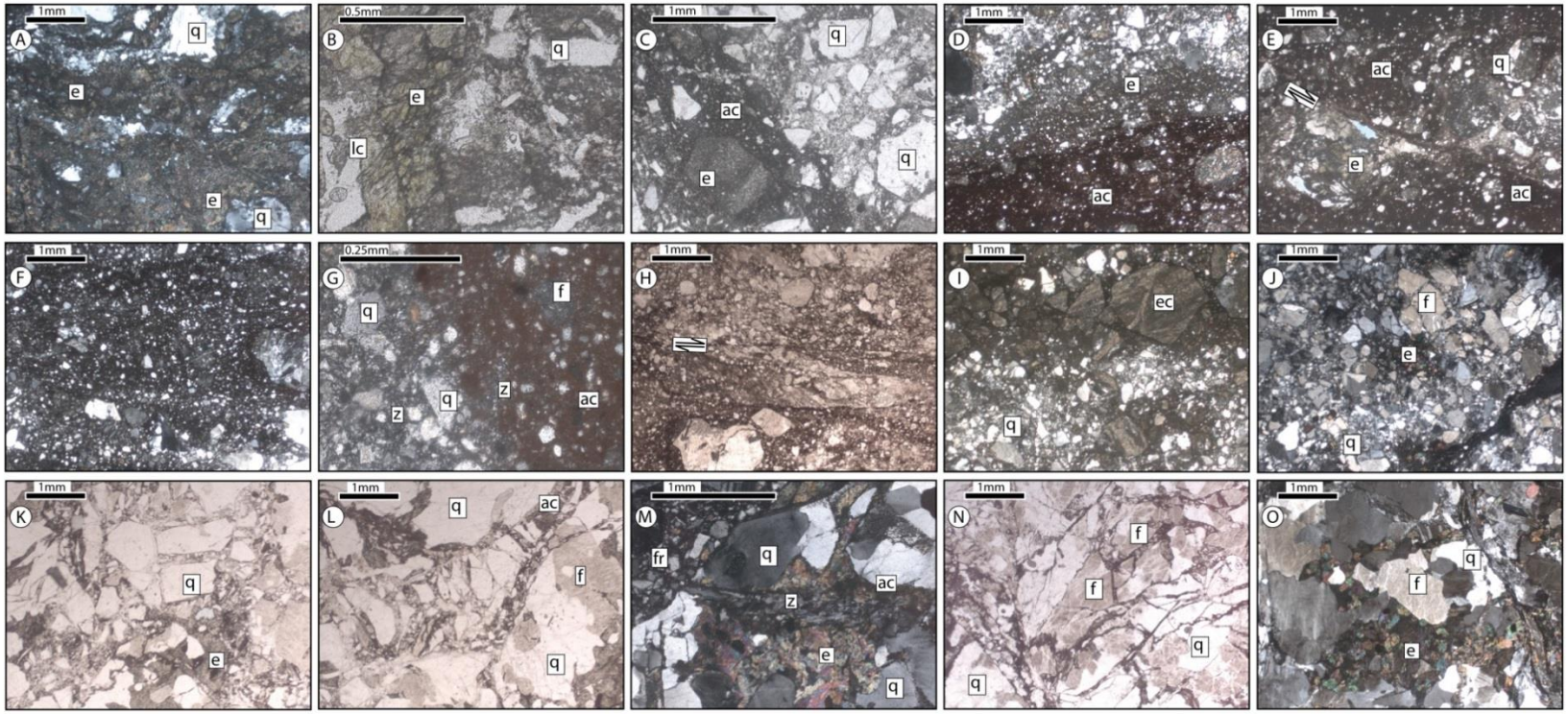
A
1mm
q
e
e
q
B
0.5mm
q
e
lc
C
1mm
q
ac
e
q
D
1mm
e
ac
E
1mm
ac
q
e
ac
F
1mm
G
0.25mm
f
q
z
q
z
ac
H
1mm
I
1mm
ec
q
J
1mm
f
e
q
K
1mm
q
e
L
1mm
q
ac
f
q
M
1mm
fr
q
ac
z
e
q
N
1mm
f
f
q
q
O
1mm
q
f
e

Figure 3.42 (previous page): Setting of Mesozoic fault at Suardail. (**i, ii, iii**) outcrop images. (**i, ii**) Two faults clearly cut both Stornoway Formation and Lewisian basement rocks, indicating that these faults are Mesozoic or younger. Purple box shows position of image iii. (**iii**) Red arrow shows section through fault rock sequence. (**A-N**) Photomicrographs of fault rock samples: (**A**) XPL. Clasts of quartz-epidote reworked within finer grained epidote ultracataclasite. (**B**) PPL. Breccia along epidote vein adjacent to lithic clast, also containing epidote. Quartz is ingrown with epidote, which probably formed at the expense of calcic feldspars. (**C**) PPL. Two breccia sets: RHS shows first phase epidote-cemented breccia of a pre-existing quartz-epidote bearing cataclasite, followed by second phase breccia containing authigenic brown clays that cement lithic clasts. (**D**) XPL. Contact between the latest (Mesozoic or younger) cataclasite high strain zone (bottom of image, with authigenic clays (ac) cementing epidote cataclasite clasts), and earlier epidote-cemented cataclasite (top of image, e). (**E**) PPL. Mesozoic or younger fault rock core. Authigenic clay (ac) supported clasts of quartz (q) and epidote (e) within principal slip zone (offset indicated). (**F**) XPL. Authigenic clay supported quartz, epidote and feldspar clasts in Mesozoic or younger fault rock. Note not as fine-grained as in D (the highest strain zone). (**G**) XPL. Fine-grained cataclasite, with highly altered feldspar. Zeolite occurs alongside authigenic clays and independently (at left), cementing the cataclasite. (**H**) PPL. Fine cataclasite and authigenic clay-rich zone, with normal shear sense indicators. Clasts are quartz and altered feldspar, surrounded by authigenic clay. (**I**) XPL. Clast of epidote ultracataclasite (ec), surrounded by brown clay. Quartz cataclasite (q) lacks clay alteration. (**J**) XPL. Fine-grained chaotic breccia derived from immediately adjacent country rock. (**K**) PPL. Crackle, mosaic and chaotic breccias developed with relative increasing proximity to the principal slip surface. (**L**) PPL. Mosaic and chaotic breccia along fractures within country rock clasts forming a coarse breccia portion of the fault. Minor authigenic clays developed from epidote. Feldspar is altered within large country rock clasts. (**M**) XPL. Zeolite veins within country rock clast. The vein is not continuous into the surrounding fault rock outside the clast (fr). Note also presence of authigenic clays (ac) around rim of zeolite vein. (**N**) PPL. Crackle breccia. Fractures are associated with epidote mineralisation and later authigenic clay alteration. (**O**) XPL. Unfractured country rock, comprised of coarse quartz-feldspar gneiss with partial alteration of feldspar to epidote.

3.4.4.1 Fault rock types

Five principal groups of cataclastic faults have been identified within the Lewisian Gneiss of the Stornoway region. In chronological order (earliest to latest) these are:

1. **Pseudotachylite and early ultracataclasites.** The fault rocks are widespread across the region, and are commonly difficult to distinguish from each other in the field (e.g. Imber, 1998). Both are predominantly associated with early top-to-the-NW thrusting, agreeing with previous observations (e.g. Sibson, 1977b; Imber et al., 2001). Pseudotachylite is visible in outcrop as black to purple-grey aphanitic veins with abrupt margins that are concordant and discordant with the foliation of the surrounding Lewisian Gneiss. Veins of pseudotachylite originate from fault planes and intrude discordantly into the surrounding gneiss (Sibson, 1977b). Pseudotachylite is also commonly seen parallel with foliation and local fault planes (Figure 3.43). In thin section, pseudotachylite consists of ultra-fine grained matrix with clasts of quartz and feldspar up to 1-2 mm across, the quartz displays more angular margins than those associated with feldspar. Margins are abrupt and embayed where pseudotachylite encounters

amphibole or chlorite crystals (Figure 3.43A and E). The fine-grained matrix contains flow structures (Figure 3.43C) and is at times devitrified with spherulite forms (Figure 3.43D).

The early ultracataclasites are similar in appearance to the pseudotachylites, being very fine-grained and extremely well indurated. The 'Mashed Gneiss' of the OHFZ is associated with movement on pseudotachylite-bearing faults (Fettes et al., 1992; Stevens, 1914; Coward, 1972; Macinnes et al., 2000), and is seen in the Stornoway region in the hangingwall of a major thrust. These are zones of intense crushing residing in the hangingwalls of large scale thrusts. In some cases, cataclasites clearly pre-date the formation of pseudotachylite. For example, in Figure 3.43E pseudotachylite veins truncate a chlorite-bearing, very fine-grained cataclasite that is shown in Figure 3.43F. The proximity of these two fault rocks may indicate that the pseudotachylite formed along pre-existing cataclasite-bearing fault (e.g. Passchier and Trouw, 1996). No porosity is seen within this fault rock type. Figure 3.43G-H shows high-resolution BSEM images of pseudotachylite. The very fine nature of the rock is clearly visible, with later adularia and authigenic clay formation.

Pseudotachylite is generally accepted to form at depths in the crust deeper than most other cohesive and incohesive brittle fault rocks (e.g. Sibson, 1977a; Passchier and Trouw, 1996). Fettes et al. (1992) estimate a depth of 13.5 km for the formation of pseudotachylite within the OHFZ of east Lewis, and Sibson (1975) suggests a minimum depth of formation of 5 km. In eastern Lewis, pseudotachylite veins and faults are cut and overprinted by epidote cataclasites. Ar-Ar dating undertaken on these fault rocks across the OHFZ (Kelley et al., 1994; Sherlock et al., 2009) have given ages of 430 ma and earlier Proterozoic dates, the latest of which are generally thought to result from Caledonian top-to-the-NW thrusting (e.g. Macinnes et al., 2000). The pseudotachylite cuts chlorite bearing cataclasites. Chlorite forms at temperatures >120°C in hydrothermal systems (e.g. Reyes, 1990) and it seems likely that it formed at considerable depth, given that it is cross-cut by pseudotachylite.

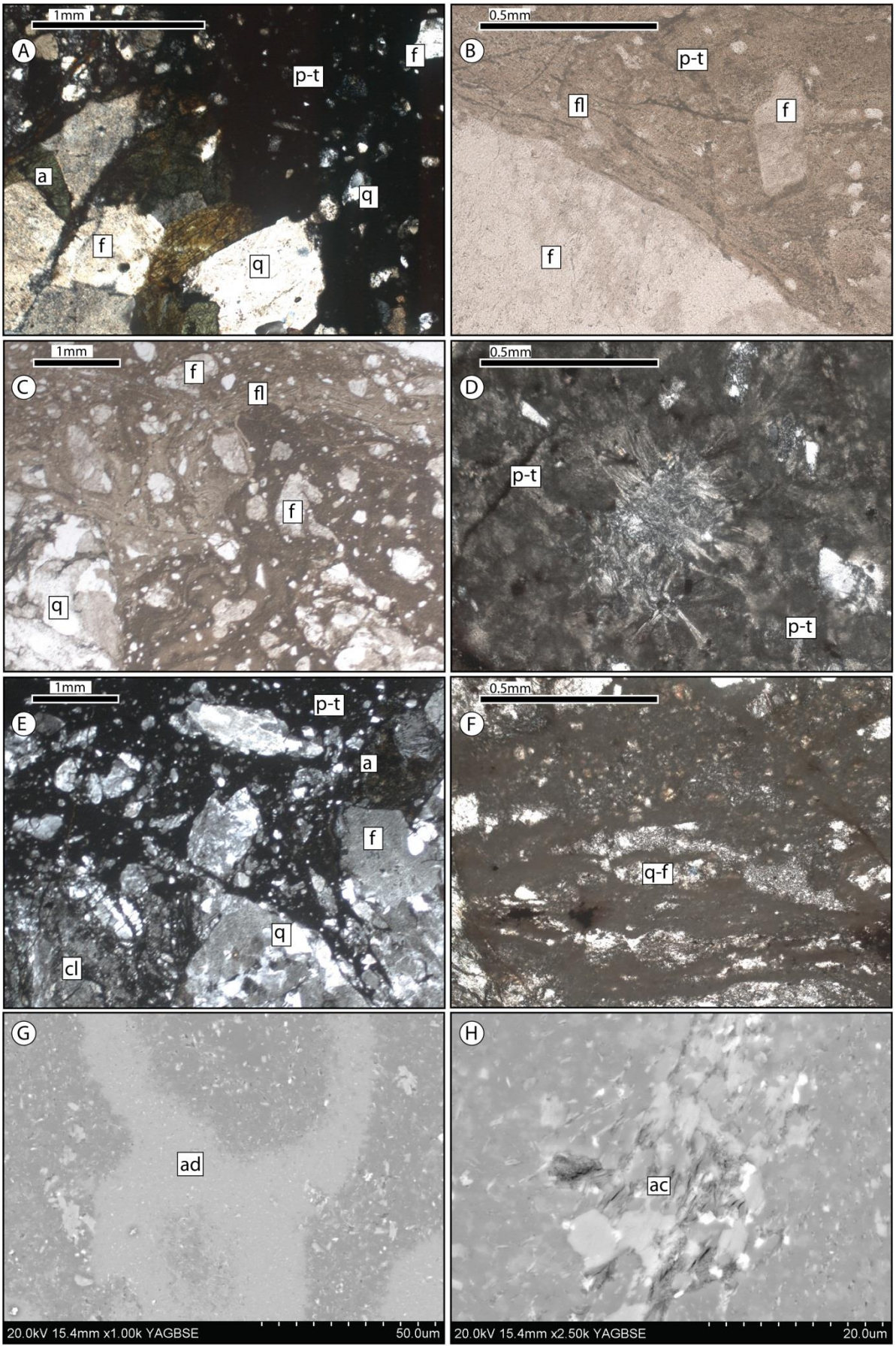
1mm
A
p-t
f
a
q
f
q
0.5mm
B
p-t
fl
f
f
1mm
C
f
fl
f
q
0.5mm
D
p-t
p-t
1mm
E
p-t
a
f
q
cl
0.5mm
F
q-f
G
ad
20.0kV 15.4mm x1.00k YAGBSE
50.0um
H
ac
20.0kV 15.4mm x2.50k YAGBSE
20.0um

Figure 3.43 (previous page): Group 1 fault rocks, all from Pabail South. Pseudotachylite-bearing faults. (**A**) XPL. Pseudotachylite contact with amphibolite wall rock. Note ill-defined boundaries with amphibole clasts (a), and angular well-defined contacts with quartz (q). p-t = pseudotachylite. (**B**) PPL. Abrupt wall-rock contact with subtle flow structures (fl). Feldspar is altered with rounded margins. (**C**) PPL. Flow structures (fl) within pseudotachylite. (**D**) PPL. Devitrification structures visible within pseudotachylite with acicular spherulitic forms. (**E**) XPL. Pseudotachylite (p-t) truncates a chlorite-bearing cataclasite (cl) and incorporates feldspar (f), quartz (q) and amphibole (a) grains. (**F**) XPL. Chloritic cataclasite from E. Very fine quartz-feldspar aggregate. Grain size is not uniform, and embayed margins indicate a degree of recrystallization. (**G**) BSEM image. Pseudotachylite with ring-like adularia-rich zoning. (**H**) BSEM image. Late authigenic clay alteration of pseudotachylite groundmass.

2. **Epidote cataclasites and ultracataclasites**. These faults are very widespread and occur in areas that are outside the region interpreted by the BGS to be the OHFZ. They occur in multiple fault sets with both normal and reverse kinematics. Epidote-bearing faults are indurated and usually appear in the field as discrete surfaces with a veneer of fine-grained epidote or cataclasite seams 1-2 cm thick. In thin section, epidote-bearing faults can also have a dispersed zone of well-cemented epidote breccia in the wall rock (e.g. Figure 3.44A-D). These two different styles of faulting are probably attributable to different fracture sets and differing conditions of faulting that have not been distinguished here. Well-developed epidote-bearing fault zones often occur as dual slip surfaces separated by a core of brecciated rock 0.5-1.0 m thick.

   Epidote-bearing faults cross-cut pseudotachylite structures in eastern Lewis (e.g. Figure 3.44). Epidote alteration within the gneiss country rock is linked with epidote-bearing veins and faults, indicating conditions at the time of faulting and post-faulting are sufficient for epidotisation of feldspars and amphiboles in the surrounding gneiss.

   Figure 3.44E-H are taken from a discrete epidote-bearing fault, more clearly composed of epidote crystals at lower magnification. The angular nature of these crystals and their random orientations suggests that the fabrics of these fault-rocks originated from post-tectonic grain growth. This is confirmed by euhedral epidote crystals observed locally growing into vug-like pore space, with the remainder of the porosity entirely cemented with quartz. As can be seen in Figure 3.44E, multiple high strain slip surfaces are present and represented by a fining of the crystal size towards and within them, indicating that these faults can record a complex history of slip and mineralisation. Adularia veining is visible post-dating epidote faulting and veining (see below), with a later adularia vein visible in Figure 3.44F. At higher magnification (Figure 3.44G-H), the epidote is visible as crystalline clasts with some very minor fracturing. Quartz clearly infills pre-existing porosity and fining of epidote crystals towards the high strain slip surfaces is visible.

The widespread presence of epidote suggests temperatures and pressures generally greater than those of later zeolite and authigenic clay-bearing faults with temperatures above 200°C (Liou, 1993), and hence if a normal geothermal gradient of 30°C km^{-1} is assumed, the samples are representative of faulting deeper than 6-7 km. Formation depths of close to 10 km have been suggested for epidote cataclasites within Norwegian Caledonides (Fossen and Hurich, 2005). If the geothermal gradient is raised during formation, the position of stability of epidote would have been closer to the surface. In places, epidote-bearing faults are linked to phyllonites that have been interpreted as Caledonian in age (Imber et al., 2001).

Reactivation of epidote cataclasite faults by later faulting is common. The fault shown in Figure 3.44A-D is reactivated with a light brown thin (<1 cm thick) gouge, with normal kinematics identified from steps on the hangingwall surface.

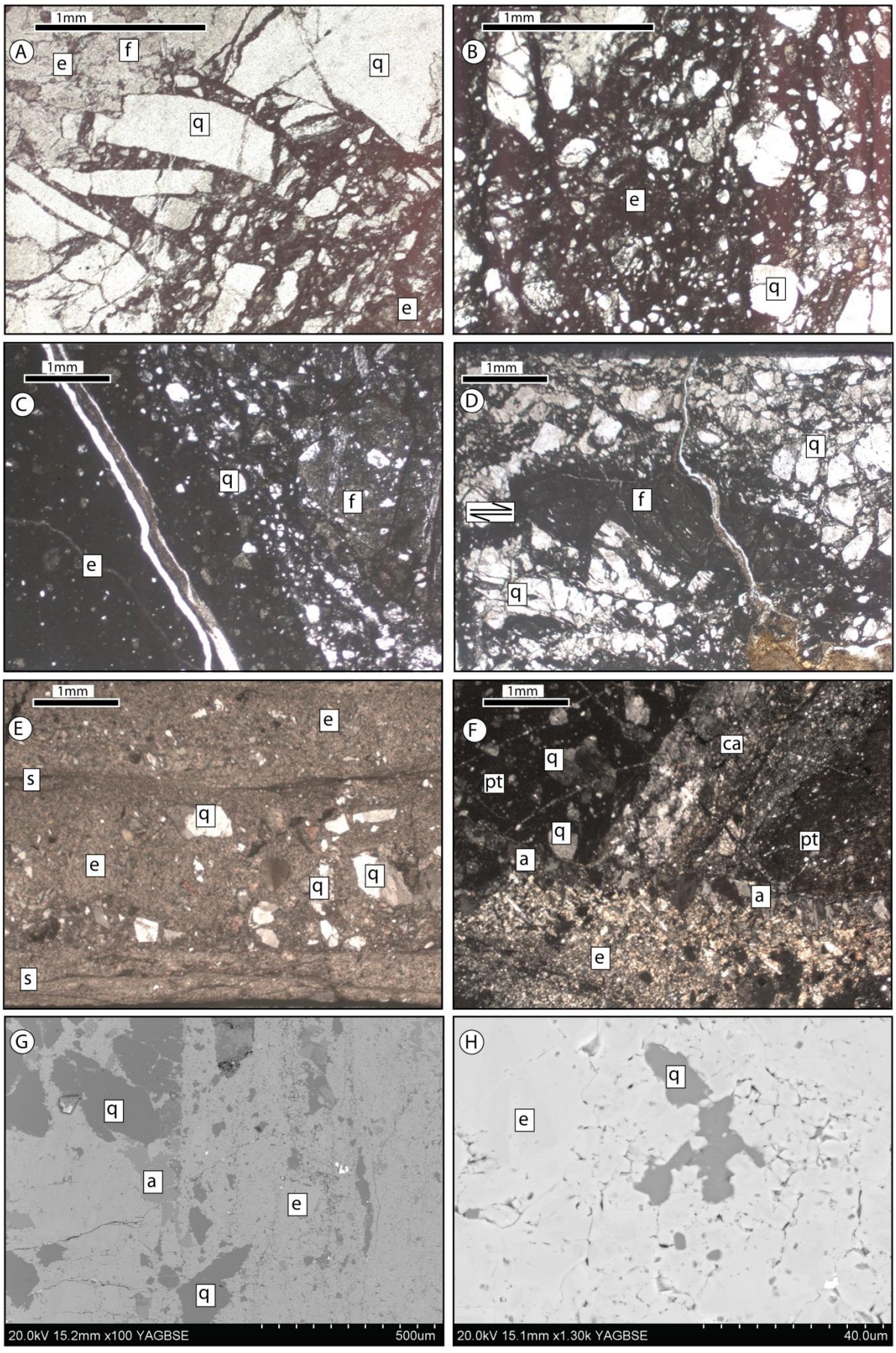
A
1mm
e
f
q
q
e
B
1mm
e
q
C
1mm
q
f
e
D
1mm
q
f
q
E
1mm
e
s
q
e
q
q
s
F
1mm
ca
q
pt
q
pt
a
a
e
G
q
a
e
q
20.0kV 15.2mm x100 YAGBSE
500um
H
q
e
20.0kV 15.1mm x1.30k YAGBSE
40.0um

Figure 3.44 (previous page): Epidote-cemented fault rocks (Group 2 faults). (**A**) PPL. (From Tob Leireabhaigh) 2.5 cm from fault surface, quartz-feldspar mosaic to chaotic breccia. Feldspar (f) is altered to sericite and patches of epidote (e). The quartz (q) is polycrystalline and highly strained, representing earlier ductile deformation. (**B**) (From Tob Leireabhaigh) PPL. 0.7 cm from fault surface, clasts of quartz and feldspar are surrounded by a matrix of very fine epidote. (**C**) (From Tob Leireabhaigh) PPL. 0.3 cm from fault surface: the boundary between matrix supported micro-breccia (right, seen in B) and very fine-grained cataclasite (at left of image). Very fine matrix is composed entirely of epidote (e) with alteration to clays in places. Feldspar is heavily altered (f). (**D**) (From Tob Leireabhaigh) PPL. Domino-faulted altered feldspar clast, showing reverse shear sense. Feldspar is mostly altered to very fine epidote. (**E**) (From Pabail North) PPL. Fine-grained epidote cataclasite, supporting clasts of quartz, epidote, and strained quartz clasts. Multiple slip surfaces are highlighted by darker bands of ultrafine epidote cutting E-W across the image. (**F**) (From Pabail North) XPL. Epidote cataclasite (e) cuts pseudotachylites of at least two distinct phases (pt) and a quartzo-feldspathic cataclasite (ca). Quartz within the pseudotachylite is rounded (q). The margin of the epidote body has been reactivated by an adularia vein associated with porosity and probable Na-stilbite. (**G, H**) (From Pabail North) BSEM images of epidote cataclasite, showing very little pore space. Epidote (e) appears crystalline, with some areas exhibiting minor fractures (visible in H).

3. **Pumpellyite/clinozoisite fault rock**. This fault rock was encountered within a single fault cutting an amphibolite at the Memorial Cairn locality in the footwall of Fault A (Figure 3.35, Figure 3.36, photomicrographs shown in (Figure 3.45). The pumpellyite mineralisation clearly pre-dates zeolite (Figure 3.45B), carbonate and authigenic clay formation associated with later fault movements. In Figure 3.45A, lithic clasts of amphibole, altered feldspar, and epidote are surrounded with haloes of pumpellyite mineralisation. The large crystal sizes associated (up to 0.5 mm across) indicate post-tectonic grain growth, or syntectonic mineralisation associated with high velocity fluid flux through the rock (S. Cox, 2011, pers. comm.). In the surrounding country rocks, amphibole is partly altered to epidote, supporting the occurrence of this pumpellyite mineralisation postdating the formation of epidote. SEM analysis shows pumpellyite alongside adularia, albite, and authigenic clay of near chloritic composition, possibly formed as a result of chlorite alteration, and suggesting P-T conditions above those associated with zeolite mineralisation; the presence of pumpellyite alongside chlorite is common within the prehnite-pumpellyite facies (Deer et al., 1992). Hence, the conditions of formation of this fault rock are tentatively assigned to the Prehnite-Pumpellyite facies, with temperatures in the range of 200-300°C and pressures from 2-8kbar (Best, 2003), suggesting a minimum depth in the crust of around 6 km.

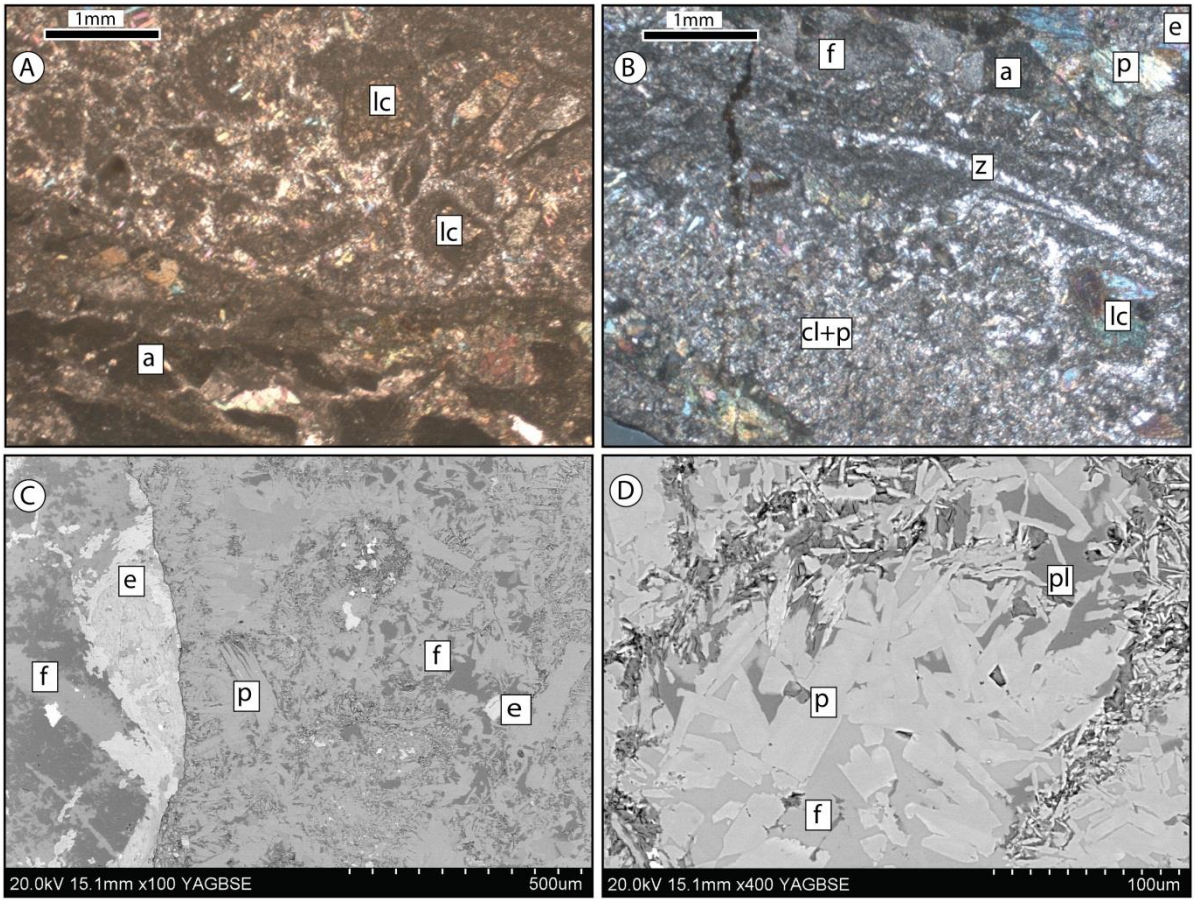

Figure 3.45: Pumpellyite/clinozoisite-bearing fault rock (Group 3 fault rock), all from Memorial Cairn. (**A**) XPL. Pumpellyite-mineralised breccia, composed of lithic clasts (lc) of mainly amphibole surrounded with pumpellyite haloes. Amphibolite country rock is composed of amphibole (a) and altered sericitised feldspar. Several phases of fault rock are visible with multiple fault rock boundaries. (**B**) XPL. Same slide as A, mineralised fault breccia with later zeolite veining (z). Country rock is amphibolite, with altered amphibole (a), and sericitised feldspar (f). Amphibole appears to be altered to pumpellyite (p) and epidote (e). Fault rock contains lithic clasts of mainly amphibole (lc). Main mass of fault rock is clinozoisite and pumpellyite with (cl+p) albite and adularia below the resolution of optical microscopy. (**C**) BSEM image of fault rock/wall rock interface. Wall rock is composed of epidotised amphibole (e) and albite and k-feldspar (f). The fault rock is composed of masses of pumpellyite laths with contemporaneous albite , k-feldspar, and clinozoisite, surrounding clasts of epidote and amphibole derived from the wall rock. (**D**) BSEM image. Fault rock shown in C at higher magnification. Laths of pumpellyite are surrounded by albite (pl) and k-feldspar (f).

4. **Zeolite-filled fractures**. Zeolite has been identified through optical microscopy, although the specific zeolite species could not be determined. The presence of zeolite mineralisation along faults in the basement differs from that observed in the cover, with complex and extensive zeolite veining associated with fractures up to 1 cm away from the fault surface (e.g. Figure 3.46E). This is in addition to zeolite cemented breccias and cataclasites that are also found within the basement. Figure 3.46 shows optical microscope images of several phases of zeolite-filled fractures, often associated with porosity, appearing in the field as pink to light

grey veins up to 2 mm thick. Zeolite crystals show euhedral terminations inward from the vein walls, indicating growth into fluid-filled pore spaces. These fills are post-dated by authigenic clay development (see below) - in Figure 3.50B clasts of zeolite-cemented breccia are entrained within later authigenic clay-cemented breccia. Zeolite commonly forms a fine-grained matrix within fault cores, cementing fault rocks similar to fault rocks within the Stornoway Formation, and is commonly associated with calcite (e.g. Figure 3.46C and D) and open pore spaces (here termed 'vuggy porosity'). Calcite is typically dispersed across the centre of zeolite veins (Figure 3.46D) over several mm, yet still possesses parallel extinction. Serrated margins on some of the calcite crystals within these veins indicate dissolution, which may contribute to the observed porosity, and this may have facilitated zeolite crystallisation. However, the presence of calcite in the centre of veins, rimmed with zeolite would suggest that zeolite mineralisation pre-dates that of calcite. In an isolated example, sparry calcite is seen entirely enclosing zeolite crystals. Hence, several phases of calcite may be associated with pre- and post-zeolite mineralisation. Zeolite in one slide is clearly composed of several phases (Z1 and Z2, Figure 3.46E-F). Z1 is comprised of colourless crystals generally 0.05 mm across, whilst Z2 is associated with oil staining, a greater amount of porosity and larger crystals up to 0.1 mm thick that have clear radial extinction patterns.

Open pore space is consistent with a low temperature/low pressure origin of these veins - i.e. P/T conditions were low enough for porosity to remain open, presumably as fluid filled cavities.

Zeolites are commonly associated with a volume increase relative to the primary dominant feldspar minerals within a rock (e.g. Weisenberger, 2009). Porosity formation may be associated with another process such as tensile fracturing or zeolite-precipitating fluids may have led to dissolution of calcite.

Brown staining (possible oil) is seen along open undulatory fractures and along porous Z2 veins seen within one sample and is very similar to fractures with oil-staining observed in samples from the Clair Field. This potential oil staining has been observed in five samples, and in particular two samples from Seisiadar South, the closest onshore position to the Minch Fault (Figure 3.20). Oil staining and flow may be synchronous with Z2 veining or may post-date it, i.e. it is the latest mineralisation observed.

Adularia is pure K Feldspar found in low temperature veining (e.g. Steiner, 1970; Halliday and Mitchell, 1976), and can form at depths lower than or alongside analcime (zeolite) in burial diagenesis and hydrothermal systems (Goodwin, 1973; Hay, 1978). Adularia-bearing fractures

and fault rocks are also associated with zeolite mineralisation and also authigenic clays. Figure 3.47 and Figure 3.48 show optical microscope and BSEM images of adularia/zeolite/authigenic clay-bearing fracture infills and fault rocks. Images in Figure 3.48 are taken from the same fault rock as Figure 3.47A-B and Figure 3.47E-F, from a fault rock taken from a NW-SE striking fault with vuggy porosity up to 5 mm wide in the fault core visible in the field. These images show that authigenic clay formation and adularia veining appear to be contemporaneous, with a mutually cross cutting relationship that is synchronous with the faulting. In Figure 3.47C- D, fine grained adularia, zeolite, and authigenic clay are injected into the surrounding country rock from the fault plane.

As can be seen in Figure 3.47A-B and E-F, grain size is again very fine and nearly unresolvable with an optical microscope, with grain sizes less than 0.05 mm across. In the BSEM images (Figure 3.48), the syntectonic nature of the authigenic clay is clearly visible, with blades of iron-rich possibly smectitic clay uniformly aligned parallel with the fault surface and wrapping fault clasts (Figure 3.48A-B). Figure 3.47E-F and Figure 3.48C-F show porosity associated with these adularia-rich faults. Similar to the zeolite-bearing rocks in Figure 3.46, euhedral crystals indicate growth into pore spaces, in this case adularia with possible albite and zeolite, and authigenic clay mineralisation. It seems likely that, given the syn-tectonic origin of adularia, zeolite, and authigenic clay, that there is also a syn-tectonic origin for the production of this porosity, likely related to extensive fluid flow within the rock. Oil seen within these fault rocks is mostly associated with brecciation of the country rock, and hence it seems unlikely that these are near-surface oil-like seeps originating from the Holocene peat cover, rather than oil that was present during fracturing. It is interesting to note that oil has been observed in thin sections derived from six fault rocks at five localities, each of which is within, or immediately adjacent to major faults in the region (Figure 3.51).

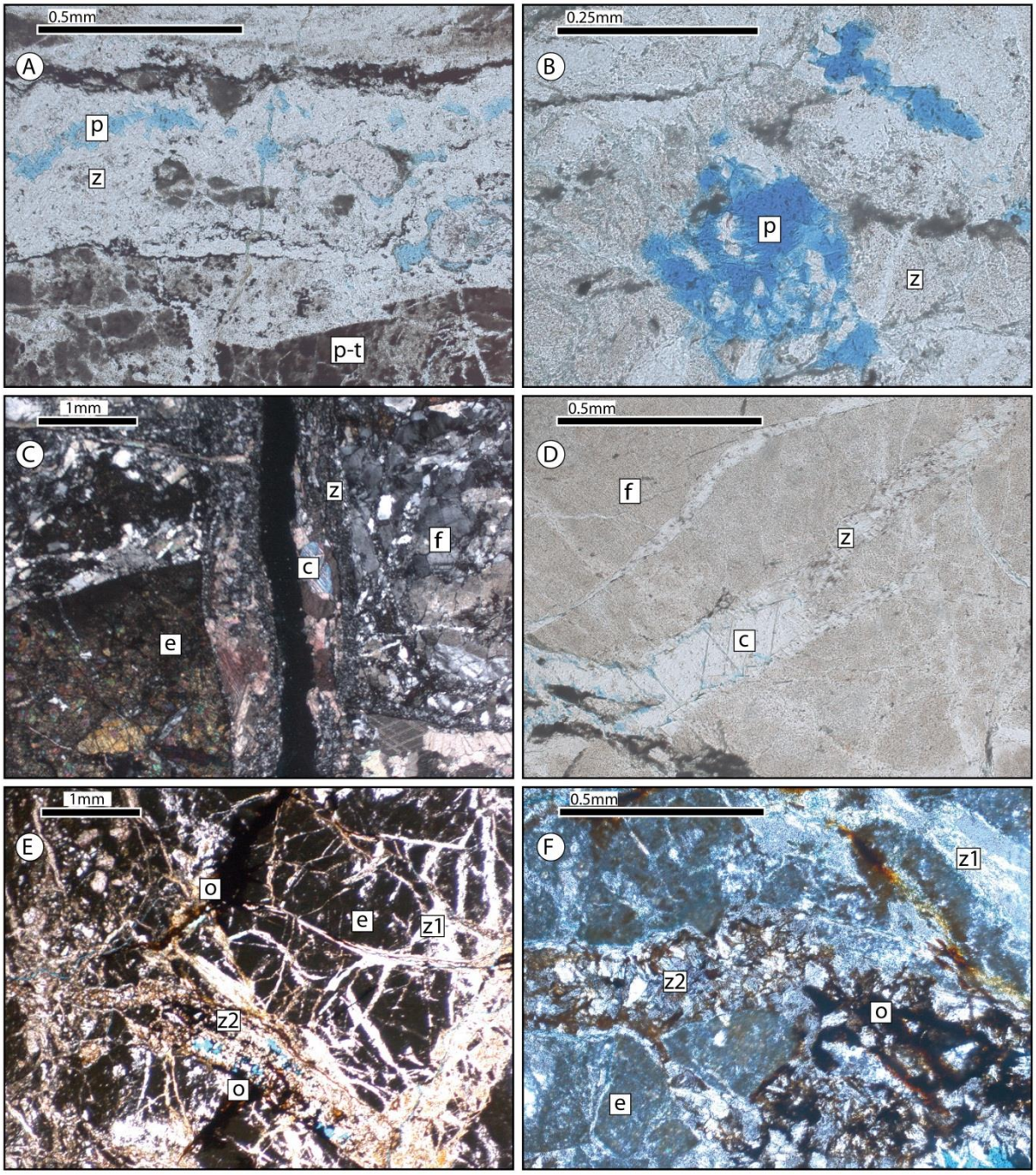

Figure 3.46: Zeolite bearing faults, lacking adularia and albite (Group 4 fault rocks), all from Seisiadar South. Several phases of zeolite veining are evident, with the latest phase associated with hydrocarbon staining. (**A** and **B**) PPL. Zeolite veining associated with faulting (z) cutting an earlier heavily fractured and altered pseudotachylite (p-t). Porosity (p) is common in zeolite veins. (**C**) XPL. Fault related mineralisation. Calcite (c) veining reactivates a zeolite vein (z) that cuts epidote cataclasite (e). Surrounding rock is heavily fractured and composed of cataclastic quartz-feldspar epidote (altered) gneiss. (**D**) PPL. Fault-related calcite (c) and zeolite (z) cutting altered feldspar (f). Note porosity (in blue), which calcite infills. (**E**) PPL. Two phases of fault related zeolite veins cut altered epidote cataclasite. The early phase of zeolite (z1) comprises a finer crystal size (0.05 mm or smaller), whilst the second phase of zeolite comprises of larger crystals (up to 0.1 mm) that display radial extinction, and are associated with porosity (in blue) and hydrocarbon staining (o). (**F**) XPL. Higher magnification of image E, showing Z1 and Z2 phases. Z2 is associated with oil (o).

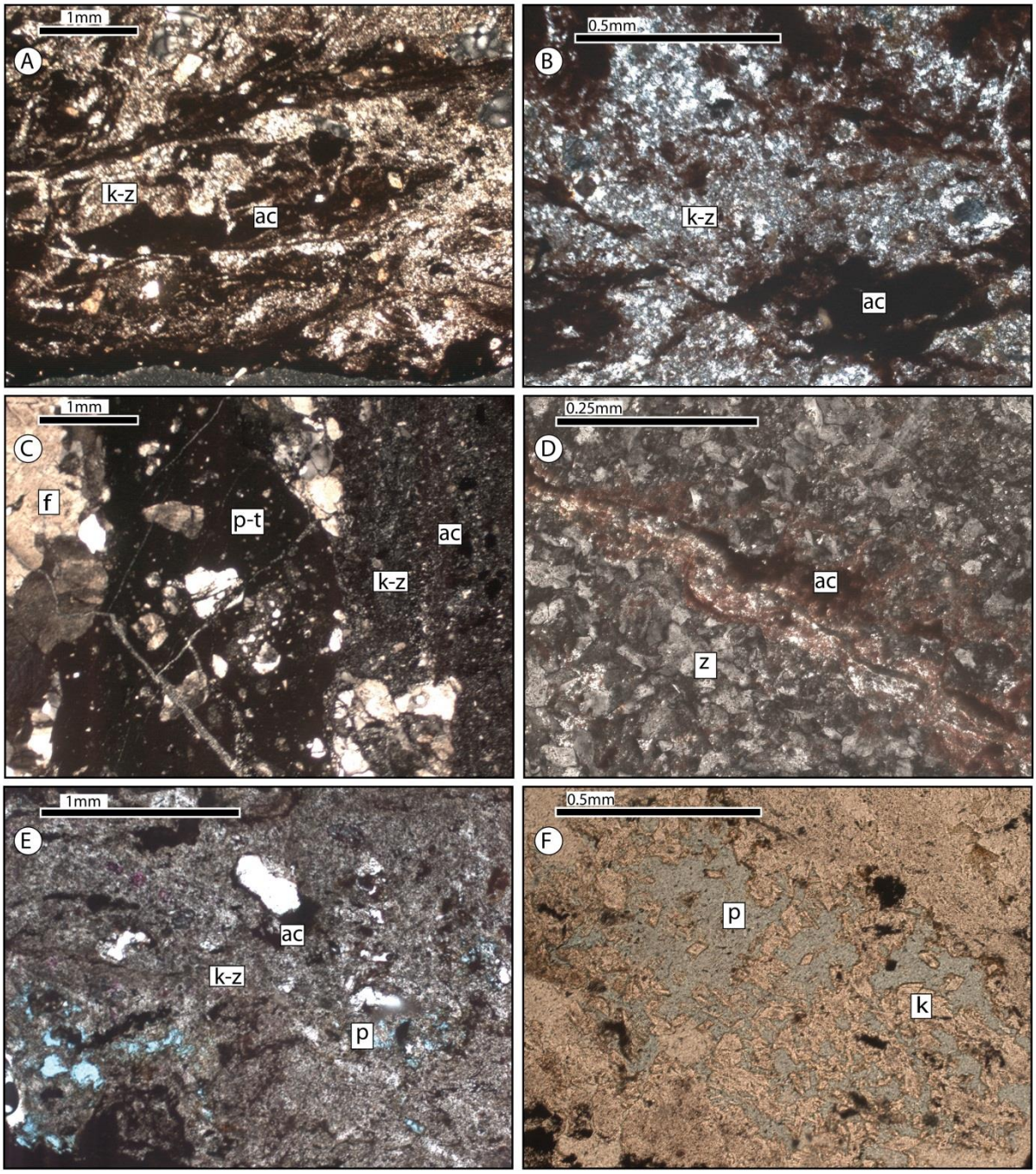

Figure 3.47: Adularia – zeolite – authigenic clay faults (Group 4 fault rocks), all from Tob Leireabhaigh. (**A**) PPL. Very fine-grained adularia-zeolite (k-z) and authigenic clay-bearing (ac) fault rock, with minor sphene. These phases appear to be syntectonic. (**B**) XPL. Higher magnification of image A, showing fine-grained nature of the fault rock. (**C**) XPL. Adularia-zeolite (k-z) and authigenic clay (ac) emplaced into surrounding country rock from the fault plane. Appearance is very similar to fault rocks in A and B. Country rock is composed of pseudotachylite (p-t), and quartz-feldspar gneiss (f). (**D**) XPL. Higher magnification of RHS of image C, shows low birefringence, very low relief zeolite (z) and a cross cutting fracture associated with authigenic clay (ac). (**E**) PPL. Pore space (p) associated with adularia-zeolite and authigenic clay fault rock. (**F**) PPL. Higher magnification of E. Showing pore space (p) and adularia crystals (a).

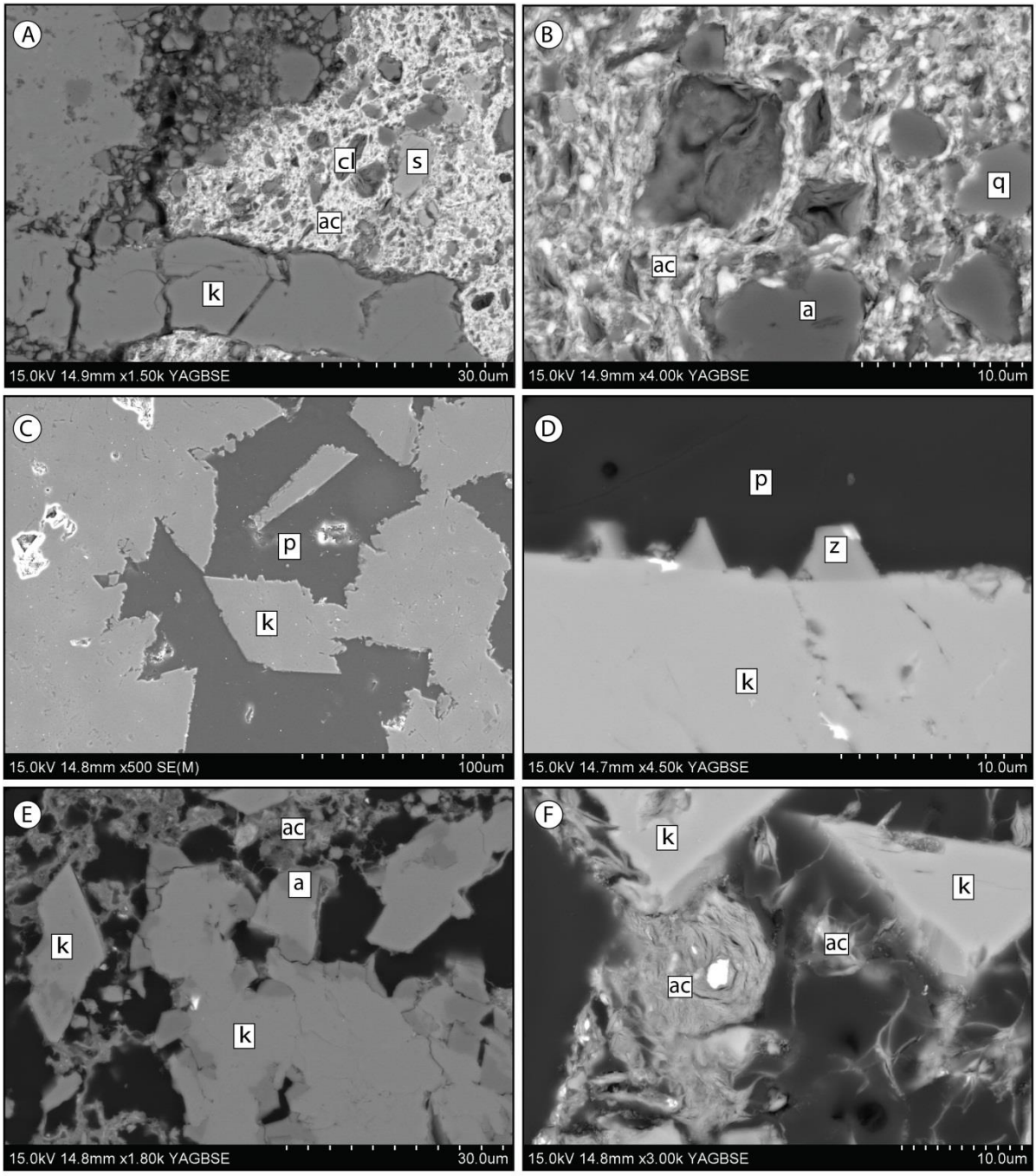

Figure 3.48: Adularia, zeolite, and authigenic clay, porous fault rocks under SEM (Group 4 fault rocks), all from Tob Leireabhaigh. (**A**) BSEM image. Showing adularia veining (k) cross cutting bright white authigenic clay fault rock, with Fe rich clay wrapping clasts of sphene (s) and chlorite (cl). (**B**) BSEM image. Higher magnification image of Fe rich clay (ac) wrapping clasts of amphibole (a) and quartz (q). (**C** and **D**) SE (M) and BSEM images. Euhedral adularia crystals (k) with overgrowths of possible zeolite (z), crystallising within pore space (p). (**E** and **F**) BSEM images. Adularia (k) with albite (a) and authigenic clay (ac) crystallising within porosity.

5. **Clay-rich gouges and cataclasites/microbreccias** (Figure 3.42, Figure 3.49 and Figure 3.50). These fault rocks are associated with calcite mineralisation, and also zeolite veining of a more discontinuous nature than that seen in Group 4, and with accessory haematite. These fault-

rocks cross-cut and reactivate earlier pseudotachylite-, peppery cataclasite- and epidote-bearing faults and veins, with earlier phases of fault rock often visible as clasts within the faults (e.g. Figure 3.50B-C). Group 5 faults are visible in the field as moderately to poorly indurated dark brown gouges, cataclasites, and breccias often lying along the plane of the local foliation (e.g. Figure 3.50E-F) and reactivating earlier faults. In thin section, calcite and zeolite are commonly present within the matrix of the fault rocks and cementing microfractures. Principal slip surfaces are always localised along the margins of the damage zones, which are up to 2 m wide on major structures such as those observed just onshore from the Minch Fault and at the Memorial Cairn locality. Lithic clasts of surrounding wall rocks are common, as are clasts of pre-existing green epidotic cataclasites and microbreccias from Group 2, where reactivation has occurred on pre-existing faults. In thin section they have a similar appearance to fault rocks cutting the Stornoway Formation, and their development also appears to be similar, with initial fracturing along mineral boundaries and initial porosity production, followed by authigenic clay development and formation of very fine grained aggregates of quartz and feldspar (Figure 3.49A-D). A high proportion of clay within the matrix surrounds and cements disaggregated clasts of country rock in places alternating with quartz-feldspar aggregates to produce foliated cataclasites, e.g. Figure 3.49D. Amphiboles, micas and epidote are often visible altering to brown clays that are high in iron content (e.g. Figure 3.50A). Syntectonic alteration to clays and the presence of clasts of heavily altered feldspars incorporated into large Group 5 faults indicates the presence of a free fluid phase during faulting (e.g. Watts et al., 2007). Figure 3.49E-H shows BSEM images of the same fault rock show in Figure 3.49A-D. As in the Stornoway Formation, there is often an association between zeolite presence and the presence of porosity (Figure 3.50D).

A difference in the level of fracturing is noticeable between quartz and feldspar minerals, with feldspar having an obviously more fractured appearance, and with open fractures and cataclasis occurring along cleavage planes during initial cataclasis whilst quartz remains intact. This contrast in mechanical strength is indicative of temperatures below 300°C (Passchier and Trouw, 1996). Figure 3.49G-H show authigenic iron rich clays of near smectitic composition wrapping clasts within the cataclasite. It seems likely that areas particularly rich in authigenic clays are forming from altered mafic minerals. The dominance of authigenic clays within the fault rocks is indicative of low temperature and low pressure conditions (e.g. Velde, 1985; Reyes, 1990; Frey, 1987; Frey and Robinson, 1999), with temperatures generally less than 180°C. With a normal geothermal gradient this temperature suggests crustal depths of no more than 6 km. Some localities display fault rocks associated with localised zeolite, most commonly occurring as discontinuous veins up to 0.2 mm thick that are parallel with wall rock

margins of the fault core/principal slip zone. In Figure 3.42, the fault has a margin of brecciated gneiss on the hangingwall side of the fault, with progressive strain towards the fault core producing crackle, mosaic and chaotic breccias across about 5 cm. Oil staining is also found in Group 5 faults at Earabhig and the Memorial Cairn.

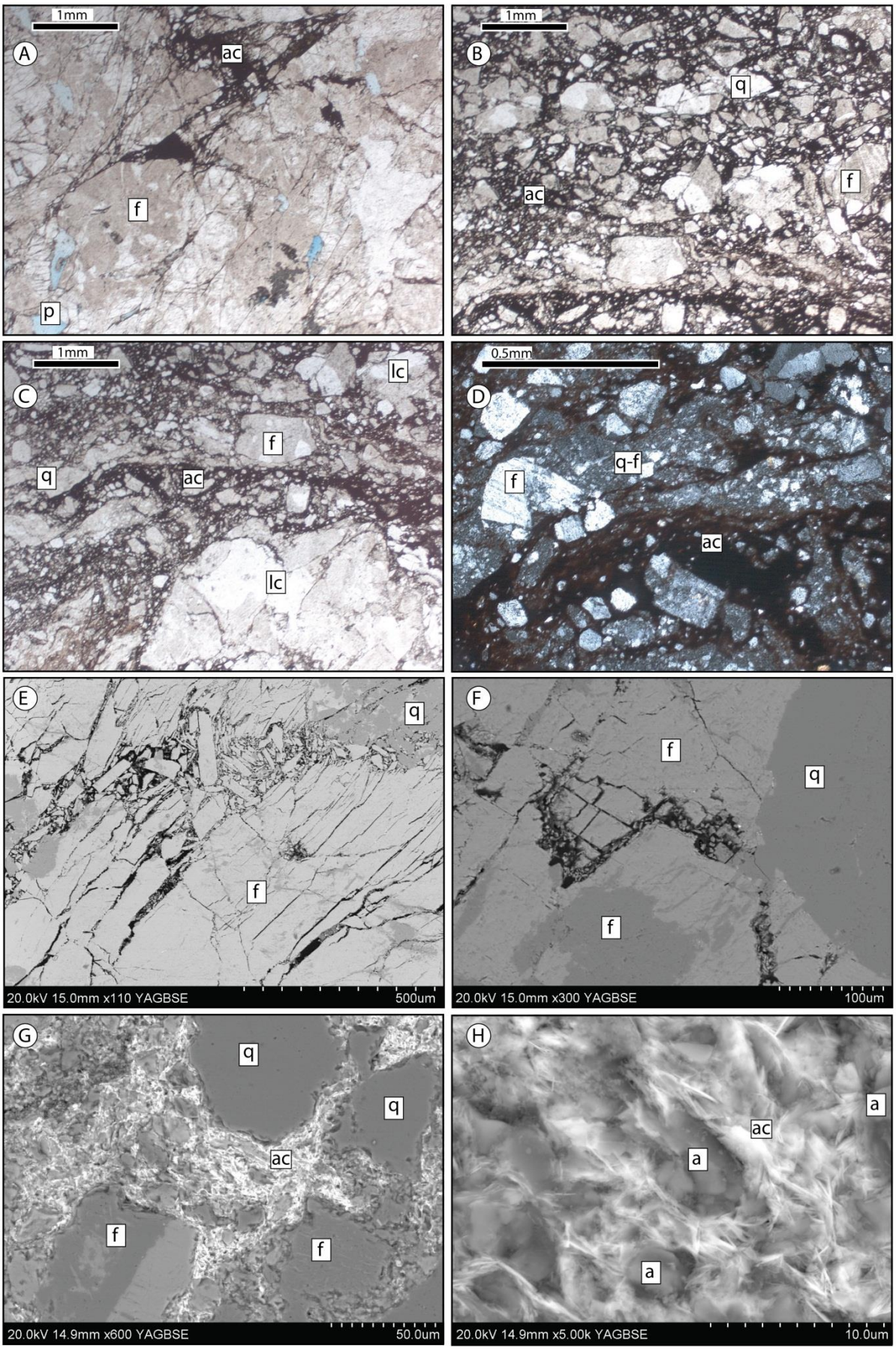

Figure 3.49: Clay-bearing gouge and cataclasite developed along the major SE dipping fault at Seisiadar South (Group 5 fault rock, Figure 3.27G - I). (**A**) PPL. Crackle and mosaic breccias cut

individual minerals and exist along mineral boundaries. These fractures produce porosity (p) that in some cases is infilled with authigenic clay (ac). (**B**) PPL. Chaotic breccia with grain size-reduced lithic clasts forming mono-mineralic grains. In places the breccia is supported by a matrix of dark authigenic clay. (**C**) PPL. With increased strain localisation and alteration banding of alternating quartz-feldspar (q and f) rich layers with authigenic clay-bearing layers (ac) develop. (**D**) XPL. Fine-grained areas are aggregates of quartz and feldspar (q-f). Clay appears to be authigenic (ac). (**E**) BSEM image. From fault margin, showing fractures in feldspar clasts (f) but not quartz (q). Fractures along cleavage planes resulting in production of porosity (in black). (**F**) BSEM image. Chaotic breccias fill crackle breccia fractures. Again a clear difference is visible in deformation of quartz (q, undeformed) and feldspar (f, brecciated) is evident. (**G**) BSEM image. Within chaotic breccia from a fault core, from same fault as image D. Bright Fe-rich authigenic clay (ac) wraps angular clasts of chaotic breccia composed of quartz and feldspar. (**H**) BSEM image. Blades of authigenic clay altered from and wrap amphibole clasts that are not visible via optical microscopy.

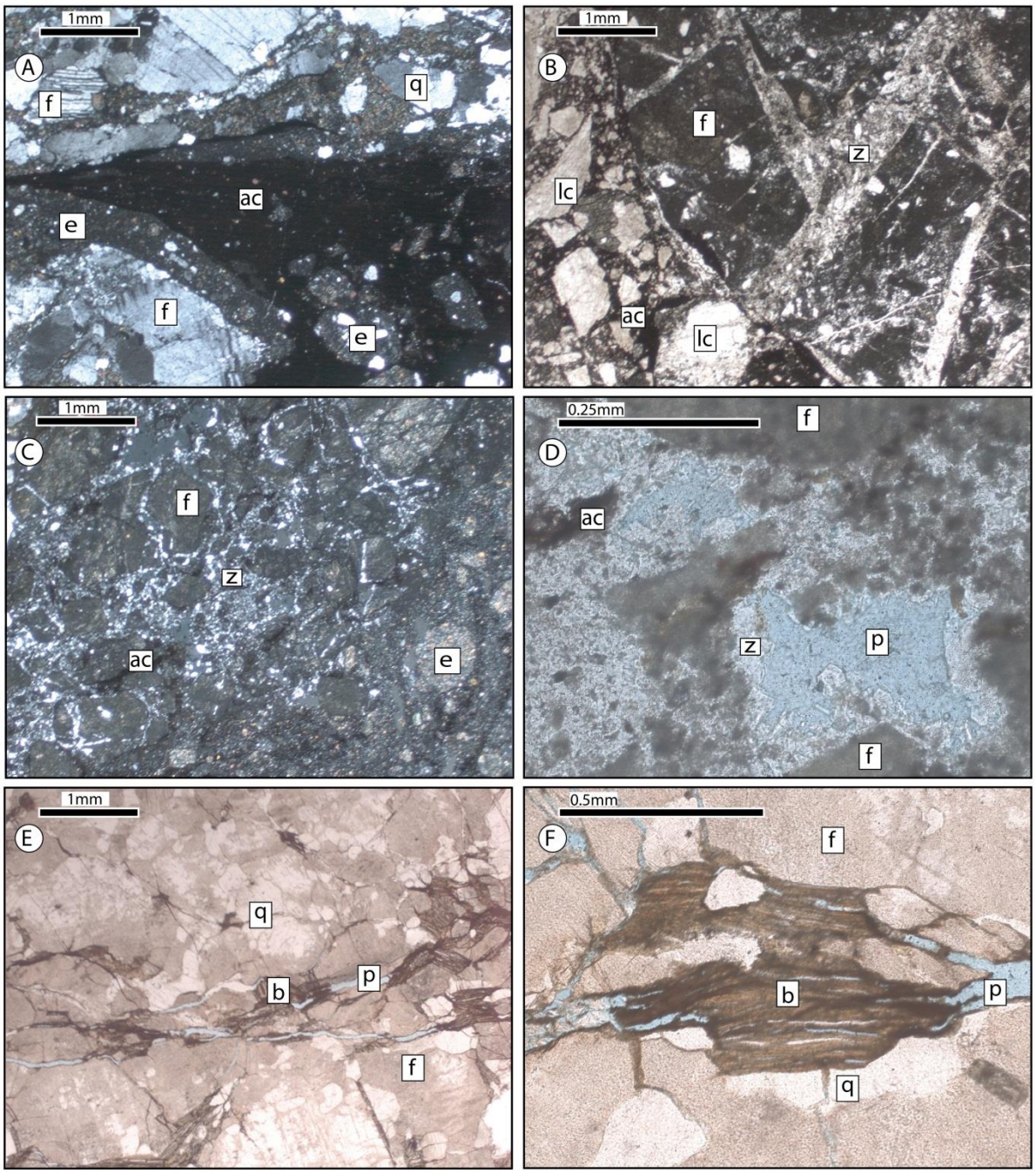

Figure 3.50: Characteristics of faults with clay-bearing gouges (Group 5 fault rocks), all from Garrabost. (**A**) XPL. Breccia of pre-existing epidote cataclasite (e), with clasts of feldspar (f) and quartz (q) in late-phase authigenic clay (ac) matrix. (**B**) PPL. Clast containing highly altered brecciated feldspar (f) altered to clinozoisite and epidote, and cemented with zeolite (z). Brecciated altered feldspar is itself brecciated within a later chaotic breccia cemented with authigenic clay (ac). (**C**) XPL. Altered feldspar (f) composed primarily of clinozoisite and epidote cemented in a matrix of zeolite (z). (**D**) PPL. Porosity (p) associated with zeolite (z) and authigenic clay (ac). F = altered feldspar. (**E** and **F**) PPL. Sample taken from the immediate footwall of a fault containing authigenic clay. Rock is a quartz (q), feldspar (f), biotite (b) gneiss, with biotite defining a foliation. Note formation of porous fractures along and parallel with the biotite cleavage planes.

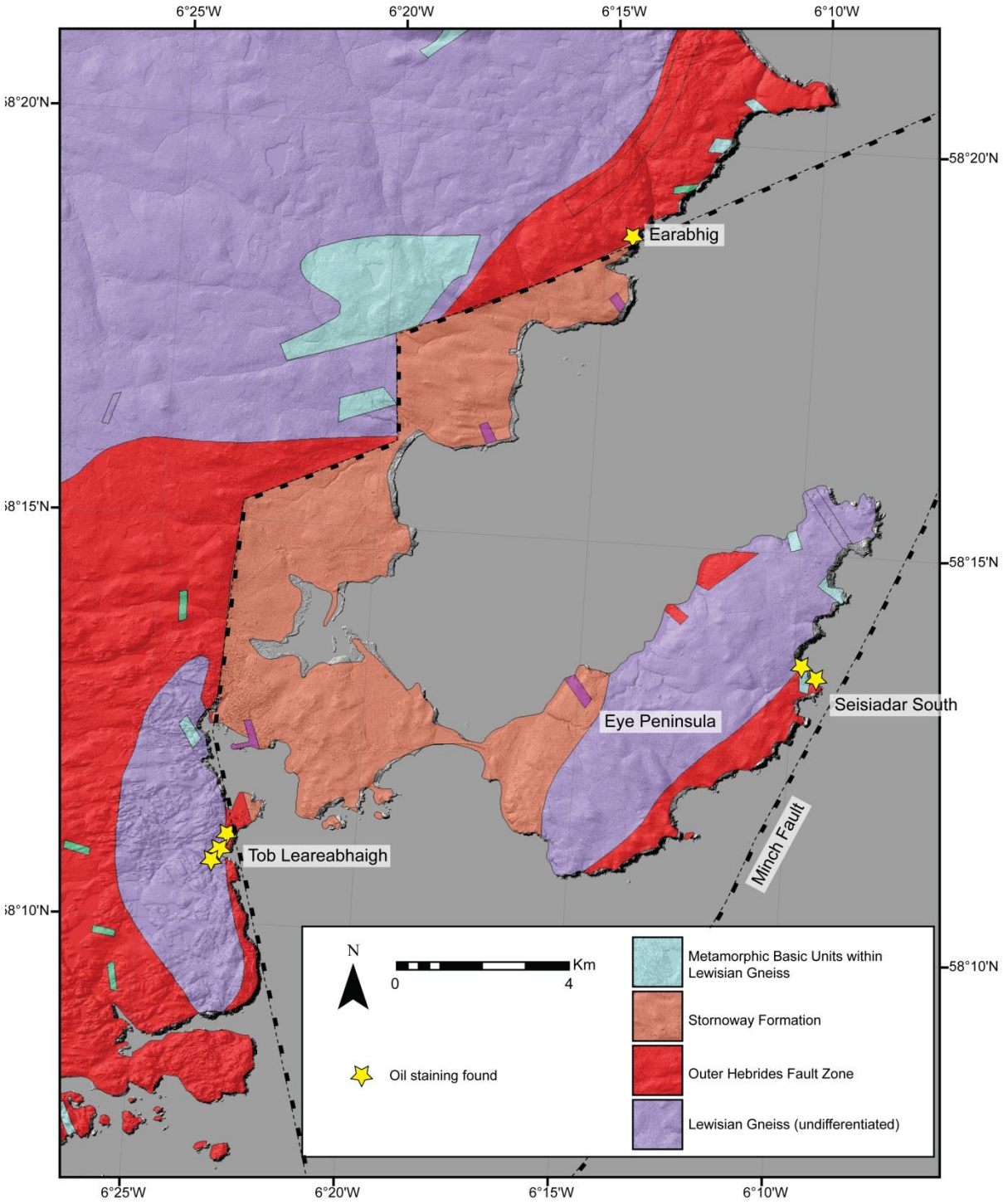

Figure 3.51: Map showing localities found with oil staining.

3.4.4.2 Fault rock discussion

The sequence of faulting described in section 3.4.3 reflects a decrease in temperature and pressure conditions through time. The sequence of brittle faulting described above probably initiated in the Caledonian orogeny or earlier (Imber et al., 2001), and includes phases of post-

Caledonian fault movements. In summary, the following fault rock sequence is recognised (oldest to youngest):

1. Pseudotachylite, recording conditions of brittle faulting at depths of 13.5 km (Fettes et al., 1992), determined from samples from SE Lewis. Probably deeper than those associated with later fault rocks (Passchier and Trouw, 1996). One example of a chlorite-bearing fault was seen, cut by pseudotachylite. This is indicative of temperatures >120°, and probably substantially higher given that it is cut by pseudotachylite that is believed to have formed at depth.
2. Epidote cataclasites/ultracataclasites recording multiple phases of faulting overlapping pseudotachylite formation. In some cases epidote cataclasites are overprinted with later granular epidote crystal growth. Epidote faulting is likely related to local epidotisation of the Lewisian Gneiss at depths greater than 6-7 km.
3. Pumpellyite-bearing faulting, brecciating patchily epidotised amphibolite, with later authigenic clay alteration. The presence of brecciated epidote and later authigenic clay alteration suggests conditions around 6 km depth.
4. Zeolite/adularia mineralisation associated fracturing and faulting, with authigenic clay and vuggy porosity development, requiring depths shallower than 6 km. Oil is locally observed in these rocks in areas adjacent to major basin-bounding (faults Figure 3.51).
5. Authigenic clay-bearing faults with zeolite mineralisation formed at shallower depths than those associated with adularia. Oil is also observed in some of these fault rocks.

The aim of this analysis was to identify Mesozoic aged fault rocks within the Lewisian. Clasts of fault rock derived from Groups 1, and 2 are widespread within the conglomerates of the Stornoway Formation (e.g. Butler, 1995; Imber, 1998) and intact faults bearing these assemblages do not pass up into the cover sequence. Epidote-bearing fault-rock clasts in particular are very common within the Lewisian, and this may be expected given the wide range of temperature-pressure stability of epidote (Liou, 1993). Fault rocks of Groups 3 and 4 are present locally within the basement. Authigenic clays and zeolites are seen within the Stornoway Formation, but not associated with adularia. The fault at Suardail that cuts both basement and cover sequence has been studied in depth (see Figure 3.42 caption) and is found to contain Group 5 fault rocks, comprised of an authigenic clay-bearing matrix supporting breccia and cataclasite, with associated zeolite veining. As mentioned above, the conditions indicated by the minerals in this fault group could indicate a formation depth of up to 6 km, but as these fault rocks are at times present with soft gouge, it seems likely that the depths of formation of these faults are considerably less. Denudation over Lewis in the Palaeocene alone has been estimated to be 2250 ± 750m on the 799m high mountain of Cliseam in the centre of the island (Persano et al., 2007). This provides a

minimum depth estimate of Group 5 faulting now exposed in the Lewisian of the Stornoway Region.

In the Stornoway Formation, zeolite is found in close association with calcite. Some calcite pre-dates the zeolite, displaying dissolution textures and occurring in the centre of zeolite haloes. In the Lewisian, there is evidence for multiple zeolite and calcite veining events. Zeolite crystals are observed growing into porous vein centres from the vein walls. Calcite, at times, appears to post-date this zeolite growth. A phase of zeolite mineralisation may precede the formation of authigenic clay-rich faulting, visible in Figure 3.50B.

A key question of interest is why does porosity exist within veins and faults in the Lewisian, and also within fault rocks of the Stornoway Formation? As mentioned above, porosity is associated primarily with calcite, zeolite, and adularia mineralisation occurring alongside authigenic clay minerals. Zeolite formation is enabled through the dissolution of material from the surrounding rocks and incorporation into zeolite minerals (Hay, 1978). In faults within the Stornoway Formation, fluid flow and cataclasis within these fractures may have enabled zeolite formation from fine gouge and cataclasite derived from clasts of the basement, whilst also contributing to dissolution of calcite. In addition to porosity increase due to microfracturing during faulting, the presence of porosity associated with these large molar volume minerals suggests that material has been moved out of the system through dissolution, or there has been a porosity decrease in other components of the rock. Retrogression or alteration reactions may have contributed to a volume decrease. One particular mechanism for volume decrease is albitisation of plagioclase feldspar (Weisenberger, 2009). Albite is found alongside adularia mineralisation (Figure 3.48E), and its formation within the gneiss may have reduced the overall rock volume and allowed formation of porosity. However, adularia represents a molar volume increase when forming from alteration of albite (Booden and Mauk, 2011). Hence it seems most likely that porosity results from the dissolution and removal of material from the rock. As described above, this process has occurred synchronously with faulting and localised oil migration into open fractures. Using the above information, it is possible to group faults in the Lewisian and order them by their relative ages according to their fault rock assemblages and cross-cutting relationships.

3.4.5 Fieldwork Fault Orientation Results – splitting using fault rock analysis

Fieldwork fault orientation data show similarities with orientation trends identified in the lineament analyses (Figure 3.17). The wider spread of field data is attributed to the higher resolution obtained from fieldwork, and the mapping of low-angle structures that are absent from the lineament analysis. The dominant trend is NNW-SSE, with weaker N-S and broadly E-W trends. Using the fault rock characterisation described above it is possible to group faults on the basis of their fault rocks. Figure 3.52 shows faults split between Pre-Mesozoic (fault rock Groups 1-4) and Mesozoic or younger aged fault rocks (fault rock Group 5). This grouping reveals that Pre-Mesozoic faults strike mainly NE-SW with the strongest grouping of faults dipping gently to the southeast. These trends seem to most clearly reflect the regional trend of the OHFZ in eastern Lewis. Mesozoic and younger faults show a strong NNW-SSE trend, which is prominently developed in the Stornoway Region. Faults with authigenic clay gouges and cataclasites (i.e. Mesozoic/Cenozoic structures) commonly lie sub-parallel to the local foliation in the gneisses (e.g. Figure 3.52). Palaeostress analysis performed on Mesozoic and younger faults in the Lewisian show very similar results to those of Set 1 and Set 2 within the Stornoway Formation, with ENE-WSW directed extension.

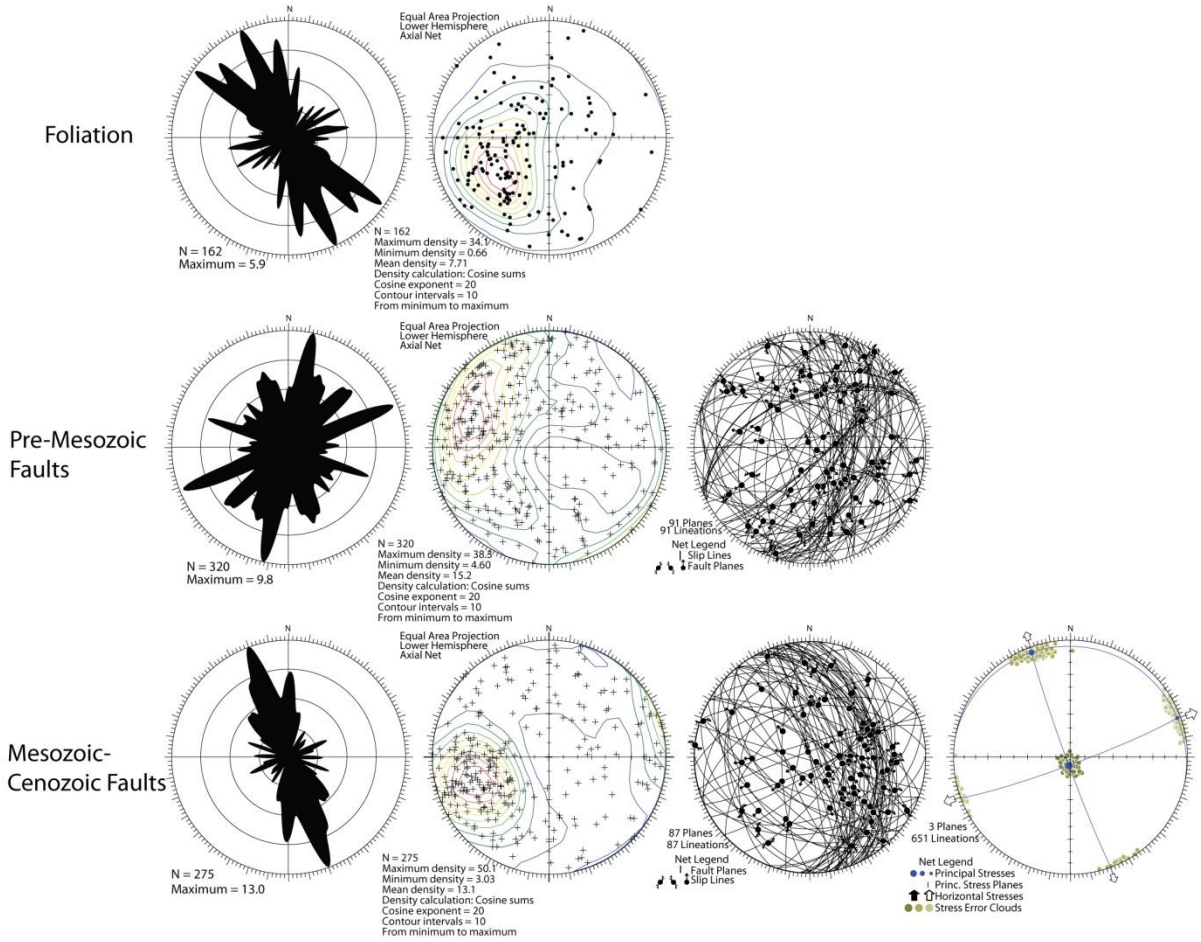

Figure 3.52: Fieldwork orientation results, showing foliation; faults are identified as pre-Mesozoic, and Mesozoic-Cenozoic age.

3.4.6 Effect of Foliation

Field observations reveal that foliation can comprise phyllosilicate rich layers such as Older or Younger Basics and pre-existing phyllonite bands, in addition to biotite as part of the gneissic layering. Phyllosilicates can have lower frictional coefficients ($\mu<0.6$) (Imber et al., 2008; Lockner et al., 2011), compared to the most intact rocks and hence parallelism of phyllosilicate rich layers with faulting may be expected to occur. The effect of foliation can be analysed quantitatively by determining the eigenvalue ratios 'C' and 'K', derived from the orientation matrix (Woodcock and Naylor, 1983; Beacom et al., 2001) of fault and foliation data, in order to plot and compare these values. The 'C' value indicates the strength of the preferred orientation, with higher values representing more organized samples of data and a zero value representing a perfectly uniform distribution. The 'K' represents the shape of the orientation data distribution, where K values approaching zero represent uniaxial girdle distributions of data, and K values towards infinity represent uniaxial clusters. Hence a positive correlation between K values of faults and foliation, and C values of faults and foliation, will be consistent with geometric coincidence. C and K values

both show R^2 values of 0.44 (Figure.3.53), with a weak positive correlation that is not statistically significant. However, there is a positive correlation as indicated by the regression. Several localities have anomalous values due to a lack of data, such as Tolstadh Beach, where a lack of foliation data has produced an anomalously high C value for the foliation.

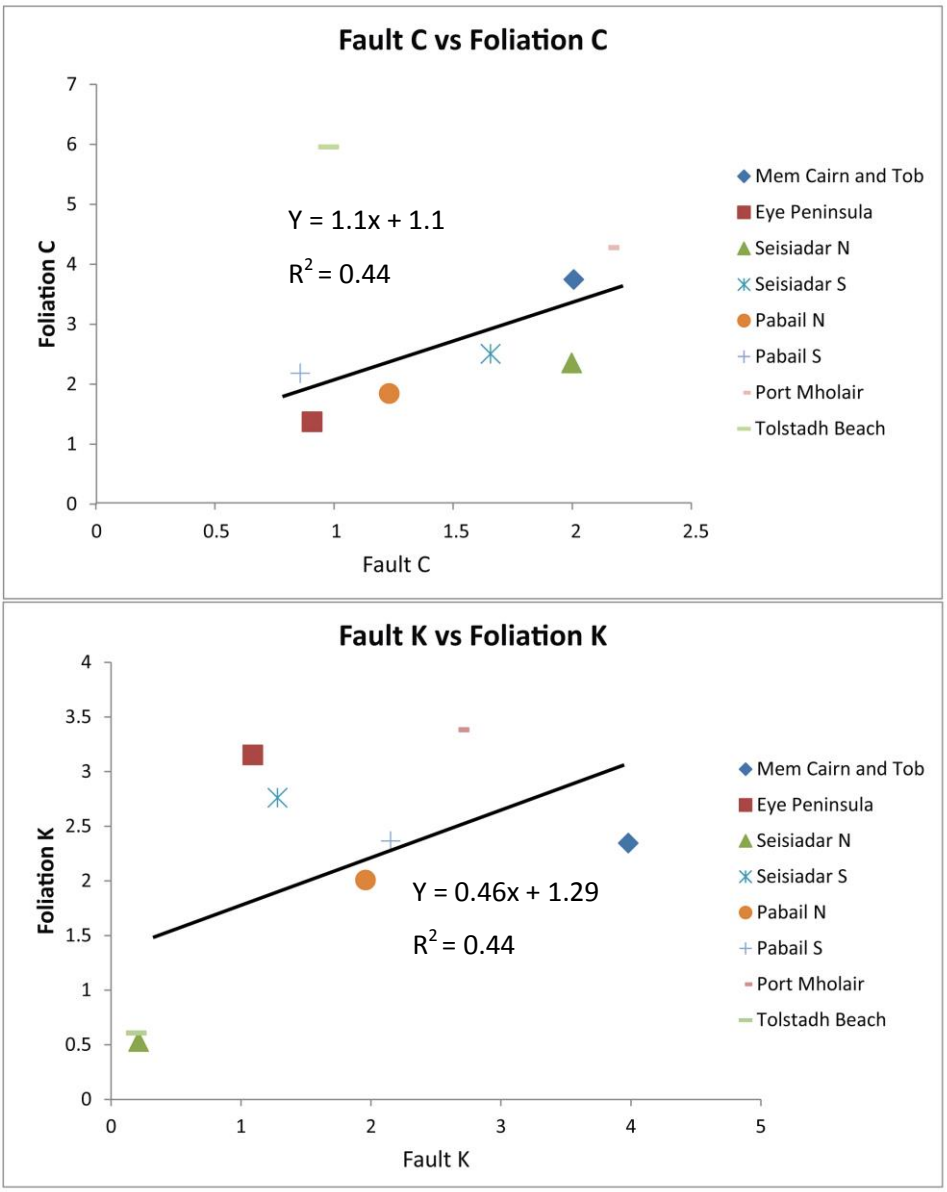

Figure 3.53: Graphs showing fault C value vs. foliation C value (top), and fault K value vs. foliation K value (bottom), with a linear regression line fitted to all of the data.

3.5 Basement cover interface

The exposures at the margins of the Stornoway Formation show the basement/cover interface to be a complex zone of erosional unconformity surfaces, faults, alteration, and carbonate/injected sediment veins. Four localities were visited where the basement cover interface can be directly observed. At all localities faulting exists close to or at the contact. Previous studies (Steel and Wilson, 1975) have determined the Stornoway Formation to be a half graben system with the conglomerates onlapping onto the basement in the east on the Eye Peninsula. The exposures of the contact at Dun Mor and Suardail show that this is broadly correct, but with a degree of faulting localised along and locally modifying the interface.

3.5.1 Basement cover interface field localities

3.5.1.1 Garrabost

The contact at Garrabost (NB 5113 3380) is formed by normal faults that post-date deposition of the Stornoway Formation (Figure 3.54). In detail, the unconformity is sheared with normal kinematics, and immediately adjacent to a sub-parallel fault (e.g. Butler, 1995). The adjacent fault displays a more planar, wider zone of fault gouge when compared to the sheared contact, probably indicating that more displacement has occurred along it than the actual unconformity (Figure 3.54). This situation is similar to that observed at Suardail, where shear planes localised parallel to the unconformity, but within the Stornoway Formation (e.g. see Figure 3.59F). Bedding is weakly defined due to the massive nature of the conglomerate, and is at a high angle to the faulting at this locality. The main fault surface in Figure 3.54D strikes NNW-SSE with normal oblique dextral slickenlines. In thin section, faulting at Garrabost seems contemporaneous with carbonate and zeolite veins/mineralisation (Figure 3.64A-B). About 2-3 m below the unconformity within the Lewisian Gneiss a fault is lined with a veneer of epidote, but contains a soft brown, easily eroded fault rock. Carbonate mineralisation is also associated with this fault. Given the orientation and kinematics, the main fault within the Stornoway Formation is probably part of the Set 1 faults observed within the Stornoway Formation (section 3.3.3.2). Other faults (e.g. on the right of Figure 3.54A) may be conjugates to the faults observed at the contact.

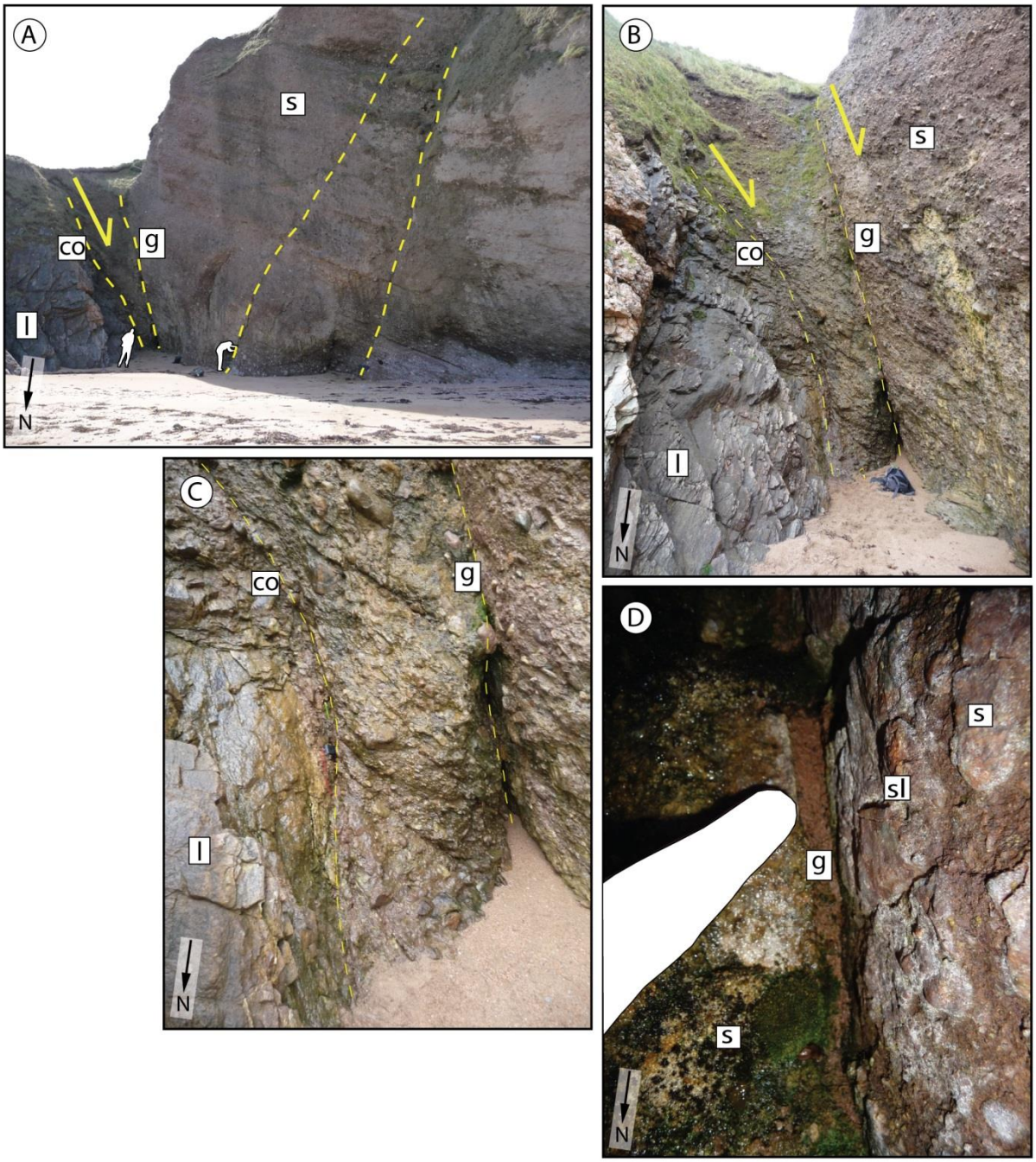

Figure 3.54: s = Stornoway Formation, l = Lewisian Gneiss, yellow dashed lines = faults. (**A**) View of the contact (co), with adjacent gouge-bearing fault (g). Faults shown here with opposite dips may be conjugates to the contact fault. (**B** and **C**) Contact (co) and gouge-bearing fault (g). (**D**) Gouge-bearing fault with finger for scale. Slickenlines are visible on the hangingwall surface (s).

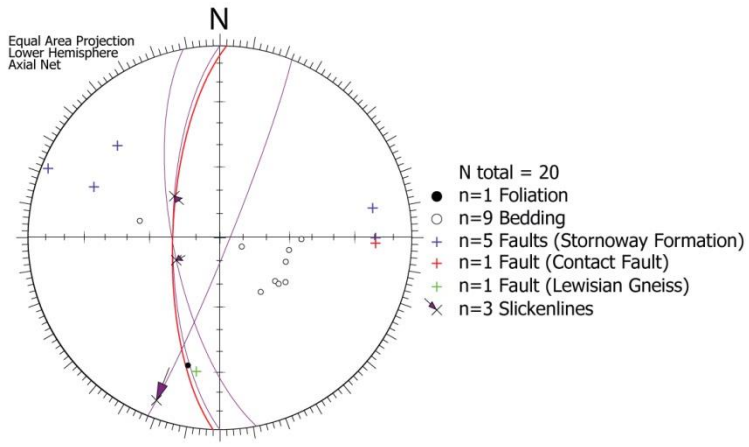

Figure 3.55: Stereonet of data collected from the Garrabost contact and immediate surroundings. Faults with slip data recorded are shown with a great circle in addition to the pole.

3.5.1.2 Dun Mor

At Dun Mor (NB 5150 3400, location shown in Figure 3.1), the contact is composed of Stornoway Formation conglomerate overlying a Younger Basic amphibolite (Figure 3.56), forming a small headland. The amphibolite contains multiple epidote veins and epidote ultracataclasite-bearing minor faults, cut and reactivated by carbonate and clastic-infilled veins that presumably originate from the interface and intrude up to 6 m down into the fractured basement rocks. Within the veined amphibolite there is an eastward dipping fault and in the immediate fault hangingwall an approximately 1 m thick zone of heavily altered, highly fractured basement amphibolite that is overlain by the Stornoway Formation (Imber, 1998). This disrupted zone is visible on both sides of the headland (Figure 3.56A-F). Within the disrupted zone in the fault hangingwall, multiple sets of sediment- and carbonate-dominated veins occur, with clasts of carbonate and sediment visibly enclosed by both vein types (Figure 3.56G). Veins are truncated against the fault and are also found parallel with the fault in the fault core. The fault consists of a zone of heavily altered amphibolite approximately 10 cm thick with parallel carbonate veins along a thin (1 cm thick) clayey principal slip zone (Figure 3.56G), which contains fractured epidote – indicating that an epidote filled fracture has been reactivated with the later carbonate-associated faults. Faulting at this locality has resulted in the formation of the disrupted zone with localisation of carbonate veining and sediment injection possibly due to extension in the fault hangingwall. At the point where the Stornoway Formation contacts the basement, clastic intrusions are also observed. Therefore it would appear that faulting is not the sole cause of clastic intrusions, but has allowed their concentration into the disrupted zone through overpressure that may be linked to fault movements. The presence of shattered carbonate veins within clastic veins and vice versa likely indicates the presence of repeated overpressure events probably linked to repeated motions on the fault.

Figure 3.57 shows orientation data collected from Dun Mor. The NE-SW trending faults with slickenlines dipping towards the northeast are all epidote-bearing faults within the amphibolite that clearly pre-date the formation of the interface. Bedding is coincident with the unconformity surface, and these are markedly different in orientation from the eastward dipping fault discussed above. Orientation data from carbonate and clastic veins at Dun Mor were also collected (Figure 3.58). Clastic veins are near vertical, strike E-W and NW-SE, and lie at approximately 90° to the fault surface. Vein distribution is concentrated in the fault hangingwall. Carbonate veins show a notably different distribution from the clastic vein data, with dominant trends of N-S and NE-SW. N-S trending carbonate veining seems to be linked to the main eastward dipping fault at this locality. NE-SW trending carbonate veins closely mirror the orientation of the unconformity surface and may be linked to gravitational slumping along the contact surface and the contact-parallel fault (shown in Figure 3.56C).

Clastic veins are fine-grained comprising mud-sized clasts up to half a millimetre across, with at least two phases of carbonate veins and also later carbonate-zeolite mineralisation that wholly or partially infills voids (Figure 3.64C-D). At all localities carbonate forms a cement in the cataclasites and injection veins, with additional probable zeolite.

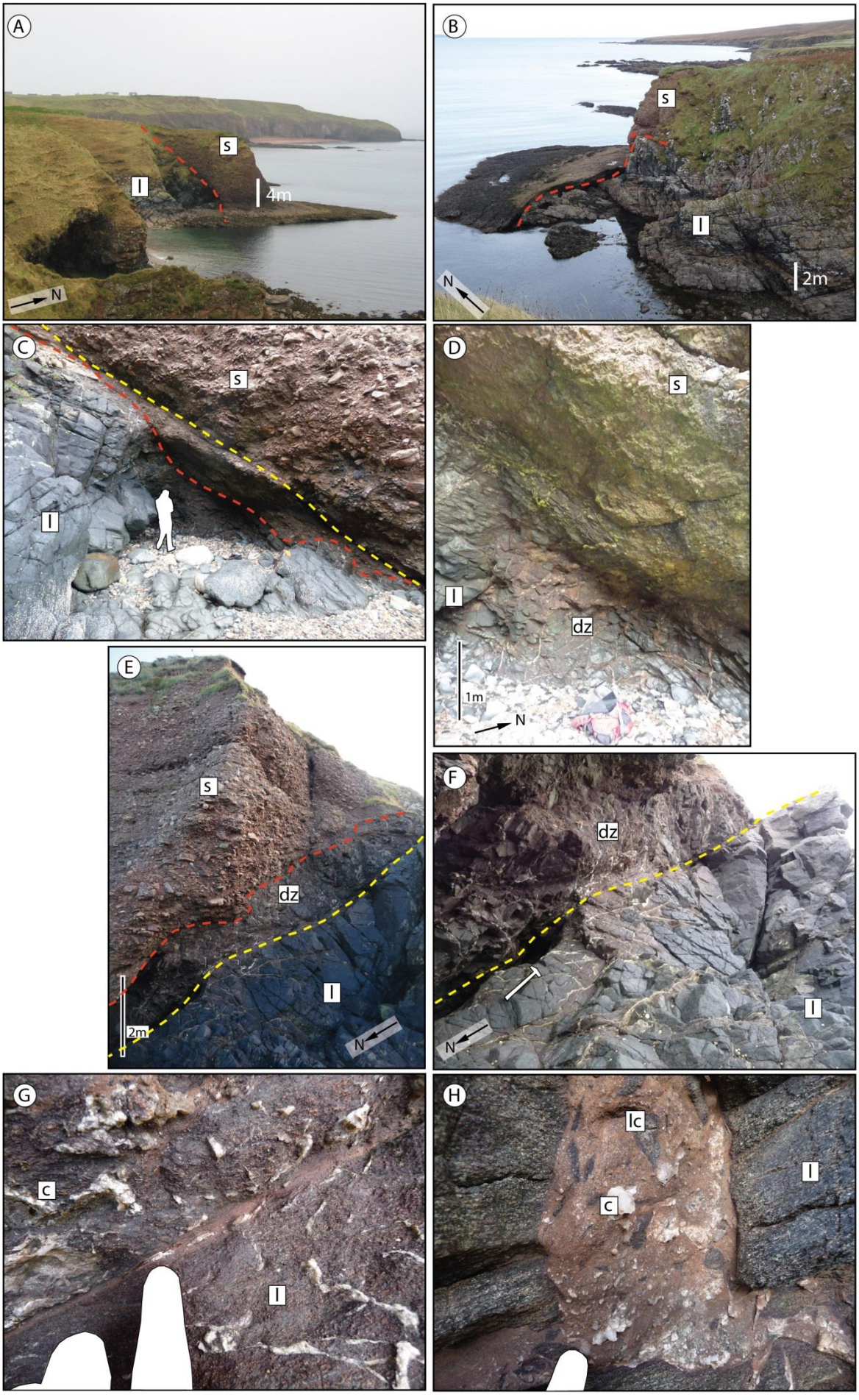
A
s
l
4m
N
B
s
l
2m
N
C
s
l
D
s
l
dz
1m
N
E
s
dz
l
2m
N
F
dz
l
N
G
c
l
H
lc
c
l

Figure 3.56 (previous page): Outcrop of Stornoway Formation 'cake' at Dun Mor. S=Stornoway Formation, l = Lewisian, dz = disrupted zone, red dashed line = unconformity, yellow dashed line = fault, c = calcite, lc = lithic clast. (**A** and **B**) Cliffside views of the contact at Dun Mor, viewed from the northeast (A) and the southwest (B). (**C**) On the northeast side of the cake, minor shears are visible (yellow) 20-40 cm above, and parallel with, the unconformity surface (red). (**D**) Unconformity between the disrupted zone and Stornoway Formation. (**E**) View of the 'cake' from the southeastern side of the outcrop. Disrupted zone between the Stornoway Formation proper and the amphibolite of the Lewisian is clearly visible. (**F**) Fault is localised along the base of the disrupted zone. Alteration of the amphibolite around epidote veins reactivated with calcite and clastic veins is evident. (**G**) Fault shown in images E and F. Discrete surface of thin (<1 cm) gouge, with associated carbonate mineralisation. This fault diverges from the unconformity surface. (**H**) Clastic veins within the Lewisian amphibolite.

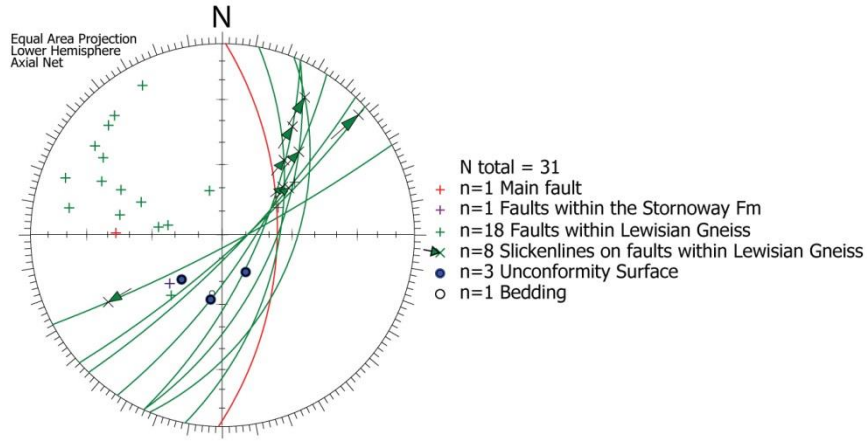

Figure 3.57: Stereonet of data collected at Dun Mor. Main eastward dipping fault shown in red. Faults with slip data recorded are shown with a great circle in addition to the pole.

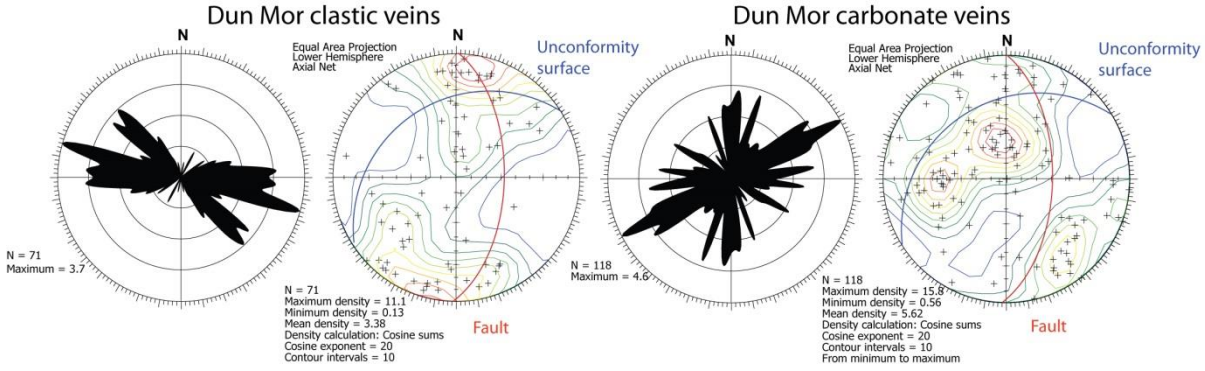

Figure 3.58: Clastic and carbonate veins measured at Dun Mor.

3.5.1.3 Suardail

At Suardail (NB 4958 3007), the contact is partly composed of a large-scale fault striking NNW-SSE and dipping to the east, with a normal-oblique (dextral) sense of motion, and a series of linked

faults and fractures visible in the Stornoway Formation immediately overlying the fault (Figure 3.59A-E). This fault dips to the east and diverges away from the actual unconformity surface as it is traced around the peninsula from west to east. This is similar to Dun Mor. Elsewhere the unconformable contact is preserved, but is closely paralleled by a discrete fault that passes through the cover (Figure 3.59F), again similar to Dun Mor. The syntectonic nature of carbonate veining is visible at Suardail where euhedral masses of calcite up to 8 cm across are preserved in fractures that are hard-linked to the main fault at that locality. In thin section, calcite veining also emanates from the principal slip zone and intrudes the surrounding rock normal to the fault plane. The main fault (shown in red, Figure 3.60) is closely paralleled by a series of faults within the Stornoway Formation, and linked with non-parallel faults through a series of lateral ramps and splays. Fault zone thickness along the main fault diminishes southwards along the outcrop, from over 40 cm to about 5 cm in thickness, probably as displacement along this surface is transferred onto the lateral ramps (Figure 3.59A-B). The conglomerate at Suardail notably contains clasts of sedimentary rock (Figure 3.59G-I). It is unclear what the origins of these clasts are, and they may be Torridonian, Devonian or Permo-Triassic (reworked Stornoway Formation) in age.

Faults that cut Stornoway Formation and Lewisian Gneiss post-date epidote cataclasite and pseudotachylite-bearing faults within the gneiss at this locality. All these early fault rocks are also preserved in boulders within the conglomerates and are truncated by the sandy sedimentary matrix at the edges of the pebbles. The main fault displays motions compatible with Set 1 faulting identified within the Stornoway Formation. A series of low angle faults are linked with the main fault within the Stornoway Formation with varying orientations and with generally very incohesive, but thin (< 1 cm thick), fault rocks. An exception is an eastward-dipping fault that is sub-parallel with the main fault, with fault rock that is extremely well indurated with carbonate. To investigate the possible effects of bed tilt at Suardail, faults within the Stornoway Formation were back rotated to correspond with horizontal bedding (Figure 3.60). The main fault and associated sub-parallel faulting steepen slightly in dip, and kinematics become more obviously oblique-dextral. Two low angle faults are shown dipping in an opposite directions when back rotated (highlighted light blue, Figure 3.60). These faults are lateral ramps linked with the main fault and hence are not believed to have been active with the back rotated opposing sense of dip. Thus it seems likely that these faults, and by inference the main fault, formed after some rotation of the bedding.

The main fault and linked structures are offset across later E-W oblique dextral faults that may be linked to fault Set 3 identified within the Stornoway Formation. The faults that cut the Stornoway Formation and Lewisian Gneiss display NNW-SSE and N-S trends, with one fault showing kinematics and orientation compatible with those of fault set 2 within the Stornoway Formation.

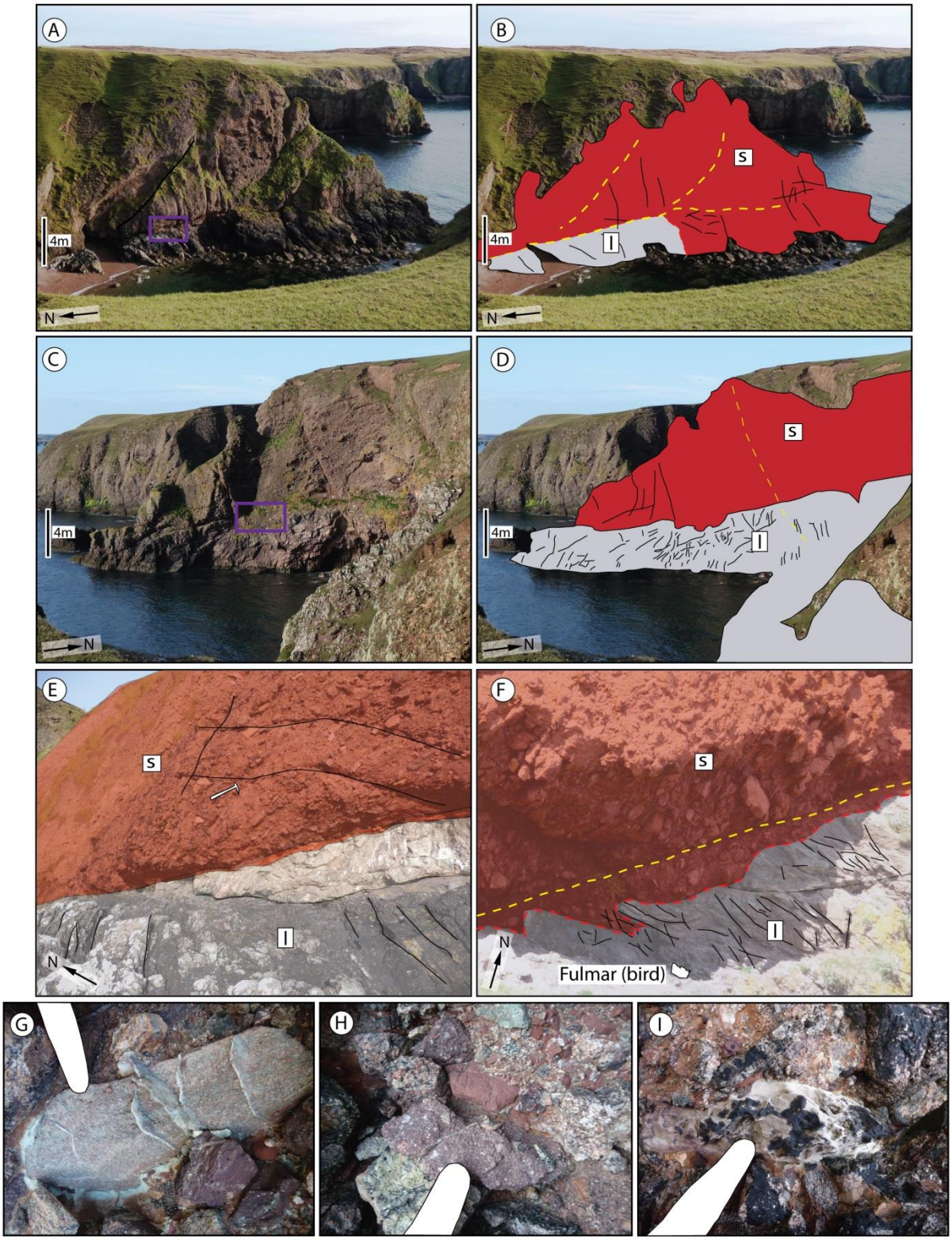

Figure 3.59: Suardail outcrop images. (**A** and **B**) Showing Suardail headland, looking east. Purple box shows location of image E. (**C** and **D**) Showing Suardail headland looking west. Purple box shows position of image F. (**E**) Fault forming the contact between the Stornoway Formation (red) and the Lewisian Gneiss (grey). Red = cataclasite, white = lense of faulted altered Lewisian Gneiss within the fault. (**F**) Fault parallel with and partly localising along the unconformity surface. (**G** - **I**) 'Exotic' clasts within the Stornoway Formation close (within 1 m) to the unconformity surface.

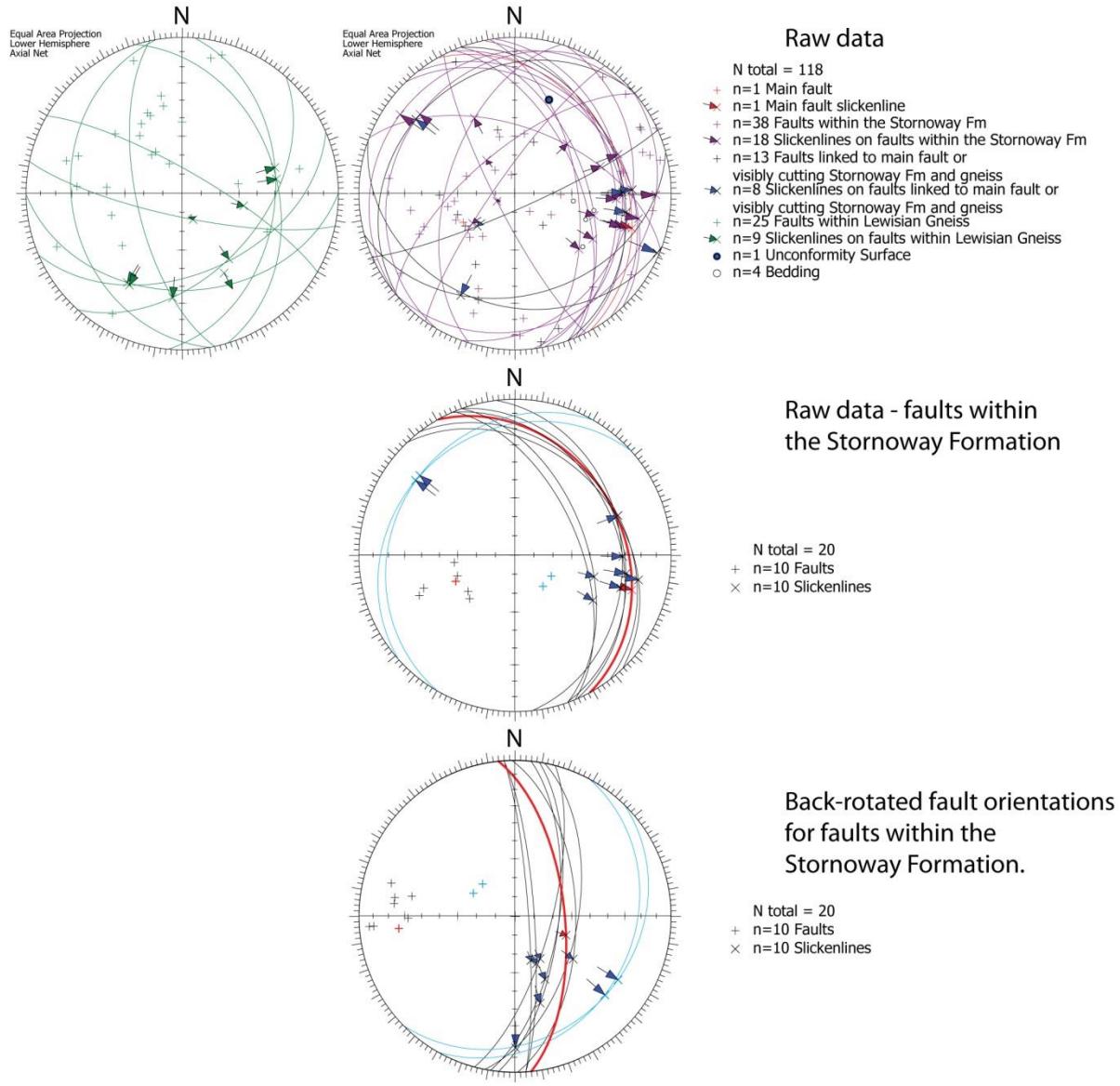

Figure 3.60: Data collected at Suardail within the Stornoway Formation and Lewisian Gneiss. Main fault shown in red. Light blue highlights two faults with an opposite sense of dip when back rotated. Faults with slip data recorded are shown with a great circle in addition to the pole.

3.5.1.4 Earabhig

Earabhig (NB 5180 4380) is the only exposed section of a Stornoway Formation bounding fault (Figure 3.62). The contact comprises an E-W striking major fault that has localised along a chloritic shear zone visible in the immediate footwall (Figure 3.61). The green colouration of the basement here is due to shear on a chlorite-rich phyllonite that has boudinaged pink K-feldspar rich gneiss (Figure 3.62D). This lithology may reflect an early-stage Older Basic unit within the Lewisian

Gneiss that has undergone shearing and alteration related to movements on the Outer Hebrides Fault Zone.

Slip has occurred in the basement along gouge-bearing fault planes with chlorite mineralisation interspersed with quartz-feldspar breccia. The chlorite present in these fault rocks appears to be directly derived from the pre-existing phyllonitic shear zone at this locality. As can be seen on the stereonet in Figure 3.61, the southward-dipping fault closely parallels the approximate orientation of the foliation of the shear zone within the basement at this locality. Other minor fault planes were also measured in the footwall of the main fault.

Calcite is again associated with the contact, and is visible as fault rock cement and as cataclastic clasts, confirming a syn-faulting origin and syn-deformational fluid flow.

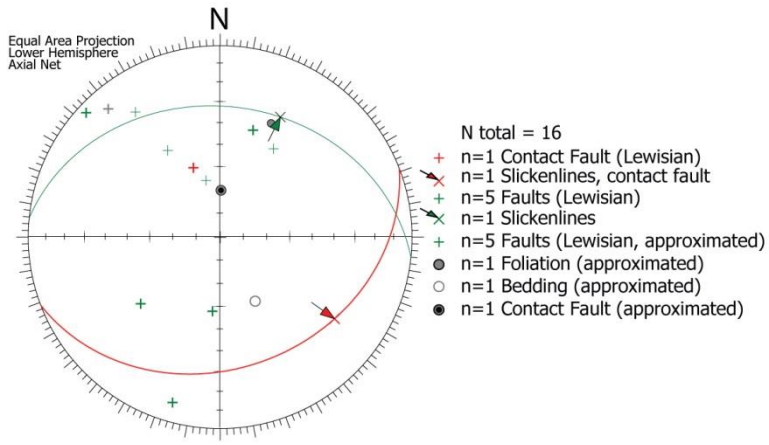

Figure 3.61: Fault orientation data collected from Earabhig. Faults with slip data recorded are shown with a great circle in addition to the pole.

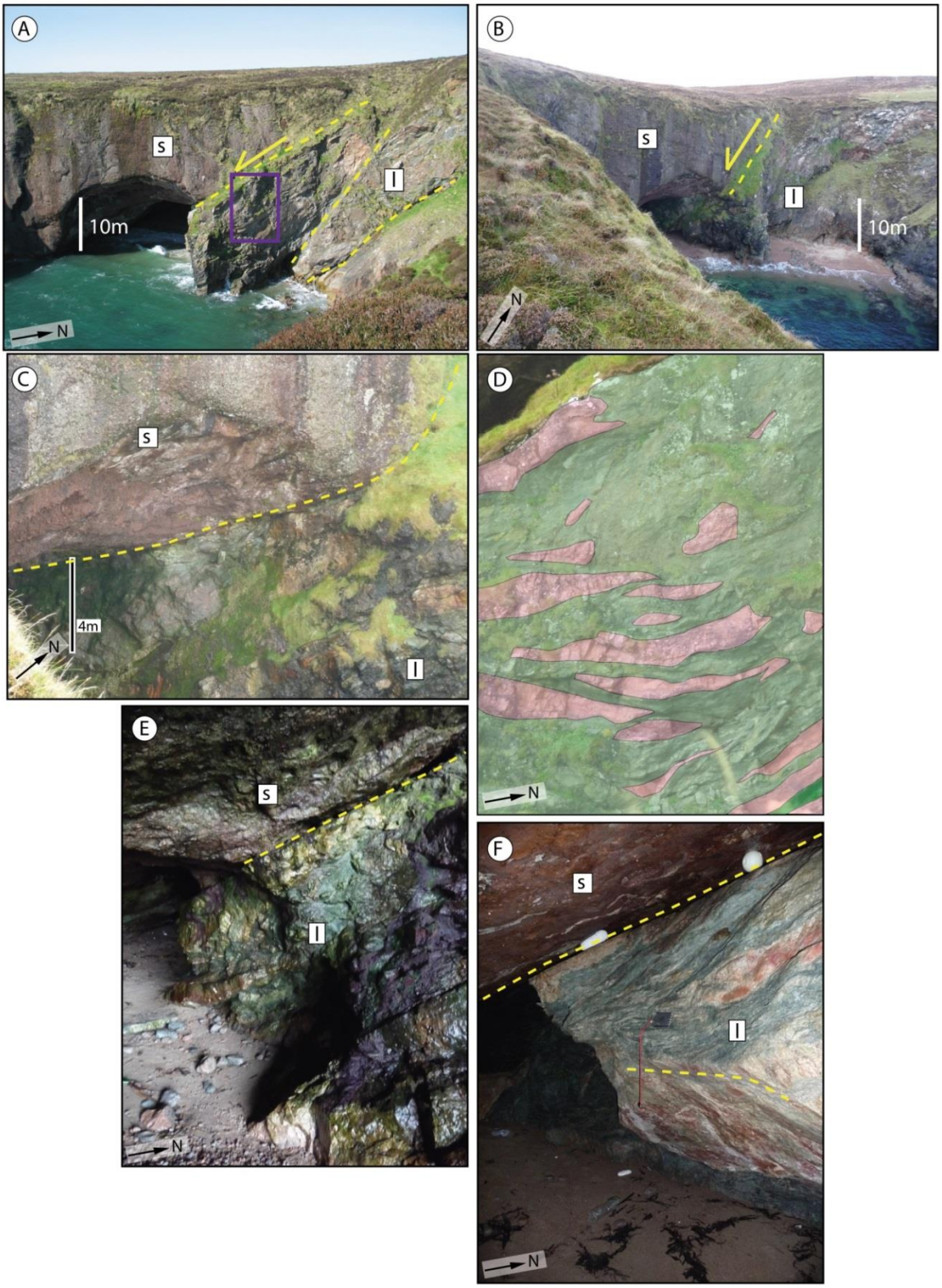

Figure 3.62: Earabhig basement-cover interface images. S=Stornoway Formation, l = Lewisian, yellow dashed line = fault. (**A**) Cliff-top view of the contact looking west. Stornoway Formation is in faulted contact with highly altered, ductiley and brittley deformed Lewisian Gneiss. Purple box indicates position of image D. (**B**) Cliff-top looking north at contact. (**C**) Contact at higher magnification. Green colouration within the Lewisian is due to the presence of chlorite. (**D**) Cliff face immediately below the faulted contact is composed of boudinaged k-feldspar dominated gneiss (pink) within chlorite rich sheared gneiss (green). (**E** and **F**) Within cave, Contact is clearly defined fault surface with dip-slip slickenlines. Strong green colouration is due to chlorite within basement shear zone.

3.5.2 Summary of faulting at the basement-cover contact

The basement/cover interfaces observed in the Stornoway region record complex phases of faulting. At the 'onlap' localities on the Eye Peninsula, faults are widely localised at low angles to or sub-parallel with the unconformity through formation of discrete structures in the Stornoway Formation, within 1 m of the unconformity surface.

Clastic vein injection into the basement at Dun Mor may at least be partly controlled by faulting with veins concentrated in the fault hangingwall perpendicular to the fault surface. Faulting at Dun Mor may be linked to both the clastic and carbonate veins, formed during repeated cycles of fluid overpressure possibly linked to fault movement. At Suardail similar evidence is present in the form of euhedral calcite mineralisation and carbonate veins.

Grouping faults between those measured in the basement and those measured in the cover (Figure 3.63) confirms the pattern identified previously. Lewisian-hosted faults tend to be pre-Mesozoic in age and display NE-SW trends and often dip to the southwest. Younger faulting within the Stornoway Formation displays the typical NNW-SSE trend identified above, as well as subsidiary N-S and E-W structures.

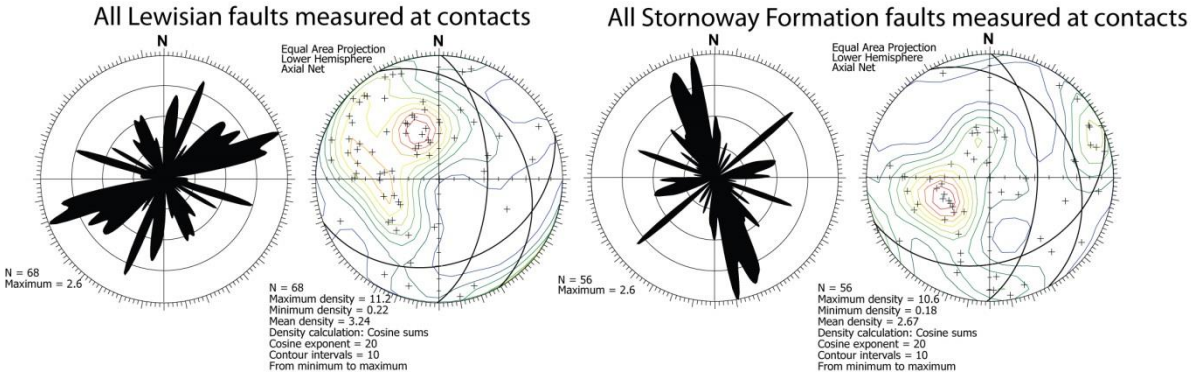

Figure 3.63: Stereonets of data collected from Dun Mor, Earabhig and Suardail, black lines show the three main fault structures at these localities.

3.5.3 Basement-cover interface microstructures

Carbonate veins are pervasive, cementing micro fractures in the fault and wall rocks that are associated with the initial stages of fracturing (Figure 3.64A-B). Sediment injection observed at Dun Mor is coarse-grained sand with clasts up to 0.5 mm across (Figure 3.64C). Multiple calcite phases are present within the clastic veins, with masses of fine crystals of around 0.1 mm across, and sparry crystalline calcite, with crystals up to 1 cm across. Porosity within the clastic injections is filled with carbonate that also has a 0.1 mm thick rim of zeolite followed by a 0.1 mm thick rim of brown authigenic clay alteration. In Figure 3.64D, feldspars display very heavy alteration, a feature not generally observed within the Stornoway Formation rocks, and probably reflecting the influence of fluids in these veins.

At Suardail, calcite fills faults and microfractures. Along the principal slip zone, very fine-grained quartz-feldspar aggregates alternate with bands of authigenic clay minerals. The main fault is comprised of a clay-bearing fault rock comprised of very fine grained aggregates of quartz and feldspar within a clay-bearing matrix (Figure 3.64E). Vertical, discontinuous carbonate veins < 0.2 mm thick cut the fault rock. These veins are perpendicular to the fault surface, and indicate a vertical maximum principal stress orientation during calcite vein formation. Kinematic indicators within the fault rock confirm normal kinematics on the main fault. This fault rock is similar to Group 5 fault rocks seen in the Lewisian Gneiss and fault rocks within the Stornoway Formation cover.

At Earabhig (Figure 3.64F-H), calcite cements microfractures within a pre-existing zeolite-cemented cataclasite, and minor chlorite linked to the pre-existing shear zone, is dispersed through the rock. Cataclastic sheared gneiss exists for at least 2 m below the principal contact surface. Also at Earabhig (Figure 3.64G), oil staining is visible associated with porosity within the zeolite cemented cataclasite, and cross cuts all other structures. Oil surrounds brecciated fault rock in some areas, suggesting that oil influx occurred during faulting or at high pore fluid pressure (Figure 3.64G), or both.

In general, fault microstructures observed at the basement-cover interfaces are similar to those seen within the Stornoway Formation and in fault rock Group 5 in the Lewisian Gneiss.

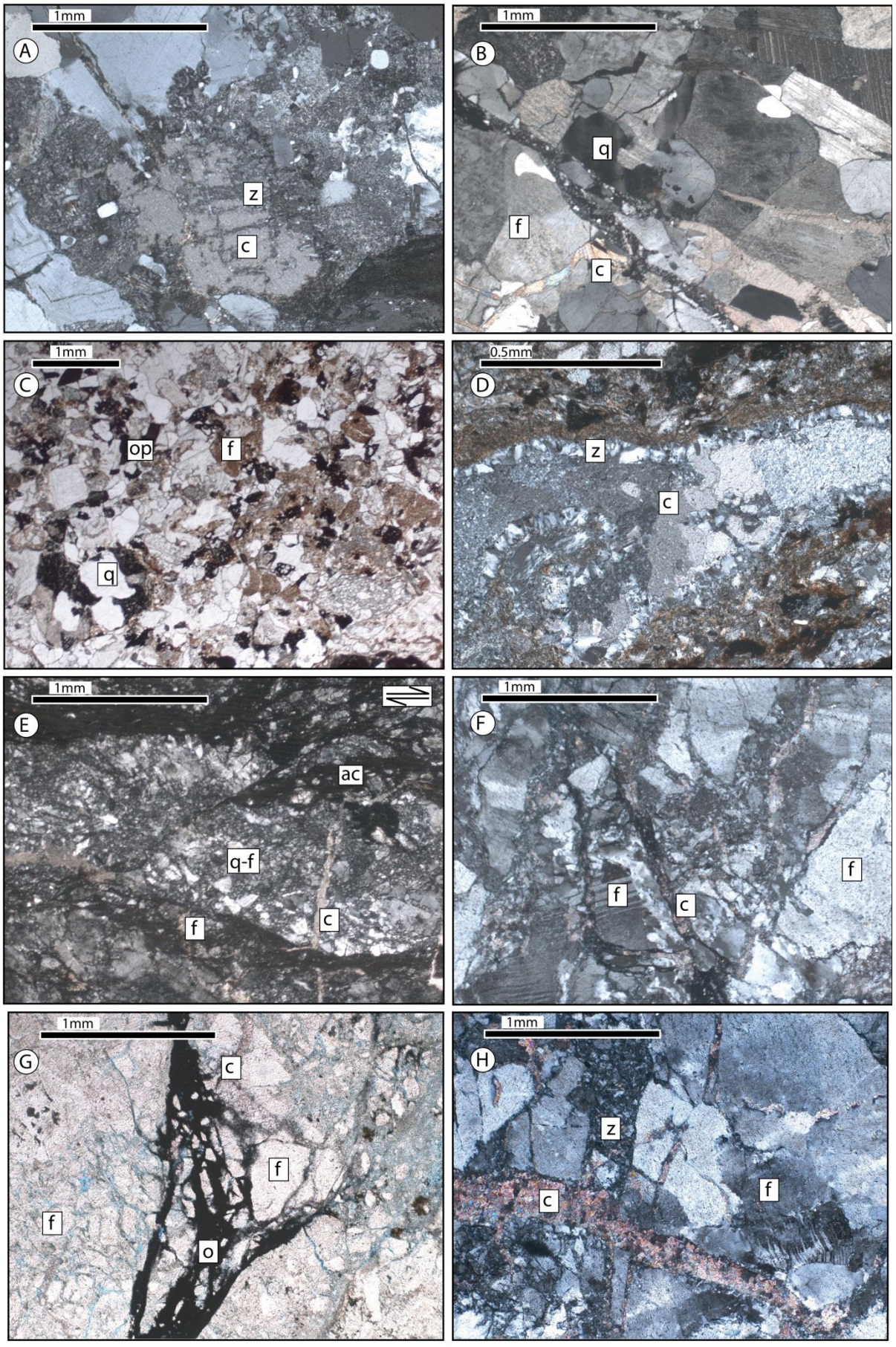
1mm
A
z
c
1mm
B
q
f
c
1mm
C
op
f
q
0.5mm
D
z
c
1mm
E
ac
q-f
f
c
1mm
F
f
f
c
1mm
G
c
f
f
o
1mm
H
z
c
f

Figure 3.64 (previous page): Photomicrographs from the basement-cover interface. (**A**) (From Garrabost) XPL. Carbonate-zeolite mass in altered cataclasite from the immediate hangingwall of the sheared unconformity. (**B**) (From Garrabost) XPL. Fractures and cataclasites in the fault-adjacent country rock, and carbonate veins. (**C**) (From Dun Mor) PPL. Injected material from adjacent to the unconformity surface. With heavily altered feldspar (f), quartz (q), and opaques (op). The matrix also contains several phases of calcite. (**D**) (From Dun Mor) XPL. From 1 m below contact, carbonate-zeolite veining, with calcite core and margins of zeolite. Surrounding material is the injection material shown in C. (**E**) (From Suardail) XPL. The main fault cataclasite: normal offset quartz-feldspar aggregate, cut by carbonate veins perpendicular to the fault surface (c). Authigenic clay bands (ac) alternate with very fine-grained quartz-feldspar aggregates (q-f). (**F**) (From Earabhig) XPL. Showing mass of carbonate cemented fractures (c) and cataclastic fault products. (**G**) (From Earabhig) PPL. 1 m below main fault surface: quartz-feldspar gneiss cataclasite (f) with minor chlorite, heavily fractured and cemented with zeolite and carbonate (c), cross cut by oil bearing veins (o). (**H**) (From Earabhig) XPL. Carbonate veins (c) cut cataclasite and zeolite veins (z).

3.6 Synthesis of Results

3.6.1 Lineaments

Lineament analysis results from the cover sequence fit well with geometric data obtained from fieldwork, with the same major fault sets represented. Stornoway Formation bedding dips to the NW and steepens across the formation from around 10-15° adjacent to the bounding faults in the west to up 45° on the Eye Peninsula; changes in bedding dip do not appear to be mirrored by changes in fault orientations. Lineament analyses show a concentration of bounding fault-parallel faults in the Stornoway Formation adjacent to those main bounding faults. This relationship, and steepening of the bedding, is consistent with the Stornoway Formation being a synrift sequence and suggests that in most cases, faulting occurred during or shortly after deposition in the basin. The bounding fault at Earabhig appears to be controlled by a pre-existing basement structure, and the bounding faults at other sites are parallel to sub-parallel with the local foliations. This parallelism of faulting in the Stornoway Formation with the bounding faults highlights at least the local basement foliation control on faulting in the cover sequence.

The longest lineaments appear to cut across multiple foliation orientations across the island, and if the assumption that they are faults is correct, they will also cut across and offset pre-existing faults and fractures. This carries with it the implication that the longest, most continuous lineaments are also the youngest features on the island. This seems to be confirmed by the fact that the longest lineaments mainly trend NNW-SSE and E-W. These orientations correspond to those of the fault sets that have been identified by fieldwork as the youngest faulting events in the region.

The very prominent NNW-SSE trending faulting/fractures found in both the Stornoway Formation and surrounding Lewisian Gneiss are attributed to normal faulting parallel to the local foliation within the Lewisian. The strong ENE-WSW trending signal within the Lewisian, particularly at 1:1000 scale, can be attributed to minor and intermediate scale early ductile shear zones, which are common on the Eye Peninsula. E-W striking structures are attributed to late (post Tertiary dyke) E-W strike-slip faults, particularly over the south of the Stornoway Formation region.

3.6.2 Fieldwork

Mesozoic and Cenozoic brittle deformation has produced discrete faults and fractures in the Stornoway Formation and underlying Lewisian Gneisses. Damage zones are lacking within the Stornoway Formation, with only a handful of faults having fault rocks of greater than 5 cm thickness. Carbonate found within the faults themselves may originate from the surrounding sediments, redistributed by fluids associated with faulting, and may also be partly related to later

dyke emplacement (Steel, 1971). Throughout the Stornoway Formation it is evident that post-depositional fluids have been important. Regular patches of crystalline calcite cemented conglomerate must have developed in response to high fluid fluxes through the sediment and removal of interstitial matrix particles. The fact that fault rocks in the Stornoway Formation are generally indistinguishable between the identified fault sets would suggest that they formed under the similar conditions, originating from shallow depths in the crust. The exception to this is the lack of foliated cataclasites or zeolite cement identified in Set 3 (post Tertiary dyke) faults within the Stornoway Formation, indicating lower temperature and pressure conditions, and less well-developed faults probably formed over a more restricted time period. This late strike-slip faulting is concentrated spatially in the south of the Stornoway Formation across Arnish and Holm (see Figure 3.6 for localities).

Stress inversions performed on the fault data collected from the Stornoway Formation indicate a recorded history of at least 3 stress regimes. Set 1 and Set 2 both pre-date the emplacement of Tertiary dykes (which were emplaced ca. 61-55 Ma; Hansen et al., 2009) and produce ENE-WSW to E-W horizontal extension, suggesting a direct relationship with extension associated with the early onset of Atlantic rifting. In the Minch Basin, Permo-Triassic sediments are overlain by horizontally bedded post-rift Jurassic sediments (Stein, 1992) so it seems unlikely that Set 2 records Jurassic rifting. Rather, the two fault sets more likely record Permo-Triassic phases of faulting associated with rifting and production of units 1, 2 and 3 in the model of Steel and Wilson (1975).

Tertiary dykes of the North Atlantic Igneous Province (Fettes et al., 1992; Hansen et al., 2009) are observed to intrude along Set 1 and Set 2 faults, and are clearly cross-cut by Set 3 sinistral and dextral conjugate strike-slip faults. Their emplacement in a NNW-SSE orientation also indicates the orientation of the minimum principal stress to be ENE-WSW, and this is readily related to extension along the NE Atlantic margin (e.g. England, 1988).

Stress inversion of fault data collected from Set 3 faults that cross cut the Tertiary dykes produces an ENE-WSW directed compression and NNW-SSE extension. This is different to the earlier stress regimes, and is relatively young. It may be related to post-breakup compression and either ridge push or a change in opening orientation (e.g. Dore et al., 1997). Tertiary strike-slip fault movements have been postulated on the mainland on the Great Glen Fault (Underhill, 1991) as a result of NE Atlantic opening**.** It is interesting to note that these late (post-Tertiary dyke) strike-slip faults have been found on North or South Uist during fieldwork conducted by the author.

When compared with the basement faults, there is a clear correlation between fault rock type and orientation, with the major trends of Mesozoic structures found in the Stornoway Formation

also being present in the Lewisian. Faults with clay-rich cataclasites, microbreccias and gouges are widespread in the basement. They cut ductile structures, reactivate pre-existing cataclasites, and have an associated mineralogy and kinematics very similar to faults seen within the Stornoway Formation. It is clear from the rose plots that the very strong NNW-SSE and weaker N-S trends identified in the Lewisian match the orientations of Set 1 and 2 faults identified in the Stornoway Formation. Set 3 structures are common in the Stornoway Formation but not in the Lewisian basement; this is probably reflecting the localised nature of E-W faulting in the Stornoway Formation, whereas faulting associated with Sets 1 and 2 affected the entire area. At Seisiadar, a large (2-3 m wide) NNE-SSW striking fault was observed parallel to the Minch fault. Given the proximity to the Minch Fault at Seisiadar, faulting related to movement on the Minch Fault may be expected at this locality. If the regional NNW-SSE trending normal faulting is contemporaneous with extension on the Minch Fault, a polymodal fault organisation must be present.

Detachments were observed along several phyllonite bands at Seisiadar and Pabail North, in agreement with observations made by other authors further south in southeast Lewis and Harris (e.g. Butler, 1995; Imber, 1998). These detachments seem to post-date pseudotachylite development. In addition, the bounding fault at Earabhig lies along a thick (>2 m wide) zone of phyllonite. Detachments lying parallel to the phyllonitic foliation were also observed, and although observations were limited to three outcrops, two main types are present; green, discrete fractures of uncertain displacement, and a clay-bearing dip-slip normal motion detachment set. These two groups may correspond to Type 1 and Type 2 detachments as identified on North Uist by Imber (1998). The earliest phase was poorly developed, and so little can be concluded from it. The latest detachment phase seems to be cut by the prevalent NNW-SSE striking faulting observed at most localities, and hence seems to pre-date it. However, it seems likely that movement on these detachments would have coincided with movement on the nearby Minch Fault, and a Mesozoic age can be postulated for them.

Stereoplots of data taken from Dun Mor show that carbonate veins tend to lie parallel with the main east-dipping fault at that locality, and perpendicular to the unconformity surface. These two vein orientations probably represent separate phases that are linked to the unconformity and development of the fault. Clastic veins show a preferred WNW-ESE orientation, and are localised to the hangingwall of the east-dipping fault. Clastic injections must have occurred during lithification, and were emplaced into fractures that were optimally orientated to the local stress orientations. This would indicate that the σ_3 direction trended NNE-SSW to NE-SW at this locality, and this could be associated with Set 1 faulting. Alternatively, this could reflect gravity-driven slumping off the basement high of the Eye Peninsula into Broad Bay north of the Eye Peninsula.

Shearing near to or along the unconformity surface was observed at Garrabost, Dun Mor, and Suardail. It is possible that shearing parallel with the unconformity occurred due to gravity-driven slumping, since the fault surface and contact at these localities all slope away from the basement high of the Eye Peninsula. Slumping may have occurred either during lithification or afterwards, during rotation of the bedding. Notably at all three localities shearing was localised to a discrete fault surface within the Stornoway Formation that parallels the unconformity in a zone up to 2 m up into the Stornoway formation. High pore fluid pressures would also have lowered the shear stress magnitudes needed for failure along both the contact interface and the faults seen at these localities, possibly enabling slumping. Carbonate veining is contemporary with sediment veining and seems to be partly controlled by the presence of pre-existing ENE-WSW trending epidote-filled fractures that the carbonate veins reactivate.

Oil within basement rocks of the Stornoway Region seems closely related to proximity to major structures, and may be derived from phases of oil generation in the Minch (e.g. Stein, 1992). At the bounding fault of the Stornoway Formation at Earabhig, oil is seen surrounding breccia, indicating that oil influx may have occurred during faulting or under high pore fluid pressure during Mesozoic faulting. This constrains the Group 4 fault rock, identified in the basement and associated with oil, to the Mesozoic if the oil is of the same age.

In summary the Stornoway Formation contains three distinguishable faulting events that can be relatively dated. Stress regimes through time have generally been directed with a vertical/sub-vertical maximum principal stress during the Mesozoic, followed by a switch to an E-W orientation, in the early Tertiary. These phases could be linked to Atlantic rifting and continental breakup, and the age of these faulting events is likely to be equivalent to those seen within the Minch itself, giving phases of deformation during the Permo-Triassic and Tertiary. Jurassic faulting has not been identified along the Minch Fault and seismic lines show horizontally bedded strata interpreted as post-rift deposits (Stein, 1992).

Within the basement, Mesozoic and younger faulting is evidently at least partly controlled by pre-existing foliation in the gneisses and faults within the OHFZ. Most noticeably early epidote-rich cataclasites and epidote-cemented breccias are reactivated by zeolite and authigenic clay-bearing fault rocks that are continuous through into the cover sequence. Hence faulting within the Stornoway Formation was at least locally directly controlled by structures within the Lewisian basement.

3.6.3 Microscope Results

In areas where the country rock of the Stornoway Formation contains porosity, faulting appears to noticeably decrease local rock porosities through mafic, phyllosilicate, and epidote minerals altering to clays, and due to the very fine grain sizes produced through cataclasis. Set 1 and 2 faults in the Stornoway Formation have been found to contain crystalline zeolite in the form of veins and haloes, often associated with carbonate dissolution and porosity in the fault rock. The process of formation of porosity is clearly linked to zeolite production and fluid flow, and possibly to the associated dissolution of calcite.

Zeolite mineralisation indicates fluid circulation at temperatures of up to 200°C (Frey, 1987; Watts et al., 2007), and zeolite is the dominant secondary mineral that forms at these temperatures in crystalline rocks (e.g. Weisenberger, 2009). This suggests that zeolite formed at depths < 6 km, if a normal geothermal gradient is assumed. It seems very likely that depths of burial are much less than this, with an estimated denudation on Lewis of 2250 +/- 750 m during the uplift of the Palaeocene due to igneous underplating (Brodie and White, 1994; Tiley et al., 2004; Persano et al., 2007)**.** Low temperatures are also confirmed by calcite type 1 deformation twinning within the fault rocks, indicating temperatures of less than 170°C (Passchier and Trouw, 1996). The presence of authigenic clay minerals also confirms low temperature and low pressure conditions (e.g. Velde, 1985).

Set 3 faulting occurred alongside carbonate mineralisation, and it is noticeable that Set 3 faults do *not* contain crystalline zeolite in the form described above, but rather, have incorporated zeolite into the fault rock as clasts, potentially indicating shallower (and more recent) conditions of faulting. This may partly be a reflection of the regional denudation described above. Clearly conditions throughout the depositional history of the Stornoway Formation have been consistently low enough to prevent epidote formation, confirming temperatures lower than 200°C (Liou, 1993).

In the basement, Mesozoic faulting is associated with carbonate and zeolite mineralisation occurring alongside syntectonic authigenic clay formation. Mesozoic faulting is associated very clearly with porosity that is directly associated with zeolite and adularia mineralisation. The origins of this porosity are not entirely clear, but it is once again clearly associated with the partial dissolution of calcite. It is clear that throughout the phases of Mesozoic/Cenozoic faulting identified, fluids played a major role, with hydration and alteration of mineral phases and transport of species to produce clay and zeolite phases.

Fluids also played an important role in the development of the basement-cover interface. Carbonate veining is directly attributable to the faulting seen at all contact localities, with multiple

phases of local veining and fault movements preserved. Carbonate veining occurred contemporaneously with sediment injection into the basement, seen most conspicuously at Dun Mor. As sediments were still mobile, injections must have occurred during lithification and clastic veining is associated with an east-dipping fault. Multiple phases of sediment injection indicate repeated cycles of fluid overpressure and fracturing of the basement rock, probably during dewatering and subsequent pore fluid overpressure.

3.6.4 Synthesis

Figure 3.65 shows the interpreted structures from the lineament analysis of the Stornoway Region based on fieldwork results. As can be seen, there is agreement between lineaments from the Stornoway Formation, and those from the Lewisian Gneiss with the exception of NE-SW striking shear zones and pre-Mesozoic faults encountered within the Lewisian that are not through-going into the Stornoway Formation.

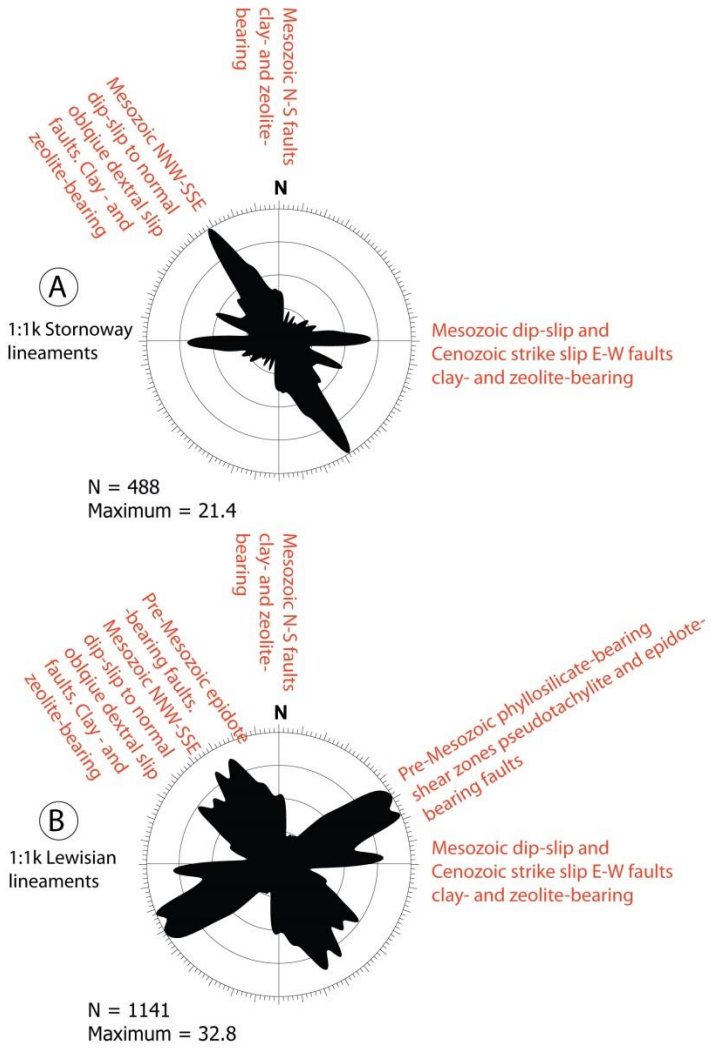

Figure 3.65: Lineament analysis orientation results with interpretations ascertained from fieldwork shown in red. (**A**) Lineaments picked from the Stornoway Formation. (**B**) Lineaments picked from Lewisian of the Stornoway region.

The structural analysis of Suardail (sections 3.4.2.1.7, 3.4.4 and 3.5.1.3) provides important insights into the structure of the region as a whole, confirmed through the fieldwork described above. The headland at Suardail is shown in Figure 3.66, with interpreted faults indicated and presented in 3D in the bottom image. On the western side of the headland, lateral ramps (in orange) link to the main fault surface (in red) that is partly coincident with the basement-cover interface at this locality. On the eastern side of the headland, another likely lateral ramp (in orange) passes through the basement-cover interface, that is closely approximated by a low angle shear (in yellow). A NNW-SSE striking fault (light blue) is visible truncated against the interface, whilst other faults (dark blue) are through-going. From these observations at Suardail and from other localities, it is possible to produce a conceptual model for faulting in the Stornoway region, shown in Figure 3.67 with major relationships observed in the field indicated.

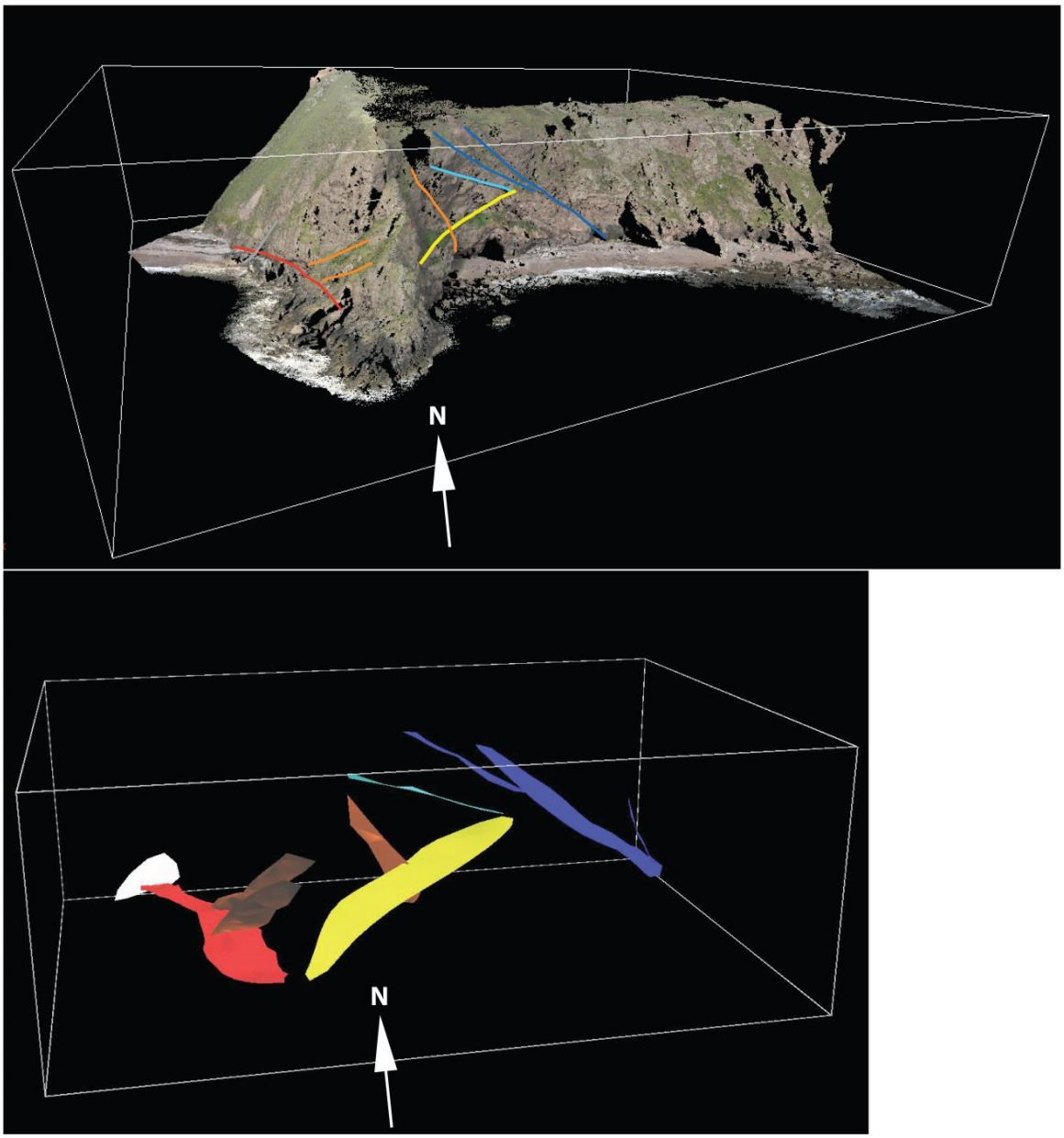

Figure 3.66 (previous page): Terrestrial laser scan data from Suardail, with viewpoint looking from the sea towards the headland (top), with interpreted surfaces indicated and shown in bottom image. Red = main fault, dipping to the east, orange = lateral ramps from main fault, yellow = low angle shear, dark blue – ENE dipping faults cutting basement and cover, light blue = ENE dipping fault localised to the Stornoway Formation only, grey = possible late E-W striking strike-slip fault.

Thin sections from typical faults are also presented in Figure 3.67, corresponding with the faults indicated in the block diagram. From microscopy analysis it is apparent that porosity and permeability are enhanced in Mesozoic faults and associated fractures, particularly with the presence of open porosity associated with adularia and zeolite mineralisation that occurs alongside the development of authigenic clays. This observation is important as it correlates with direct observations of porosity in the basement rocks of the Clair core (chapter 6), and indicates that faulting of Mesozoic and younger age occurred under roughly the same conditions on the Hebrides and at the Clair Field.

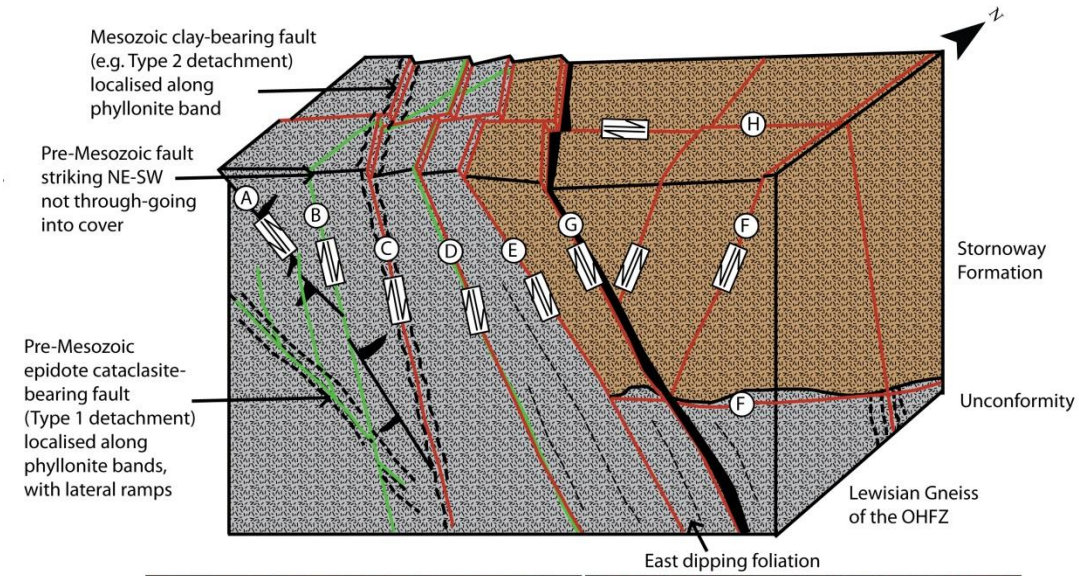

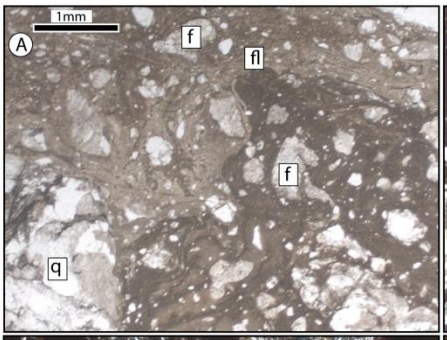

Pseudotachylite fault rock - no porosity

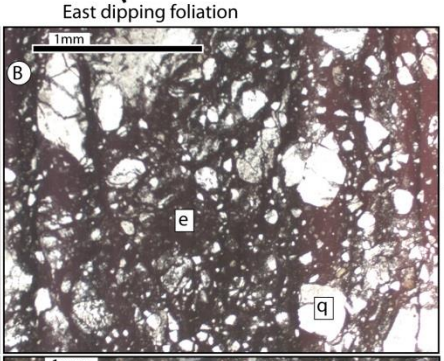

Epidote cataclasite fault rock - no porosity

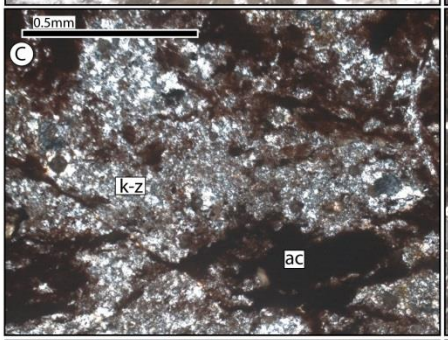

Clay-, adularia-, zeolite-bearing fault rock with porosity

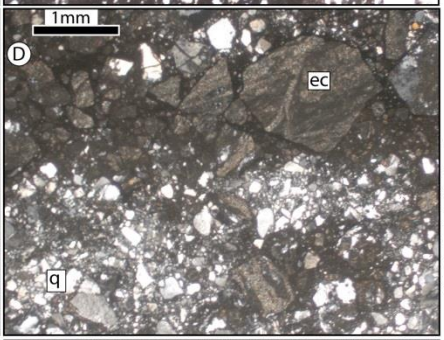

Clay-, adularia-, zeolite-bearing fault rock with porosity, reactivating epidote-bearing fault rock

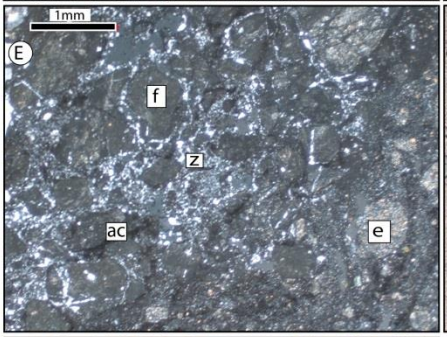

Bounding fault zeolite and clay-bearing fault rock, with porosity

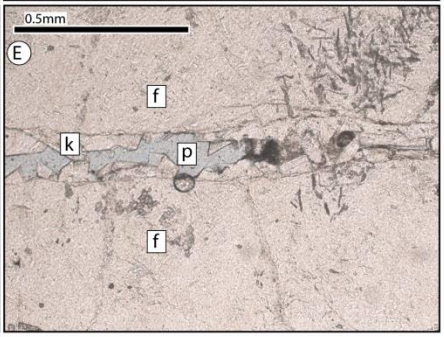

Open porosity along partially filled fractures assocaited with bounding faults

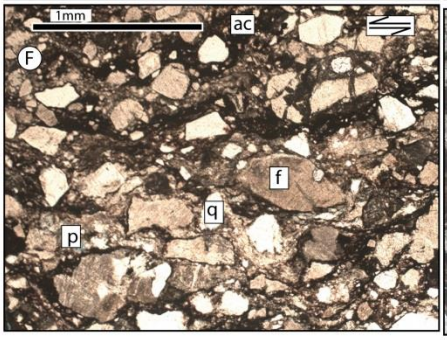

Zeolite and clay-bearing fault rocks

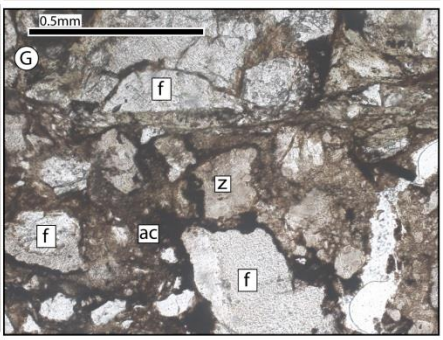

Zeolite and clay-bearing fault rocks. Enriched in zeolite following dyke intrusion

Figure 3.67 (previous page): Conceptual model of faulting in the Stornoway Region with accompanying fault rock images. A-B, Pre-Mesozoic faults, C-G Mesozoic age faults. f = feldspar, fl = flow structures, q = quartz, e = epidote, ac = authigenic clay, ec = epidote cataclasite, z = zeolite, p = porosity, k = adularia. (**A**) Early pseudotachylite both parallel with and cutting the foliation. (**B**) Epidote cataclasite bearing faults, striking NE-SW and NW-SE, offsetting foliation and pseudotachylites. (**C**) Clay-bearing Mesozoic age faulting localising along phyllonite bands. Pre-Mesozoic faults also localise along and splay from phyllonite bands. (**D**) Clay-bearing Mesozoic age faulting localising along pre-existing epidote-bearing fault. (**E**) Bounding faults of the Stornoway Formation localised along local foliation planes. (**F**) NNW-SSE and N-S striking Mesozoic age conjugate faulting developed within the Stornoway Formation, probably linked with or terminating at the basement-cover interface. (**G**) Tertiary dykes (in black) intruded along NNW-SSE and N-S striking faults in the Lewisian and Stornoway Formation. (**H**) Post-Tertiary dyke strike-slip faulting.

3.6.5 Conclusions

The following have been demonstrated during the present work:

- *What are the characteristics of faulting within the cover sequence?*

  Faulting in the Stornoway Formation cover sequence is comprised of at least two and probably three sets of Mesozoic and younger faults: Those that pre-date and those that post-date the Tertiary dykes. Faulting in the cover is dominated by relatively thin (<5 cm thick), relatively steeply dipping clay gouge-bearing faults, at times cemented with calcite. Faults within the cover strike NNW-SSE, N-S and E-W, with all sets being represented by conjugate faulting.

- *Is faulting in the cover controlled by faulting within the basement?*

  The basement-hosted OHFZ has also influenced the distribution of the fault-bounded Stornoway Formation. Major bounding faults in the west and north lie along foliated rocks that formed during earlier phases of motion on the OHFZ. Mesozoic (Set 1 and 2) aged faults in the Stornoway Formation often directly reactivate epidote cataclasite faults in the basement, and also locally reactivate the basement foliation. The localisation of E-W faulting within the Stornoway Formation may be due to the localised presence of E-W to ENE-WSW trending early shear zones in the Lewisian that were identified during fieldwork on the Eye Peninsula. Mesozoic faults within the basement are dominated by the same NNW-SSE trend found within the cover rocks, indicating continuity from basement to cover.

- *Is faulting of Mesozoic age distinguishable within the basement?*

Mesozoic and younger faulting is observed within the basement and Permo-Triassic cover sequences with characteristics noticeably different to older fault rock assemblages (e.g. pseudotachylite and epidote cataclasites) that are only preserved in the basement rocks.

The sequence of fault rock assemblages identified within the Lewisian Gneiss are indicative of a system undergoing exhumation through time, from ductile movements along shear zones and production of mylonites and phyllonites, followed by brittle pseudotachylite faulting (possibly 13.5 km depth, Fettes et al., 1992) epidote cataclasites (>7 km depth e.g. Fossen and Hurich, 2005), and adularia, zeolite, and clay-bearing faults (< 6 km depth). Mesozoic and younger faults identified within the Lewisian are generally discrete fractures lacking any macroscopic damage zones. Zeolite and clay bearing faults have been identified as Mesozoic in age on the basis that they are continuous through into the cover sequence, and are most easily distinguished by their colour, often poorly indurated nature, and presence of calcite and zeolite.

- *What controls are there on faulting within the basement?*

  Field observations and existing geological maps show that local foliations are parallel with the bounding faults of the Stornoway Formation. Mesozoic and younger faulting is at least partially controlled by pre-existing structures in the basement (gneissose foliation, shear zones, faults). In many cases, the presence of weak phyllonites has enabled localisation of extension onto these surfaces with the formation of detachments.

- *What is the nature of the basement-cover interface?*

  The basement-cover unconformities studied on the Eye Peninsula at Dun Mor and Suardail preserve an association with faulting approximately 1 m into the cover sequence that parallels the unconformity. It seems likely this shearing occurred shortly after the sediments were deposited, possibly under the influence of tectonically-induced gravity-driven slumping. Other faults may be localising along the basement cover interface, and at both Suardail and Dun Mor Mesozoic age faults are present. At Dun Mor extensive clastic and calcite veining occur within the Lewisian. Multiple phases of both vein types are present, and this is likely to be indicative of repeated phases of pore fluid overpressure and tensile fracture, which may be related to movements on the fault.

Chapter 4: Brittle faulting and fracturing within Lewis

4.1 Introduction

The Isles of Lewis and Harris lie along-strike from the Clair Field (Figure 1.5). Clair crystalline basement is considered to be analogous to that of the Lewisian Gneiss Complex (e.g. Pless, 2011). The Outer Hebrides lie in the uplifted footwall of the Mesozoic Minch Fault (Roberts and Holdsworth, 1999) making study of this area of basement rock particularly relevant to the Clair Field. In addition, the OHFZ may underlie the Clair Field at depth (e.g. Ritchie and Darbyshire, 1984; Duindam and Van Hoorn, 1987; Dore et al., 1997; Dean et al., 1999), and hence understanding fracture properties within the onshore Outer Hebrides Fault Zone will also potentially contribute to better constraining fracture properties in the Clair Field basement in the subsurface. Fracture sets on Lewis are poorly understood, with no existing island-wide studies that report on fracture attributes such as orientation, spacing, and aperture and their links to lithology, foliation, and fault rocks/age. This chapter attempts to bridge this knowledge gap.

4.1.1 Objectives

The main questions posed here are:

- What are the characteristics and possible ages of faults on Lewis?
- What are the characteristics of post-Caledonian faulting on Lewis?
- How do the geological characteristics of faulting and fracturing differ between the rocks of the Outer Hebrides Fault Zone and rocks located to the west?
- What controls possible Mesozoic-aged faulting on Lewis?

These questions have been studied using remotely sensed data analysis, fieldwork, and thin section analysis, presented below.

4.2 Geological background

Lewis is dominated by the presence of the OHFZ in the east, and a major lineament – the Seaforth Lineament - forms a prominent divide approximately between Lewis and Harris across which topography, geology (Figure 4.1), and predominant fracture orientations change. The area south of this lineament is described and discussed in Chapter 5.

4.2.1 Regional Geology

As discussed in chapter 2, the Isles of Lewis and Harris are composed predominantly of quartzo – feldspathic 'grey' gneisses. In the west, the area is dominated by Laxfordian migmatites, granite intrusions, and pegmatite veins (Fettes et al., 1992). These granites and pegmatites generally cut the foliation, and granite bodies are mostly irregular in shape (Fettes et al., 1992). In northernmost Lewis, supracrustal rocks are preserved, including metasediments and anorthositic remnants (Watson, 1969). These rocks comprise an assemblage very similar to the Langavat belt of South Harris (Coward et al., 1969) and have a similar metamorphic history (Whitehouse, 1990; Whitehouse and Bridgwater, 2001), possibly representing an accreted arc terrane. To the south and southwest, the region studied here is bounded by the Seaforth Lineament.

4.2.1.1 OHFZ

The Outer Hebrides Fault Zone trends NE-SW across the eastward margin of the Outer Hebrides and Lewis. This major structure was initiated in the Proterozoic and has been reactivated multiple times since with phases of ductile and brittle deformation (Butler, 1995; Butler et al., 1995; Imber et al., 1997; Imber, 1998; Imber et al., 2001; Imber et al., 2002).

4.2.1.2 Post-Caledonian Faulting

Brittle faulting postdating Caledonian structures is little studied on Lewis and Harris. Mendum (2009) mentions that late cataclasites, gouges and breccias may be related to Devonian, Carboniferous, and Mesozoic age faulting within the Minch. In chapter 3, Mesozoic and Cenozoic faults were identified within the Stornoway Region of the OHFZ. These faults strike NW-SE, N-S and E-W, and display near dip-slip normal motion. Tertiary dykes often intrude down NNW-SSE to N-S striking fault cores, and a late phase of E-W strike-slip faults cross-cuts these dykes. Mesozoic and Cenozoic aged fault rocks are mainly composed of calcite cemented syntectonic authigenic clay gouges and cataclasites that show varying degrees of development (section 3.4). Large scale features that cross the islands and hence presumably post-date large-scale movements on the OHFZ, such as the Seaforth Lineament and the Tarbert and Loch Liurbost Faults (Mendum, 2009), are often marked on maps but are not closely studied or described in any detail.

4.2.2 Study Sites and methods

Due to the large areal extent of the Lewisian Gneiss on Lewis, fieldwork was targeted to accessible zones of specific interest and exceptional exposure. Similarly with Chapters 3 and 5, the study of

faulting has been achieved through regional lineament analysis, local fieldwork, and thin section analysis of selected fault rocks. A total of 422 sites were visited within the Lewisian Gneiss Complex and OHFZ on Lewis and Harris (Figure 4.1), including sites discussed in Chapter 3. Exposure is mostly limited to the coast, and within quarries and along road cuttings or stream sections inland, which dictates data collection site distribution. Elsewhere, faults and fractures are difficult to study due to intense weathering and Quaternary peat cover.

This chapter has been subdivided into two main areas – east Lewis, and west Lewis (Figure 4.1).

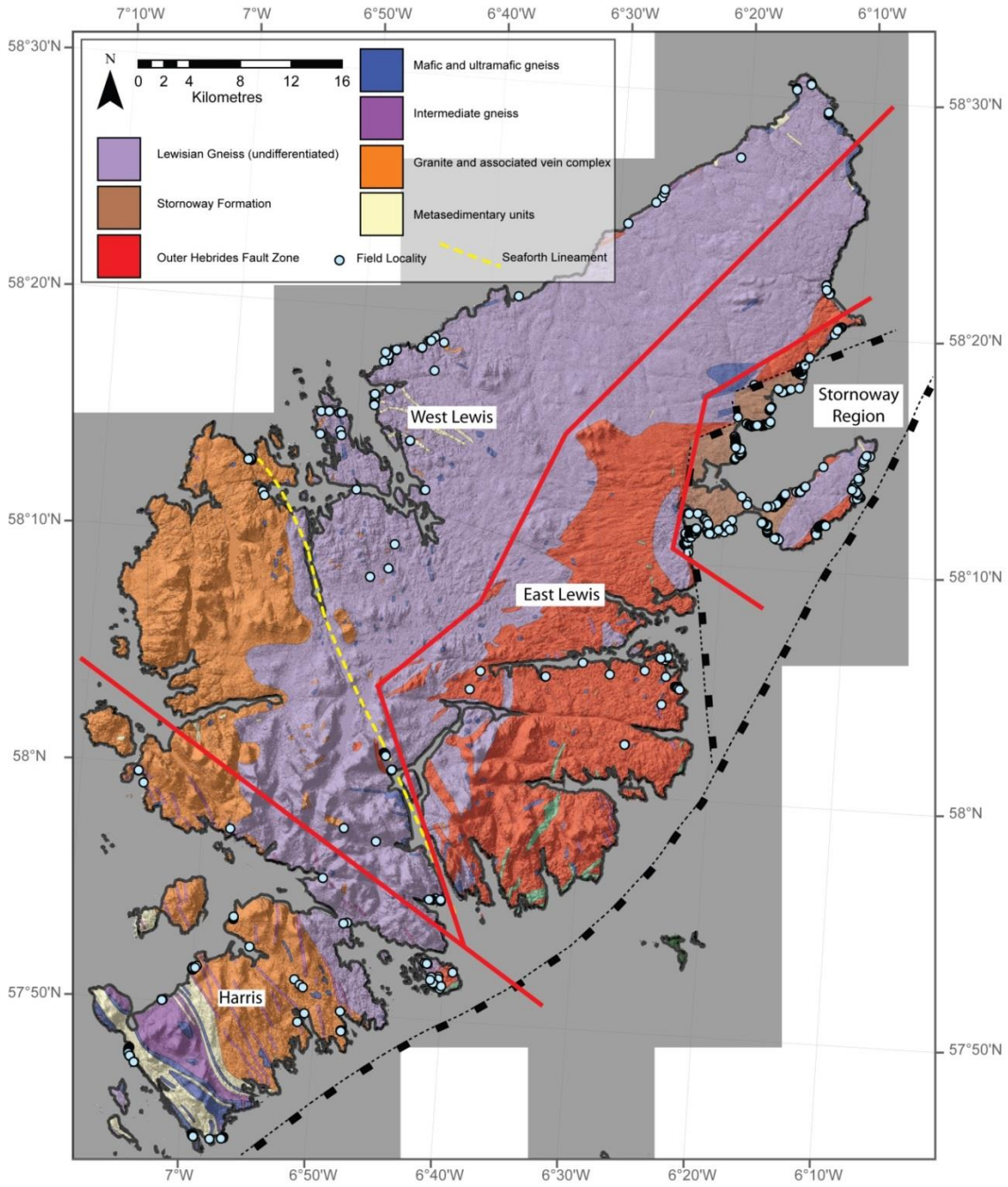

Figure 4.1: Showing geology of Lewis and Harris underlain by digital surface model (DSM) processed from Nextmap ® data. Red lines indication division of the island. West and east Lewis

are covered in this chapter. The Minch Fault and major faulting associated with the Stornoway Formation are indicated. Seaforth lineament is indicated in yellow.

4.3 Lineament analysis

Lineament analysis was performed with the aim of identifying major faults and zones of interest, in addition to giving an indication of fault lengths and orientations. In order to undertake the lineament analysis, the foliation was first digitised across Lewis and Harris in order to eliminate foliation related lineaments (Figure 4.2). The same methodology and limitations apply to this analysis as mentioned in section 3.4.1, and importantly, low angle structures are not distinguishable. Splitting and comparing these results between west and east Lewis (Figure 4.3 and Figure 4.4 respectively) shows only minor variation between the different resolutions at 1:25k, 1:50k, 1:100k, indicating a degree of scale invariance with respect to lineament orientation. In west and east Lewis, both datasets show a strong NNW-SSE trend, and a weaker ENE-WSW trend that is more pronounced in west Lewis. These results compare favourably with fieldwork results (section 4.4 and section 4.5) that show the same major orientations, supporting the assumption that the majority of picked lineaments represent the surface expression of faults. In west Lewis, additional NW-SE structures are likely related to faults of this trend widely developed in northwest Harris (see section 5.3). Northern Lewis notably lacks lineaments due to a thick peat cover that precludes any topographic expression of faults.

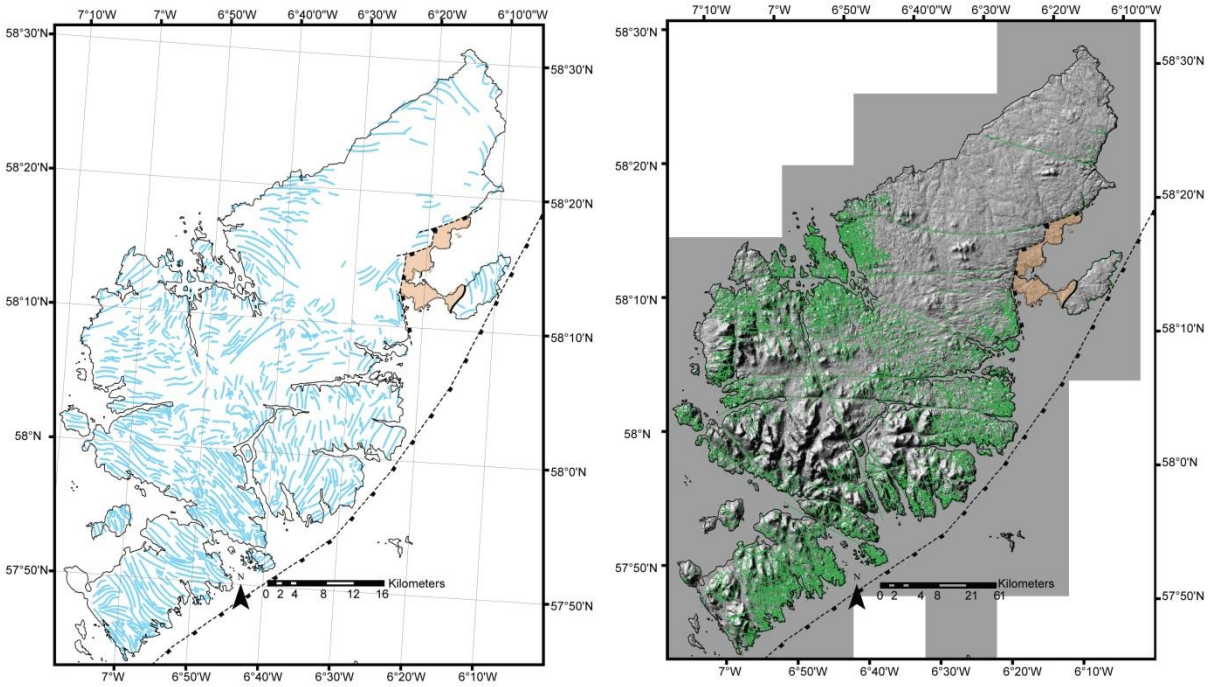

Figure 4.2: Digitised Foliation trend from Lewis and Harris (left, in blue) and lineaments picked from DSM (right, in green). Stornoway Formation shown in brown with major faults indicated.

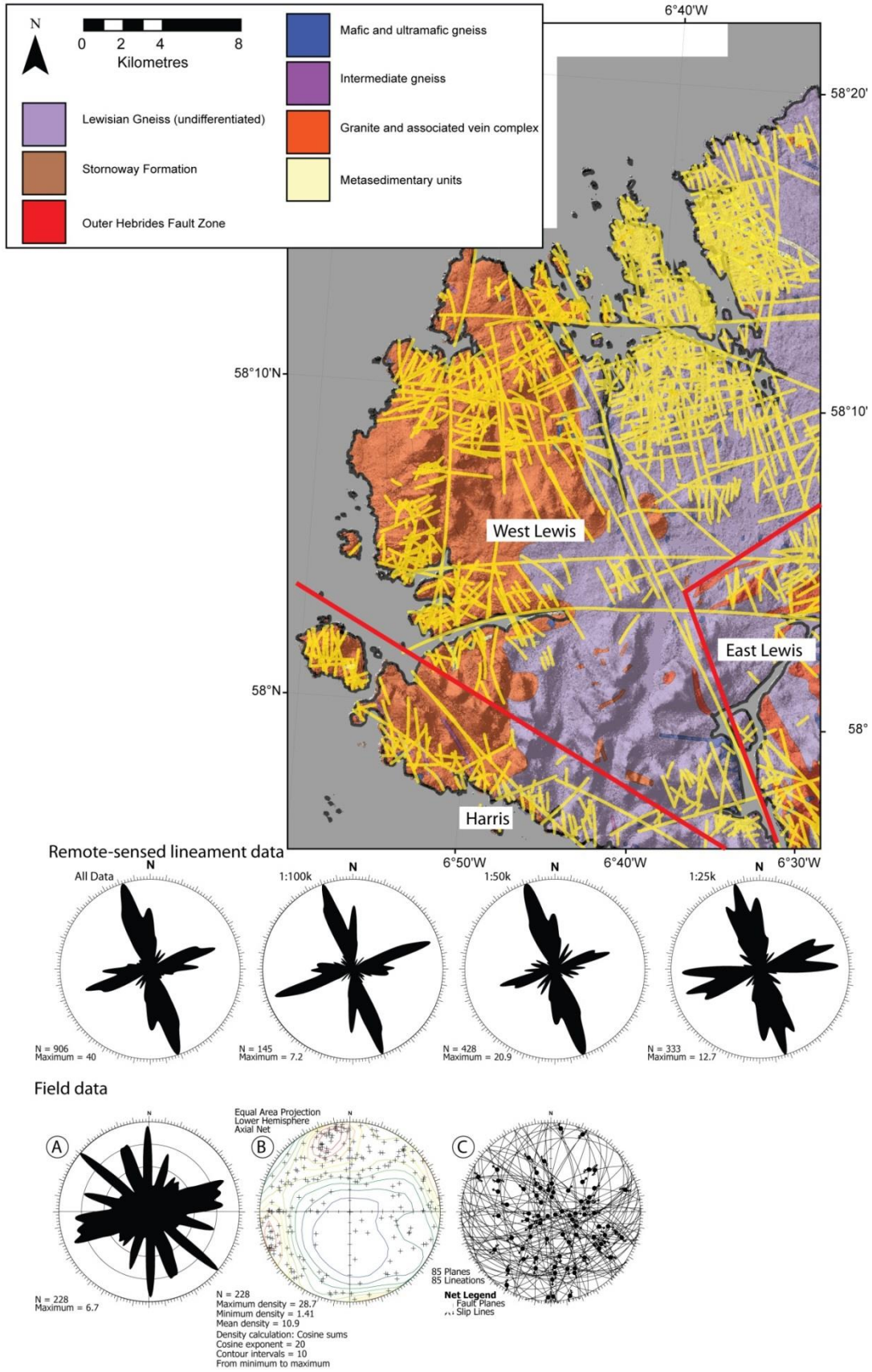

Figure 4.3: Western Lewis lineament analysis and fieldwork results comparison. Map shows geology of western Lewis overlain by lineaments picked from the remote sensed DEM data (in yellow). DEM data was analysed at 1:100k, 1:50k and 1:25k (top row of plots). Fieldwork results are shown in the bottom row of plots.

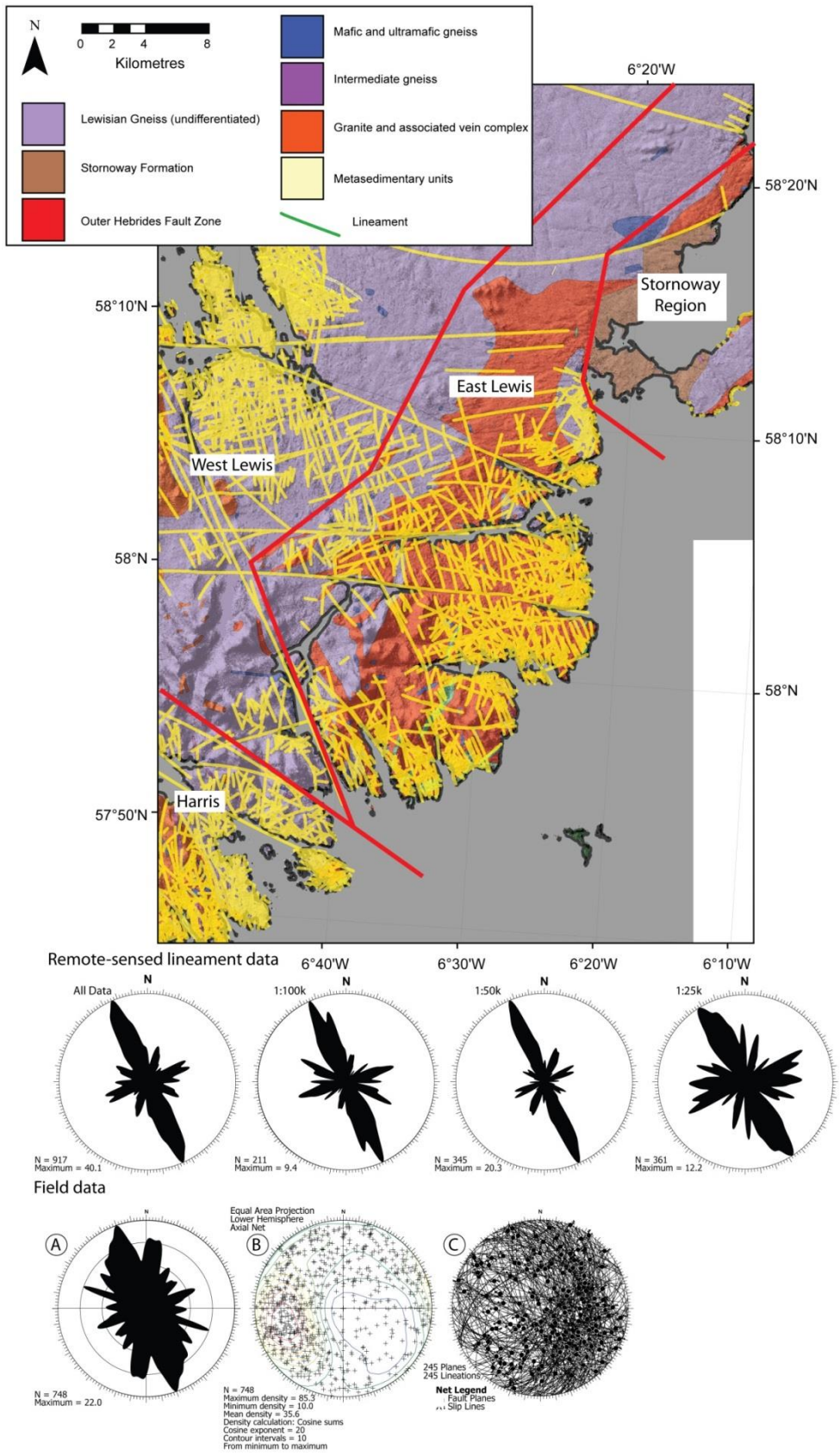

Figure 4.4: Eastern Lewis lineament analysis and fieldwork results comparison. Results include those from the Stornoway Region. Map shows geology of eastern Lewis overlain by lineaments picked from the remote sensed DEM data (in yellow). DEM data was analysed at 1:100k, 1:50k and 1:25k (top row of plots). Fieldwork results are shown in the bottom row of plots.

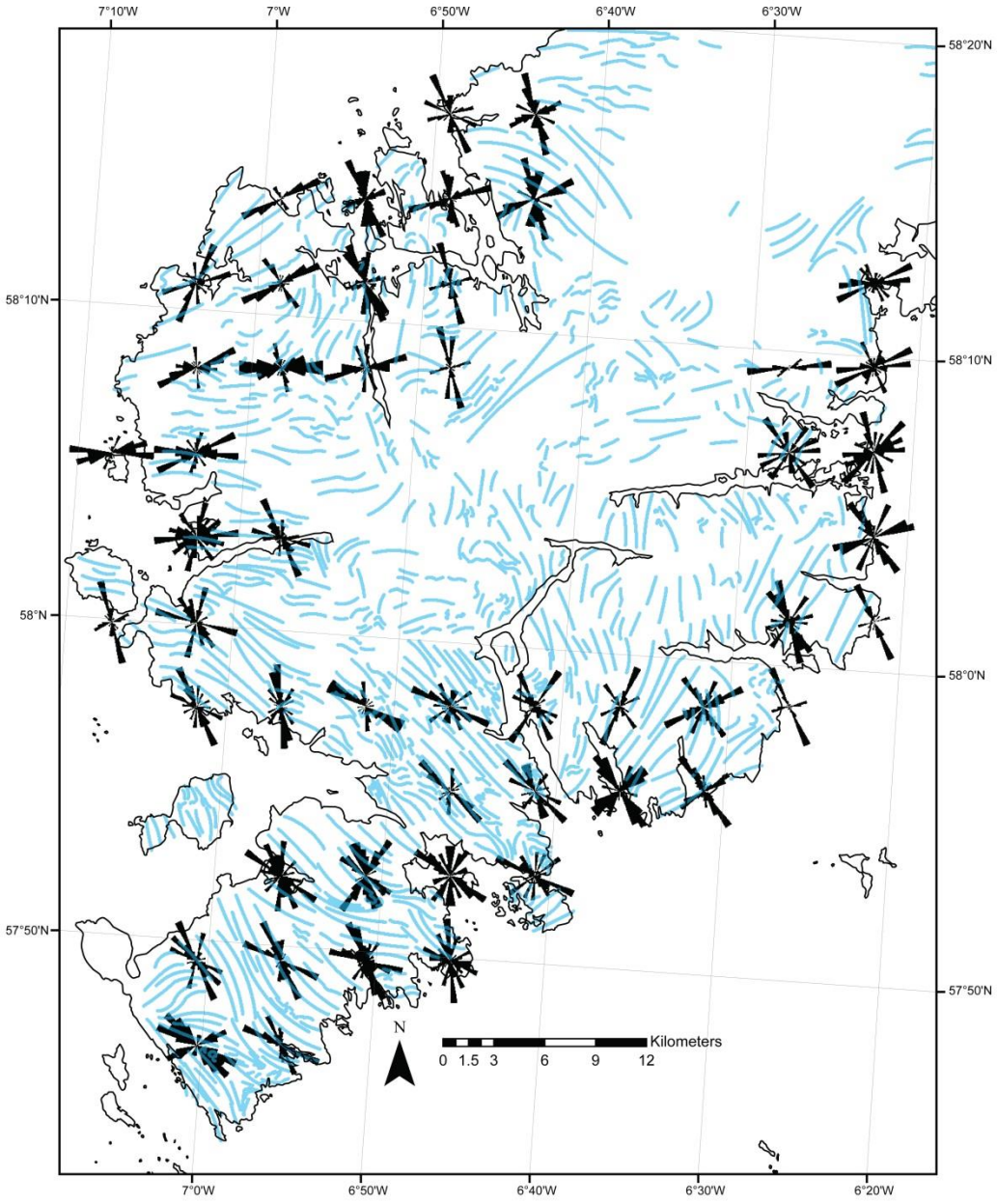

Figure 4.5: Variation in lineament orientation overlying foliation trend (in blue).

4.4 Fieldwork Results – West Lewis and North Lewis

Fault analysis in West Lewis has concentrated on the identification of dominant lineament trends with fieldwork targeted on this basis, together with accessibility and exposure, in order to characterise specific fault sets.

4.4.1 North Lewis: Cunndal/Port Stoth E-W faulting

Three localities were studied in the North of Lewis: Cunndal, Port Stoth, and Port Ness. These were chosen for good exposure and accessibility (Figure 4.6). Foliation is sub-horizontal, which is

notably different from that seen in the South Harris Shear Zones, to which the area has been equated (Whitehouse, 1990). The country rock is composed of strongly banded gneiss, with metasedimentary and anorthositic pre-cursors (Watson, 1969). The rocks are all highly deformed under amphibolite facies conditions (Watson, 1969). Immediately inland no exposures of rock are available for study due to peat cover.

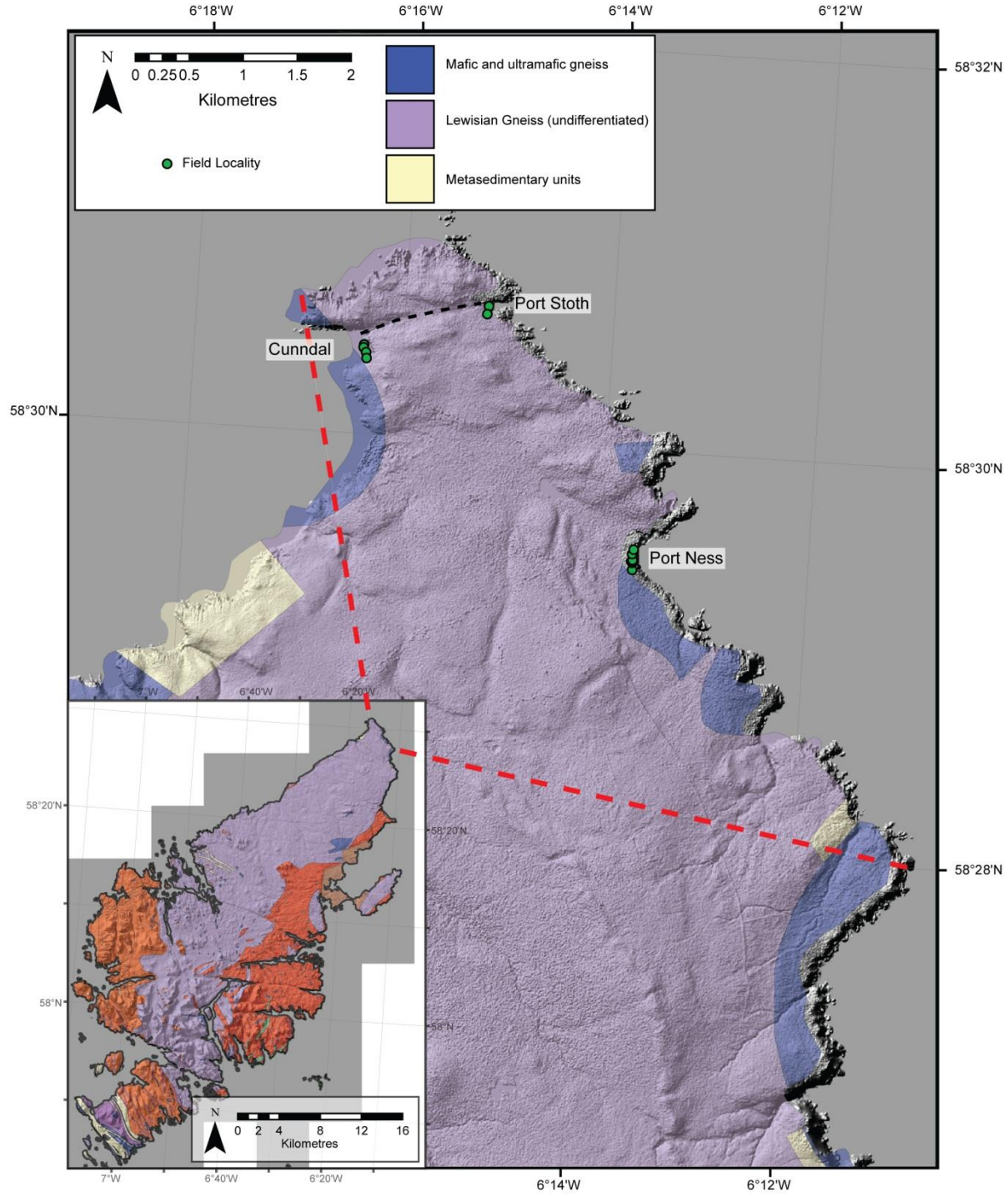

Figure 4.6: Geological map of N Lewis overlying a digital surface model of the island, and showing field localities.

4.4.1.1 Cunndal

The bay at Cunndal (NB 5124 6553) lies on the western tip of north Lewis, facing west. The studied area encompasses ~200 m of ~8 m high cliffs. The area is dominated by amphibole-bearing coarse-grained quartzo-feldspathic gneisses, with pods and lenses of pegmatite and amphibolites that are boudinaged. Foliation is sub-horizontal, dipping shallowly towards the east, and is finely banded at a sub-centimetre scale.

Several phases of faulting are visible at Cunndal. Pseudotachylites up to 5 cm thick are seen lying sub-parallel to the foliation and are associated with injection veins that cut the foliation (Figure 4.7A). Other relatively early faulting is associated with epidote veneers and cataclasite (Figure 4.7B). Epidote-bearing faults tend to cut the foliation at a high angle and dip to the southeast, with dip-slip normal kinematics. A third phase of faulting that hosts clayey gouge (Figure 4.7C-H), cross cuts the foliation and earlier faults, and in some cases these faults are sub-parallel with epidote-cataclasite faults. Reactivation of pre-existing epidote cataclasite bearing faults by clay gouges was suspected but not proven in the field, however in thin section it is apparent that zeolite, calcite and clay bearing faulting brecciates pre-existing epidote cataclasite fault rock (section 4.6.1). Clay-bearing faults dip moderately to steeply towards the south (Figure 4.8), with normal offsets.

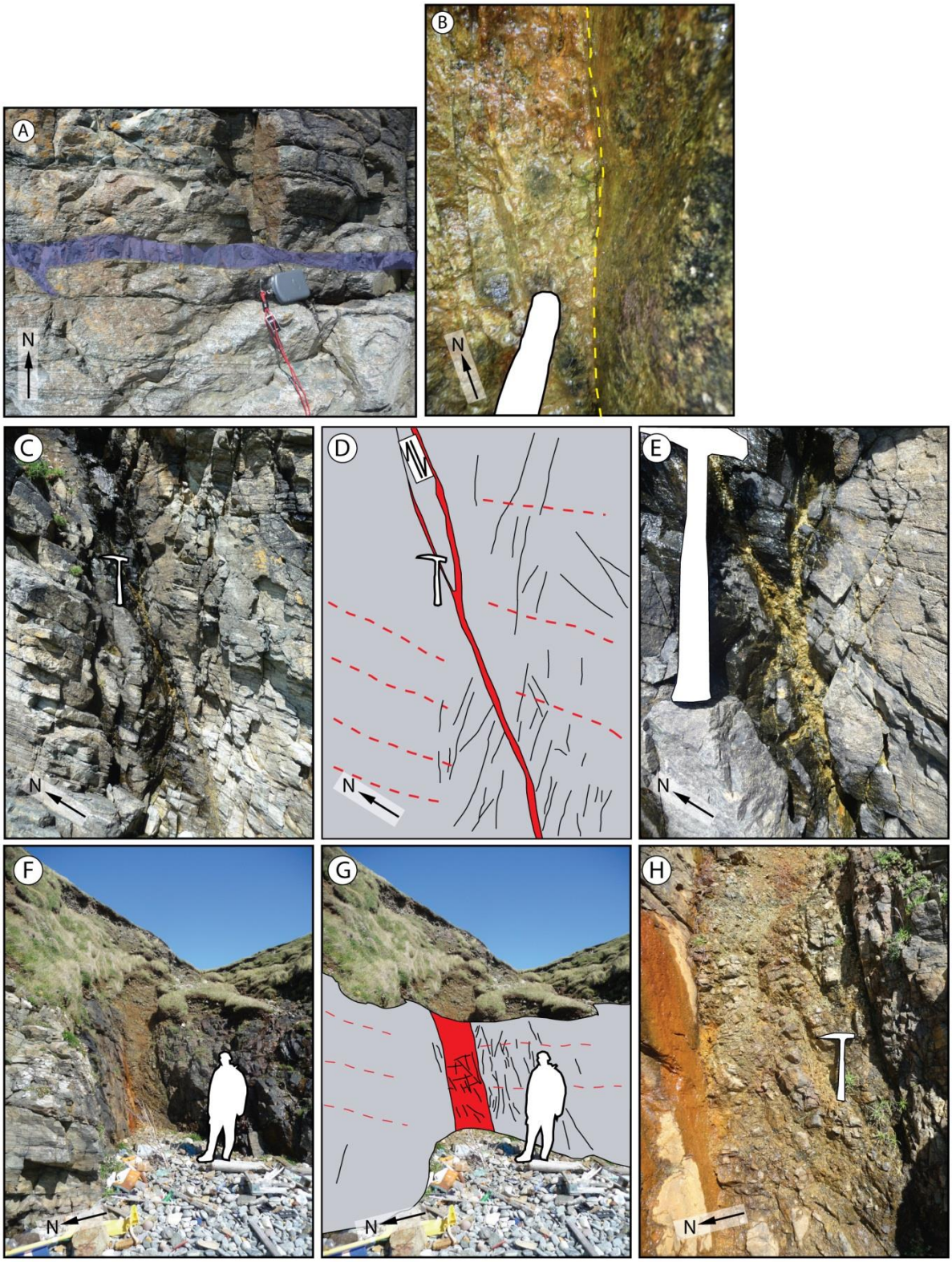

Figure 4.7: Outcrop at Cunndal. Purple = pseudotachylite, red = clayey gouge and breccia, yellow dashed line = fault, red dashed line = foliation, light grey = grey gneiss. (**A** - **B**) NB 5122 6558. (**A**) Foliation-parallel pseudotachylite with injection vein cutting the foliation at the left of the image. (**B**) Epidote-bearing slip surface (right of dashed yellow line) and breccia (left of dashed yellow line). (**C** – **H**) NB 5124 6553. (**C** - **E**) Clay-bearing fault cutting the foliation at a high angle, with subsidiary fractures indicated. Dip-slip normal kinematics were observed on this fault. (**F** – **H**) One-metre wide zone of steeply southward dipping clayey chaotic breccia with normal kinematics.

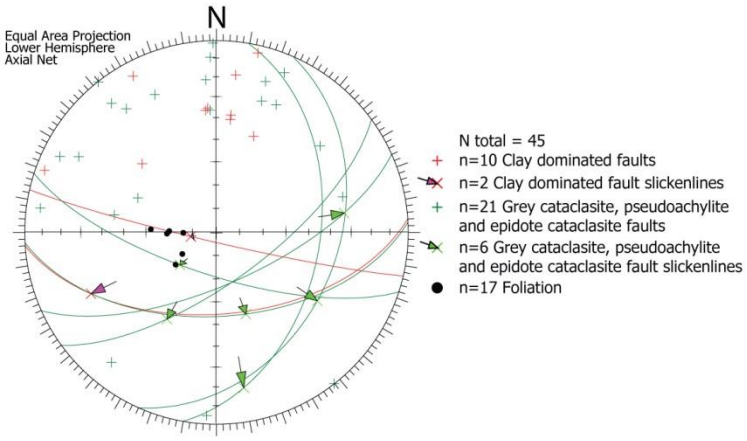

Figure 4.8: Stereonet of data collected at Cunndal. Faults with slip data recorded are shown with a great circle in addition to the pole.

4.4.1.2 Port Stoth

Port Stoth (NB 5239 6596) is situated on the eastern tip of northern Lewis (Figure 4.6). Outcrop is limited to ~70 m of Lewisian Gneiss in cliffs up to about 6 m high, which face east. The country rock is composed of grey gneisses with foliation dipping shallowly to the east (Figure 4.10) with bands of concordant amphibolite and more granitic composition, K-feldspar-rich gneiss.

On closer inspection, the foliation is commonly defined by mylonitic and proto-mylonitic banding, and dips moderately to the east (Figure 4.9A). Several phases of faulting are visible, with reactivation evident. Early pseudotachylite bands lie parallel with the foliation, with associated cross-cutting injection veins (Figure 4.9A). Later faulting is dominated by steeply and moderately northward dipping faults with epidote cataclasites and veneers (Figure 4.9B) overprinted and reactivated by carbonate-rich clay gouges (Figure 4.9C-E). Epidote cataclasite-bearing faults and clay-bearing faults were not observed to follow the foliation in the gneisses. Epidote cataclasite-bearing faults are dominated by pairs of fault cores, with two parallel fault planes usually less than 1 m apart. Carbonate veins associated with faults cross-cut earlier epidote veins (Figure 4.9F-G).

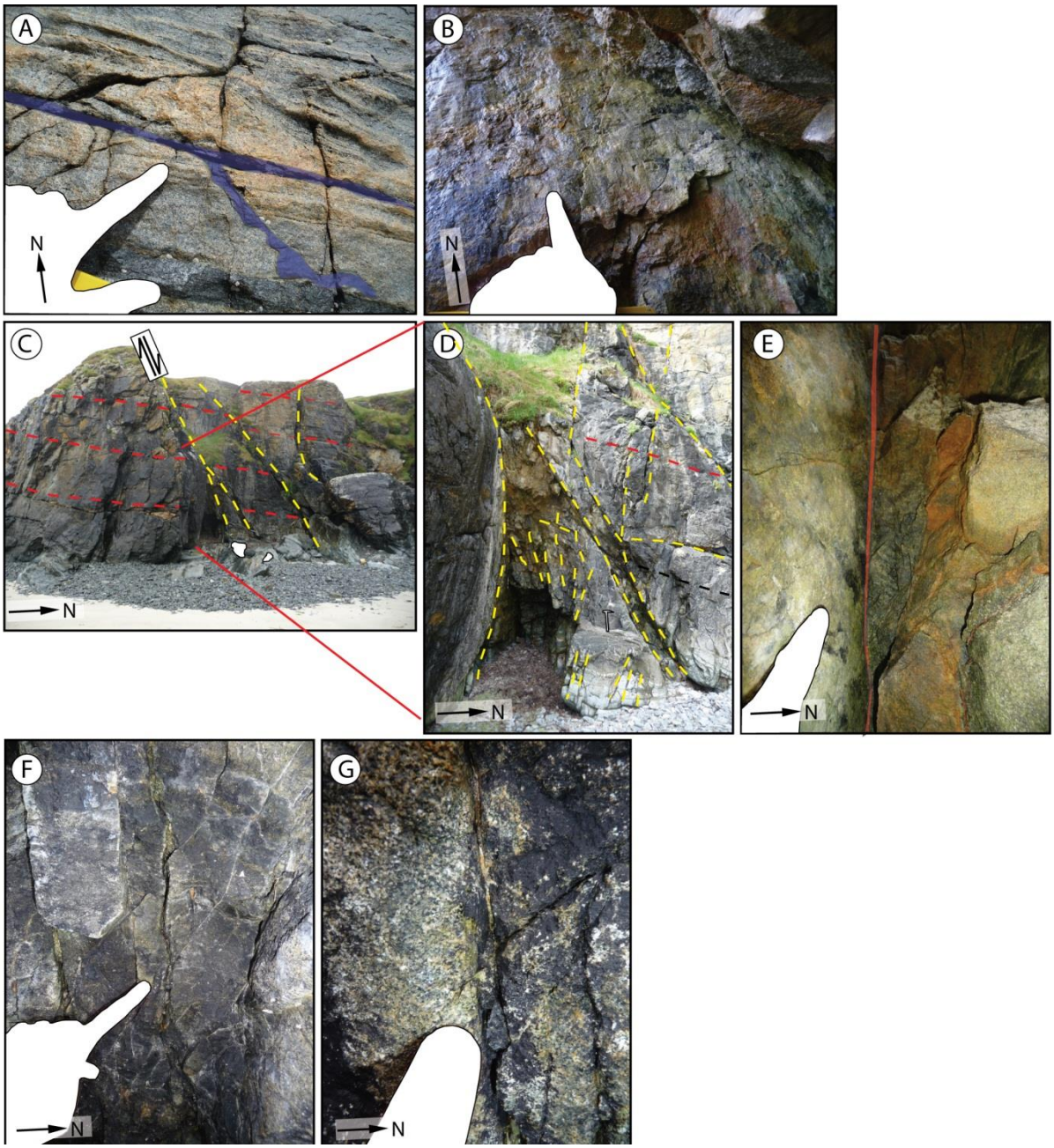

Figure 4.9: Outcrop at Port Stoth. NB 5239 6596. Blue = pseudotachylite, red = clay gouge, yellow dashed line = fault, red dashed line = foliation. (**A**) Pseudotachylite lying parallel with the foliation and injection vein. (**B**) Epidote veneered fault surface with dip-slip kinematics. (**C – E**) Well exposed northward dipping fault with dip-slip normal kinematics. Epidote bearing veins and the fault surface are cross cut by a later clayey gouge and carbonate veining. (**F – G**) Carbonate veining cross-cutting pre-existing epidote veins.

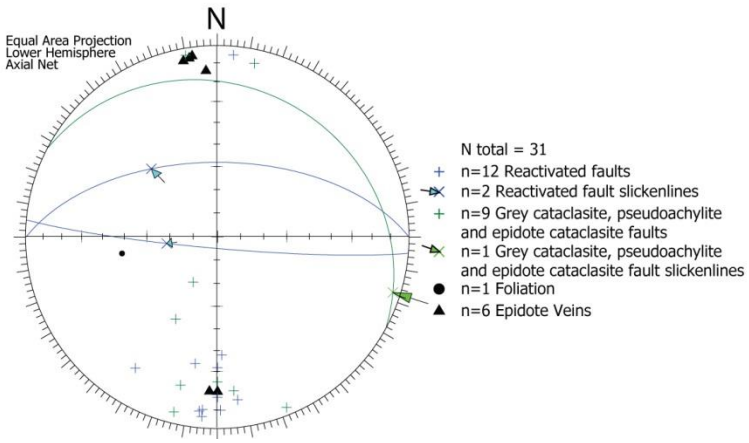

Figure 4.10: Orientation data collected from Port Stoth. Faults with slip data recorded are shown with a great circle in addition to the pole. Reactivated faults are comprised of epidote cataclasites reactivated by clay gouges.

4.4.1.3 Port Ness

Lewisian Gneiss at Port Ness (around NB 5372 6357) is exposed as low (<3 m) cliffs in the bay of the harbour, for about 300 m. The country rock is dominantly composed of finely (sub-centimetre) foliated and mylonitic gneisses, referred to by Watson (1969) as 'pelitic augen gneiss'. Amphibolites are common and generally laterally continuous. Long wavelength (10s of metres) recumbent folds verging to the northwest are visible in an amphibolite at the southern end of Port Ness beach (Figure 4.11A). Phyllonitic lenses are also observed parallel with the foliation (e.g. Figure 4.11B) with sigma-clasts indicating an up-dip, top to the NNW shear sense. The upper phyllonite in Figure 4.11B appears to have formed from altered amphibolite, and the lower unit probably originated from phyllosilicate-rich pelitic gneiss.

Orientation data collected from Port Ness is shown in Figure 4.12. Foliation is sub-horizontal and dips shallowly to the north and south. Although two groups of poles are discernible in the data, the overall foliation appears to define a large scale monocline.

Port Ness is dominated by clay- and zeolite-bearing faults, dipping moderately steeply to the north and south (Figure 4.12), cutting the foliation (Figure 4.11C-E). As seen elsewhere, clay-bearing faults tend to be discrete structures with 2 cm thick gouge and microbreccia that is poorly indurated. Clay-bearing structures do not appear to be related to a sub-parallel, very well-indurated, and more dispersed set of quartz-cemented faults (e.g. Figure 4.11E). Clay-bearing faults were found to contain carbonate cements within the gouges. One example was seen of a fault with two phases of soft different coloured gouge reactivating a fine grained grey cataclasite bearing fault (Figure 4.11I-K), i.e. the clay gouge (2 cm thick) was parallel with and brecciating the

fine grained cataclasite. Strike-slip kinematic data associated with epidote cataclasites (Figure 4.12) were obtained from a small group of epidote faults.

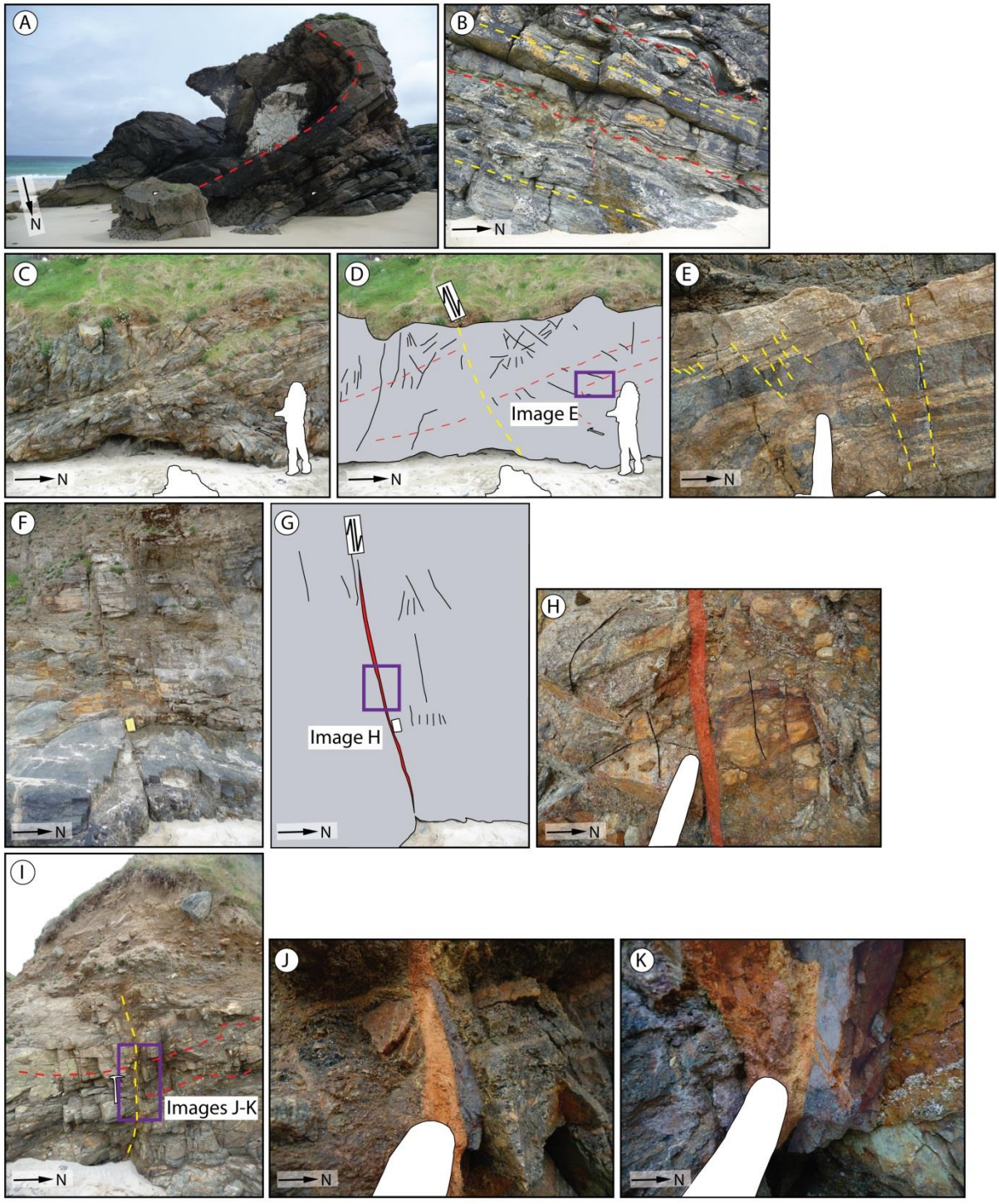

Figure 4.11: Outcrop at Port Ness. Red = fault gouge, grey = grey gneiss, yellow dashed lines = faults, red dashed lines = foliation. (**A** – **B**) NB 5373 6349. (**A**) Large scale folded amphibolite verging to the northwest. (**B**) Wavy phyllonitic bands within planar foliated gneiss. (**C** - **H**) NB 5371 6359. (**C** – **E**)Late normal fault cutting foliation, parallel with earlier dispersed quartz/epidote cemented faults (shown in **E,** hand for scale). (**F** - **H**) Late high-angle normal fault, dipping to the north with dip-slip normal motion and approximately 10 -15 cm offset. 1 cm of clay-bearing reddy brown fault gouge is shown in image H. (**I** - **K**) NB 5372 6365. High-angle normal fault cutting

foliation. Several phases of highlighted fault rock are visible: blue = grey, very fine cataclasites; red and orange = clay-bearing faults, containing breccia of the earlier grey cataclasite.

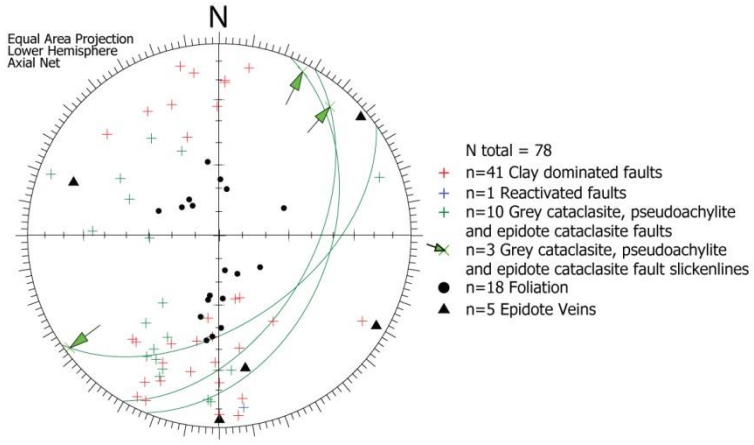

Figure 4.12: Structural data collected from Port Ness. Faults with slip data recorded are shown with a great circle in addition to the pole.

4.4.1.4 Summary of N Lewis

North Lewis is dominated by E-W striking faults. Flat-lying foliation that comprises amphibolite bands, folds, and pseudotachylite, and which is often mylonitic, shows a top to the NW motion. Epidote cataclasite and clay-bearing faults cut the foliation at a high angle. Clay-bearing faults are the youngest phase of faulting, which are observed to reactivate earlier epidote-bearing fault planes.

4.4.2 West Lewis and Bernera: NNW and ENE trending lineaments

Nine main areas were visited in western Lewis: Mealabost/Siadar, Bragar, Dail Beag, Dail Mhor, Garenin, Carloway, Bernera, Cliobh, Seaforth, plus several road-cut localities. As in other areas, good exposure of faults and fractures inland is limited mainly to road cuttings, and so fieldwork has concentrated on areas with accessible exposure (cliffs) adjacent to faults interpreted on the lineament analysis (Figure 4.13). The majority of the studied localities lie in the area interpreted as 'undifferentiated Lewisian Gneiss', comprised mainly of grey gneisses, with amphibole and biotite constituting the mafic component of the rock (Myers, 1970; Fettes et al., 1992). Lineaments identified on west Lewis dominantly trend NNW-SSE and ENE-WSW and field localities were chosen to investigate these features.

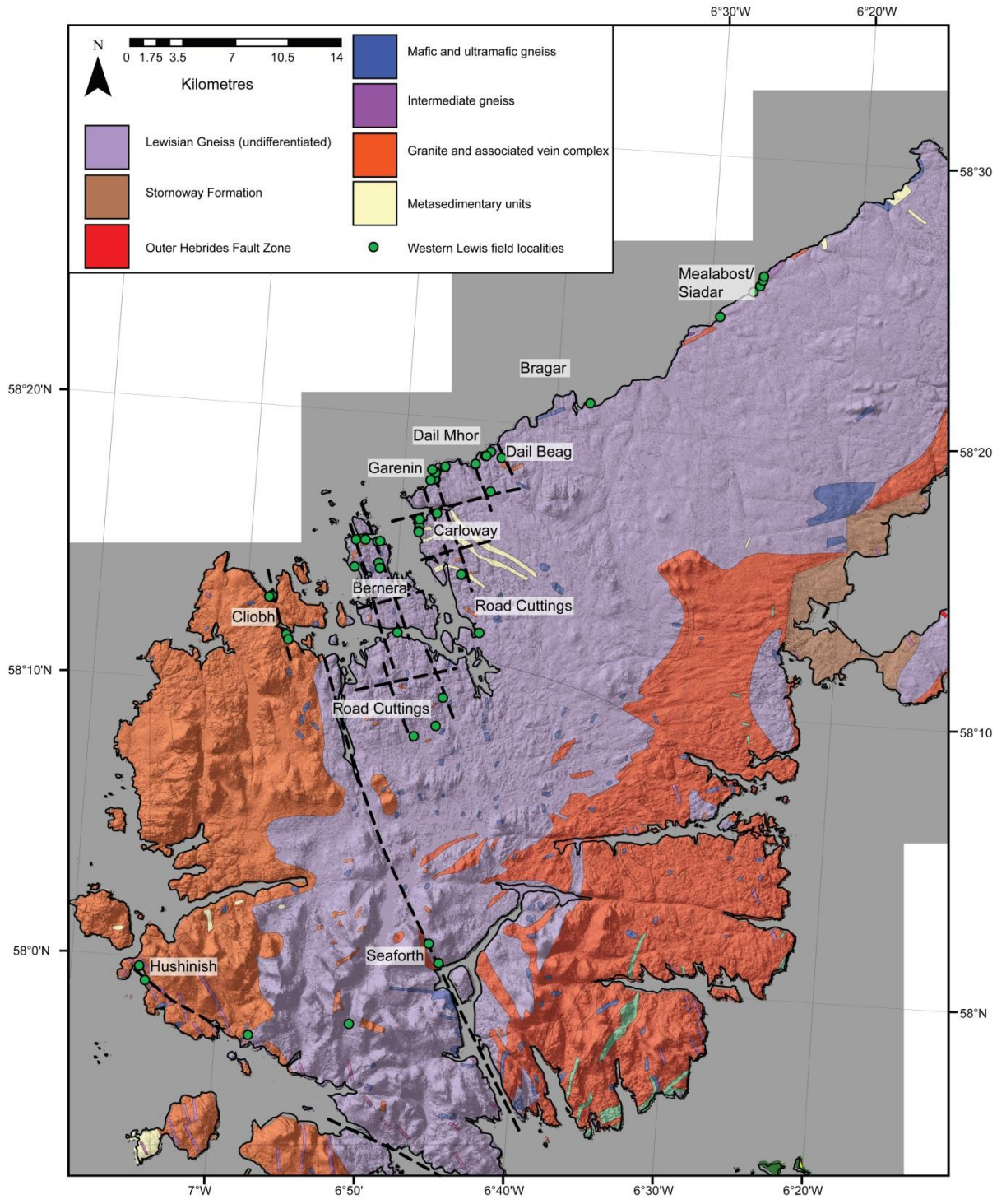

Figure 4.13: Field localities in western Lewis and northwest Harris. Selected lineaments indicated.

4.4.2.1 Mealabost, Siadar and Bragar

Mealabost (NB 40134 5661), Siadar (NB 3795 5496) and Bragar (NB 2931 4923) were only briefly visited in order to ascertain the presence, or absence, of fault exposures. Exposure was found to be relatively poor compared to elsewhere, although several faults were encountered. The most notable of these is shown in Figure 4.14 from Siadar, where north dipping clay-bearing faults

reactivate and offset a pre-existing network of epidote veins and faults. The latest phase of faulting at Siadar lies sub-parallel to the foliation and normally offsets a reactivated epidote-bearing fault by approximately 40 cm (Figure 4.14). E-W trending clay-bearing faults show a similar pattern to that seen at Cunndal, Port Stoth and Port Ness. However, slickenlines were not observed from the clay-bearing faults at this locality. Surfaces of epidote cataclasite have clear slickenlines (Figure 4.15), indicating a dominantly dextral strike-slip motion with a minor normal component like those of this type observed at Port Ness.

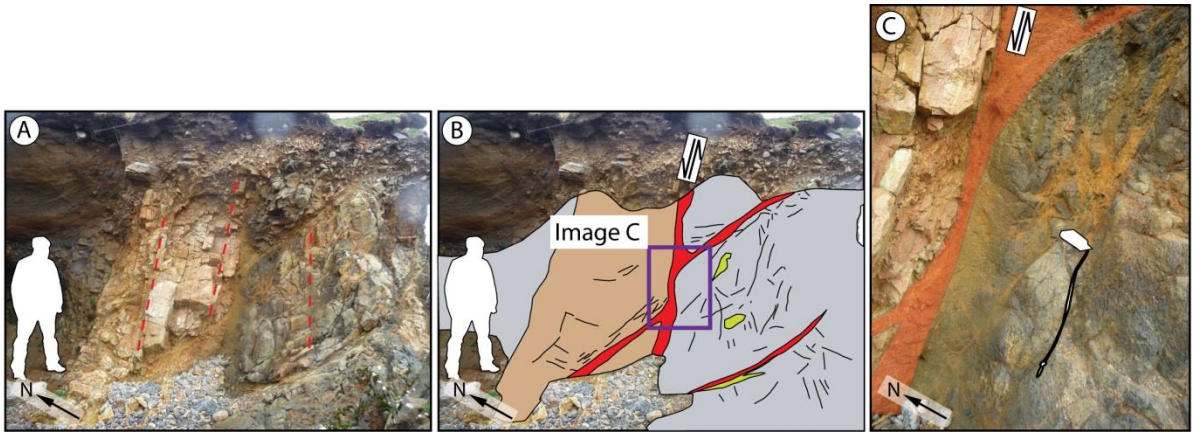

Figure 4.14: Outcrop at Siadar. NB 3795 5496. Red = clay-bearing fault rock, green = epidote bearing fault rock, brown = bleached gneiss, grey = intermediate gneiss, red dashed line = foliation. Other outcrop along this stretch of coast is limited to low cliffs with poor exposure. (**A – C**) showing clay-bearing fault with apparent normal motion, offsets an epidote-bearing fault reactivated by a clay-bearing fault.

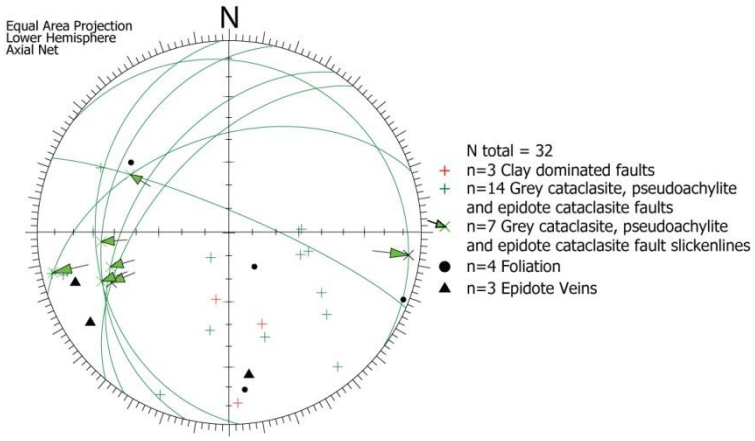

Figure 4.15: Orientation data collected from Siadar and Mealabost. Epidote bearing fault surfaces showed clear slickenlines. Faults with slip data recorded are shown with a great circle in addition to the pole.

4.4.2.2 Dail Beag and Dail Mhor

Outcrops at Dail Beag and Dail Mhor occur in three small bays (NB 2242 4574, NB 2273 4601, NB 2169 4512) and one quarry (NB 2343 4561) (Figure 4.16, orientation data shown in Figure 4.18). Country rock in the area is marked as undifferentiated grey gneisses on the BGS maps, but as at other localities pods and lenses of amphibolite and pegmatite are also preserved. Outcrop in the quarry exposes a well-developed coarse-grained augen gneiss/mylonite dipping shallowly to the south with intervening brecciated poorly indurated reddy-brown stained zones that are poorly exposed and post-date the mylonite (Figure 4.17A-C). These features appear to be sub-parallel with the foliation and may be later detachments. They appear to cross-cut a zone of steeply eastward-dipping fractures that may be equivalent to the steeply eastward dipping set of joints and faults seen at Dail Beag.

The bay at Dail Beag is dominated by joints and fracture zones that cut the foliation at a high angle (Figure 4.17D-F). The country rock is biotite-rich, quartzo-feldspathic gneiss, with foliation that dips shallowly to the southwest. Several phases of fracturing are evident, with possible exploitation of pre-existing quartz veins and joints by younger clayey gouge-bearing faults. Joints increase in density towards zones that are highly fractured and well cemented, composed of tabular blocks of gneiss that are also fractured perpendicular to the joint surfaces, with occasional very thin (1 mm) bands of gouge. These faults and joints are near vertical and strike NNW-SSE. Epidote-cemented faults are also seen at Dail Beag with the NNW-SSE striking fractures, and normal-oblique sinistral and normal-oblique dextral kinematics. Other epidote-bearing faults were observed trending ENE-WSW and may be part of another fault set. A WNW-ESE-striking dolerite dyke of assumed Tertiary age cuts these epidote veins and faults. Carbonate veins were also observed, exploiting two pre-existing epidote cataclasite bearing fault cores, trending NNW-SSE.

At Dail Mhor, exposure is dominated by a zone of massive breccia at least 80 m thick. Boulders of gneiss up to 1 m across are wrapped with chaotic breccia and foliated calcite-rich cataclasites that are parallel with NNW-SSE striking dolerite dykes of assumed Tertiary age, that intrude the breccia (Figure 4.17G-L). The dykes are undeformed relative to the surrounding breccia, but have been subject to localised faulting, with carbonate-rich cataclasites several centimetres thick that reactivate the dyke margins and also the core of a compound dyke (Figure 4.17J-L).

In summary the following earlier phases of faulting have been identified at Dail Beag and Dail Mhor:

1. Shallowly southward dipping mylonite formation postdated by a concordant low angle reddy-brown breccia (Figure 4.17C showing mylonite).

2. N-S striking fractures associated with quartz mineralisation (e.g. the quarry and at Dail Beag Figure 4.17E-F).
3. Epidote cataclasite-bearing, NNW-SSE and ENE-WSW striking faults of uncertain age relative to 2. These relatively early fracture sets are reactivated by later NNW-SSE striking gouge-bearing faults.
4. Carbonate-bearing faulting with breccia formation and foliated gouges, followed by Tertiary dyke intrusion. Within 1 m of the dyke body the breccia is much more highly indurated, indicating that dyke intrusion has probably baked the fault breccia (left of Figure 4.17H).
5. Detachment faults at Dail Beag, cross-cut NNW-SSE striking fracture zones (Figure 4.17A-B).
6. Tertiary dyke margins are themselves faulted/reactivated by dip-slip normal motion faulting (Figure 4.17J-L).

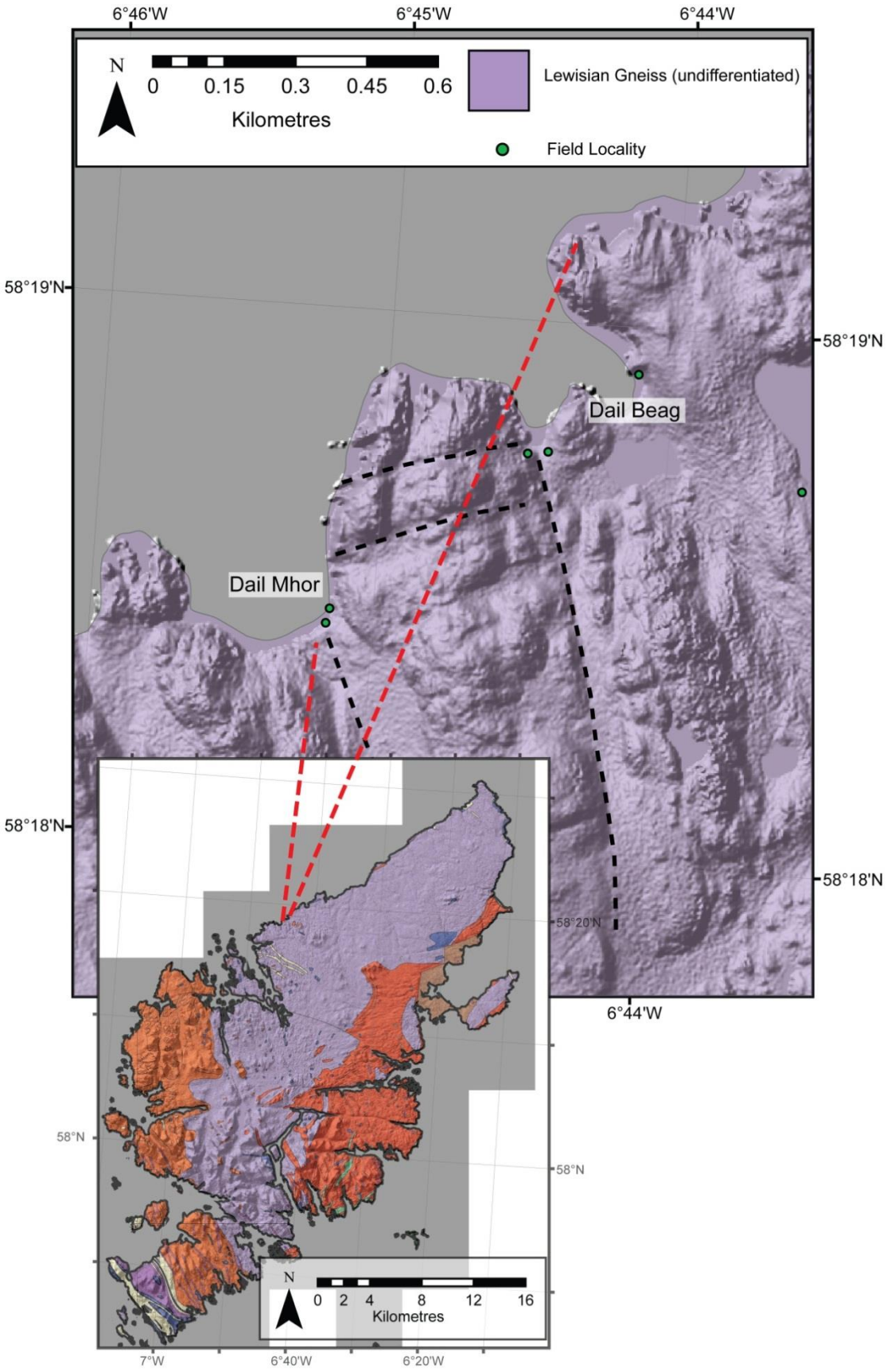

Figure 4.16: Location of Dail Beag and Dail Mhor localities with selected lineaments shown.

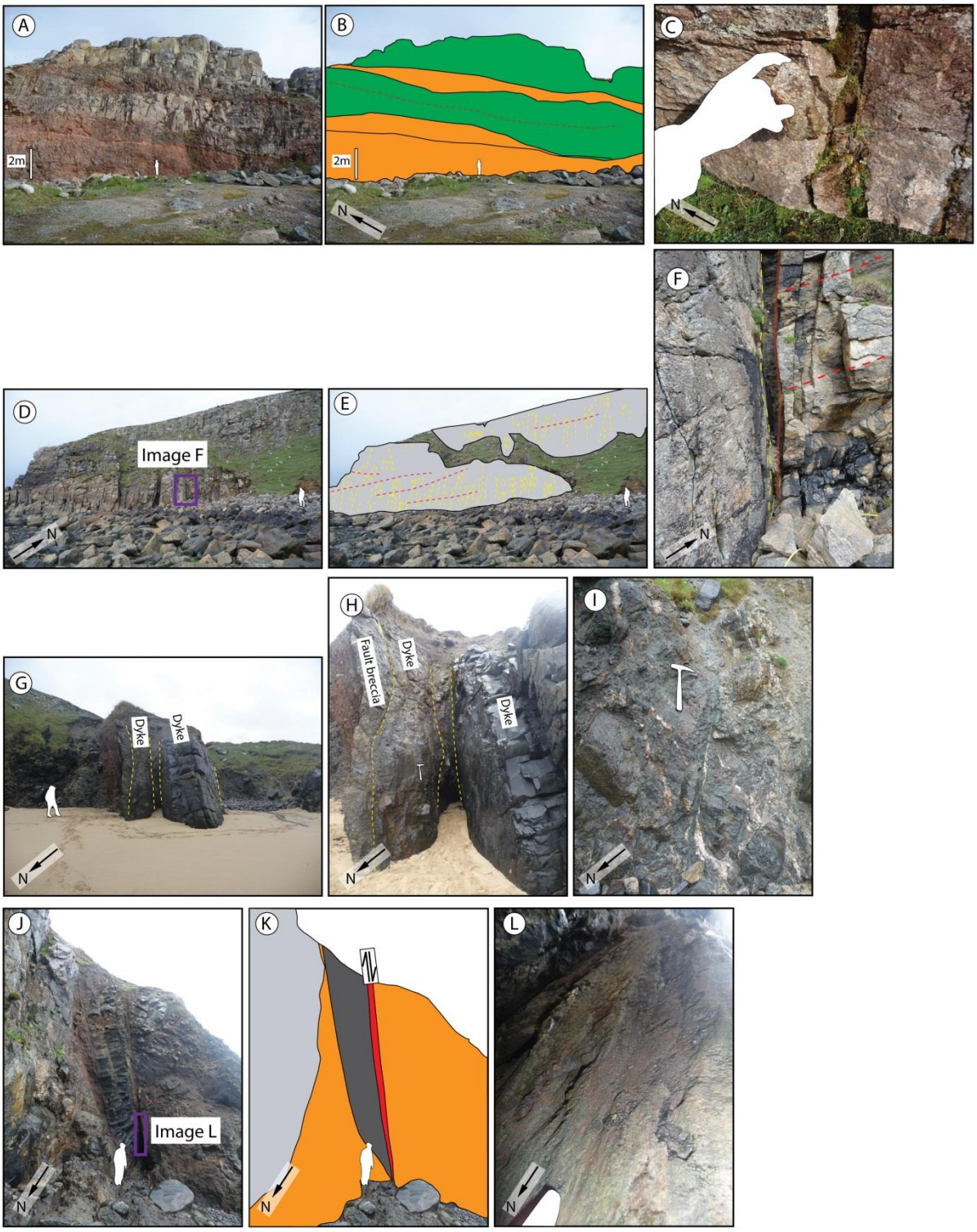

Figure 4.17: Outcrops at Dail Beag and Dail Mhor. Green = mylonite, grey = grey gneiss, dark grey = dolerite dyke, orange = breccia, red = fault gouge, yellow dashed line = fault, red dashed line = foliation. (**A** - **C**)Quarry outcrop, NB 2343 4561. Mylonite with shallowly dipping foliation cut by concordant red breccia zones. (**D – F**) Outcrop at Dail Beag, NB 2273 4601. Showing joint-dominated outcrop with occasional thin gouge seams. (**G** - **I**) Compound dyke at Dail Mhor (NB 2169 4517) intruded into chaotic massive breccia (shown in I). Fault breccia adjacent to the dyke (indicated) is more indurated than the adjacent breccia. (**J – L**) Dolerite dyke intrudes the margin of same breccia zone at Dail Beag. Side of dyke is reactivated and displays slickenlines (L).

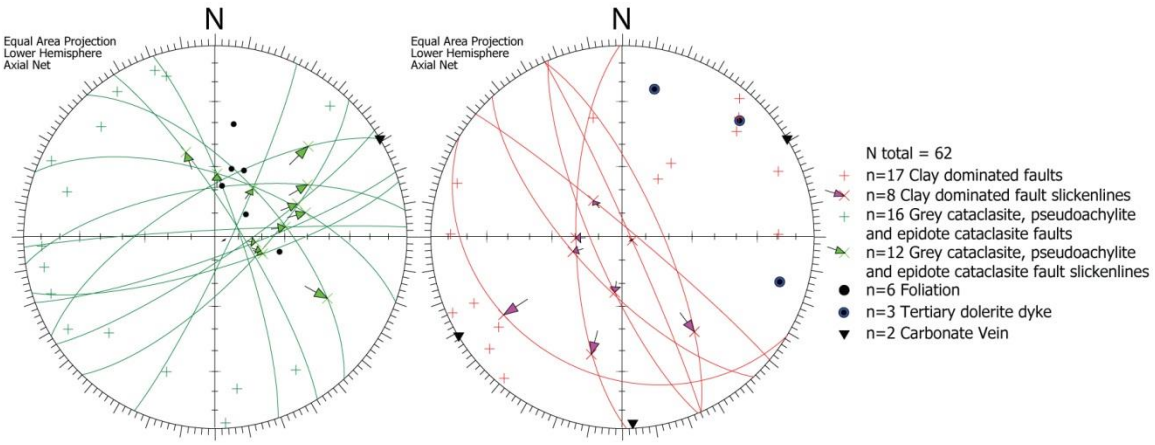

Figure 4.18: Orientation data collected from Dail Beag and Dail Mhor. Faults with slip data recorded are shown with a great circle in addition to the pole.

4.4.2.3 Garenin

Garenin is situated on the west coast of Lewis with localities in two small bays (NB 1968 4502, NB 1904 4416). Lineaments interpreted in the region trend dominantly NNW-SSE and ENE-WSW (Figure 4.19). Exposure is good, but where cliffs are high (over 30 m), access is limited to gullies. The country rocks are dominated by biotite-bearing quartzo-feldspathic gneisses with amphibolite and pegmatite lenses. Foliation in the area generally dips to the southeast with variable steepness.

The main faults studied at Garenin include a large scale N-S trending structure (Figure 4.20A-C), comprising a fault breccia at least 5 m across, which contains brecciated clasts of country rock and brecciated epidote veining and cataclasite. A principal slip surface was identified on the hangingwall side of the fault zone, with a thick band (5-10 cm thick) of clay-bearing foliated gouge, immediately adjacent to earlier, parallel quartz veins (Figure 4.20B, left hand side). This fault zone can be traced across the bay (Figure 4.20D-G)**,** where a similar fault style was observed. However, a thick zone of gouge exists on the footwall surface (Figure 4.20F) in this locality and the fault is also associated with calcite mineralisation/brecciation and veining that weathers to a rusty orange colour (Figure 4.20G). When broken apart this rock is revealed to be a carbonate-supported breccia, probably dominated by siderite. This fault cross cuts and offsets epidote veins and epidote cataclasite bearing faults that dip to the SSE.

A set of ENE-WSW striking, SSE dipping faults exist at multiple localities associated with calcite mineralisation (Figure 4.20H). These faults occupy gullies in the cliff faces, and show evidence of parallel epidote and quartz-bearing faults that predate a later phase of gouge-bearing faults that may have been contemporaneous with large carbonate vein formation (veins are up to 30 cm across) and oblique slip. The carbonate veins are usually highly brecciated (e.g. Figure 4.20J),

indicating that calcite mineralisation occurred synchronously with or pre-date faulting. Brecciated calcite mineralisation is also seen in the eastern-most bay, associated with a northwest dipping normal fault. A phase of faulting post-dates dolerite dyke intrusion at Garenin, with near strike-slip and also dip-slip kinematics recorded at one dyke margin (Figure 4.21).

The sequence of faulting determined at Garenin is as follows, with faulting of probable similar age sharing the same numeric:

1. Epidote cataclasite-bearing faulting. These faults are minor, and cross-cut by larger, younger structures (Figure 4.20I).
2. Quartz veining/faulting. This may be post-epidote, and must occur prior to the formation of clay bearing gouges and carbonate mineralisation (Figure 4.20B).

3.a In the N-S fault that was studied (Figure 4.20A-C), slickenlines and riedel shear geometry indicate dip-slip normal kinematics. The foliation varies in dip across the fault, probably indicating some component of offset down to the east.

3.b Carbonate-associated faulting with gouge formation; strong ENE-WSW trend with normal kinematics (Figure 4.20H and J).

4. Dyke intrusion followed by dip-slip and oblique slip along WNW-ESE trending dyke margin (in bold, Figure 4.21).

In Figure 4.21, the dominance of southward dipping structures is evident, cross-cutting the foliation.

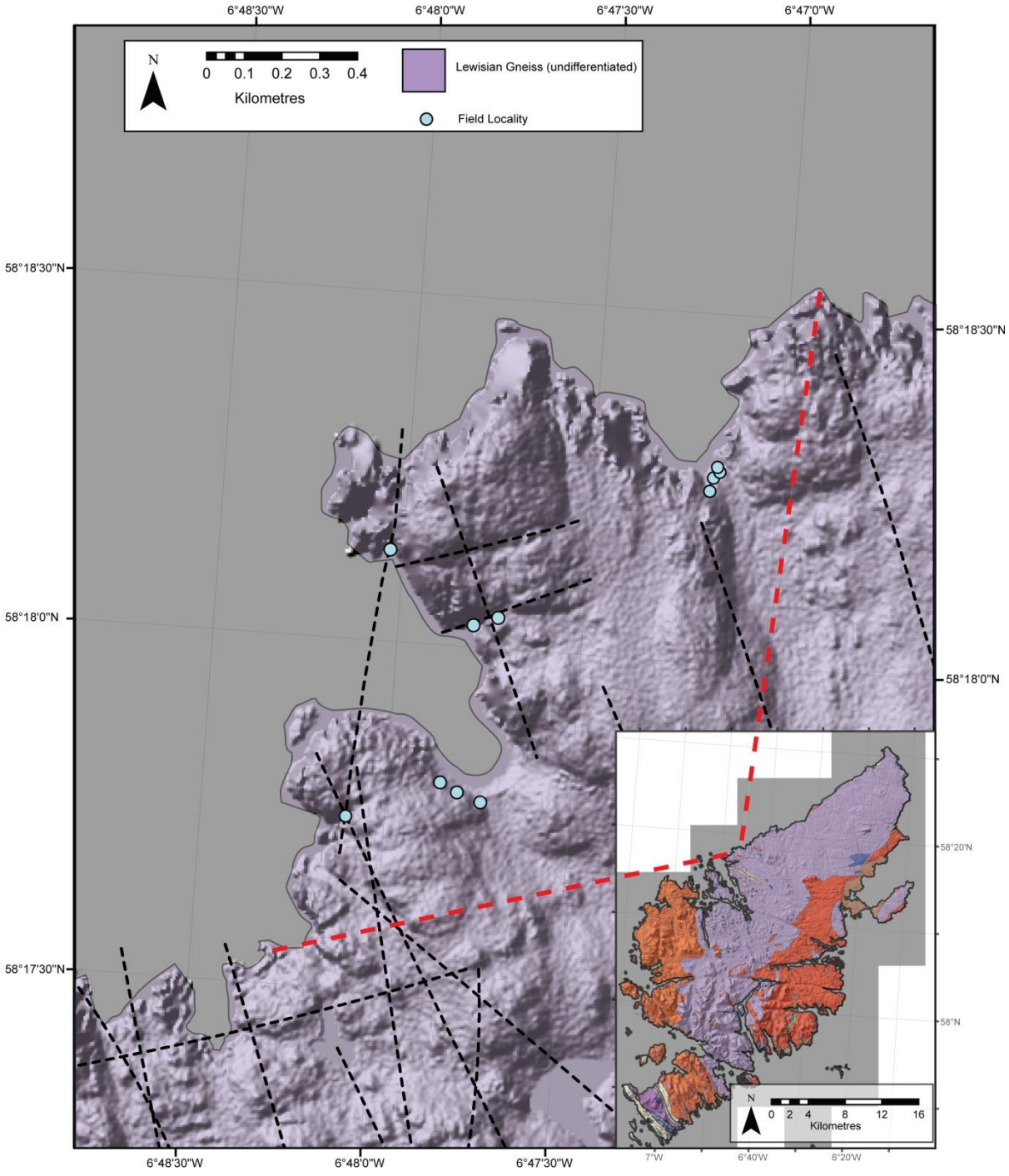

Figure 4.19: Map of field localities at Garenin. Lineaments indicated.

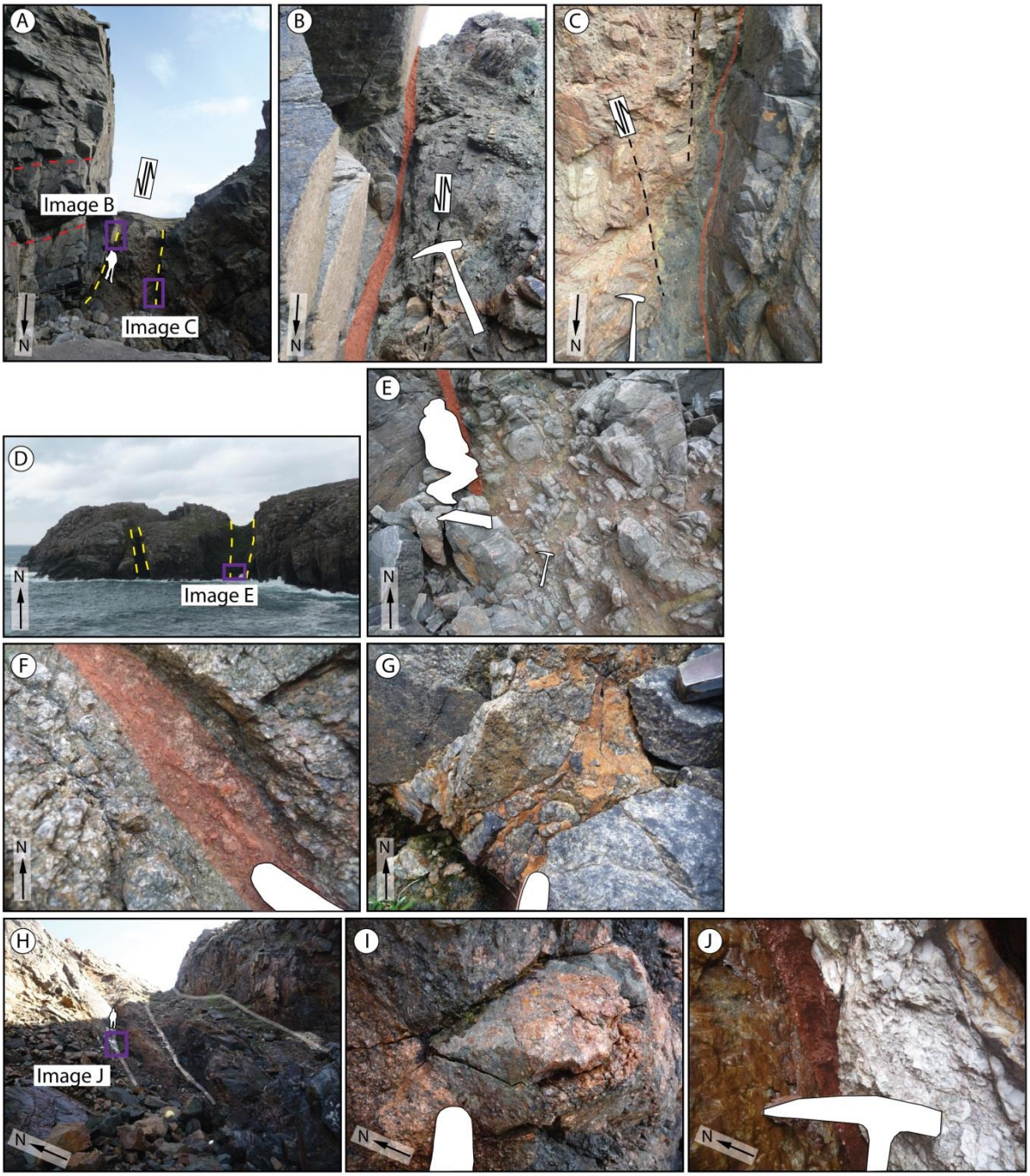

Figure 4.20: Outcrop at Garenin. Red = gouge seams, white = cataclastic calcite vein. (**A – C**) NB1870 4412. N-S striking fault with thick (5 m) wide zone of breccia and gouges with normal offset. (**D – G**) NB 1882 4483. N-S striking faults, showing fault rock (e-f) and probable siderite supported breccia (G). (**H**) Brecciated calcite veins associated with normal offset ENE-WSW trending faults. (**I**) Epidote-supported brecciated pegmatitic gneiss in footwall of faults shown in H. (**J**) Heavily brecciated carbonate vein with associated gouge seam up to 5 cm thick.

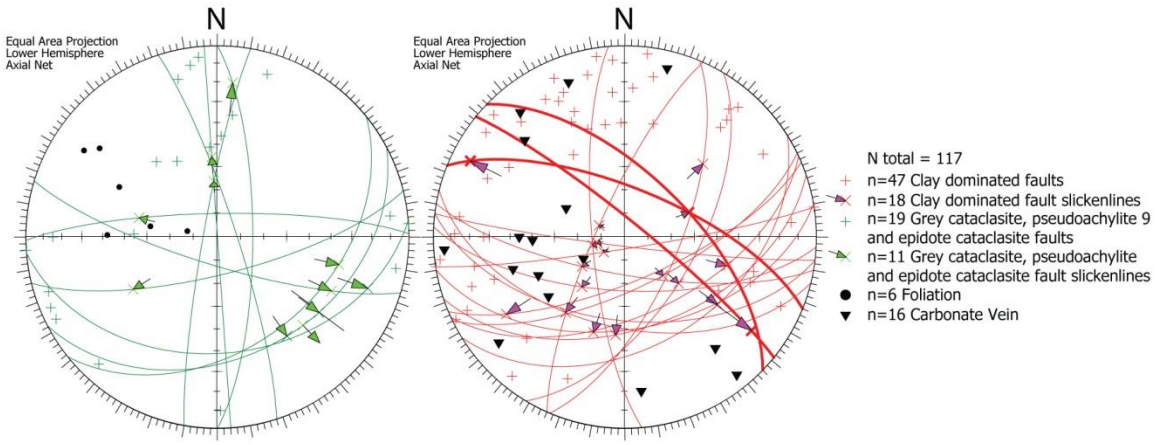

Figure 4.21: Orientation data collected from Garenin. Faults with slip data recorded are shown with a great circle in addition to the pole. Measurements in bold are taken from one single fault plane adjacent to a dolerite dyke.

4.4.2.4 Carloway and Breascleit

Outcrops at Carloway (NB 1790 4097) were visited in order to study ENE-WSW lineaments identified in the area (Figure 4.22). Outcrops at Breascleit (NB 2068 3784) form prominent roadside exposures. At Carloway, the country rock is comprised of standard grey gneisses with foliation that dips steeply to the south-southwest. Minor migmatisation is seen associated with pegmatites (e.g. bottom left of Figure 4.23E). At Breascleit, the foliation trends NE-SW and dips steeply. Orientation data are shown in Figure 4.24.

Outcrops at Carloway are shown in Figure 4.23. The dominant faulting at Carloway dips to the south and south-southeast and is at times seen lying parallel and sub-parallel with the foliation (Figure 4.23A, Figure 4.24). These faults typically have soft gouges (e.g. Figure 4.23D, G, I), and are associated with carbonate veins along the faults and carbonate cementation within the breccias and cataclasites. As seen at other localities, epidote cataclasites commonly dip steeply to the southeast and appear to be localised with thin (<1 cm) fault rocks. In seven instances, clay-bearing southward dipping faults were observed with a veneer of epidote lining the wall rocks, and at times epidote cataclasite clasts are incorporated into the soft authigenic clay gouges. Faulting must have occurred at epidote stability conditions, followed by fault reactivation under lower temperature conditions necessary for the existence of clay minerals.

Two clay gouge- and calcite-bearing south and southwest dipping faults at Carloway were observed with slickenlines on the wall rock surfaces giving oblique, near strike-slip kinematics (Figure 4.23E-G). This is similar to some of the faulting observed at Garenin (section 4.4.2.3, Figure 4.21). A major southward dipping fault at Carloway visibly offsets a pegmatite vein sinistrally and is associated with a fault zone 5 m across (Figure 4.23A-D) with <5 cm soft clayey gouge (Figure 4.23D), and clay-rich breccia and cataclasites constituting the remainder of the fault. These fault

rocks are all rich in milky carbonate, which is visible infilling microfractures within clasts in the fault, in addition to carbonate veins that cross-cut the fault rock and are incorporated into it.

Observations from Carloway are similar to those found at Garenin (section 4.4.2.3). Carbonate veins outcrop extensively, associated with ENE-WSW (south-southeast) dipping faults. Carbonate veins are often highly brecciated against these fault surfaces that display probable dip-slip normal motion (Figure 4.23H-I).

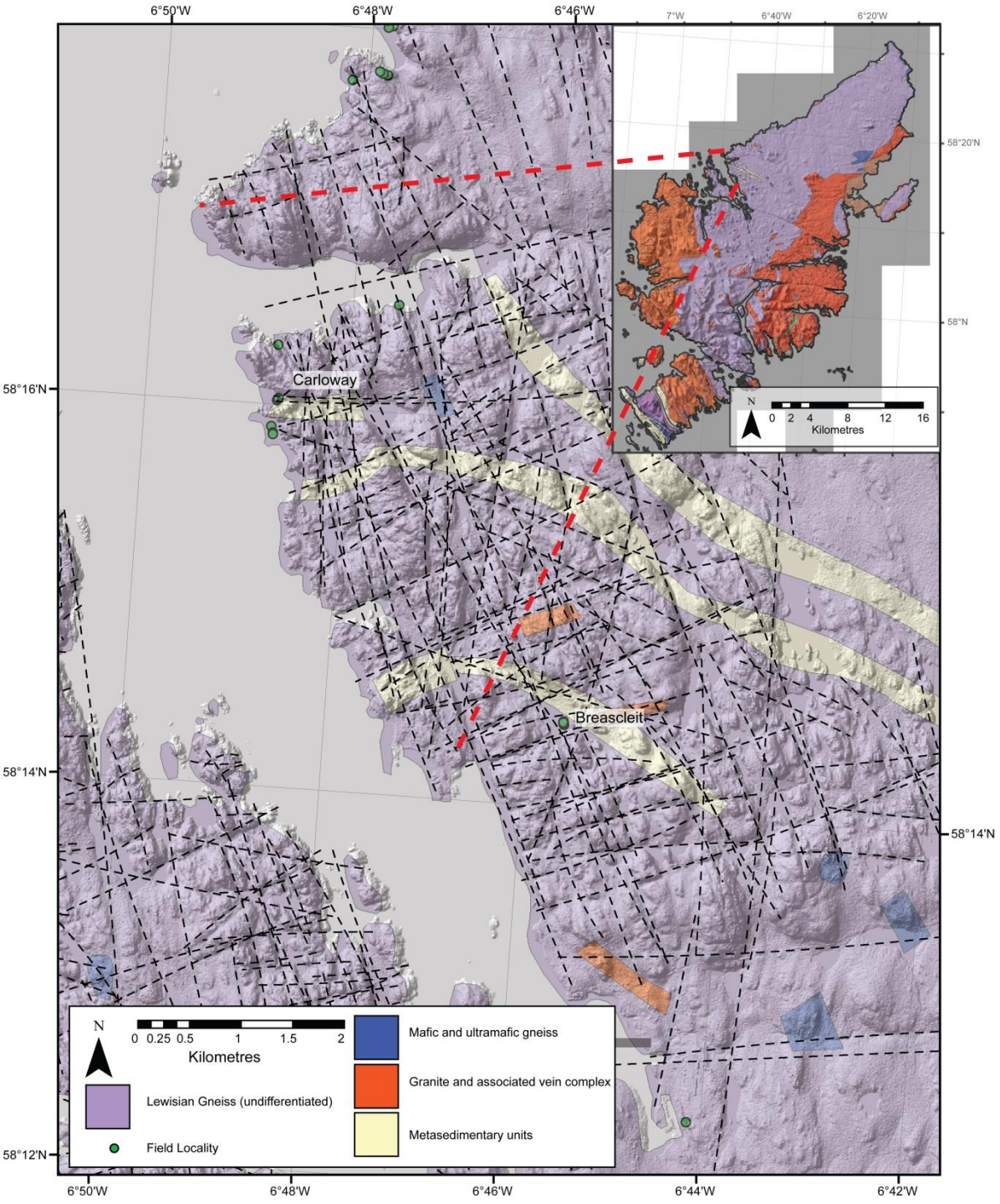

Figure 4.22: Carloway and Breascleit field localities. Lineaments indicated with dashed lines.

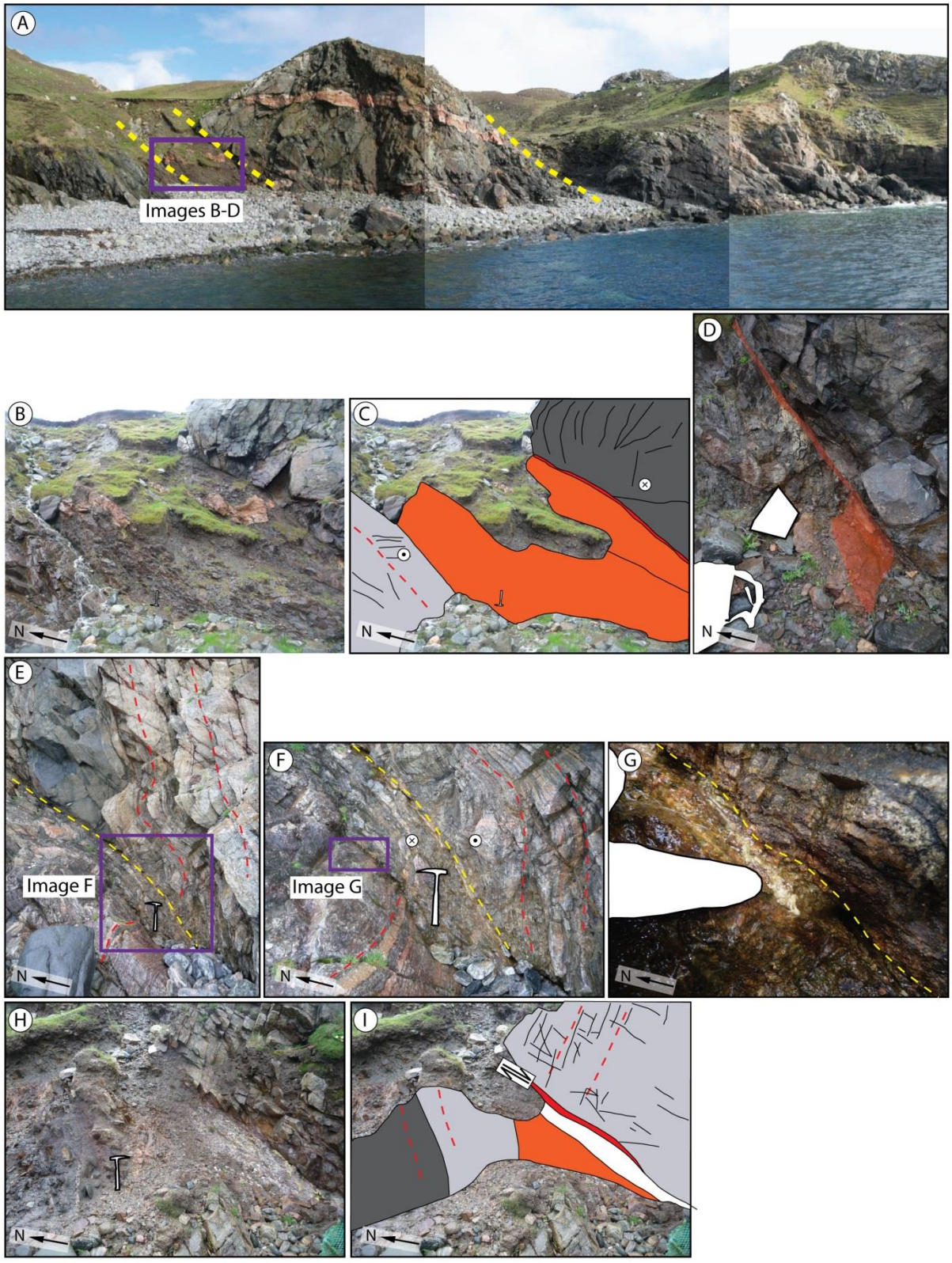

Figure 4.23: Field localities at Carloway (NB 1790 4097). Grey = grey gneiss, dark grey = amphibolite, orange = chaotic fault breccia, red = fault gouge and cataclasite, white = brecciated calcite, red dashed lines= foliation, yellow dashed line = fault. (**A**) Major lineaments picked on Nextmap data are expressed as valleys, exposed here at the coast. Purple box shows area from images B-D. (**B** - **C**) 5 m wide zone of chaotic breccia clearly faulted and offsetting pegmatite veining. (**D**) The hangingwall of the fault preserves a carbonate rich gouge approximately 4 cm thick. (**E** - **G**) A southwest dipping fault preserves oblique dextral kinematics and carbonate rich clay gouge fault core. (**H - I**) Reworked carbonate vein, faulted with red gouge.

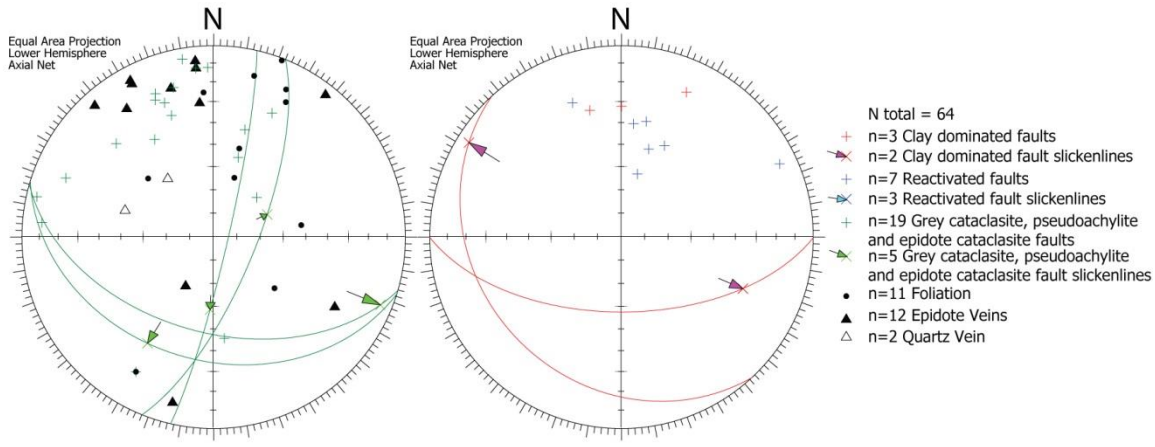

Figure 4.24: Orientation data collected from the Carloway and Breascleit outcrops. Faults with slip data recorded are shown with a great circle in addition to the pole.

4.4.2.5 Bernera

Outcrops were visited at Bernera due to the existence of strong NNW and ENE-WSW trending lineaments on the island. However, around the coast exposure was found to be relatively poor with low cliffs and a lack of good fault exposure (localities were visited at NB 1536 4009, NB 1438 4019, NB 1367 3841). Several quarries (NB 1526 3865, NB 1534 3830) and road cuttings (NB 1651 3401, NB 19534 2970, NB 1759 2714, NB 1905 2781) were visited in the area.

The country rock is composed of grey gneisses. The spread of foliation orientation data (Figure 4.27) represents clusters of data from east and west Bernera together falling along a great circle, indicating the existence of a possible large scale open fold, with a fold axis plunging shallowly to the southeast. The earliest phase of tectonism postdating gneiss formation episodes is represented by mylonitic and proto-mylonitic foliation seen at two localities dipping shallowly to the south-southwest with thrust kinematics. Evidence of low angle, top-to-the-northwest thrusting was also observed associated with brecciated gneiss in fault hangingwalls. One of these thrust faults is clearly reactivated by normal dip-slip faulting.

Faulting with multiple inheritance is common. Within one quarry (NB 1519 4006), pseudotachylite is seen injecting into mylonite, and is itself cut by steeply dipping and low angle normal faults with breccia, cataclasite and gouges (Figure 4.26A-C). Further ENE-dipping normal faults with gouge and breccia were also observed (Figure 4.26D-F), and these may be equivalent to the NNW-SSE striking faults identified on western Lewis, e.g. at Garenin (section 4.4.2.3).

Younger faults that postdate epidote veining and faulting and are associated with clay-rich gouges and cataclasites tend to dip to the east-northeast or south with apparent normal dip-slip kinematics. An example of an E-W strike-slip fault was seen with 10-30 cm of soft poorly

indurated fault breccia (Figure 4.26G-I), believed to be relatively young in age and possibly equivalent to E-W strike-slip faulting that is Tertiary in age observed on East Lewis in the Stornoway Region. This E-W striking fault cuts gneiss that is highly disrupted and migmatised.

Major NNW-SSE trending lineaments are poorly exposed. One example (at NB 1519 4006) with accessible exposure was visited, and was found to be represented by a zone of faulting several metres across, with phyllosilicate-rich breccias and cataclasites that may represent the reworking of a pre-existing phyllonitic shear zone. Cataclasites associated with this fault contained a high proportion of biotite with little evidence of alteration to clays, and clear dip-slip normal kinematics. This large-scale fault may be related to other NNW-SSE trending faults such as those discussed in section 4.4.3.2 and the ENE dipping normal faults identified above.

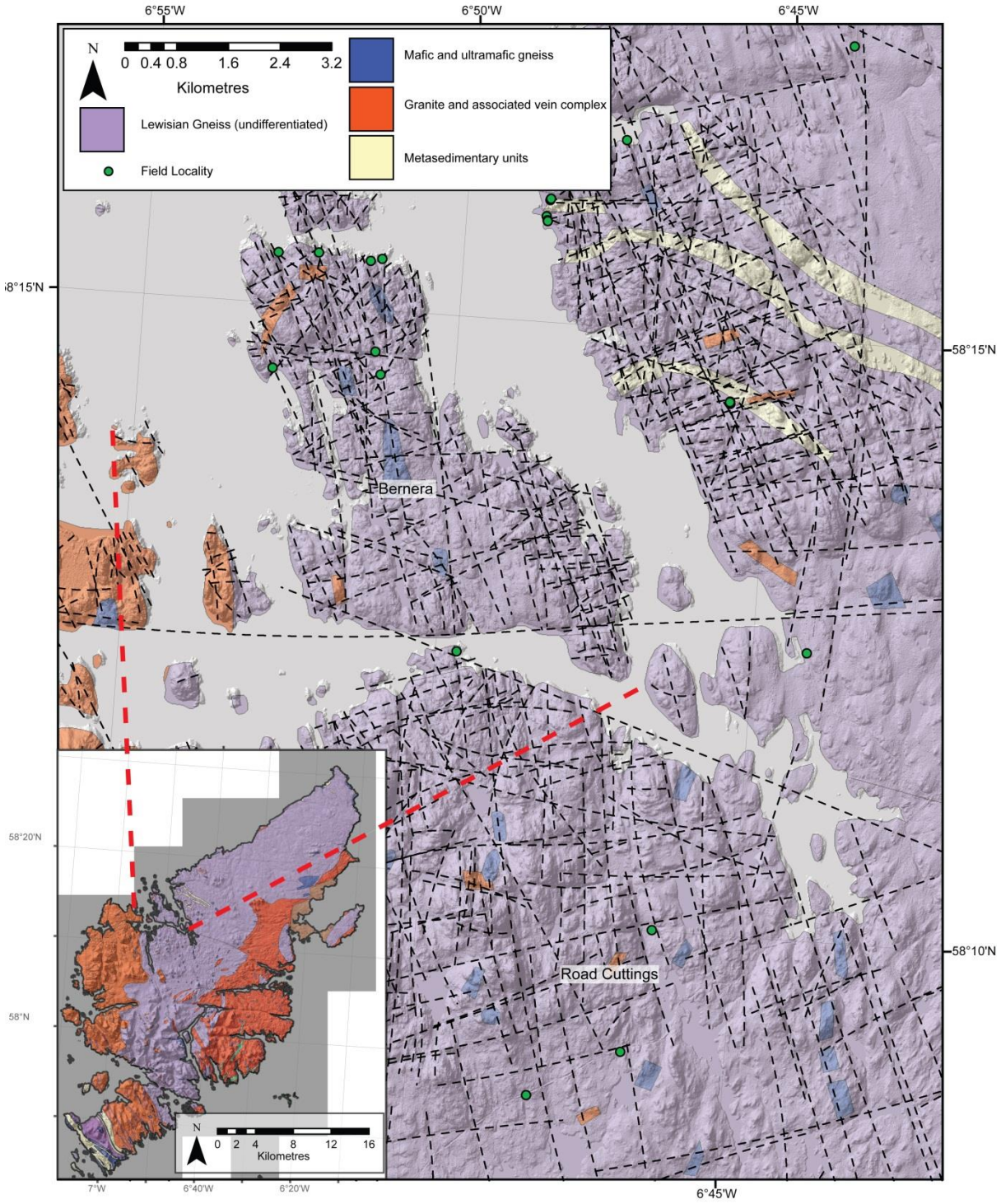

Figure 4.25: Field localities at Bernera. Lineaments indicated with dashed lines.

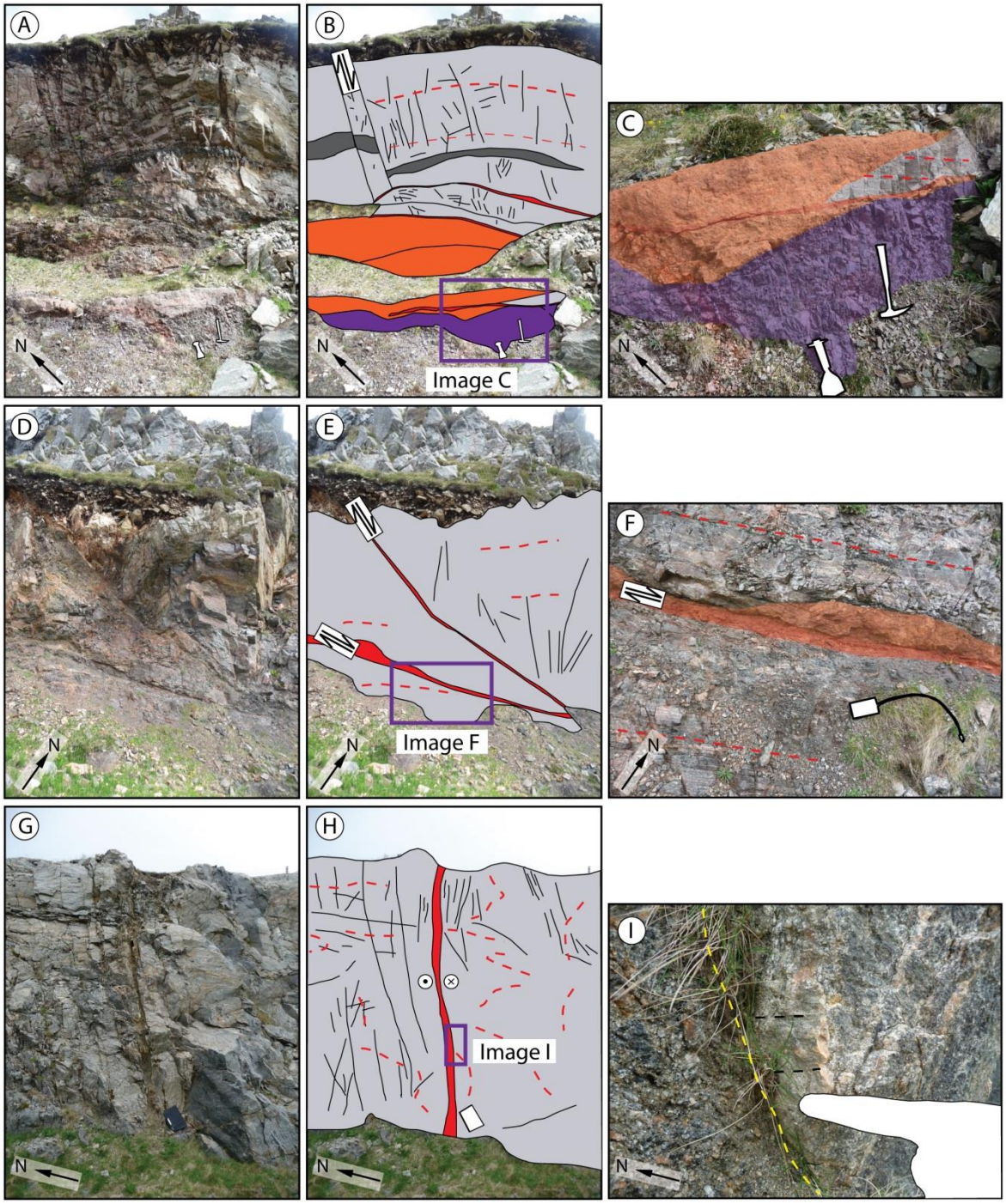

Figure 4.26: Outcrop at Bernera. Purple = pseudotachylite, orange = breccia, red = gouge, grey = migmatised grey gneiss and mylonite, dark grey = amphibolite, yellow dashed lines = faults, red dashed lines = foliation. (**A** - **F**) NB 1519 4006. Outcrop at quarry. (**A** – **C**) With low angle gougey clay bearing faults dipping to the east-northeast, brecciating pre-existing pseudotachylite faults. Higher angle normal fault in the main quarry wall dips to the SW. (**D** - **F**) Clay bearing normal faults dipping to the east-northeast with dip-slip motion. (**G** - **I**) NB 1615 3401. E-W strike-slip faulting with soft gouge and chaotic breccia up to 10cm thick, with horizontal slickenlines visible on a quartz vein on the wall rock (black dashed lines).

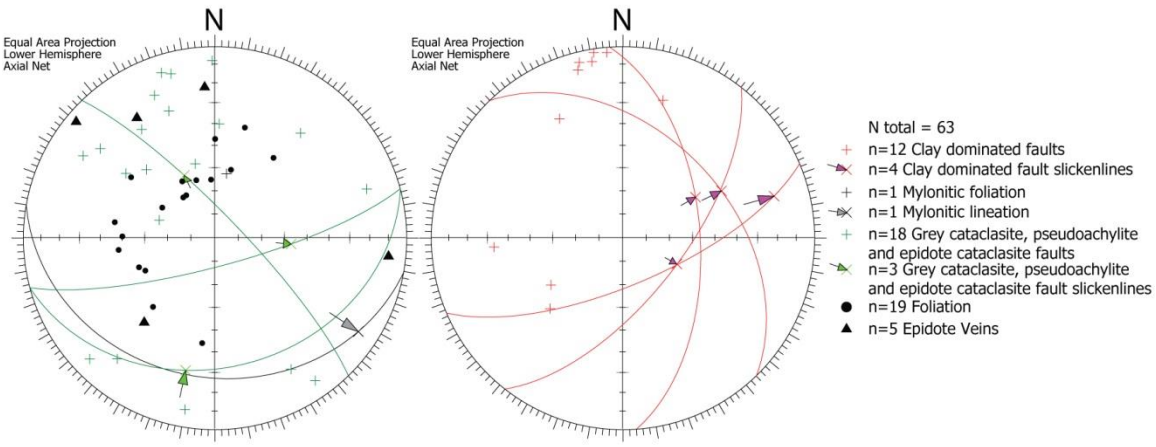

Figure 4.27: Orientation data collected from Bernera and nearby road cuts. Faults with slip data recorded are shown with a great circle in addition to the pole.

4.4.2.6 W Lewis summary

The following features were identified in the region, ordered chronologically, with faulting of probable similar age sharing the same numeric:

1. *Mylonite and pseudotachylite development.* Mylonites generally dip shallowly to the south, and are associated with foliation parallel pseudotachylite and cross-cutting pseudotachylite veining.

2.a *NNW-SSE striking faulting*. Dipping to the ENE and WSW and associated with normal kinematics. At Dail Mhor a major fault belonging to this set has produced a massive zone of breccia.

2.b *ENE-WSW striking faults*. Dipping moderately to the SSE are associated with massive carbonate mineralisation not seen on east Lewis. These calcite veins were seen at multiple localities at Garenin and Carloway, and may have formed synchronous with dip-slip faulting parallel with their margins that has brecciated the veins and produced soft clay gouges.

2.c *N-S striking faults.* A major N-S striking normal fault was seen at Garenin dipping steeply to the east, with east side down kinematics. Fault rock with is composed of poorly indurated breccia with soft gouge and cross cutting and reworking of pre-existing epidote veins and cataclasites.

2.d *Detachments.* Localised along mylonitic country rock at Dail Beag quarry, mylonite appears to be reactivated by later poorly exposed detachments that cross-cuts NNW-SSE striking faults. Dips shallowly to the south with poorly indurated breccia.

3. *Dolerite dyke intrusion.* Dykes intrude into gneissic country and faults zones, striking NNW-SSE.

4. *Post-dolerite dyke faulting.* Dyke intrusion was post-dated by faulting along dyke margins,

dominated by normal kinematics. At Garenin, a WNW-ESE trending dyke displays near strike-slip, and dip-slip motion along its margins. Near strike-slip motion seen on steep, E-W striking clay-bearing faults at Carloway and Bernera may be related to this phase of motion. E-W striking faults with strike-slip kinematics may be associated with strike-slip faulting observed in East Lewis (e.g. section 4.5.2.3) and in the Stornoway Region (e.g. section 3.3.2.2).

4.4.3 Seaforth Lineament and related outcrops

Three field localities show faulting that may be associated with this lineament: Cliobh, Seaforth Valley, and Rhenigidale. The Seaforth lineament is situated in southeast Lewis, forming Loch Rog Beag and part of Loch Seaforth (Figure 4.31), and is a very prominent valley feature cutting the island, with variation in geology and topography across it. Direct exposures of the lineament are localised to a road cutting with low banks of gneiss up to three metres high that become increasingly fractured towards the lineament, and a steeply incised valley with erosional exposure of a major east-northeast dipping fault core and immediately adjacent wall rocks.

To the northeast of the lineament (the hangingwall), north and east Lewis are generally low lying, with a small group of hills in southeast Lewis reaching an elevation of 572 m at Beinn Mhor, which probably relates to the exposure of weather-resistant OHFZ fault rocks (Fettes et al., 1992). The OHFZ outcrops over a wide area of the Parc District of southeast Lewis in the fault hangingwall. To the immediate southwest of the lineament (the fault footwall), the Uig Hills and mountains of north Harris rise to 799 m at the Cliseam, and the topography is notably much more elevated compared to the hangingwall side of the fault. Exposure of the OHFZ in the footwall is much more limited and much of the fault zone must lie immediately offshore. The footwall country rock is dominated by the Uig Hills – Harris granite and granite vein complex (Fettes et al., 1992). These observations suggest that significant offset has occurred across the Seaforth Fault, with the hangingwall moving down relative to the footwall (i.e. SW side up).

4.4.3.1 Cliobh and road cuttings

Cliobh (NB 0820 3644 to NB 0800 3640) and road cuttings nearby (NB 0918 3390, NB 0926 3357) were studied for the exposure of major NNW-SSE trending lineaments in the area, and the localities lie within 1 km SW of the Seaforth Lineament and within 250 m NE of another NNW-SSE trending lineament that is parallel with the Seaforth Lineament. Cliobh lies within the granitic vein complex area of the Uig Hills - Harris granite complex (Fettes et al., 1992, Figure 4.28). The area is

heavily intruded with granitic and pegmatitic veins up to several metres across, intruding into typical grey gneisses with foliation that dips moderately to steeply to the west. All fractures observed at Cliobh cross-cut the foliation in the gneisses. Dolerite dykes of probable Tertiary age are present at the beach and in the road cutting.

Epidote veining and faulting is common, with epidote alteration seen along the margins of pegmatite veins, and at the road cutting, pegmatites show evidence of soft body deformation during top-to-the NNW thrusting. Epidote faults were found to dip towards the southeast, southwest and northwest, and it is possible that these may relate to multiple faulting and fracturing events.

A prominent southeast dipping fault at Cliobh has a thick fault rock, 1-2 m across, with a dominantly sinistral offset of at least 1.5 m obtained from offset clasts (Figure 4.29A-B), although slickenlines could not be obtained. The NE-SW strike of this fault is also evident in the epidote-bearing faults, and this fault may be associated with them. The fault rock is composed of very heavily altered amphibole or possible biotite, and seems likely to have originated from an Older Basic or Younger Basic amphibolite unit within the gneiss.

Nearing the major NNW-SSE trending lineament at Cliobh Beach, from approximately 60 m perpendicular to it, the dominant fault set trends NNW-SSE and is near vertical. It is likely that this reflects the same phase of faulting that has produced the major lineament. Faults of this orientation are sub-parallel to the lineament and associated with an apparent dextral offset that has been observed across one of these faults (Figure 4.29C-D). Fracture intensity increases towards fault planes with breccia up to 10-15 cm across (Figure 4.29E-F). This breccia is red and orange in colour, clast-supported, with a fine clay gouge matrix. Related fractures are associated with a red staining of the surrounding gneiss (Figure 4.29E - G), due to secondary mineral formation (probably haematite or clay). Dykes are locally intruded along this fracture set, concentrated in fractures with clay-rich fault rock, probably due to mechanical weakness of these structures compared to the better cemented epidote-bearing and red-stained fractures. The dykes contain vesicles, and incorporate wall rock clasts. Vesicles are rounded, which suggests their formation occurred after flow had stopped, or that flow had ceased before cooling (solidification). There is a lack of any faulting post-dating intrusion of the dykes. It hence seems likely that the major lineament here is composed of a major fault zone with later Tertiary dyke intrusion along it. Orientation data is shown in Figure 4.30.

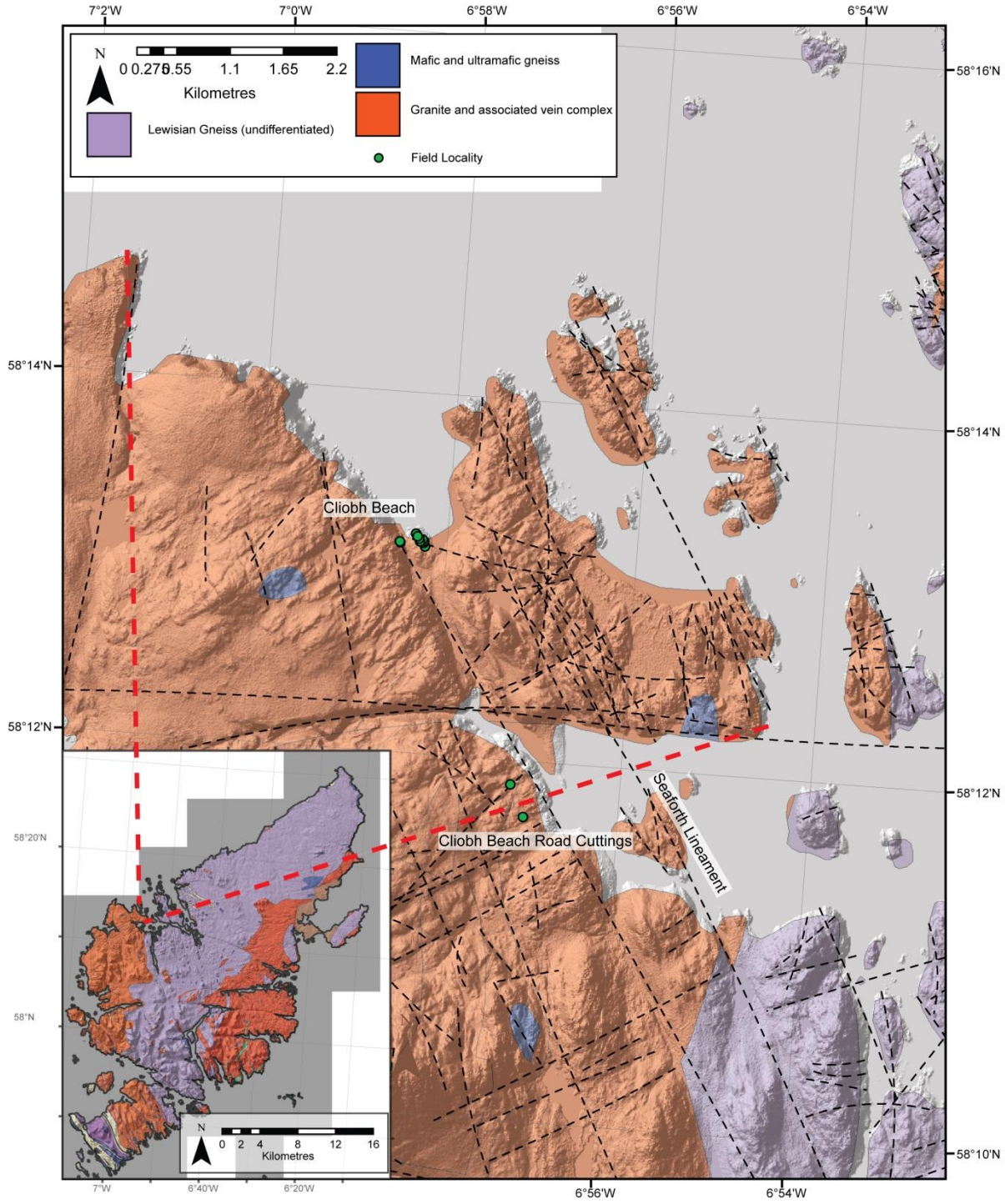

Figure 4.28: Field localities at Cliobh. Lineaments indicated - note major lineament at Cliobh beach trending NNW-SSE.

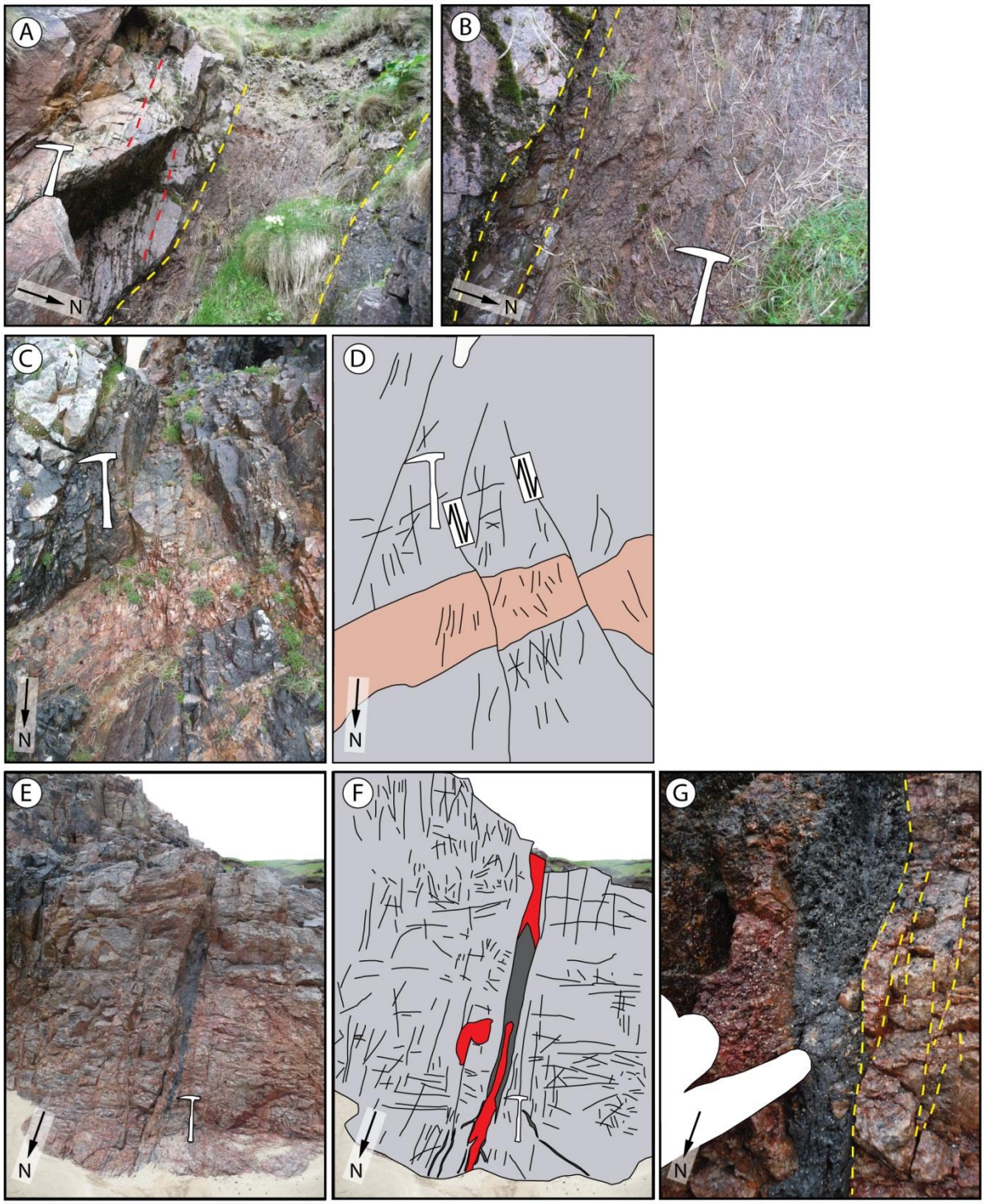

Figure 4.29: Outcrop at Cliobh. Light grey = grey gneisses, pink = pegmatite, black = Tertiary dolerite dyke, red = fault breccia, yellow dashed lines = faults. (**A** - **B**) NB 0820 3644. 1-2 m wide zone of faulted altered amphibolite with major sinistral component to slip. (**D** - **G**) NB 0800 3640. (**C** - **D**) Plan view of sheared gneiss, pegmatite vein showing apparent dextral offset of approximately 30 cm. (**E** - **G**) Dyke intrudes along pre-existing fractures of the same set shown in images C-D. Dykes are spatially associated with zones of fault breccia and fractures that show red staining. The dyke itself is highly vesicular and altered, with clasts of country rock and fault breccia incorporated into the dyke.

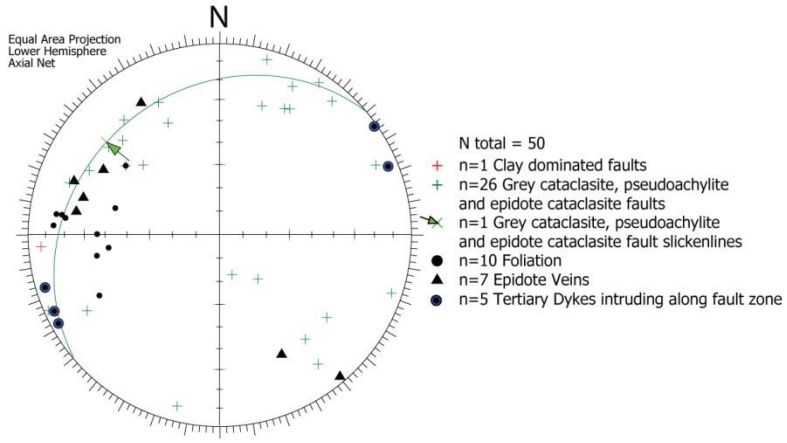

Figure 4.30: Orientation data collected from Cliobh. Faults with slip data recorded are shown with a great circle in addition to the pole. Note that dykes are intruding along clay dominated breccias.

4.4.3.2 Seaforth Valley

A 12 m wide fault core of foliated gouge and breccia outcrops in the Seaforth Valley (NB 1868 1329 to NB 1880 1311). The hangingwall country rock is comprised of quarto-feldspathic gneiss with a biotite mafic component that locally constitutes approximately 50% of the rock. In the hangingwall, the foliation is continuous, sub-centimetre banded and in places it is protomylonitic to mylonitic, with k-feldspar clasts up to 2-3 mm across wrapped by chlorite. The hangingwall foliation dips shallowly to the west. No evidence of mylonite was observed in the fault footwall.

Within the footwall at 15 m on the log (Figure 4.33), biotite-bearing brecciated gneiss grades into intact chlorite gneiss toward the fault core. The chloritic gneiss is composed of chlorite crystals up to 1 cm across defining a foliation within plagioclase feldspar, K feldspar and quartz groundmass, and dips steeply to the northeast. This steeply dipping foliation is found on the footwall side of the fault, and within intact gneiss blocks within the fault that appear to have only suffered minor amounts of rotation, relative to the footwall. Within the chlorite gneiss at the end of log 1 (Figure 4.32G, Figure 4.33), chlorite constitutes up to 80% of the rock and the foliation is sub-parallel to the foliated gouge bands and other faults at this locality. Elsewhere in the footwall side of the valley, grey gneiss with boudinaged amphibolite is visible (Figure 4.32H). The presence of chlorite gneiss and boudinaged amphibolites may indicate the presence of a pre-existing shear zone composed of retrogressed chlorite gneiss that has been reactivated by faulting.

On the hangingwall side of the fault, the foliation within the biotite gneiss and protomylonitic and mylonitic gneisses generally dips shallowly to the west, and is clearly cross cut by the faulting at this locality. Although these rocks may have undergone a degree of local rotation caused by the fault, these observations are in agreement with the BGS maps of the area, that show a clear change in the orientation of the foliation across the fault (Fettes et al., 1992).

The locality records several phases of brittle faulting, and the wall rock is cut by several fracture sets. In postulated chronological order (oldest to youngest) these are:

1. NNW-SSE striking fault gouges dominate the outcrops with 12 m of fault rock exposed within the fault core (Figure 4.33). Two localities are found within the valley with exposures of foliated gouge (Figure 4.32A - B, Figure 4.33) of approximately the same dip direction, matching the overall trend of the lineament. At these localities, foliated, light to dark green, orange, brown, red, pink, and black gouges dip steeply to the northeast (Figure 4.32C - D) with normal kinematic indicators (e.g. Figure 4.32C) that include rotated clasts close to the hangingwall country rock, and normal oblique sinistral slickenlines. A small component of sinistral motion is also suggested by several weakly sheared breccia clasts. Figure 4.32E shows Riedel shears cutting the foliation and indicating overall normal (northeast-side-down) fault movement. Varying degrees of induration are dependent on the presence of calcite that cements the breccia and gouges in lenses, but no discrete carbonate veining was observed. Carbonate mineralisation is syn-faulting (see below).

   Within the fault core, an olive-green band of fault gouge with normal oblique dextral slickenlines truncates the west-southwest dipping fault rock and has emplaced it against brecciated grey gneiss and foliated grey gneiss of the footwall, seen at 8.8 m on log 1 (also, Figure 4.32F). As can also be seen on the log within the main east-northeast dipping gouge and breccia band, several minor faults and bands of gouge were observed cutting the main foliated gouge trend, dipping to the east-southeast, and these are also visible as a prominent group of faults on the stereonet (Figure 4.34). The relationship between these faults and the main ENE dipping foliated gouges and breccias is not clear, however it is possible that east-southeast dipping faults represent reactivation of the structure.

2. In the hangingwall country rocks, quartz veins display centimetres of sinistral offset with apparent reverse motion along southward dipping faults with thin (0.5 cm) gouge. It is not clear whether these faults pass directly into the main foliated fault rock at this locality, but the markedly different kinematic style suggests that these faults may be a later set. These late E-W trending faults are seen cutting the mylonitic fabric and are associated with soft milky white non-effervescent mineralisation that is probably zeolite.
   Within the main NNW-SSE striking zone of foliated fault rocks, minor northeast and southwest dipping apparent strike-slip faults with less than 3 cm of offset and 1 mm of soft grey gouge cut the prevalent fault rock foliations, and may be associated with this latest phase of faulting.

Two structural logs were recorded at Seaforth at localities 689 (A) and 690A (Figure 4.32B), with locality 690A being 50 m along the strike of the lineament to the southeast of 689 (Figure 4.31). These logs show common lithologies that may indicate continuity of a Younger Basic (Scourie Dyke) within the fault zone and the continuation of chlorite gneiss (Figure 4.33). Transects through the Seaforth Valley Fault zone exposed at the side of the road are presented in section 7.3.2.2.

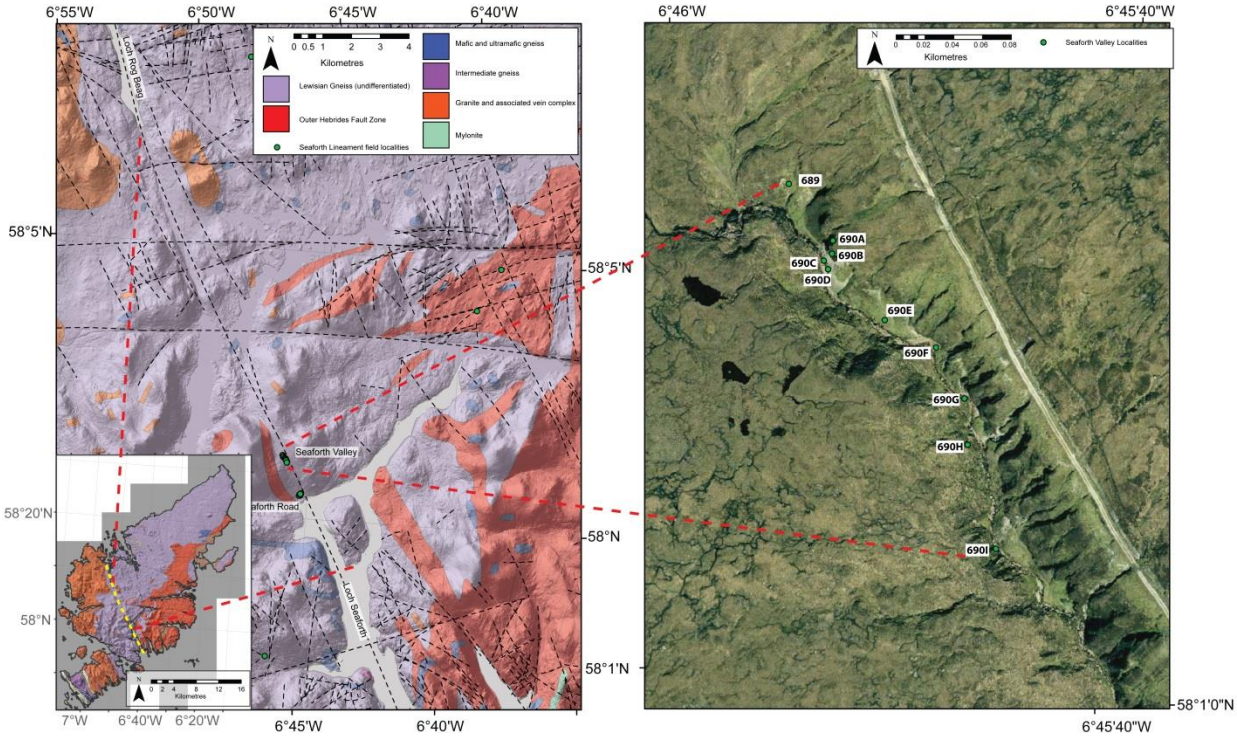

Figure 4.31: Field Localities on the Seaforth Lineament. Left hand image shows geological map of central Lewis, with red dashed lines indicating position of image on inset geological map of Lewis. Lineaments marked as black dashed lines.

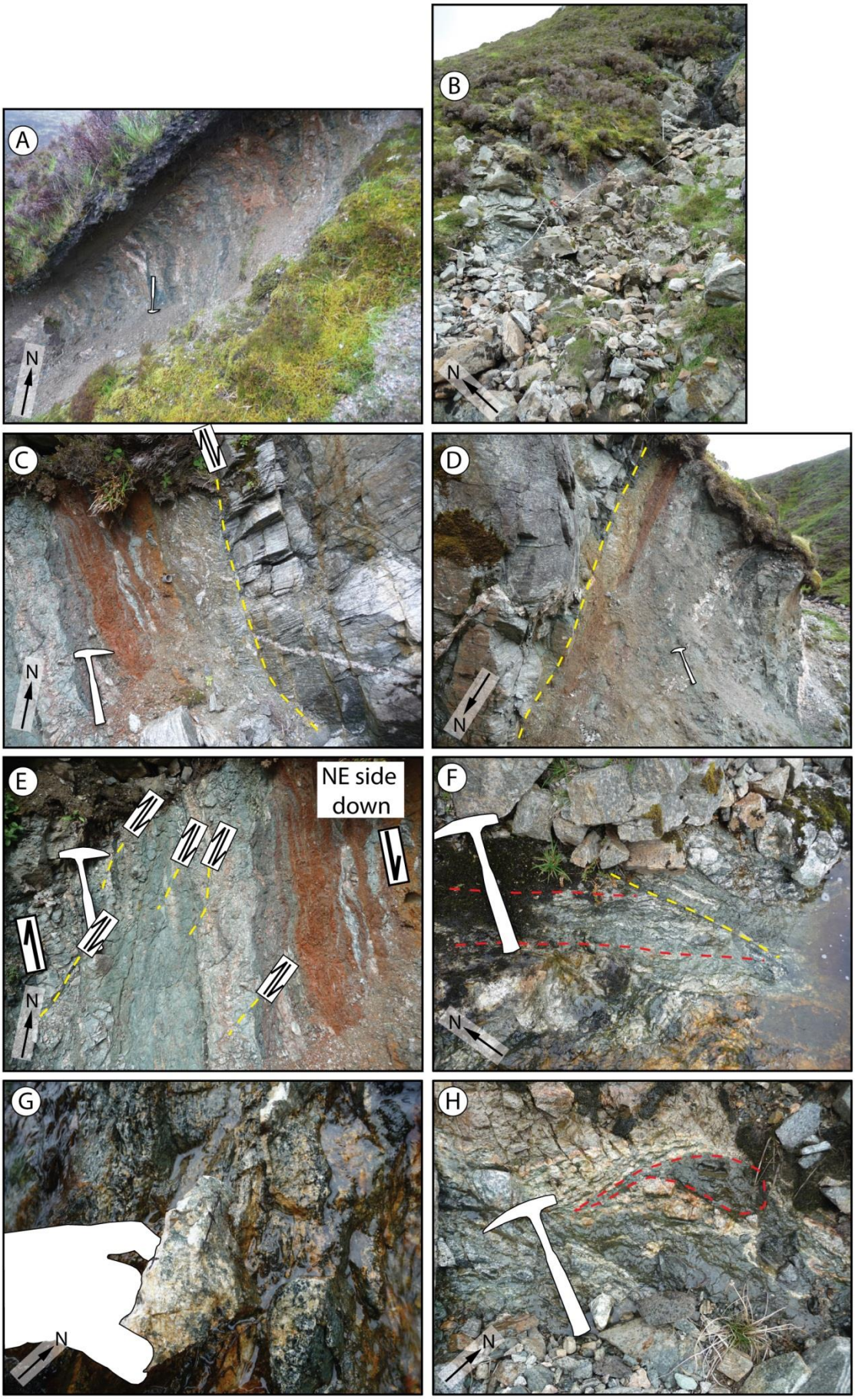
A
N
B
N
C
N
D
N
E
NE side
down
N
F
N
G
N
H
N

Figure 4.32 (previous page): Main field localities in the Seaforth Valley, (**A**) From locality 689 NB 1868 1329. (**B** - **H**) From locality 690A, NB 1871 1325. (**A**) Outcrops of foliated gouge, breccia and fault rock in the valley side at locality 689, shown in Figures 35 and 37. (**B**) Outcrop of foliated gouge and cataclasite at 690A. (**C**) Locality 690A, looking north-northwest on valley side at foliated gouge, cataclasite and breccias, and wall rock (right). (**D**) Locality 690A, looking south-southeast on valley side at foliated gouge, cataclasite, breccias, and wall rock (left). (**E**) Locality 690A, foliated gouge and cataclasite with Riedel shears, confirming normal offset on fault. (**F**) Locality 690A, olive green fault (in yellow) at 8.8 m on log cutting main gouge bands (in red). (**G**) Coarse grained chloritised gneiss from 13 m on log 1. (**H**) Boudinaged amphibolite (highlighted with red) within grey gneiss in the main fault footwall.

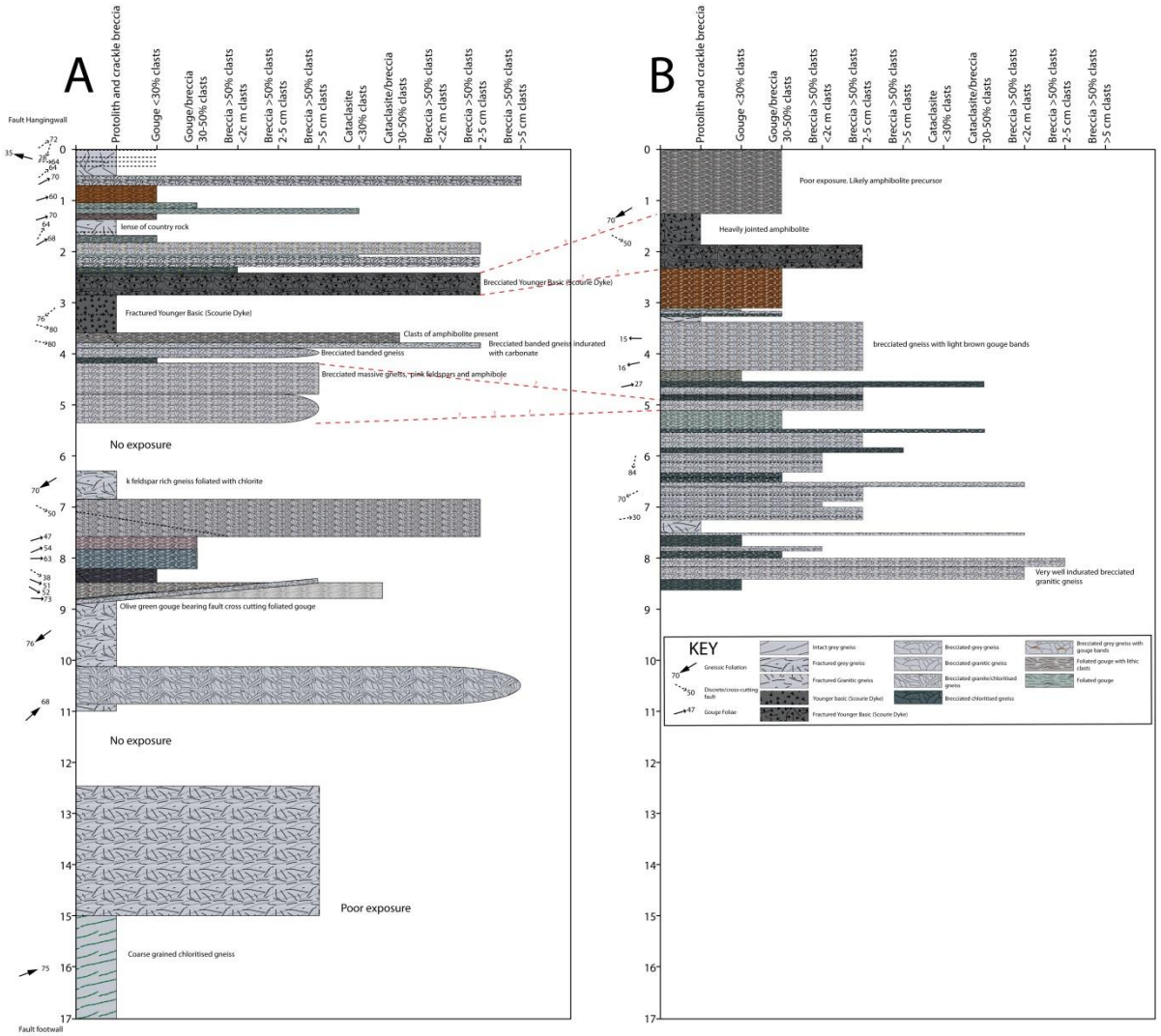

Figure 4.33: Structural log collected across the Seaforth Valley fault, at approximately ninety degrees to the hangingwall surface. Log positions are shown in Figure 4.32A and B and correspond to localities 689 and 690A (Figure 4.31). See appendix for electronic version.

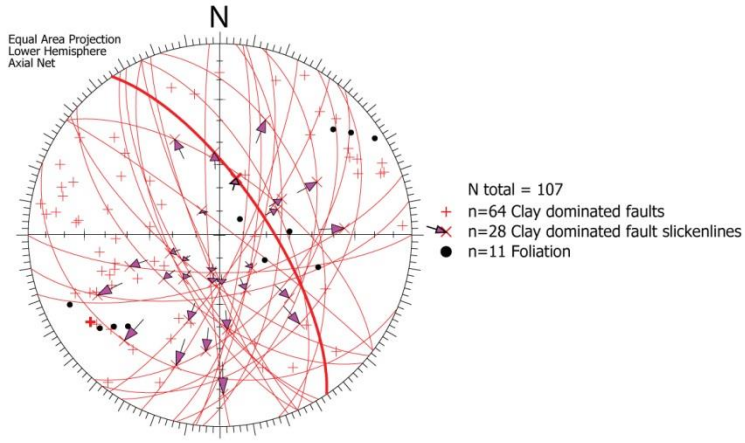

Figure 4.34: Orientation data collected from the Seaforth Valley. Faults with slip data recorded are shown with a great circle in addition to the pole. Main fault measurement shown in bold, taken from the hangingwall surface of the fault.

4.4.3.3 Rhenigidale

Rhenigidale (NB 2223 0173 to NB 2316 0172) is situated in northeast Harris along the trend of the Seaforth lineament (Figure 4.35), southeast of the Seaforth Valley localities described above (section 4.4.3.2). The outcrops visited lie 600–1400 m SW from the Seaforth Lineament. Lineaments picked in the area immediately around Rhenigidale do not show any major topographic features, but faults show a dominant NNW-SSE trend.

The country rock is composed of banded grey gneisses, cross cut by several dolerite dykes that parallel the trend of the Seaforth Lineament and lie sub-parallel with the majority of faults (Figure 4.36). Foliation varies from near horizontal at 1400 m from the Seaforth Lineament, to dipping 45°NE 600 m from the lineament. NNW-SSE striking faulting dominates, dipping to the NE and SW (Figure 4.37). The group of epidote cataclasites dipping to the northeast (Figure 4.37) were minor faults measured at one locality with strike-slip and oblique normal motion slip senses. Epidote cataclasites were observed to be cut by later carbonate-bearing minor faults.

Dip-slip normal, SW-dipping carbonate and zeolite-cemented faults dominate the area, and form a set that parallels the Seaforth Valley Fault (Figure 4.36A). Fault rocks are calcite-rich gouges (Figure 4.36B), and calcite-supported breccias (Figure 4.36F). Veins associated with these faults contain a soft grey to milky white mineral that may be zeolite, enclosing euhedral calcite (e.g. Figure 4.36C). Figure 4.36D-F shows an intermediate scale fault locality with two principal slip zones. The principal slip surfaces of the faults are localised along the hangingwall contacts, where clay-gouge can be found adjacent to chaotic breccia (Figure 4.36F). In the footwall, calcite-supported chaotic breccia grades into mosaic breccia/crackle breccias (Figure 4.36E). Faulting is contemporaneous with calcite mineralisation.

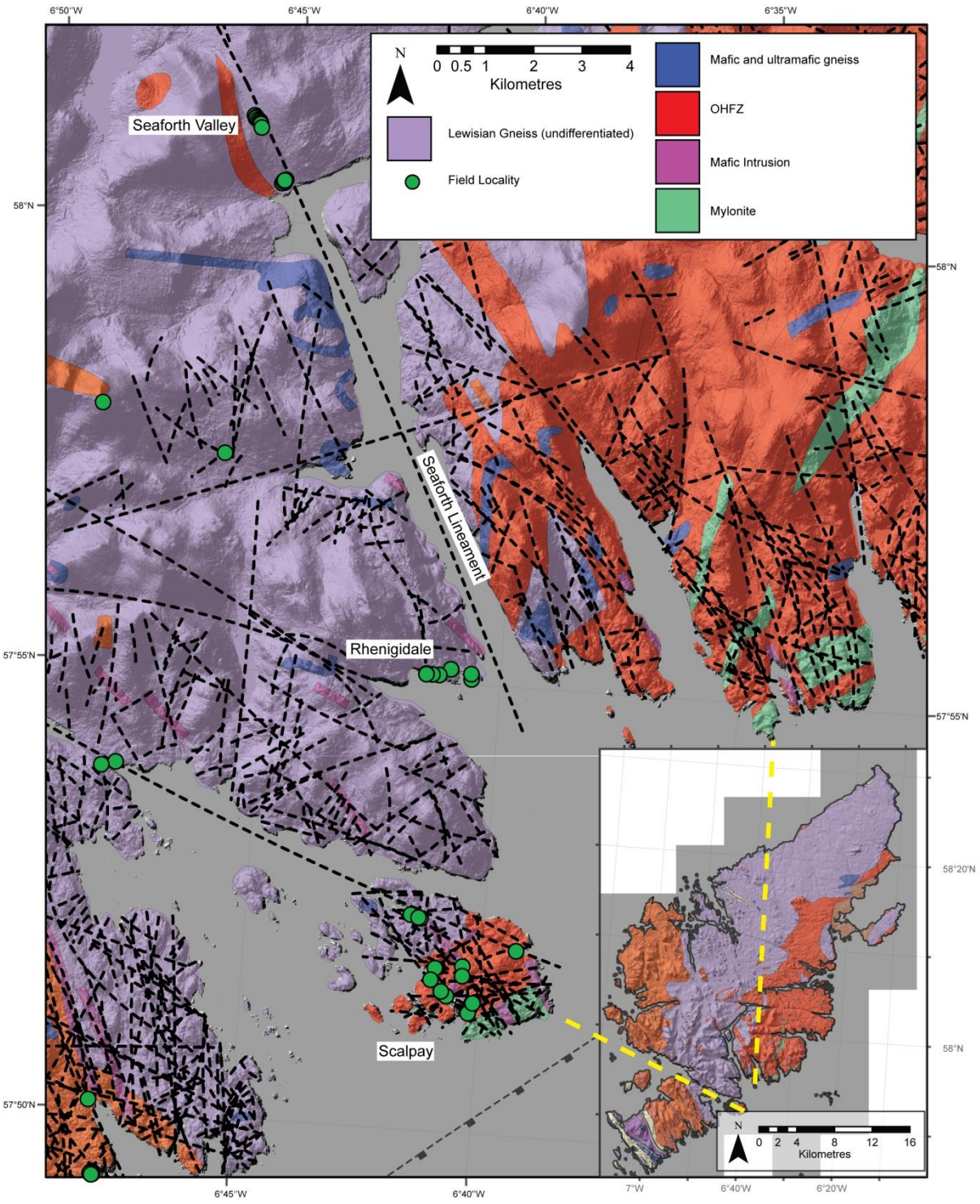

Figure 4.35: Localities at Rhenigidale and Scalpay. Note position relative to Seaforth Lineament.

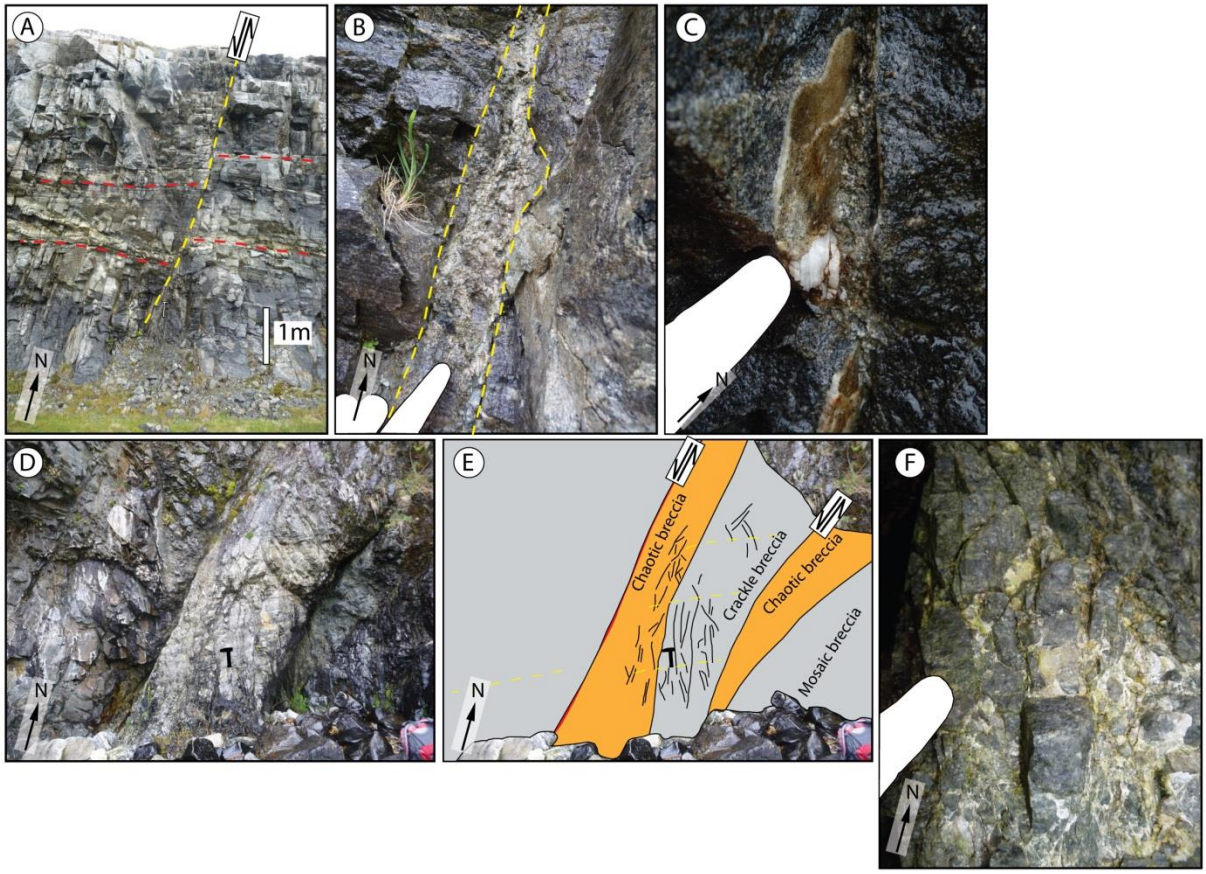

Figure 4.36: Field outcrops at Rhenigidale. Red = carbonate rich gouge, orange = chaotic breccia, grey = grey gneiss, yellow- dashed line = faulting, red dashed line = foliation. (**A** - **C**) NB 2274 0182, Normal offset across a clay gouge bearing fault, with associated calcite and probable zeolite mineralisation (image c). (**D** - **F**) NB 2223 0173. Complex fault zone with calcite cemented chaotic breccia associated with two principal slip surfaces.

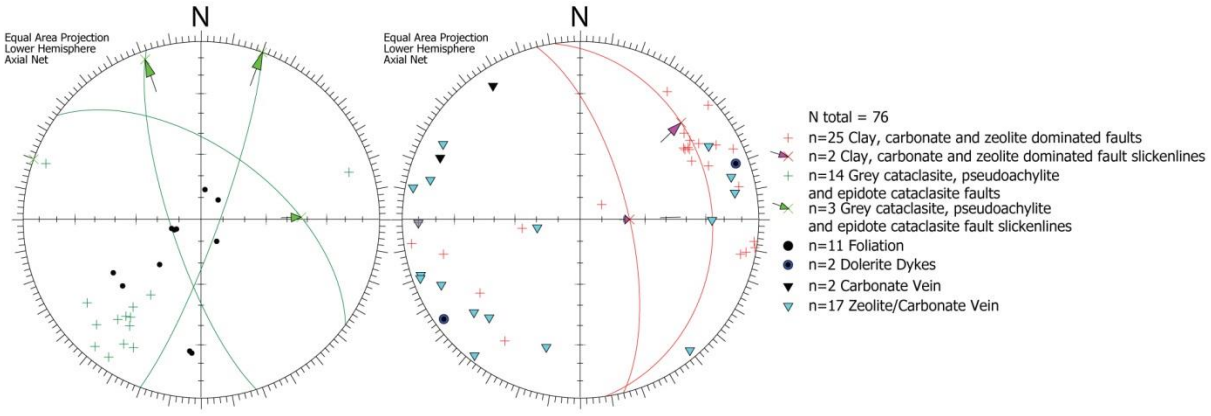

Figure 4.37: Orientation data collected from Rhenigidale. Faults with slip data recorded are shown with a great circle in addition to the pole.

4.4.3.4 Seaforth Lineament Summary

The Seaforth Lineament is a major structural feature that accommodates significant displacement. The presence of zeolite and authigenic clay development indicates relatively shallow depths in the crust, mirroring results determined for faults of this orientation and kinematics observed in the Stornoway Region (Chapter 3). Several phases of faulting have been identified at localities close to and at the Seaforth Fault:

1. At Cliobh, the majority of faults encountered were NE-SW striking epidote cataclasite bearing faults. This trend is equivalent to that identified elsewhere on both west and east Lewis. NW-SE striking epidote cataclasite faults are also widespread, possibly indicating a structural trend that has been reactivated by later clay-bearing faulting.
2. NNW-SSE faulting cuts epidote cataclasites and is associated with clay-dominated chaotic breccias and gouges. In the Seaforth Valley, the fault core of the Seaforth Lineament is exposed and the fault rock is dominated by well-developed foliated gouges.
3. Dyke intrusion along the NNW-SSE striking faults at Cliobh probably indicates the presence of dykes along some of these NNW-SSE trending lineaments.
4. At Seaforth, E-W probable strike-slip faults postdate NNW-SSE striking faults, probably representing the same later phase identified elsewhere in east and west Lewis.

Major faults with soft gouge are also associated with zeolite and carbonate mineralisation, indicating fluid flow and mineralisation are associated with these faults. It is possible that at Seaforth the fault reactivates a much earlier ?Laxfordian shear zone.

4.5 Fieldwork Results from eastern Lewis

Four main areas were visited in eastern Lewis (not including the Stornoway region which is discussed in chapter 3): Cearsiadar, Marbhig, Orasaigh, and Tolstadh Gob Thais (Figure 4.39). As in other areas, good exposure of faults and fractures inland is limited to road cuttings and quarries, and so fieldwork has concentrated on these areas. The majority of the studied localities lie in the area interpreted to be deformed within the OHFZ, and comprise variably cataclastic and mylonitic grey gneisses and fault rock (Fettes et al., 1992).

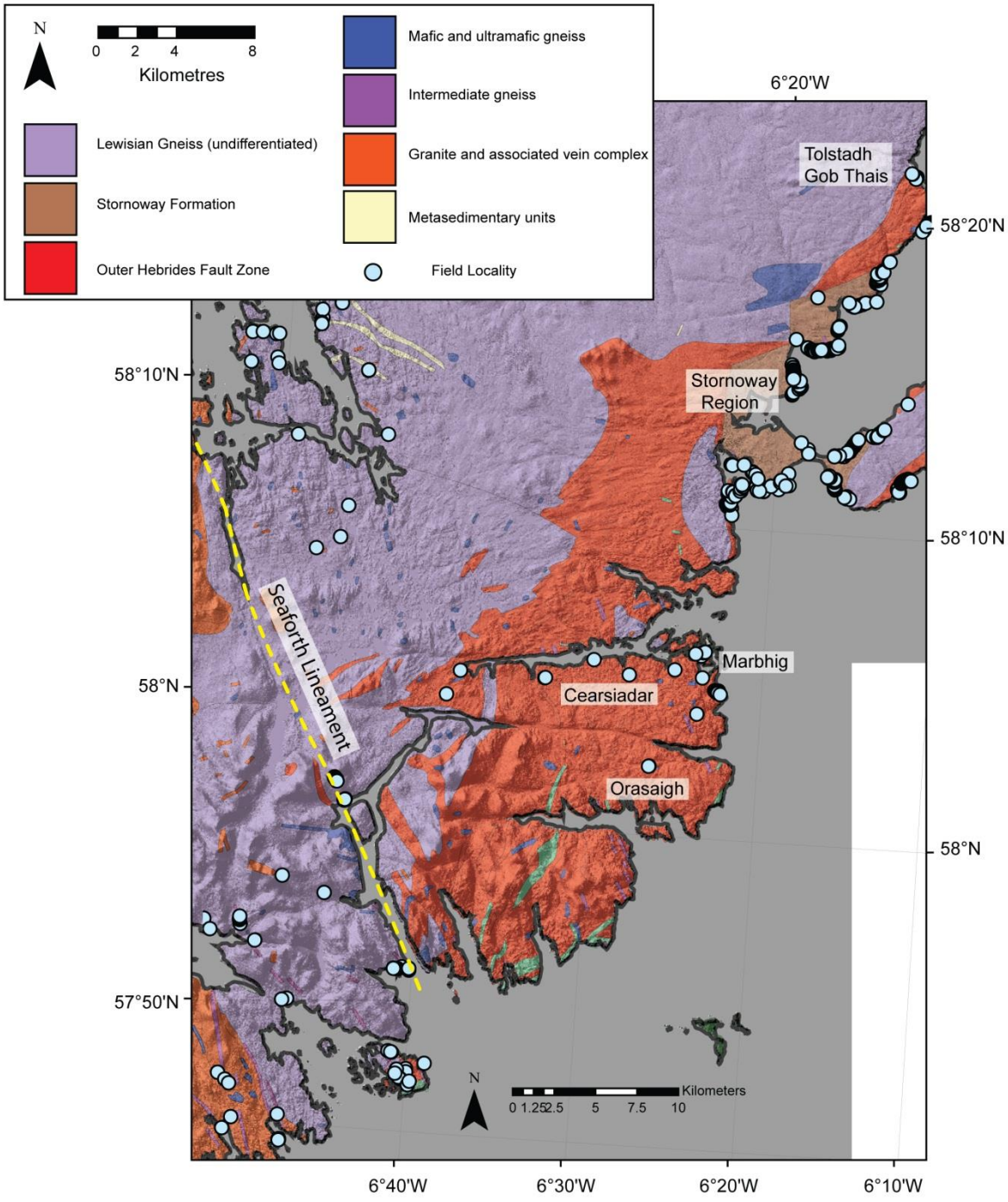

Figure 4.38: Field localities of east Lewis. Seaforth Lineament indicated.

4.5.1 Tolstadh Gob Thais

Gob Thais (NB 4380 4943 to NB 53540 4005) is located 3 km north of other localities studied at Tolstadh (discussed in chapter 3 section 3.4.2.3, Figure 4.39). Localities are located within and outside the area indicated as the Outer Hebrides Fault Zone, although the boundary between the two was not accessible. In the area of the OHFZ, there is a notable increase in fracture intensity, including joints and faults (described below), within the country rock. The country rock is

composed dominantly of grey gneisses with bands of pegmatite and amphibolite that are concordant with the foliation, dipping shallowly to the southeast (Figure 4.41).

Although exposure is limited, the gneissose foliation is demonstrably cut by several generations of faults (Figure 4.40 and Figure 4.41). Epidote cataclasite-bearing faults (e.g. Figure 4.41A-C) are observed, accommodating apparent normal displacements. Several of these faults are sub-parallel with later clay-bearing faults, and one epidote cataclasite-bearing fault is clearly reactivated, with clasts of epidote cataclasite found within clay-cemented chaotic breccia (Figure 4.40D-F). Orientations match those observed further south in the Stornoway region (chapter 3), where NNW-SSE striking faults are dominated by clay-bearing gouges and cataclasites that are of Mesozoic age.

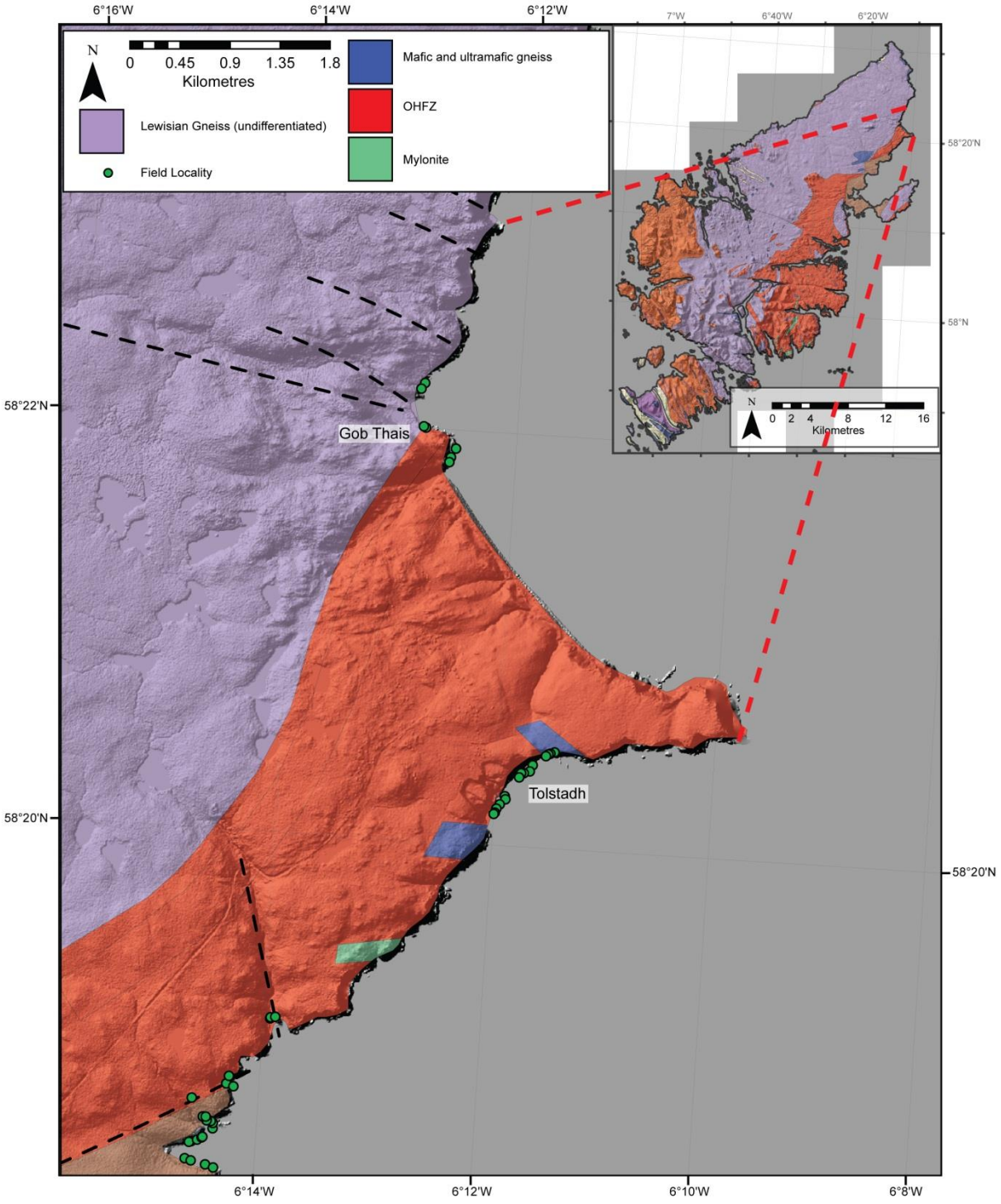

Figure 4.39: Map of localities at Gob Thais, with lineaments indicated. Localities at Tolstadh are covered in section 3.4.2.3.

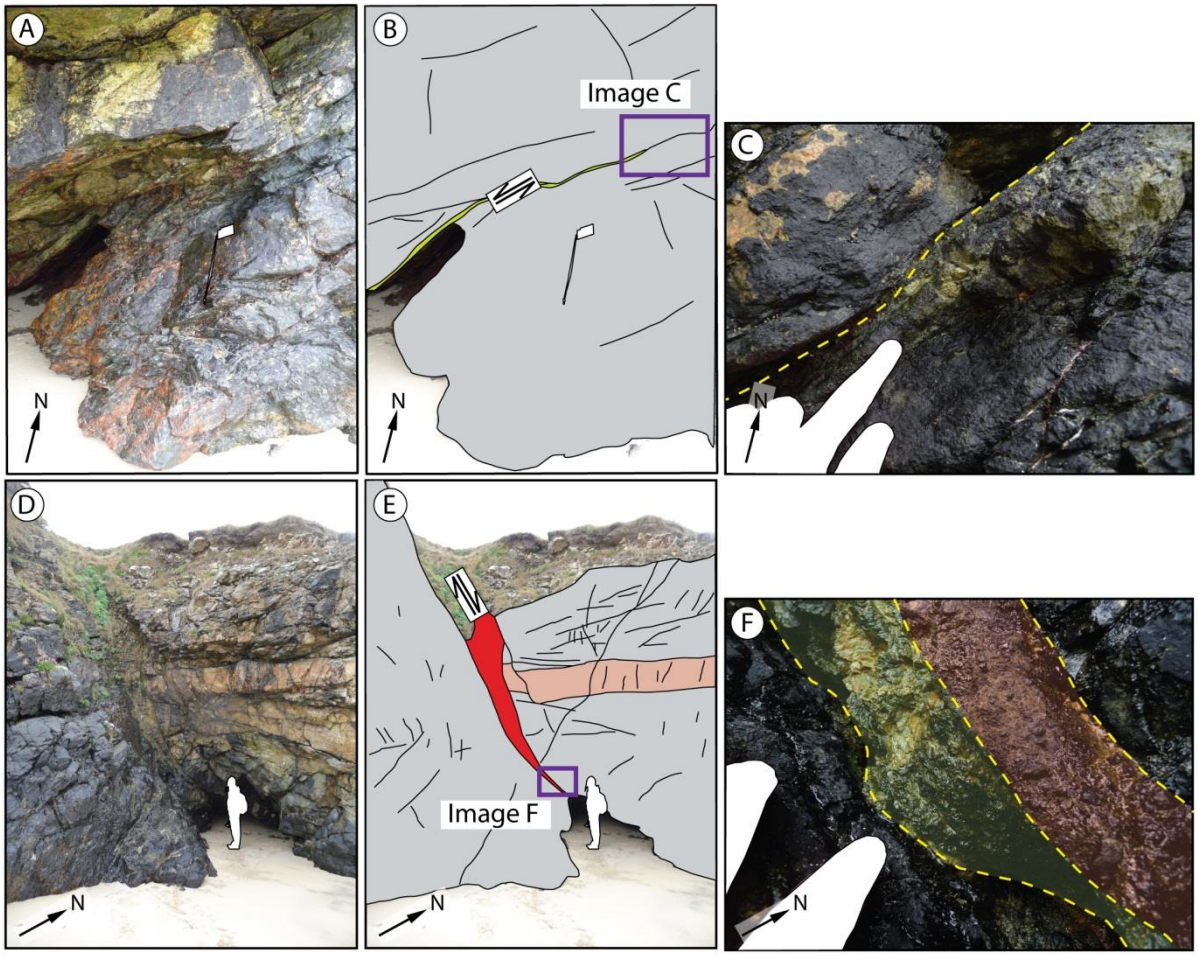

Figure 4.40: Field localities at Gob Thais within the OHFZ, NB 5380 4939. Grey = grey gneiss, pink = pegmatite, red – clay dominated fault gouge and breccia with calcite, green = epidote cataclasite. (**A** - **C**) Well indurated epidote cataclasite cutting epidotised silicic grey gneiss. Image C shows fault rock with zone of epidote developed in the footwall, up to 8 cm thick. Normal kinematics implied by minor pegmatite offset. (**D – F**) Clay-dominated fault with poorly indurated gouge and breccia with minor amounts of carbonate. Image F shows fault rock associated with this fault. A layer of epidotised crackle breccia (highlighted green) is overlain by a 5 cm thick zone of chaotic breccia of epidote clasts within a clay cement (highlighted red).

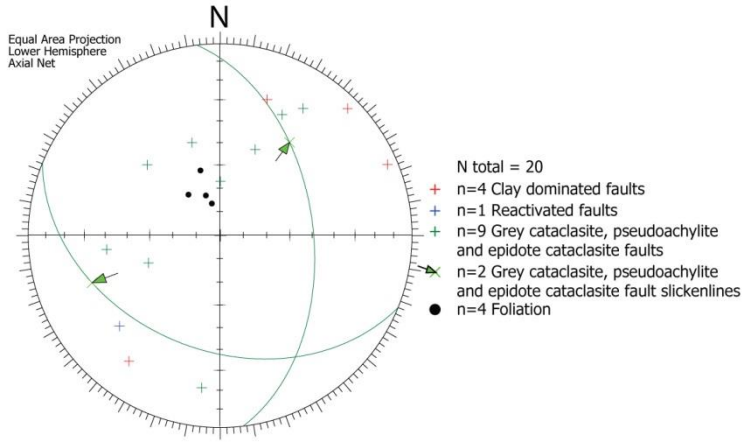

Figure 4.41: Orientation data collected from Gob Thais. Faults with slip data recorded are shown with a great circle in addition to the pole.

4.5.2 Parc District, East Lewis

The Parc District lies entirely within the region of Lewisian rocks deformed by the OHFZ (Figure 4.42). Outcrops are mostly limited to road cuttings and quarries. Cearsiadar Quarry and Orasaigh Quarry contain prominent fault exposures that are easily accessible. Exposure at Marbhig is limited to the coast and road cuttings. The country rock is composed of grey gneisses with varying degrees of mylonitisation, commonly accompanied by chlorite and epidote alteration. The foliation dips shallowly to the east-southeast and is cut by fractures and faults that postdate mylonitisation of the gneiss (Imber, 1998). Dolerite dykes of assumed Tertiary age, dipping at a high angle and trending NNW-SSE are common.

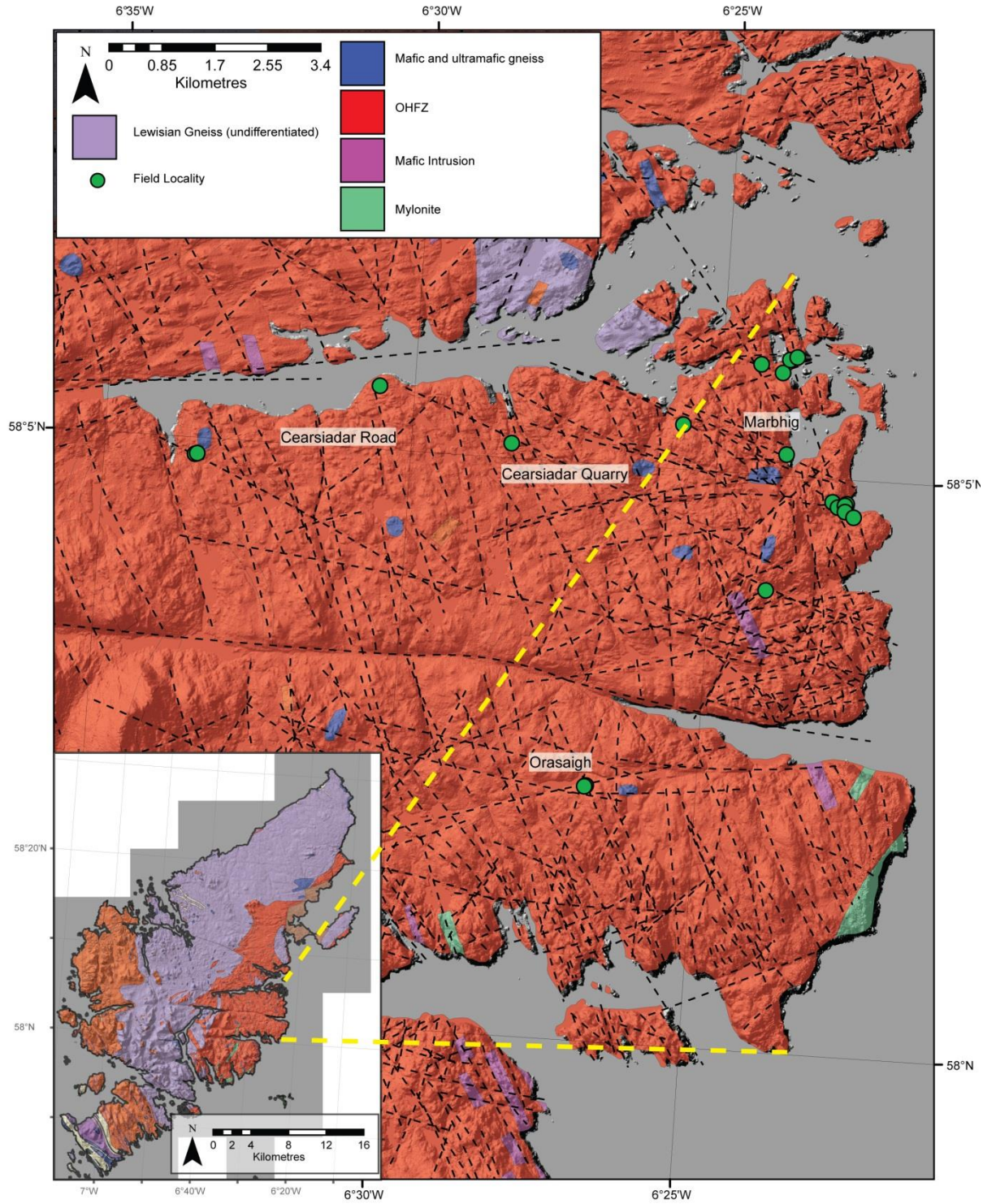

Figure 4.42: Field localities in the Parc District. Lineaments indicated.

4.5.2.1 Cearsiadar Road and Cearsiadar Quarry

The Cearsiadar area lies within the OHFZ, and exhibits intense fracturing with multiple fault sets. Cearsiadar Road cuts (NB 3138 1928 to NB 3436 2037) contain several N-S to NNW-SSE trending lineaments (Figure 4.42). In outcrop, pseudotachylite injection veins cut the surrounding gneiss, alongside quartz-chlorite veins (Figure 4.43G), and later sulphide-bearing calcite veins (Figure

4.43H). In places both the chlorite and calcite veins support brecciated gneiss in a similar manner to that seen at Cearsiadar Quarry and Orasaigh Quarry associated with faulting (section 4.5.2.3). The chlorite veins are associated with a steep, southeast-dipping fault plane, but it is not possible to identify a fault plane that the calcite veins are associated with. Given the brecciation of the gneiss it is probable that these veins originated under high pore fluid pressure conditions. Dolerite dykes, up to 2.5 m thick, are probably Tertiary age (Fettes et al., 1992) (Figure 4.43I). Dykes are observed with brecciated margins, confirming the development of a late phase of faulting along the dyke margins, as is also seen at Dail Mhor (section 4.4.2.2) and elsewhere in west Lewis. Carbonate veins everywhere cross-cut epidote and chlorite veins.

Cearsiadar Quarry (NB 3647 1945) lies along a prominent WNW-ESE trending lineament (Figure 4.42). Outcrop in the quarry wall exposes a large fault plane dipping shallowly to the NNE that is localised along 10-15 cm of mylonite/phyllonite (Figure 4.43A-C). Two slickenline sets are visible on surfaces within the fault (Figure 4.44, bold green), with slickenfibres indicating reverse slip and oblique (sinistral) slip. Four other fault planes exposed along the walls of the quarry lie sub-parallel with this main fault. Fracture intensity within the hangingwall of the main fault is visibly much greater than that in the footwall. Another fault displays clear reactivation of an E-W striking thin (<30 cm thick) mylonite zone with clayey, carbonate-rich gouge (Figure 4.44, bold blue great circles). Younger faulting hence appears to often be localised along lithological contacts, and it appears as though the WNW-ESE trending lineament may represent reactivation of mylonites/phyllonites occurring along that trend.

The latest phase of faulting in the quarry has produced a breccia zone that dips steeply eastwards (Figure 4.43D). This zone of poorly indurated breccia is 30-150 cm thick, with clay, carbonate and probable zeolite cementing angular clasts derived from the surrounding gneiss that are up to 15 cm across (Figure 4.43E-F). Dip-slip slickenlines confirm a normal slip of 50 cm observed across the zone. Other young clay-bearing faults in the Cearsiadar area are often very discrete structures lacking a damage zone (Figure 4.43J-K).

In summary, the following phases of deformation are represented at Cearsiadar:

1. Mylonite/phyllonite development, locally along discrete zones less than 30 cm thick striking ENE-WSW.
2. Chlorite/epidote bearing faults, often localising along lithological contacts. There is a greater intensity of fracturing of the country rock in the hangingwall of the faults. Two sets of slickenlines were identified within one shallowly NNE dipping epidote-chlorite bearing fault rock displaying both thrust and oblique sinistral motion.

3. Brecciation and carbonate/zeolite mineralisation, along steeply eastward dipping normal faults.
4. NNW-SSE trending dolerite dyke intrusion of assumed Tertiary age, followed by brecciation along some dyke margins.

It is inferred that the series of ENE-WSW trending faults produce the ENE-WSE lineament trend identified through the quarry.

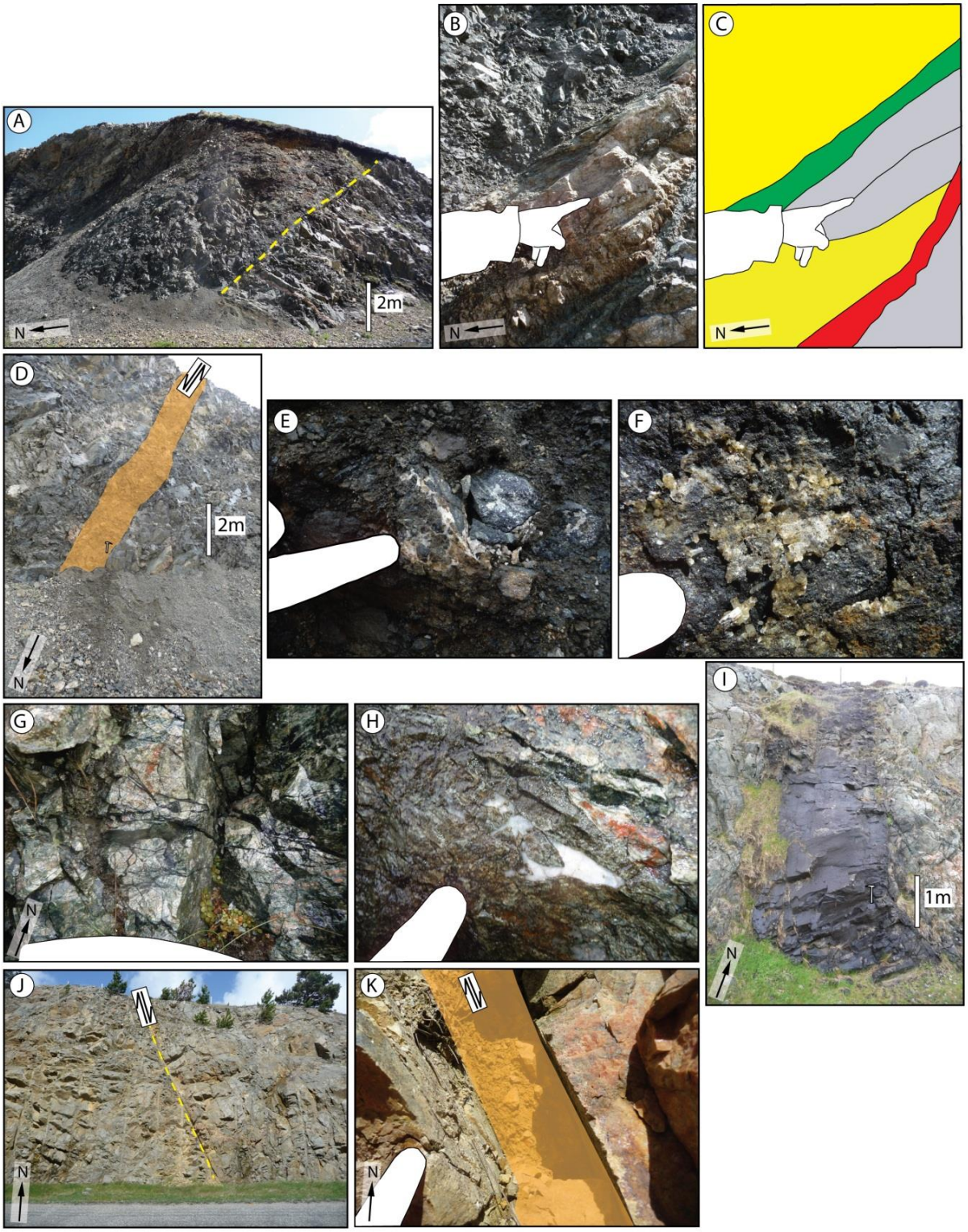

Figure 4.43 (previous page): Field outcrops along road to Cearsiadar and at Cearsiadar Quarry. Yellow dashed line = fault, red dashed line =foliation, yellow = crackle and mosaic breccia, green = phyllonite, red = gouge, grey = relatively intact grey gneiss, orange = breccia zone cemented with clay and calcite. (**A** - **C**) Main fault at Cearsiadar Quarry. (**D** – **F**) Breccia zone: youngest phase of faulting visible in Cearsiadar Quarry. Image E shows calcite cementing breccia. Image F shows possible zeolite mineralisation. (**G**) Cearsiadar Road chlorite veins. (**H**) Cearsiadar Road, calcite-cemented breccia. (**I**) Dolerite dyke. (**J** - **K**) Discrete fault with epidote veneer on hangingwall and footwall surfaces both sides of the fault gouge; fault rock is very poorly indurated clay-bearing breccia.

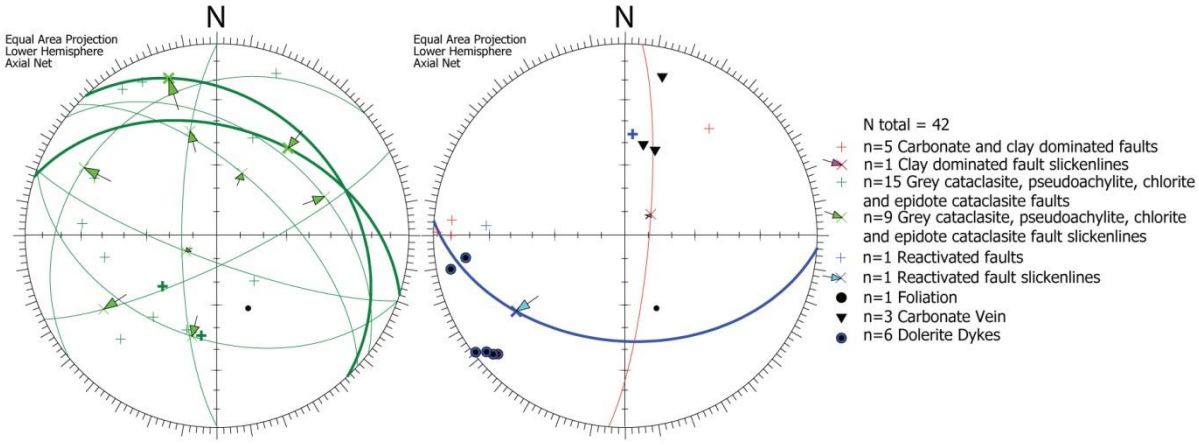

Figure 4.44: Orientation data collected from Cearsiadar Road and Quarry. Faults with slip data recorded are shown with a great circle in addition to the pole. Prominent fault plane containing two slickenline sets is shown in bold green. Bold blue = reactivation of mylonite by carbonate bearing fault.

4.5.2.2 Marbhig

The outcrop at Marbhig is dominated by coastal exposure (around NB 4095 2079 and NB 4183 1834) and road cuts (NB 4056 1708 and NB 3923 1974). Lineaments in the area trend strongly NNW-SSE (Figure 4.42), and fault attitude data show corresponding trends of epidote cataclasite faults and younger clay-gouge bearing structures. The foliation in the gneisses is often pervasively mylonitic (e.g. Figure 4.45B), with chlorite and epidote alteration. Locally, chlorite gneiss is present with the same composition and texture as that seen in the Seaforth Valley (section 4.4.3.2), with chlorite crystals up to 0.5 cm across constituting 50 - 80% of the rock, with quartz, plagioclase and K feldspar comprising the silicic component (Figure 4.45A). Mylonites found at two localities show clear lineations, which combined with asymmetric porphyroblasts indicate near sinistral strike-slip motion (Figure 4.46).

Most faults at Marbhig are epidote cataclasite-bearing (e.g. Figure 4.45C) and lie sub-parallel to the foliation (Figure 4.46), reactivating the mylonitic fabric and dipping to the ENE. One example of a minor epidote cataclasite fault with thrust kinematics is observed that reactivates the margin

of a foliation-concordant amphibolite body (Figure 4.45D). Epidote-cataclasite bearing faults (generally <2 cm thick) show normal oblique kinematics (Figure 4.46), with three measurements that are sub-parallel with lineations observed on mylonitic foliation. This parallelism may represent a continuation of the same deformation event from the formation of the ductile lineation to the formation of epidote cataclasites.

Later clay-bearing faults reactivate epidote cataclasite at one locality. These faults are again sub-parallel with the foliation, dipping to the northeast, and also the southwest, sub-parallel with the dominant clay-bearing faults identified in other areas of the island. Clay-bearing breccias are up to 20 cm across (Figure 4.45F). Dolerite dykes locally separate planar foliated chlorite-rich gneiss from migmatitic highly variable gneiss (Figure 4.45E). This lithological contact may represent a pre-existing plane of weakness along which the dykes were intruded. Some dyke margins are brecciated, indicating some post-intrusion brittle deformation. This matches observations along Cearsiadar road and at Dail Mhor.

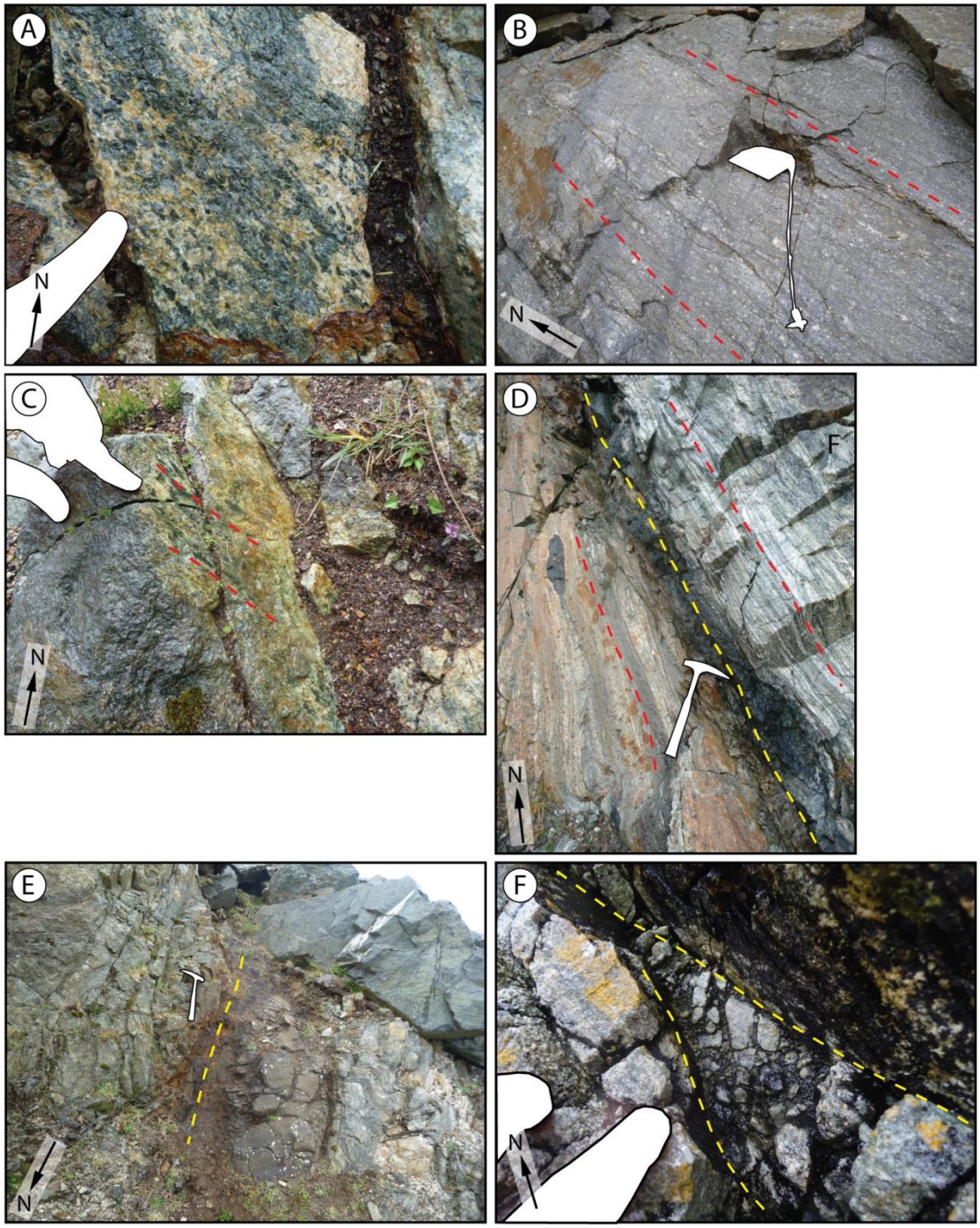

Figure 4.45: Field localities at Marbhig. Red dashed lines = foliation, yellow dashed lines = faults. (**A**) NB 2923 1974. Coarse chlorite gneiss. (**B**) NB 4056 1708. Pervasive mylonite of intermediate composition. (**C – D**) NB 2923 1974. (**C**) Epidote-chlorite fault plane; slickenlines shown. (**D**) Amphibolite forming boundary between silicic K feldspar-dominated mylonite with boudinaged amphibolite pod (left) and chloritic mylonite (right). A minor epidote cataclasite-bearing thrust fault localised along the amphibolite. (**E**) NB 3923 1974. Dolerite dyke (centre) along the lithological contact between chloritic gneiss (left) and migmatitic gneiss (right). Breccia and slickenlines at the dyke margin indicate presence of post-dyke faulting. (**F**) NB 4186 1847, Clay-bearing breccia with epidote cataclasite veneer on fault hangingwall.

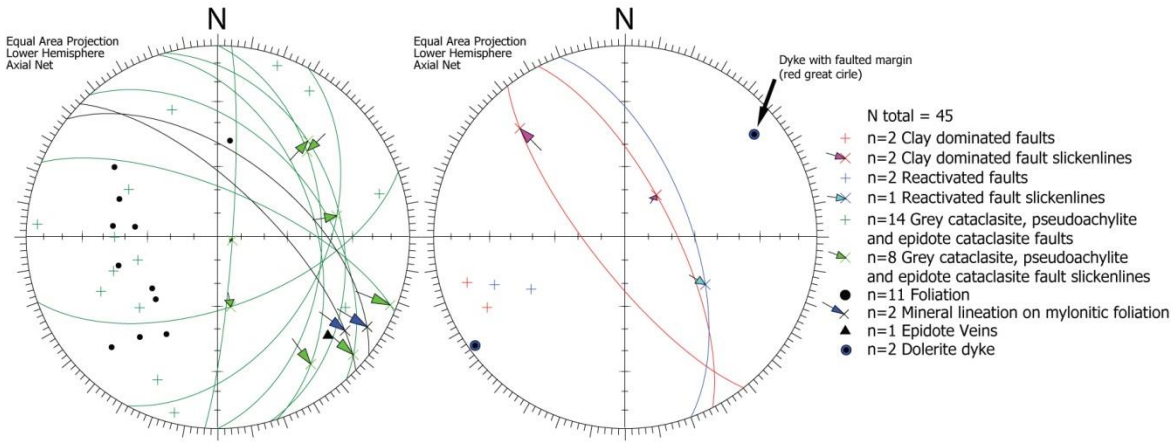

Figure 4.46: Orientation data collected from Marbhig. Faults with slip data recorded are shown with a great circle in addition to the pole.

4.5.2.3 Orasaigh Quarry

Orasaigh Quarry (NB 3766 1394) is located on a major E-W trending lineament in the Parc District. The quarry exposes an E-W striking cliff face that has excavated part of a significant E-W fault zone. The quarry face is characterised by near vertical slip surfaces with near-horizontal slickenlines. In addition, hundreds of joints dip steeply to the north, south, east and west. North-south striking joints may represent north-south directed lineaments in the area, but it is clear that the main east-west faults cut all prior structures along the entire length of the quarry (approximately 150 m, Figure 4.47A-B). Five main E-W-striking faults outcrop along the face of the quarry, each with associated gouge and breccia, stepping in an echelon pattern slightly oblique to the trend of the lineament fault zone that trends more ENE-WSW.

The country rock foliation generally dips shallowly to the east with some variation along the quarry face. The foliation is pervasively mylonitic with continuous foliation spaced at <0.5 cm intervals. Bands of pegmatite and Older and Younger Basics are also evident, with the Younger Basics showing boudinage concordant with the mylonitic foliation. Two late dolerite dykes striking NW-SE are evident in the quarry face, truncated against the fault surfaces and displaying brecciation.

Two phases of faulting are evident at Orasaigh:

1. A discrete band of foliation-parallel phyllonite at the western end of the outcrop (Figure 4.47C-D) is associated with sub-parallel quartz veining, dipping moderately to the southeast. This phyllonite is also associated with a parallel epidote-bearing cataclasite (Figure 4.49) nearby that forms a contact between amphibolite and mylonitic quartzo-feldspathic gneiss. These faults are probably earlier than the second phase of faulting

identified here. Logged fault rock from the eastern end of the quarry (Figure 4.48, from 0.7 – 1.1 m) has remains of a continuous biotite foliation that may be inherited from an earlier structure oriented subparallel with the current fault core, possibly related to this phyllonite.

2. Main faulting exposed at Orasaigh (Figure 4.47E-H). An E-W en-echelon fault set with calcite-rich foliated gouge and breccias that form much of the quarry face. This stage of faulting has produced a series of at least 5 irregularly spaced en-echelon faults that are at least 30 m long each, with associated joints and carbonate veins splaying from these faults. Most evidence indicates sinistral motion in the form of offset markers, subsidiary fractures and rotated clasts within the fault gouges. However the orientations of associated carbonate veins and joint orientations often trend ENE-WSW, suggesting dextral shear if they formed contemporaneously with faulting at this locality (i.e. parallel with maximum principal stress). At the easternmost end of the quarry, a cross section through one of these faults is preserved, displaying 20 cm of foliated gouge and metres of chaotic breccia (e.g. Figure 4.47E-G) (Figure 4.48). In places calcite is visible forming a matrix-supported breccia with clasts of angular country rock (e.g. Figure 4.47H).

NNW-SSE striking dolerite dykes of assumed Tertiary age outcrop in the quarry face. These dykes appear to pre-date the second stage of faulting described here. They are truncated against the fault surfaces, and display evidence of faulting along ENE-WSW trending fractures associated with the main faults. This would suggest that this fault set is Cenozoic in age and may match faults with this trend observed in the Stornoway Region further north (Chapter 3).

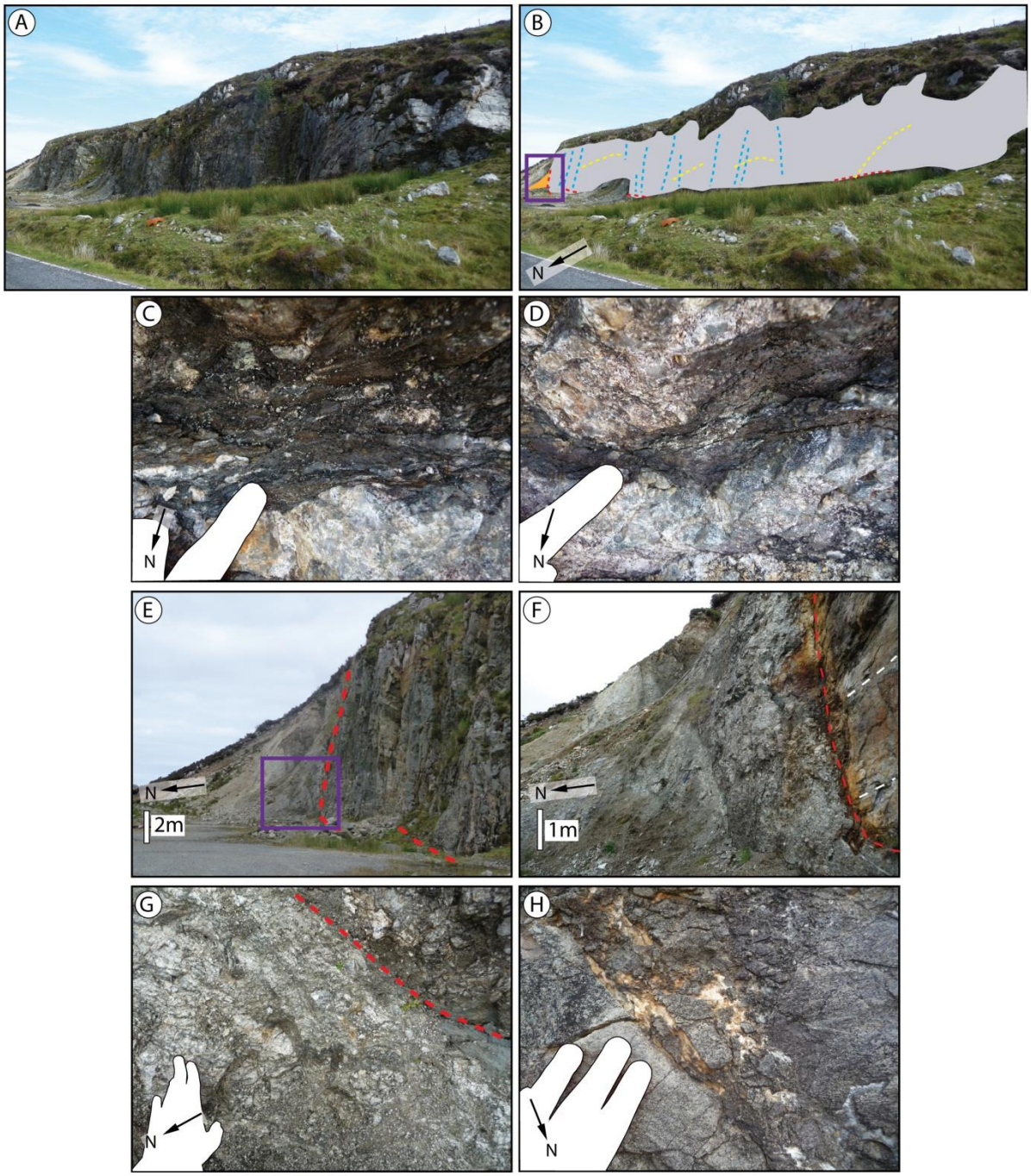

Figure 4.47: Field locality at Orasaigh Quarry. Orange = fault rock, red dashed line = fault surface, yellow dashed line = foliation, blue dashed line = jointing. (**A** - **B**) View looking southeast at Orasaigh quarry. Purple box shows area enlarged in image E. (**C** – **D**) Phyllonite dipping to the southeast. (**E** – **F**) Purple box shows area enlarged in image F. (**G**) Fault rock at Orasaigh, breccia (foreground) and grey-green clay gouge (red line). (**H**) Calcite cemented fault breccia adjacent to one of the main fault surfaces.

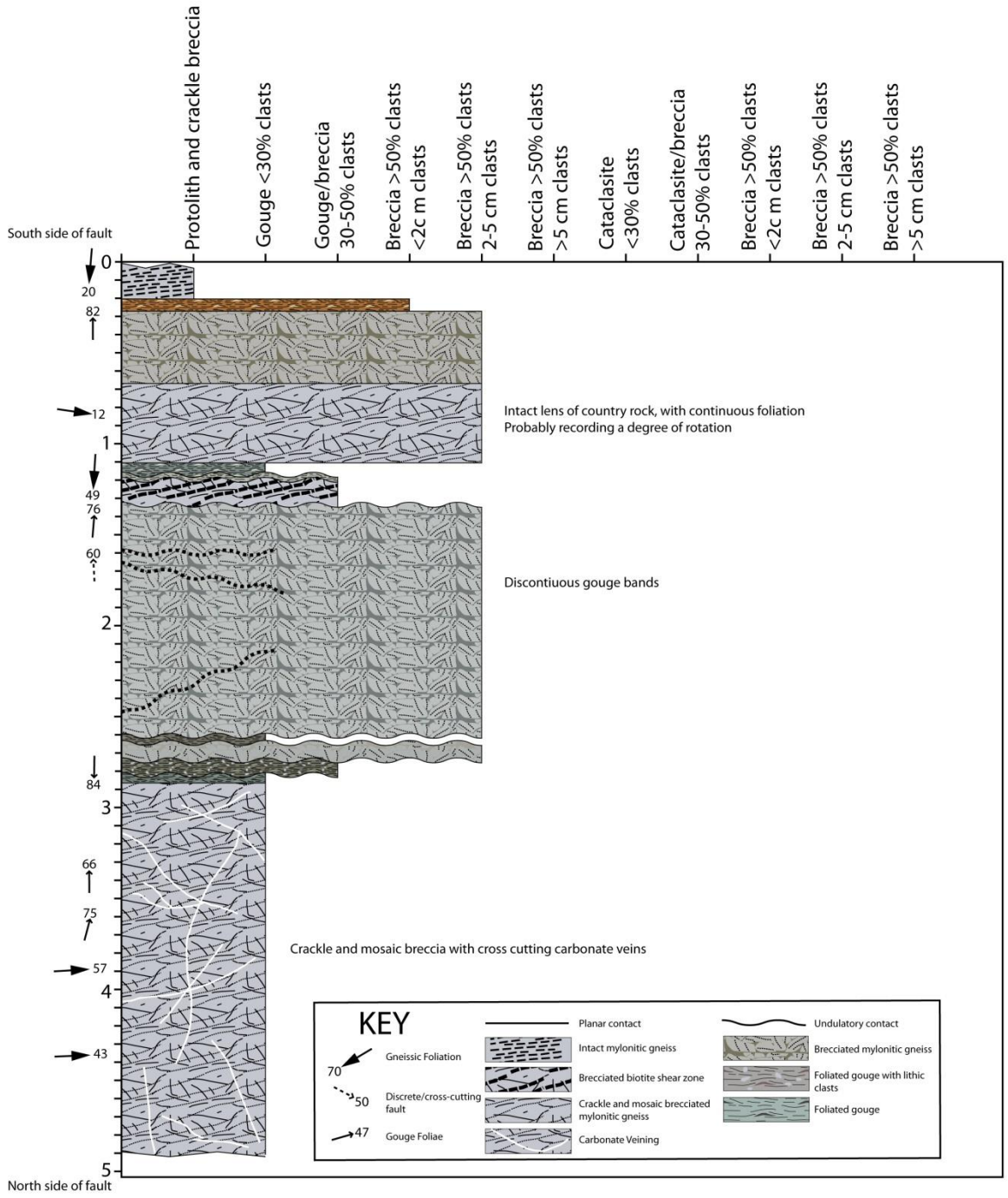

Figure 4.48: Orasaigh structural log taken perpendicular to the main fault surface at the locality shown in Figure 4.47F. See appendix for electronic version.

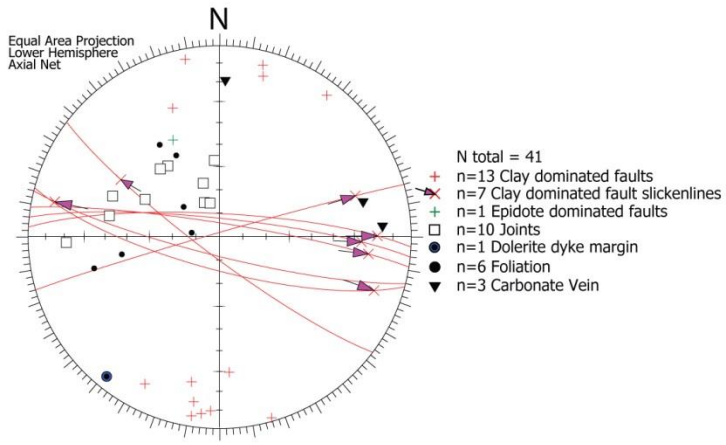

Figure 4.49: Orientation data collected from Orasaigh. Faults with slip data recorded are shown with a great circle in addition to the pole.

4.5.3 Summary of fieldwork results

Multiple phases of faulting are observed on Lewis. The earliest phases of tectonism identified agree with those seen in Chapter 3 in the Stornoway region. Phases of mylonite formation and ductile deformation were followed by the development of pseudotachylite, grey cataclasite, and epidote cataclasite faulting. Although phyllonites were not found extensively in the area covered by this chapter, they were studied in the Stornoway region and on Harris (at Rubha Vallerip), and at the latter locality phyllonite formation is visible cross-cutting pseudotachylite. Epidote cataclasite is locally associated with pseudotachylite-bearing faults and phyllonite bands. A discrete phyllonite/mylonite at Cearsiadar Road Quarry displayed both strike-slip and thrust kinematics. At Orasaigh Quarry, a southeast dipping phyllonite band occurs parallel to and spatially associated with epidote cataclasites, and epidote cataclasites have also been identified with dip-slip, thrust and strike-slip offsets. These faults likely represent multiple phases of faulting that are not possible to separate out into distinct episodes here.

The dominant phase of later faulting identified on Lewis corresponds with the fault trend observed at Seaforth Valley with large scale NNW-SSE striking faults with near dip-slip kinematics. These faults often seem to have at least locally developed along pre-existing structures such as basement shear zones or epidote cataclasite bearing faults. Other regionally extensive normal faulting with soft gouges includes E-W dip-slip faulting seen in the north at Cunndal, Port Stoth and Port Ness, ENE-WSW striking faulting in the west at Carloway and Garenin, and N-S striking faulting occasionally present in the west and east of the island. Following these phases of faulting, dolerite dykes of assumed Tertiary age were intruded across the island, and are found at most localities trending NNW-SSE and often intruding along the cores of pre-existing faults with this

trend – this is particularly evident at Cliobh. Cross-cutting these dykes are E-W striking strike-slip faults, a major example of which may be present at Orasaigh.

Combining the field observations in this chapter with those made in Chapter 3, it is possible to ascribe broad ages to the various faulting phases identified:

1. Pre-Mesozoic faults:
    a. Pervasive green mylonites of the OHFZ, generally dipping shallowly to the east and ESE (e.g. Imber, 1998), as well as phyllonites and 'cataclastic gneiss'.
    b. Pseudotachylite, often lying along the foliation plane with sporadic injection veins into the surrounding gneiss.
    c. Grey cataclasites and chlorite and epidote cataclasite-bearing thrust, strike-slip, and normal faults. These structures often lie along lithological contacts, e.g. at mylonite boundaries. NE-SW and NW-SE trending epidote cataclasite faults are common in the OHFZ
2. Mesozoic(?) faulting:
    a. E-W striking dip-slip normal faults in the north, with phases of zeolite, clay and carbonate mineralisation visibly reactivating epidote cataclasite-bearing faults.
    b. NNW-SSE striking normal faults, found across the island, excluding the north. With clay-rich gouges, breccias and cataclasites, foliated in some of the larger cases of faulting studied (e.g. at Dail Mhor, Garenin, and Seaforth). These commonly occur along (i.e., reactivating) a NNW-SSE set of epidote cataclasite faults, particularly in the OHFZ. NNW-SSE trending Tertiary dykes often lie along these faults.
    c. ENE-WSW trending normal faults, mostly widely preserved in the west.
    d. N-S breccia zones and faults, seen in both the west (Garenin) and east (Cearsiadar Quarry) of Lewis.
3. Post-Mesozoic faulting:
    a. Reactivation of NNW-SSE dyke margins by dip-slip normal faults, seen at multiple localities.
    b. Late (?) strike-slip faults seen in the OHFZ (Stornoway region and Orasaigh), and possibly present in the west (seen at Bernera), striking E-W to ENE-WSW. Late, near strike-slip faults are also seen in west Lewis at Carloway and Garenin.

4.6 Fault rock characterisation

Samples were collected during fieldwork to characterise post-Caledonian fault microstructures. 24 thin sections were produced from fault rocks from the following locations:

- Fault rocks from Cunndal and Port Stoth – E-W dip-slip faulting localised to the north of the island.
- Fault rocks from Rhenigidale and Seaforth Valley – NNW-SSE striking faults that are dominant across the island.
- Fault rocks from Orasaigh – a major example of post-Mesozoic, post Tertiary dyke E-W striking strike-slip faulting associated with calcite mineralisation.

4.6.1 E-W dip-slip faults: North Lewis

At Cunndal and Port Stoth, hand specimens and thin sections show multiple inheritance of tectonic fabrics. At Port Stoth, the gneiss consists of finely banded (<0.25 mm thick foliae) mylonite and proto-mylonitic rocks that are cut by epidote veins with evidence of thrust offset along them (Figure 4.50A-B) indicating top-to-the west motion. Similarly to Port Stoth, Cunndal also records early phases of epidote veining and faulting, with multiple epidote fault phases (e.g. Figure 4.50C). Epidote cataclasite at Cunndal is cut and brecciated within a later brown cataclasite.

Zeolite-bearing faults and veins post-date epidote mineralisation and represent the youngest identifiable fault-related mineralization phase. Figure 4.50D shows zeolite-bearing cataclasite cutting quartzo-feldspathic epidote gneiss. Clasts of country rock are up to 1 mm across, angular and with no clear sorting. The boundaries of these faults are notably discrete, consistent with observations made in the field. Within zeolite-bearing faults, very fine clasts of country rock material and incorporated veins are often cemented by crystalline zeolite with a grain size generally less than 0.05 mm (Figure 4.50E-F). Zeolite-bearing faults are the latest phase of mineralisation and faulting visible, and zeolite is also observed at Port Ness within similar E-W striking normal faults, suggesting that these faults are the same age, assuming similar conditions were present at the same time at these localities.

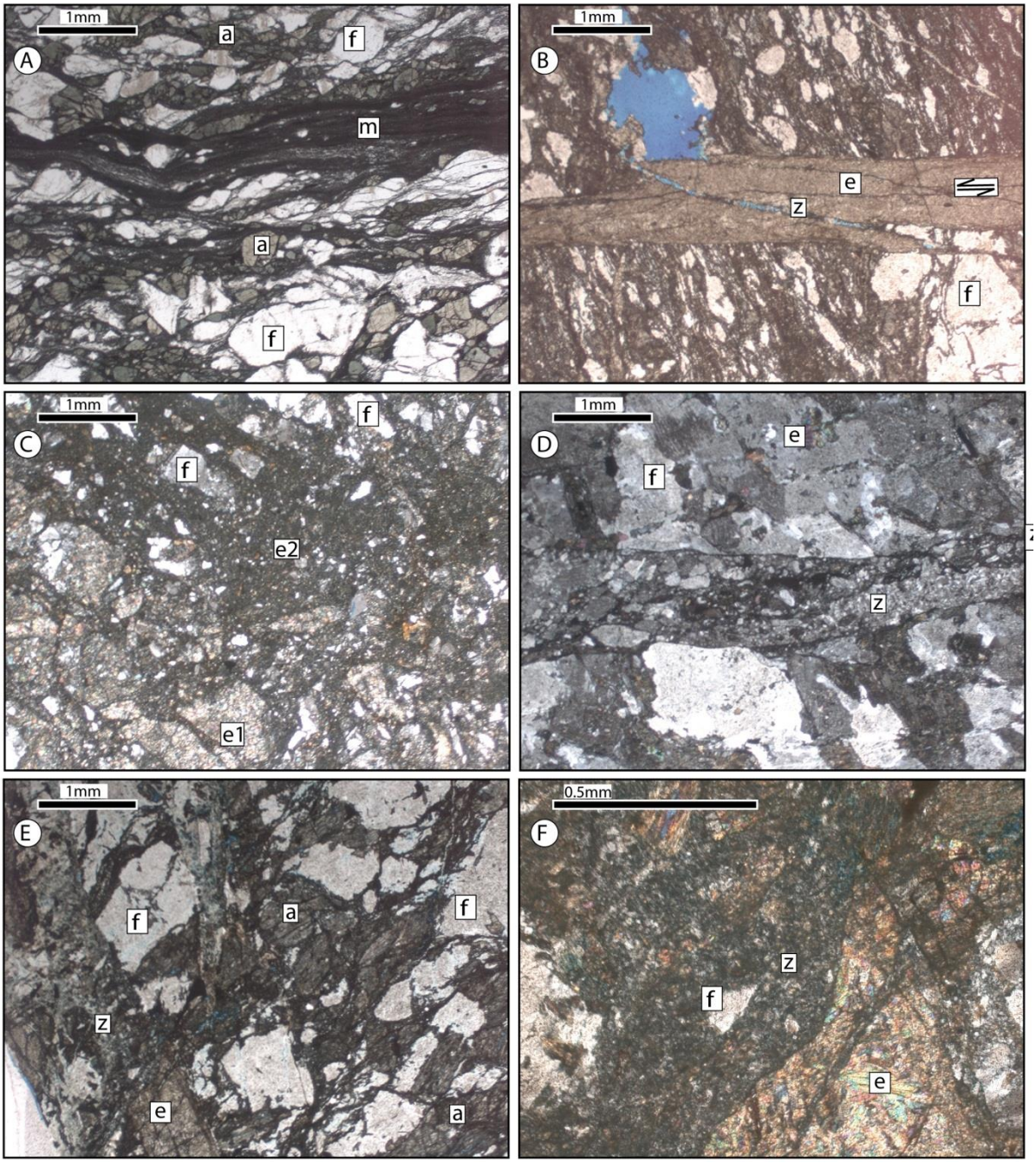

Figure 4.50: Photomicrographs of faults at Cunndal and Port Stoth, northern region of Lewis. (**A** – **B**) From Port Stoth NB 5239 6596. (**A**) PPL. Country rock is composed of mylonitic quartz-feldspar amphibole gneiss. (**B**) PPL. Epidote vein (e) cutting mylonitic gneiss, offset normally across a patchy zeolite-bearing vein (z), also associated with porosity (blue). (**C** – **D**) From Cunndal NB 51243 6553, fault rock obtained from fault shown in Figure 4.7F-H. (**C**) XPL. Multiple phases of epidote cataclasite within a single fault, with one phase (e1) brecciated within a second phase (e2) that also incorporates brecciated feldspar (f). (**D**) XPL. Zeolite-bearing cataclasite, cementing irregularly shaped clasts of country rock. (**E** - **F**) From Port Stoth NB 5239 6596. Fault rock obtained from faults shown in Figure 4.7C-E. (**E**) XPL. Zeolite-bearing cataclasite (z) cuts an epidote vein (e) and quartzo-feldspathic amphibole gneiss. (a) = amphiboles, (f) = feldspar. (**F**) XPL. Epidote vein visible in bottom left of (E), cut by zeolite-bearing cataclasite and microbreccia. (f) = feldspar clast incorporated into fault rock.

4.6.2 NNW-SSE trending structures – Rhenigidale and Seaforth

Thin sections were produced from NNW-SSE striking faults at Rhenigidale (carbonate-cemented breccia) and Seaforth (foliated clay gouges). Samples from Seaforth were collected from 1.02 m (orange-brown gouge, Figure 4.51 A-B) and 8.92 m (olive-green fault cutting other foliated gouges, Figure 4.51 C-F) on the log (Figure 4.33).

At Seaforth, foliated gouge bands are distinguished by colour, clast size distributions, and proportion of clay minerals. Assemblages of calcite, sericite, probable zeolite, and larger clasts of quartz and feldspar form the light bands, and epidote and amphibole form the darker bands, with authigenic clay alteration (Figure 4.51E). Clast sizes vary from very fine-grained clay gouge to micro-breccias with clasts up to 1 mm across, which also causes colour variation. The bright orange colouration of some gouges at Seaforth is due to iron-rich authigenic clay development with a relatively small proportion of the rock being composed of country rock clasts (Figure 4.51B). Zeolite is associated with authigenic clay and calcite in both thin sections produced at this locality (Figure 4.51B-C), and may be replacing calcite.

In the olive-green fault that cuts other foliated gouges, disaggregated primary chlorite is present with minor alteration to clay minerals (Figure 4.51F), and in both fault rocks multiple phases of gouge are visible, probably resulting from multiple slip events. Boundaries between adjacent gouge bands are notably abrupt (e.g. at left of Figure 4.51C-D).

As seen elsewhere, zeolite, clay mineralisation and carbonate are closely associated. Figure 4.51B shows calcite that is very closely associated with low birefringence, low relief, probable zeolite mineralisation that may have partially replaced the calcite crystal. Calcite mineralisation is syntectonic, shown by the presence of carbonate that appears to have undergone cataclasis (Figure 4.52D). Figure 4.51C-D show generally colourless zeolite mineralisation and authigenic clay concentrated within one band of gouge.

Feldspar clasts within both the rocks at Rhenigidale and within the Seaforth fault are highly altered and sericitised, often with yellow, probable clay alteration (e.g. Figure 4.51A, E, H). At Rhenigidale, the faults cut mylonitic gneiss with sericitised feldspar and ribbon quartz. There is little alteration of the mylonite to clay minerals, and the fault rock is cemented with sericite and calcite. Sericite dominates the fault rock (Figure 4.51G), which is probably directly derived from the surrounding altered feldspars. There is some slight yellowing to clay minerals of the country rock clasts associated with the calcite veining, but this is only minor, i.e. <<1 % of the fault rock. Calcite typically has a blocky polygonal texture.

Under the SEM, clays wrap clasts within the fault rock and are often aligned parallel and sub-parallel to the fault margins (Figure 4.52A-B, Figure 4.53C-E). These authigenic clays are likely to

be smectite and illite based on EDX analyses (section 2.4.1 and appendix). Areas of gouge are seen where authigenic clays are not present with a defined foliation (Figure 4.52C-D). These fault rocks may have developed in a relatively lower stress environment, or may have been better cemented with calcite (Figure 4.52D). It is possible that these patches are isolated pockets within the fault that have not undergone shearing to the same extent as surrounding fault rock, or alteration and clay development may have been initiated after fault movement had ceased. The later olive-green fault rock is dominated by non-foliated gouge composed of relatively clay-poor breccia (Figure 4.53) when compared to the fault rocks in Figure 4.52. Figure 4.53A-B show fault rock dominated by clasts (as opposed to authigenic clay). Primary clasts of chlorite are disaggregated and kinked with little evidence of alteration to clay minerals. However elsewhere in the slide, patches of authigenic clay mineralisation are localised and wrap country rock clasts of feldspar and quartz. Figure 4.53C-D show clay gouge minerals wrapping clasts of feldspar. As the constituent elements necessary for production of clays are not present in these minerals, it is most likely that fluids allowed mobilisation of material through the fault, but this was relatively localised. Elsewhere in the slide narrow bands of foliated clay-bearing gouge do exist with very fine clasts of country rock incorporated into it (Figure 4.53E). Authigenic clay development appears to be syntectonic, based on the observations of clay wrapping clasts of country rock within the faults and crystals aligning parallel with the fault margins.

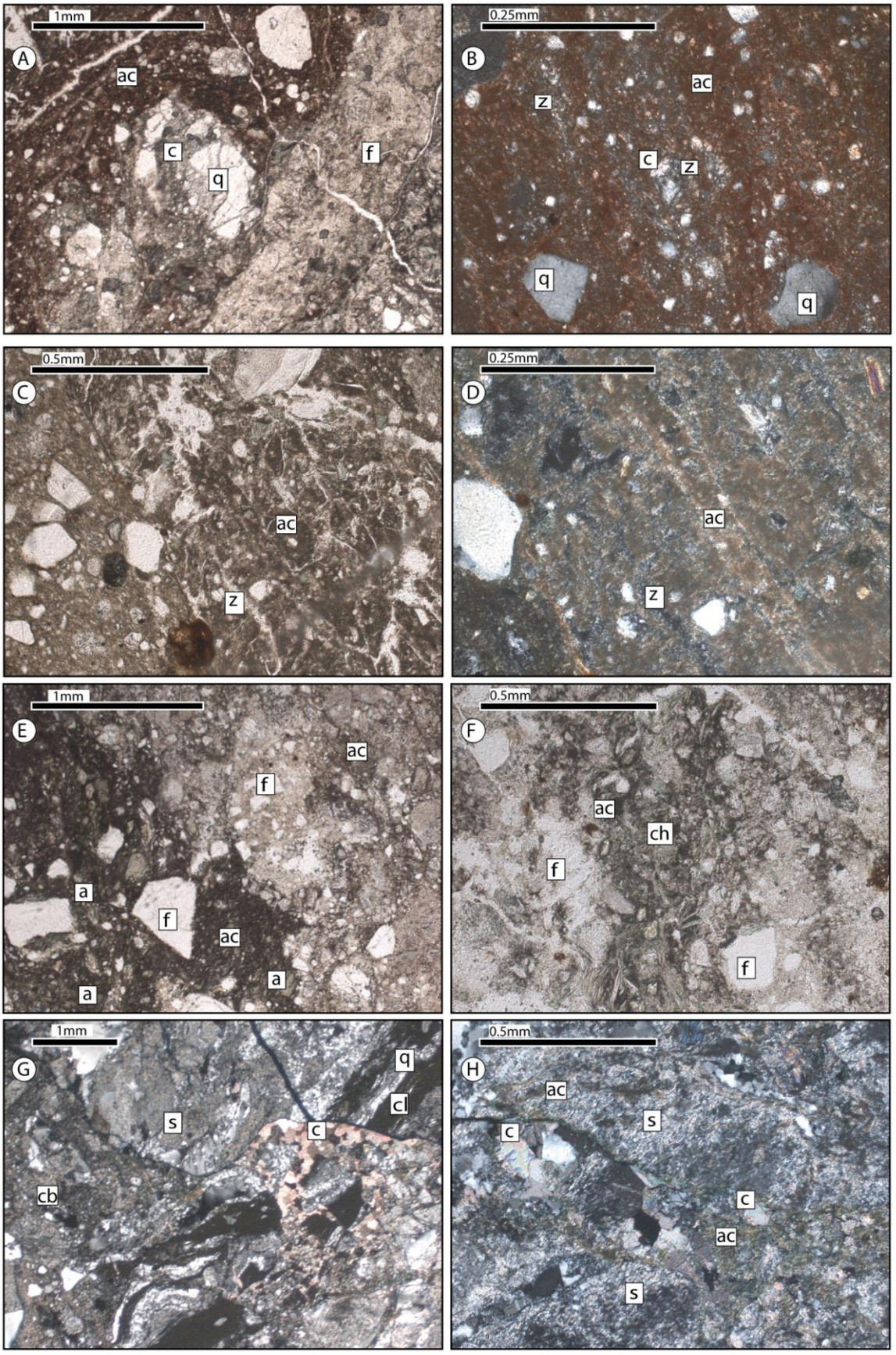

Figure 4.51: Photomicrographs from Seaforth (images A-F, NB 1871 1325) and Rhenigidale (images G-H, from fault shown in Figure 4.36D-F, NB 2223 0173). Log positions refer to Figure 4.33. (**A**) PPL. From 0.7 m on log. Boundary between light coloured fault rock at right, and darker clay dominated faulted rock at left. Light coloured fault rock is composed of altered feldspar

dominated breccia (f) that also contains clasts of calcite and probably zeolite cement, with minor authigenic clay. Darker fault rock is composed of much authigenic clay (ac), wrapping clasts of quartz (q) and calcite + zeolite (c). (**B**) XPL. From 0.7 m on log within orangey-brown clay rich gouge. Angular clasts of quartz (q) and altered feldspar are entirely enclosed by authigenic clay (ac). A calcite clast (c) is associated with probable zeolite (z). (**C**) PPL. From 8.9 m on log. Authigenic clays (ac) are associated with zeolite (z) mineralisation. (**D**) XPL. From 8.9 m on log showing variation in colour. Higher resolution image of A. (**E**) PPL. From 8.9 m on log. Amphiboles (a) altered partially altered to authigenic clay (ac). Feldspar (f) cataclasis and alteration shows yellowy colour, probably due to sericite or other phyllosilicates. (**F**) PPL. From 8.9m on log. Disaggregated chlorite (ch) with alteration to brown authigenic clays (c), surrounded by sericitised feldspar (f). (**G**) XPL. From Rhenigidale fault breccia, carbonate – sericite breccia (cb) cementing clasts of mylonitic gneiss with bands of ribbon quartz (q) and very fine grained clinozoisite (cl). Calcite varies from crystals up to 0.25 mm across to very fine calcite dispersed throughout a cement also composed of very fine sericite probably derived from cataclastic sericitised feldspar clasts (s). (**H**) XPL. From Rhenigidale fault breccia. Calcite veining (c) cutting sericitised feldspar (s), with a thin (<0.05 mm) yellow authigenic clay (ac) alteration halo around the calcite.

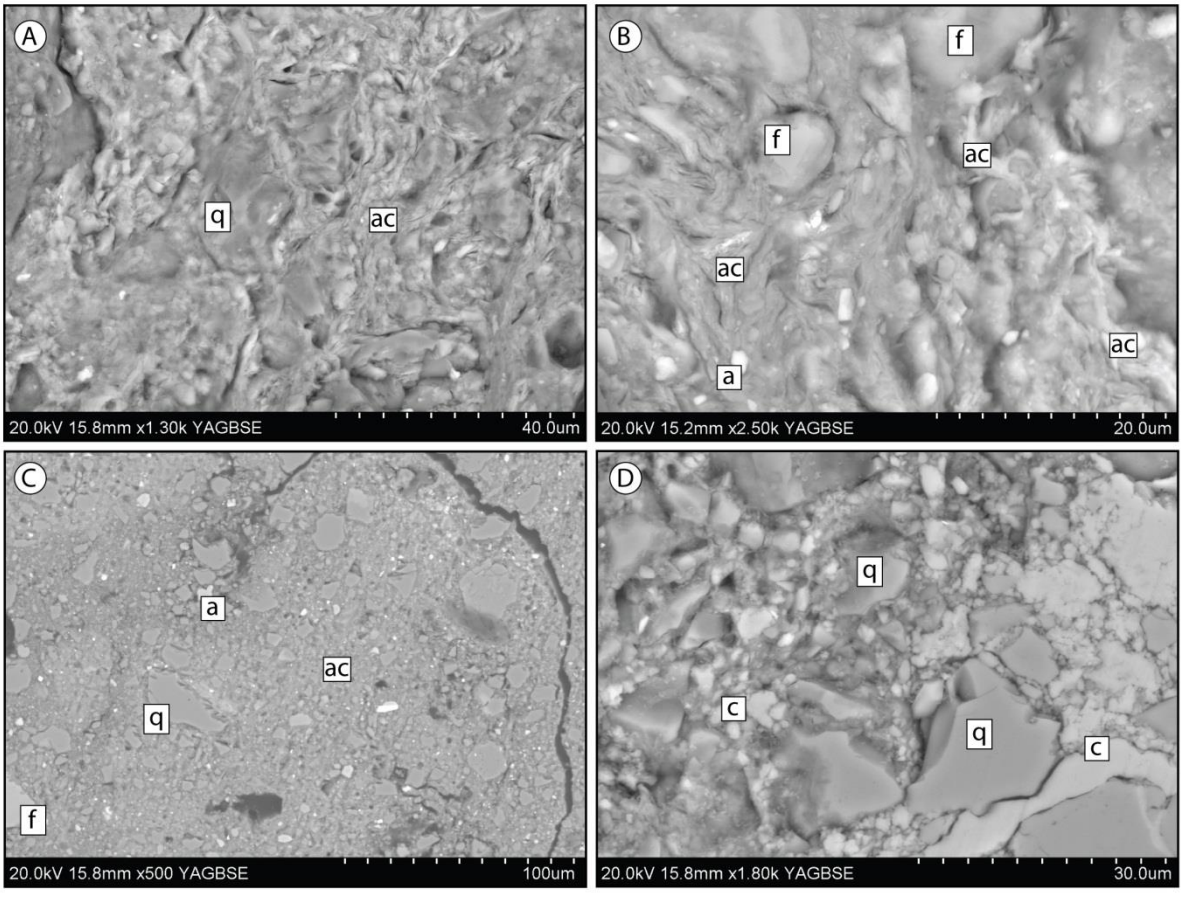

Figure 4.52: BSEM images from Seaforth, from 1.02 m on log (Figure 4.33). (**A** - **B**) Authigenic clay (ac) wrapping quartz (q), feldspar (f) and amphibole (a) clasts. (**C** - **D**) Non foliated gouge area with authigenic clay. Calcite (c) cement has also undergone cataclasis.

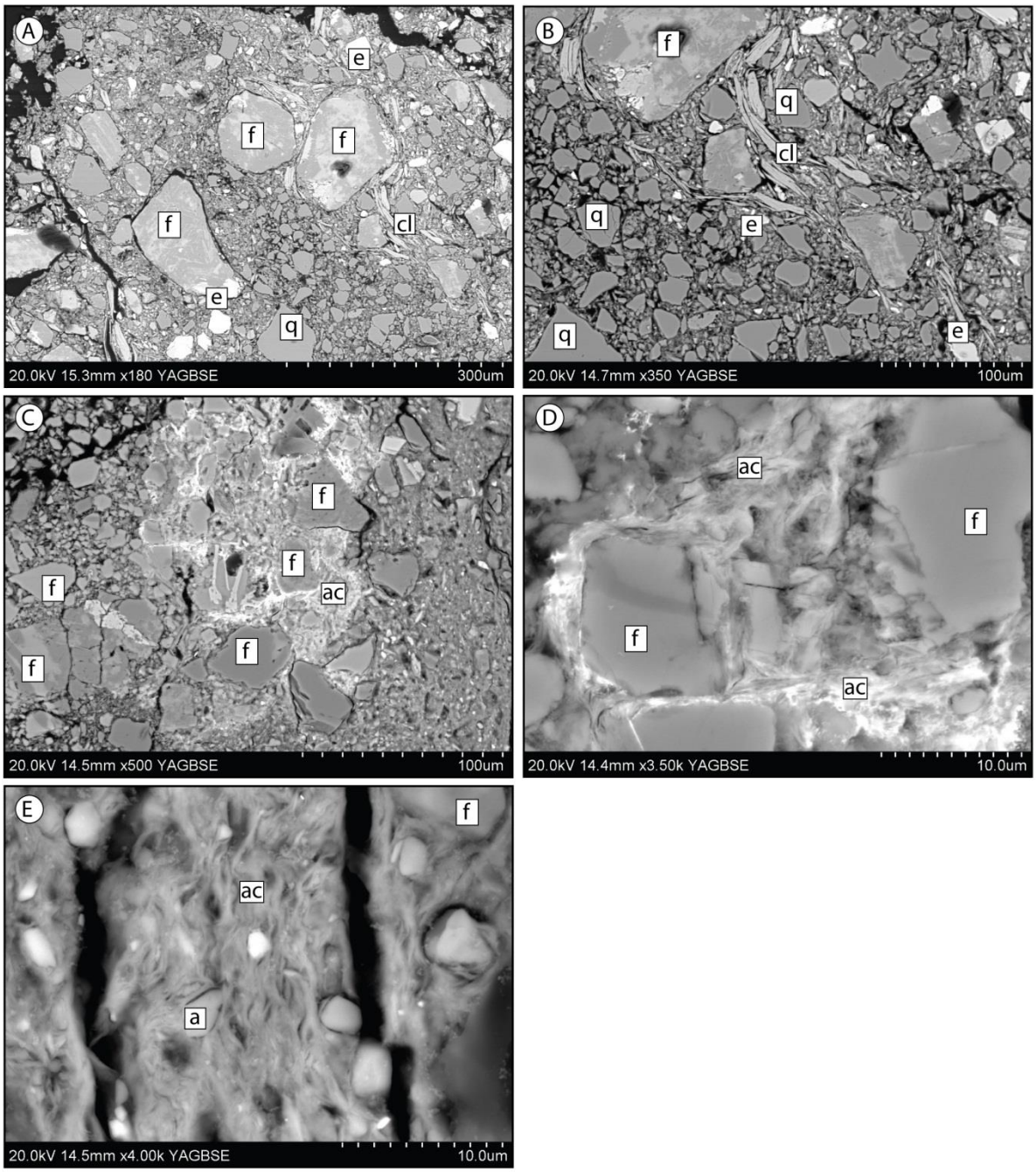

Figure 4.53: BSEM images from Seaforth, from 8.92 m on log (Figure 4.33), olive-green fault. (**A** – **B**) Clastic dominated fault rock with clasts of epidote (e), feldspar (f), quartz (q) and chlorite (cl). (**C** – **D**) Authigenic clay (ac) syntectonically wrapping alkali feldspar clasts (f). (**E**) Foliated authigenic clay (ac) with clasts of very fine amphibole (a) and feldspar (f).

4.6.3 E-W structures, strike-slip - Orasaigh

Fault rocks at Orasaigh vary from coarse crackle breccias to very fine gouges. Breccias at Orasaigh are cemented with clay and calcite, although the latter mineral occurs as both matrix and clasts. The country rock is composed of quartz-feldspar amphibole gneiss at the locality of the log (Figure

4.48) with a mylonitic texture and alteration of amphiboles to chlorite and epidote and sericitisation of feldspar. Quartz shows ribbon textures and feldspars are highly altered and sericitised (Figure 4.54A). In patches, the calcite is coarser with crystals up to 1 mm across (Figure 4.54A). Sinistral offsets of the main fault are visible in offset clasts within the fault rock (e.g. Figure 4.54A), confirming observations recorded in the field. Poorly cemented breccia within the fault is composed of clasts of mylonite up to several cm across, and in places almost entirely cemented with calcite (Figure 4.54B). Calcite also occurs as clasts within the fault rock. Darker coloured patches in the matrix of this breccia are due to smaller grain sizes of calcite that has undergone cataclasis. In other areas of gouge and breccia, calcite is widely dispersed and forms a very fine-grained matrix alongside very fine crystals of sericite (Figure 4.54C-D) that may be derived from sericitised feldspars present in the country rock, as clasts of sericitised feldspar are relatively rare within the gouge. Sericitised feldspars within the gouge often appear to have gradational contacts with the sericite-rich matrix. The main gouge band at 1.15 m on the log (Figure 4.48) is composed of angular clasts of country rock up to several cm across set in a sericite-dominated matrix also enclosing clasts of quartz usually <1 mm across, rarer calcite <0.5 mm across, and feldspar <1 mm across (Figure 4.54C gouge is at left hand side, Figure 4.54F). Also within the gouge, disaggregated chlorite is present, again probably derived from the country rock, with partial alteration to a murky yellow low relief low birefringence probable clay mineral (Figure 4.54E).

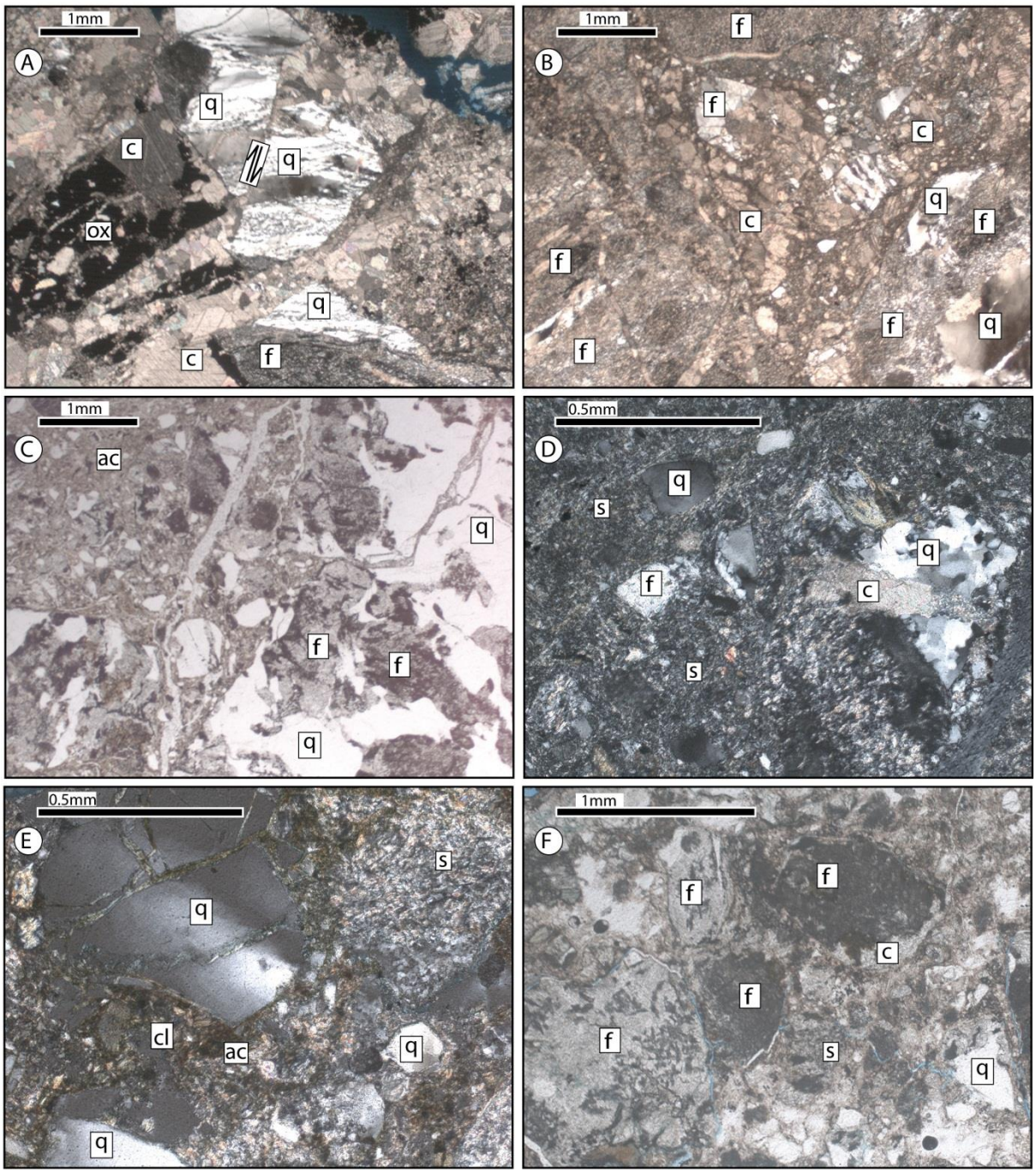

Figure 4.54: Photomicrographs of fault rocks collected from Orasaigh Quarry shown in Figure 4.47E-G. Positions refer to sampling point on the log (Figure 4.48). (**A**) XPL. Breccia from 4m on the log (Figure 4.48). Calcite (c) cemented mosaic and chaotic breccia. Country rock is mylonitic gneiss with ribboned quartz (q) and highly altered feldspar (f). Sinistral offset of the fault is indicated. Ox = Iron oxide. (**B**) XPL. Breccia from 0.9m on log. Calcite (c) supported chaotic breccia, with calcite that has also undergone cataclasis. Slightly darker colouration is due to smaller clast sizes of calcite. Q = ribbon quartz, f = altered feldspar. (**C**) PPL. Gouge from 1.15m on log (**D**) XPL. Gouge from 1.15m on log. Sericite (s) and calcite (c) rich cement enclosing clasts of feldspar (f), quartz (q). Calcite c is present within clasts and within the matrix. (**E**) XPL. Breccia from 2.4m on log. Sericitised feldspar (s) associated with a sericite/clay rich cement cementing clasts of quartz (q). Chlorite (cl) partially altered to brown authigenic clay (ac). (**F**) PPL. Gouge from 1.15m on log. Sericitised feldspar (f) and quartz (q) cemented in sericite with yellow alteration.

4.6.4 Summary of rock microstructures

As observed elsewhere, multiple reactivation of both ductile and brittle features is common. In the north of the island, zeolite-bearing faults reactivate older epidote cataclasite-bearing fault surfaces, and the major fault at Seaforth reactivates a chlorite-bearing shear zone in the gneisses, producing spectacularly coloured gouges. At Orasaigh, the main fault studied may have reactivated a pre-existing phyllonitic shear zone. Fault rock composition dependence on the country rock composition is clearly shown at Rhenigidale and Orasaigh where faults are dominated by sericitic gouges that are probably derived from sericitised feldspar in the country rock.

The microstructures in the fault rocks examined here are similar to those observed in the Stornoway area (Chapter 3), with calcite, authigenic clay and zeolite mineralisation occurring contemporaneously with later phases of faulting. Foliated authigenic clays are observed wrapping clasts derived from the country rock, confirming a syntectonic origin. Patches of gouge and cataclasite with non-foliated authigenic clays appear to form isolated domains within the fault rock around which foliated gouge may develop, possibly due to a very localised (sub cm) increase in shear resistance probably due to the presence of a greater strength of calcite-cemented patches of fault rock. In all the faults, calcite has a syntectonic origin, evidenced by clastic occurrences of calcite within authigenic clays and breccias, alongside intact calcite veining that also looks contemporaneous with faulting. The calcite zeolite relationship is less clear, but in some rocks it does appear as though zeolite mineralisation post-dates calcite, confirming observations made in the Stornoway region. In some of the youngest fault rocks, a relative lack of authigenic clays is observed. This may be due to a lack of available transporting fluids within specific faults.

4.6.4.1 Conditions of faulting

As discussed in chapter 3, epidote cataclasite is indicative of temperatures of >200°C (Liou, 1993), indicative of depths in the crust of >6 km assuming a normal geothermal gradient (Watts et al., 2007). Epidote bearing veins and faults are cross cut by zeolite bearing faults, indicative of temperatures of <150°C (Frey, 1987), indicative of crustal depths of <5 km. Authigenic clay bearing fault rocks (e.g. at Seaforth) are indicative of similarly low pressure and temperature conditions (e.g. Reyes, 1990). These observations indicate that zeolite and clay formation occurred at lower temperature and probably lower pressure conditions (i.e. higher in the crust) than epidote bearing fractures.

4.7 Discussion

4.7.1 Lineament analysis

Similar to chapter 3, the lineament analysis was used as a guide to the orientations of faulting and the location of major lineaments on the island. The limitations of this analysis are discussed in chapter 3. The analysis shows little variation between east and west Lewis, with the same NNW-SSE and ENE-WSW trends represented. In the field these lineaments were found to be the surface expression of faults and also dolerite dykes, although the latter often intrude along pre-existing fault cores and are themselves often faulted along their margins.

4.7.2 Fieldwork: Faulting Synthesis

It is possible to group faults on the basis of their associated fault rocks, given the assumption that similar fault rocks will form at similar crustal conditions and hence at similar times. Ages can be assigned to these faults on the basis of cross-cutting relationships, regional considerations and comparison to previous work. On this basis, the following phases of deformation have been identified on Lewis from a combination of this work concentrating on post-Caledonian brittle deformation, and work concentrating on Caledonian and older deformation (e.g. Butler, 1995; Imber, 1998):

1.a *Mylonite formation – Proterozoic (Imber et al., 2002).* Thrusting synchronous with granite intrusion in west Lewis would suggest initiation during the Laxfordian. Mylonite formation was postdated by formation of a cataclastic texture within the gneiss (e.g. Butler et al., 1995). Mylonite is found within gneisses in north, west, and east Lewis.

1.b *Chlorite gneiss formation – Proterozoic?* Recognised at Seaforth and at Marbhig, this gneiss is relatively localised. The very high degree of alteration and localisation of these gneisses is suggestive of the existence of them along shear zones, e.g. as seen at Seaforth.

1.c *Pseudotachylite and ultracataclasite formation – Proterozoic?* Similar rocks are referred to as the crush mélange by Sibson (1977) on North Uist. Related to thrusting in the OHFZ (e.g. Imber et al., 2001). These fault rocks are seen at multiple localities but are most obvious in the Parc District of the OHFZ east of the Seaforth Lineament, in addition to being present in the Stornoway Region. Pseudotachylites have also been linked to Grenvillian and older phases of deformation (e.g. Sherlock et al., 2009). Fettes et al. (1992) determine a depth of formation of pseudotachylites in SE Lewis of 13.5 km.

2.a *Phyllonite formation – Caledonian (Butler et al., 1995).* Developed as NE-SW striking sinistral shear zones with later extension (e.g. Butler et al., 1995; Imber et al., 1997). Phyllonites are known to post-date pseudotachylite and cataclastic gneisses. Lineations observed on mylonite at Marbhig indicate down to the SE motion that may be linked with this later phase of phyllonite formation.

2.b *Chlorite-bearing faults – Caledonian age?* Within the OHFZ, with multiple phases of movement represented by thrust and strike-slip kinematics. These chlorite bearing faults are linked with phyllonites at Cearsiadar Quarry. Probably related to thrusting during the Caledonian Orogeny.

3. *Epidote-bearing faults – Caledonian and late Caledonian age?* There are several phases of epidote-bearing faults that are consistently cross cut by fault rocks containing authigenic clay, zeolite and carbonate. Ordered by region, these are:

a. In the OHFZ region, these commonly trend NW-SE and NE-SW with normal oblique offsets. Epidote cataclasite faults are commonly linked to mylonitic and phyllonitic shear zones, representing reactivation of these ductile fabrics. In the Stornoway Region, epidote cataclasite faults are linked with extensional ductile features (folds at Arnish) and with phyllonites (Seisiadar). These fault rocks record motions of top-to-the-east and southeast extensional collapse, postdating fault rocks associated with the Caledonian Orogeny.

b. Epidote cataclasite faults are also seen in the west of the island, often with trends parallel/sub-parallel to those of later clay-bearing faults. At Garenin, for example, epidote cataclasite-bearing faults strike N-S and ENE-WSW, and at Dail Beag and Dail Mhor epidote cataclasite-bearing faults strike ENE-WSW to NE-SW. Epidote cataclasites have dominantly normal to normal oblique kinematics.

c. In north Lewis, epidote cataclasite faults strike NE-SW with near strike-slip offsets. These strike-slip faults may relate to a phase of faulting strike-slip motion identified in the OHFZ and attributed to the late Caledonian (e.g. Imber, 1998). NE-SW striking epidote cataclasite-bearing faults with strike-slip motion were also found at several localities in the Stornoway Region (Chapter 3), where epidote cataclasites were also seen related to phyllonites. It is possible that the phase of strike-slip movement identified on these phyllonites (Butler, 1995; Imber, 1998) may also be linked to the strike-slip faulting associated with these epidote cataclasites.

Temperature conditions associated with epidote are typically >200°C (Liou, 1993), indicating depths generally greater than 6 km in the crust, assuming a normal geothermal gradient. In

the Caledonides of Norway, epidote-filled fractures represent a depth of formation of around 10 km (Fossen and Hurich, 2005).

4. *Zeolite, calcite and clay-bearing faults – Mesozoic and Cenozoic.*

- **a.** In the OHFZ, zeolite is found in NNW-SSE striking faults that contain soft clay gouges and calcite (e.g. Rhenigidale, Seaforth, Stornoway Region (chapter 3)) predominantly striking NNW-SSE, that consistently cross cut earlier structures (phases 1-4). In Cearsiadar Quarry, zeolite is found within a breccia zone of post-Caledonian age that trends N-S. The low temperatures and pressures necessary for the formation of zeolite would also suggest this mineralisation post-dates that of epidote, given a history of continuous exhumation of the Lewisian Complex. Calcite is also strongly associated with authigenic clay-bearing fault rocks and zeolite. Whilst the exact relationship between calcite and zeolite growth is not always clear, in some cases calcite appears to be partially replaced by zeolite. Calcite is particularly strongly associated with faulting at Rhenigidale (NNW-SSE striking dip-slip normal faulting) where the fault rock is also cemented with sericite.
- **b.** In the west, ENE-WSW striking, SSE dipping faults are strongly associated with sub-parallel calcite veins that are heavily brecciated and associated with soft red clay gouge. At Dail Mhor and Cliobh large scale NNW-SSE striking faulting was observed. Large examples of these faults cross the island (e.g. Seaforth) and are associated with foliated clay gouges. These faults have near dip-slip normal offsets. The relationship between NNW-SSE striking faults and ENE-WSW striking faults is not clear. However, within the Stornoway Region, the Mesozoic bounding faults of the Stornoway Formation strike N-S and ENE-WSW with normal kinematics, and are believed to be contemporaneous (Chapter 3).
- **c.** In north Lewis, the dominant faults are E-W striking, with dip-slip normal kinematics. Fault rocks are zeolite-bearing, often reactivating epidote bearing structures.

Temperature and pressure conditions of formation of zeolite bearing faults are less than that of epidote bearing faults (<150°C, Frey (1987)). Mendum (2009) mentions that late cataclasites, gouges and breccias may be related to Devonian, Carboniferous, and Mesozoic age faulting within the Minch. The presence of faulting within the Stornoway Formation indicates that NNW-SSE, ENE-WSW, N-W, and E-W striking clay, calcite and zeolite bearing faults are Mesozoic and younger in age. These faults formed at relatively shallow depths in the crust, and denudation of Lewis is around 2 – 3 km (Persano et al., 2007).

5. *Dolerite Dyke Intrusion – Palaeogene.* Generally trend NNW-SSE across the island and intrude

along NNW-SSE striking faults

6.a *E-W striking strike-slip faulting – Cenozoic*. At Orasaigh, the fault rocks are also composed of sericite probably directly derived from the wall rock. Faulting at Orasaigh clearly cuts all other structures at that locality, including NNW-SSE striking breccias and gouges, and Tertiary dolerite dykes, suggesting the presence of a widespread Tertiary aged strike-slip fault phase. This agrees with observations from within the Stornoway Region (Chapter 3). Late stage Tertiary or younger faulting is also observed reactivating NNW-SSE trending dolerite dyke margins at many localities, e.g. Dail Mhor, Garenin, Cearsiadar Road, and Marbhig.

6.b *NNW-SSE striking dip-slip normal faulting.* Minor faults (<2 cm thick) are seen reactivating dyke margins with brown cataclasite and breccia. These are observed in the west at Dail Mhor, Dail Beag, Garenin and in the east at Marbhig and Cearsiadar Road.

Whilst similarities exist across the island, there are also some important differences. Dominant faults and fractures in the central areas of Lewis and Stornoway strike NNW-SSE and likely reflect Mesozoic-aged deformation. In the north, phases of faulting with similar fault rocks are heavily dominated by E-W dip-slip faulting, and this is also seen in the north of the Stornoway Region where the bounding faults of the Stornoway Formation trend E-W. In the west, faulting of assumed Mesozoic and Cenozoic age shows a strong tendency to strike E-W to ENE-WSW with both dip-slip normal and strike-slip offsets. This faulting may be contemporary with that identified in the north of Lewis and also in the north of the Stornoway Region, and strike-slip kinematics are likely to be recording the phase of E-W strike-slip faulting recorded elsewhere (e.g. at Seaforth, Orasaigh). The NNW-SSE normal motion faults and E-W to ENE-WSW striking normal faults could be part of the same set, representing polymodal faulting (e.g. Reches, 1983).

4.7.3 Basement structural controls on faulting

The reactivation of basement structures is a feature observed at many localities, whether of pre-existing faults, or of the actual foliation in the gneisses/mylonites. Within the OHFZ, faults often form along pre-existing structures - epidote cataclasites often form at lithological contacts, and authigenic clay bearing rocks often form localising along the foliation (e.g. in the Stornoway Region). The relative lack of phyllonites in the west of the island relative to their abundance in the region of the OHFZ means that low angle detachments were not observed there. At Dail Beag Quarry, low angle red-brown cataclasites and breccias were observed localising along the plane of mylonitic foliation, but it was not possible to determine a sense of offset. In the Seaforth Valley,

the presence of a narrow band of fault parallel chlorite dominated mylonitic gneiss suggests that the fault may have localised along this relatively weak lithological zone. It is possible that this structure represents an earlier Laxfordian shear zone formed along at least part of the Seaforth Lineament.

4.7.4 Brittle fault rocks: conditions of formation

As discussed in the faulting synthesis above (section 4.7.2), conditions of faulting illustrate the exhumation of the Lewisian Complex through time. Pseudotachylites, believed to have formed at depths of 13.5 km (Fettes et al., 1992), are postdated by epidote cataclasites (> 6 km depth) and authigenic clay (< 6 km depth).

As seen in the Stornoway Region, NNW-SSE striking faults have a tendency to reactivate pre-existing structures carrying epidote cataclasites. The latest phases of motion on these authigenic clay bearing faults are normal near dip-slip, agreeing with the kinematics identified in the Stornoway Region. Fault rocks are composed of foliated gouges, cataclasites, and breccias, with zeolite, calcite and clay mineralisation that are closely associated. The relationship of zeolite with calcite and possibly replacement of calcite with zeolite is similar to the relationship observed in the Stornoway region. Foliated gouges were not found at Rhenigidale. For authigenic clays to form, the presence of fluids is required for the transport of species to form the new minerals (e.g. Weisenberger and Bucher, 2010). Although calcite mineralisation has occurred at Rhenigidale, the movement of species necessary for the formation of clays did not. This suggests that separate phases of fluid flow and mineralisation occurred, with calcite mineralisation perhaps occurring separately to authigenic clay development at Seaforth. This would agree with observations of zeolite replacement/dissolution of calcite, particularly in the Stornoway region, with zeolite associated with authigenic clay development. Alternatively, conditions at Rhenigidale did not enable the development of clay minerals, perhaps suggesting it is of a different fault set to the Seaforth lineament. This seems rather unlikely, given the similarities between faulting at Rhenigidale and the nearby major Seaforth Fault**.** The impact of country rock also plays a part in determining the composition of the fault rocks. At Orasaigh and Rhenigidale there are heavily sericitised feldspar clasts within the fault rock that, at times, show a gradational contact with the sericite matrix. This suggests that sericitic material in the matrices of these faults is not primary, but may be directly derived from the country rock.

4.7.5 Differences between east and west Lewis

Although the OHFZ forms a zone of intense fracturing and faulting encompassing both ductile (mylonites and phyllonites) and brittle fault rocks, these early fault rocks are also found locally

right across the island. Intense fracturing and production of 'cataclastic-(smashed) gneiss', is common in the OHFZ and is also seen in the west, although it is much less intense in its development. Areas outside the OHFZ are also often characterised by relatively unfaulted, joint dominated fracture sets (e.g. at Dail Beag beach). In the west of the island, distinctive features such as mylonites are not as common as those seen in the east. As mentioned above, low angle detachments of probable Mesozoic age are seen in the Stornoway region, Scalpay, and Harris, within the OHFZ localising along phyllonites. Although possible detachments were seen along mylonite at Dail Beag Quarry (section 4.4.2.2), it was not possible to conclusively identify them.

Whilst there is an overall difference in intensity of the fracturing from west to east, clay-, calcite-, and zeolite-bearing faults are relatively common throughout the island. These faults have been identified as being Mesozoic or younger.

4.7.6 Seaforth Lineament

The major Seaforth Fault contains similar fault rocks to those identified in the Stornoway region, with similar kinematics and orientation to demonstrably Mesozoic faults, i.e. those cutting the Stornoway Formation. On this basis, and the fact that it clearly cuts OHFZ structures of older age, it seems likely that this fault is Mesozoic in age. Significant variation in topography and lithology across the fault suggests major amounts of offset have occurred along this structure. Along with the 12 m of gouge studied at outcrop, this suggests the Seaforth Fault is a major structure with perhaps tens to hundreds of metres of displacement. The OHFZ shows a separation of 6.6 km directly across the fault. Given that near dip-slip normal kinematics were observed in the field on the fault, it is likely that this separation is due to mostly vertical displacement (top-to-the NE) on the Seaforth Fault. According to Imber et al. (2001), the OHFZ dips at 20-30 ° to the east. Hence, assuming an average dip of 25° down to the east and pure dip-slip motion on the Seaforth Fault, this suggests a vertical top-to-the NE displacement of 1.7 km (through trigonometry). Using a more conservative estimate of 4 km offset of the OHFZ (Figure 4.57), 1 km of vertical displacement occurred across this fault. If there was a small sinistral component to the motion on this fault as observed in the field, vertical displacement will be reduced. However, it is apparent that at least hundreds of metres of displacement have occurred across the Seaforth Fault.

Dip-slip normal faulting has been observed along NNW-SSE striking faults along Tertiary dyke margins across Lewis. This raises the possibility that some degree of normal displacement could also have occurred along the NNW-SSE striking Seaforth Fault during the Tertiary. This may account for part of the 2250 ± 750 m denudation found to have occurred at the top of the Cliseam mountain (Persano et al., 2007), which lies in the immediate uplifted footwall of the fault.

The Seaforth Fault and Minch fault may form part of a polymodal fault set, and it is possible that both faults were active simultaneously in a manner similar to that of the bounding faults of the Stornoway Formation in eastern Lewis (chapter 3) that are likely to have been active simultaneously and are at approximately the same orientation relative to each other as the Seaforth and Minch faults. The Minch Fault is postulated to have been reactivated during a phase of faulting in the Oligocene (Evans et al., 1991) in an event that may have produced a basin offshore SE Harris (Figure 4.57). If displacement on the Seaforth Fault is linked to movement on the Minch Fault, movement may also have occurred on the Seaforth Fault during Oligocene basin formation.

It is interesting to note that the fault west of Lewis (labelled, Figure 4.57) is not believed to extend beyond the extrapolated trend of the Seaforth Fault (e.g. Stoker et al., 1993). This may be due to displacement being transferred onto the Seaforth Fault, thus preventing the occurrence of faulting offshore NW Lewis. In central Lewis, sinistral offset within the OHFZ is postulated across a prominent WNW-ESE trending lineament between Loch Leurbost and Callanish (Fettes et al., 1992). This fault is shown in Figure 4.57 with question marks. Similar to the Seaforth lineament, this structure could represent a normal fault, downthrowing to the NNE. Unfortunately it was found to be poorly exposed in the field during reconnaissance and was therefore not visited as a locality.

4.7.7 Synthesis

Structures found in the field that correspond with the lineament analysis results are indicated in Figure 4.55. These results compared with Figure 3.65 from eastern Lewis show little variation. NNW-SSE striking structures are the dominant feature across the island due to their relatively young age and large strain concentrated on structures such as the Seaforth Fault (section 4.4.3). In the field, E-W striking structures are found to be relatively young, post-dating epidote cataclasites. In eastern Lewis, basement shear zones of this orientation are common and it is possible that Mesozoic brittle faulting has reactivated pre-existing basement shear zones during polymodal faulting similar to the Stornoway Formation bounding faults.

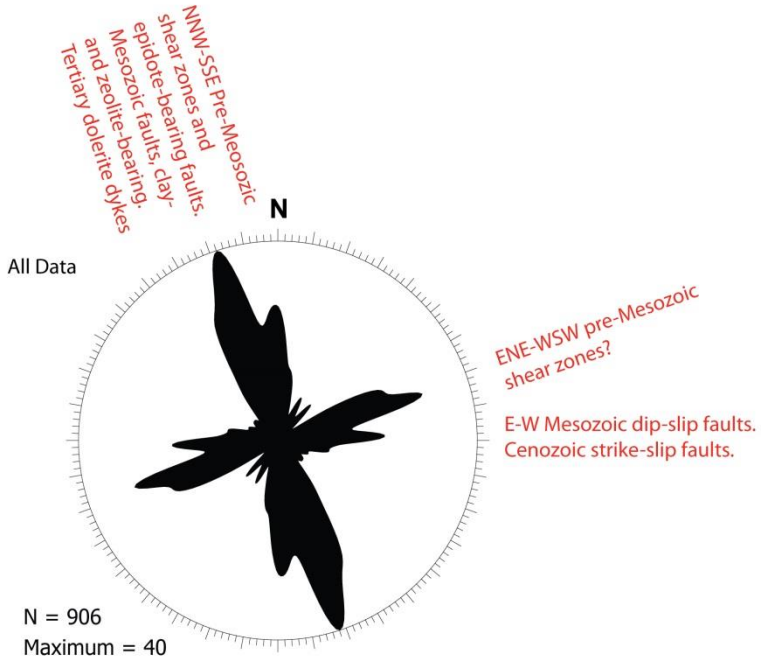

Figure 4.55: Lineament analysis results from west Lewis, with interpreted structures from fieldwork indicated in red text.

The cross-cutting relationships and structural analysis described in this chapter allow construction of a conceptual model for Lewis, shown in Figure 4.56. The longest lineaments identified on Lewis trend NNW-SSE and ENE-WSW/E-W and it is likely that these orientation correspond with Mesozoic age NNW-SSE and ENE-WSW striking dip-slip faults, E-W striking Cenozoic strike-slip faults and NNW-SSE striking Tertiary dykes identified in the field.

The geological observations recorded in the field and presented in this chapter allow construction of a conceptual structural fault model for Harris, shown in Figure 4.56 with associated fault rock photomicrographs. Fault rocks are similar to those identified in Chapter 3, with pre-Mesozoic mylonite, phyllonite, pseudotachylite and epidote/chlorite bearing-cataclasites. Mesozoic fault rocks are indicative of a lowering of the temperature and pressure conditions across Lewis during exhumation attributable to movement on the Minch Fault during exhumation attributable to Atlantic breakup. Structures identified as Mesozoic in age are associated with calcite, zeolite, and adularia mineralisation alongside open porosity.

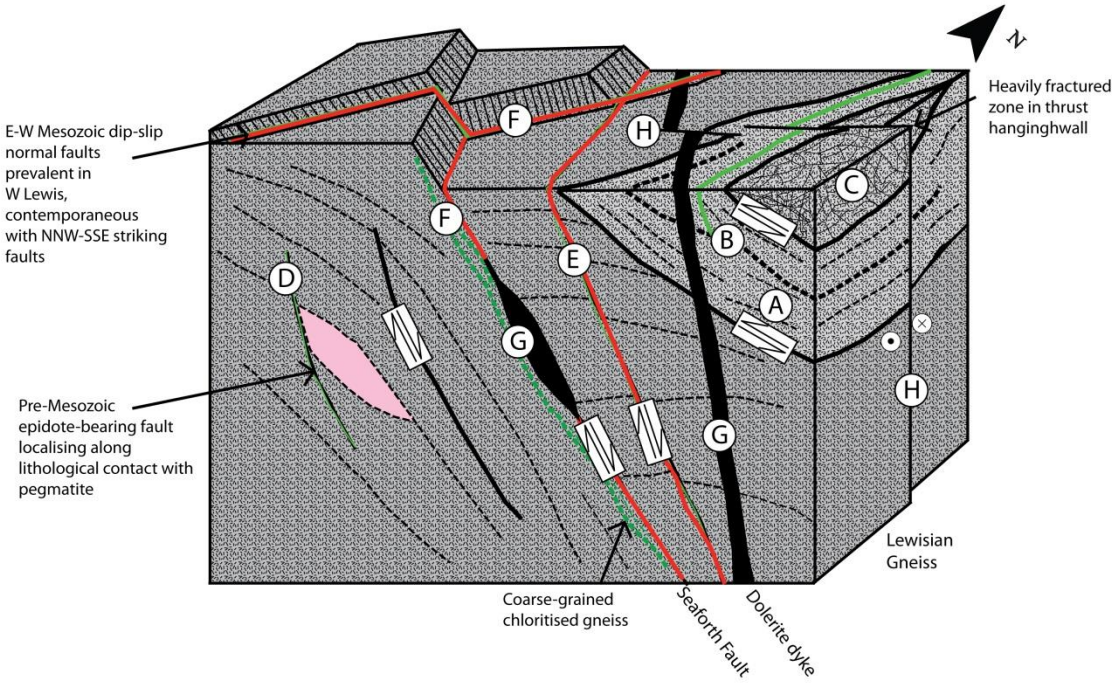

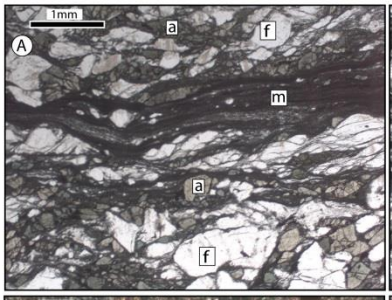

Mylonitic foliation particularly common in OHFZ

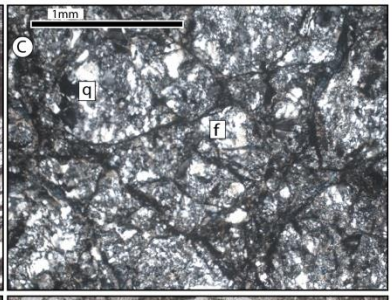

Highly fractured quartzo-feldspathic gneiss from the 'crush melange', with very fine grained re-crystallised fabric

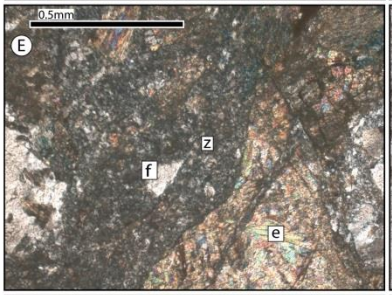

Epidote-bearing vein associated with epidote-bearing faults truncated against zeolite and carbonate-bearing fault

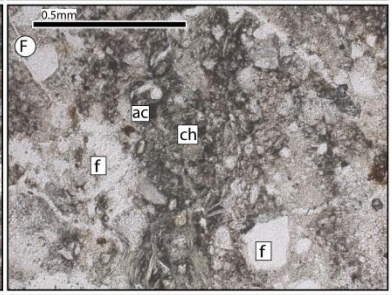

Chlorite from chloritised gneiss reworked within the Mesozoic NNW-SSE striking Seaforth Fault

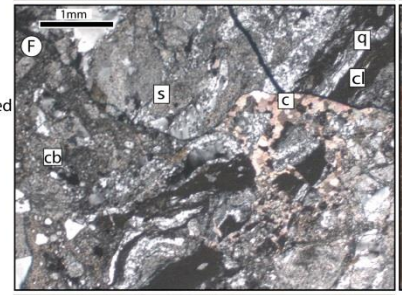

Carbonate-sericite cemented breccia with clasts of mylonitic wall rock from a Mesozoic NNW-SSE striking fault in the OHFZ

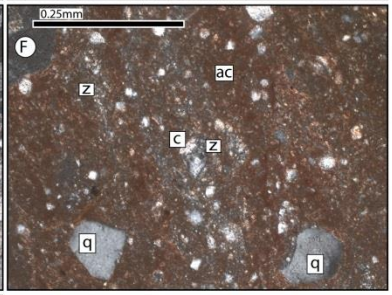

Foliated clay-rich gouge from the Seaforth Fault with calcite and zeolite mineralisation

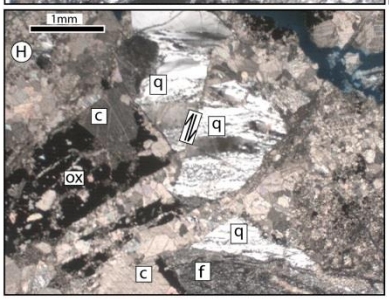

Calcite cemented cataclasite from the Cenozoic E-W striking fault at Orasaigh

Figure 4.56 (previous page): Conceptual structural model of faulting in Lewis with accompanying fault rock sections where available. Block diagram: Light grey = OHFZ, dark grey = grey gneiss. Thin section images: f = feldspar, a = amphibole, m = mylonitic foliation, z = zeolite, e = epidote, ac = authigenic clay, ch = chlorite, cb = calcite-sericite cement, s = sericite, c = calcite, cl = clinozoisite, q = quartz, ox = iron oxide. (**A**) Pre-Mesozoic mylonitic foliation prevalent in the OHFZ, cut by later brittle deformation. (**B**) Pre-Mesozoic phyllonite band with linked epidote cataclasite-bearing fault. (**C**) Pre-Mesozoic 'crush melange', common in the hangingwall of thrusts faults within the OHFZ. (**D**) Pre-Mesozoic epidote cataclasite-bearing faults often present at lithological boundaries, e.g. with pegmatite and grey gneiss. (**E**) NNW-SSE and E-W striking clay-bearing dip-slip faults (red) are probably contemporaneous and reactivate epidote bearing cataclasites (green). (**F**) Mesozoic age Seaforth fault with foliated gouge, localised along and reworking chloritised gneiss shear zone (green dashed line). (**G**) Tertiary dyke intrusion along pre-existing NNW-SSE striking structures across central Lewis. (**H**) Cenozoic E-W striking strike-slip faults with carbonate dominated fault rock.

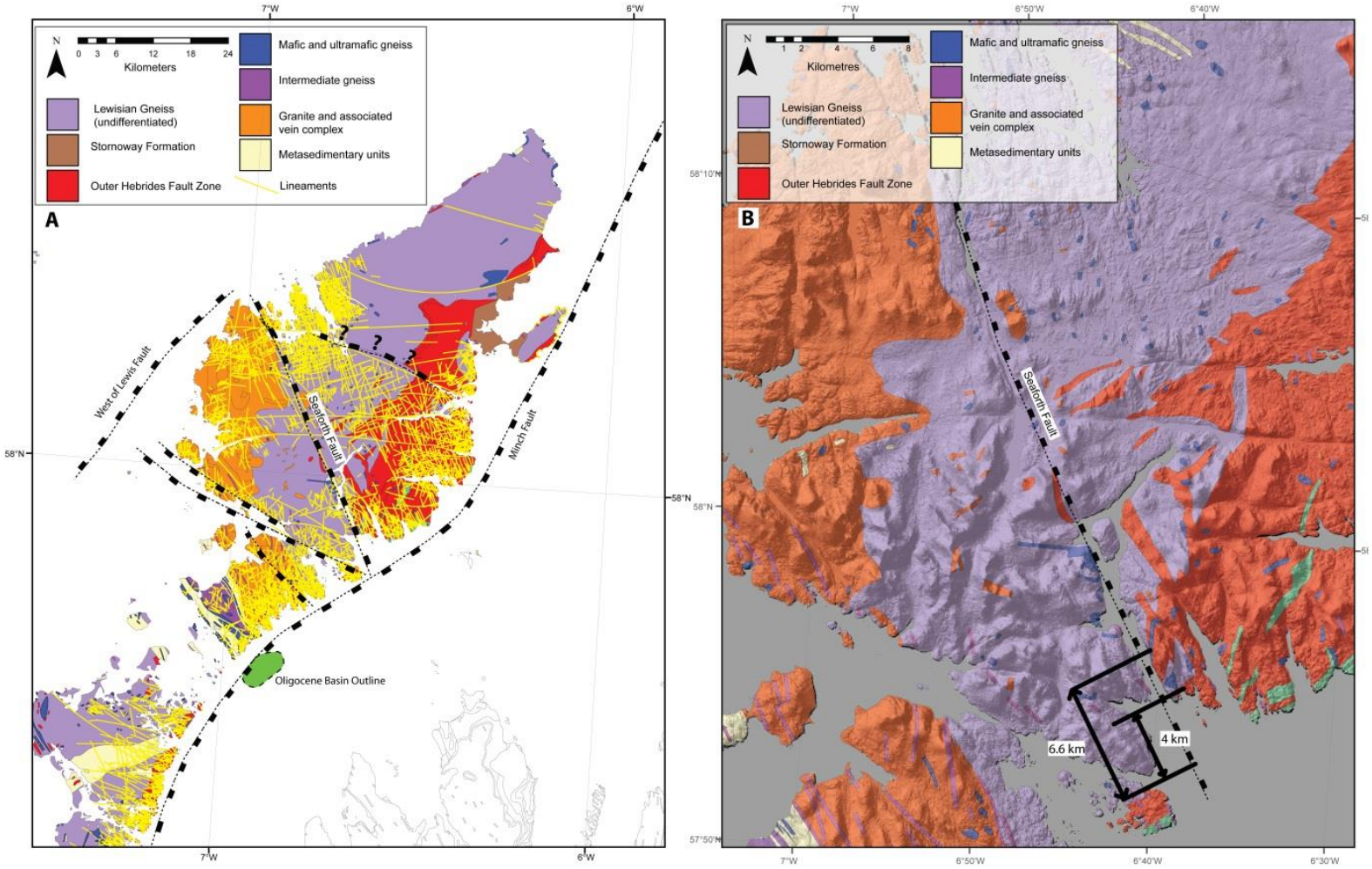

Figure 4.57: (**A**) The Seaforth Fault and digitised major offshore structures (Stoker et al., 1993). Possible fault across central Lewis that displays sinistral offset of the OHFZ is shown with question marks (Oligocene basin outline digitised from Evans et al., 1991). (**B**) Offset of the OHFZ across the Seaforth Fault.

On mainland Scotland, major NW-SE structures have been interpreted as transfer faults (e.g. the Loch Maree Fault, Roberts and Holdsworth, 1999), and have been similarly interpreted as such in the Clair region linking NE-SW Mesozoic normal faults (e.g. Hitchen and Ritchie, 1987; Dore et al., 1997). There have been suggestions that Palaeocene compression may be concentrated along these structures (Dean et al., 1999). NW-SE trending lineaments offshore have also been interpreted as intrusions and hydrothermal vent complexes (Moy and Imber, 2009). It is possible that the Seaforth Fault acted as a transfer structure in the past, linking displacement on the Minch Fault offshore NE Harris to movement on the fault west of Lewis (e.g. Stoker et al., 1993; Roberts and Holdsworth, 1999) (Figure 4.57), i.e. with a dominantly strike-slip displacement. However, no evidence for this could be ascertained from field and the aforementioned topographical and displacement observations, from which it seems most likely that the most recent phase of substantial motion (i.e. tens of metres or more offset) is Mesozoic, or even as young as the Oligocene, with a dominantly dip-slip component of normal motion.

There are many faults parallel with the Seaforth Fault within the basement (e.g. at Cliobh and Rhenigidale) and the spatial attributes of the structures associated with the fault damage zone are examined in Chapter 7.

4.8 Conclusions

- *What are the characteristics and possible ages of faults on Lewis?*

  Multiple phases of faulting are present on Lewis, representing exhumation of the Lewisian Complex through time. The 'crush melange' breccias and cataclasites are found throughout the OHFZ, associated with pseudotachylites. Pseudotachylites are usually found along foliation planes, and are relatively discrete, indicative of deep seismic faulting in the crust (Sibson, 1975; Fettes et al., 1992). Epidote cataclasites are usually discrete structures, dominantly trending NE-SW, NW-SE with normal and normal oblique kinematics. These faults may represent post-Caledonian collapse. The 'crush melange' and epidote cataclasites are all consistently cross cut by clay bearing faults of probable Mesozoic and Cenozoic age. The latest phase of faulting is represented by E-W trending structures with strike-slip kinematics.

- *What are the characteristics of post-Caledonian faulting on Lewis?*

  Major structures post-date the Caledonian Orogeny on Lewis. Zeolite, calcite, clay mineralisation occur on features of dominantly NNW-SSE and ENE-WSW to E-W trends, with dominantly near dip-slip normal motion identified as Mesozoic in age. Two phases of

faulting have also been found to post-date the intrusion of Tertiary dolerite dykes: Strike-slip motion has been identified on E-W and ENE-WSW trending structures, and dip-slip normal motion faulting striking NNW-SSE has occurred reactivating and at times brecciating dyke margins. Calcite mineralisation at times appears to predate zeolite mineralisation, however both are associated with Mesozoic and younger structures. Post-Caledonian age structures have a tendency to lie along pre-existing structures, particularly pre-existing epidote cataclasite faults and, in the case of the Seaforth lineament, possible Laxfordian shear zones.

- *How do the geological characteristics of faulting and fracturing differ between the rocks of the Outer Hebrides Fault Zone and rocks located to the west?*

  Fracturing of pre-Mesozoic age is more common in the OHFZ, whilst Mesozoic age structures are found throughout the islands. Within the OHFZ, the presence of weak fabrics such as phyllonites can lead to localisation of faulting along them, and these structures are often low-angle. Low angle structures reactivating basement fabrics were not identified in west Lewis.

- *What controls* possible *Mesozoic-aged faulting on Lewis?*

  Mesozoic age faulting is present across the island, both cutting and reactivating features of the OHFZ. Reactivation of epidote cataclasite bearing faults is common, and the latest (Mesozoic and Cenozoic) phases of faulting are characterised by zeolite, clay and calcite mineralisation. The presence of existing structures is particularly important in the east where detachments often localise along phyllonites within the OHFZ, in addition to local faulting along the plane of the foliation that is not present to the same extent in the west.

Chapter 5: Brittle faulting and fracturing within Harris and Scalpay

5.1 Introduction

The Isle of Lewis and Harris lies along structural trend from the Clair Field, and the basement at Clair is believed to be analogous to that of the Lewisian Gneiss Complex (e.g. Pless, 2011). Harris exhibits a significantly different range of lithologies to those of Lewis, with a large area of the island dominated by the Laxfordian granite complex, and, in the south, the South Harris Igneous Complex and associated shear zones. The shear zones cause a change in the overall trend of the foliation to a steeply dipping, very dominant NW-SE trend that is not observed on Lewis. These rock types and foliation trends may plausibly exist in the basement of the Clair Field and for these reasons Harris and Lewis are presented in separate chapters.

Fracturing on Harris is generally poorly understood, and there are no island-wide studies of Lewis and Harris that report on fracture attributes such as orientation, spacing, aperture and their links to lithology, foliation, and fault rocks/age. Studies of brittle fracturing of post-Caledonian age in Harris are extremely limited, restricted to the recognition of dip-slip Mesozoic faulting with down to the west kinematics, identified within the OHFZ (e.g. Imber et al., 2002). This chapter attempts to bridge this knowledge gap and present a more in depth study of post-Caledonian faulting and fracturing.

5.1.1 Objectives

The following objectives are discussed:

- What are the characteristics and possible ages of faults present on Harris?
- What are the characteristics of post-Caledonian faulting on Harris?
- How do the geological characteristics of faulting and fracturing differ between the rocks of the Outer Hebrides Fault Zone and rocks located to the west?
- What controls possible Mesozoic-aged faulting on Harris?

These questions are addressed below using data from remote sensing, fieldwork, and thin section analysis.

5.2 Geology

5.2.1 Regional Geology

As discussed in chapter 2, the Isle of Harris is dominated by the Laxfordian granite complex, and in the south, the South Harris Shear Zones and South Harris Igneous Complex. The Outer Hebrides Fault Zone (OHFZ) lies mostly offshore and to the east, but is present outcropping on Scalpay and at a handful of other sites in the extreme east of South Harris. A large number of granites and pegmatites generally cut the foliation in the host gneisses, and granite bodies are typically irregular in shape (Fettes et al., 1992). Island-wide foliations dip steeply to sub-vertically and trend NW-SE, and a similarly oriented weak fabric is present in some outcrops of the granite complex (Fettes et al., 1992).

5.2.1.1 Outer Hebrides Fault Zone

The Outer Hebrides Fault Zone (OHFZ) trends NE-SW across the extreme eastward margin of the region, and is best exposed on Scalpay. This major structure was likely initiated in the Proterozoic and reactivated multiple times. Pre-existing structures within the OHFZ may be expected to localise later faults and fractures along them, in addition to allowing fluid flow and alteration (e.g. Butler, 1995; Butler et al., 1995; Imber et al., 1997; Imber, 1998; Imber et al., 2001). Five major deformation events have been recognised in the northern segment of the OHFZ, that includes the Isles of Lewis and Harris (Imber, 1998; Imber et al., 2002):

1. Top to the NW thrusting within a broad mylonitic shear zone.
2. Brittle top to the W thrusting, producing widespread cataclasite and pseudotachylite.
3. Sinistral top to the NE strike-slip occurring within phyllonitic shear zones.
4. Brittle-ductile top to the SE extension within phyllonitic shear zones.
5. Brittle top to the east extension along steeply dipping normal faults.

This study builds on the identification of these deformation phases and identifies further brittle deformation within the Lewisian Gneiss.

5.2.1.2 South Harris Shear Zones (SHSZ)

The South Harris shear zones (coincident with the metasedimentary Leverburgh and Langavat belts) enclose the antiformal structure of the South Harris Igneous Complex (Graham, 1980; Fettes et al., 1992). Rocks within these belts are highly deformed, planar flaggy gneisses of amphibolite facies grade' (Graham, 1980). Work in this chapter has concentrated in part on the Leverburgh Belt for reasons of accessibility and outcrop. The Leverburgh Belt incorporates a series of metasedimentary units (Baba, 2002) with local shear zones and a penetrative planar fabric.

Between these two belts, the Palaeo-proterozoic South Harris Igneous Complex occupies an antiformal setting that was formed after it's discordant intrusion into the metasediments of the Langavat and Leverburgh belts (e.g. Fettes et al., 1992 and references therein). The South Harris Shear Zones mark the boundary between the northern and southern segments of the OHFZ (Butler et al., 1995; Imber et al., 2002).

5.2.1.3 Post-Caledonian Faulting

Brittle faulting postdating Caledonian-aged structures is little studied on Lewis and Harris. Mendum (2009) mentions briefly that late cataclasites, gouges and breccias may be related to Devonian, Carboniferous, and Mesozoic age faulting within the Minch, but there is currently no further evidence available to confirm the hypothesis of Devonian/Carboniferous age faulting within the literature. Large scale features that cross the island, such as the North Harbour Fault at Scalpay and its NW continuation the Tarbert Fault (Figure 5.18; Szulc et al., 2008; Mendum, 2009), are often marked on maps (e.g. Fettes et al., 1992) but are not described. Mesozoic dip-slip extension along steeply dipping normal faults has been noted in the literature but not studied in depth (e.g. Butler et al., 1995; Imber et al., 2001; Imber et al., 2002). The area studied here resides in the footwall of the major Mesozoic Seaforth Fault, examined in chapter 4 (section 4.4.3).

5.2.2 Study Sites and methods

Due to the large areal extent of the Lewisian Gneiss on Harris, fieldwork was targeted to accessible zones of specific interest and exceptional exposure. Similarly with earlier chapters, the study of faulting has been achieved through regional lineament analysis, local fieldwork, and thin section analysis of selected fault rocks. A total of 103 sites were visited within the Lewisian Gneiss Complex and OHFZ on Harris and Scalpay (Figure 4.1). Visited localities are mostly coastal (shown in Figure 5.3), with inland access limited to sites within quarries and along road cuts. Faults and fractures are difficult to study through the remainder of Harris and Scalpay due to intense weathering and Quaternary peat cover.

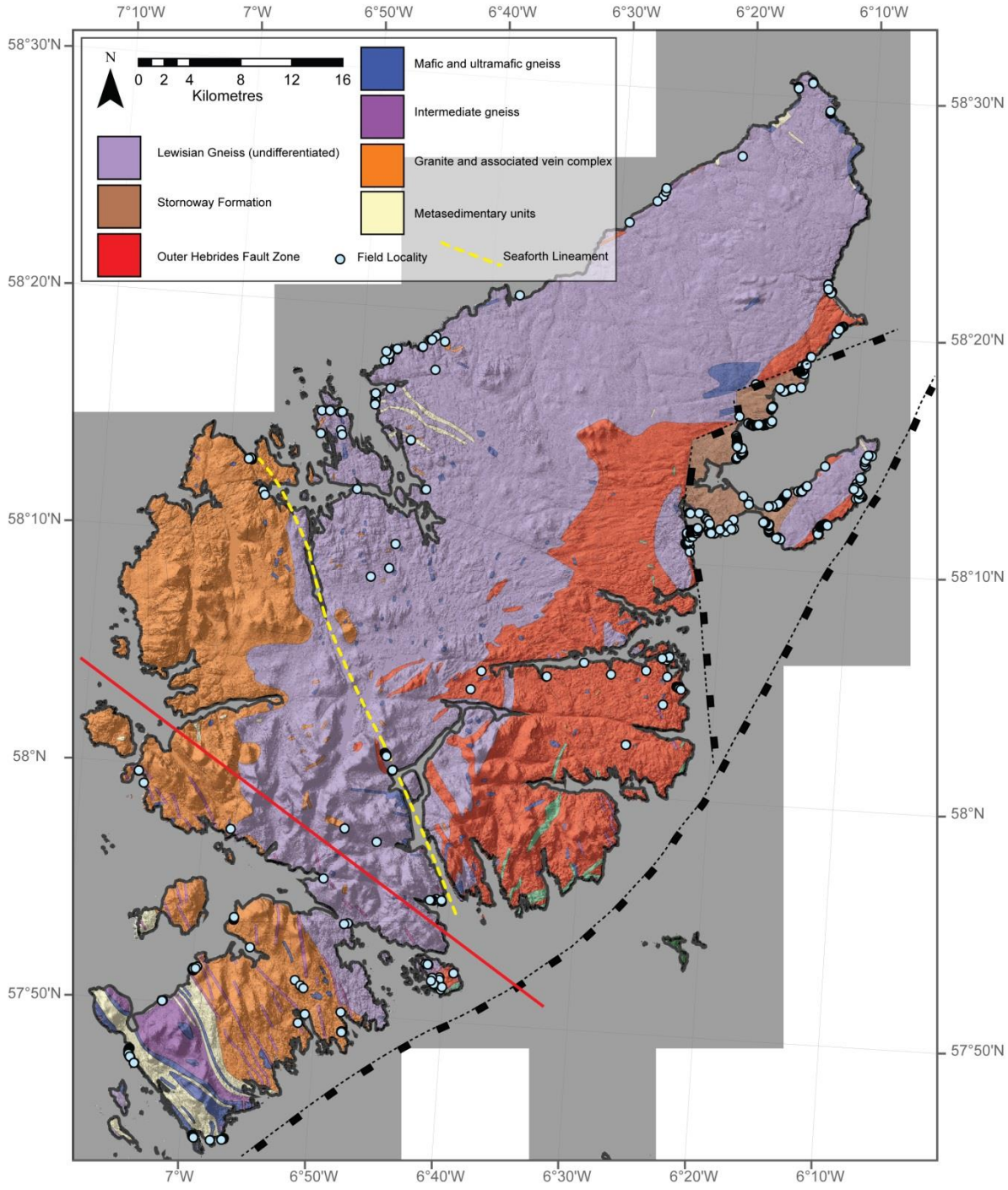

Figure 5.1: Showing geology of Lewis and Harris underlain by digital surface model (DSM) processed from Nextmap ® data. This chapter covers data collected from south of the red line.

5.3 Lineament analysis

Lineament analysis was performed with the aim of identifying major faults and zones of interest, in addition to giving an overview of fault lengths and orientations. In order to undertake the lineament analysis, the foliation from published BGS maps was digitised across Lewis and Harris (Figure 5.2). Results are shown in Figure 5.3 compared to data collected in the field, and in Figure 5.4 displayed by area.

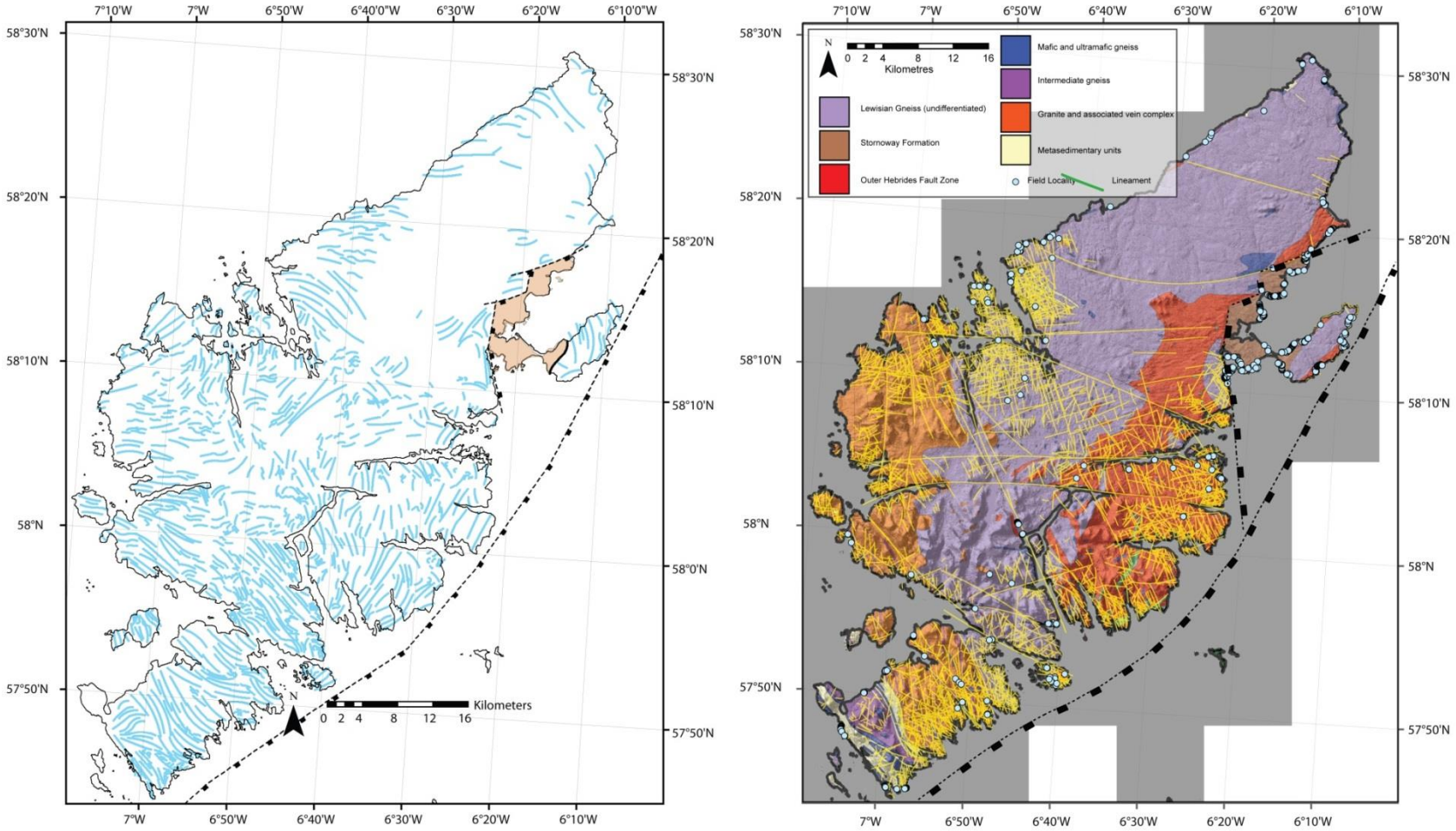

Figure 5.2: Digitised foliation trend on Lewis and Harris based on BGS data (left, in blue). Lineaments picked from DSM (right, in yellow). Stornoway Formation shown in brown with major faults indicated.

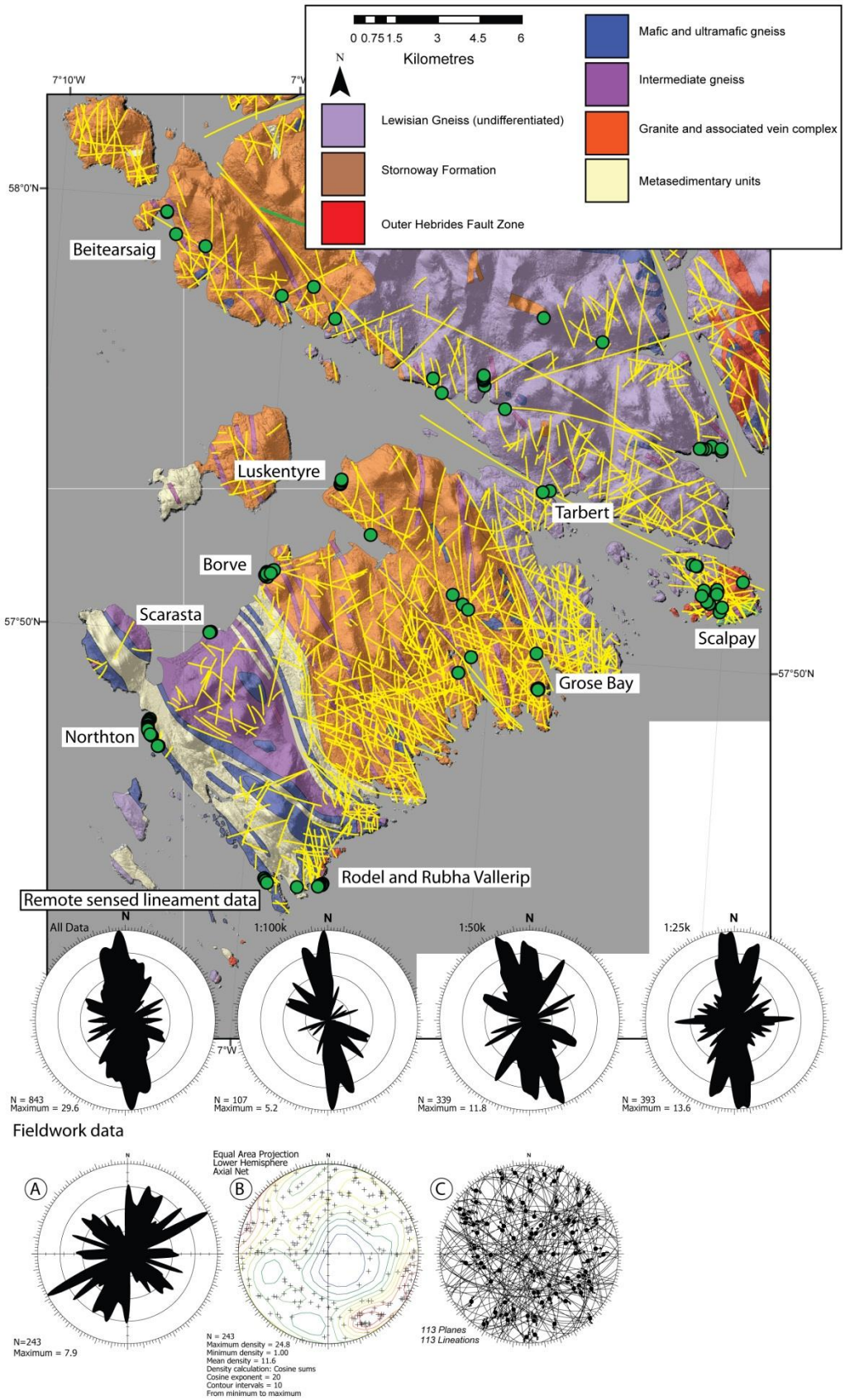

Figure 5.3: South Harris lineament analysis data (top row of rose diagrams) and fieldwork data comparison (bottom row of plots).

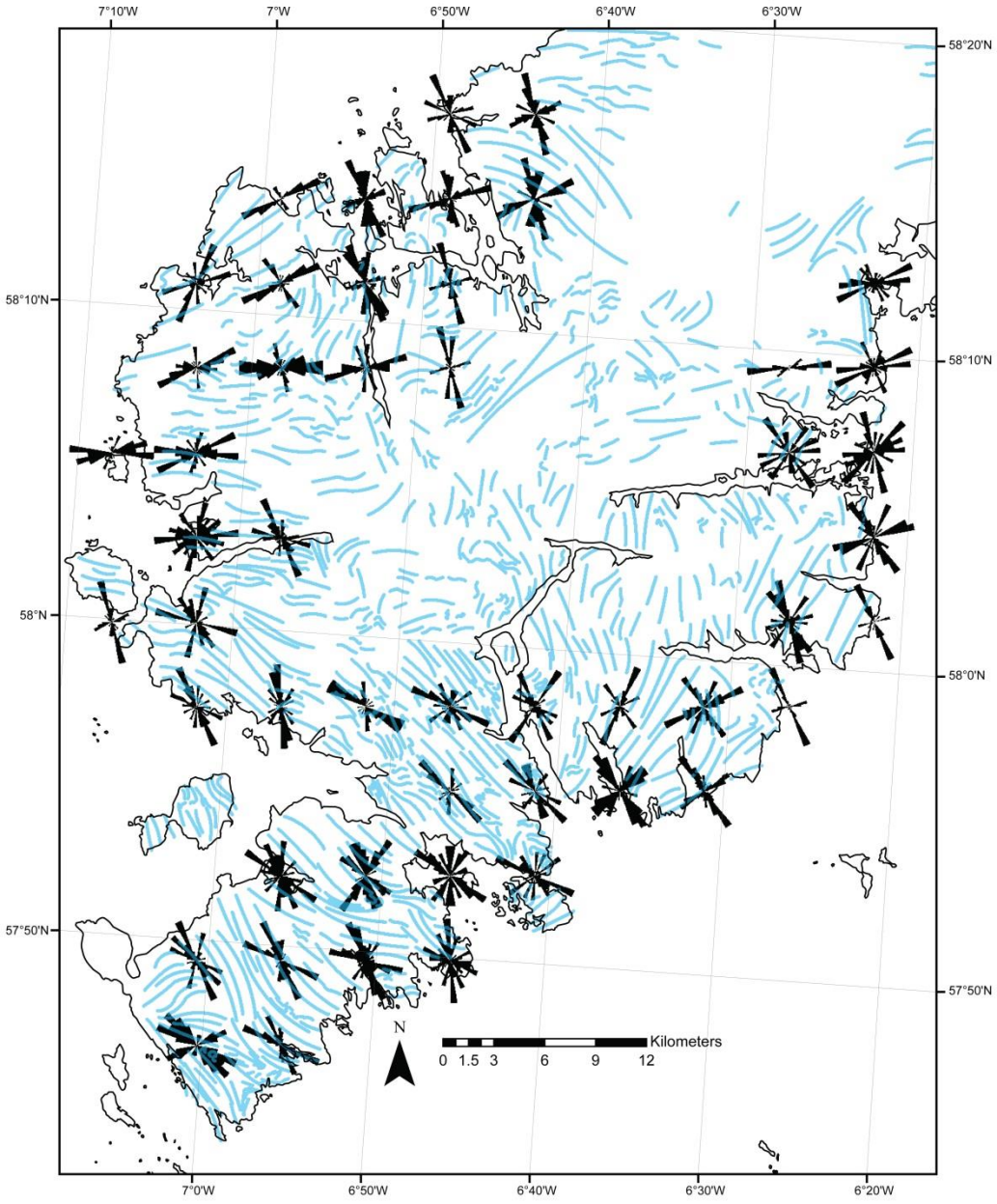

Figure 5.4: Variation of lineament orientation overlying foliation trend. Minimum number of lineaments in a rose diagram is 13.

Grouping lineaments by the resolution they were picked at (Figure 5.3) shows only minor variations between the different resolutions at 1:25k, 1:50k, 1:100k, indicating a degree of scale invariance with respect to lineament orientation. As discussed in chapter 4 and shown in Figure 5.4, picked lineaments across Lewis show a very strong NNW-SSE trend and a slightly weaker ENE-WSW trend. Results from Harris are markedly different, with the strongest most dominant lineament trend identified being N-S to NNE-SSW, and a weaker NW-SE trend. When compared to data collected during fieldwork (Figure 5.3) there are some differences, e.g. a strong NE-SW trend evident during fieldwork is not as strong in the lineament analysis results. This is because in

regions like Northton (SW Harris, Figure 5.3) relatively few lineaments have been picked in the lineament analysis (due to poor exposure) and this has not illuminated the faulting orientations discovered in the field in that area. Also, low angle detachments found at Rubha Vallerip (section 5.5.1) and Scalpay (section 5.5.2) in the limited exposures of the OHFZ are not well represented on the lineament analysis as it is not possible to easily identify low angle features in the lidar data. Low angle detachment faults in the OHFZ were found to trend dominantly NE-SW. NW-SE striking faults identified on fieldwork represent localities at Scalpay, Beitearsaig, and Grose Bay/Luskentyre where major NW-SE trending lineaments were sampled. As seen on the map, the longest lineaments are those trending NW-SE (Figure 5.3 and Figure 5.5), and there are several of these that cross the whole of Harris.

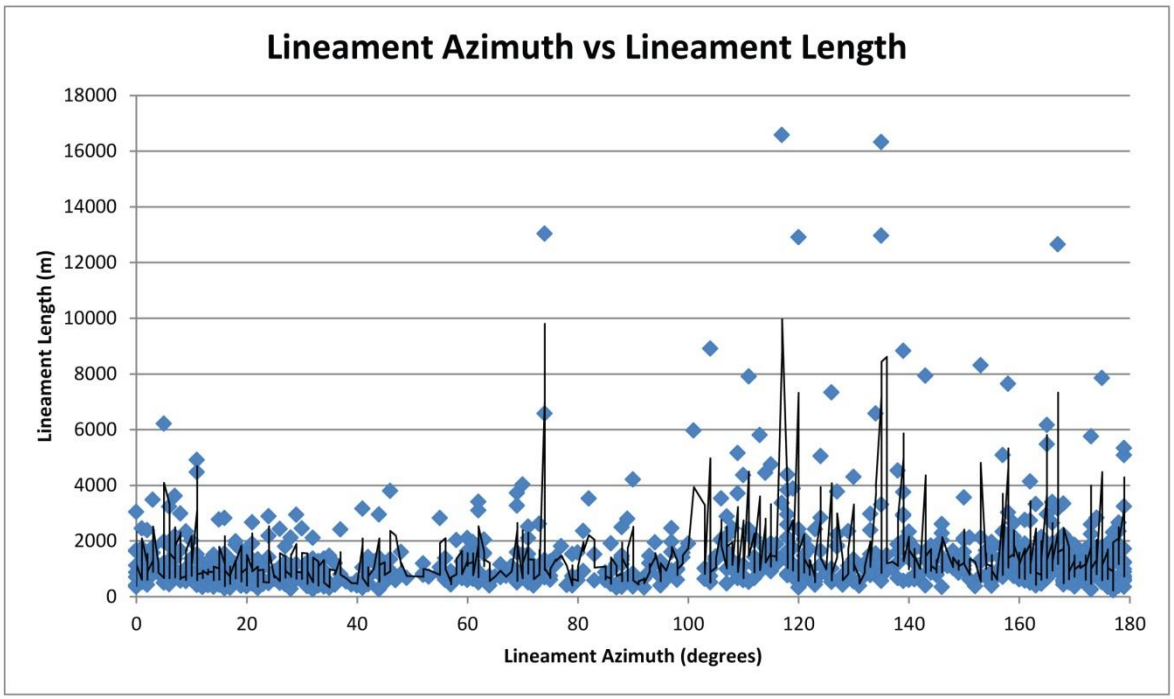

Figure 5.5: Lineament azimuth vs. lineament length for lineaments picked on Harris. Points represent individual lineaments, line = 2 point moving average.

5.4 Fieldwork results outside the OHFZ

Localities across Harris were selected in order to gain insights into the areas of study identified in Section 5.1.1. The areas studied by fieldwork outside the OHFZ were selected for the following reasons:

- *Beitearsaig*: Located in close proximity to a major NW-SE trending lineament.
- *Luskentyre/Grose Bay*: Located in close proximity to a major NW-SE trending lineament.

- *Borve and Scarasta*: Selected for the presence of a Permo-Carboniferous camptonite dyke (Fettes et al., 1992) in order to ascertain the age of faulting relative to this. Also at Borve, massive granite is juxtaposed against banded gneiss, enabling fractures characteristics to be compared/contrasted between these lithologies (section 7.3.2.4.1).
- *Northton*: Within the Leverburgh Belt of the South Harris Shear Zones, selected for the presence of a strong penetrative fabric and examination of the potential effects on faulting.

5.4.1 Beitearsaig and Hushinish Road, NW Harris

The localities studied on the Hushinish Road are concentrated along a set of lineaments trending NW-SE (Figure 5.6). The main locality occurs at the north-western end of the lineament near Beitearsaig where a thick zone of fault rock is exposed (GR NA 9974 1095).

Country rocks in the area are grey gneisses with biotite constituting the dominant mafic component towards the northern end of the lineament in the area around Beitearsaig. The gneiss varies between pervasively biotite banded gneiss to dispersed biotite defining the foliation of massive gneiss (Myers, 1970). Amphibolite and pegmatite banded biotite gneisses are found in the region further south and east (Myers, 1970). Foliation dips shallowly to the southwest in the area around Beitearsaig and steepens towards the south.

Multiple phases of faulting are present along the Hushinish Road, and these are most obvious at the exposures at Beitearsaig. At this locality NW-SE to N-S epidote cataclasites are very obviously reactivated by clay bearing foliated gouges, cataclasite and chaotic breccia that contain clasts of epidote cataclasite in a zone approximately 4-5 m wide adjacent to a main fault surface that strikes NW-SE (Figure 5.7C-E, see section 5.7.1 for further fault rock study). Eleven examples were recorded of clay gouge-bearing faults reactivating and brecciating earlier epidote cataclasite bearing faults (e.g. Figure 5.7B), including the main fault at this locality. The faults are associated with fault-parallel epidote veins (Figure 5.8) that are typically concentrated in the hangingwalls (Figure 5.7F-G), with footwall epidote veining rare. The reactivated epidote cataclasite-bearing faults dip steeply to the east, west, northeast and southwest with normal oblique kinematics. Slickenline steps are present on a north-south-trending steeply dipping epidote cataclasite bearing fault giving reverse motion, however this fault does not appear to be related to the main NW-SE striking fault at this locality.

The main clay-bearing fault core dips moderately to the WSW with dextral oblique normal kinematics (Figure 5.8, in bold) ascertained from a principal slip surface that exists between a

hangingwall of intensely epidote veined country rock and the fault core. Slickenlines from other clay-bearing faults are clustered in the same orientation as the main fault slickenlines, indicating that they are probably part of the same set and subsidiary to the main fault. These faults all lack carbonate mineralisation. One example of a clay gouge-bearing fault with two sets of slickenlines was observed, with one down-dip slickenline set and another near sinistral strike-slip set (Figure 5.8, blue dashed lines). It is not possible to tell which overprints the other as the sequence of slickenline layers does not indicate the sequence of slip events (Sperner and Zweigel, 2010). However, it seems likely to the author that strike-slip faulting has reactivated earlier dip slip faults as strike-slip faulting has been found to be the latest phase of faulting at other localities on Lewis (e.g. section 4.5.3.3).

At the locality north of Beitearsaig (Figure 5.6), intensely fractured ENE-WSW trending faults and joints are associated with carbonate mineralisation. This carbonate cements brecciated angular wall rock clasts and fills fractures with apertures up to 2 cm across. Some of these fractures are faults, with well indurated reddy-brown veneers on the wall rock surfaces that are probably clay or haematite (Figure 5.7H-I). The age of these reddy-brown fractures relative to the main lineament is not clear, but their association with carbonate mineralisation suggests they may be relatively young (i.e. Mesozoic) (see sections 3.3.3.5 and 3.4.3). These ENE-WSW trending fractures may also be related to the carbonate associated faults seen on the west coast of Lewis at Garenin (section 4.4.3.3) and Carloway (4.4.3.4). For further quantitative fracture details see section 7.3.2.1.1.

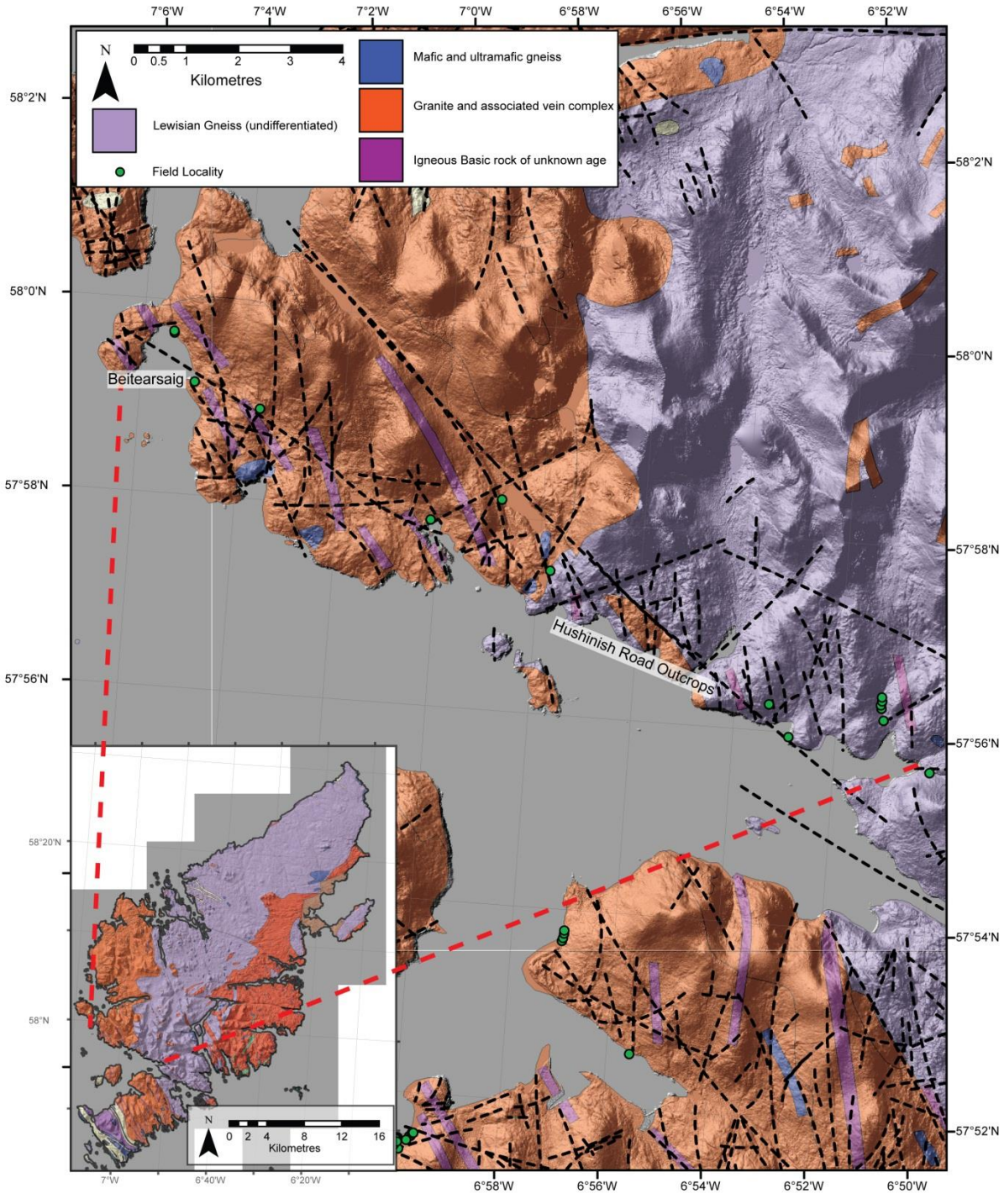

Figure 5.6: Field localities at Beitearsaig and along Hushinish Road with interpreted lineaments in black.

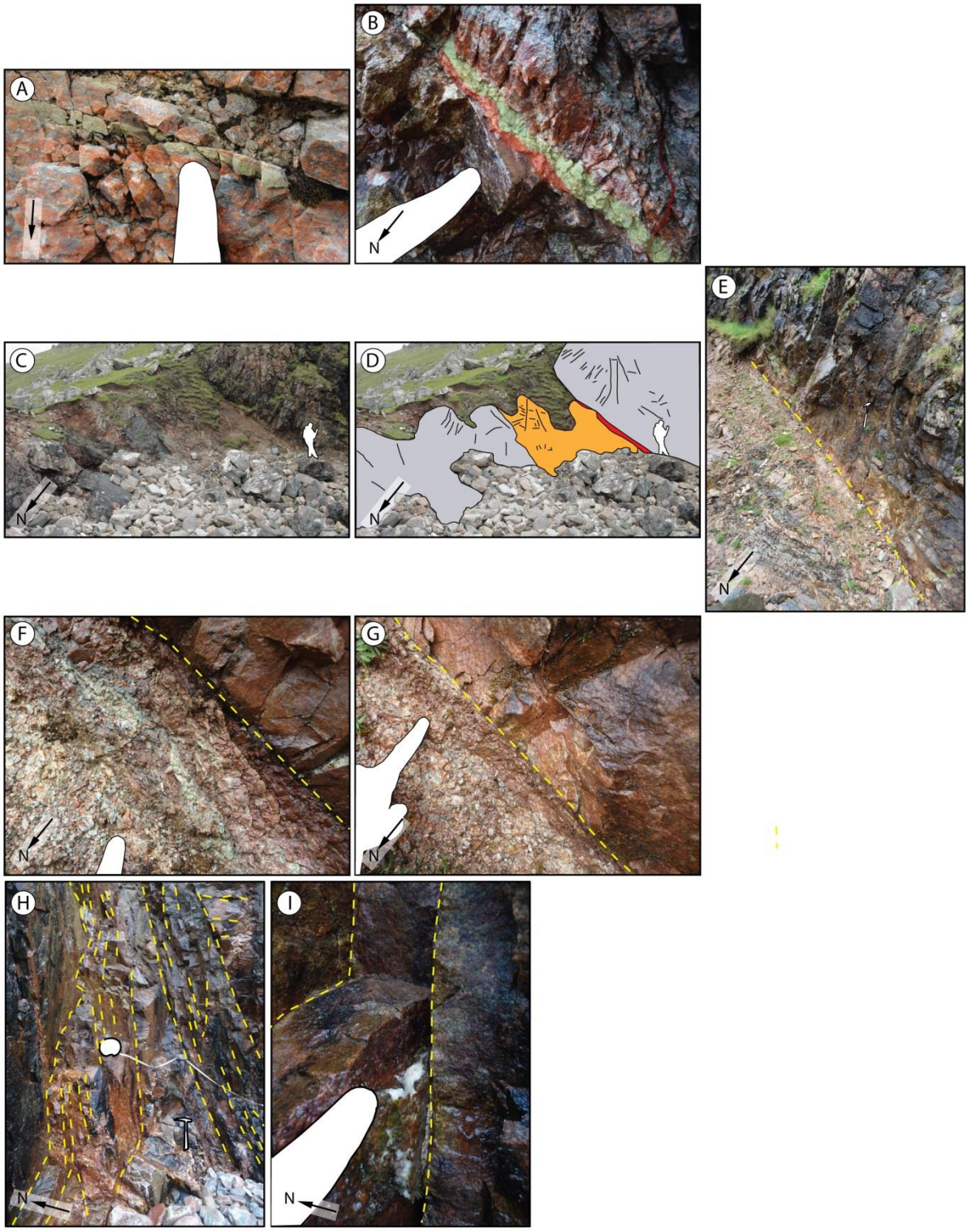

Figure 5.7: Outcrop at Beitearsaig. Red = red soft clay rich gouge, green = epidote cataclasite, orange = breccia, grey = grey gneiss banded with pegmatites, yellow dashed line = main fault surface. (**A** – **G**) GR: NA 9975 1095 (**A**) Epidote cataclasite cementing brecciated pegmatitic gneiss. (**B**) Fault showing epidote cataclasite reactivated with soft gouge. Note intact footwall surface and brecciated hangingwall. (**C** - **E**) Major lineament at Beitearsaig, approximately 4.5 m of breccia and up to 20 cm of foliated gouge. (**F** – **G**) Foliated gouge at the hangingwall contact of the fault. (**H** – **I**) GR: NA 9936 1193, NE-SW striking steeply dipping faults with carbonate mineralisation and well indurated reddy veneer on the fracture surface (I).

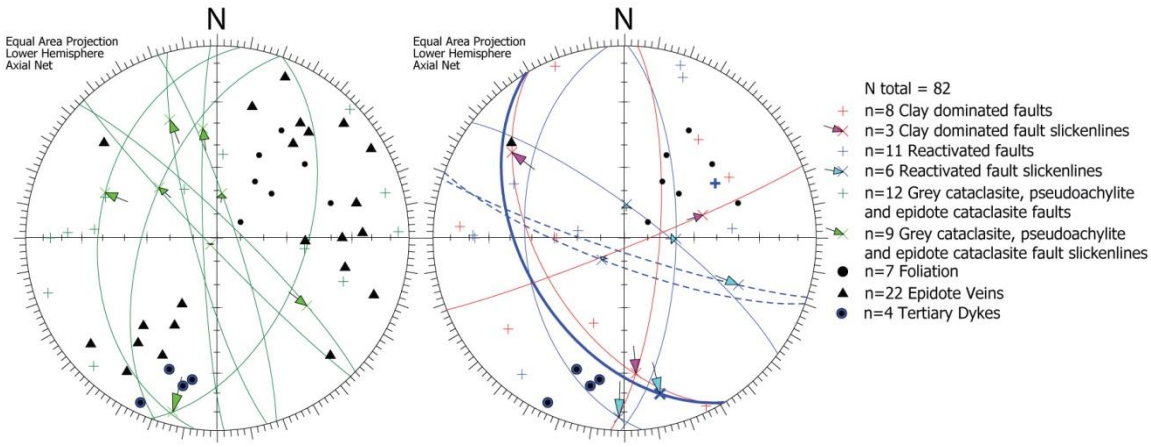

Figure 5.8: Orientation data collected from Beitearsaig and Hushinish Road. Main fault with slickenlines at Beitearsaig marked in bold. Faults with slickenline data are drawn with a great circle. Dashed great circles indicate a clay gouge bearing fault with two slickenlines that is reactivating an epidote cataclasite bearing fault.

5.4.2 Luskentyre, Luskentyre Old Road and Grose Bay

Luskentyre (NB 0681 0020), Luskentyre Old Road (NB 1162 9545) and Grose Bay (NG 1528 9139) lie along the trend of the same NW-SE trending lineament (Figure 5.3), and so are discussed together here. On BGS maps of the area, at the northern end of the lineament, the foliation trends sub-parallel to the main fault observed along the old Luskentyre Road outcrops, dipping steeply towards the southwest. In the region of the Old Luskentyre Road the foliation rotates to a more east-west orientation dipping towards the south at an angle to the lineament marked on the BGS maps. From these observations, it appears the fault does not parallel the foliation along its entire length.

These localities lie within the area identified by Fettes et al. (1992) as the Uig Hills – Harris Granite Complex (Figure 5.9). At Luskentyre, compound dolerite dykes intrude into a fault rock that is at least 4 m wide, trending NW-SE. Foliation in the nearby country rocks dip to the south (i.e. is not fault parallel), with boudinaged pinch and swell structures indicating high strain, but the foliation orientation varies along the length of the lineament. The country rock is comprised of strongly foliated grey gneisses with lenses of Older and Younger Basics concordant with the foliation with varying degrees of massive granitic and pegmatitic veins. In the north at Luskentyre Beach, the country rock is more dominantly composed of massive granite. At Grose Bay, a very well indurated zone of breccia is observed in the valley sides, parallel with a fine mylonitic foliation in the country rock that generally dips towards the southwest. The core of the lineament is not exposed.

At Luskentyre, a zone of fault breccia at least 4 m wide steeply dipping to the southwest is comprised of clasts of country rock gneiss with a very well indurated green-tinged breccia displaying slickenlines with oblique sinistral kinematics on slip surfaces. This breccia has a similar appearance to the breccia at Grose Bay (discussed below), and is intruded by parallel dolerite dykes (Figure 5.10A-B). Pseudotachylite-bearing faulting is also present with pseudotachylite intruding into steeply dipping epidote cataclasite that strikes NW-SE (Figure 5.10D-F). The country rock is at times massively epidotised with alteration of feldspars seen in zones several metres across that are likely to parallel the NW-SE striking epidote cataclasites. Epidote cataclasites represent an early phases of faulting that is parallel with later clay-bearing faults and the overall trend of the lineament. The light grey-green fault breccia is cut by 1-2 mm thick milky white and cloudy carbonate-zeolite veining and light grey-green foliated gouge up to 3 - 4 cm thick with surrounding fault breccia 5 - 10 cm thick (Figure 5.10C), displaying clear dextral strike-slip kinematics measured from probable zeolite slickenfibres. Soft clay gouge, fault orientation and kinematics are similar to those observed at Beitearsaig (section 5.4.1). Faulting is also locally seen along dolerite dyke margins, with foliated brown and creamy gouge up to 10 cm thick. This suggests that a phase of faulting postdates the emplacement of Tertiary dykes, but poor exposure precludes further study.

At Grose Bay, a zone of NW-SE striking fault breccia at least 3 m wide is truncated against a NW-SE striking fault footwall surface (Figure 5.10G-I) of intact pale green mylonitic rock that dips to the southwest. Local foliation is parallel to sub-parallel with the exposed fault plane, and the mylonite grades into pegmatite and granitic gneiss country rock <5 m from the main fault surface. 20 m into the country rock, the foliation is variable and displays folds verging to the southeast with wavelengths of 50 – 100 cm. The country rock also shows evidence of alteration to epidote. The main fault breccia is composed of angular clasts of mylonitic country rock up to 5 cm across that are very well indurated by white non-effervescent probable phyllosilicate mineralisation (?sericite) that is easily scratched (see section 5.7.2 for fault rock study), with a similar appearance to the well indurated breccia found at Luskentyre Old Road (Figure 5.10B). Multiple fractures within the brecciated zone are suggestive of a subsidiary set of Riedel shears developed during dextral shear on the main fault plane. The centre of the brecciated zone is obscured by a stream exiting the valley, and it is not known whether the fault zone at Grose Bay contains foliated gouge or dolerite dykes of the kind seen at Luskentyre Old Road. Poles to jointing measured at Grose Bay lie in four broad groups. A large proportion of poles to the joint surfaces are parallel/sub-parallel to the orientation of the lineations in this area. This may be an indication that there is a degree of kinematic coupling between the joints and the main fault in this area, with at least some joint sets produced through tensile fracturing resulting from fault movements and associated stresses.

In summary, the outcrops at Luskentyre and Grose Bay represent several phases of tectonism:

1. Pegmatite/gneiss intrusion associated with the Uig Hills granite complex followed by formation of down dip southeast verging folds in granitic gneiss.
2. Formation of localised zone of pale green mylonite < 10 m thick, with foliation striking NW-SE and dipping steeply to the southwest. It seems likely that this mylonite is related to relatively early shearing along the OHFZ or across the South Harris Shear Zones.
3. Brittle faulting with epidote cataclasite and pseudotachylite development along the same trend.
4. Formation of white (probable sericite) cemented breccia, oriented parallel to sub-parallel with the mylonitic foliation at Grose Bay.
5. Formation of soft clay gouge-bearing faults dipping steeply to the southwest, associated with zeolite veining and mineralisation along the fault planes, preserving dextral strike-slip kinematics.

For further fault rock details see section 5.7.2.

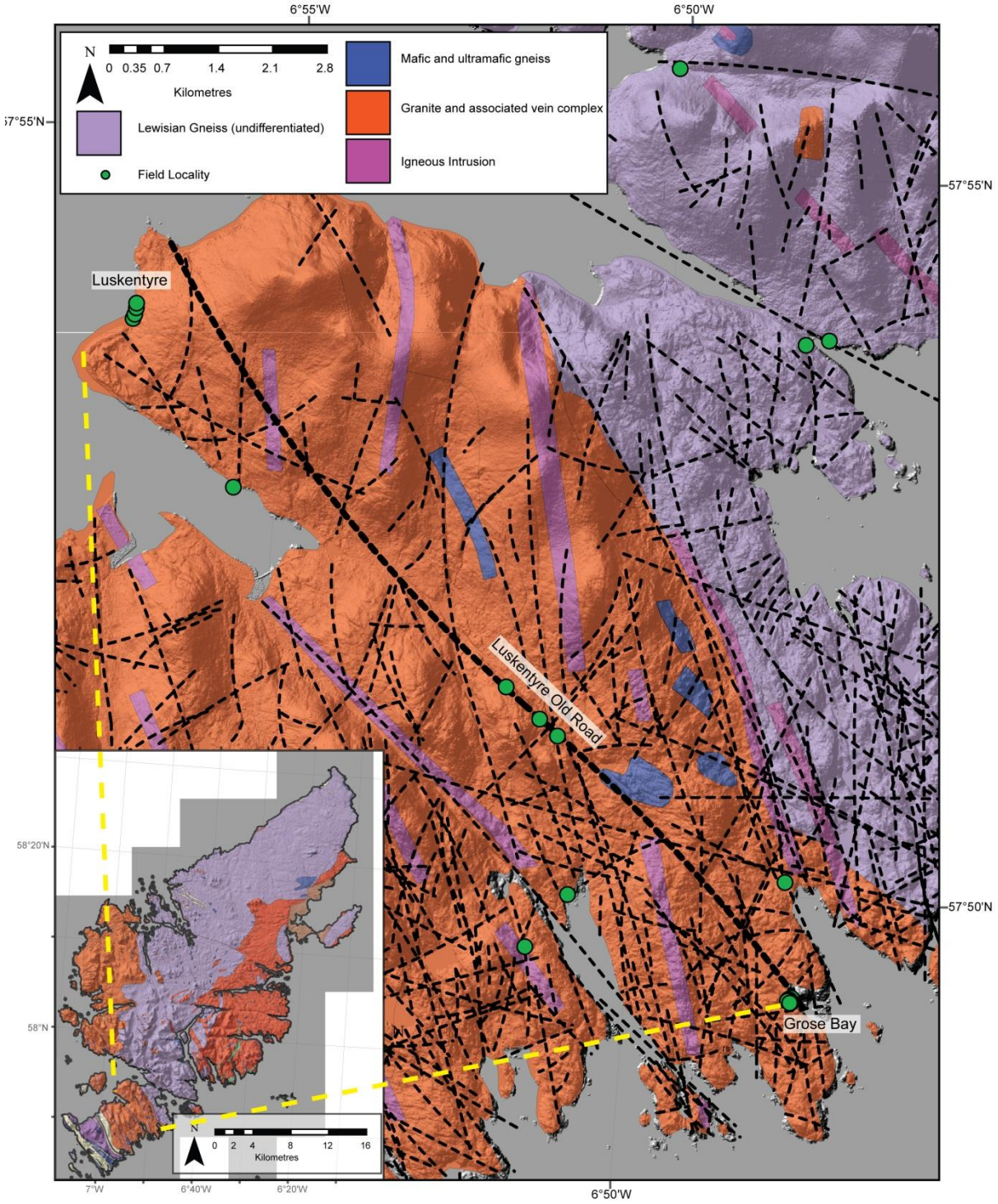

Figure 5.9: Field Localities at Grose Bay and Luskentyre. Interpreted lineaments displayed. Lineament of interest highlighted in bold.

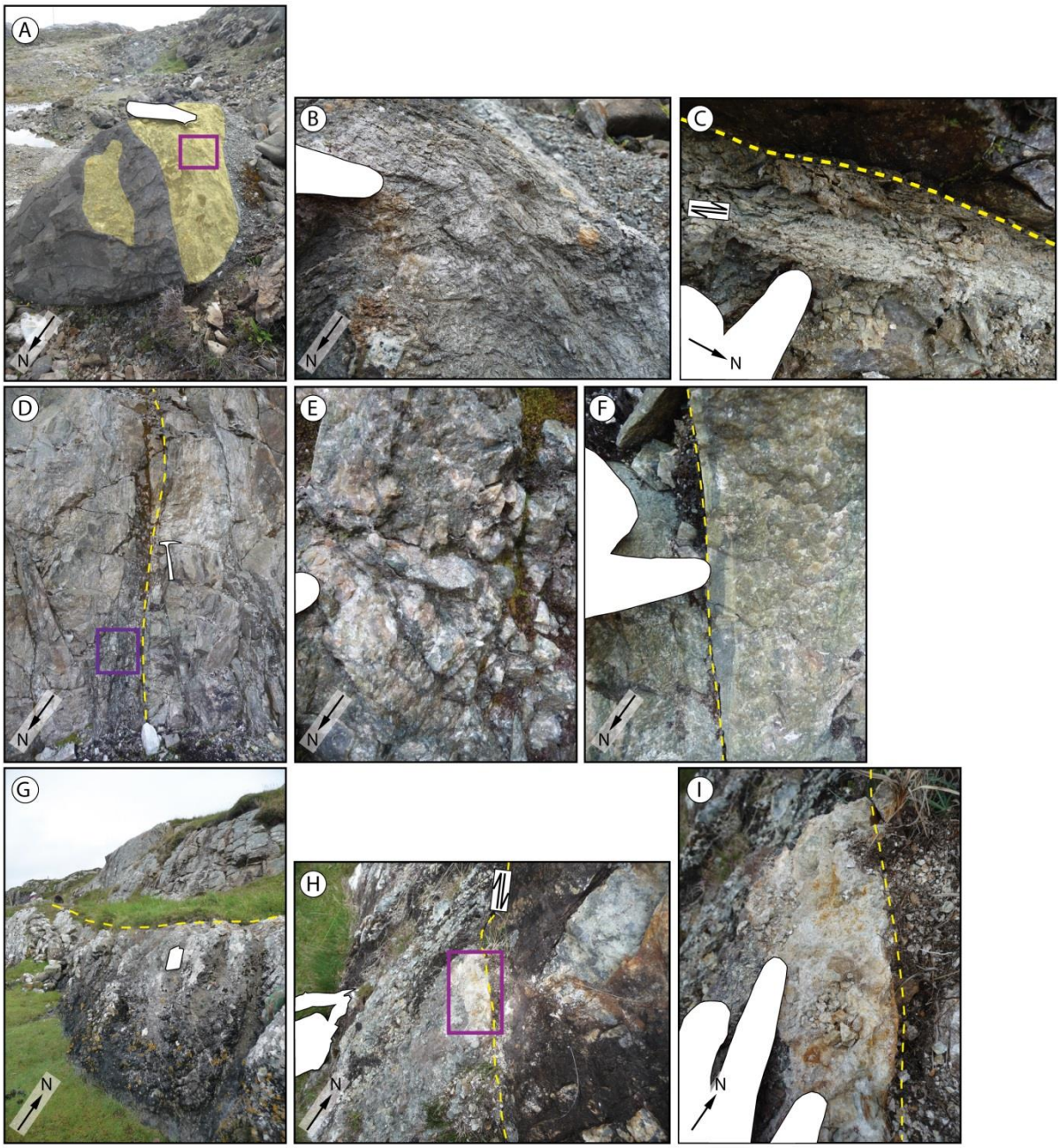

Figure 5.10: Outcrops at Luskentyre and Grose Bay. Purple box = higher resolution photo. yellow = fault breccia, grey = dolerite dyke, yellow dashed line = fault, red dashed line - foliation. (**A -F**) Luskentyre Old Road. (**A** - **C**) NB 1162 9545. (**A** - **B**) Dolerite dyke intruding well indurated light grey fault breccia (image B) with clasts usually < 2 cm across. Purple box in image A = image B. (**C**) Nearby dyke-parallel fault surfaces with soft foliated gouge up to 3 cm across show dextral near strike-slip motion. (**D** - **F**) NG 1228 9481. Parallel with the lineament, pseudotachylite (dark grey) bearing faulting postdating epidote cataclasite fault rock (green). Surrounding rock is highly epidotised. (**H** - **I**) NG 1528 9139. (**G** - **H**) Outcrop at Grose Bay. (**G**) View along the outcrop showing fault breccia (foreground, below yellow line), and relatively unfractured country rock behind. (**H**) Plan view of the footwall contact of the fault breccia with country rock. (**I**) Fault breccia, showing highly altered lens of fault rock likely composed of material altered to phyllosilicates.

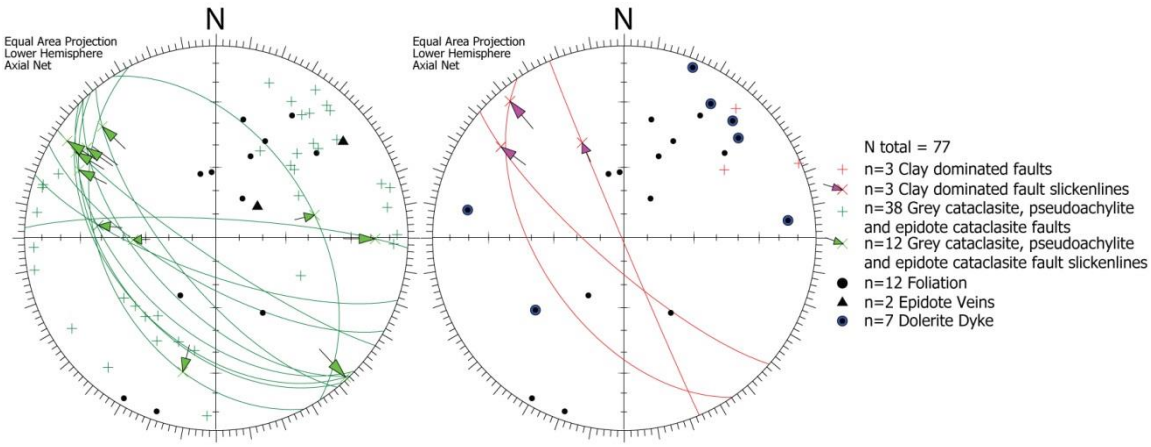

Figure 5.11: Orientation data collected from Luskentyre, Luskentyre Old Road and Grose Bay. Main fault at Grose Bay highlighted in bold green, and the foliated gouge-bearing fault at Luskentyre Old Road is shown in bold red. Faults with slickenline data are drawn with a great circle.

5.4.3 Borve and Scarasta

Lithologies in the area studied comprise massive, biotite-Laxfordian granite sheets intruded into Archaean banded felsic gneisses (Mendum et al., 2009) in the area around Rubha Romaighidh near Borve. The presence of lithological variation between massive gneisses and banded gniesses at Borve has enabled quantitative comparison of spacing attributes and other characteristics in these two very different rock types (section 7.3.2.4.1). Qualitatively, faulting at Borve (NG 0357 9620) is concentrated in banded gneisses, as opposed to the massive granitic units. South of this, the area around Scarasta (NG 0118 9383) was studied due to the presence of a Camptonite-Monchiquite dyke assumed to be of Permo-Carboniferous age (e.g. Baxter and Mitchell, 1984; Fettes et al., 1992) intruded into metadioritic rocks of the South Harris Igneous Complex (SHIC). Foliation in the area dips moderately to steeply towards the southwest.

Faulting at Borve is dominated by a set of faults that dip to the southeast and cut the foliation at low angles or are sub-parallel with it (Figure 5.13). Figure 5.12A-B shows one of these faults cutting the foliation obliquely and partly localising along it, giving a 'ramp and flat' geometry. This faulting often forms along lithological contacts between banded felsic gneisses and granite sheets. A zone of pseudotachylite-cemented breccia that is up to 5- 10 m lies in the immediate footwall of a relatively discrete group of these southeast-dipping faults (Figure 5.12C-D). In the hanging wall of the faults, foliation is sub-parallel with faulting, undulatory and closely spaced (< 0.5 cm), composed of biotite wrapping quartz and feldspar. Feldspar sigma-type clasts indicate thrust kinematics (top-to-the-north), however it is not clear if these are representative of movement on the fault plane. The fault rock is up to 5 cm thick and composed of light yellow-grey (epidote?) cataclasite cementing clasts of pseudotachylite up to 2 cm across, itself enclosing clasts of felsic

gneiss generally < 0.5 cm across. In the massive pseudotachylite breccia that exists in the fault foot wall, clasts of country rock are up to 10-15 cm across (Figure 5.12E). The presence of clasts of pseudotachylite cementing fine clasts of banded gneiss within the fault rock suggests that the fault may originally have been a pseudotachylite-generating fault surface reactivated by the yellow-grey cataclasite-bearing faulting.

At Scarasta, a camptonite dyke intrudes into metadiorite of the South Harris Igneous Complex. The dyke is not faulted and is continuous through the surrounding gneiss (Figure 5.12F, highlighted by white lichen). Close to the margin of the main dyke, a minor spur of the dyke intrudes a fault breccia, but the dyke itself is not brecciated (Figure 5.12G-H). The fault dips to the south-southeast and fault rock characteristics are very similar to a large number of faults observed at Northton to the south (see section 5.4.4). This observation suggests that camptonite dykes postdate the phase of faulting seen at Northton. Several dolerite dykes of assumed Tertiary age were encountered trending NW-SE, in one example intruding parallel with the foliation. Dolerite dykes were not observed to be faulted.

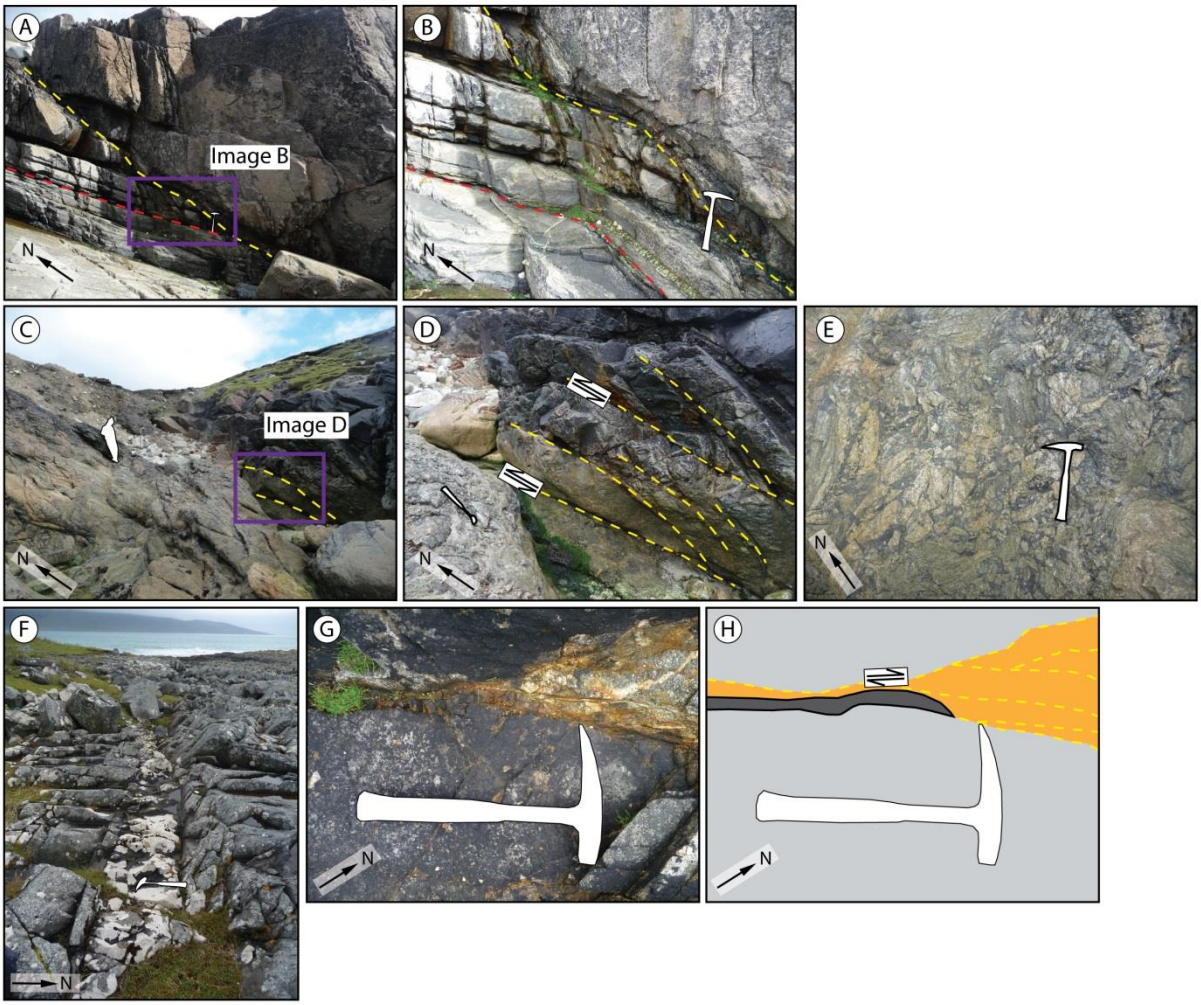

Figure 5.12: Outcrops at Borve and Scarasta. Dark grey = camptonite dyke spur, orange = zeolite cemented breccia, light grey = meta-igneous gneiss, red dashed line = foliation, yellow dashed line = fault. In images A-D the fault footwall is banded felsic gneiss and hangingwall is granite. (**A – E**) NG 0357 9620. (**A – B**) Fault obliquely cutting the foliation and forming ramp and flat geometry. (**C – E**) Fault associated with massive pseudotachylite in the immediate footwall. Postulated thrust offset indicated. (**F - H**) NG 0118 9383. Permo-carboniferous camptonite dyke highlighted by white lichen, and intruding a zeolite bearing fault with zeolite slickenfibres.

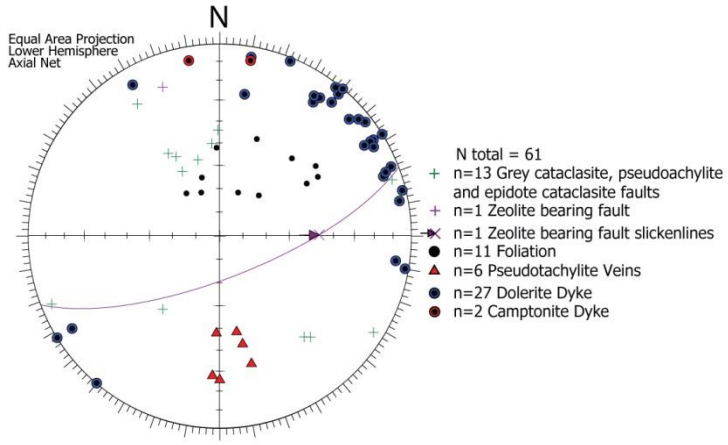

Figure 5.13: Orientation data from Borve and Scarasta. Faults with slickenline data are drawn with a great circle.

5.4.4 Northton

Localities at Northton lie within the Leverburgh Shear Zone of South Harris (localities from NF 9862 9012 to NF 9896 8895). Lithologies at Northton vary from amphibolite-facies pelitic gneisses to meta-norite rocks. Foliation is pervasive and dips steeply to the northeast, with evidence of dextral ductile kinematics. Sparse pegmatite veins 20-30 cm across of assumed Laxfordian age cross-cut the foliation.

Several minor epidote- and chlorite-bearing faults were observed lying parallel to sub parallel with the foliation (e.g. Figure 5.14D). These faults showed evidence of dextral shear, possibly as a continuation of dextral ductile shear identified within the foliation. Epidote cataclasite-bearing faults were not observed cutting camptonite dykes of assumed Permo-Carboniferous age, hence these faults are assumed to pre-date these dykes. Faulting at Northton is dominated by a group of zeolite- (and rare carbonate) and grey cataclasite-bearing, steeply-dipping conjugate faults that strike NNE-SSW to NE-SW with near strike-slip mostly dextral kinematics. These faults are not observed cutting the camptonite dykes, but do however cross-cut epidote veins and epidote-bearing fault rocks. These faults are characterised by dual slip surfaces usually around 30 cm apart, surrounding a core of highly fractured and veined crackle to mosaic breccia (Figure 5.14A-C). The faults are found in both meta-igneous and meta-sedimentary rock units. Non-foliated, soft, orange gouge was found in six separate faults (e.g. Figure 5.14E- I) that are believed to be part of this fault set. These faults often exist alongside well-indurated breccias and cataclasites and are associated with zeolite.

Orientation data (Figure 5.15) show that very few of the dominant set of zeolite bearing faults lie sub-parallel to the foliation plane. Within the fault breccias of the fault cores, tensile fractures are common and also do not reactivate the foliation. However, several examples were seen of continuous faults stepping obliquely through the foliation, with the largest example shown in Figure 5.14H - I. This fault contains soft, orange gouge lenses up to 5 cm across, similar to that seen elsewhere associated with the main fault set at Northton (described above).

The dominant faulting style seen at Northton is not observed elsewhere in Harris, with the exception of Scarasta where the camptonite dyke intrudes one of these faults (section 5.4.3). Presumed zeolite veining within the fault zones and surrounding them appears to be syntaxial.

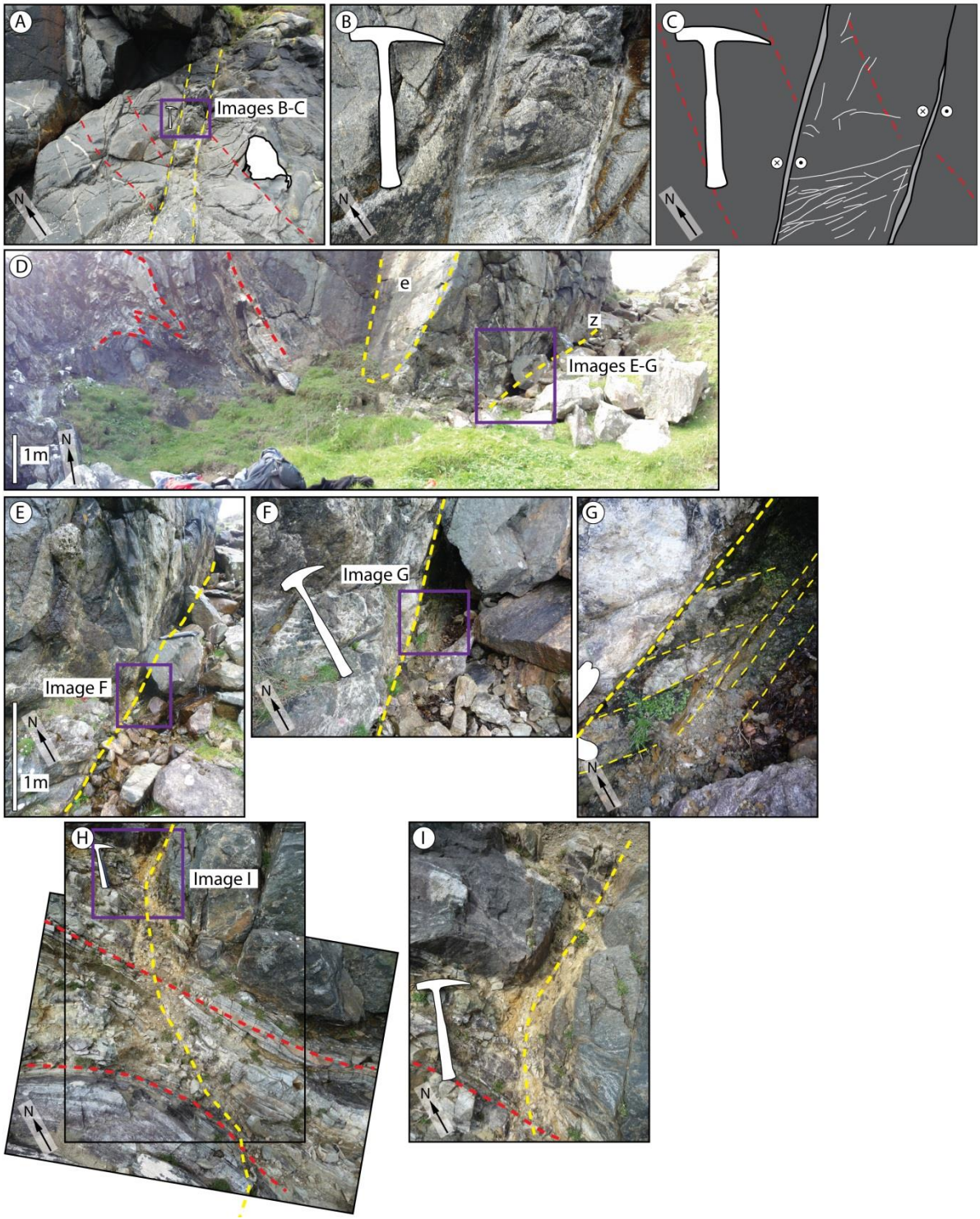

Figure 5.14: Outcrop at Northton . Dark grey = metanorite, light grey = light grey cataclasite, yellow dashed line = fault, yellow dashed line = foliation, purple box = enlarged in subsequent image. (**A – C**) NF 9897 8895. (**A – C**) Typical zeolite bearing fault with two parallel relatively discrete slip surfaces and a core of crackle/mosaic breccia cut by much zeolite veining. Faults have dextral kinematics. (**D – I**) NF 9867 8942. (**D**) Zeolite bearing fault (z) cutting the foliation and epidote bearing fault (e) at high angle. (**E – G**) Zeolite bearing fault with much random zeolite veining in the fault hangingwall (visible at left of F and G). The fault contains several slip surfaces and subsidiary fractures (**G**). (**H – I**) Fault cutting the foliation at a high angle and stepping obliquely through the foliation before continuing. Fault rock is composed of orangey gouge.

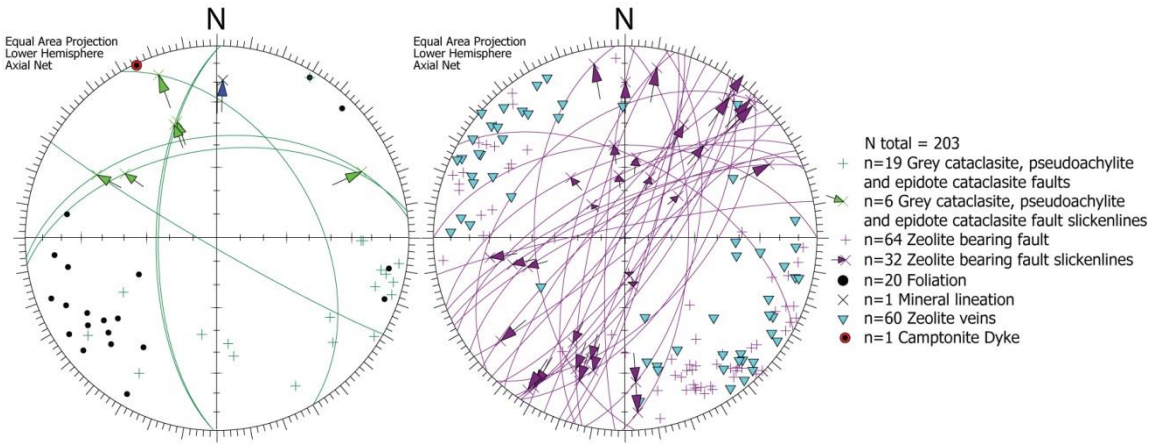

Figure 5.15: Orientation data from Northton. Faults with slickenline data are drawn with a great circle.

5.4.5 Summary of fieldwork outside the OHFZ

Several phases of brittle faulting have been identified in the region of Lewisian rocks located outside and to the NW of the OHFZ. These are chronologically ordered below, as determined by cross cutting relationships. Features that are believed to be contemporaneous share the same numeric:

1.a. *Pale green epidote- and probable chlorite-bearing cataclasites.* These are widespread, often parallel to sub-parallel with the local foliation, and forming lithological contacts. These faults are often steeply dipping and strike NE-SW and NW-SE with near strike-slip kinematics.

1.b. *Pseudotachylite breccias and fault planes.* Seen reactivating/cutting a near vertical NNW-SSE striking epidote cataclasite-bearing fault in one instance at Luskentyre Road. Postdate mylonitic gneiss showing top to the north thrust kinematics at Borve.

2. *Zeolite-bearing NE-SW striking strike-slip faults.* Zeolite is seen associated with a locally intense fault set of NE-SW striking steeply dipping, dominantly dextral strike-slip faults found only in SW Harris. Soft clay gouge-bearing faults were found associated with these faults, but were not foliated.

3. *Camptonite dyke intrusion.* E-W trending camptonite dyke intrusion into the South Harris Complex postdates the zeolite bearing faults. Permo-Carboniferous age (Baxter and Mitchell, 1984; Fettes et al., 1992)

4. *Light grey phyllosilicate cemented breccias*. Found at Grose Bay and probably Luskentyre Old Road. The breccia-bearing faults at both localities are associated with dextral strike-slip kinematics.

5. *Clay-bearing gouges and cataclasites*. Found associated with moderately to steeply

southwest dipping faults, at Luskentyre Old Road and Beitearsaig. Found with dip-slip normal and strike-slip kinematics.

6. *Dolerite dyke intrusion.* NW-SE trending dolerite dyke intrusion. Tertiary age (Fettes et al., 1992). Fault rock was observed along one dolerite dyke margin, indicating a possible phase of NW-SE striking faults that postdate these dykes.

Older faults (1.a. and 1.b.) were observed to have a tendency to localise along the foliation and lithological contacts, and clay-bearing gouges and cataclasites are very often seen reactivating pre-existing fault structures.

5.5 Fieldwork results within the OHFZ

Localities across Harris were selected in order to gain insight into the areas of study identified in Section 5.1.1 . The areas studied on fieldwork inside the OHFZ were selected for the following reasons:

- *Rubha Vallerip*: Selected due to the presence of low angle detachment faults potentially localising along foliation planes or pre-existing faults (e.g. Imber, 1998).
- *Scalpay*: Sections within and outside of the OHFZ (Butler, 1995; Imber et al., 2002), also sections along the 'North Harbour Fault' (Szulc et al., 2008) that follows a major NW-SE trending lineament.

5.5.1 Rubha Vallerip

Rubha Vallerip and Rubha Quidnish (not visited here) record the only outcrops of the OHFZ on South Harris (Fettes et al., 1992; Imber, 1998). Rocks at Rubha Vallerip (around NG 0590 8297) are entirely derived from the meta-anorthosite of the Roinebhal massif (Imber, 1998), varying from intact meta-anorthosite to breccia zones of pseudotachylite and meta-anorthosite blocks, and light green cataclasites. These features are cut by discrete (up to 1 m thick) and pervasive (over 10 m thick) phyllonites and protophyllonites that wrap more intact clasts of meta-anorthosite (Imber, 1998). Phyllonites are mainly bright green in colour, and often display detachment faults that have localised parallel to the foliation. The foliation dips uniformly to the south-southeast within blocks of relatively unaltered meta-anorthosite, and phyllonites are concordant with the surrounding foliation with NW-SE and E-W trending mineral lineations (Imber, 1998). Several examples of southeast verging folds were identified within the phyllonites of Rubha Vallerip, suggestive of extensional top-to-the-SE shear at some point during phyllonite formation. This agrees with observations by Butler (1995) and Imber (1998). An en echelon set of dolerite dykes is

visible intruding the meta-anorthosite and cross cutting the phyllonites. Between en-echelon dyke pairs intense random fracturing and carbonate mineralisation is visible (Figure 5.16I).

The SE-dipping phyllonites were observed to cross-cut pseudotachylites, a zone of steeply dipping extremely well cemented crackle and mosaic brecciation of the meta-anorthosite up to 10 m across that trends NNE-SSW (e.g. Figure 5.16E-H). The phyllonites are cut by discrete SW and SE dipping (<2 cm thick) epidote cataclasite that cut the pseudotachylite and crush zones. Quartz-chlorite-bearing, steeply dipping N-S trending veins cross-cut the pseudotachylite.

Phyllonites have abrupt country rock contacts and contain foliation-parallel detachments (Figure 5.17). Two groups of detachment may be distinguished, in broad agreement with Imber's (1998) Type 1 and Type 2 classifications of the detachments found within phyllonites of North Uist:

- Type 1 detachments (Figure 5.16A-D) are foliation-parallel faults developed during 'macroscopically ductile shear' (Imber, 1998). These faults are associated with very well indurated light green cataclasites. The N-S striking chlorite and quartz veining mutually cross-cuts these faults, indicating that they are probably contemporaneous. Type 1 fault rocks are up to 10 cm thick, and comprise brecciated phyllonites cemented with pale green cataclasite. More discrete (>2cm thick) undulatory detachment surfaces also exist wrapping clasts of country rock (often protophyllonite). These detachments on Rubha Vallerip are found particularly localised along the margins of the phyllonite bands.
- Type 2 detachments (Figure 5.16E-H) are very different, comprising brittle clay gouge-filled faults localising along the foliation within and at the margins of the phyllonite bands. These faults can be undulatory and often exhibit subsidiary Riedel fracture sets indicative of normal kinematics. Figure 5.16H shows highly fractured phyllonite brecciated by Type 2 detachments.

In chronological order as determined from cross cutting relationships, the following faulting sequence has been established at Rubha Vallerip:

1. *Pseudotachylite faulting and brecciated meta-anorthosite.* Random pseudotachylite veining cutting the foliation. Brecciated ('crushed') anorthosite zones are up to 10 m across, trending NE-SW. Probably related to early movements on the OHFZ (e.g. Imber, 1998).

2.a. *Phyllonite formation*. Light green phyllonites dipping shallowly to the ESE. Down dip verging folds indicate an early phase of ductile top-to-the-SE extension.

2.c. *Type 1 detachments.* Quartz-chlorite-epidote-bearing cataclasites and breccias 2-10 cm thick that reactivate some phyllonite boundaries. Kinematics could not be determined. Imber (1998) notes that Type 1 detachments on North Uist are extensional, and likely

formed during extensional ductile shear on the phyllonites. Hence it seems possible that the down-dip verging folds may be contemporary with Type 1 detachment formation.

2.b. *Epidote cataclasite bearing faulting*. Typically discrete structures (<2 cm thick) dipping to the SW and SE, cross-cutting pseudotachylite and brecciated meta-anorthosite. Strike-slip kinematics identified on one fault plane. Age relationships with the phyllonite development are not entirely clear, however epidote cataclasite bearing faulting has been associated with phyllonites on Lewis (section 3.4.2.1.4) and epidote is found within Type 1 detachment fault rocks. It is also likely that there are multiple phases of faulting associated with this fault rock (e.g. section 3.4.4.1).

3. *Type 2 detachments.* Clay-bearing gouges and cataclasites 2-5 cm thick reactivating phyllonites with down-dip, top-to-the-SE normal motion.

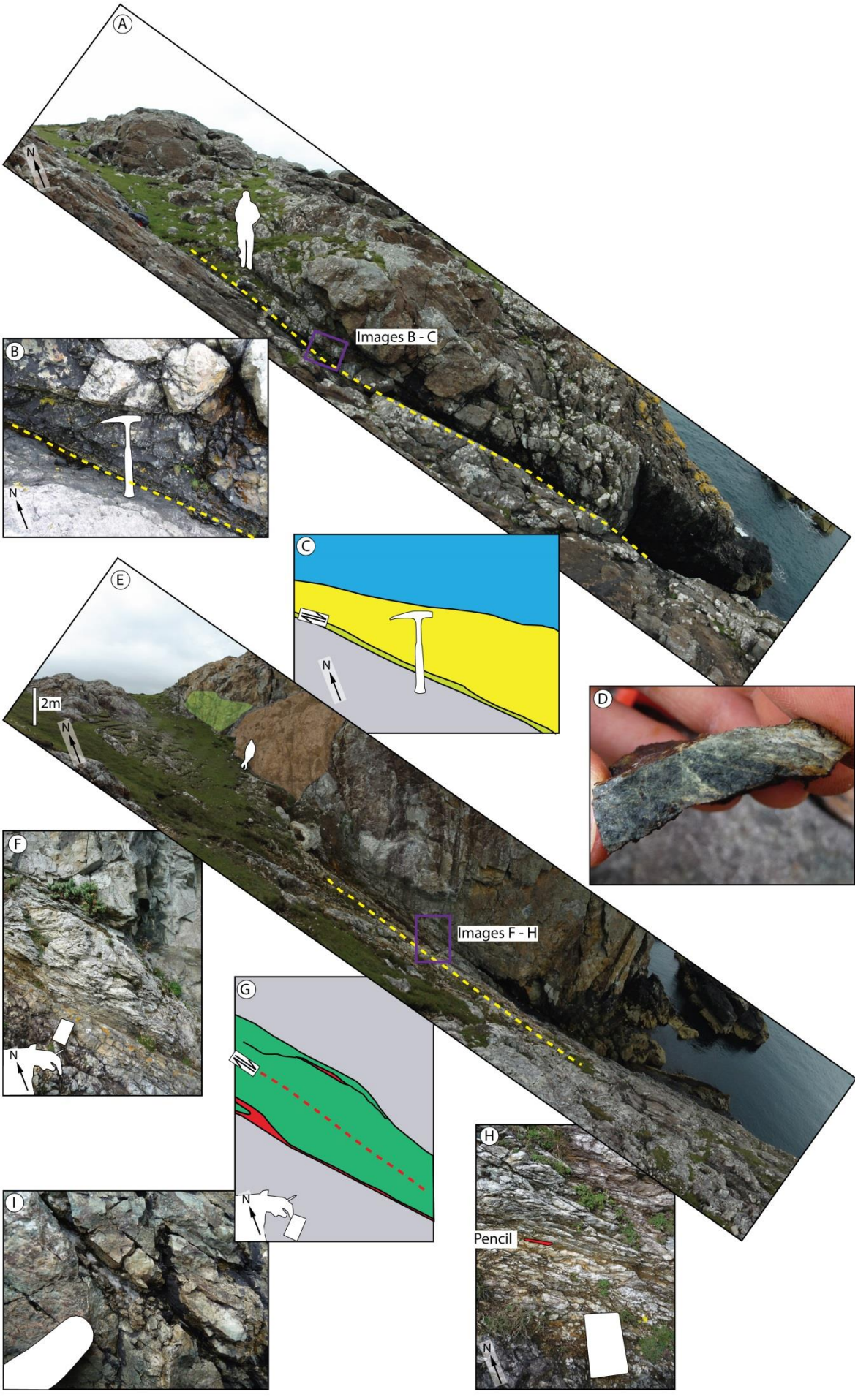
A
N
Images B - C
B
N
C
N
E
2m
N
D
F
N
Images F - H
G
N
H
Pencil
N
I

Figure 5.16 (previous page): Outcrop at Rubha Vallerip. Blue = protophyllonites, dark green = phyllonite, light green = type 1 detachment with epidote cataclasite/ultracataclasite, yellow = well indurated crackle and mosaic breccia composed of clasts of protophyllonite, grey = anorthosite, red = type 2 detachment fault gouge, red dashed line = phyllonitic foliation, yellow dashed line = fault. (**A** – **D**) NF 0598 8298. Type 1 detachment fault. (**B** - **C**) 20-30 cm of brecciated protophyllonite and phyllonite localising at lithological boundary. (**D**) Pale green epidote rich cataclasite from fault core. (**E** – **H**) NG 0590 8297. Type 2 detachment fault with 1 – 1.5 m of discrete phyllonite with clay rich type 2 detachments localising within it. (**E**) Zone of brecciated anorthosite (highlighted brown) and light green cataclasite (highlighted light green) faulting cut by phyllonite. (**F** –**G**) Phyllonite body showing abrupt contacts with anorthosite country rock. (**H**) Phyllonite with multiple brown clay rich detachment surfaces - the yellow pencil is protruding from one such fault. (**I**) Carbonate mineralisation associated with dyke intrusion.

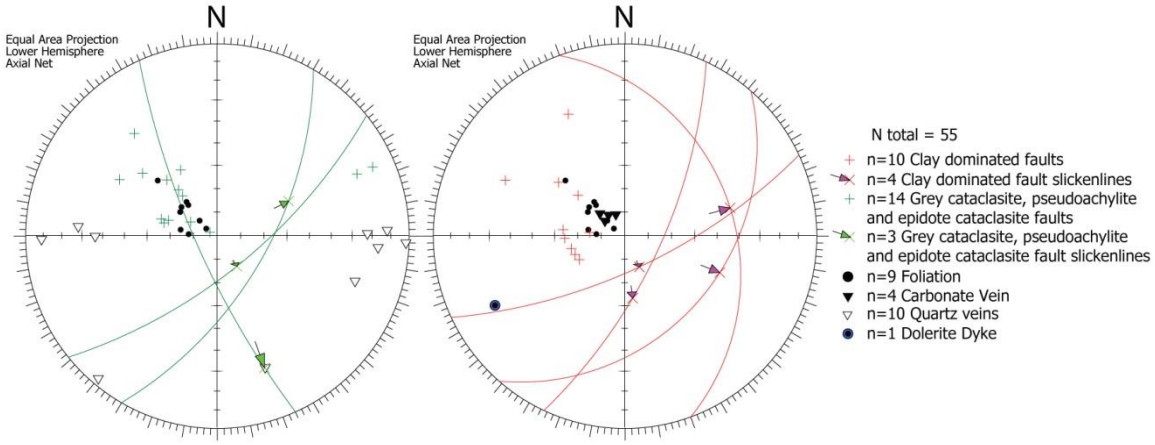

Figure 5.17: Orientation data collected from Rubha Vallerip. Faults with slickenline data are drawn with a great circle.

5.5.2 Scalpay

Scalpay is situated off the coast of northeast Harris, along strike from the NW-SE lineament that passes through Tarbert (Figure 5.18). On Scalpay, this lineament is called the 'North Harbour Fault' by Szulc et al. (2008). Scalpay is dominated by rocks associated with the Outer Hebrides Fault Zone (e.g. Imber et al., 2002; Szulc et al., 2008) (Figure 5.18). The north-western part of the island is comprised of quartzo-feldspathic amphibole gneiss (grey gneisses), which have a gradational contact with mylonitic gneisses of the OHFZ (e.g. Sibson, 1977b; Butler, 1995; Imber, 1998), and the south-western part of the island is dominated by pervasive mylonite (e.g. Imber, 1998; Szulc et al., 2008). Phyllonites are interbanded with the mylonite (Sibson, 1977a; Butler, 1995; Imber, 1998; Szulc et al., 2008), showing evidence of dip-slip thrust motion and sinistral strike-slip motion localised within the phyllonites (Butler, 1995; Imber et al., 1997; Imber, 1998). Imber (1998) and Szulc et al. (2008) note the presence of extensional detachments that are localised within the phyllonites. The foliation is concordant between the gneiss, mylonite, and phyllonite units and dips to the southeast. Within the mylonite zone, asymmetric sigma clasts and

NW verging folds within the mylonite confirm top to the NW thrusting (Figure 5.19B), and en-echelon veins of epidote, cross cut by parallel en-echelon veins of quartz and sulphide, confirm NNW-SSE directed compression associated with this mineralisation. Sub-vertical dolerite dykes are present at several localities cutting the foliation at a high angle, and striking NW-SE.

A major WNW-ESE trending lineament cuts the island and is exposed in the North Harbour of Scalpay as a significant fault zone, termed the 'North Harbour Fault' (Szulc et al., 2008). This fault is noted by Sibson (1977) as a 30 m wide zone of iron stained 'crush breccia', with an apparent sinistral offset of the mylonites. Butler (1995) notes the presence of soft indurated clay gouge on this fault, and 200-300 m sinistral offset along it has been suggested. Very late movement is postulated on this fault as it is observed to cut two Tertiary dykes (Sibson, 1977b), however these were not located in the present work. The North Harbour Fault has been linked to the Mesozoic Minch Basin offshore (Szulc et al., 2008), and other prominent lineaments (probable faults) on Scalpay trend E-W, N-S and WNW-ESE.

In the field, at least three phases of faulting were observed at Scalpay. Within and parallel to the phyllonites, Type 2 detachment faults bearing soft gouges and poorly indurated breccias up to 8 cm thick are present. These postdate ductile phases of movement represented within the phyllonite (Figure 5.19D-F). Detachment faults are concordant with the foliation and dip to the southeast and preserve near dip-slip extensional kinematics. Fault rocks are up to 2 cm thick dominated by soft clay gouge surrounding misoriented clasts of country rock.

Figure 5.19A-C show a N-S striking epidote and quartz bearing cataclasite that is reactivated with thin (<0.5 cm) gouge and patchy carbonate mineralisation (Figure 5.19C, also shown in blue, Figure 5.20), truncated against a carbonate cemented breccia and gouge associated with an E-W strike-slip fault with dextral kinematics. Late strike-slip faulting is evident in Figure 5.20 with a strong E-W trend, and these are associated with fault-parallel carbonate veining. This later phase of faulting may be coincident with that identified in the Stornoway region (e.g. section 3.3.2.2 and section 4.5.2.3), where they were found to postdate Tertiary (Palaeogene) dolerite dykes.

Figure 5.19G-I show the large, steeply southwards dipping fault zone encountered at North Harbour at the locality coincident with the major lineament that crosses the island (Figure 5.18). This is comprised of at least 50 cm of orange and green foliated gouge with asymmetric deformation features indicating a sinistral motion (Figure 5.19H). In the fault hangingwall (visible in Figure 5.19G), the rock is mostly intact grey gneiss with patches of crackle breccia and numerous orange, fault-parallel carbonate veins that are probably siderite (Figure 5.19I), giving the rock and gouge the rusty colouration. These veins are up to 1-2 cm thick and in places support angular clasts of brecciated gneiss. At Tarbert harbour, >50 cm of orange foliated fault gouge was

observed, in addition to breccia and fault parallel carbonate veining of very similar appearance to that seen on Scalpay. This indicates a continuation of this fault to at least this locality, confirming suggestions by Sibson (1977) and Szulc et al. (2008). The apparent slight misorientation of this fault on Scalpay relative to the WNW-ESE trend of the lineament may be due to en-echelon faulting of the same style as that seen at Orasaigh (section 4.5.2.3).

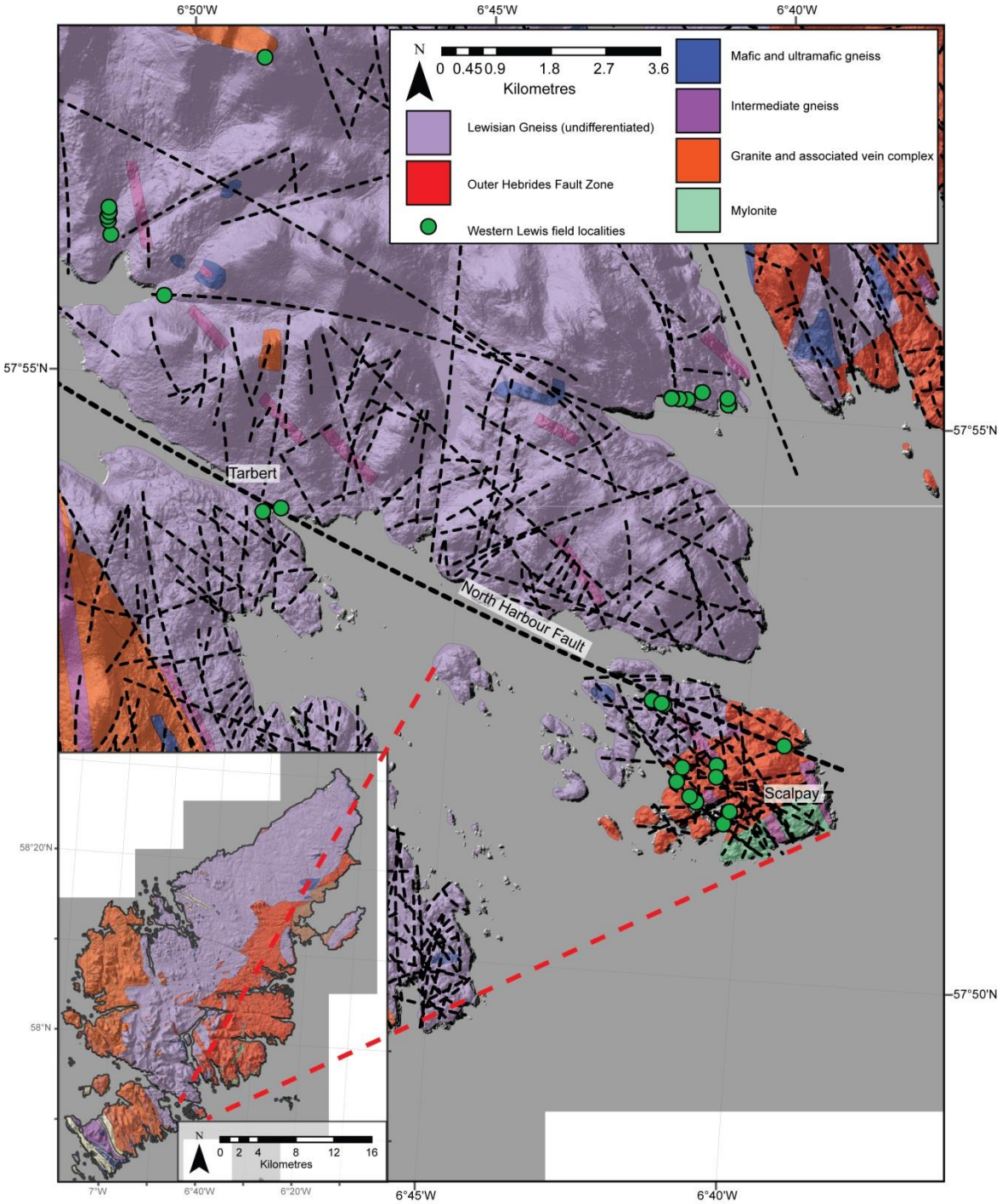

Figure 5.18: Map of field localities at Scalpay. Interpreted lineaments shown in black. North Harbour Fault associated lineament shown in bold.

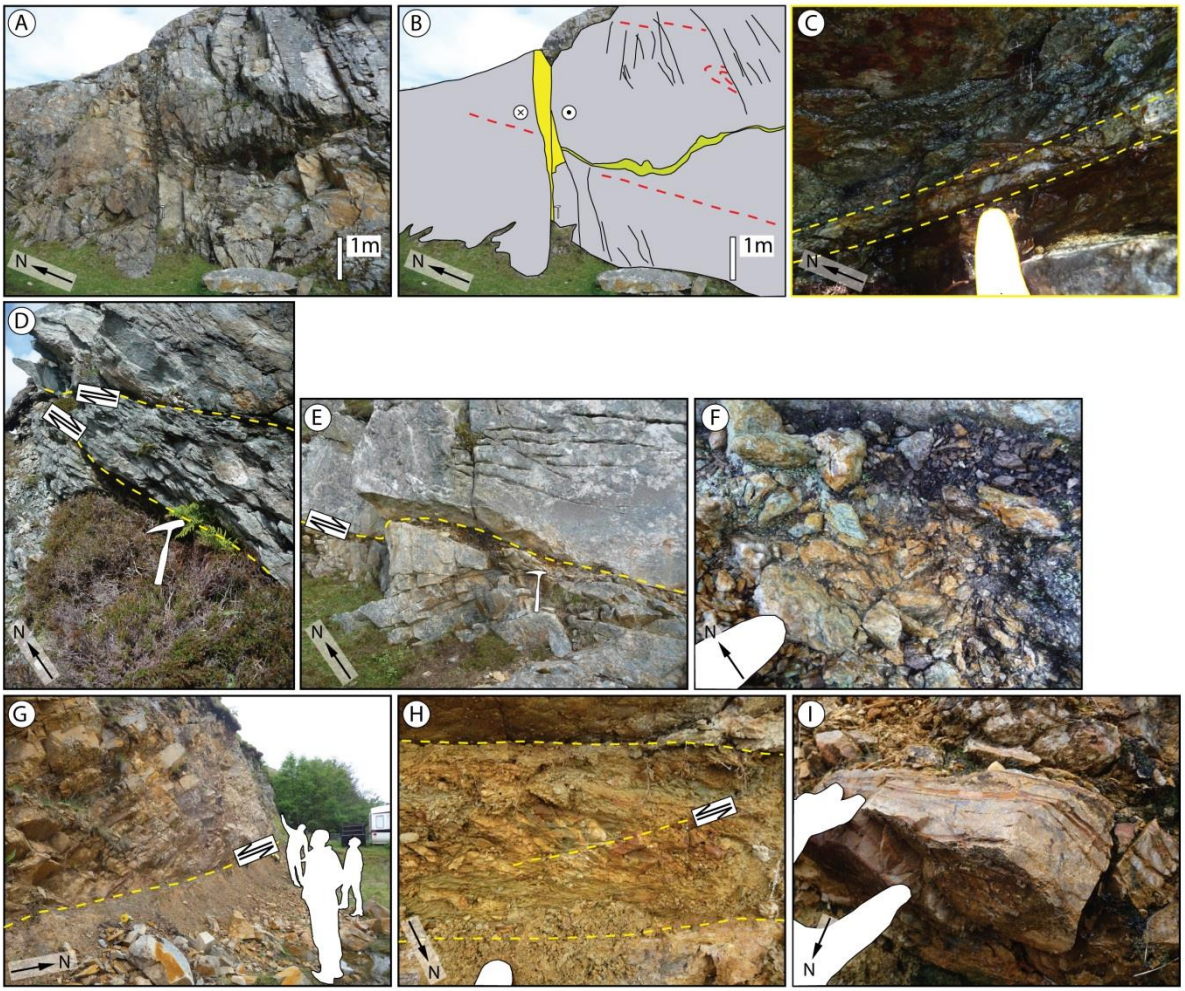

Figure 5.19: Field localities on Scalpay. Yellow = carbonate cemented breccia and gouge, green = quartz-epidote cataclasite, red dashed line = foliation, yellow dashed line = faults. (**A – C**) NG 22314 9539. Calcite rich E-W strike-slip fault truncating a reactivated N-S quartz-epidote cataclasite bearing fault. Note NW verging folding. (**D – F**) NG 2192 9674. (**D**) Detachments with soft gouge, localising within and parallel to a green phyllonite. (**E – F**) Detachment fault with soft gouge offsetting proto-mylonitic rocks. Fault core contains chaotic breccia and authigenic clay. (**G - I**) NB 2191 9674. North Harbour Fault, showing fault gouge with sinistral kinematics (**H**) and adjacent intensive siderite veining (**I**).

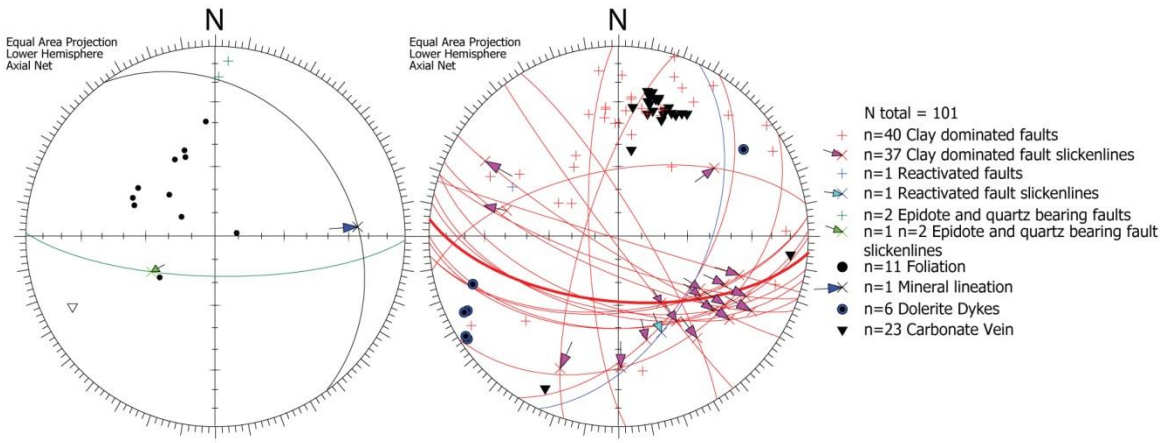

Figure 5.20: Orientation data collected from Scalpay. The main fault is marked in bold red. Faults with slickenline data are drawn with a great circle.

5.5.3 Summary of Fieldwork inside OHFZ

Multiple phases of faulting are present on Harris and Scalpay with several phases being similar to those identified on Lewis. These are chronologically ordered below, as determined by cross cutting relationships. Features that are believed to be broadly contemporaneous share the same numeric.

1.a. *Pale green epidote- and probable chlorite-bearing cataclasites.* Within the OHFZ, the earliest evidence for brittle tectonism is represented by the presence of epidote cataclasites cutting and reactivating the 'pervasive mylonites'. These faults trend NE-SW and NW-SE. Epidote also occurs as en-echelon veins orientated consistently with the maximum stress directed NW-SE probably related to thrusting. Epidote cataclasites are seen cutting pseudotachylites at Rubha Vallerip.

1.b. *Pseudotachylite breccias and fault planes.* Seen reactivating/cutting epidote cataclasite bearing faults in one instance at Luskentyre Road. Associated with mylonitic gneiss showing thrust (top-to-the-north) kinematics at Borve. Likely to be roughly contemporary with mylonite development.

1.c. *Crush breccias/cataclastic gneiss.* Zones of extremely well indurated cataclastic gneiss observed at Rubha Vallerip trending NE-SW, cut by epidote cataclasites. Likely similar to the 'crush melange' of Sibson (1977a) and Imber (1998) in North Uist.

2.a. *Phyllonite formation.* Believed to have occurred postdating the formation of pseudotachylites, with thrust, strike-slip and extensional kinematics recorded within the phyllonites by other authors (e.g. Imber, 1998; Imber et al., 1997), similar to observations made on Lewis (e.g. section 4.5.2) and the Uists (e.g. Imber et al., 1997; Imber, 1998). Phyllonites cut epidote cataclasites and crush breccias of the OHFZ.

2.b. *Type 1 detachments.* Composed of pale green epidote-chlorite-quartz cataclasite fault rocks, often localising along lithological contacts parallel to the mylonitic/phyllonitic foliation, dipping moderately to the southeast with fault rocks 2-10 cm thick.

2. c. *Epidote cataclasite bearing faulting*. Typically discrete structures (<2 cm thick) dipping to the SW and SE, cross-cutting pseudotachylite and phyllonite. It is also likely that there are multiple phases of faulting associated with this fault rock as seen on Lewis.

3.a. *Type 2 detachments.* Composed of soft authigenic clay-rich fault rocks 2-5 cm thick, localising within phyllonite zones with down-dip slickenlines and top-to-the-SE shear sense criteria.

3.b. *Reactivation of epidote cataclasite bearing faults.* At Scalpay, a N-S trending discrete (<2 cm thick) epidote cataclasite bearing fault is seen reactivated by a clay and calcite bearing fault. This pattern is similar to that observed across Lewis and Harris, where clay-bearing

faults trending NW-SE to N-S often reactivate epidote cataclasite-bearing faults.

4 *Late E-W strike-slip faulting along E-W to WNW-ESE striking faults.* Associated with carbonate mineralisation and truncating earlier structures. Dominated by sinistral strike-slip faulting. The major North Harbour Fault at Scalpay is continuous through to at least Tarbert and may be an en-echelon structure.

5.6 Fieldwork results synthesis

5.6.1 Pre-Mesozoic structures

The earliest identified brittle fracturing is associated with randomly oriented and foliation-parallel pseudotachylite veining, epidote cataclasite formation, and 'crush' breccias found most commonly within the OHFZ. These fault rocks also occur outside the OHFZ (e.g. at Borve, section 5.4.3), but are more infrequent. Pseudotachylite fault rocks from across the Outer Hebrides yield a range of ages from the Proterozoic to the Caledonian (e.g. Kelley et al., 1994; Sherlock et al., 2009). It seems likely that many pseudotachylite, epidote cataclasites and crush melanges formed during the Caledonian Orogeny (e.g. Imber, 1998; Imber et al., 2002). There is a tendency for pseudotachylite and epidote cataclasites to localise along pre-existing lithological contacts and along the foliation.

Epidote and pseudotachylite bearing fault rocks are postdated by the formation of phyllonites that developed during ductile shear within the OHFZ (e.g. Imber, 1998), and these phyllosilicate-rich fault rocks are visible cutting other pseudotachylite, epidote cataclasite-bearing faults and crush breccia at Rubha Vallerip.

Type 1 detachments are the first phase of faulting that locally postdate the phyllonitic fabrics, and may be contemporaneous with them (Imber, 1998). These were identified at Rubha Vallerip, and appear to have formed under very similar conditions to the phyllonite itself with epidote-/chlorite-bearing fault rocks and associated veining. It is possible that these faults may be contemporaneous with phyllonite formation and represent transient overpressure or high strain rate conditions that led to brittle failure (Imber, 1998).

In southwest Harris, NNE-SSW to NE-SW-striking zeolite-bearing faults with near strike-slip dextral kinematics are common. This faulting appears to be composed of conjugate pairs, and in several instances, light orange non-foliated clay gouges were observed lying along these faults. Rarely, the zeolite is also associated with calcite mineralisation. NNE-SSW to NE-SW striking zeolite-bearing faults often have a dual slip surface architecture with two parallel principal slip surfaces

enclosing a 30 cm wide core of highly fractured and zeolite veined country rock, with thin (< 2 cm thick) principal slip surfaces. At Scarasta, a fault of this group is intruded by a (non-faulted) camptonite dyke, suggesting that they pre-date the intrusion of these late Carboniferous-early Permian dykes. These faults are localised to southwest Harris and were not found elsewhere. Unlike other identified fault sets, this set is relatively unaffected by pre-existing structures. No examples were seen of these faults reactivating pre-existing faults, and the majority do not localise along the foliation. One example of a fault attributed to this group and stepping obliquely through the foliation was observed, and very minor 'ladder'-type fracturing was also present in the SHSZ, but not to the extent present in shear zones on the mainland (e.g. in the Canisp shear zone, see Pless, 2011).

5.6.2 Mesozoic and younger structures

Unlike Lewis, where most faults identified as Mesozoic in age strike NNW-SSE, on Harris there is a marked rotation anticlockwise of these clay-bearing faults so that many of the prominent lineaments on Harris trend more NW-SE to WNW-ESE. Kinematics on many of these faults are enigmatic, with dip-slip normal and strike-slip dextral and sinistral motions observed, with the relative ages of these different movement senses being unclear. Strike-slip motion is not seen on NNW-SSE striking faults identified in Lewis. At Beitearsaig and Grose Bay/Luskentyre, clay gouge-bearing faults reactivate earlier epidote bearing structures, and at Grose Bay, the lineament clearly reactivates and brecciates a localised zone of pre-existing mylonite. Hence, similar to faulting identified on Lewis (Chapters 2 and 3), reactivation of earlier structures by clay gouge-bearing faults seems common. The strike-slip motions identified on at least some of these NW-SE striking faults may be related to Tertiary strike-slip movements identified elsewhere (e.g. Chapter 3 and Chapter 4). Several examples of steeply southward dipping strike-slip faults were identified on Scalpay, the North Harbour Fault being the most prominent example. Movement on this fault may be linked to phases of E-W strike-slip faulting seen elsewhere on Lewis, and these phases of faulting are amongst the youngest identified (e.g. 4.5.3.3). Alternatively, major NW-SE striking faults on Harris with strike-slip kinematics may represent transfer faults linking faults offshore west and east of Harris.

Two types of dyke are present within the Lewisian of Harris thus enabling relative ages to be attributed to most faulting. Dolerite dykes of assumed Tertiary age (Fettes et al., 1992) were found throughout the island, consistently trending NW-SE, again slightly rotated (anti-clockwise) from the dolerite dykes seen on Lewis (e.g. see section 3.3.2.2). Three camptonite dykes were visited in southwest Harris at Borve and Northton, oriented E-W. On the basis of the cross cutting relationships described here and in addition to the relative age observations made in Chapters 3

and 4, it is possible to ascribe broad ages to the various brittle deformation events identified above. These relative ages are summarised here:

Pre-Mesozoic faults:

1. Green pervasive mylonites in the OHFZ striking NE-SW with top to the north and northwest, seen on Scalpay alongside cataclastic gneiss of the 'crush melange' (Sibson, 1977a).

2.a Pseudotachylite and grey cataclasites, found particularly in the OHFZ, often running parallel with the foliation and also found as random veining. Postdated by phyllonite formation on Rubha Vallerip.

2.b Chlorite- and epidote cataclasite-bearing normal, thrust and strike-slip faults in the OHFZ, in addition to chlorite- and epidote cataclasite-bearing Type 1 detachments at the margins of phyllonite shear zones on Rubha Vallerip. Epidote cataclasite-bearing faults are usually steeply dipping and predominantly strike NW-SE and NE-SW.

3. Zeolite- and orange gouge-bearing faults localised in southwest Harris, cutting the foliation of the Leverburgh Belt and epidote cataclasite-bearing faults. These faults strike NNE-SSW to NE-SW, and are observed to be cross-cut by Camptonite (Permo-Carboniferous) dykes.

Mesozoic and Cenozoic faulting:

1. WNW-ESE- to NW-SE-striking normal faulting, found at Beitearsaig. This phase of clay-rich foliated gouge-bearing faulting at Beitearsaig was observed to be reactivating an earlier epidote cataclasite-bearing fault surface. Although normal kinematics were not observed on major lineaments at Luskentyre and Grose Bay, it is possible that this movement phase may have been obscured by later strike-slip faulting.

2. NE-SW striking clay gouge-bearing Type 2 detachments, localising within pre-existing phyllonites on Scalpay and Rubha Vallerip.

3. WNW-ESE- to NW-SE-striking oblique slip to strike-slip faulting, found at Beitearsaig, Scalpay, and Luskentyre Old Road localities. On Scalpay, the North Harbour Fault has been observed to cut the mylonites and sinistrally offset Tertiary dykes (Sibson, 1977b; Butler, 1995). This may coincide with the phase of E-W strike-slip faulting on Lewis that is known to cross cut Tertiary dykes. The North Harbour Fault may also be a Mesozoic transfer fault that links major faults east and west of the island.

5.7 Fault rock characterisation

Samples were collected during fieldwork in order to characterise specific faulting within the Lewisian basement rocks of Harris. The following thin sections were obtained:

- Five thin sections of pre-Permo-Carboniferous zeolite-bearing faults at Northton.
- Three thin sections from fault rocks at Grose Bay – two from the fault breccia and one from the country rock mylonite. Faults here show evidence of reactivation of parallel basement foliation within the mylonite.
- One thin section of soft gouge at Beitearsaig, and one section from soft gouge from the North Harbour Fault, Scalpay. These faults are at least superficially similar to NNW-SSE striking foliated clay gouge bearing faults observed on Lewis.

Three thin sections of soft fault gouge from Scalpay, Beitearsaig, and Northton were studied with SEM. The aim of thin sections work was to determine:

- The broad characteristics of different post-Caledonian faulting on Harris and Scalpay.
- Any differences between fault rocks obtained along NW-SE trending lineaments. Fault rocks from these lineaments could be expected to be similar given they originate on structures with the same orientation and with similar cross-cutting relationships.
- The differences or similarities between clay-bearing gouges along different faults.
- Any controls on faulting on Harris and Scalpay, e.g. weakening mechanisms.
- The conditions of faulting and depth of formation of fault rocks within the Lewisian basement rocks of Harris.

5.7.1 NW-SE striking faults with soft gouge – Scalpay and Beitearsaig

5.7.1.1 Scalpay

Fault rocks at Scalpay and Beitearsaig are dominated by very fine grained foliated clay-bearing gouges and cataclasites, together with significant probable siderite mineralisation at Scalpay. Thin sections were produced from the soft foliated gouges at both localities in order to compare them to each other and other samples. At Beitearsaig, the gouge is reddy brown in colour, and at Scalpay it is bright yellow-orange, suggesting some difference in mineralogy.

Soft clay-bearing gouge from the North Harbour Fault (Figure 5.19G-H) was used to produce the thin section from Scalpay. The fabric is defined by a low relief, low birefringence, very fine grained groundmass with occasional clasts of quartz or feldspar. The groundmass is composed of very fine (< 0.01 mm) clasts of probable smectite-illite gouge (Figure 5.21A) that are brecciated and

cemented in a groundmass of finer, paler-coloured, very fine grained smectite-illite or possible illite-chlorite in crackle and mosaic breccias. Under SEM (Figure 5.21C-F), the groundmass is revealed to be dominantly composed of probable smectite- illite and illite-chlorite of varying iron content. This wraps ultrafine clasts of quartz, feldspar and rare phyllosilicates, indicating that most authigenic clay formation is syntectonic. The majority of the rock is composed of relatively iron-poor, probable smectite-illite with minor probable illite-chlorite, wrapping ultrafine grains of cataclastic quartz and other minerals (Figure 5.21E-F).

Quartz and feldspar are present as randomly dispersed clasts constituting <5% of the rock. Throughout most of the rock, these clasts are smaller than 0.1 mm across (visible in Figure 5.21B-D). Quartz clasts are usually mono-crystalline and rounded, whereas feldspars exhibit greater fracturing and disaggregation with several bands of chaotically brecciated feldspar that may have originally represented contiguous clasts (e.g. Figure 5.21B). These bands tend to contain coarser clasts up to 0.2 – 0.3 mm across.

Dark brown veins <0.1 mm across cross-cut the fault rock obliquely at approximately 30 degrees to the foliation in thin section view (visible in Figure 5.21A-B and in C-D as bright white mineral) . These veins are at times visibly syntaxial, with a dark band down their centres. In bands of fault rock with a higher proportion of clastic quartz and feldspar relative to illite/phyllosilicate, this veining is much more intense (Figure 5.21B) and brown veining seems to emanate from these areas. The reasons for this are unclear, but as these veins cross-cut the banded fault rock, it may be the product of later fluid flow that was concentrated in more porous, clast rich areas of the fault rock (e.g. Chang and Chang, 2000), with fluid that spread from these areas. Under the SEM, these veins are revealed to be smectitic in composition and exhibit elongate undeformed 'book' crystal geometry, indicating post-tectonic formation (Figure 5.21C-D). Bands of iron-rich clay enclose areas of iron-poor clay and ultrafine clasts of cataclastic country rock that appear to be syntectonic. Hence, this later phase of brown authigenic smectitic clay veining represents a phase of fracturing, fluid flow and crystal growth that postdates faulting.

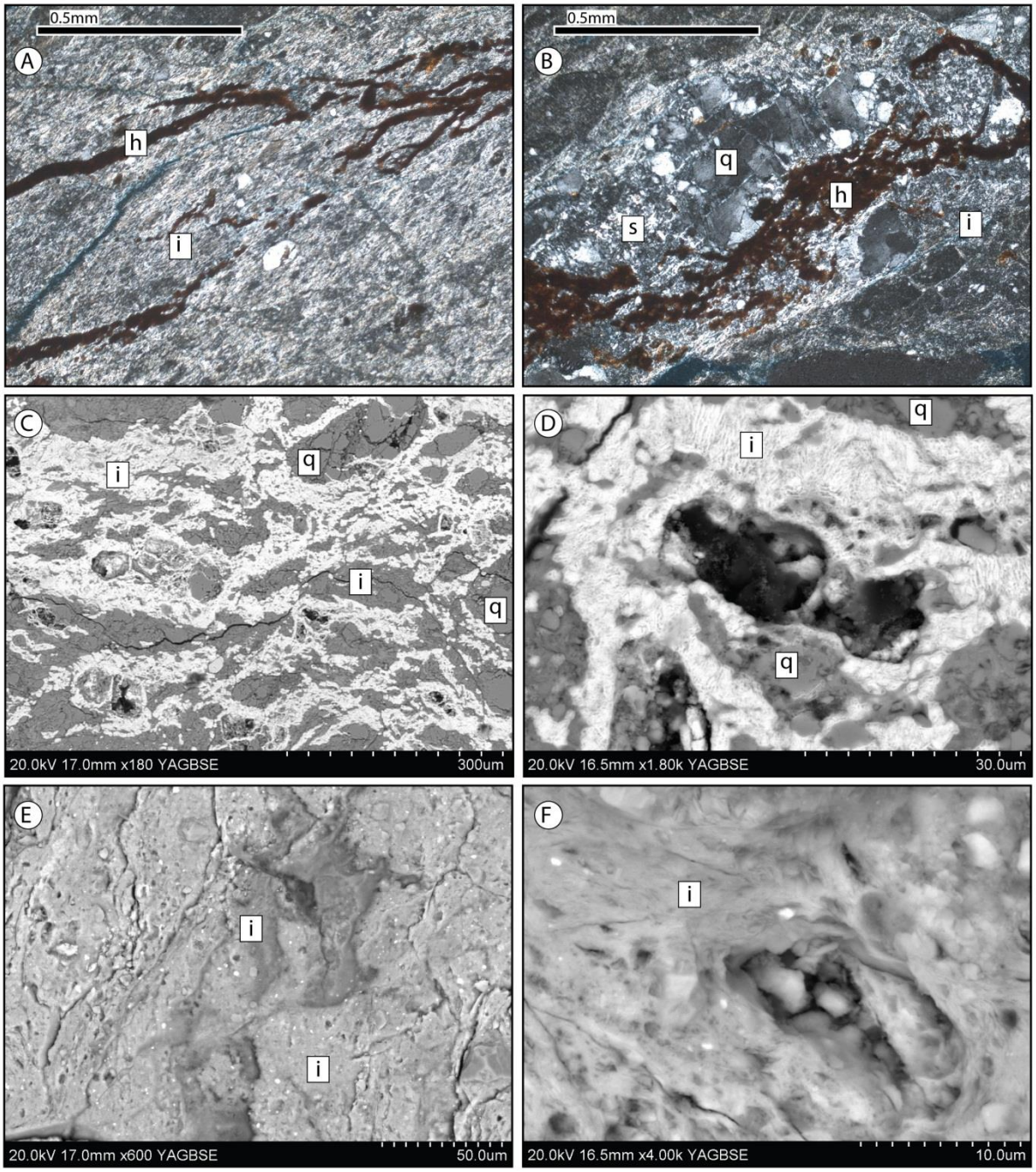

Figure 5.21 (previous page): Photomicrographs of foliated fault gouge from Scalpay North Harbour Fault (NB 2191 9674, shown in Figure 5.19H-I). (**A**) XPL. Fault rock overview - smectite-illite ground mass cut obliquely by reddy-brown veins. (**B**) XPL. Reddy-brown mineral (iron rich clay shown in C and D) concentrating in clastic dominated band of fault rock – surrounded by cataclastic quartz and feldspar. (**C - D**) BSEM images. Bands of iron rich smectite-illite wrapping more clastic dominated bands with relatively iron-poor illite. (**E**) BSEM image. Syntectonic illite and ultrafine chaotic breccia clasts supported by smectite-illite matrix. (**F**) BSEM image. Higher magnification image of E, smectite-illite and ultrafine clasts of country rock.

5.7.1.1.1 Conditions of faulting at Scalpay

Authigenic illite-smectite, chlorite and smectite are known to form under low temperature and pressure conditions, probably at temperatures less than 200°C but possibly higher (Reyes, 1990).

Later smectitic veining may have formed at temperatures less than 120°C (e.g. Warr and Cox, 2001). Greater disaggregation of feldspar relative to quartz is indicative of low temperature (<300°C) conditions (Passchier and Trouw, 1996 p62).

5.7.1.2 Beitearsaig

The thin section was produced from red foliated fault gouge shown in Figure 5.7F-G. In thin section, the fault rock is bright red-brown, alternating with yellow-brown and pale green bands up to 0.75 cm across. These bands are themselves very finely foliated with foliae of << 0.1 mm in most areas. The fault rock is composed dominantly of brown matrix-cementing clasts of rounded quartz and feldspar (Figure 5.22A-D). Under the SEM, the brown matrix is revealed to be composed dominantly of ultrafine monomineralic clasts of country rock generally less than 10 µm (Figure 5.22E-H), cemented in authigenic syntectonic clay cement. The clay matrix is smectitic clay and is probably altered from phyllosilicate minerals such as biotite and muscovite, which are visibly 'shredded' in thin section (Figure 5.22G). Clay development is syntectonic and wraps individual clasts and groups of clasts. Sigma clasts in the fault rock and offset clasts (e.g. Figure 5.22H) indicate sinistral kinematics, agreeing with measurements obtained from slip surfaces nearby. Fractures cross-cut the foliated gouge and are themselves filled with illite/clay flakes < 0.1 mm across, and these also indicate a sinistral sense of motion from offsets of < 1 mm. It is not clear if these fractures are contemporary with the faulting that produced the foliated gouge or postdate it.

Clasts at optical microscopy resolution (up to 50x) are dominantly composed of quartz, and the breakdown into clay minerals and cataclasis of feldspar into very fine cataclastic bands up to 0.1 mm across is widespread (e.g. visible in Figure 5.22A and D). The latter are interspersed with more clay-dominated foliae, and are composed of very fine, irregularly shaped, fractured feldspars that exhibit strained extinction patterns. These fractured feldspar clasts are likely to have originally been contiguous. Quartz clasts occur usually as rounded mono-mineralic clasts surrounded by more clay-rich matrix, with the largest clasts up to 0.2 mm across (e.g. Figure 5.22A). In addition to quartz and feldspar, there are also clasts of epidote cataclasite fault rock, up to 1 mm across (Figure 5.22C). These are dominantly composed of angular fragments of quartz cemented in a very fine matrix of epidote. The presence of pre-existing fault rocks within the gouge confirms observations in the field that the clay gouges reactivate earlier pale green epidote cataclasite bearing faults.

A network of veins cut the foliated fault rock, possibly composed of illite (identified from EDX spectra). It is not clear whether these are contemporaneous or later than the main phase of

faulting and foliated gouge formation. In addition to these fractures, foliation-parallel veins of low birefringence zeolite are present, up to 0.1 mm across (Figure 5.22D) and composed of randomly orientated crystals < 0.5 mm across. These are not affected by cataclasis and hence probably postdate faulting. The parallelism of these veins with the foliated gouge may be indicative of reactivation of the weak clay-rich fabric by later veining.

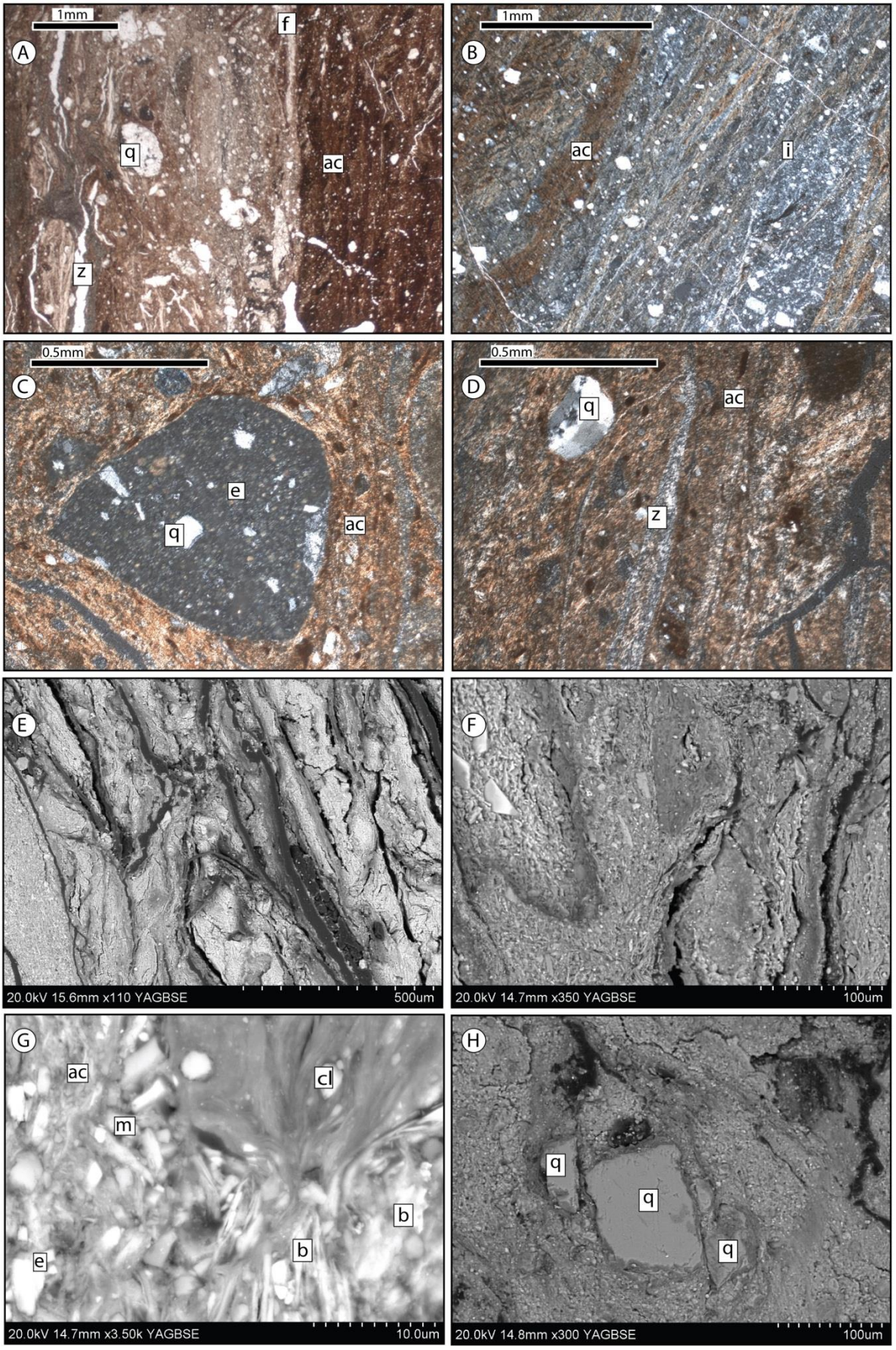
A
1mm
f
q
ac
z
B
1mm
ac
i
C
0.5mm
e
q
ac
D
0.5mm
q
ac
z
E
20.0kV 15.6mm x110 YAGBSE
500um
F
20.0kV 14.7mm x350 YAGBSE
100um
G
ac
cl
m
b
b
e
20.0kV 14.7mm x3.50k YAGBSE
10.0um
H
q
q
q
20.0kV 14.8mm x300 YAGBSE
100um

Figure 5.22 (previous page): Photomicrographs of sample collected from Beitearsaig foliated fault rock (GR NA 9974 1095, shown in Figure 5.7C-G). (**A**) PPL. Showing foliated fault gouge composed of authigenic clay (ac), likely smectitic in composition. Quartz (q) forms majority of clasts within the fault rock, whilst feldspar (f) is highly brecciated. Zeolite (z) veining is parallel with the foliation within the gouge. (**B**) XPL. Lighter area of fault rock, still tightly foliated. Probably more dominantly composed of illite (i). (**C**) XPL. Clast of epidote cataclasite (e) cementing angular quartz fragments, itself entirely wrapped by authigenic clay rich matrix of the foliated gouge (ac). (**D**) XPL. Quartz fragment (q) wrapped by authigenic clays (ac), with intact foliation parallel zeolite vein (z). (**E - G**) BSEM images. Foliated very fine grained gouge at progressively higher magnification. Foliation bands running diagonally from top left to bottom middle. Biotite is undergoing disaggregation (b), and most clasts are mono-mineralic. m = muscovite, e = epidote, cl = chlorite, ac = authigenic clay. (**H**) BSEM image. Offset disaggregated quartz clast in matrix of ultrafine clay cemented gouge.

5.7.1.2.1 Conditions of faulting at Beitearsaig

Fault rocks at Beitearsaig contain syntectonic smectitic clays, although they are dominated by brecciated clasts. Smectite is suggestive of low temperatures that may be less than 120°C (Reyes, 1990; Warr and Cox, 2001), and, if this was the case, could indicate depths of faulting less than 4 km in the crust assuming a normal 30°Ckm^{-1} geothermal gradient (e.g. Watts et al., 2007).

5.7.1.3 Summary and comparison of fault rocks from Beitearsaig and Scalpay

Faulting at Beitearsaig has produced a very fine grained clastic supported breccia of mono-mineralic clasts cemented with authigenic clay. Fault rocks at Scalpay are lighter in colour, and the illite-dominated fault rock is cut by veins of iron-rich smectite that is concentrated around and seems to emanate from zones of cataclastic feldspar, likely due to increased porosity/permeability in those areas. Fault rocks at Scalpay are very heavily dominated by authigenic clays with illite composition and clasts are less abundant. These differences may be an indication that the fault rock at Beitearsaig is less 'developed', i.e. deformation, fluid flow and alteration processes have not progressed to the same point as at Scalpay. This may be expected given that the sample at Beitearsaig was taken from a thinner zone of gouge (< 20 cm) than that at Scalpay (> 50 cm). Alternatively, illite in the North Harbour Fault at Scalpay may indicate the occurrence of faulting at that locality at depths deeper than those associated with faulting at Beitearsaig.

Both faults exhibit sinistral kinematics and are composed of very finely foliated gouges, and in both faults, feldspars appear weak relative to quartz, indicating 'very low grade conditions' with temperatures less than 300°C (Passchier and Trouw, 1996, p62). At Beitearsaig, gouge-bearing faulting post-dates epidote cataclasite-bearing faulting, but no evidence of reactivation was seen at Scalpay.

5.7.2 NW-SE striking faults with basement inheritance from mylonite – Grose Bay

Samples at Grose Bay were collected from the exposed fault breccia and country rocks. The fault breccia collected from Grose Bay is derived directly from very finely foliated mylonite derived from granitic gneiss and pegmatites. In thin section, the mylonite is nearly entirely composed of quartz and feldspar (often sericitised) with elongate foliation-parallel patches of darker epidotised feldspars and sericite (Figure 5.23A). The largest crystals are composed of feldspar and are up to 0.3 mm across, often with mantles of very fine grained feldspar with crystal sizes << 0.1 mm. These appear to be the product of bulging recrystallisation (Passchier and Trouw, 1996, p42). Quartz is polycrystalline, strained, and displays irregular margins, with some fabric indicative of subgrain rotation crystallisation. Bulging recrystallisation and evidence for subgrain recrystallisation are indicative of lower temperatures and higher strain rates than grain boundary migration recrystallisation (Passchier and Trouw, 1996, p43). In places, sericite appears altered to a dark brown clay mineral (Figure 5.23A). Sigma porphyroclasts indicate a NE side up component to the SW dipping foliation, i.e. top to the south.

Within the fault breccia, lithic clasts of country rock displaying mylonitic foliation are evident (Figure 5.23B). The rock is a clast-supported chaotic breccia comprised of angular fragments of country rock up to 1 mm across cemented by a yellow-brown phyllosilicate-rich matrix (Figure 5.23C). This matrix is composed of very fine grained sericite and chlorite, possibly formed from the incorporation and alteration of sericitised feldspar in the country rock. In places, there is a darker brown colouration to the matrix, caused by the overprinting of alteration to authigenic clays (Figure 5.23C). In addition, open fractures cross-cut the sericite-chlorite fault rock, with porosity constituting up to 5% of the rock volume, based on thin section observations (Figure 5.23B). Clasts of mylonite with straight foliation-parallel sides and elongate axes parallel with the direction of the foliation indicate the tendency of the country rock to fracture along the foliation (Figure 5.23B).

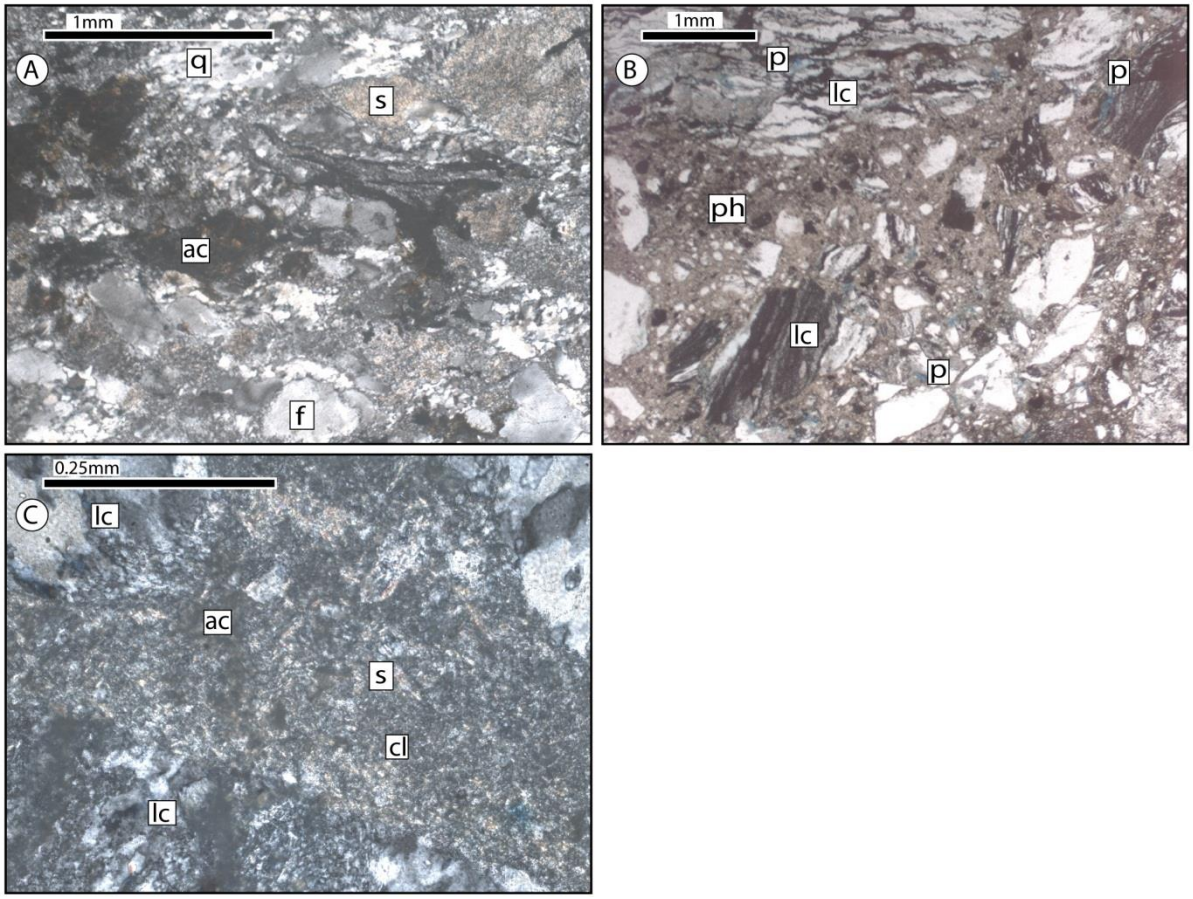

Figure 5.23: Photomicrographs of fault samples from Grose Bay (NG 1528 9139). (**A**) XPL. Mylonitic foliation with secondary alteration of sericitised feldspar (s) to authigenic clay (ac). Quartz is ribboned and polycrystalline (q), and feldspar (f) is surrounded by a halo of very fine feldspar crystals (bulging recrystallisation). Authigenic clays (ac) are associated with sericitised feldspar. (**B**) PPL. Clast supported breccia of lithic clasts (lc) in a phyllosilicate (ph) dominated matrix of very fine low relief low birefringence tabular mineral. Porosity is shown in blue (p). (**C**) XPL. Showing fine grained matrix of chlorite (cl, darker patches) and higher birefringence sericite (s) between lithic clasts (lc). The matrix shows late alteration to authigenic clays (ac).

5.7.2.1 Conditions of faulting at Grose Bay

The sericite-chlorite cataclasite fault rock is suggestive of lower greenschist facies conditions with temperatures of around 250 – 300 °C (e.g. Watts et al., 2007 and references therein). It is interesting to note that faulting on North Uist has been observed with normal kinematics associated with similar fault rocks (White, 1998). Lower greenschist facies conditions exceed those associated with authigenic clay development, with the late authigenic clay overprint indicating lower temperature and pressure alteration of the original fault rock. Open fractures cross-cutting the sericite-chlorite breccia are probably associated with a later phase of faulting that is not directly exposed at Grose Bay. Any later stage of faulting at Grose Bay may be the phase of clay bearing faulting identified at Luskentyre Old Road where authigenic clay-bearing foliated gouges were observed reactivating a pale green/grey breccia.

5.7.3 NNE-SSW striking faults with zeolite mineralisation – SW Harris

Studied samples of the NNE-SSW to NE-SW striking zeolite-bearing fault rocks and associated rocks at Northton (see section 5.4.4) include soft gouge-bearing faults, grey cataclasite-bearing faults and tension fractures. Samples were taken from faults that cut metanorite and metasedimentary 'semi-pelites' (Mendum, 1982), both previously metamorphosed at amphibolite facies (Fettes and Mendum, 1987). Within the metasediments, the country rock is composed of garnet-biotite gneisses, with additional amphibole present in the metanorite. The grey cataclasites sampled are of similar mineralogy in the meta-pelites and meta-igneous rocks, being dominated by zeolites.

5.7.3.1 Fault rocks from the meta-sediments

Three thin sections were obtained from metasedimentary rocks at Northton; one of soft gouge from a NNE-SSW striking fault core, and two samples from a dual slip surface fault with the fault rock from a principal slip surface and tension fractures in the fractured interval sampled.

The boundary between the fault and country rocks is abrupt (Figure 5.24A) with minor fracturing and zeolite-bearing veins << 0.1 mm thick extending into the country rock oblique to the fault rock contact. The gneiss is composed of fine grained biotite (most clasts are 0.1 – 0.2 mm across) and quartz-feldspar masses (crystals <0.1 mm), with feldspar showing alteration to probable sericite. Garnet constitutes < 5% of the rock with crystals < 0.5 mm across. The foliation is poorly defined by discontinuous bands of biotite crystals < 0.5 mm across. Biotite is also seen in random orientations in the intervening quartz-feldspar masses. Quartz bands are up to 1 mm across and display intragranular fracturing, probably as a result of proximity to the fault surface. A large quartz vein with some transgranular fracturing and chaotic brecciation cuts the biotite foliation and is oblique to the fault surface (similar veins are visible in Figure 5.24A).

The fault surface is defined by an abrupt change in lithology to zeolite veins, zeolite cataclasites, and disaggregated country rock clasts, with minor authigenic clay development (Figure 5.24A). Within the veins, zeolite crystals are euhedral, up to 1 mm across and random orientated, with pore space existing in some areas (Figure 5.24B). It seems likely from these observations that zeolite veins developed under high pore fluid pressure conditions and grew into open fluid-filled cavities. Much of the matrix of the cataclasite is composed of brecciated, randomly orientated zeolite crystals generally less than 0.1 mm across. These are, however, cross cut by veins of euhedral randomly orientated zeolite crystals up to 0.2 mm across that do not appear to be deformed (Figure 5.24B). This indicates a degree of crystal growth and mineralisation post-dating

brittle faulting. These euhedral crystals are seen surrounding clasts of chaotically brecciated country rock up to 0.2 mm across. Cross cutting this latest zeolite, and associated with clay-filled porosity, are nearly isotropic crystals of probable analcime (Figure 5.24B), up to 0.4 mm across. These crystals are again in-growing into pore spaces, which, in some cases, have been infilled with authigenic clay. Further brown authigenic clay alteration is seen in patches and in a poorly defined bands sub-parallel to the wall rock contact (Figure 5.24C). Biotite crystals within the fault core are partially disaggregated and 'shredded' with fracturing along cleavage planes. Quartz clasts within the fault are much disaggregated.

In the area between these dual slip surfaces, zeolite veining propagating from the fault surfaces cuts intact gneiss and quartz veins. Multiple phases of veins appear to be present, with parallel thinner zeolite veins (< 0.2 mm thick) and two larger veins (up to 2 mm across) oblique to the thinner veins. Within the larger veins, zeolite crystals around 0.2 – 1 mm across support disaggregated crystals derived from the immediate country rock that are up to 0.3 mm across. Other zeolite veining in the area shows this same relationship (e.g. Figure 5.24E - F), indicating that a degree of brecciation occurred with emplacement of the veining fluids. This suggests these fractures may be related to tensile hydrofracture and transiently high pore fluid pressures existing along the fault planes.

One thin section was produced from soft gouge taken from a fault cutting metasedimentary country rock and was also studied using SEM (Figure 5.25). As observed in the field, the gouge is not foliated (Figure 5.25A - B). Clasts up to around 1 cm across entrained into the gouge are assumed to have originated from the country rock and are composed of quartz-biotite gneiss, with biotite constituting approximately 40% of the clasts, with the remainder being composed of quartz. These clasts are wrapped by a yellow-brown clay-rich mass (Figure 5.25A - B) that supports a chaotic breccia of disaggregated quartz, dominantly altered feldspar, and altered biotite crystals. Biotite appears to be altering to brown clay minerals, and these constitute approximately 40 % of the matrix. Patches (constituting < 10% of the rock) of cataclasite are composed of quartz-feldspar aggregates with crystal sizes < 0.1 mm. In these areas, feldspars appear unaltered, but in the majority of the matrix feldspar is totally sericitised and highly altered, constituting approximately 20-30% of the matrix. The remainder of the matrix is composed of angular quartz fragments up to 1mm across that are entirely surrounded by authigenic clay and fine grained sericitised, highly altered feldspar fragments. A calcium-rich zeolite dominated vein (determined from EDX) with radial crystals up to 1.5 mm in length is surrounded by altered feldspars and is brecciated (Figure 5.25A and C-D). Other zeolite veins are also brecciated within the matrix, indicating that this phase of zeolite veining is pre- or syntectonic. Under SEM, the zeolite vein clasts are chaotically brecciated and cemented in a surrounding matrix of authigenic

clay, probably of the smectite group, that apparently lacks a syntectonic foliation (Figure 5.25C – D). Altered biotite shows evidence of kinking deformation, whilst feldspar is highly altered to sericite (Figure 5.25E – F). The lack of foliation or wrapping of clasts by clay minerals in the clay rich matrix indicates clay mineralisation was post-tectonic.

5.7.3.2 Fault rocks from the metanorite

Two samples were obtained from an intermediate-scale fault within metanorite rocks shown in Figure 5.14D-G, and one sample was obtained from a zeolite-calcite vein nearby. Within the metanorite, amphibole is more common than biotite, but the rock texture and composition is very similar to that described above for the meta-sedimentary rocks. In the field, the wall rock contacts with faults were observed to be abrupt with multiple zeolite veins of seemingly random orientations propagating away from the contact. In thin section, the fault rock is similar to that described within the metapelite - it is heavily veined and the majority of the fault rock (at least 60%) is constituted of fine grained zeolite crystals that are generally less than 0.1 mm across. This zeolite matrix supports disaggregated clasts of country rock, and further large lithic clasts (larger than slide dimensions) of cataclasite that are very similar in texture and appearance to the background matrix. A mass of quartz crystals 5 mm across and composed of crystals of approximately 0.5 mm size may have existed as a vein within the country rock originally. This quartz displays transgranular fractures following grain boundaries and cutting through the crystals. These fractures are often open, and associated with cavities up to 0.05 mm across. It seems unlikely that this porosity production would have pre-dated zeolite crystallisation, and this may represent a late fracturing event. This quartz is surrounded by the equant zeolite matrix and chaotically brecciated lithic clasts.

Several examples of zeolite-calcite veins were observed in the field. In thin section these are revealed to be radial growths of zeolites up to 5-6 mm across that must have grown into a fluid filled cavity (Figure 5.24D). Zeolite is visible supporting chaotically brecciated country rock (Figure 5.24E - F), again suggesting high pore fluid pressures. Calcite envelops laths of zeolite in the cores of zeolite veins (Figure 5.24F), indicating that its formation post-dates zeolite mineralisation and fills remaining porosity.

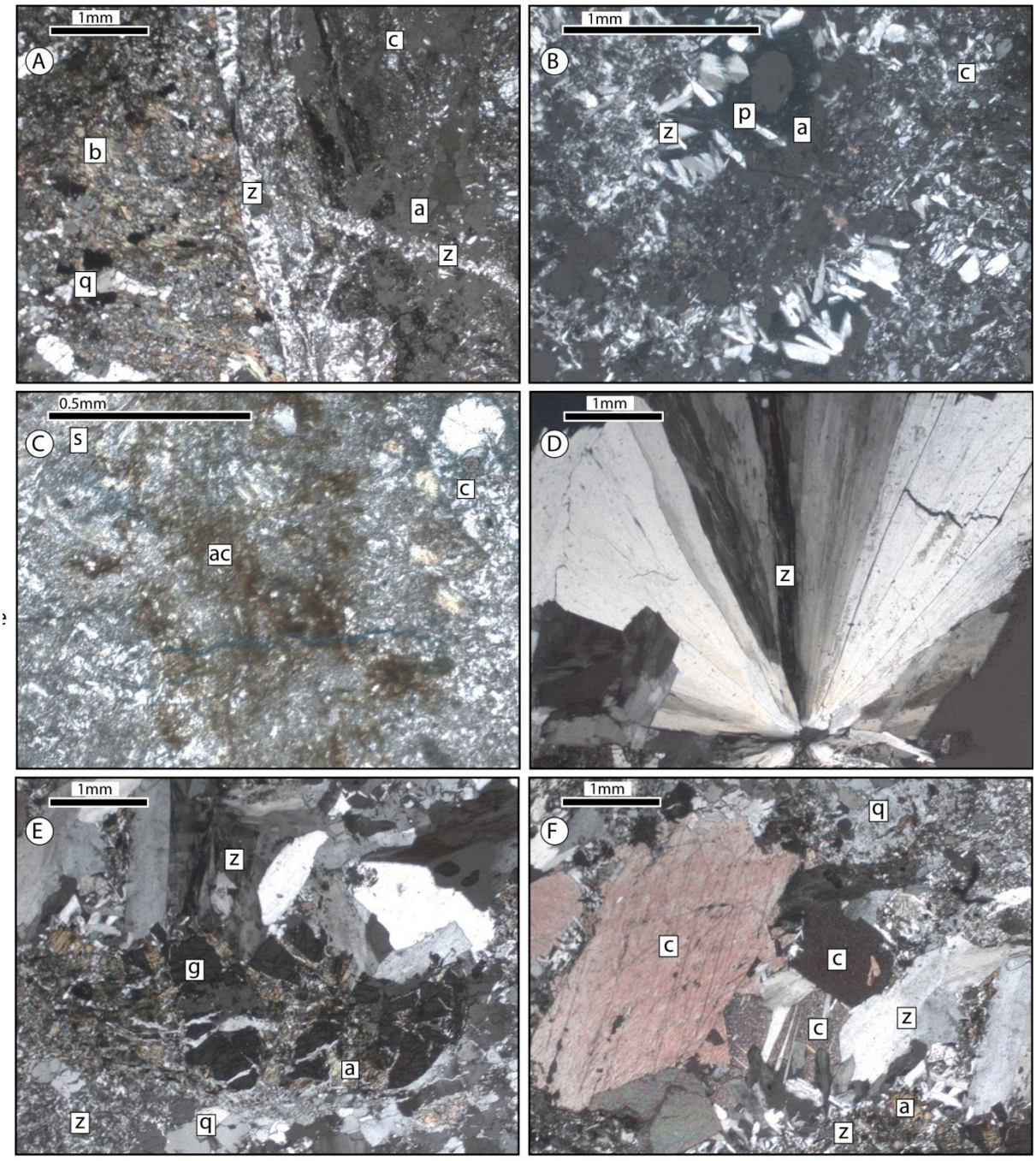

Figure 5.24: Photomicrographs of cataclasite and vein samples from Northton (localities from NF 9862 9012 to NF 9896 8895). (**A**) XPL. Biotite gneiss (b) with quartz veining (q) cut by zeolite (z) and analcime (a) veined cataclasite (c). (**B**) XPL. Higher resolution of cataclasite (c), showing much zeolite mineralisation (z) and analcime (a) crystallised within porosity (p). (**C**) XPL. Authigenic clay (ac) associated with sericitised feldspar (c) and zeolite. (**D**) XPL. Part of zeolite vein showing large zeolite (z) crystal with radial extinction. (**E**) XPL. Large zeolite crystals (z) cementing brecciated amphibole (a), garnet (g) and quartz (q). (**F**) XPL. Sporadic calcite mineralisation (c) associated with zeolites (z).

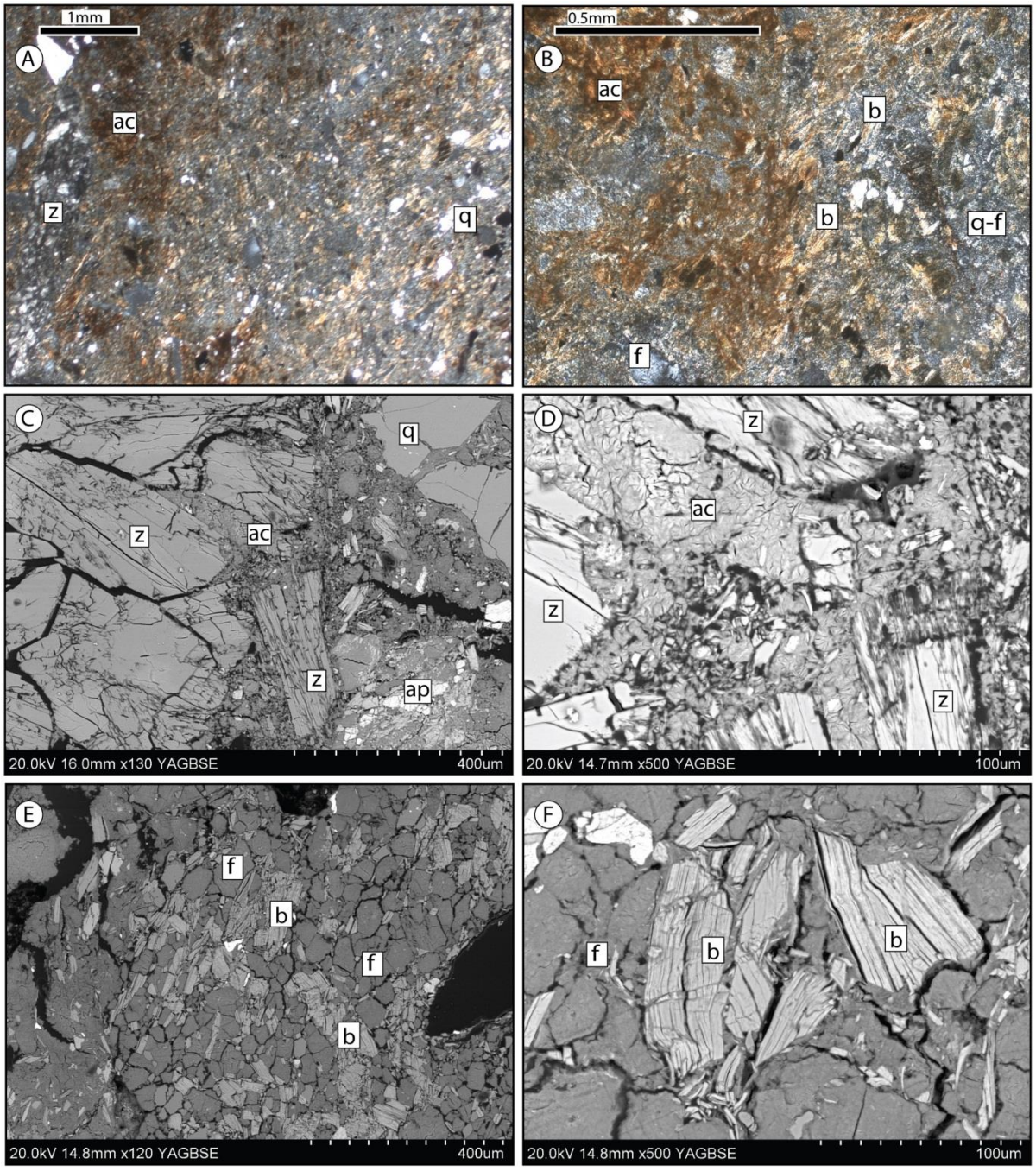

Figure 5.25: Photomicrographs of gouge collected from fault at Northton (from fault at NF 9854 8976). (**A**) XPL. Fault rock overview, showing authigenic clay with no overall foliation. Fragments of quartz (q) and feldspar are present. Zeolite mineralisation is brecciated (z). (**B**) XPL. Higher resolution image of (A). Authigenic clay (ac) developing from relict biotite grains (b). The matrix is composed of fine grained quartz-feldspar masses (q-f) where feldspar is highly altered. (**C**) BSEM image. Brecciated Ca-rich zeolite vein (z) brecciated in authigenic clay-bearing fault rock with clasts of country rock (q = quartz). Bright white mineral is apatite (ap), probably incorporated from the wall rock. (**D**) BSEM image. Higher magnification image of C, showing brecciated zeolite (z) within authigenic clay (ac) with a post-tectonic fabric. (**E**) BSEM image. Altered incorporated wall rock, with highly altered feldspar (f) and biotite (b). (**F**) BSEM image. Higher resolution image of E, showing highly altered feldspar (f) and kinked bioite (b).

5.7.3.2.1 Conditions of faulting at Northton

The presence of analcime in the cataclasites suggests temperatures of less than 150°C (Frey, 1987). It is likely that the earlier phase of zeolite, which the analcime cross-cuts, represents similar conditions. With a normal geothermal gradient of 30°C km^{-1}, this is indicative of depths of 5 km. Within the gouge, authigenic clay with no fabric indicates post-tectonic overgrowth. Smectitic clays have been known to form at temperatures as low as 120°C within hydrothermal systems and fault zones (Steiner, 1968; Warr and Cox, 2001), indicating depths of 4 km. This clay may have formed from an altered ultrafine matrix of fault rock, similar to the fault rock seen at Beitearsaig.

5.7.4 Summary of microscopy observations

The following points can be summarised from the above observations from microscopy work:

- The NW-SE striking sericite-chlorite fault breccia at Grose Bay is indicative of higher temperature and pressure conditions than those associated with fault rocks of post-Caledonian age, with the presence of chlorite indicating relatively higher temperature and pressure conditions. This breccia is associated with a lineament that also displays zeolite- and foliated clay-bearing faulting (seen at Luskentyre Old Road). Evidence for the presence of this zeolite and clay bearing phase of faulting at Grose Bay may be represented by late authigenic clay alteration and open porous fractures in this breccia that cross-cut the earlier fault rock.

- NNE-SSW to NE-SW striking post-Caledonian faults that pre-date camptonite dykes in the area of SW Harris (Northton area) are characterised by zeolite and analcime mineralisation crystallised within open porosity, most likely associated with high pore fluid pressures. Soft gouge-bearing faults at Northton are not foliated, implying that the smectitic clays observed developed after faulting had ceased. High pore fluid pressures are confirmed by the common presence of zeolite-filled tension fractures. Calcite mineralisation postdates zeolite mineralisation.

- Mesozoic and younger faults are dominated by syntectonic clay gouges and cataclasites with calcite, zeolite and authigenic clay mineralisation. Faulting must have been accompanied by fluid flow, necessary for the transport of species in the formation of these new minerals, occurring at low temperatures and pressures. Clay-dominated gouges and breccias linked with NW-SE striking faults do not necessarily have the same mineralogy- the Scalpay North Harbour Fault contains illite-dominated fault rock, and that

at Beitearsaig is associated with smectite. Fault rocks from the North Harbour Fault are suggestive of potentially higher temperature and pressure conditions than those at Beitearsaig.

The fault rocks studied are brittley deformed, with deformation mechanisms dominated by cataclasis. The rounding of quartz grains within faults at Scalpay and Beitearsaig is indicative of rolling and attrition during cataclastic flow within the fault, and the relative weakness of feldspar to quartz is indicative of low temperature deformation (<300°C (Passchier and Trouw, 1996 p62)). Disaggregation of feldspar was enhanced by rotation within the fault rock and disaggregation along cleavage planes.

5.8 Discussion

5.8.1 Lineament analysis

Similar to chapters 3 and 4, the lineament analysis was used as a guide to determine the dominant orientations of faulting and the location of major lineaments on the island. This analysis indicated that two main trends exist on Harris: N-S to NNE-SSW, and NW-SE trending lineaments. As seen in Figure 5.5, the longest lineaments are NW-SE trending, and are probably the youngest in age. Although N-S/NNE-SSW trending lineaments are common, they are relatively short features. These lineaments may be subsidiary features hard-linked to the major NW-SE lineaments, or maybe related to the faulting observed in SW Harris that post-dates camptonite dykes. When compared to the fieldwork data (Figure 5.3), disparities can be explained by a lack of sampling of lineaments from specific areas of fieldwork such as SW Harris, and the lack of lower angle structures picked during the lineament analysis such as detachments found at Rubha Vallerip.

5.8.2 Fieldwork: Faulting synthesis for Harris

Faults have been grouped on the basis that similar fault rocks will form under similar conditions and hence at similar times. The mineralogy of clay-rich fault rocks have been found to be dominated by their environments of formation, with only minor influence from the country rock composition (e.g. Klima et al., 1988). Hence these faults can be grouped and ages can be assigned to these faults on the basis of their mineralogy, cross cutting relationships, comparison to previous work and results from other chapters. On this basis, the following fault phases have been identified on Harris (from section 5.4.5 and section 5.6). These are chronologically ordered below, as determined by cross cutting relationships. Features that are believed to be broadly contemporaneous share the same numeric.

1.a *Formation of the South Harris Igneous Complex (SHIC), South Harris Shear Zones (SHSZ) and mylonite within the OHFZ - Proterozoic.* Intrusion of the SHIC into pelitic rocks of the Leverburgh and Langavat Belts occurred during the Proterozoic (Friend et al., 2001). Shearing along these belts, forming the SHSZ, also occurred during the Proterozoic (Imber et al., 2002). The origin of the reactivated steeply-dipping NW-SE striking mylonitic foliation at Grose Bay is not clear, but is likely to be early. The north side up kinematics identified here could indicate uplift to the north contemporary with Laxfordian and Grenvillian age across the SHSZ (Cliff and Rex, 1989; Imber et al., 2002).

1.b *Pseudotachylite-, epidote- and chlorite-bearing faulting associated with crush zone development – Caledonian or older.* Massive pseudotachylite was observed on western Harris, and although it is not possible to give this faulting an age, it seems likely this is related to Precambrian and Palaeozoic events discussed elsewhere (e.g. Kelley et al., 1994; Imber, 1998; Sherlock et al., 2009; Imber et al., 2002). Pseudotachylite was cut by a probable epidote-bearing thrust fault at Borve. These faults often localise along pre-existing lithological contacts with reverse offsets. At Rubha Vallerip (within the OHFZ), very well indurated zones of cataclasite, breccia and pseudotachylite occur, cross cut by epidote-bearing faults and phyllonites (Imber, 1998). These zones may be similar to the 'crush melange' of North Uist (Sibson, 1977a).

1.c/ 2.c? *Epidote-bearing faults – Caledonian and late Caledonian age.* Similarly with Lewis, there are likely to be several phases of epidote cataclasite bearing faults: Epidote cataclasite is found predominantly associated with NW-SE and NE-SW striking structures with strike-slip or near strike-slip kinematics. Faults with these characteristics are found at Beitearsaig, Grose Bay, Rubha Vallerip, and Northton. The faults cross-cut earlier pseudotachylite and 'crush breccias' and the phyllonite at Rubha Vallerip, however at Luskentyre, epidote cataclasite is cut by pseudotachylite. Hence, multiple phases of this faulting are present or faulting or pseudotachylite development and epidote cataclasite fault developed contemporaneously. As the type 1 detachments fault rocks are epidote bearing, it is possibly that epidote cataclasite faulting occurred around the time of Type 1 detachments (phase 2.b). Clay gouge bearing later faulting often reactivates pre-existing epidote-bearing faults (e.g. at Beitearsaig) and some epidote cataclasites are cut by phyllonites and related detachments.

2.a *Phyllonite development – late Caledonian? (Imber, 1998).* Phyllonites observed by Butler (1995) and Imber (1998) show evidence for thrust, strike-slip and normal kinematics. In fieldwork carried out here, down-dip verging folds and other kinematic indicators were

found to be dominant, probably representing the late extensional (top-to-the-SE) overprint (Imber, 1998).

2.b *Epidote cataclasite-bearing detachments late- to post-Caledonian?* Pale green epidote-bearing cataclasites with normal kinematics were found associated with Type 1 detachments with normal down-dip top-to-the-SE kinematics localising along phyllonites within the OHFZ at Rubha Vallerip (possibly coincident with Type 1 detachments of Imber, 1998). This phase of extensional motion must have occurred at higher temperatures and pressures than subsequent clay-bearing detachment faults, possibly due to collapse following the Caledonian orogeny. On North Uist, these brittle detachments have been attributed to increases in pore fluid pressure during ductile movement on phyllonites by Imber (1998).

2.c? *Epidote cataclasite bearing faults – late- to post-Caledonian?* See phase 1.c/2.c above.

3. *Zeolite-dominated faulting – pre-dating the intrusion of Permo-Carboniferous dykes.* This distinct set of N-S to NE-SW striking faults is prevalent in the Northton region of SW Harris, with calcium-rich zeolite mineralisation overprinted by analcime. These faults cut the foliation at a high angle with only minimal interaction between the faults and the foliation observed. Dominantly dextral strike-slip kinematics were observed on these faults. Fault rock style did not alter between differing lithologies, and is suggestive of low temperatures (< 150°C, Frey, 1987) and low pressure conditions with zeolite and analcime crystallising into pore spaces that were probably open under fluid overpressure conditions.

4.a *Authigenic clay-dominated faults – Mesozoic and Cenozoic dip-slip normal motion faulting along NW-SE lineaments*. There appears to be an anticlockwise rotation from Mesozoic faulting trends observed on Lewis from NNW-SSE, to a NW-SE trend on Harris. On Harris, these NW-SE striking clay-bearing faults are also locally associated with strike-slip motion, found at Luskentyre Old Road, Beitearsaig and Scalpay. Faulting at Beitearsaig and Luskentyre Old Road reactivate pre-existing epidote cataclasite- and pseudotachylite-bearing faults. At Beitearsaig, strike-slip and dip-slip normal kinematics were observed in the same fault rock. It seems likely that strike-slip motion followed normal motion (see below). Smectitic fault rocks represent conditions with temperatures less than 200°C (e.g. Reyes, 1990). Syn-tectonic and post-tectonic zeolite mineralisation observed at Luskentyre Old Road and Beitearsaig indicates temperature conditions of possibly less than 150°C (e.g. Frey, 1987).

4.b *Authigenic clay-dominated faults – Mesozoic and Cenozoic aged detachment faults dipping to the east*. Found localising within phyllonite units within the OHFZ at Rubha Vallerip and Scalpay with normal down-dip kinematics. These faults are composed of soft clay rich gouges and cataclasites incorporating chaotic clasts of country rock. These fault rocks are not foliated, suggesting that these faults may be relatively undeveloped relative to the NW-SE striking faults of 4.c (below). These detachment faults could also be related to very late (Tertiary) faulting on the Minch Fault associated with the development of an Oligocene basin immediately offshore (Figure 5.26, Evans et al., 1991).

4.c *Authigenic clay dominated faults – Mesozoic or Tertiary strike-slip faulting.* Strike-slip kinematics found on E-W, WNW-ESE and NW-SE faults at Luskentyre, Beitearsaig and the North Harbour Fault of Scalpay/Tarbert Harbour may represent late strike-slip faulting that has also been identified in Lewis, or Mesozoic-age transfer faulting between the Minch Fault and faults offshore western Lewis. The most prominent example of this was seen in Scalpay, where the North Harbour Fault shows sinistral strike-slip kinematics. Foliated clay gouge-bearing NW-SE striking faults at Beitearsaig also displayed sinistral kinematics, whilst at Luskentyre dextral kinematics are preserved. Strike-slip faulting was not observed on NNW-SSE striking clay gouge-bearing Mesozoic aged faults in Lewis.

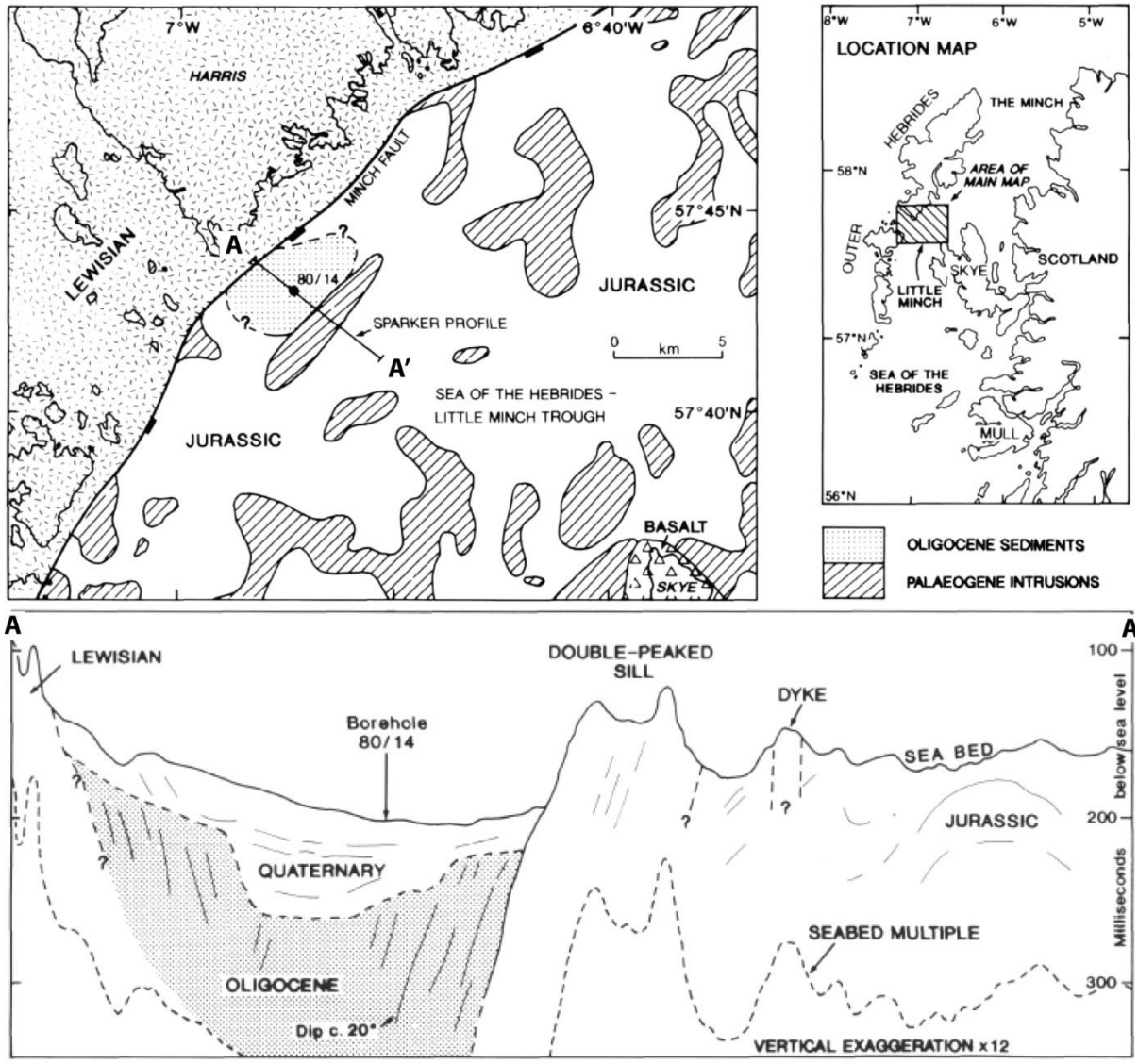

Figure 5.26: From Evans et al. (1991), showing postulated Oligocene Basin immediately offshore SE Harris.

The map in Figure 5.27 shows three soft clay gouge bearing faults identified on Harris with probable significant sinistral displacement (the North Harbour Fault, faulting at Beitearsaig, and faulting at Luskentyre/Grose Bay). WNW-ESE to NW-SE trending faults with sinistral displacements were not observed on Lewis, and are only present within the hangingwall of the Seaforth Fault. The WNW-ESE to NW-SE trend of faults on Harris is rotated approximately 20 degrees anticlockwise from the dominant NNW-SSE trend on Lewis. Several WNW-ESE to NW-SE striking clay gouge-bearing faults are known to reactivate pre-existing faults (e.g. epidote cataclasite-bearing faults at Beitearsaig), and it seems likely that the presence of pre-existing faults striking WNW-ESE to NW-SE lead to Mesozoic and possibly Cenozoic faulting localising along them.

There are three possible explanations for sinistral displacement along NW-SE striking clay bearing faults on Harris:

1. Strike-slip faulting along these structures may indicate that these faults acted as transfers or lateral ramps between the Minch Fault in the east and faults offshore western Harris during extension on these structures. The fault west of Lewis/Harris has not been interpreted as continuing north of the extrapolated continuation of the Seaforth Fault (Stoker et al., 1993). As discussed in chapter 4, displacement may have been transferred onto the Seaforth Fault from the fault west of Lewis/Harris. Displacement along the Seaforth Fault may also explain the lack of WNW-ESE to NW-SE striking faults on Lewis east of the Seaforth Fault.
2. On Lewis, Tertiary strike-slip faulting has been identified in the OHFZ at Orasaigh (Chapter 4) and in the Stornoway Region (Chapter 3) along steeply dipping E-W striking structures. It is possible that this phase of faulting is contemporary with strike-slip faulting on the NW-SE to E-W striking faults on Harris and Scalpay, whilst on Lewis the misorientation of Mesozoic NNW-SSE striking faults relative to the principal stress orientations during the Tertiary prevented their reactivation as strike-slip faults at this time. The North Harbour Fault is believed to truncate two (Palaeocene-Eocene) dykes (Sibson, 1977b), indicating a Cenozoic age for displacement along it. In addition to late E-W strike-slip faulting on Lewis and Harris, E-W strike-slip faults have also been observed on North and South Uist in work not presented here (see also Sibson, 1977b; Imber, 1998).
3. A basin of Oligocene age is postulated to be present off SE Harris (Figure 5.26) that has been linked to normal movement on the Minch Fault (Evans et al., 1991). If displacement was occurring along the Minch Fault during the Oligocene, the North Harbour Fault at Scalpay may also have been active as a transfer fault. It is possible that strain may have been partitioned between the detachment faults and the WNW-ESE striking North Harbour Fault.

Two principal differences exist between east and west Harris:

- *NNE-SSW trending, zeolite-bearing faults are localised to SW Harris*. The area at Northton where these faults are present is approximately 10 km from the Minch Fault. It seems likely that this area is at the limit of exhumation caused by the Minch Fault, as uplift in individual normal fault footwalls rarely affects areas exceeding 10-15 km distance from the fault (King et al., 1988). It is therefore possible that fault rocks formed across Harris in the zeolite stability zone as seen at Northton, before the intrusion of Permo-Carboniferous camptonite dykes and Mesozoic exhumation due to movement on the

Minch Fault. Zeolite bearing fault rocks may since have been exhumed and eroded on east Harris during Mesozoic normal faulting on the Minch and Seaforth Faults, and some epidote cataclasites may represent the same phase of faulting found in SW Harris associated with zeolite. Unfortunately no camptonite dykes were observed in east Harris, so this hypothesis could not be tested to see if epidote cataclasite faults cross-cut camptonite dykes.

- *The localisation of detachment surfaces onto phyllonites within the OHFZ.* Phyllonites are weak relative to the surrounding intact quartzo-feldspathic gneisses. Their proximity to the major Mesozoic and possibly Cenozoic Minch Fault just offshore is likely to explain their reactivation with normal faulting.

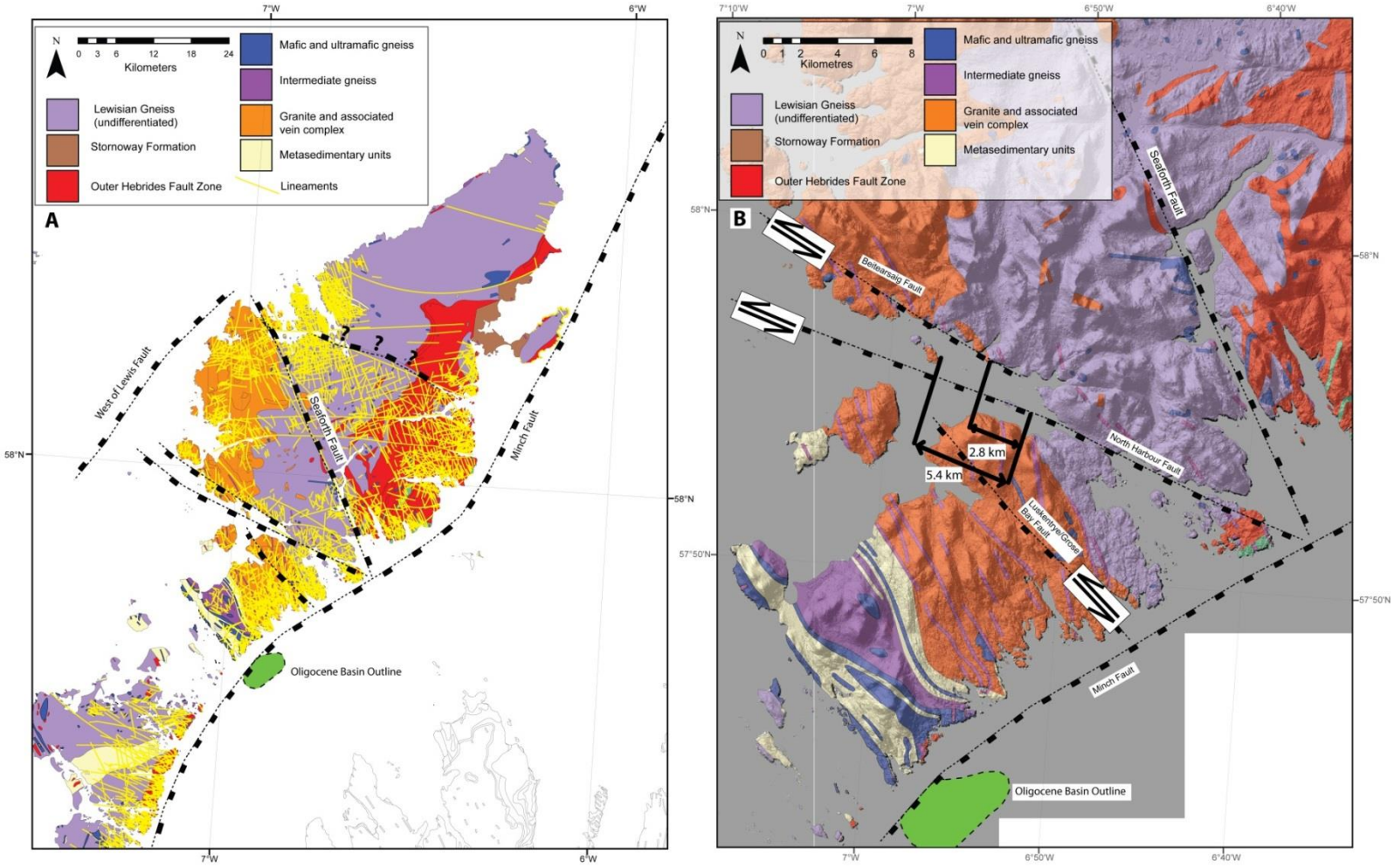

Figure 5.27: (**A**) Digitised major structures on Lewis and Harris. (**B**) Sinistral dominantly strike-slip displacements on faults indicated. Potential measurable offset across the North Harbour Fault is shown.

5.8.3 Basement structural controls on faulting

The effect of the basement foliation on faulting is most obvious within the OHFZ at Scalpay and Rubha Vallerip, where phyllonites and mylonites are often observed being reactivated by brittle foliation-parallel detachments. At Rubha Vallerip and Scalpay, detachments are localised along phyllonite foliation planes. Detachments are also present to a lesser extent within the pervasive mylonite of Scalpay, although this may be due to the presence of now reworked discrete phyllonites (e.g. Imber, 1998). These faults are not observed elsewhere, and their dominant localisation within weak phyllosilicate-dominated units suggests that weak foliation is very important in their development. Elsewhere, the gneissose foliation is locally reactivated by faulting. At Borve and Scarasta, relatively old faults (epidote and pseudotachylite bearing) are observed cutting the foliation obliquely and reactivating the foliation in places as part of ramp and flat structures. At Grose Bay, a large breccia zone reactivates the foliation of a mylonite zone < 10 m thick. The fault is probably continuous along the lineament that cuts through this locality and is continuous with outcrops on Luskentyre Old Road, where epidote cataclasites and soft foliated gouges were also found parallel with the trend of the lineament. More generally, foliation-parallel faulting and reactivation of the foliation has been important throughout the history of the OHFZ and the Lewisian Gneiss Complex of Harris in general.

On the Scottish mainland, 'ladder fracturing' was found to be important within the major ductile Canisp shear zone (Pless, 2011), where fracturing across the foliation and fracturing along the foliation produce a mesh-like geometry (Pless, 2011). In the Leverburgh Belt, only very limited occurrences of 'ladder fractures' of the type seen at the Canisp Shear Zone on the mainland are present. Otherwise, this geometry was not observed in the Outer Hebrides.

5.8.4 Brittle fault rocks: conditions of formation

The earliest brittle deformation is visible in the form of pseudotachylites, probably formed at minimum depths of 4-5 km and possibly deeper (Sibson, 1975). Fettes et al. (1992) suggest a depth of 13.5 km for the formation of pseudotachylite in SE Lewis. Epidote cataclasites are likely to be associated with temperatures of at least 200°C associated with the formation of epidote (e.g.Bird et al., 1984; Frey, 1987; Reyes, 1990; Liou, 1993), suggesting depths of at least 6-7 km with a normal geothermal gradient of 30°C km^{-1}. However, the geothermal gradient is likely to have been higher during periods of tectonic activity, particularly associated with normal faulting and rifting where geothermal gradients may have been > 50°C km^{-1} (Allen and Allen, 1990), and so epidote mineralisation could have occurred closer to the surface.

At Northton, soft gouge-bearing faults are present with a post-tectonic fabric (i.e., clay within the faults developed after fault movements). This suggests that the present phase of clay mineralisation has replaced the fault rock matrix, likely composed of very fine grained gouge. The presence of syntectonic zeolite mineralisation alongside analcime confirms low temperature and pressure conditions for the formation of these rocks. Extensive zeolite mineralisation is found as non-brecciated veins, cataclasite cement, and brecciated within fault rocks dominated by zeolite with high Ca:Na ratios. Temperature, pressure, pCO_2, ionic strength and water activity all influence the kind of zeolite produced (e.g. Hay, 1978; Weisenberger, 2009). Increasing the chemical activity of water, pCO_2, and ionic strength (i.e. concentration of ions in solution) all favour the crystallisation of less hydrous zeolites over more hydrous ones, including calcium-rich zeolites such as laumontite. High Ca content zeolites are stable only if the pCO_2 of a fluid is very high, and this also destabilises carbonates (Frey, 1987), possibly explaining the relative paucity of carbonates cements discovered in the Northton area. However, alongside the Ca zeolites, analcime is also present, possibly post-dating the Ca-rich zeolite. As analcime is an entirely Na zeolite, it seems unlikely that this formed from the same fluid as Ca zeolite, and instead represents a different fluid composition with higher pCO_2 and Na content, possibly indicating the influx of saline water, i.e. several phases of fluid migration have occurred through the faults. It was not possible using the techniques available to identify which species of Ca zeolite exists.

At Grose Bay, the presence of porosity along fractures cutting sericite-chlorite cemented fault breccia appears unrelated to the faulting that produced very well indurated sericite cemented breccia. This is suggestive of a later phase of fracturing reactivating this fault. At Luskentyre Old Road, soft foliated gouge-bearing faults were discovered along the same lineament, and this same faulting may also be present at Grose Bay reactivating the fault breccia. Authigenic clay-bearing faults were observed at multiple localities, commonly with syntectonic smectitic clays constituting the fault rock matrix. As discussed in previous chapters, authigenic clays are associated with low temperature and pressure conditions, probably less than 200°C (e.g. Frey, 1987; Reyes, 1990).

It is interesting to note that faulting at Beitearsaig has not produced the same fault rock as observed at the Scalpay North Harbour/Tarbert Harbour Fault, despite being associated with a near parallel major lineament along strike from the Scalpay lineament, and with similar kinematics. The illite present on the North Harbour Fault is likely to be indicative of higher temperature and pressure conditions than those seen associated with smectitic clays at Beitearsaig (e.g. Frey, 1987; Reyes, 1990). The presence of a higher-grade fault rock may be explained by later exhumation on the Minch Fault with uplift localised to the immediate footwall area (King et al., 1988), perhaps also associated with the Oligocene-age basin postulated off SE Harris (Evans et al., 1991) (Figure 5.27). Scalpay's position in the footwall of the major Seaforth

Fault (chapter 4) may also account for a greater degree of exhumation at Scalpay compared to Beitearsaig.

Soft gouges from Scalpay North Harbour Fault and Beitearsaig are indicative of the formation of fault rock under low temperature and pressure conditions. Work by Klima (1988) suggests that the dominant control on clay-rich fault rock composition is dependent on tectonic setting, rather than the composition of the parent rock. This suggests that these two localities experienced different styles of faulting, agreeing with observations of solely strike-slip faulting at Scalpay, and dip-slip and strike-slip faulting at Beitearsaig. At both localities it is clear that fluids have migrated along the faults, enabling formation of clay minerals. As suggested by Chang and Chang (2000), initial cataclasis may have enabled fluid flow, with subsequent clay mineral formation reducing the porosity. This is confirmed by observations at Scalpay, where veining radiates from clast-dominated regions in the fault rock. The presence of swelling clays (i.e. smectite) along prominent faults may well have enabled their reactivation as weak faults (e.g. Warr and Cox, 2001).

Taking these fault rock observations into account, the overall P-T history of the region during brittle faulting is one of progressive exhumation that follows on from the earlier ductile exhumation (e.g. Dickinson and Watson, 1976; Fettes et al., 1992; Imber et al., 2001).

5.8.5 Synthesis

Structures found in the field that correspond with prominent orientations in the lineament analysis are shown in Figure 5.28. Disparities in the results between lineament analysis and fieldwork are caused by poor resolution in the remotely sensed data. The results are different to those obtained north of the Seaforth Fault (Chapters 3 and 4), and this may be partly a result of the pervasive NW-SE striking foliation present on Harris that is not generally present on Lewis. In addition, this difference in fault orientations occurs across of the Seaforth Fault, confirming its interpretation as a major structural feature (Chapter 3).

The longest structures on Harris have been found to trend NW-SE. This orientation may well reflect the latest stage of deformation represented by possible Cenozoic strike-slip faulting along WNW-ESE to NW-SE structures observed in the field. This orientation also corresponds with the orientation of the Tertiary dolerite dykes on Harris. Mesozoic faulting is controlled to a large extent by pre-existing structures in the form of pre-existing faults and phyllonite bands.

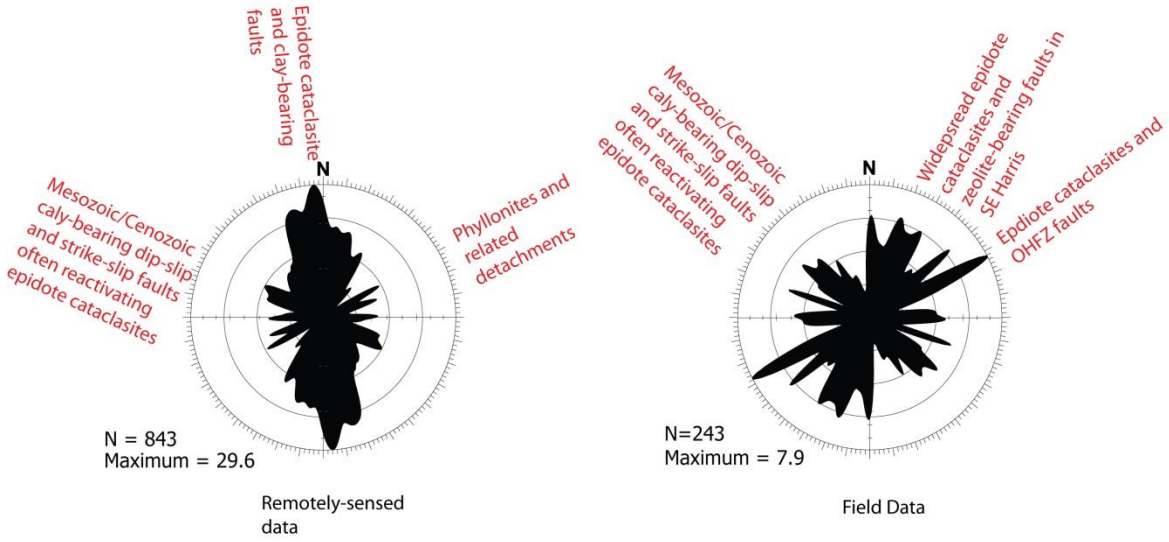

Figure 5.28: Lineament analysis results and fieldwork results from Harris, with interpreted structures from fieldwork indicated in red text.

The geological observations recorded in the field and presented in this chapter allow construction of a conceptual structural fault model for Harris, shown in Figure 5.29 alongside associated fault rock photomicrographs. Fault rocks are similar to those identified in chapters 3 and 4. Pre-Mesozoic fault rocks include pseudotachylite; epidote/chlorite/sericite-bearing cataclasites; and zeolite/analcime-bearing cataclasites (localised to SE Harris). As on Lewis, the youngest groups of faults are fond with authigenic clay, calcite, and zeolite cements and are subsequently dated as Mesozoic/Cenozoic based on similar observation on Lewis (Chapter 3). Porosity is associated with zeolite-bearing faults around Northton, and relatively young (Mesozoic/Cenozoic) structures, whilst earlier fault rocks have no porosity detectable under optical microscopy. Conditions represented by these fault rocks indicate general exhumation of the region since the Caledonian and before. Zeolite-bearing fault rocks along NNE-SSW striking fault localised to SE Harris that predate Permo-Carboniferous dykes may be represented elsewhere on Harris by epidote-bearing cataclasites in areas that closer to and more affected by exhumation in the footwall of the Minch Fault.

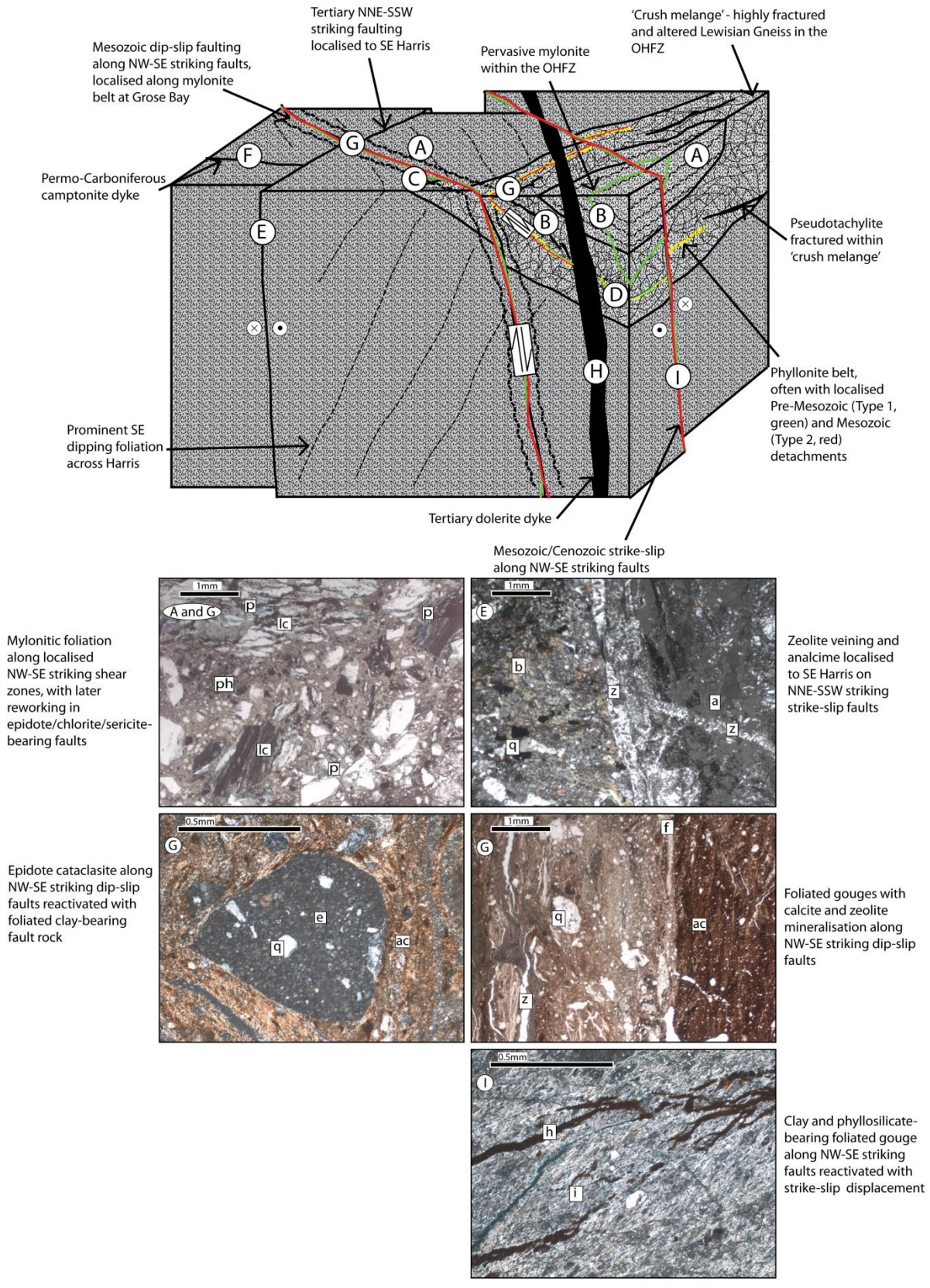

Figure 5.29: Conceptual block model of fault in Harris with accompanying fault rock sections where available. Block diagram: Light grey = OHFZ, dark grey = grey gneiss. Thin section images: p = porosity, lc = lithic clasts of country rock mylonite, ph = phyllosilicate cement, b = biotite, q = quartz, z = zeolite, a = analcime-bearing cataclasite, e = epidote cataclasite, ac = authigenic clay, f = feldspar, h = haematite, i = illite. (**A**) Proterozoic age mylonite in the OHFZ and localised

mylonite band formation. (**B**) Epidote cataclasite-bearing faults, formation of 'crush melange' associated with thrusting in the OHFZ. (**C**) Pre-Mesozoic epidote and chlorite-bearing faults with normal, strike-slip and reverse displacements. (**D**) Phyllonite formation in the OHFZ, with accompanying epidote-bearing (Type 1) detachments. (**E**) Pre-Mesozoic NNE-SSW striking strike-slip zeolite-bearing faults localised to SE Harris. (**F**) Permo-Carboniferous camptonite dyke. (**G**) Mesozoic reactivation of NW-SE striking epidote cataclasite-bearing faults with normal displacement and clay-bearing fault rock, and clay-bearing detachments (Type 2) localising along phyllonites in the OHFZ. (**H**) Tertiary dolerite dyke. (**I**) Cenozoic reactivation of NW-SE striking Mesozoic dip-slip faults and pre-Mesozoic epidote-bearing faults with strike-slip displacement.

5.9 Conclusions

- *What are the ages of faults present on Harris?*

  Multiple fault ages are present on Harris, with pseudotachylites and epidote cataclasites outcropping in similar styles to those noted in the north. Epidote cataclasite-bearing faulting generally strikes NW-SE and NE-SW, and clay-bearing faults commonly reactivate earlier epidote cataclasite-bearing structures. Zeolite-bearing faults that pre-date the emplacement of Permo-Carboniferous dykes are locally widespread in SW Harris.

- *What are the characteristics of post-Caledonian faulting on Harris?*

  NW-SE-striking regional scale faults are found across Harris, with authigenic clay development of smectitic composition and dip-slip normal kinematics that are probably followed by strike-slip motion during the Tertiary. On Lewis, strike-slip faulting was not observed along the main group of Mesozoic faults that trend NNW-SSE, and it is possible that these faults were misorientated for strike-slip reactivation. In SW Harris, zeolite-bearing faults of Permo-Carboniferous age are prevalent. The reason for the localisation of these faults to SW Harris is not clear, but the lack of zeolite mineralisation associated with faults in S and SE Harris may be related to their exhumation (and erosion) due to uplift on the Minch Fault.

- *How does faulting differ between the rocks of the Outer Hebrides Fault Zone and rocks to the west?*

  The main difference in faulting between the OHFZ and area of west Harris is a change in the intensity of faulting. Fault rocks classically associated with the OHFZ are still found in the west, notably a very thick interval of pseudotachylite at Borve. The west does, however, lack the very well indurated Caledonian-aged 'cataclastic gneiss' (e.g. crush breccia, abundant pseudotachylite) that is localised in the OHFZ, observed at Rubha Vallerip. Also, the presence of the OHFZ rocks has allowed localisation of low-angle detachments onto phyllonites – these are not seen in the west.

- *What controls Mesozoic aged faulting on Harris?*

  Pre-existing basement structures are important in controlling the orientation of Mesozoic faults on Harris. The influence of the country rock is most evident within phyllonites of the OHFZ where detachments have localised. Elsewhere, it is very common for authigenic clay-bearing faults of low temperature and pressure conditions to reactivate earlier epidote cataclasites and mylonites. In the west, epidote cataclasite-bearing faults are often observed forming the contact between different lithologies. An exception is the Permo-Carboniferous aged faults of SW Harris. These faults cut the foliation at a high angle, with only one example of a fault 'stepping' through the foliation obliquely. The lack of reactivation of the foliation at these localities is most likely due to the misorientation of the fabric relative to these faults. The dominant NW-SE trending foliation of Harris is paralleled by a series of faults that are most likely at least partly Mesozoic in age.

Chapter 6: Brittle faulting and fracturing in the Clair core

6.1 Introduction

The Clair Field is situated 75 km west of the Shetland Islands (Figure 6.1) and is composed of a ridge of Devonian-Carboniferous red beds of the Clair Group overlying Lewisian-like basement (the Rona Ridge) (Coney et al., 1993). The field contains more than 5 billion barrels of stock tank original oil in place (STOOIP) (Witt et al., 2010), and is one the last giant fields to be exploited on the UK continental shelf. The Clair Field is a nationally important asset, highlighted by the recent (October 2011) announcement by BP of a £4.5 billion investment in the field. Oil at Clair is found primarily within the Devonian-Carboniferous Clair Group, but the oil-water contact lies below the level of the basement high, and connection is suspected across the field through fractures within basement rocks (A Conway, 2010, pers. comm.). Fractures are also known to be important in the cover sequence, which also contains matrix porosity in sandstone units (e.g. Barr et al., 2007).

The large size of the Clair Field has led to it being developed in stages – Phase 1, already in production, comprises the Core, Horst and Graben areas (Figure 6.2). Phase 2 will be composed of the Ridge area. Vertical wells drilled up until 1991 culminated with the 206/8-8 well that proved a success, and this and further wells revealed a linked fracture network that contributed significantly to oil flow (Barr et al., 2007). Wells have since been drilled to target good porosity matrix units and natural fractures identified from seismic data, particularly aimed at intersecting the dominant fracture trends discovered in the wells (Witt et al., 2010; Morton and Milne, 2012). For example, well 206/8-10z was drilled horizontally and was targeted to intersect WNW-ESE striking fractures discovered in well 206/8-8, and was a success (Barr et al., 2007).

Wells at Clair that intersect areas with high matrix porosity and well-developed fracture systems are the most productive. It is therefore important to further understand the fracture systems that exist within the reservoir at Clair, with particular emphasis here on those in the basement – are there transmissive fractures identifiable under the microscope, and why are they transmissible?

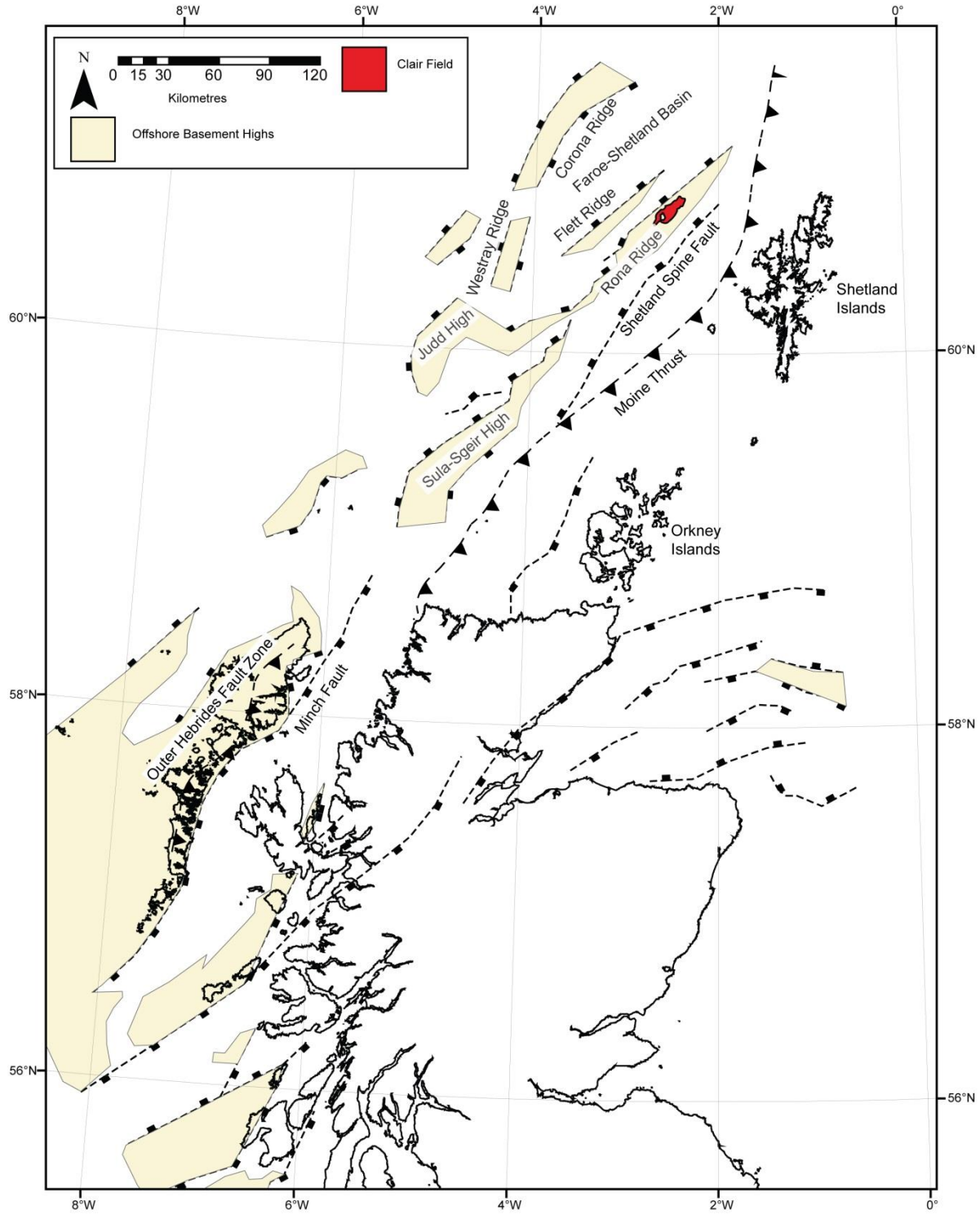

Figure 6.1: Map of basement highs and related Mesozoic faults, showing outline of Scotland. Moine Thrust also shown. Modified from Stoker et al., 1993; Roberts and Holdsworth, 1999; Sorensen, 2003.

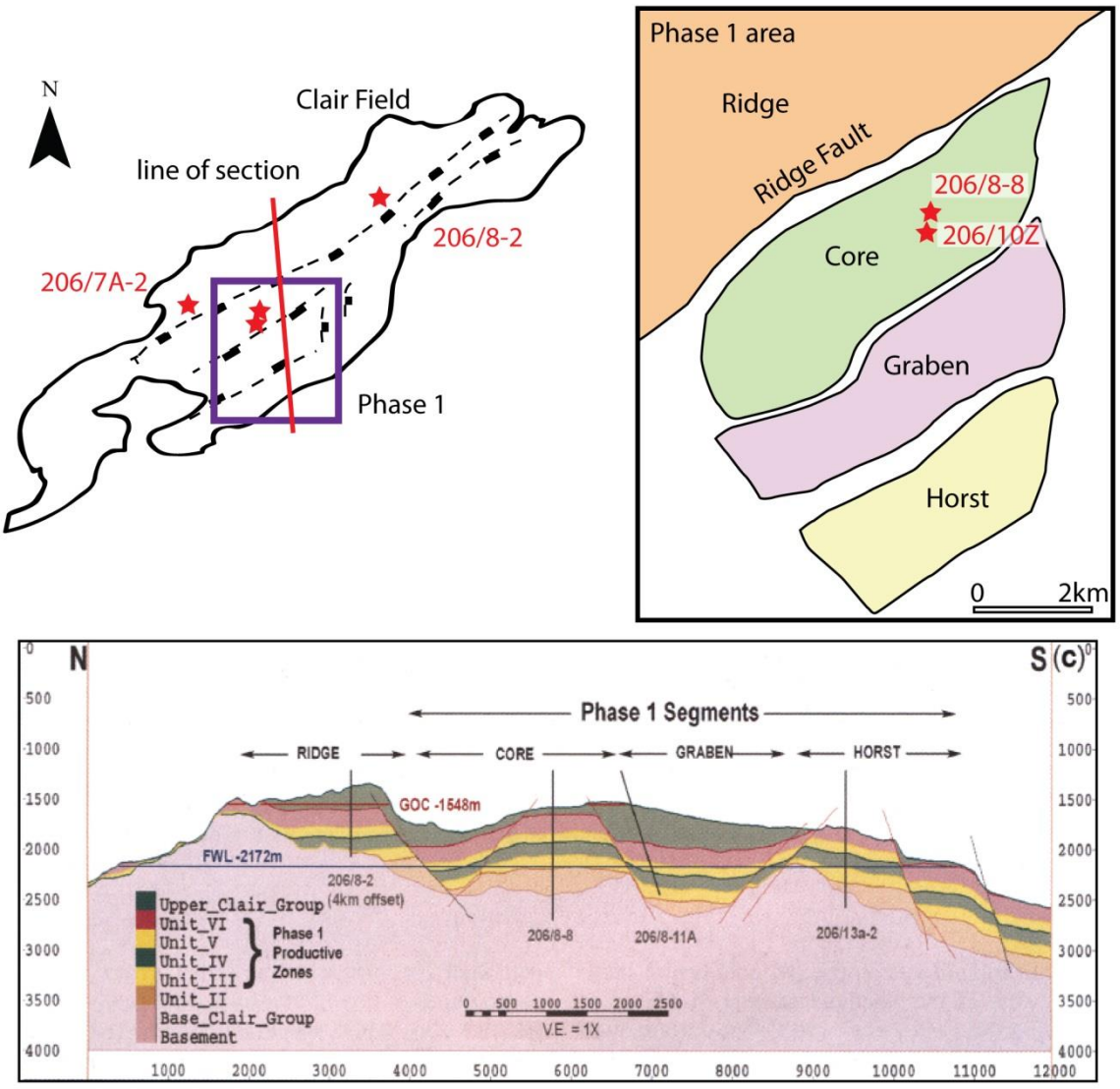

Figure 6.2: Clair Field phase 1 development area, from Witt (2010) and Barr (2007). Wells studied in this work are marked. FWL = Free Water Level (i.e. oil present above this level).

6.1.1 Rationale and Objectives

For the reasons described above, understanding fractures in the Clair Field is important. Hence, core was studied at the Iron Mountain Core Store in Aberdeen over the course of a week, in order to collect both qualitative and quantitative data (i.e. line transect data, see sections 7.4 and 7.6) to address the following questions:

- What are the characteristics and age of faulting and fractures in the Clair Group?
- What are the characteristics and age of faulting and fractures in the Clair basement?
- What are the characteristics of porosity within the Clair Field?
- How does fracturing within the Clair Field compare to the Outer Hebrides?
- What are the controls on fracturing?

These questions have been investigated through a visit to the core store, collection of line transect data, and collection of samples for thin section analysis.

6.2 Geology and Previous Work

6.2.1 Regional Geology

The Faroe-Shetland Basin lies between Shetland and the Faroe Islands on the northeast Atlantic margin. The basin is bounded to the southeast by the Shetland Spine Fault, to the northeast by the Corona Ridge, and to the west by the Westray Ridge. Within the basin, crystalline basement rocks are interpreted to be an along strike continuation of the Lewisian Complex of NW Scotland (Ritchie and Darbyshire, 1984; Hitchen and Ritchie, 1987; Dean et al., 1999).

The basement is overlain by a succession of rocks related to repeated episodes of faulting during the Phanerozoic. This faulting has produced the dominant structures in the Faroe-Shetland Basin, comprised of fault parallel NE-SW to NNE-SSW trending structural highs that were up-faulted in phases. These structural highs may be bounded by reactivated Caledonian structures (e.g. Enfield and Coward, 1987; Dore et al., 1997), or formed as a result of transtension on regional strike-slip faults (Allen and Mange-Rajetzky, 1992). The structural highs contain basement in their cores. The Rona Ridge is one of these structural highs (Figure 6.1), bounded by faults that may have been initiated in the Devonian as the Caledonian mountain belt underwent extensional collapse (Bartholomew et al., 1993; Hinz et al., 1993; Knott et al., 1993). The Devonian-Carboniferous Clair Group is believed to have formed within an endorheic basin in the late- to post-Caledonian orogenic setting (Nichols, 2005), possibly as a result of this extensional collapse (Scotchman et al., 2006). After deposition of the Clair Group, the area was supposedly affected by at least 5 rift events from the Permo-Triassic to the Palaeocene (Dean et al., 1999).

Major NW-SE trending lineaments cross the Faroe-Shetland basin that have been suggested to be transport-parallel transfer zones related to Caledonian thrusting (Enfield and Coward, 1987) and Mesozoic rifting (e.g. Dore et al., 1997). It has also been suggested that these lineaments may represent hydrothermal vent complexes and gas chimneys (Moy and Imber, 2009). NW-SE striking faults offset the ridge-forming NE-SW striking structures (e.g. Goodchild et al., 1999). Following Cretaceous rifting and faulting, Cenozoic inversion attributed to ridge push forces is marked by fault reactivation, folding and the development of unconformities in the Faroe-Shetland Basin (Barr et al., 2007). Igneous rocks of the North Atlantic Tertiary Igneous Province (NATIP) were erupted and emplaced during the period from 62 – 54 Ma (Saunders et al., 1997), with significant hiatuses in activity including sill emplacement and eruption of flood basalts. This magmatism is attributed to the impact of the proto-Iceland plume on the base of the crust (Trewin, 2004).

The Clair Field is situated primarily within Devonian-Carboniferous sediments overlying Lewisian-like basement rocks (e.g. Ritchie and Darbyshire, 1984) of the Rona Ridge, itself considered a potential hydrocarbon reservoir (e.g. Ridd, 1981, note presence of FWL level below the level of the basement rocks of the ridge in Figure 6.2). The Rona Ridge is an elongate NE-SW trending up-faulted basement high that separates the West Shetland Basin from the Faroe Trough. The Ridge Fault separates the ridge (in its footwall) from the core, horst and graben areas of the phase 1 development (Figure 6.2). The Ridge Fault is believed to have initiated during the Devonian (Knott et al., 1993), with the current configuration of ridges and basins of the Faroe-Shetland Basin formed during Cretaceous faulting (Goodchild et al., 1999; Moy and Imber, 2009). Major fault movements elsewhere in the phase 1 area pre-date the Cretaceous, but the ridge bounding faults were active during the Cretaceous and Cenozoic (Barr et al., 2007). The hydrocarbon trap is a four-way dip closure of Late Cretaceous mudstones (Witt et al., 2010). The Clair Group is overlain by the Base Cretaceous unconformity and a thick sequence of Cretaceous mudstones of the Shetland Group, forming the oil system seal (Barr et al., 2007). Overlying the Clair Group, shallow marine sands are overlain by deep-water Shetland Group mudstones (Barr et al., 2007), with further shallow water Cenozoic sands and mudstones.

6.2.1.1 Basement Geology

The geological history of the basement rocks is poorly understood due to a lack of data (i.e., sparse well sampling). Ritchie and Darbyshire (1984) used Rb-Sr dating to produce an age of 2527 ± 73 Ma for basement rocks on the Rona Ridge SW along structural trend from Clair, confirming that the rocks are Archaean in age, and this is very broadly equivalent to the ages determined for the Inverian and Badcallian metamorphic events identified within the onshore Lewisian Complex (Kinny et al., 2005). Quartzo-feldspathic gneisses, granitic gneisses, tonalitic grey gneiss, diorite gneiss and pegmatites identified within the Clair core are similar to lithologies present with the Lewisian Complex onshore mainland Scotland (Pless, 2011). Deep seismic analysis in the basin has determined two-layer continental crust with seismic wave velocities equivalent to those found within mainland gneisses. The upper unit has been inferred to be Laxfordian gneiss, and the lower Scourian (Smith and Bott, 1975).

The Faroe-Shetland Basin lies along strike from the Moine and Lewisian Belts of NW Scotland (Dean et al., 1999). The Moine Thrust has been traced under the Shetland Platform to link with the Great Glen Fault/Walls Boundary Fault Zone (e.g. Ritchie et al., 1987). As the area is along the main structural trend NE of the Outer Hebrides, the Outer Hebrides Fault Zone (OHFZ) has been postulated to underlie the Rona Ridge (e.g. Hitchen and Ritchie, 1987), making study of the Outer Hebrides particularly relevant to the Clair Field.

6.2.1.2 Clair Group Geology

The Devonian-Carboniferous Clair Group onlaps the basement of the Rona Ridge (Allen and Mange-Rajetzky, 1992) and has been divided into upper (units VII-X) and lower (units I-VI) groups comprised of ten lithostratigraphical units (Allen and Mange-Rajetzky, 1992; Nichols, 2005).

In the Upper Clair Group, conductive fractures are thought to be relatively unimportant and the group contains abundant smectite, giving poor porosity/permeability characteristics (Barr et al., 2007). For these reasons it has not been targeted in the current development (Barr et al., 2007; Witt et al., 2010) or studied here. The Lower Clair Group forms the main reservoir (Witt et al., 2010). Details of each unit are shown in Figure 6.3**.**

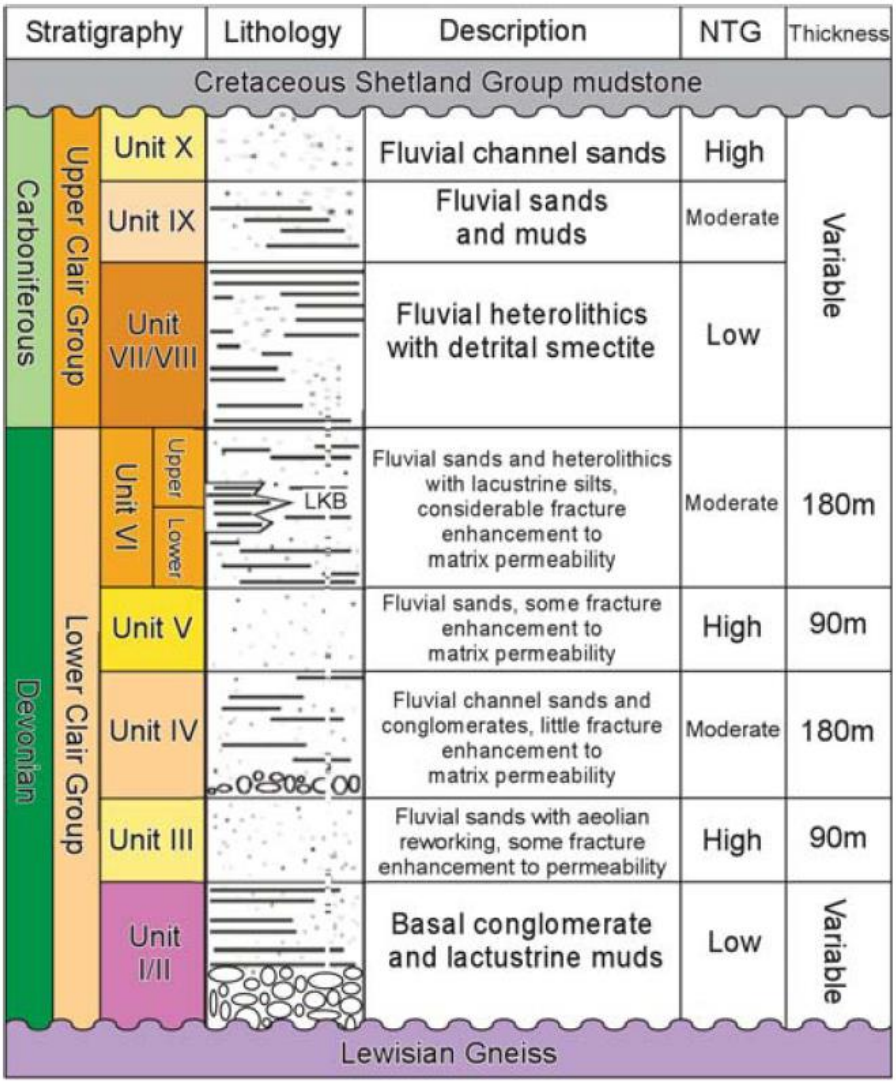

Figure 6.3: Stratigraphic details of the Clair Group (Witt et al., 2010).

6.2.1.3 Fractures in the Clair Field

Fractures at Clair are extremely important in controlling fluid flow and are developed in all units, to varying degrees (Barr et al., 2007; Witt et al., 2010), decreasing in density upwards from the basement (Coney et al., 1993). In the basement, fractures on the ridge are dominated by two main sets: NNE-SSW fractures that truncate the Rona Ridge, and NE-SW to ENE-WSW normal faults (Coney et al., 1993). In northern Scotland, Devonian red beds overlie Moinian basement, studied as an analogue for the Clair Field by Coney et al. (1993). In higher intensity 'fracture corridors' within the Moine basement, fractures were observed to pass up into the cover sequences, but with a general decrease in fracture intensity from 10-30 to 5-10 fractures per metre, with a general background intensity of 1 fracture per m in the red beds and 1-2 fractures per metre in the basement rocks.

6.2.1.3.1 Fracturing in the Basement

Within the basement at Clair, Coney et al., (1993) found the major fault trends to be NNE-SSW and NE-SW to ENE-WSW. The NNE-SSW faults truncate the NE-SW ridge forming faults, producing a 'diamond-shaped' (rhomboidal shaped) fracture network (Coney et al., 1993). It seems likely that these two trends form a polymodal conjugate fault set related to rifting (e.g. Johnson, 1995). Open fractures within well 206/8-8 in the 'core' part of the field were found to trend WNW-ESE and NNW-SSE (Coney et al., 1993). More recently picked fractures within the basement show a predominant strong NE-SW trend (Pless, 2011), originating from ridge parallel faulting, a weaker NW-SE trend, and weak N-S and E-W trends (bottom of Figure 6.4). Pless (2011) does not distinguish the two sets of fracturing identified within the basement by Coney et al. (1993), however this may be due to seismic resolution being too low to distinguish these orientations.

6.2.1.3.2 Fracturing in the Cover (Clair Group)

In the cover sequence, orientated core has been logged for fracture orientation (Coney et al., 1993) and fracture orientations have also been logged from well data (Barr et al., 2007) (Figure 6.5). This has shown that the orientation of open fractures is variable from well to well (Figure 6.5A). Within well 206/8-8, the dominant trend of fractures were found to be NE-SW, parallel with the trend described in the basement above, with a fairly even spread of fractures at other orientations. Open fractures however are concentrated in a WNW-ESE orientation, a trend that is not evidenced in the seismic horizon maps from Pless (2011), shown in Figure 6.4. In the seismic horizon maps (Figure 6.4), the most prominent orientation is NE-SW, matching the orientation

determined from well data by Coney et al., (1993), and believed to be representative of Cretaceous rifting (Pless, 2011).

The increased relative dominance of the N-S trend within the Lower Clair Group may indicate that these faults were initiated in the Devonian as part of the N-S trending rift faults that were active at this time (e.g. Duindam and Van Hoorn, 1987). However, the presence of this orientation of faulting in the overlying Cretaceous rocks does suggest a component of Mesozoic reactivation, possibly representing Jurassic normal faulting (Pless, 2011).

It has been suggested that E-W trending structures reactivate basement fabrics, given their 'clustered distribution' (Pless, 2011). However, while it is likely that these faults are through going into the basement, they do not necessarily have to reactivate pre-existing basement structures.

NW-SE trending structures, close to the trend identified by Coney et al. (1993) as being 'open' and permitting fluid flow, are poorly sampled within the cover sequence seismic horizons of Pless (2011). However, this trend of faulting is much more evident within the basement and several of these faults may offset the Ridge Fault (Pless, 2011). As NW-SE trending structures are not present in the cover sequence seismic horizon maps, they must be early-Devonian or older in age (Pless, 2011). Most of these structures are attributed to pre-Devonian faulting and likened to NW-SE trending shear zones present within the Lewisian Complex onshore (Pless, 2011). However, major lineaments of this orientation cross the Mesozoic Faroe-Shetland Basin, with some clearly displaying a degree of offset (e.g. Moy and Imber, 2009). As Cretaceous faulting formed the current geometry in the basin, it seems likely that if the Ridge Fault is offset by NW-SE trending structures, that these structures are relatively young (i.e. Cretaceous or younger in age). This would agree with the observation of relatively young open fractures within the Clair cores that trend WNW-ESE to NW-SE (Barr et al., 2007). Pless (2011) shows that the longest faults within the basement trend NE-SW (Figure 4.6, page 217), indicating that these structures are the youngest on the Clair Field. It is possible that WNW-ESE to NW-SE open fractures within the Clair Field may be linked to the latest phase of faulting along the NE-SW striking faults.

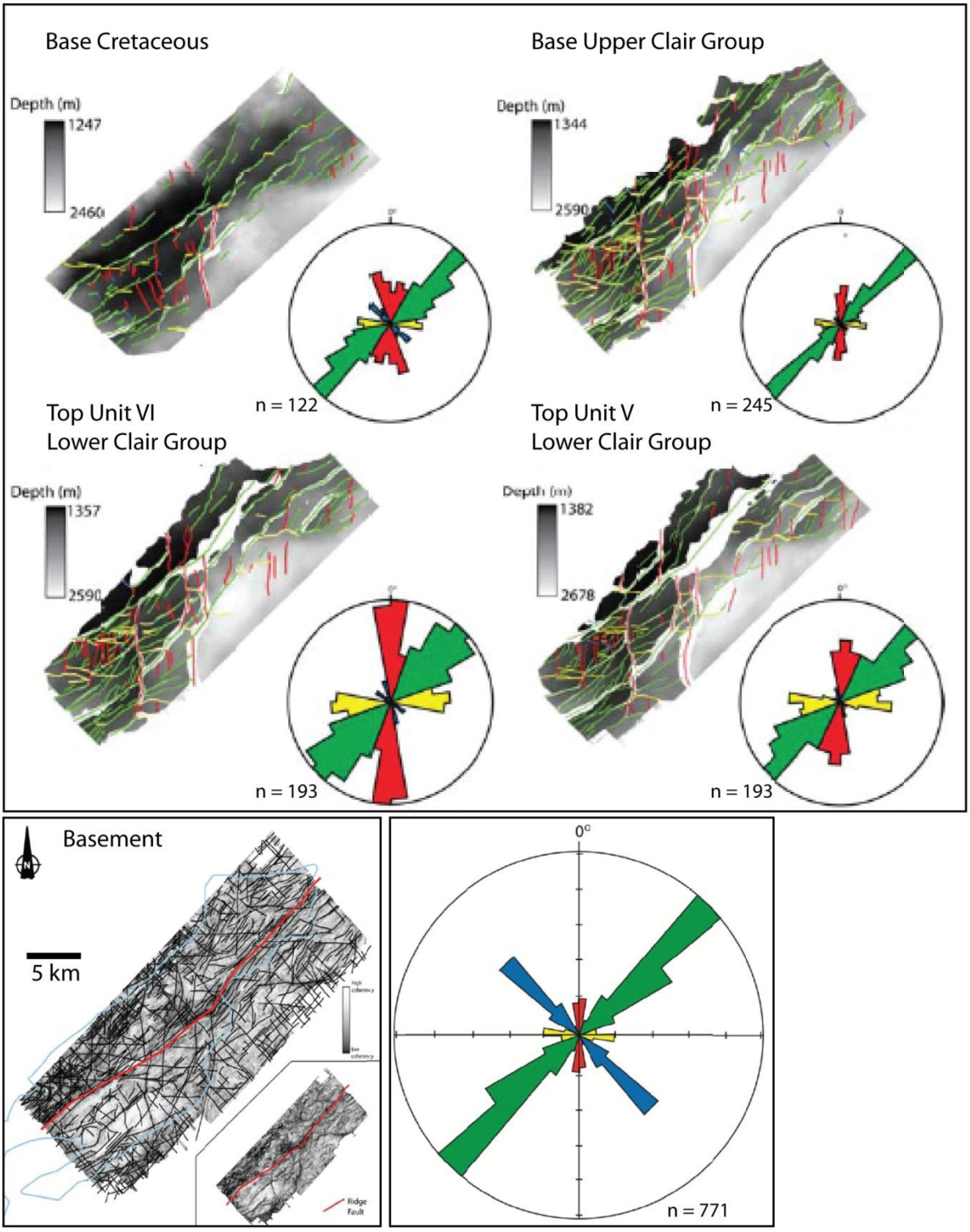

Figure 6.4: Lineaments picked from the cover sequence (top) and basement (bottom) from 3D seismic horizon analysis. From Pless (2011). Basement map picked from coherency attribute.

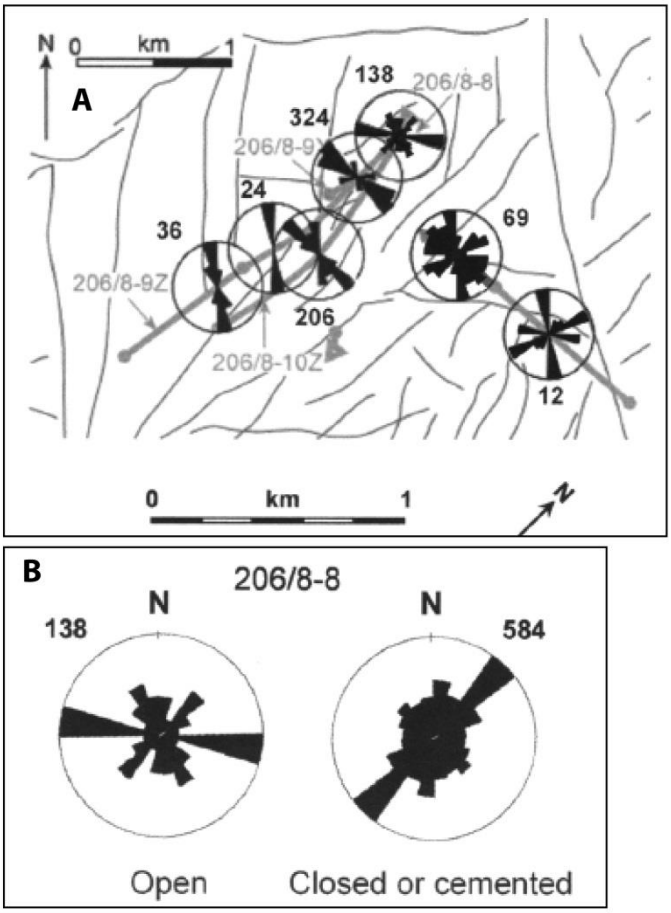

Figure 6.5: From Barr et al. (2007). (**A**) Open fracture strike from well data with number of open fractures seen in each well. (**B**) Open and closed fractures from well 206/8-8.

6.2.1.3.3 Fracture fills

Previous work in the Clair Group cover sequence has analysed fracture mineralisation and chronology in depth (Milodowski et al., 1998), with ten stages recognised in the evolution of fractures in the cover sequence at Clair. From earliest to latest, these are:

1. *Granulation seam development* - Believed to have occurred during the Carboniferous.
2. *Sulphide I mineralisation associated hydrofractures.*
3. *Calcite I mineralisation associated hydrofractures.*
4. *Fluorite mineralisation associated hydro fractures*.
5. *Calcite II mineralisation associated fractures* – Fracturing and mineralisation synchronous with hydrocarbon migration.
6. *Sulphide II mineralisation associated fractures* –Roughly coeval with Calcite II.
7. *Sulphide III mineralisation associated fractures* – Typically found lining open fractures. Synchronous with hydrocarbon migration.

8. *Calcite III mineralisation associated fractures* – Typically found lining open fractures, synchronous with hydrocarbon migration.
9. *Hydrocarbon filling of the Clair Reservoir* – Formation of open fractures.
10. *Late stage fracturing* – Fault brecciation after hydrocarbon filling.

Other phases of veining and alteration are visible within the underlying basement rocks, discussed by Pless (2011) and studied further in this chapter (see section 6.3.4 and section 6.4.2).

6.2.1.4 Oil at Clair

Based on geochemical analysis, the Late Jurassic Kimmeridge Clay Formation is thought to form the source rock for oil at the Clair Field and much of the Faroe-Shetland Basin (Scotchman et al., 1998). Burial history is dominated by extension (Scotchman et al., 2002). Multiple phases of hydrocarbon charges have been identified in the Faroe-Shetland Basin. At the Foinaven Field approximately 100 km southwest of Clair, three phases of hydrocarbon charges have been identified, each associated with rifting and subsidence, and Oligocene-Miocene inversion events (Scotchman et al., 2006). At Foinaven, reactivation of Mesozoic faults allowed migration of the oil into Cenozoic strata. At Clair, observations of the core and Re-Os dating has revealed the following chronology (from Finlay et al., 2011):

1. Basement becomes fractured at or before 72 ± 5 Ma.
2. Pyrite and calcite precipitate as hydrocarbon migrates through basement fracture network to Clair and other West of Shetland fields at 72 ± 5 Ma.
3. A second significant pulse of hydrocarbon migrated through secondary permeability in the fracture network and into the Clair and other West of Shetland fields at 64.4 ± 2 Ma.
4. Later pulses of hydrocarbon occurred further west in the West of Shetland area at 53 ± 14 and 42 ± 6 Ma.

6.2.2 The Clair Cores and Study Locations

These were selected to give a representative sample of faulting within the cover sequence, in addition to sections within the basement and basal conglomerate for comparison to the Outer Hebrides. The locations of these wells are shown in Figure 6.2**.** Cores from the Clair Group were selected for the presence of fault zones as identified by Milodowski (1998). Within the basement and basal conglomerate, only six returned cores contain basement rocks. The three with the longest returned intact basement cores were studied. The selection of cores studied here are:

Cover

- 206/8-8 (vertical well): 1729-1767 m depth, unit VI faulted section.

- 206/8-8 (vertical well): 1887-1905 m depth, unit V faulted section.
- 206/8-8 (vertical well): 2096-2098 m, units III and IV faulted section.
- 206/8-10Z (horizontal well): 2313-2325.8 m, unit V faulted section.

Basement and Basal Conglomerate

- 206/8-8 (vertical well): 2291.5 – 2355 m, basal conglomerate.
- 206/8-8 (vertical well): 2484 – 2500 basement and faulting.
- 206/8-2 (vertical well): 1787 – 1810 m basal conglomerate.
- 206/8-2 (vertical well): 1854 – 1864 m basement.
- 206/7A-2 (horizontal well): Spot cores from basement on the ridge between 2140 – 2600 m.

6.3 Macroscopic Core Observations

6.3.1 Clair Group

Four fault zones identified by Milodowski (1998) were studied within the cover sequence (listed above). The sections studied are described in detail in the appendix (Appendix) and summarised here. The sections are within fluviatile sandstone of Units III – VI within the Lower Clair Group. Milodowski (1998) describes the Lower Clair Group as:

> ''At least 325 m thick, consisting of mainly poorly sorted, very fine to medium grained braided fluvial sandstones with rare pebble lag and fine grained overbank deposits. The sandstone display well-developed horizontal lamination and rough cross-bedded sets, the latter typically forming stacked sequences 10 to 20 cm thick. Thin aeolian sandstones occur towards the top of the unit.''

Grain size varies from shaley laminated mudstone and siltstones with clay lenses, to thickly bedded coarse-grained sandstone. Within fine-grained units porosity is relatively reduced, and this is obvious in the colour of the rock – coarser grained and more porous units are brown with oil staining, whereas carbonate cemented areas and fine grained rocks are not stained. Contacts between oil stained and non-oil stained rock are often abrupt (Figure 6.6A).

The following sequence of fracturing and mineralisation has been determined from observation of the core:

1. *Granulation seam development, particularly in porous sandstones*. May also have occurred after/during initial calcite matrix formation (see 2 below). Granulation seams are planar to anastomosing, usually < 0.5 cm thick and black in colour. This colouration is

believed to result from reduced grain size within the seams and possible clay development, alongside oil staining. In several instances normal kinematics were identifiable from duplex development between overlapping granulation seams, however offset on most of these seams is likely to be small (<5 cm). Larger examples of granulation seams were observed with up to 1 cm of probable authigenic clay within their cores (e.g. Figure 6.6C). This either represents a continuation of shearing along granulation seams, or a reactivation of granulation seams by later faulting (e.g. Fossen and Hesthammer, 1998).

2. *Calcite mineralisation of the matrix and fine grained calcite vein formation*. The earliest calcite veining intensity increases around some of the faults in 206/8-8, and reactivates some granulation seams. (Calcite I; Milodowski 1998). Veins are typically thin (<0.5 cm thick) and white in appearance, with crystals that are difficult to distinguish with the naked eye, and are occasionally associated with fine-grained pyrite (Pyrite I). These veins are more dispersed throughout the cores than later calcite-pyrite veining (see 4 below).
3. *Fluorite veining around some faults in 206/8-8*. (Fluorite I and II mineralisation; Milodowski 1998). Minor amounts of thin (<5 mm thick) discontinuous purple fluorite veins are concentrated around several faults. For further details the reader is directed to Milodowski (1998).
4. *Sparry calcite-pyrite veins concentrated around oil stained areas.* These are associated with faulting and porosity (Figure 6.6E and G) (Calcite II and III; Milodowski 1998). Veins are up to 30 mm across, and are cloudy white to brown in colour. Individual crystals have been observed up to 5 mm across. This coarse sparry calcite occurs alongside euhedral grains of pyrite, with individual pyrite mineralisation up to 30 mm across. Calcite-pyrite veins are surrounded by reduced (green) haloes in the country rock.
5. *Late brecciation.* Late open fractures are present, particularly easily observed within the studied section of well 206/8-10z. The fractures are associated with particularly coarse calcite and pyrite mineralisation as described above, although it is not clear if these open fractures are linked to stage 4 mineralisation. Vuggy porosity up to 1 mm across is found within 1 m of normal faulting that has produced discrete (<1 mm thick) brown, very poorly indurated gouge fault rock.

Granulation seams are present in both porous and non-porous sandstones that are cemented with calcite, but in general granulation seams are much more dominantly observed within the porous, oil filled rocks. This is probably due to the maintenance of open porosity in these rocks. Calcite cemented sandstones that are faulted often develop dispersed zones of breccia cemented with calcite up to 50 cm thick (e.g. Figure 6.6D), rather than the granulation seams seen in the porous rock. This difference in faulting style is likely due to the porous versus non porous nature

of the oil-filled and calcite cemented sandstones (e.g. Aydin, 1978). Granulation seams are thin (~1 mm to 5 mm thick) and appear black within the core, in some areas intense networks of granulation seams are present over ~1 m of core. Later faulting at times localises around the granulation seams, with production of light brown cataclasite that is probably clay rich. Granulation seams are certainly reactivated themselves by faults and cross cut by later calcite-pyrite and fluorite mineralisation (e.g. Figure 6.6C). There is a marked difference in fracturing between sandstones and shales. Within the sandstones, veining is prevalent, oriented perpendicular to the bedding (Figure 6.6E). In the shales veining becomes dispersed, and faulting has produced clay-rich gouges (Figure 6.6E-F). It is not possible to properly assess the thickness of these gouges due to poor recovery but they may be up to 10 cm across. The gouges fizz with acid, indicating the presence of carbonate, and contain slickenlines but these are not preserved in their original orientation. Gouge is also locally injected into the surrounding country rock. In general the faults observed within the cores are not major structures and most of the offsets observed are at the centimetre scale. Faulting and fracturing within the cores is clustered to areas around faults that are associated predominantly with sparry calcite-pyrite veining (stage 4 mineralisation given above). Sparry calcite-pyrite veins often increase in intensity towards faults and calcite-pyrite mineralisation is often found within fault cores (e.g. Figure 6.6B).

Within well 206/8-10z, open elongate pore space (up to 1mm width x 50 mm length) is observed (Figure 6.6H) at times associated with late phase sparry calcite crystals. However, the lack of mineralisation suggests that they post-date phase 4, late calcite-pyrite mineralisation. Faults are also seen with no apparent mineralisation. This suggests a phase of faulting that may post-date late stage calcite mineralisation (Figure 6.6I), agreeing with the observations of Milodowski (1998).

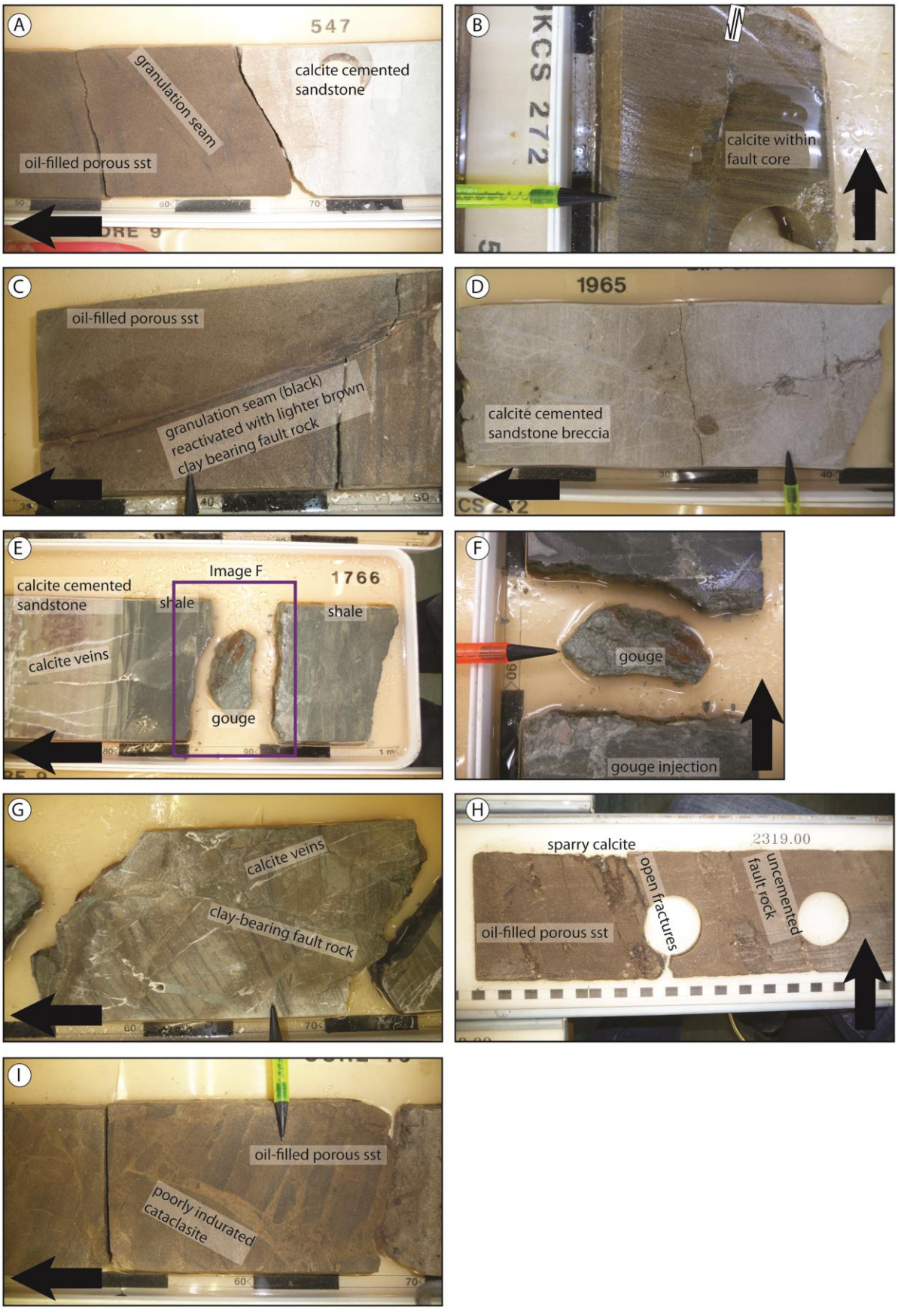
A
547
granulation seam
calcite cemented sandstone
oil-filled porous sst
B
calcite within fault core
C
oil-filled porous sst
granulation seam (black) reactivated with lighter brown clay bearing fault rock
D
1965
calcite cemented sandstone breccia
E
Image F
1766
calcite cemented sandstone
shale
shale
calcite veins
gouge
F
gouge
gouge injection
G
calcite veins
clay-bearing fault rock
H
sparry calcite
2319.00
open fractures
uncemented fault rock
oil-filled porous sst
I
oil-filled porous sst
poorly indurated cataclasite

Figure 6.6 (previous page): Observations from cores of the Lower Clair Group. Arrow marks bedding upwards direction. (**A**) Abrupt boundary between porous oil filled sandstone and tight calcite cemented sandstone. (**B**) Normal faulting associated with calcite mineralisation in the fault core. (**C**) Porous oil-filled sandstone cut by granulation seam (black) reactivated by late possibly clay rich cataclasite. (**D**) Calcite cemented sandstone and breccia. (**E**) Clay gouge localising within shale layer. Note also porous sparry calcite veining localising within more competent fine sandstone unit (left). (**F**) Higher resolution image of (E) showing fault gouge. Brecciated clasts of intact country rock within the gouge. (**G**) Porous sparry calcite veining localised within fault breccia. (**H**) Sparry calcite and pyrite mineralisation localised around minor normal faulting with normal offsets. Note presence of vuggy porosity associated with this faulting. (**I**) Uncemented fault rock, with lighter brown matrix composed of clasts derived from the country rock and probable clay.

6.3.2 Basal Conglomerate and Basement-Cover Interface

6.3.2.1 Basal conglomerate

The basal conglomerate of the lower Clair Group overlies Lewisian basement unconformably. Milodowski (1998) describes this conglomerate as follows:

> "This breccia ranges in thickness from 30 to 120 m in thickness. It consists of proximal to mid-fan conglomerates interbedded with flat to cross-bedded and pebbly, sheetflood sandstones, and thin red mudstones deposited in inter-fan lakes."

The basal conglomerate has been studied in cores 206/8-2 (22 m) and 206/8-8 (63 m and 2 m from separate cores). The conglomerates are clast supported and comprised of clasts with highly variable lithology (e.g. Figure 6.7H). Clasts are derived from crystalline basement rocks with occasional clasts of sandstone. Silicic, intermediate, and mafic composition rocks are present, including granitic and granodiorite gneisses, pegmatites, amphibolites with epidotisation, and diorite gneisses (e.g. Pless, 2011). Clasts are sub-angular to sub-rounded and vary in size from greater than 50 cm to less than 1 cm, and are typically around 10 cm across in size. In 206/8-2, clast size is generally smaller (typically 0.5 – 10 cm across) and bands of conglomerate are interspersed coarse-grained, bedded red sandstones up to 2. 5 m thick. Within the 206/8-8-core, the conglomerate clearly fines upward from the basal unconformity, where gneiss blocks are up to 60 cm across, to clast sizes of less than 10 cm transitioning into sandstones at the top of the conglomerate. Clasts are set within a fine to medium sand, compositionally immature interstitial matrix inter-bedded with coarse sandstone units.

The conglomerate matrix is reddy-brown to olive-green. Clasts within this matrix are angular, and dominated by quartz (> 80 %), with the rest being composed of plagioclase, bed-aligned muscovite, opaques, authigenic clays and patchy calcite-cement. Sparry calcite veining up to 5 mm across cuts the matrix, and also replaces areas of the matrix entirely with masses of calcite up

to 3 cm across (e.g. Figure 6.7C). Vertical sparry calcite-pyrite veins within and between clasts are common in both 206/8-2 and 206/8-8, and may be associated with proximity to faulting (Figure 6.7F).

Faulting within the basal conglomerate is associated with authigenic clay development and a reduction in grain size, and displays varying degrees of development. An interval of well-developed faulting within the basal conglomerate was observed between 2335 – 2337 m within core 206/8-8 (Figure 6.7A-E). This faulting was represented by three parallel, well defined clay gouge-filled principal slip surfaces up to 2- 3 cm across, surrounded by up to 40 cm thick chaotic angular clast supported breccias with clay-rich matrix that at times displays a weak foliation sub-parallel with the bounding faults. Some minor offsets on these faults are apparent with several centimetres of normal motion. Poorly developed faults are also present, displaying the same colour gouge development, but with limited apparent fault damage in the surrounding rock that also lacks a clay-rich matrix (Figure 6.7G).

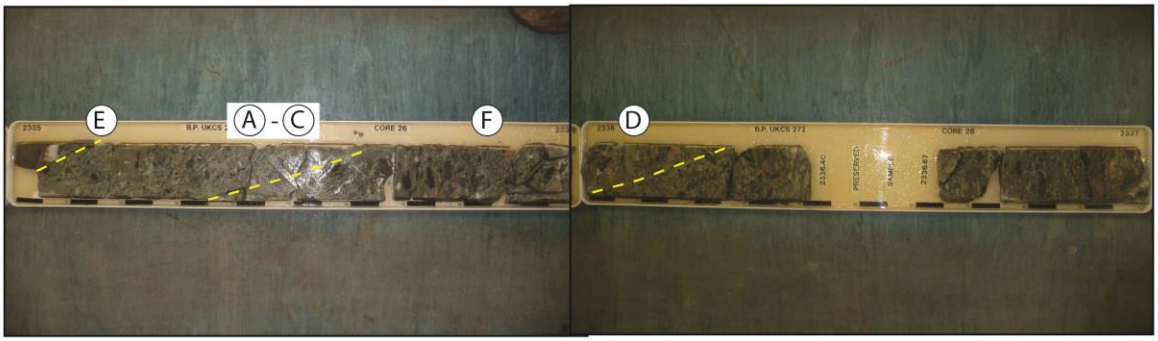
E
A - C
F
D

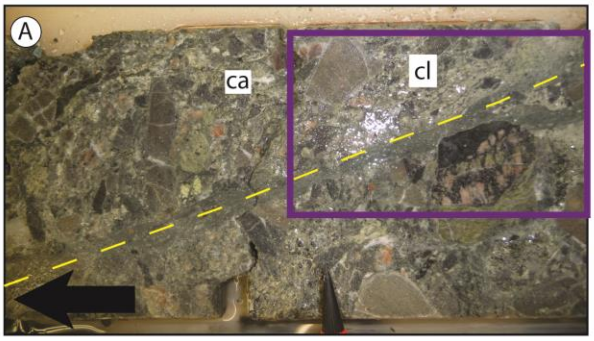
A
ca
cl

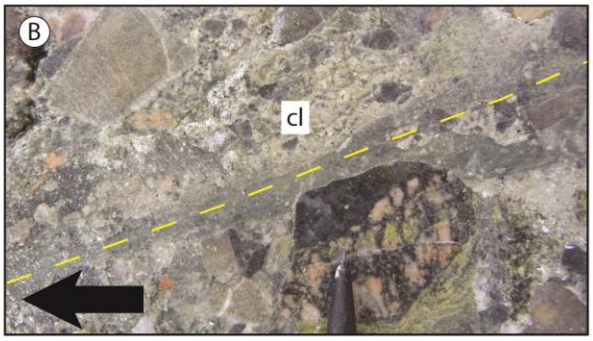
B
cl

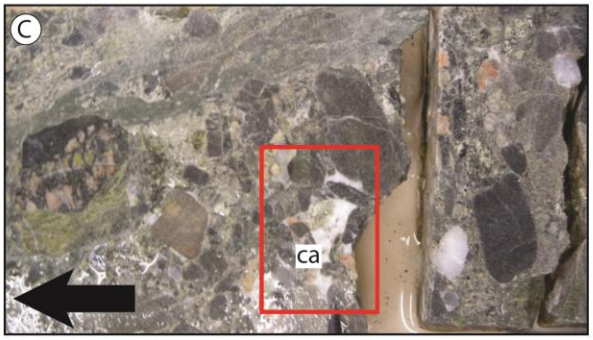
C
ca

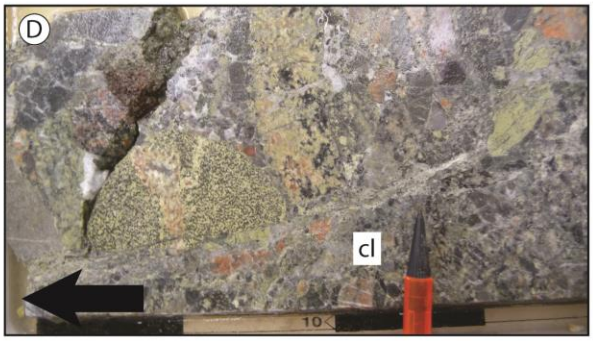
D
cl

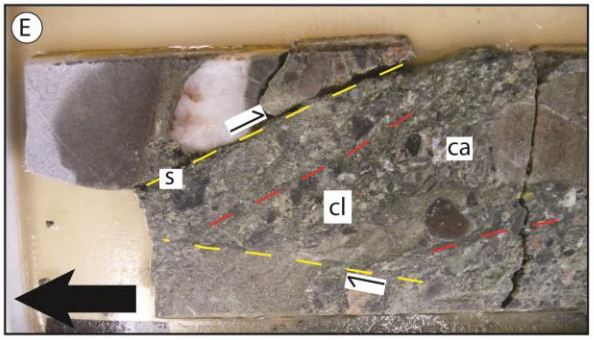
E
ca
s
cl

F
ca

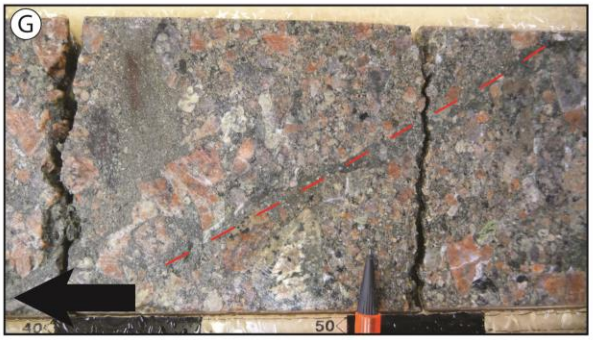
G

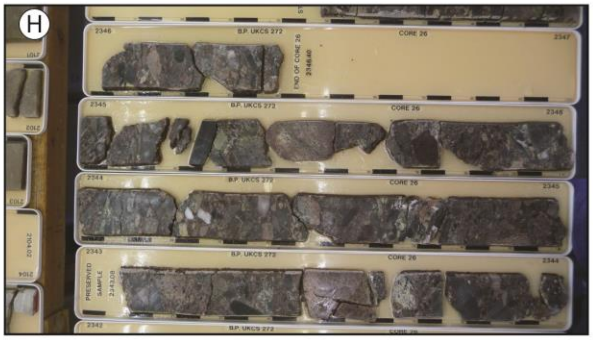
H

Figure 6.7 (previous page): Observations from the basal conglomerate, Lower Clair Group. cl = clay dominated breccia, ca = sparry calcite mineralisation, s = slip surface, red dashed line = foliation, yellow dashed line = slip surface. (**TOP**) Faulted section between 2335 – 2337 m, showing position of three parallel faults, images A-F. (**A - B**) grey-green cataclasite surrounded by clay rich breccia. Fine to very fine grain size visible within cataclasite. Purple box indicates position of B. (**C**) Sparry calcite replacement of part of the matrix (within red box). (**D**) Thin (approximately 1 cm thick) band of grey-green cataclasite cutting and offsetting clasts within the basal conglomerate. (**E**) Dispersed clay rich fault breccia, with a weak foliation parallel to a more significant slip surface. Normal movement offset visible (black dashed line). (**F**) Vertical calcite veining visible cutting clasts and becoming more dispersed within the matrix. (**G**) Poorly developed fault at 2315.5 m in granitic gneiss conglomerate with grey-green cataclasite surrounded by unfractured basal conglomerate. (**H**) Typical basal conglomerate with varied lithology.

6.3.2.2 Basement-cover interface

The basement-cover interface is exposed in core 206/8-8 at 2486.4 m depth, where a basement amphibolite is overlain by the basal conglomerate (Figure 6.8A). The contact between these two units is abrupt, defined by a final band of fine-grained sandstone matrix of the conglomerate that encloses 2 – 5 cm sized clasts of gneiss. Above this, the basal conglomerate is composed of gneiss boulders up to 60 cm across and probably larger, with smaller interstitial clasts that are cemented in a grey-green fine sandstone matrix (e.g. Figure 6.8B). These fine-grained sandstones in places appear primary with clear banding, however in several cases, clasts of gneiss appear to be brecciated within them, and one example of a sinuous vein of matrix material is present within a gneiss boulder (Figure 6.8E), indicating sediment injection. It seems likely that if sediment injection occurred within boulders, sediment injection also occurred into the basement. The fine sandstone matrix is often partially replaced in places with sparry calcite with pyrite, but in some of these veins the calcite also seems brecciated (Figure 6.8C). As noted by Pless (2011), epidote veins within gneiss clasts are truncated against clast margins, indicating that epidote and red-brown 'haematite' veining predates the deposition of the conglomerate. However, in thin section (e.g. section 6.4.2.1) haematite is only present as very (<<0.1 mm across) fine grained clasts within veins in the basement, and instead this feature appears to be a speckled adularia vein, containing fine-grained pyrite, iron oxide and clay.

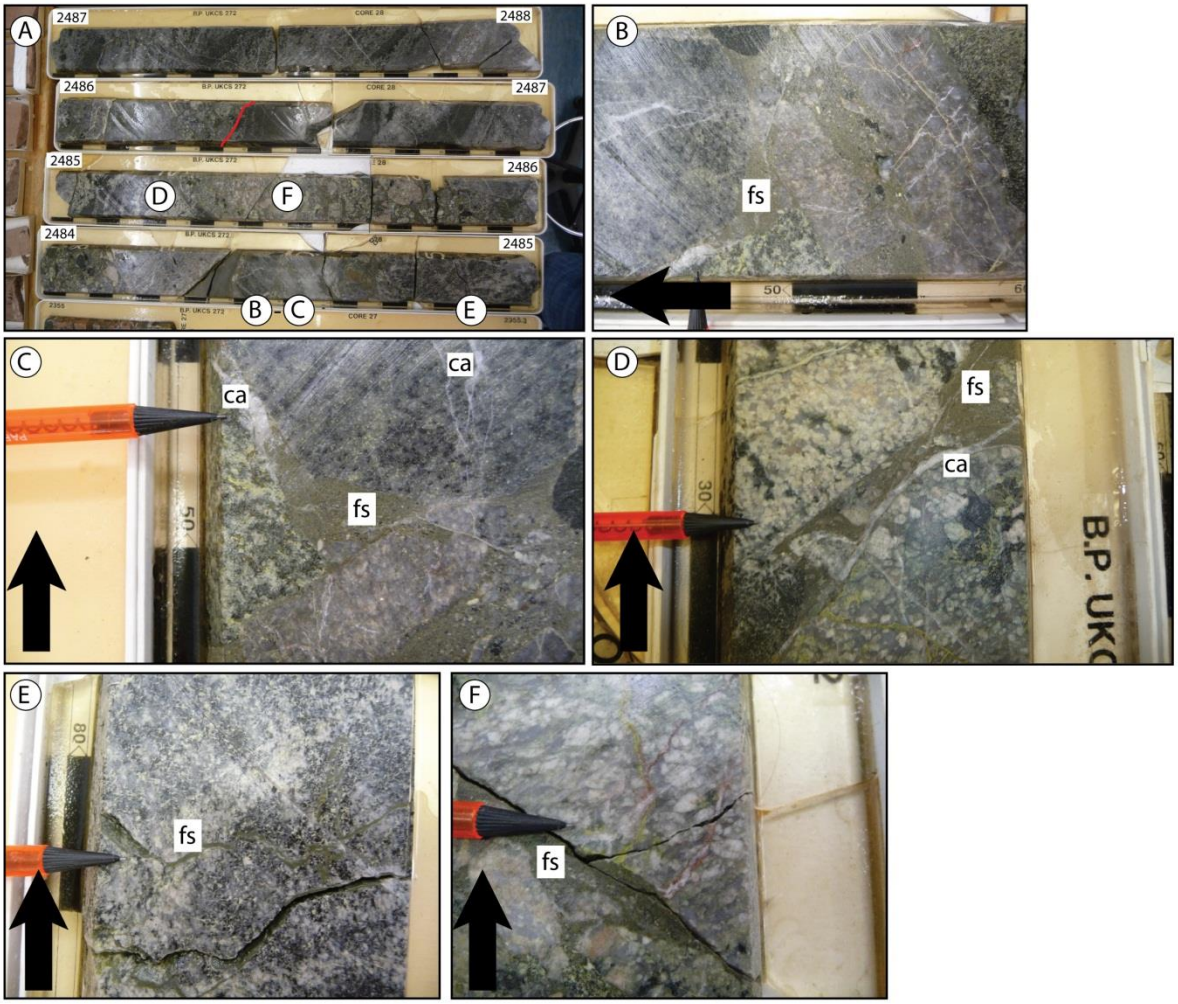

Figure 6.8: Observations from the basement-cover interface of the basal conglomerate (Lower Clair Group) and Lewisian basement in well 206/8-8. Fs = fine sandstone, ca = calcite. Arrows point upwell (vertically upward). (**A**) Basement cover interface (red line), showing locations of photos from within the basal conglomerate. (**B** - **C**) Fine sandstone with brecciated gneiss clasts and calcite veining that may also be partially brecciated, indicated by pencil. (**D**) Fine sandstone cut by later calcite vein. (**E**) Injection of fine sandstone and probable clay into a large (60 cm across) clast within the basal conglomerate.

6.3.3 Summary of findings from the cover

Within porous (now oil-filled) sandstones, granulation seams have developed, and likely formed barriers to fluid flow due to extensive grain size reduction (e.g. Antonellini and Aydina, 1994). In zones of calcite-cemented sandstone (not oil stained), the typical faulting style is of well-cemented cataclasites and calcite-cemented breccias. Clay dominated gouges are only found within shale layers. From these observations it is apparent that there is a strong lithological control on faulting and fault rock style in the Clair Field, and most of these faults described above have a tendency to act as baffles – they are not associated with significant macro-scale porosity development except within sparry calcite-pyrite veining that is at times spatially associated with faulting (e.g. Figure6.6E and G). Within well 206/8-10z, the latest stage of fracturing is associated

with the development of open elongate pores (up to 1 mm x 50 mm) within the Clair Group that cluster around faults displaying normal displacements. These faults contain uncemented breccia that post-dates the latest phase of mineralisation. Apparent normal kinematics have been determined within several of the faults identified on the basis of visible offset of the Clair Group and fault duplex-type structures.

Within the basal conglomerate, calcite replacement of the matrix and vertical calcite veining is seen up to 130 m or more above the basement-cover contact in an area associated with faulting. Assuming that the bedding was horizontal, such vertical veins indicate that the maximum principal stress at the time of formation of these veins was vertical, consistent with a normal faulting regime. This also agrees with the observed kinematics of the faults. Vertical calcite veins are most evident within gneiss clasts, becoming more irregular and dispersed within the matrix.

At the basement-cover interface, sediment injection is observed into blocks of gneiss within the basal conglomerate, with intrusion of fine grained sandstone and possible brecciation of sparry calcite. This was not observed in the basement rock immediately below the conglomerate in the core, but sparry calcite veining is present cementing angular clasts of gneiss (see below). Epidote and adularia veins within gneiss clasts are truncated at the clast margins, suggesting that these veins at least predate the Devonian. This observation agrees with those of the Outer Hebrides where some epidote cataclasites are associated with Caledonian fault movements, and calcite has been associated with normal faulting that postdates the Caledonian structures.

6.3.4 Basement

The following wells have returned basement core from the Clair Field:

- 206/7a-1: Cored 160 m of basement, and returned samples in rubble form not of value in for fracture studies.
- 206/7a-2: Horizontally drilled 400 m of basement and returned orientated spot core totalling 77 m in length, **studied here**.
- 206/8-2: Cored 10 m of basement, **studied here**.
- 206/8-8: Cored 14 m of basement, **studied here**.
- 206/9-2: Cored 4.5 m of basement.
- 206/12-1: Cored 10 m of basement.

Studied core was selected as these are the longest, most continuous core sections available.

Lithologies within the basement are similar to those identified within clasts of the basal conglomerate unit, with granitic and granodiorite gneisses, pegmatites, amphibolites with

epidotisation, and diorite gneisses occurring in lenses and bands indicative of amphibolite facies or above (Pless, 2011). Lithology is highly variable over metre scales (e.g. Figure 6.9, Figure 6.10A-B), and for detailed lithological descriptions of the basement rocks the reader is directed to Pless (2011). Foliation is typically weakly defined predominantly by the alignment of biotite and amphibole within some units. Within well 206/7a-2 (the only orientated core), foliation has been found to be steeply dipping and strikes NW-SE to NNW-SSE (Pless, 2011).

Multiple phases of faulting and mineralisation exist within the basement, with epidote veining, red-brown veining (identified as haematite by Pless, 2011) (e.g. Figure 6.10D), and several phases of calcite and pyrite veining. The following sequence of fracturing and mineralisation was determined by Pless (2011) (oldest to youngest):

- Red-brown ('haematite') veining associated with epidote veining, epidote-cemented cataclasites, and quartz veining.
- Several phases of calcite-pyrite mineralisation.
- Oil is associated with vug-like porosity in carbonate mineralised fractures and also along open fractures.

This study builds on these observations to investigate fracture mineralisation within the basement rocks and the association of porosity and oil presence.

Much of the basement is highly altered – within well 206/8-8 and 206/8-2, epidote veining and epidote-cemented cataclasites are common and there are areas of core up to 40-50 cm in length that show alteration of feldspars to a light green mineral identified as epidote by Pless (2011) (e.g. Figure 6.10B and D). Porosity is common within the basement rocks of well 206/7a-2 and 206/8-2, forming along fractures and as elongate voids 1-2 cm long and up to 2-3 mm wide (e.g. Figure 6.10I-J). Porosity associated with oil staining is often found alongside calcite-pyrite mineralisation that is similar in appearance to the late stage calcite-pyrite veining observed in the cover sequence (e.g. Figure 6.10F-H). No evidence of reactivation of the foliation by faulting or veining was observed, but fractures are often reactivated by multiple phases of mineralisation (e.g. Figure 6.10E).

From my own direct observations of the core, the following chronological sequence of fracturing and mineralisation has been determined (oldest to youngest):

1 Epidote cataclasite-bearing faults are up to 2 cm across and incorporate clasts of country rock, constituting ≤ 20 % of the total cataclasite volume. The remaining volume of the cataclasites are composed of very fine grained epidote with grain sizes that are not discernible to the naked eye (Figure 6.10C). It is probable that locally widespread epidote

alteration of the gneiss occurred contemporaneously with epidote cataclasite formation.

2 Dark grey/black ultracataclasite bearing faults are visible exploiting and cutting pre-existing epidote cataclasite bearing fractures (Figure 6.10C). These faults are up to 0.5 cm across and offset epidote cataclasite faults and veins.

3 Alteration of feldspar within the gneiss to a pale green mineral – appearing superficially like epidote (Figure 6.10B and D). This alteration is pervasive over a minimum 10 m of gneiss, but probably extending further as 10 m is the maximum length of continuous core in the basement. Relative age of this alteration is constrained by microscopy (section 6.4.2).

4.a Faulting, brecciation and veining associated with red-brown matrix ('haematite') mineralisation of Pless (2011), at times seen associated with oil staining (Figure 6.10F). These red-brown veins can be up to 4 cm thick, but are more commonly <1 cm thick.

4.b Calcite-pyrite mineralisation associated with vuggy porosity, faulting and oil staining (Figure 6.10 F-H). These veins can be up to 2 cm across and pores within them measure up to 1 cm across and 2-3 cm in length. Breccias associated with much pyrite mineralisation are oil stained and therefore likely to be very porous (Figure 6.10 H).

4.c Vuggy porosity was also seen in cores 206/7a-2 and 206/8-2 that was not associated with calcite mineralisation (Figure 6.10I-J). Interestingly, this style of porosity was not observed in well 206/8-8, below the oil-water contact (Baron et al., 2008).

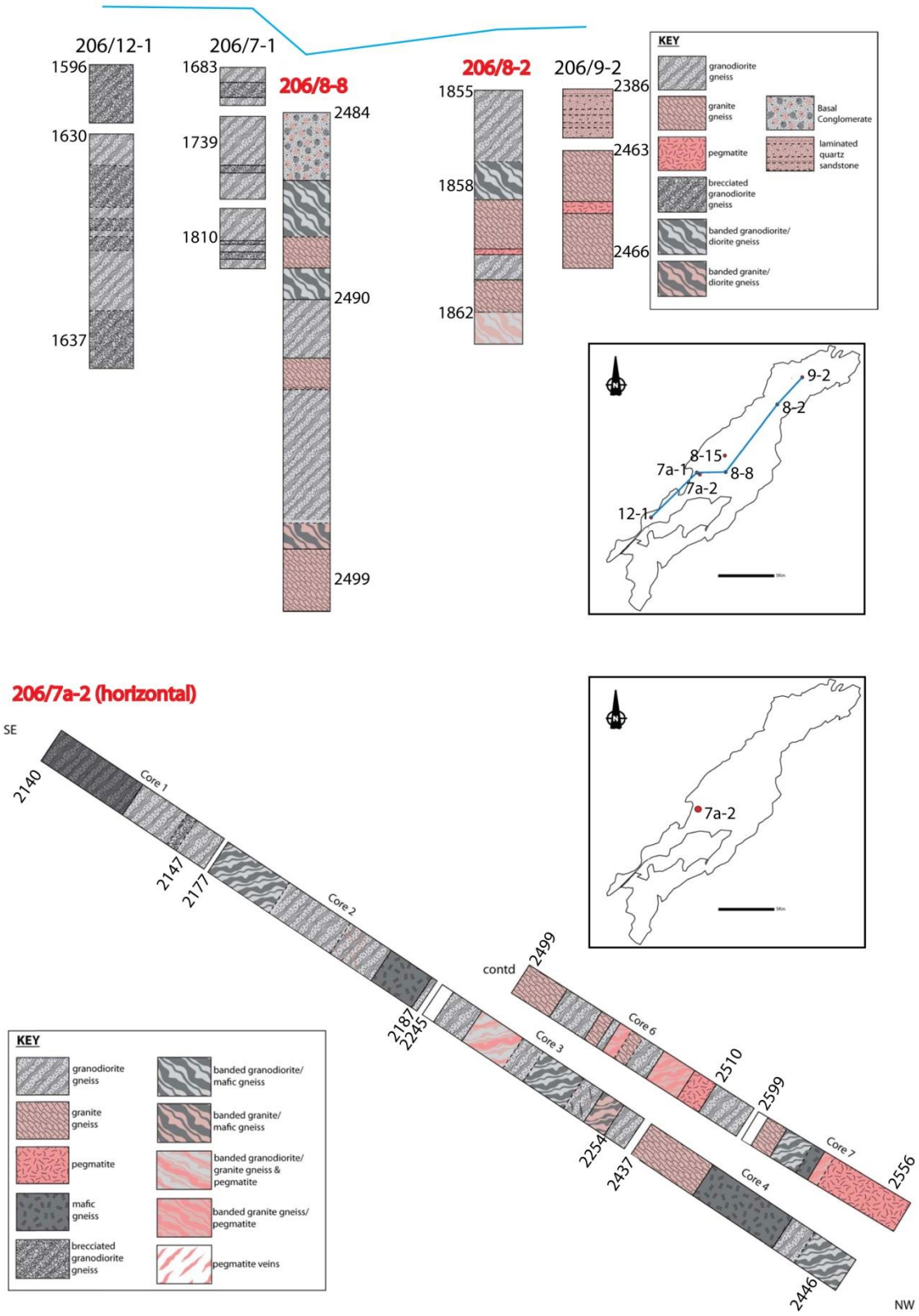

Figure 6.9: Clair basement well logs, from Pless (2011). Sections studied here are highlighted in red, with depths in metres indicated.

A
Image B
N
B
N
C
e
e
ccl
D
rb
N
E
N
F
c
rb
o
N
G
N
H
N
I
p
1864.35
J
1863.50
p
p
p
p

Figure 6.10 (previous page): Observations of the Clair basement cores. Images with a north arrow are from well 206/7a-2, drilled horizontally. Arrow in other images = upward direction. (**A** - **B**) Amphibolite and granitic gneiss in core 206/7a-2, showing lithological variation over short distances. Pink = alkali feldspar, light green = alteration of feldspar.(**C**) Dark grey very fine grained cataclasite (ccl), cutting and offsetting epidote veins (e). (**D**) Red-brown veins (rb) cutting light green altered gneiss. (**E**)) Fracture displaying multiple mineralisation: Calcite (right), red-brown vein (centre), epidote (left). (**F**) Oil staining (o) associated with brecciation, calcite mineralisation (c) and red-brown veining (rb). (**G**) Vuggy porosity associated with calcite veining. (**H**) Zone of breccia associated with calcite-pyrite mineralisation and much oil staining. (**I**) Vuggy porosity (p) within epidotised gneiss. (**J**) Vuggy porosity (p) within granodioritic gneiss.

6.3.5 Summary of findings from macroscopic observations of the core

A complex sequence of fracturing and mineralisation is present within the basement, indicating multiple phases of deformation and mineralisation, the latest phases of which are associated with porosity development and oil staining alongside red-brown veining, and calcite-pyrite veining.

Earlier phases of faulting are consistent with faulting at depth - epidote cataclasites are associated with elevated temperatures over 200°C (Liou, 1993). The second stage of fault rock development is dark grey cataclasite, followed by faulting associated with red brown mineralisation, and calcite-pyrite veining. Clay bearing faults were not observed within the basement, but this may be due to poor recovery and limited sampling.

The reasons for the association of porosity with calcite-pyrite veining and the presence of open vuggy porosity are not clear from macroscopic observations. Vuggy porosity seen on the Clair ridge in wells 206/8-2 and 206/7a-2 may be a feature associated with a period of weathering that did not last as long in the 'core' region sampled by 206/8-8 that was onlapped by sediments earlier than the ridge. Rock from the ridge also shows evidence of large-scale alteration of feldspar in the gneiss to a pale green coloured mineral that may be the result of weathering.

6.4 Microscopy

Thin sections were examined at the Iron Mountain core store in Aberdeen during a week-long visit. Samples were obtained from the core and returned to Durham University, where a further 10 slides were produced. In addition, 4 slides were available from the Pless (2011) study, giving a total of 30 thin sections that were examined.

6.4.1 Clair Group microscopic observations

Within the Clair Group, three thin sections were made in order to investigate two specific points of interest:

1. To investigate vuggy porosity within well 206/8-10z (1 thin section).
2. To investigate potential sediment injection in the basal conglomerate (2 thin sections).

6.4.1.1 Well 206/8-10z

Open fractures are particularly important in the Clair Field, and these are associated with vuggy porosity within the sandstone. For this reason one thin section was produced from the cover rocks of 206/8-10z from 2319.15 m, in order to investigate the cause of vuggy porosity that has been particularly associated with oil infill (Milodowski et al., 1998). The sandstone is coarse grained (clasts typically around 0.5 – 0.75 mm across) and comprised of subrounded to subangular clasts of quartz (60%) and feldspar and plagioclase (35%) with occasional clasts of muscovite and brown probable clay (5%). Feldspar clasts are usually relatively unaltered, but some (≤ 20%) show significant sericitisation. Clasts are cemented by patchy calcite cement. In areas lacking calcite cement, significant porosity (15-20%) exists. Elongate pores 0.5 - 1 mm across and up to 4 mm in length are discontinuous along two trends (open pore shown in Figure 6.11). No mineralisation is evident lining these pores, and fracturing of clasts is not seen, suggesting that these fractures may have resulted from dissolution. In places of narrowing or pore-closure, calcite infill is present within pores and in occasional patches around the pores in calcite-cemented areas of the rock. In places, the calcite cement displays relict margins where quartz/feldspar grains would have previously been extant. This is in agreement with observations by Milodowski (1998) who notes a late phase of feldspar and lithic clast dissolution, visible by the presence of oversized pores and partially dissolved clasts. Calcite must also have dissolved within these pores, as they frequently cut through entirely calcite cemented sandstone. The concentration of vuggy porosity around normal faults in the sandstone suggests that fluids related to or moving through these faults played a major role in the production of this secondary porosity. Within the porosity, very fine (< 0.1 mm across) clasts of pyrite are occasionally present.

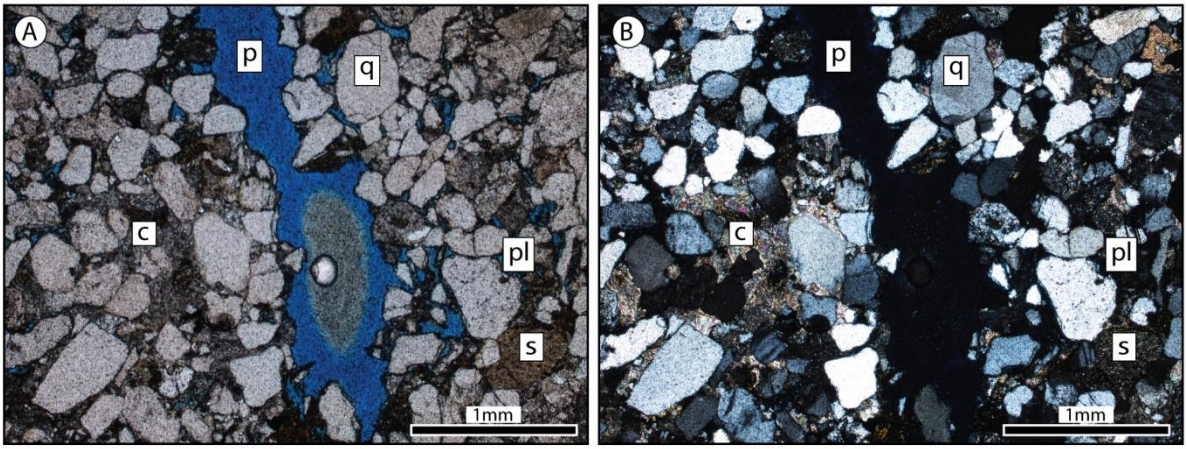

Figure 6.11: Photomicrographs of vuggy porosity within Unit V of the Lower Clair Group. (**A**) PPL (**B**) XPL. p = porosity, c = calcite, q = quartz, pl = plagioclase, f = alkali feldspar, s = sericitised feldspar. Note lack of mineralisation along margins of the pore.

6.4.1.2 Well 206/8-8

Two thin sections were produced from the basal conglomerate of well 206/8-8 from the following localities:

Depth (m)	Lithology
2484.7	Basal Conglomerate: Interstitial fine-grained clastic matrix and calcite veining between gneiss boulders (shown in Figure 6.8D).
2485.3	Basal Conglomerate: Interstitial fine grained clastic matrix and calcite veining between gneiss boulders (adjacent to veining shown in Figure 6.8B-C)

These were selected for the purpose of investigating the matrix of fine sandstone that exists between larger clasts of conglomerate in the basal conglomerate, specifically to identify whether these sandstones could have resulted from soft sediment injection as seen in the Stornoway region. In thin section, the fine sandstone is observed to be relatively well sorted, with equigranular grains of quartz (50% of the rock), feldspar (20%), chlorite (10%), muscovite and biotite (10%) crystals around 0.02 mm across interlayered with occasional bands of more muscovite enriched laminae around 0.2-0.3 mm across. Clasts are angular and cemented by an interstitial matrix of phyllosilicates such as sericite that constitutes < 10% of the rock, and in places this matrix has been replaced with calcite. Occasional larger lithic clasts up to 5 mm across are present.

Calcite mineralisation is mostly localised to the margins of the sandstone adjacent to gneissose conglomerate clasts/boulders. Calcite is sparry and up to 3 mm across with thin (< 0.05 mm) open

fractures visible along some vein margins (Figure 6.12A-B). Sparse minor pyrite crystals < 0.5 mm across are dispersed within the calcite veins. Minor pyrite mineralisation also occurs in sparse, narrow (generally < 0.1 mm) discontinuous veins of calcite that are randomly orientated and associated with narrow (< 0.05 mm) meandering open fractures that are localised along a clay/sericite rich layer. Sparry calcite veining displays sparse small porosity (0.1-0.2 mm across) with irregular margins that may have resulted from dissolution of the calcite. As mentioned above, calcite mineralisation also occurs patchily replacing the matrix, and it is also seen cementing brecciated sandstone in one example (Figure 6.12C). This may have formed as a result of formation from injection of fluids at high pore fluid pressures.

Although the fine sandstone is relatively equigranular it is compositionally immature. The well-sorted nature and layered banding of the fine sandstones suggests that they are primary features, not sediment injection veins.

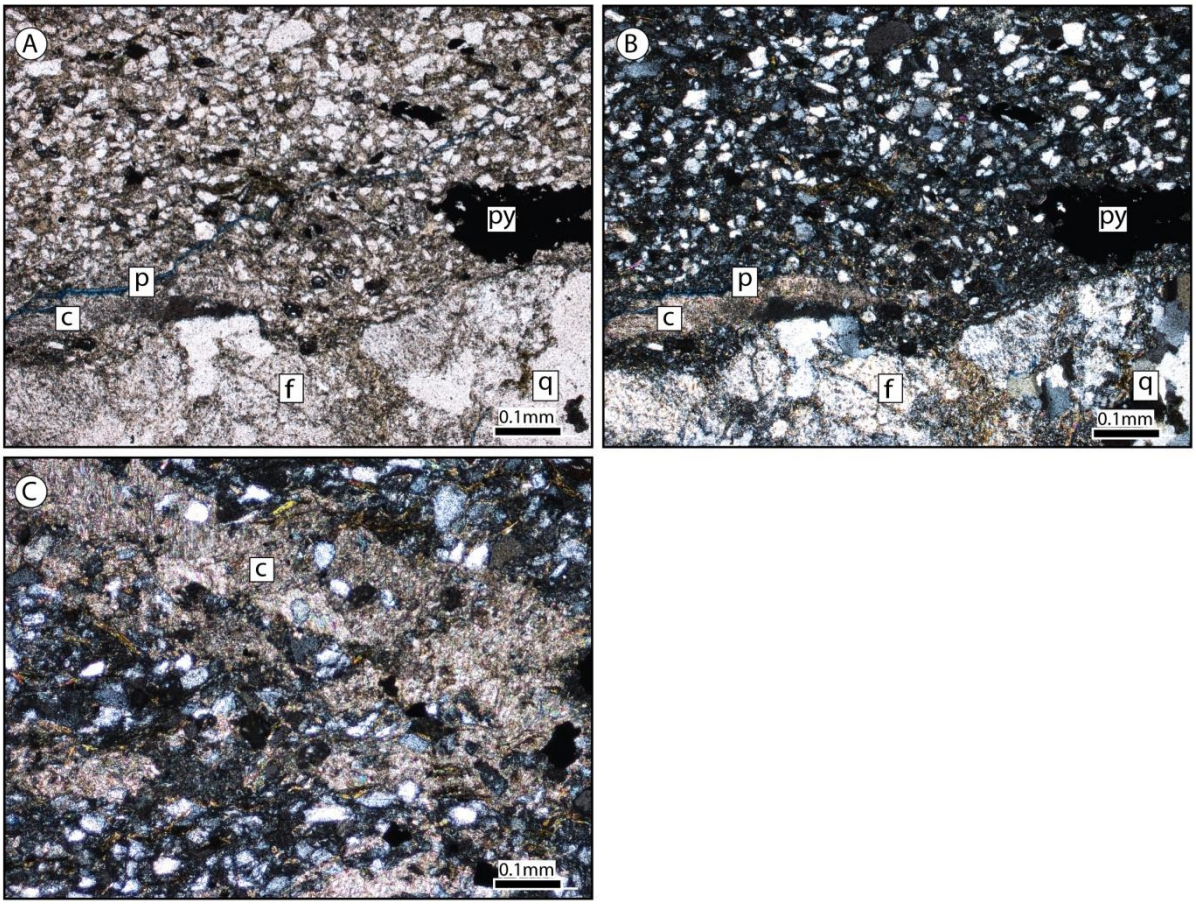

Figure 6.12: Photomicrographs of fine interstitial sandstone collected from the basal conglomerate. c = calcite, f = feldspar, p = porosity, py = pyrite, q = quartz. (**A** - **B**) PPL and XPL, respectively, from 2484.7m. Fine, well-sorted clasts, cemented with clay (top) and the margin of a large clast in the conglomerate (bottom). Open fracture localised alongside calcite vein. (**C**) XPL. From 2485.3m. Calcite containing clasts of fine sandstone.

6.4.2 Basement microscopic observations

Within the basement rock thin sections, multiple phases of mineralisation have been identified, with additional phases of veining identified under the microscope that were not recognised during macroscopic observations of the core.

6.4.2.1 Well 206/7a-2

The following slides were studied from well 206/7a-2, in addition to four thin sections held at Durham University from Pless (2011) that are not located on the core:

Depth (m)/slide number	**Lithology**
2141.4	(Prepared from collected sample) Mafic gneiss with green alteration and epidote, red-brown, and calcite veining.
2141.5	(At core store) Mafic gneiss with green feldspar alteration and epidote, red-brown, and calcite veining.
2145.8 (x2)	(At core store) Mafic gneiss with green feldspar alteration, and epidote, red-brown, and calcite veining.
2146.7	(Prepared from collected sample) Fractured granodiorite gneiss with vuggy porosity and associated oil staining. Fractures are red-brown and calcite filled.
2178	(At core store) Mafic gneiss, green alteration of feldspar and mafic mineral (amphibole).
2181.4	(Prepared from collected sample) Granodiorite gneiss with green alteration. Calcite and red-brown veins and vuggy porosity associated with oil staining.
2182	(At core store) Granodiorite gneiss with green alteration. Calcite and red-brown veins and vuggy porosity associated with oil staining.
2247.5	(At core store) Granite gneiss with green alteration of feldspar.
2249.5	(At core store) Granodiorite gneiss, with green alteration of feldspars, and calcite veining associated with oil.
2439.8	(Prepared from collected sample) Brecciated zone within mafic gneiss, heavily oil stained with pyrite and calcite mineralisation.
2594.3	(At core store) Mafic gneiss with quartz veining.
2597.5	(At core store) Granitic gneiss with green alteration of feldspars.
7-A2-1 (Pless, 2011)	Epidote veining reactivated by red-brown and calcite veining, cut by a further phase of calcite veining.
7-A2-2 x2 (Pless, 2011)	Reddy-brown cemented fault rock with calcite mineralisation.
7-A2-3 (Pless, 2011)	Sericitised granodiorite gneiss.
7-A2-4 (Pless, 2011)	Calcite vein cutting mafic gneiss.

The following description is an amalgamation of the observations from the above thin sections:

Under the microscope, the gneiss is dominated by feldspar, quartz and chloritised amphibole crystals typically 2-3 mm across. Feldspars are generally sericitised and are also altered in places to epidote. The earliest phase of fracturing is identifiable as epidote veining and epidote-cemented cataclasite. Epidote cataclasites up to 3 mm across have been observed in thin section, but in the core these are present up to 20 mm across. Within epidote-bearing faults and veins, the majority (80%) of the rock is comprised of fine (< 0.1 mm across) equigranular epidote crystals. In the epidote cataclasites, sparse clasts of angular feldspar and quartz up to 0.5 mm across are entrained, supported in the fine grained matrix. Pores up to 0.5 mm across are present, often partially/wholly infilled with calcite and adularia. Pore space development could be related to either dissolution of pre-existing minerals, or the formation of tensile fractures that have since been partially filled by mineralisation.

Phases of adularia, calcite and quartz veining reactivate epidote bearing fractures. Adularia occurs in both euhedral form lining open fractures (e.g. Figure 6.13E), and anhedrally within red-brown 'speckled' veins with pyrite, haematite and probable clays (e.g. Figure 6.13A-D), associated with patchy porosity. Euhedral adularia occurs as fine (< 0.05 mm) crystals lining open fractures, and is often entirely altered to a light green clay mineral that preserves the distinctive adularia diamond-shaped crystal form (Figure 6.13E). Alteration of the country rock gneiss to light green clay is also seen in patches throughout the 206/7a-2 core that is not associated with veining (e.g. Figure 6.13E, H), and it is this that gives the core its widespread green colouration, not epidote. Feldspars are often sericitised, and sericite within feldspars that have been altered to the light green clay are generally better preserved than the feldspars themselves.

Red-brown filled fractures are composed of speckled anhedral fine grained adularia. In red-brown veins, speckled adularia mineralisation surrounds entrained fine grained lithic clasts of country rock (largest up to 0.5 mm across). Adularia crystals in these veins are small (around 0.1 mm across), anhedral, and are accompanied by patchy calcite (20%), opaques (10%, pyrite) and faint murky brown clay and haematite found as inclusions within adularia crystals (Figure 6.13D). The red-brown colouration is derived from this clay and iron oxide. Porosity in speckled adularia veining may be due to either partial mineralisation of an open fracture or dissolution. Dissolution may be more likely, given that porosity is enhanced by dissolution in the cover. This would also explain the vug-like nature of the porosity.

Speckled adularia veining occurs alongside and mutually crosscuts calcite veining, of which two types of calcite vein may be distinguished. Speckled adularia is found both with and without calcite cement (Figure 6.13A (with), B (without)). Sparry calcites within speckled veins are up to 0.5 mm across with irregular margins, and may have precipitated within porosity. Irregular shaped porosity within calcite crystals along their planes of cleavage may also indicate a degree of

dissolution of the calcite. The presence of clay and iron oxides give speckled adularia veins a red-brown appearance in hand specimen that can lead to misidentification (as 'haematite'). Several phases of adularia veining are evident with subtle variations in the proportion of calcite, entrained clasts and clay mineralisation. Oil staining is seen associated with the porosity in these veins, and also as inclusions within aggregates of adularia (Figure 6.13C). In some cases, it appears as though specks of oil are enclosed in fine grained aggregates of adularia, suggesting that oil influx and adularia mineralisation may have been contemporaneous, or that adularia mineralisation postdates oil migration.

Open fractures are often partially infilled with patchy calcite and pyrite that are seen to overprint euhedral adularia and speckled adularia mineralisation. This late phase of calcite-pyrite mineralisation does not exhibit evidence of dissolution and occurs with oil inclusions (i.e. it may postdate dissolution of pre-existing calcite). The pyrite occurs as aggregates of euhedral individual crystals < 0.1 mm across, although crystals up to 1 cm across are observed in the core. Thin (0.1 mm) very low relief mineral veins often reactivate speckled adularia veins, with low relief and low birefringence , together with very fine, anhedral, randomly orientated crystals that may be zeolite. It is possible that the speckled adularia veins with entrained clasts of country rock may be sediment injection veins, or they may be related to faulting (i.e. fault gouge injections). These veins are, however, matrix supported by fine speckled adularia, unlike the adularia-cemented fault rock that is clast supported (see well 206/8-8, section 6.4.2.3).

The relative ages of calcite –pyrite mineralisation and speckled adularia veining is not clear. Calcite-pyrite veining that exhibits evidence of calcite dissolution mutually cross cuts speckled adularia filled fractures, but at least two and possibly three phases of calcite veins are evident. Not all calcite veins show evidence of dissolution, and some show active inclusion of oil within calcite crystals. Generally crystals within calcite veins are equigranular, and veins with no evidence of dissolution are both fine grained (crystals <0.1mm across) and sparry (crystals 2 mm across) (e.g. Figure 6.13A). Fine grained calcite veins in some cases entrain sparry calcite crystals from reactivated sparry vein margins, indicating that fine grained calcite mineralisation may be the latest phase of calcite. Calcite showing evidence of dissolution is sparry and may pre-date non-dissolved calcite. An offset of approximately 0.5 mm is visible across one sparry calcite vein, indicating that some of these fractures may have originated as shear fractures.

Quartz is often observed with syntaxial overgrowths into open to wholly calcite-filled fractures (Figure 6.13H). In places, quartz has annealed across the entirety of calcite-pyrite veins that are up to 0.5 mm across, producing quartz crystals with inclusions of calcite and pyrite (e.g. Figure 6.13G). Quartz mineralisation is observed to directly overprint both adularia and calcite-pyrite veining, and displays inclusions of calcite, pyrite, haematite, clay and probable oil. Syntaxial

overgrowths on quartz clasts within the cataclasite have produced veins of equant quartz grains up to 0.4-0.5 mm across. Crystals exhibit grain-shaped haloes of very fine grained iron oxide and probable clay inclusions in their cores which have been incorporated into the quartz during crystal growth. These inclusions are also visible within fractures that have been annealed through quartz crystals. Quartz veining is also seen reactivating the margins of sparry calcite-pyrite veining and cutting speckled adularia veins (e.g. Figure 6.13F), and in some cases euhedral quartz crystals show evidence of growth into open porosity. In Figure 6.13F this porosity has been infilled with late brown clay development. Brown clay is also seen cementing brecciated country rock and speckled adularia (Figure 6.13F), but observations of clay cemented breccia are limited to one slide. Clay-cemented faulting appears to be the latest phase of faulting present in the basement core.

As discussed above, in several thin sections sparry calcite looks partially dissolved, with pores that lie along crystal cleavage planes with rough, non-euhedral margins to the crystals. In some areas this porosity is infilled with quartz mineralisation. These quartz crystals display inclusions of calcite (Figure 6.13H). This suggests that dissolution of calcite may have been contemporary with, or, occurred before quartz overgrowths and veining.

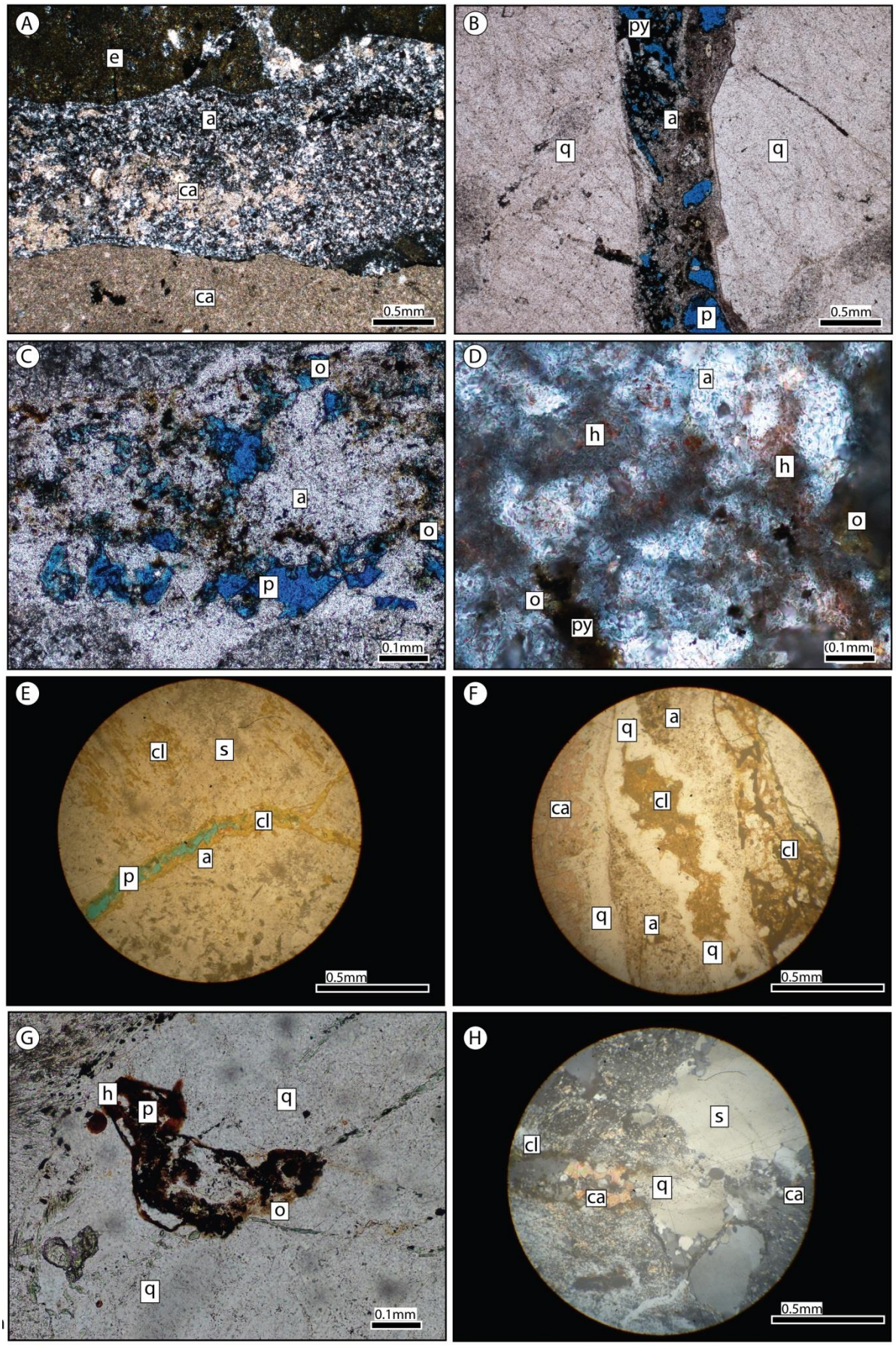
A
e
a
ca
ca
0.5mm
B
py
a
q
q
p
0.5mm
C
o
a
o
p
0.1mm
D
a
h
h
o
o
py
(0.1mm
E
cl
s
cl
a
p
0.5mm
F
q
a
ca
cl
cl
q
a
q
0.5mm
G
h
p
q
o
q
0.1mm
H
s
cl
q
ca
ca
0.5mm

Figure 6.13 (previous page): Photo micrographs from core 206/7a-2. a = adularia, ca = calcite, cl = clay mineral, p = porosity, p = oil staining, py = pyrite, q = quartz, s = sericitised feldspar. (**A**) XPL. From 2141.4 m. Top = epidote cataclasite (e), centre = speckled adularia-rich vein (a), with calcite (c), haematite, pyrite and clay, bottom = fine grained calcite-pyrite vein. (**B**) PPL. From 2146.7 m. Speckled adularia veining (a) occurring without calcite. Pyrite still present (py), with obvious porosity (p, in blue). Quartz crystals (q) at vein margins show syntaxial overgrowths, incorporating clay/haematite into the quartz. (**C**) PPL. From 2141.6 m. Within speckled adularia vein (a), with obvious porosity (p) and oil staining (o). Oil staining is found within the adularia mineralisation. (**D**) XPL. From 2181.4 m. High resolution image of speckled adularia veining (a), showing haematite (h), pyrite (py) and oil (o) inclusions. (**E**) PPL. From 2146.7 m. Euhedral adularia veining altered to yellow-green clay (a/cl) and associated with porosity (p). Feldspar in the gneiss is also altered to yellow-green clay (cl). (**F**) PPL. From 2141.5 m. Sparry calcite (ca) and speckled adularia veining (a) cut and reactivated by quartz veining (q). Quartz shows euhedral crystals into clay filled space (cl, centre). At the right of the image clay (cl) cements a breccia comprised of wall rocks clasts and clasts of speckled adularia veining. (**G**) PPL. From unmarked location within 206/7a-2, Quartz crystals (q) entirely enclosing pyrite (py) and probable oil (o). Pyrite shows alteration to probable haematite (h). (**H**) XPL. From 2141.8 m. Calcite vein (ca, left) with clay alteration halo (cl), annealed by quartz vein (q). Quartz vein shows calcite inclusions.

6.4.2.2 Well 206/8-2

One slide was prepared from a sample taken from 206/8-2 at 1864.35 m from granodiorite gneiss (from rock shown in Figure 6.10J), where vuggy porosity had been observed in the core. Similar to 206/7a-2, the rocks in 206/8-2 display oil staining associated with calcite mineralisation and vuggy porosity.

Under the microscope, the country rock is composed of coarse quartz and feldspar, cut by epidote cataclasite 5 mm thick with associated parallel epidote veins < 1 mm thick. Quartz and feldspar both show evidence of ductile recrystallisation and grain size reduction and feldspar clasts are often cut by chlorite-epidote-sericite veins <0.5 mm across. The cataclasite is composed of very fine (<0.1 mm) clasts of equigranular epidote supporting rounded clasts of relict feldspar (up to 2 mm across) altered to very fine epidote (Figure 6.14D).

Partially open fractures occur in discontinuous bands across the thin section (e.g. Figure 6.14A, C, F), up to 1.5 mm long x 0.2 mm across. Between these elongate pores, the fractures are syntaxially overgrown with both quartz (e.g. Figure 6.14C) and feldspar (e.g. Figure 6.14H), with both minerals exhibiting probable very fine fluid inclusions. Overgrowths are notably reduced through the epidote cataclasite portions of the thin section. Open fractures have serrated margins due to the presence of fine-grained euhedral adularia mineralisation growing inwards from fracture margins (Figure 6.14A-H). This adularia obscures the original open fracture boundaries and has partially filled the open fractures (Figure 6.14G-H). In Figure 6.14G-H, the original fracture boundaries are evident and abrupt. Pull-aparts are observed along one fracture suggesting a

minor component of shear (Figure 6.14A). Elsewhere, there is no evidence of shear occurring along the fractures and hence they appear to have been initiated as tensile mode 1 fractures.

Fractures are also partially filled with sparry calcite that overprints adularia (Figure 6.14B), with abrupt boundaries against open pore space. Irregularly shaped porosity is present within the calcite, aligned parallel to the calcite cleavage planes and with poorly defined margins with the calcite crystal. In Figure 6.14G-H pyrite is apparent filling porosity associated with a partially open fracture lined with adularia. At the margin of the pyrite, oil staining is evident, and oil staining is also seen in pores at the margins of the sparry calcite.

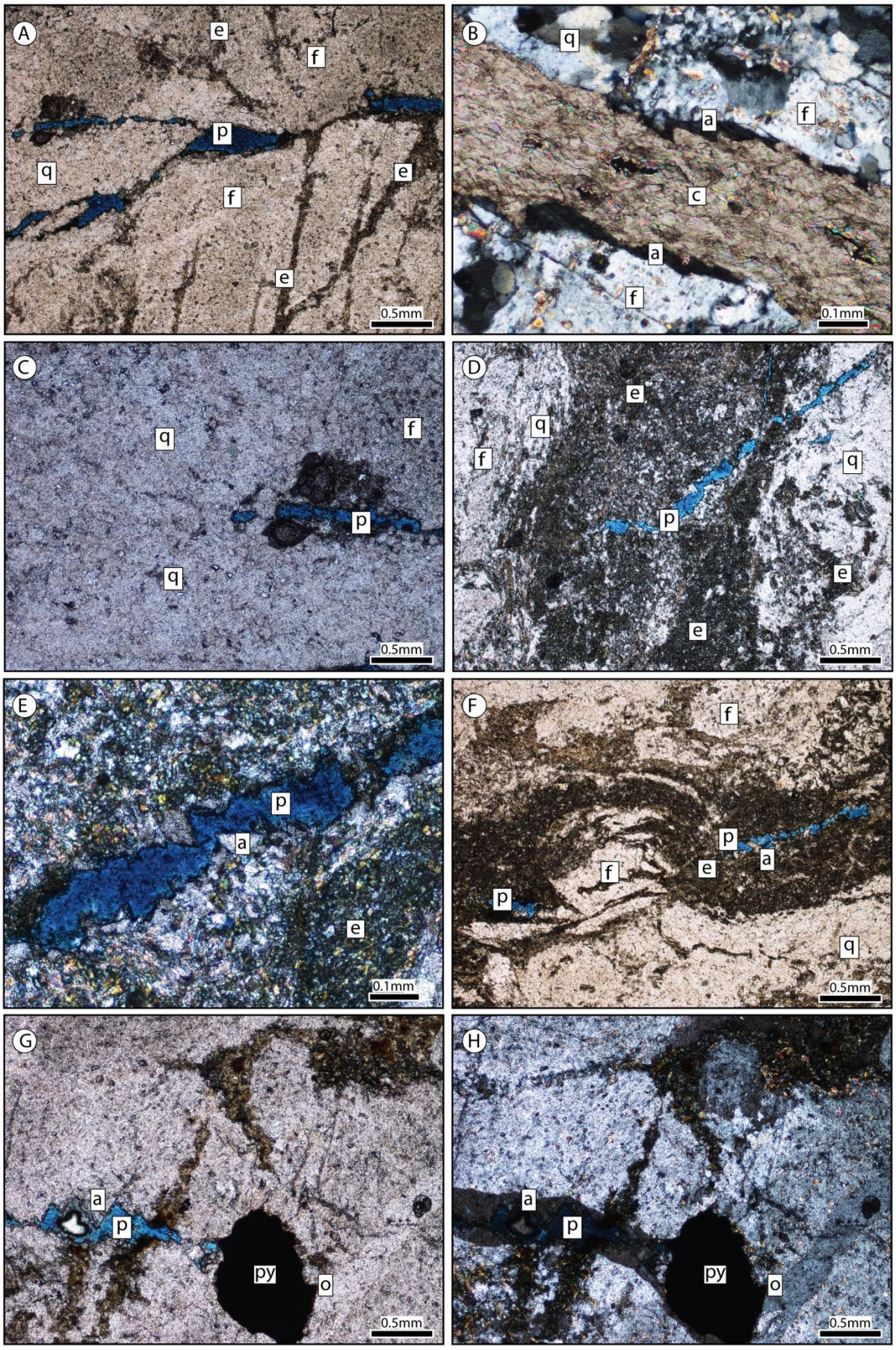
A
e
f
p
q
e
f
e
0.5mm
B
q
a
f
c
a
f
0.1mm
C
q
f
p
q
0.5mm
D
e
q
f
q
p
e
e
0.5mm
E
p
a
e
0.1mm
F
f
p
a
e
f
p
q
0.5mm
G
a
p
py
o
0.5mm
H
a
p
py
o
0.5mm

Figure 6.14 (previous page): Photomicrographs from 206/8-2. a = adularia, c = calcite, e = epidote, f = feldspar, o = oil staining, p = porosity, py = pyrite, q = quartz. (**A**) Open fracture through quartz-feldspar gneiss (q and f) formed from pull-aparts, with open porosity (p) cutting epidote veining (e). (**B**) Calcite (c) and adularia mineralisation within partially open fracture (a). (**C**) Discontinuous open fracture (p) completely annealed through quartz crystal (q) by syntaxial quartz overgrowths. (**D – E**) Open fracture (p) through epidote cataclasite (e), partially filled with euhedral adularia mineralisation (a). (**F**) Discontinuous open fractures (p) partially filled with adularia (a) and annealed through a feldspar crystal (f). (**G – H**) PPL and XPL images, respectively, of open fracture (p) partially filled with adularia (a) and pyrite (py) associated with oil staining (o) around the pyrite margins. Under XPL the original size of the open fracture is apparent (shown in H near to extinction).

6.4.2.3 Well 206/8-8

Two thin sections were produced from 2490.3 m depth in well 206/8-8 (location shown in Figure 6.10C). At this locality granodiorite gneiss is cut by multiple phases of veining and faulting. In thin section, sparry calcite veins up to 4 mm across cross-cut and cement clasts of pre-existing very fine grained cataclasite. The cataclasite displays a foliated zone (up to 2mm across) of equigranular ultrafine clasts of probable feldspar/adularia (<0.01 mm across) that grades into chaotic micro-breccia with clasts up to 1 mm across (Figure 6.15A-B). Patchy calcite cement is present within the fault rock, at times entirely enclosing clasts of breccia. The whole cataclasite zone is at least 2 cm across (limited by the width of the slide) and is composed of angular feldspar (70%) and quartz (30%) clasts with crystals ranging in size from < 0.01 mm to 2 mm across, with minor amounts of sericite. Clasts are cemented by probable adularia. The predominance of feldspar and the association with adularia veining may suggest that faulting occurred under temperature and pressure conditions of stability for adularia. Multiple phases of fault rock development are suggested by slight differences in colour from brown to yellow (Figure 6.15C).

Similarly with rocks at 206/8-2 and 206/7a-2, open fractures lined with adularia and occasional calcite cut the cataclasite. Adularia crystals within these veins are euhedral and up to 0.2 mm across, exhibiting crystals that widen into the centre of fractures. Euhedral adularia mineralisation and open fractures are truncated at the margin with the fine grained cataclasite described above, indicating a mutually cross cutting (contemporaneous) relationship, i.e. adularia is found within veins in the fault rock, and is also cut by the fault rock. Fracture centres are at times filled with sparry calcite crystals up to 0.4 mm across. These calcite infills may be associated with the larger calcite veins that cut the rock and cement brecciated clasts of very fine grained ultracataclasite and coarser clasts of breccia. The largest calcite vein is at least 4 mm across, with smaller parallel veins occurring throughout the rock. Within these sparry calcite veins, patchy discontinuous porosity exists parallel to the planes of cleavage, constituting 15-20% of the calcite. Calcite veining

contains an apparently random distribution of pyrite crystals that are up to 0.1 mm across, and crystals of euhedral pyrite up to 1.5 mm across are found within the cataclasite. The presence of euhedral pyrite within the cataclasite suggests that the cataclasite was permeable to pyrite-forming fluids, which may be confirmed by the presence of pores (generally around <0.1 mm across) in the fault rock.

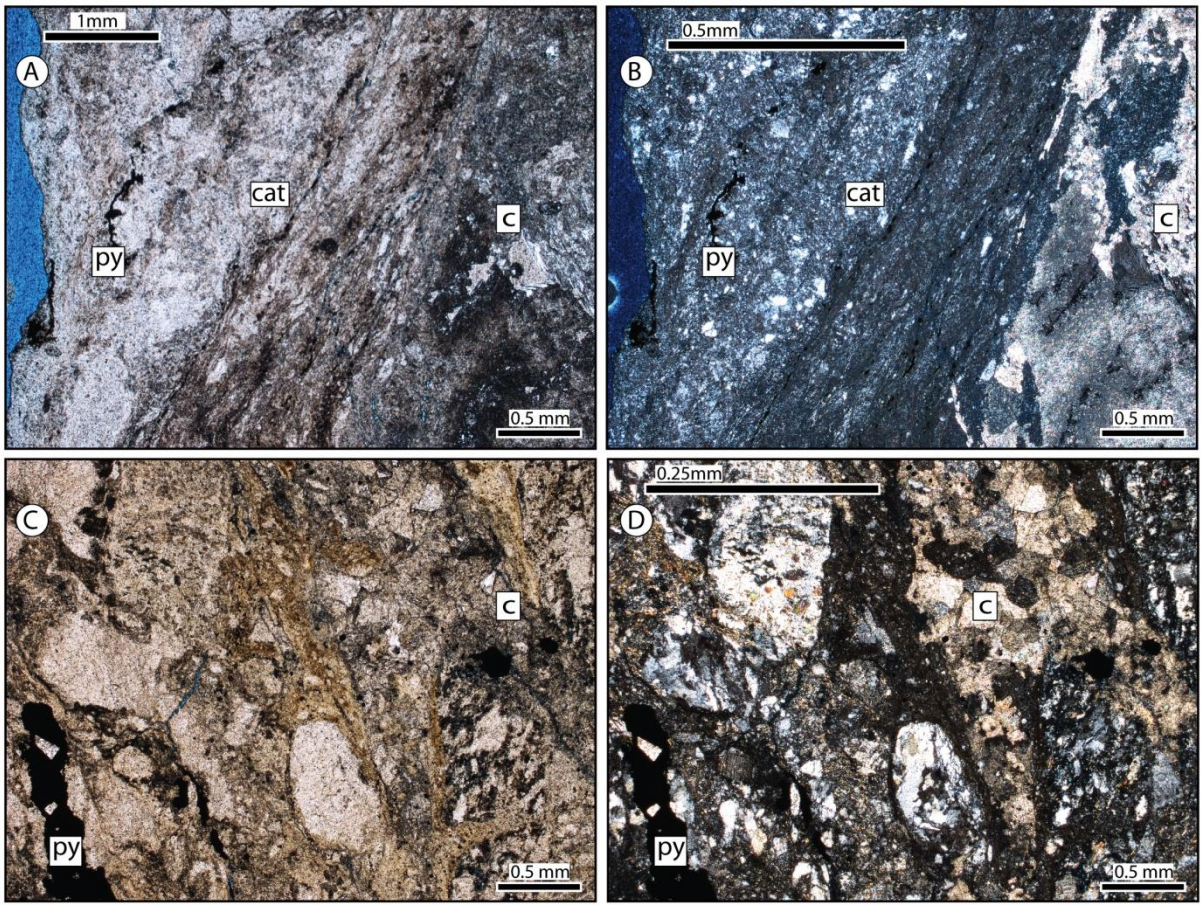

Figure 6.15: Photomicrographs from basement fault zone at 2490.3 m in well 206/8-8. c = calcite, cat = cataclasite, py = pyrite. (**A** - **B**) PPL and XPL, respectively. Very fine grained cataclasite (cat) grading into chaotic micro-breccia (**C** - **D**) PPL and XPL, respectively. Calcite mineralisation (c) supporting clasts of breccia derived from surrounding chaotic micro-breccia.

6.4.2.4 Conditions of fracture and faulting in the Clair Field

As discussed in previous chapters, the presence of epidote is indicative of temperatures above 200°C (Liou, 1993), which corresponds to depths in the crust of greater than 6 km, assuming a normal geothermal gradient existed at the time of formation. This suggests that epidote veining and cataclasis occurred before uplift of the Clair Ridge, probably during the Caledonian Orogeny or earlier.

Adularia veins and faults cut or reactivate epidote bearing fractures. Adularia is found in both euhedral form in veins associated with faulting, and in anhedral form in speckled veins alongside fine-grained pyrite, haematite, clay and probable oil. Adularia is commonly found in low

temperature veins (e.g. Steiner, 1970; Halliday and Mitchell, 1976), and can form at depths lower than or alongside analcime (zeolite) in burial diagenesis and hydrothermal systems (Goodwin, 1973; Hay, 1978). It has been found to exist at temperatures as low as 180°C in hydrothermal systems in the Philippines (Reyes, 1990), giving a possible minimum depth of 6 km with a normal geothermal gradient. The euhedral adularia-bearing phase of faulting and veining occurred mostly before oil migration and is associated with open porosity (now infilled with calcite) and euhedral adularia that has grown into porosity, probably occurring alongside high pore fluid pressure. Alteration of adularia and feldspar in the country rock to pale green clays is likely to have occurred during the period of greatest exhumation, potentially early during rift onset in the Devonian when the Rona Ridge was exposed subaerially. Geothermal gradients are elevated under rift conditions (e.g. Allen and Allen, 1990) and this could have produced adularia at depths in the crust shallower than 6 km. Upwelling relatively hot hydrothermal fluids may also have produced mineralisation at shallower depths in the crust. The rocks analysed above are from shallow depths in the basement (< 300 m), and as these veins do not contain oil and are affected by clay alteration, this indicates that euhedral adularia mineralisation is most likely to have occurred before exhumation and erosion of the Rona Ridge, probably in the Devonian. Later 'speckled' adularia veining may also be associated with faulting. Speckled adularia is seen with probable inclusions of oil, mutually cross cutting calcite-pyrite mineralisation. The association with calcite-pyrite veins and oil staining suggests that this later phase of adularia mineralisation may be Mesozoic in age (cf. Finlay et al., 2011). Reburial under the Clair Group and Mesozoic rifting may have elevated temperature and pressure conditions enough for adularia mineralisation within the basement.

The latest phase of mineralisation is that of quartz overgrowths and veining. Quartz overgrowths post-date calcite-pyrite veining and oil influx. In Iceland, quartz is present throughout the higher temperature zones in hydrothermal deposits, above about 250°C (Frey and Robinson, 1999). However, quartz crystallisation has also been associated with meteoric water at temperatures less than 100°C within sediments (Frey and Robinson, 1999). It seems likely that quartz mineralisation occurred at relatively shallow crustal levels in the Mesozoic/Cenozoic, given that it overprints late Cretaceous oil. The basement at Clair currently lies at depths of between 1800 – 2500 m and it seems probable that quartz mineralisation occurred at similar depths.

6.4.2.5 Summary of basement microscopy findings

The following sequence of veining, faulting, and mineralisation has been determined from microscopy work on samples from the basement:

1.a *Gneiss formation* was followed by alteration of amphiboles to chlorite and epidote and patchy alteration of feldspars to very fine grained sericite and epidote. This alteration may have occurred contemporaneously with 1.b.

1.b *Epidote veining and epidote cataclasites*, alongside chlorite and epidote alteration of the host rock. Epidote veins and cataclasites are very fine grained and equigranular with characteristic 'pistachio green' colour.

2.a *Grey fine grained cataclasite*, comprised predominantly of cataclastic sericite and feldspar/adularia that may have originated within the fault as veining. Associated with veins of euhedral adularia growing into open fractures (2.b). Post-dated by wide scale alteration of feldspars to green clay minerals. Within the fault rock, calcite is present infilling porosity up to 0.5 mm across.

2.b *Euhedral Adularia veining, within partially open fractures.* Crystals of adularia in these fractures are usually < 0.1 mm across, with open porosity up to 0.2 mm across and often altered to a bright green clay mineral. This alteration is common in core from 206/7a-2. Feldspar at fracture margins often exhibit syntaxial overgrowths probably associated with this phase of mineralisation.

Calcite-pyrite mineralisation is commonly observed infilling remaining fracture porosity, and appears to have been precipitated after adularia formation. Open fractures lined with euhedral adularia mineralisation are also associated with oil staining, and where calcite-pyrite mineralisation is present, oil staining can occur within pore space within calcite. No inclusions of oil were observed within euhedral masses of adularia crystals. Fracture linings of euhedral adularia display crystals that widen towards the (open) centre of the fractures, indicating nucleation at the wall rock (Cox and Etheridge, 1983).

Adularia mineralisation was followed by large scale alteration of feldspars in fractures and within the country rock to probable green clay in core 206/7a-2.

In core 206/8-8, adularia mineralisation that lines an open fracture may be associated with faulting that produced the very fine grained cataclasite (2.a).

3.a *Red-brown speckled adularia rich faults and veins.* Reddy brown veins and faults are common cutting the basement in well 206/7a-2. These fractures are up to 20 mm across in the core, and associated with calcite mineralisation. In thin section, fractures are speckled in appearance and filled with aggregates of very fine grained adularia, fine grained iron oxides, pyrite, and clay, and country rock clasts, alongside probable oil. Mutually cross cutting relationships were observed between speckled adularia-rich veins and sparry calcite-pyrite veining (3b), and quartz overgrowths overprint speckled adularia filled fractures.

Oil staining is visible within open fractures, and in some cases may be present with fine

grained aggregates of adularia crystals. Probable zeolite veining is seen reactivating speckled adularia veins.

Although this phase of veining is not associated with euhedral adularia mineralisation (as seen in 2.b) syntaxial overgrowths of country rock feldspar crystals are observed.

No evidence of faulting (cataclasis) along these veins was observed. Clasts of country rock are however entrained into the veins, but no evidence of cataclasis was observed. 'Haematite' bearing fault rocks in core from 206/7a-2 observed by Pless (2011) are very similar in appearance to the speckled adularia bearing veins discussed here and are probably one and the same.

3.b *Calcite and pyrite mineralisation*. Calcite and pyrite typically occur within the same fractures, usually with calcite hosting minor pyrite mineralisation. At least two phases of calcite-pyrite veining are present in the Clair Field basement. The earliest phase appears to be contemporary with the phase of adularia veining described above (3.a), and similarly at times also entrains clasts of country rock within it. Calcite-pyrite veining is also visible infilling fractures that are lined with euhedral adularia (stage 2.b). These relationships provide constraints on relative timings of mineralisation of these phases: Calcite mineralisation appears to have occurred after euhedral adularia mineralisation, but some developed synchronously with speckled adularia bearing fractures (3.a). Minor offset across sparry calcite veins suggests an association with faulting. 3.a and 3.b are mutually cross cutting and both show oil inclusions. Calcite within speckled adularia veins and with sparry calcite veins often exhibits evidence for dissolution, with porosity developed along cleavage planes. This dissolution may be associated with that found in the cover rocks, where feldspar, lithic clasts and calcite is known to have been dissolved, enhancing porosity of the rock prior to (or during) oil influx (e.g. Milodowski et al., 1998).

3. c *Postulated sparry calcite-pyrite mineralisation.* With oil inclusions and infilling porosity. Occurring synchronously with a phase of oil migration. Crystals are up to 5 mm across and are associated with similarly sized pyrites. These crystals lack porosity development along cleavage planes.

4 *Late quartz overgrowths*. Quartz mineralisation occurred mostly as syntaxial overgrowths on existing crystals into open porosity and across pre-existing calcite-pyrite and speckled adularia veins. Examples of quartz entirely enclosing remnant calcite crystals reduced in size from those of the original adjacent vein, are common, in addition to inclusions of pyrite and possible oil. This would suggest that calcite may have been dissolved synchronously with quartz mineralisation. Quartz overgrowths consistently postdate calcite-pyrite mineralisation and speckled adularia veins, as evidence by inclusions within quartz crystals. Hence, quartz veining and overgrowths occurred after 3.a and 3.b, and

possibly after oil migration.

5 *Orange-brown clay mineralisation and clay-bearing faulting.* Observed in one thin section filling porosity within both sparry calcite and quartz veins. In the same thin section, clay cements clasts of country rock and speckled adularia veins within a probable minor fault.

Hence, porosity is found associated with:

- Open tensile fractures, partially filled with euhedral adularia mineralisation (now green clay after alteration in well 206/7a-2).
- Speckled adularia veins with entrained clasts of country rock, showing random patchy porosity.
- Sparry calcite-pyrite veins. Also occurring as elongate irregularly shaped pores within calcite crystals growing parallel with crystal cleavage.
- Dissolved calcite (and syntaxial overgrowths of quartz).

Porosity produced during tensile fracturing has been reduced by syntaxial overgrowths of feldspar and quartz, adularia and clay mineralisation. Porosity has probably been enhanced through dissolution, noticeably within sparry-calcite crystals. Dissolution may also have affected adularia, although no conclusive evidence of this was observed.

6.5 Discussion

Combining macroscopic and microscopic observations of the core, the following chronology has been determined from section 6.3.3 and section 6.4.2.4:

Stage (age)	Basement	Cover (Devonian – Carboniferous)
1.a (Precambrian)	Gneiss formation, imposition of foliation. Age of 2527 Ma derived from whole rock Rb-Sr dating by Richie and Darbyshire (1984) for basement rocks 25 – 100 km SW of Clair.	
1.b (Precambrian/ Caledonian)	Epidote cataclasites and veining, possibly accompanying chloritisation and widespread retrogression of the gneiss.	
2.a (Post-Caledonian?)	Dark grey, very fine grained adularia/feldspar cataclasite development, alongside euhedral adularia mineralisation within open fractures.	

2.b (Devonian-Carboniferous)	Locally pervasive alteration of the feldspar in well 206/7a-2 to green clay. Probably occurred when the Rona Ridge was exposed to weathering before/during the deposition of the Clair Group.	Onset of deposition and lithification of the Clair Group. In the core (well 206/8-8) conglomerate deposition/lithification was accompanied by localised injections of fine sediment into the basement.
3.a (Mesozoic)	Possible calcite veining?	Patchy calcite mineralisation of the Clair Group, contemporaneous with/followed by development of granulation seams within still-porous sandstone. Within calcite cemented sandstone, granulation seams are much scarcer. Granulation seam development in porous sandstone was followed by formation of calcite veins with sets pre-dating oil influx (Calcite I of Milodowski, 1998).
3.b (Mesozoic)	At least two phases of calcite-pyrite veining contemporaneous with speckled adularia veins, alongside oil influx. Porosity with ragged margins within some calcite crystals suggests a degree of dissolution, possibly related to quartz overgrowth formation. Pyrite and bitumen dating by Finlay et al., (2011), gives late Cretaceous age. Probable zeolite veining often reactivating speckled adularia veins.	Calcite veining occurred synchronous with oil influx (Calcite II and III of Milodowski, 1998). Late calcite veining (Calcite III) was also synchronous with faulting, with veining increasing in intensity towards faults. In areas of shale, clay gouge formed. Dissolution of calcite was noted in sparry veins in the cover rocks. Within 206/8-10z open fractures formed from dissolution are associated with normal faulting.
4 (Mesozoic or younger)	Quartz overgrowths and quartz veining, probably following on from calcite dissolution and oil influx.	Not present in the Clair Group?
5 (Mesozoic or younger)	Clay bearing faulting.	Very poorly indurated clay bearing faulting (from 206/8-10z)?

6.5.1 Basement porosity

Barr et al., (2007) divides the fractures encountered in the Clair Group into three groups:

- Non-conductive – granulation seams and cataclasites.
- Conductive – open fractures, nearly always with some shear offset. Often containing calcite and pyrite with evidence to suggest that the fractures were open in the sub-surface.

- Cemented or filled – 'blocked' during or after formation, with sparry calcite and/or fluorite. Also oil is encountered intergrown with cement, indicating syn- or post-migration cementation.

In this chapter, porosity within conductive fractures in the basement has been found to result from several modes of formation. Later mineralisation has often occluded porosity within the basement, yet open fractures do still exist. Porosity is particularly associated with adularia mineralisation (both 'speckled' and euhedral) and calcite-pyrite veining. Calcite-pyrite veining occurred alongside oil influx, and oil may have provided the necessary CO2 and sulphide and for the formation of these veins.

Euhedral adularia that lines open fractures originates on the wall rocks of tension fractures, probably associated with faulting, that must have been open and fluid filled in the sub-surface, indicating high pore fluid pressures. This porosity has consequently been partially filled with adularia, calcite-pyrite, oil, and quartz overgrowths. The origin of these tension fractures is unknown, but they are seen to be linked with and sub-parallel to grey, fine-grained, adularia-bearing cataclasite along a fault in well 206/8-8. Thus it seems likely that tension fractures opened due to faulting, perhaps under high pore fluid pressures, and were subsequently available for fluid flow. Euhedral adularia mineralisation is postdated by alteration to a pale green mineral that is probably clay. This alteration is not observed in speckled adularia veins of Mesozoic age that occur with oil influx. Hence euhedral adularia predates oil influx and may be associated with Devonian exhumation and erosion of the Rona Ridge.

Although common in the basement, adularia has not been identified in the cover. Milodowski (1998) notes the association of porosity with what they describe as partially dissolved K feldspar in one sample from the cover. However, the figure illustrating this (page A9, Figure 17) shows crystals with the distinctive adularia form that are unlikely to be detrital. It therefore seems likely that adularia mineralisation may be present within the Clair Group. This would also imply a Devonian and younger age for some of the adularia identified within the basement rocks.

6.5.2 Comparison to the Hebrides

In the Clair cores, foliation tends to be rather poorly defined. This is in marked contrast to the majority of outcrop in the Outer Hebrides, especially within the Outer Hebrides Fault Zone where foliation is pervasive and often mylonitic. No mylonites or phyllonites were observed within the Clair Core, although this may be due to very limited sampling. Foliation in well 206/7a-2 strikes N-S to NNW-SSE and dips steeply to the east and west, although as seen within the Lewisian on

Lewis, the foliation is locally variable. Areas of more poorly defined foliation do exist within the Outer Hebrides (e.g. the Uig Hills – Harris granite vein complex) but these are outside the OHFZ.

6.5.2.1 Cover

Fault rocks in the Stornoway Formation have developed directly from the country rock, with clay-rich slip surfaces around 2 cm thick containing clay that is both derived from the matrix of the conglomerate and developed authigenically within the fault. In places the fault rock is carbonate cemented, and associated with zeolite mineralisation. In the Clair Group, fault rock composition is determined by the surrounding country rock. Within porous sandstones, granulation seams have developed, and these are reactivated by later veining within calcite cemented sandstones. As granulation seams reduce the primary porosity and permeability of sandstone, later exploitation of granulation seam margins must occur as they represent relatively weak discontinuities within calcite-cemented rock, and are hence preferentially fractured and mineralised. Elsewhere, calcite cemented sandstone does not display granulation seams, and the fault rocks are calcite-cemented breccias. In zones of shale, clay gouges have developed. Open fractures seen within well 206/8-10z were not observed within the Stornoway Formation. Calcite within the open fractures in 206/8-10z shows imprints of the location of clasts that are now missing, and oversized pores point to production of these fractures through dissolution of calcite, lithic clasts, and feldspar (Milodowski, 1998). These open fractures exist in immediate proximity to faults, where they are most intense. Hence, fracturing related to faulting is likely to have enabled significant fluid flux through the Clair Group, resulting in dissolution and porosity production in the regions surrounding normal faults. Patchy vuggy discontinuous porosity up to 0.5 mm across is seen within fault rocks in the Stornoway Formation, alongside pores at times partially infilled with calcite that displays evidence of dissolution along cleavage planes (section 3.3.3.2). Similar to the Stornoway Formation rocks, authigenic clay-bearing gouges are also present within the basal conglomerate at Clair. The lithological dependence of fault rocks on the surrounding country rock in the rest of the Clair Group suggests that the interstitial matrix of the conglomerate is very likely to have had a significant role in the development of clay gouge. Except for within the basal conglomerate (Unit 1) at Clair, clay-bearing gouge faults that were observed in the Clair Group have developed from shale-like zones. Granulation seams are not present in the Stornoway Formation.

The basal conglomerate shows some marked similarities to the Stornoway Formation. In both rocks, calcite mineralisation forms a patchy cement within the matrix. Calcite veining is common within the basal conglomerate of the Clair Group, often forming patches where calcite entirely replaces the matrix – this is also seen within the Stornoway Formation. Calcite also forms vertical

veining within gneiss clasts in the conglomerate that may be associated with normal faulting. Normal faulting of varying degrees of development was observed in both the Stornoway Formation and within the basal conglomerate.

6.5.2.2 Basement

Similar to the Outer Hebrides, epidote cataclasite within the Clair Field basement represents the earliest phase of identified faulting and veining. At Clair, porosity has been primarily found to be associated with euhedral adularia mineralisation lining open fractures. Mesozoic faulting in the Lewisian Gneiss of the Outer Hebrides is represented by authigenic clay-bearing gouges and cataclasites that are associated with calcite, zeolite and adularia mineralisation, and porosity in the Stornoway Region basement is also associated with adularia mineralisation that appears to be growing into open fractures. In the cases observed in section 3.4.4.1 (stage 4 zeolite-bearing fault rock), adularia mineralisation occurs along fault planes, crystallising within open porosity alongside clay mineralisation that was contemporaneous with adularia mineralisation. Widespread alteration of feldspar to a pale green mineral at Clair is probably related to weathering, but this has not been observed in the Outer Hebrides where weathered gneisses are often bleached to a paler colour. In general, there is a lack of authigenic clay-bearing faults in the Clair Field basement rocks but sparse sampling and poor recovery during drilling may have prevented their observation. Oil observed within Mesozoic age basement hosted faults in the Outer Hebrides (section 3.4.4.1) confirms that these structures act as conduits for the migration of fluids.

Overall, the observations in the Clair basement are similar to those of the Outer Hebrides, where epidote has been associated with Caledonian fault movements on the OHFZ, and calcite has been associated with normal faulting that postdates the Caledonian orogeny.

6.5.2.3 Basement – Cover Interface

In the Stornoway Region, the faulting has been observed to localise along the basement-cover interface, with evidence of fluid overpressure in the form of euhedral calcite mineralisation and repeated phases of sediment injection into the basement. The interface was only studied in one core from the Clair Field (206/8-8), and deformation at the basement-cover interface at Clair was much more limited than that in the Stornoway region, appearing to be a simple unconformity. The contacts observed in the Stornoway region were adjacent to the oldest exposed unit of the Stornoway Formation (at Dun Mor section 3.5.1.2 and Suardail section 3.5.1.3). Hence this area was most heavily rotated and faulted during basin development. Clair may not show such geology

at the location studied as it was from the centre of a graben (the 'core' area) but it is difficult to assess this given that no bedding data are available. A similar relationship between faulting in the basal conglomerate and calcite mineralisation was however observed at both Clair and Lewis, with vertical calcite mineralisation related to normal faulting. Although sediment injection was seen in one clast within the basal conglomerate at Clair, it was not observed within the basement itself, but this is likely to be due to poor sampling.

6.6 Conclusions

- *What are the characteristics and age of faulting and fractures in the Clair Group?*

  As reported by Milodowski (1998), multiple phases of fracturing and mineralisation exist within the Clair Group. Fault rock type is mostly strongly influenced by the host rock lithology, with granulation seams developed in porous sandstones and calcite-cemented breccias within calcite cemented sandstones. Clay gouge-bearing faults are present within shale layers.

  Dissolution clustered around normal faulting has produced a set of open fractures that are partially filled with sparry calcite and pyrite. Open fractures/porosity have been intersected in well 206/8-10z and have been identified as important for oil flow (Barr et al., 2007).

- *What are the characteristics and age of faulting and fractures in the Clair basement?*

  Multiple phases of fracturing and veining are evident within the basement at Clair. Fracturing of probable Caledonian age is represented by epidote veins and cataclasites. These are cut by grey fault rocks comprised of very fine grained adularia cemented cataclasite, associated with tensile fractures partially filled with euhedral adularia mineralisation, possibly of early Devonian age. Alteration of feldspar within the gneiss and adularia veining is believed to result from near surface weathering, possibly during the Devonian. Open fractures persisted and were partially filled by subsequent speckled adularia and calcite-pyrite veining during the Mesozoic, that was also contemporaneous with oil influx. Quartz mineralisation in the form of syntaxial overgrowths and limited veining postdate calcite-pyrite veining and oil influx. This last phase of mineralisation is not preserved in the Devonian cover.

- *What are the characteristics of porosity within the Clair Field?*

  Four types of porosity exist in the Clair field basement, ordered oldest to youngest these are:

- Open tensile fractures, partially filled with euhedral adularia mineralisation (now green clay after alteration in well 206/7a-2).
- Speckled adularia veins with entrained clasts of country rock, showing random patchy porosity.
- Sparry calcite-pyrite veins also display vuggy porosity. Elongate irregularly-shaped pores also occur within calcite crystals oriented parallel with crystal cleavage.
- Dissolution of calcite (associated with syntaxial overgrowths of quartz).

- *How does fracturing within the Clair Field compare to the Outer Hebrides?*

  Porosity in the Stornoway Region and the Clair Field is found in both locations along open fractures, partially filled with adularia, zeolite and calcite. In the Stornoway Region Lewisian Gneiss and the Clair Field basement, adularia mineralisation and porosity are associated with faulting. Mesozoic age faulting in the Outer Hebrides is clay- and calcite-bearing, but little evidence was found for clay-rich faults within the basement rocks at Clair, with the exception of one example of potential clay bearing faulting seen under the microscope. Clay-bearing fracturing is however the last phase of fracturing in the Clair Field basement and in the Lewisian Gneiss of the Outer Hebrides. No mylonite or phyllonite was observed in the Clair Field, and there was no evidence for the reactivation of foliation, a feature that is often seen in the Outer Hebrides

- *What are the controls on fracturing?*

  Foliation was not seen to be reactivated in the Clair Field. Fracturing and mineralisation do however repeatedly reactivate pre-existing fractures. Epidote-bearing cataclasites and veins are reactivated by speckled adularia, calcite-pyrite veining, and late clay bearing faulting.

  It was not possible to assess the orientations of tensile fractures, but where they were observed they were often seen to be parallel/sub parallel with each other, suggesting some kind of organisation that may be related to regional faulting.

Chapter 7: Quantification of Fracture Characteristics

7.1 Introduction

It is important to quantify fracture attributes such as length, aperture and spacing in order to fully understand fracture geometry (Chapter 2). Many authors have discussed the existence of self-similarity of these attributes across all scales in the crust and attempted to quantify these attributes (e.g. Barton and Zoback, 1992; Nicol et al., 1996; Peacock and Sanderson, 1994Gillespie et al., 1993; McCaffrey and Johnston, 1996; Sleight, 2001; Jolly and Cosgrove, 2003; McCaffrey et al., 2003; Pless, 2011). 1D line transects are an effective way of collecting fracture attribute data that can be analysed and compared to studies conducted elsewhere (e.g. Gillespie et al., 2001 Ortega et al., 2006). Data presented in this chapter have been collected along 1D line transects performed over selected outcrops on Lewis and Harris as an analogue for the Clair Field, and from selected parts of the Clair core. As discussed previously, Mesozoic faults and fracture systems within Clair are particularly important for fluid flow, and characterisation of fractures on Lewis has concentrated on Mesozoic and younger age fracture sets. Determination of spacing and aperture characteristics allows more accurate modelling of fracture populations with field simulations.

7.1.1 Rationale and Objectives

The main aim of this chapter is to quantify fracture characteristics further, in particular spacing, and aperture, in order to answer the following questions:

- What are the fracture characteristics in the Hebrides and in the Clair Field?
- Is Mesozoic faulting recognisable from its spacing characteristics?
- How does fracture spacing change between joint dominated vs. fault dominated areas?
- Is there any effect on fracture spacing due to lithology?
- How do fractures vary from basement to cover?

7.1.2 Methodology - a note on attribute vs. cumulative frequency plot interpretation

Quantifying fracture attributes such as spacing is most reliably achieved through collection of 1D line transect data (e.g. Gillespie et al., 1993; Beacom et al., 2001; Jolly and Cosgrove, 2003; McCaffrey et al., 2003) (section 2.3). Data collected along transects is plotted on fracture attribute vs. cumulative frequency plots that are used to ascertain the type of distribution represented by the data (e.g. Harris et al., 1991; Gillespie et al., 1993; Pickering et al., 1995; McCaffrey and Johnston, 1996; Beacom et al., 2001; Sleight, 2001; Jolly and Cosgrove, 2003; McCaffrey et al., 2003; Ortega et al., 2006; Olson, 2007; Pless, 2011). Fracture attribute datasets are commonly

described by three types of distribution; power-law, exponential and log-normal (e.g. Bonnet et al., 2001). These distributions plots as straight lines on log/log, log/linear, and linear/log plots, respectively (see section 2.3.2). However, if the sample does not represent the full population accurately, the sample is biased, and is not representative (Pickering et al., 1995). Two common biases are present in fracture studies, truncation and censoring (Pickering et al., 1995, see section 2.3.2.4). Because of the effects of bias on the distribution of data, it can be difficult to distinguish the type of distribution that best describe the data. On log/log plots, the curvature of individual distributions may be caused by a combination of truncation (smaller sized faults/spacings that are inadequately sampled) at the smaller scale end and censoring (larger sized faults/spacings are inadequately sampled) at the larger scale end (Odling, 1997). There is no method that corrects fully for the effects of censoring and truncation in these studies. Natural fracture characteristics such as length (Nicol et al., 1996), aperture (e.g. Marrett et al., 1999) and spacing (Gillespie et al., 1993) often can be described by power-law distributions. Hence, power-law distributions are often assumed and the curved tails present on log/log plots are simply discounted (e.g. Odling, 1997; McCaffrey et al., 2003; Pless, 2011). However, this assumption can lead to a misrepresentation of the distribution, for example if the data are best represented by an exponential distribution that the curved tails are a part of. Additionally, studies in the literature often sample limited fractures belonging to a well-defined single set of structures, a situation that does not exist within basement rocks on Lewis and Harris.

This project was not focused around the development of statistical methods for the analysis of fractures. Hence, each dataset is plotted on log/log, log/linear and linear/log to enable comparison between potential distribution types in order to determine which distribution type best fits the data. Visual comparison of these plots, the coefficient of variation (Cv, section 2.3.2.4) and the number of points excluded from each plot to produce a straight line trend with an $R^2 > 0.9$ are all taken into account when determining which distribution type is the best description. The power-law distribution type is only assigned when a sufficient straight line portion on the log/log plot is present. A straight line across ~1 order of magnitude on the x axis of the log/log plot was selected as the cut-off for the interpretation for the presence of a power-law distribution, as ideally data should span at least one order of magnitude for power-law interpretation (e.g. McCaffrey and Johnston, 1996). It is also important to bear in mind where data on each plot is densest. If curvature on the log/log plots occurs where data density is the highest, it is more likely that it will be a real representation of the data and the spacing distribution may not be power law. Determining whether a power-law is present is important as the D value provides a better characterisation of spatial distributions than other measurements such as fracture density (Belfield, 1998).

7.2 Spacing - lineament transect data

7.2.1 Methods – lineament transects

Lineaments were selected for orientation and spacing analysis, using the methodology for lineament picking discussed in section 2.1. Lineament transects were chosen to ensure that a minimum of 30 structures were intersected to enable the type of distribution represented by the data to be ascertained. Data sets with fewer than 30 data points give poorly defined distributions on graphical presentations of the data. The generally poor exposure away from coastal regions means that only four lineament transects were used to investigate the spacing characteristics of lineaments on Lewis and Harris. The general exposure levels also mean that only relatively large structures can be picked out from the available datasets.

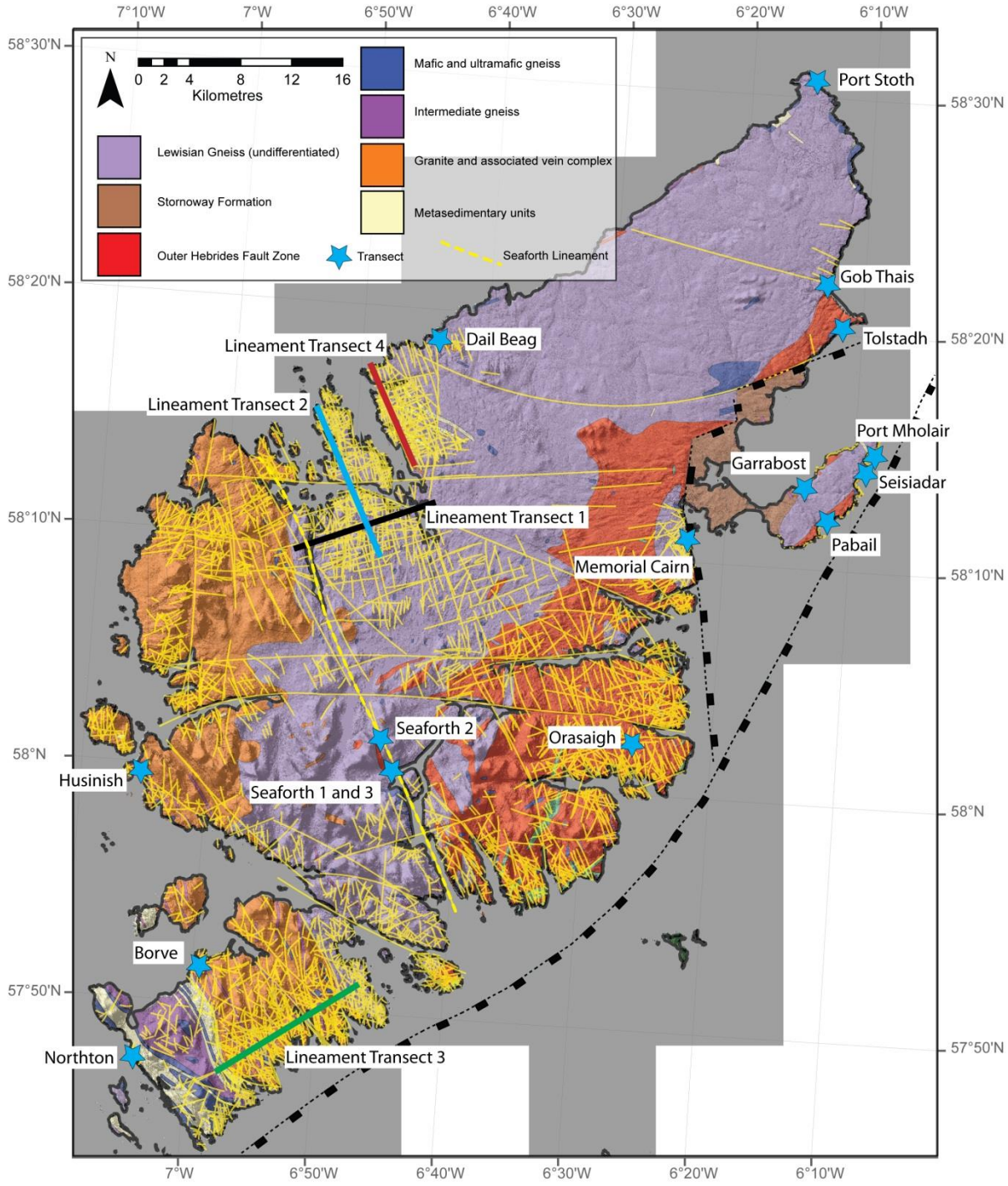

Figure 7.1: Geological map of Lewis and Harris, showing lineament transects (red, blue, black and green) and localities of transect data collected on fieldwork (blue stars).

7.2.2 Results

Cv values from transects one to four are all < 1 (Table 7.1), with transects three and four being very close to 1 (0.95 and 0.97, respectively) which would be characteristic of a random spacing distribution. Transects 1 and 2 display relatively more anticlustered spacing distributions (0.79 and 0.88, respectively). Transects 2 and 4 are adjacent and parallel (Figure 7.1), sampling fractures of similar orientations (Figure 7.2), and hence may be expected to show similar results. However

transect 4 shows a greater fracture density and decreased spacing. Although transect 3 is sub parallel with transect 1, orientations sampled by these transects are different, reflecting the difference in fracture orientation across Lewis and Harris discussed in previous chapters. The data are shown plotted with spacing (m) vs. cumulative frequency, normalised to the transect line length, on log/log, log/linear and linear/log plots (Figure 7.3).

Table 7.1: Results for lineament transects across the Lewisian Complex.

Line	Description	Line Orientation	N	length (m)	Fracture Density (fractures/m)	STD of Spacing	Mean Spacing (m)	Cv
1	WNW-ESE transect intersecting dominantly N-S striking faults of western Lewis, assumed to be related to Mesozoic normal faulting observed along N-S faults in W Lewis.	74°	34	11172	0.0030	238.04	300.32	0.79
2	NNW-SSE trending transect intersecting dominantly ENE-WSW trending lineaments, likely to be linked with Mesozoic dip-slip ENE-WSW striking faults in W Lewis.	138°	49	12800	0.0038	219.59	248.86	0.88
3	NE-SW trending transect intersecting dominantly NW-SE trending lineaments on south Harris, probably representing multiple ages of fractures.	69°	76	12730	0.0060	153.27	160.77	0.95
4	NNW-SSE trending transect, intersecting dominantly ENE-WSW trending lineaments, likely to be linked with Mesozoic dip-slip ENE-WSW striking faults in W Lewis.	135°	43	8665	0.0050	188.45	194.02	0.97

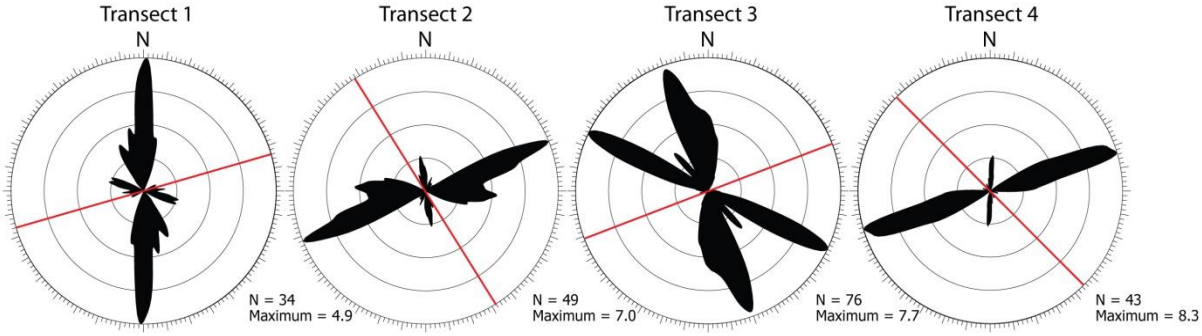

Figure 7.2: Rose diagrams of lineament orientations intersected by each transect.

No power-law trend lines have been assigned to the log/log plot due to the obviously curved nature of the distributions and the absence of a straight line portion to assign a power-law trend line to. The distributions are best described as negative exponential, with fewest data points excluded for an exponential trend line fit (Table 7.2). Log-normal trend lines on the linear/log plots are relatively difficult to fit, with >40% of data points excluded to create a log-normal trend line fit.

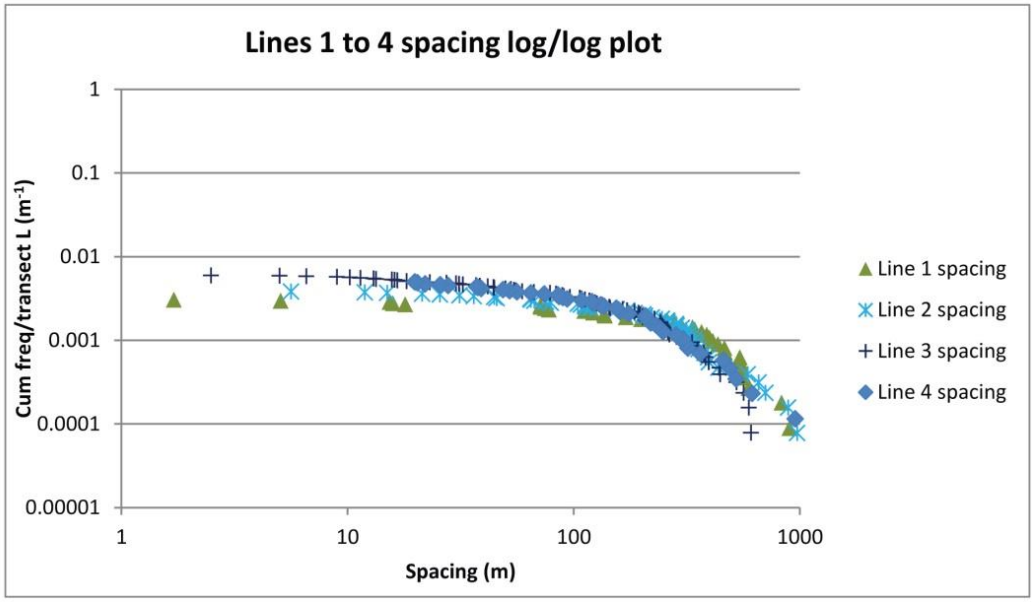

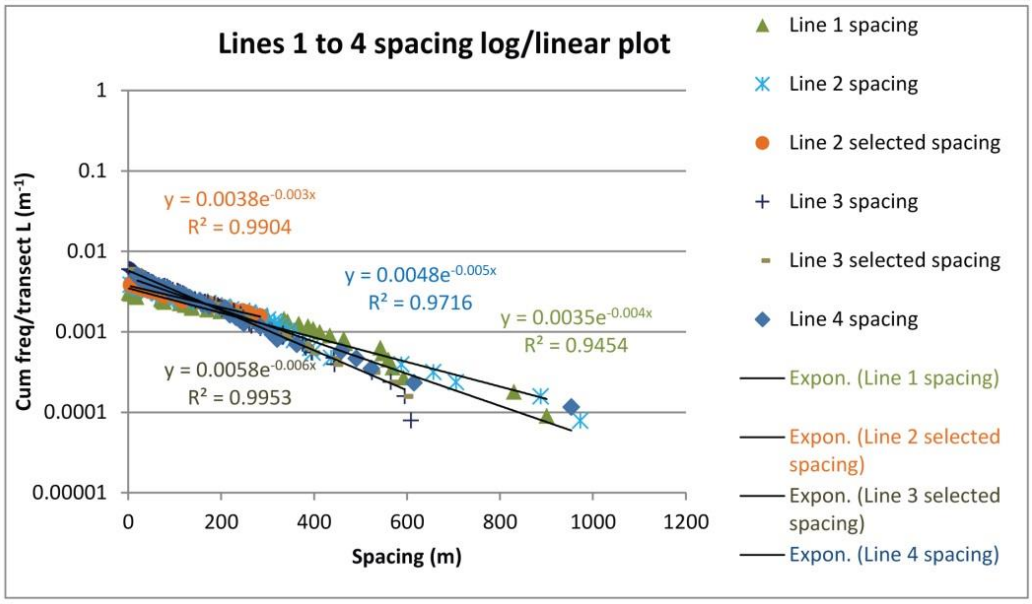

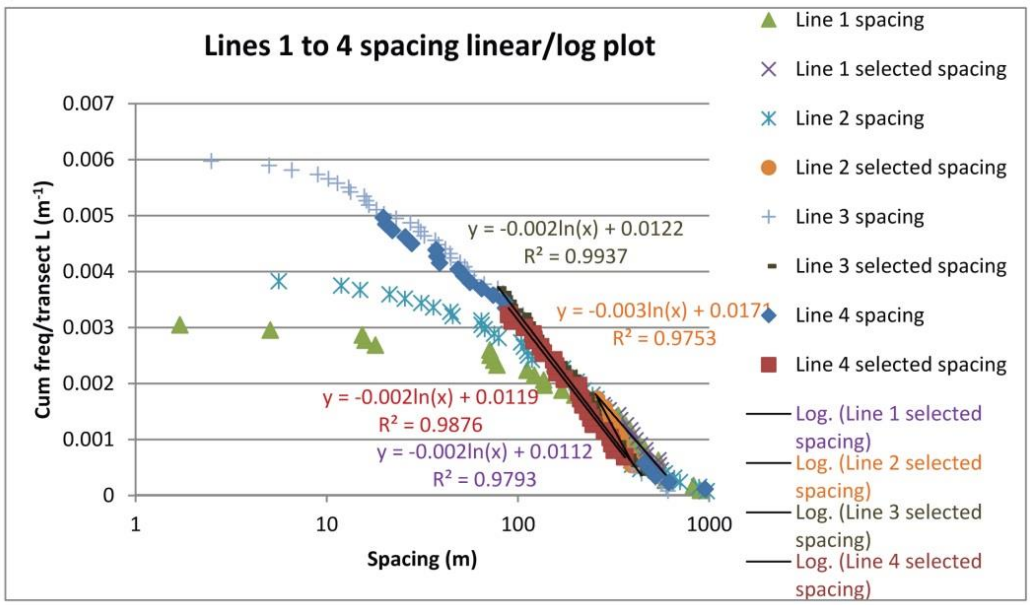

Figure 7.3: Lineament transects results, showing spacing (m) vs. cumulative frequency/transect line length.

Table 7.2: Table of number of data-points excluded from each plot type (and percentage of total data).

Distribution	Line 1	Line 2	Line 3	Line 4
Power-law	N/A	N/A	N/A	N/A
Negative exponential	0	19 (39%)	1 (1%)	0
Log-normal	17 (50%)	33 (67%)	33 (43%)	20 (47%)

7.2.2.1 Summary and discussion

The Cv values of close to 1 suggest that these data are best represented by exponential relationships. In addition, the high R^2 values of >0.945 show that the lineament spacing data is well represented by exponential trend lines. Variations in the fracture density are at least partly attributable to differences in exposure – on Harris (transect 3) exposure is better than Lewis. Pless (2011) finds exponential and weak power-law relationships on transects taken across lineaments of multiple orientations (and hence of multiple fracture sets). Splitting lineaments by orientation on the mainland and performing transects across lineaments of select orientations was found to produce stronger power-law relationships due to isolation of specific fracture sets (Pless, 2011). Due to the relatively low number of lineaments sampled in the Lewisian of Lewis and Harris, it is not possible to repeat this approach here.

7.3 Spacing – Lewis and Harris fieldwork transect data

7.3.1 Methods – fieldwork transects

Transect data were collected during extended periods of fieldwork on Lewis and Harris across outcrops selected for specific fracture sets and lithologies (Table 7.3). Where possible, transect data were collected from outcrops both parallel and perpendicular to the strike of selected fracture sets to enable direct comparison of attributes from different fracture sets at different orientations.

Data from individual localities were plotted on power-law, log-normal and exponential graphs of the variable measured vs. cumulative number (e.g. Gillespie et al., 1993; Beacom et al., 2001). These plots were studied visually and, together with the coefficient of variation (Cv) and

proportion of points excluded from straight line portions, were used to decide the distribution type (section 7.1.2). Spacing results are analysed here.

It is apparent from previous studies that the local geological context of 1D fieldwork line transects is extremely important in determining the spacing and fault attributes of any fracture sets (e.g. Beacom et al., 2001). Hence, sites are divided in this study by geological context so that inherent geological differences may be taken into account. Unfortunately due to the generally large (decimetre) spacing of faults in the Stornoway Formation and the limited coastal exposure, it was not possible to perform transects within the Stornoway Formation during either fieldwork or lineament analysis.

7.3.1.1 Study sites for transect data collection

In this section, spacing data collected from the localities shown in Table 7.3 are analysed.

Table 7.3: Transect localities from Lewis and Harris. Transects marked parallel and perpendicular were taken parallel and perpendicular to Mesozoic dominated fracture sets.

Locality	Grid ref	Orientation	Lithology	Fracture set sampled
Borve 1	NG 0387 9645	040°	Banded gneiss and granite. Outside OHFZ.	Pre-Mesozoic faults and joints.
Borve 2	NG 0388 9755	330°	Banded gneiss (adjacent to granite). Outside OHFZ	Pre-Mesozoic faults and joints.
Borve 3	NG 0381 9638	333°	Massive granite, lacking any foliation. Outside OHFZ.	Pre-Mesozoic faults and joints.
Dail Beag	NB 2274 4601	064°	Banded Gneiss. Outside the OHFZ.	Joint dominated fracture set striking NW-SE. See section 4.4.2.2.
Garrabost	NB 5104 3308	260°	Banded gneiss near the OHFZ.	Mesozoic fault dominated, NNW-SSE and N-S striking faults. See section 3.4.2.1.1.
Gob Thais	NB 5354 5005	160°	Banded gneiss. Outside the OHFZ.	Joint dominated. See section 4.5.1.
Hushinish	NA 9936 1190	170°	Granitic gneiss, adjacent to large NNW-SSE trending lineament.	Calcite vein and joint dominated. See section 5.4.1.
Memorial Cairn 1 (Parallel)	NB 4254 2988	160°	Banded gneiss with amphibolite, within OHFZ..	Mesozoic fault dominated. See section 3.4.2.2.
Memorial Cairn 2 (Perpendicular)	NB 4254 2988	067°	Banded gneiss with amphibolite, within OHFZ..	Mesozoic fault dominated. See section 3.4.2.2.
Orasaigh 1	NB 3766 3944	268°	Banded gneiss, within OHFZ.	Sub-parallel with late E-W faults, joints and veins. See section 4.5.2.3.
Orasaigh 2	NB 3766 3944	256°	Banded gneiss, within OHFZ	Sub-parallel with late E-W faults, joints and veins. See section 4.5.2.3.
Orasaigh 3	NB 3766 3944	253°	Banded gneiss, within OHFZ	Sub-parallel with late E-W faults, joints and veins. See section 4.5.2.3.
Pabail	NB 5328 3124	072°	Banded gneiss within OHFZ, adjacent to NNW-SSE Mesozoic fault with several ms of gouge.	Mesozoic calcite cemented minor fault dominated. See section 3.4.2.1.3
Port Mholair	NB 5647 3628	249 °	Banded gneiss and granite, outside the OHFZ.	Epidote bearing faulting and background jointing. See section 3.4.2.1.6
Port Stoth	NB 5239 6596	350°	Finely laminated mylonite outside the OHFZ.	Epidote bearing faults reactivated with clay bearing faulting. See section 4.4.1.2.
Seaforth 1 (Perpendicular)	NB 1925 1188	062°	Banded gneiss, outside the OHFZ. Along road cut.	Dominated by jointing (50 m from the Seaforth Fault).
Seaforth 2 (Parallel)	NB 1871 1325	150°	Mylonitic gneiss, probably within the OHFZ.	Dominated by faulting. See section 4.4.3.2.
Seaforth 3 (Perpendicular)	NB 1928 1192	062°	Banded gneiss, outside the OHFZ. Along road cut.	Dominated by clay gouge bearing faults related to the Seaforth fault.
Seisiadar 1 (Perpendicular)	NB 5593 3300	136°	Banded gneiss, within the OHFZ.	Mesozoic fault dominated. See section 3.4.2.1.4.
Seisiadar 2 (Parallel)	NB 5593 3300	032°	Banded gneiss within the OHFZ.	Joint dominated. See section 3.4.2.1.4.
SHSZ A	NF 9864 8946	147°	Foliation parallel within met	Joint dominated. See section 5.4.4.
SHSZ B	NF 9864 8946	33°	Banded gneiss, perpendicular with the foliation.	Joint dominated. See section 5.4.4.
SHSZ C	NF 9867 8943	120°	Banded gneiss.	Joint dominated adjacent to NNE-SSW striking fault. See section 5.4.4.
SHSZ D	NF 9864 8946	036°	Banded gneiss, oblique to the foliation.	Joint dominated. See section 5.4.4.
Tolstadh	NB 5412 4618	095°	Within the 'crush mélange' of the OHFZ – very heavily fractured cataclastic gneiss.	Fractures within cataclastic gneiss, cut by Mesozoic structures. See section 3.4.2.3.

7.3.2 Results

Table 7.4 shows the numerical results for all transect data collected on Lewis and Harris. These data are discussed in the sections below for specific characteristics identified in the objectives (section 7.1.1).

The number of spacing values may vary by a small amount from the number of fractures due to small exposure gaps (<50 cm) in individual transects.

Table 7.4: Line transect results.

Locality	N (fracs)	N (spacing values)	Mean spacing (m)	STD	Cv	Transect Length	Density (fracs per m)	Lithology	Fracture set sampled
Borve 1	188	186	0.39	0.56	1.45	77.58	2.42	Banded gneiss and granite. Outside the OHFZ.	Pre-Mesozoic faults and joints.
Borve 2	234	233	0.14	0.23	1.58	33.9	6.9	Banded gneiss (adjacent to granite). Outside the OHFZ	Pre-Mesozoic faults and joints.
Borve 3	17	16	0.30	0.30	0.99	61.74	0.28	Massive granite, lacking any foliation. Outside the OHFZ.	Pre-Mesozoic faults and joints.
Dail Beag	68	67	0.27	0.29	1.08	20.64	3.29	Banded Gneiss. Outside the OHFZ.	Joint dominated fracture set striking NW-SE. See section 4.4.2.2.
Garrabost	85	83	5.04	6.24	1.24	435.5	0.2	Banded gneiss within the OHFZ.	Mesozoic fault dominated, NNW-SSE and N-S striking faults. See section 3.4.2.1.1.
Gob Thais	63	62	0.38	0.30	0.81	23.47	2.68	Banded gneiss. Outside the OHFZ.	Joint dominated. See section 4.5.1.
Hushinish	108	107	0.15	0.13	0.83	9.9	10.91	Granitic gneiss, adjacent to large NNW-SSE trending lineament. Outside the OHFZ	Calcite vein and joint dominated. See section 5.4.1.
Memorial Cairn 1 (Parallel)	61	60	0.19	0.14	0.70	12.22	4.99	Banded gneiss with amphibolite, within OHFZ.	Mesozoic fault dominated. See section 3.4.2.2.
Memorial Cairn 2 (Perpendicular)	172	173	0.14	0.19	1.37	30.22	5.69	Banded gneiss with amphibolite, within OHFZ.	Mesozoic fault dominated. See section 3.4.2.2.
Orasaigh 1	238	220	0.12	0.15	1.26	31.48	7.56	Banded gneiss, within OHFZ.	Sub-parallel with late E-W faults, joints and veins. See section 4.5.2.3.
Orasaigh 2	111	104	0.12	0.14	1.16	18.33	6.06	Banded gneiss, within OHFZ	Sub-parallel with late E-W faults, joints and veins. See section 4.5.2.3.

Orasaigh 3	57	56	0.11	0.23	2.07	7.74	7.36	Banded gneiss, within OHFZ	Sub-parallel with late E-W faults, joints and veins. See section 4.5.2.3.
Pabail	63	61	0.16	0.12	0.75	10.63	5.93	Banded gneiss within OHFZ, adjacent to NNW-SSE Mesozoic fault with several ms of gouge.	Mesozoic calcite cemented minor fault dominated. See section 3.4.2.1.3
Port Mholair	149	145	0.23	0.24	1.07	33.72	4.42	Banded gneiss. Outside the OHFZ.	Epidote bearing faulting and background jointing. See section 3.4.2.1.6
Port Stoth	87	86	0.09	0.07	0.83	8.27	10.52	Finely laminated mylonite. Outside the OHFZ.	Epidote bearing faults reactivated with clay bearing faulting. See section 4.4.1.2.
Seaforth 1 (Perpendicular)	168	167	0.27	0.27	1.03	44.54	3.77	Banded gneiss, outside the OHFZ. Along road cut.	Dominated by jointing (50 m from the Seaforth Fault).
Seaforth 2 (Parallel)	46	45	0.18	0.16	0.90	8.43	5.45	Mylonitic gneiss, probably within the OHFZ.	Dominated by faulting. See section 4.4.3.2.
Seaforth 3 (perpendicular)	141	138	0.22	0.30	1.34	39.17	3.6	Banded gneiss, outside the OHFZ. Along road cut.	Dominated by clay gouge bearing faults related to the Seaforth fault.
Seisiadar 1 (Perpendicular)	67	66	0.19	0.23	1.22	13.75	4.87	Banded gneiss, within the OHFZ.	Mesozoic fault dominated. See section 3.4.2.1.4.
Seisiadar 2 (Parallel)	51	50	0.48	0.53	1.10	24.14	2.11	Banded gneiss within the OHFZ.	Joint dominated. See section 3.4.2.1.4.
SHSZ A	179	166	0.06	0.07	1.21	9.36	19.12	Banded gneiss, parallel with the foliation. Outside the OHFZ	Joint dominated. See section 5.4.4.
SHSZ B	69	61	0.13	0.11	0.86	8.72	7.91	Banded gneiss, perpendicular with the foliation. Outside the OHFZ	Joint dominated. See section 5.4.4.
SHSZ C	70	69	0.04	0.05	1.26	2.98	23.49	Banded gneiss. Outside the OHFZ, in fault footwall, foliation parallel.	Joint dominated adjacent to NNE-SSW striking fault. See section 5.4.4.
SHSZ D	69	67	0.12	0.11	0.92	9	7.67	Banded gneiss, oblique to the foliation. Outside the OHFZ	Joint dominated. See section 5.4.4.
Tolstadh	200	199	0.01	0.01	0.95	4.735	42.03	Within the 'crush mélange' of the OHFZ – very heavily fractured cataclastic gneiss.	Fractures within cataclastic gneiss, cut by Mesozoic structures. See section 3.4.2.3.

7.3.2.1 Background fracturing

A range of transects were undertaken at localities that sample joint-dominated outcrops (Table 7.5), that lack any significant faulting. At Dail Beag, Gob Thais, Hushinish and Port Mholair, the outcrops were joint dominated with little evidence of significant faulting. These localities lie outside the area of the OHFZ and display Cv values close to or <1. At Tolstadh, the transect samples intensely fractured gneiss/crackle breccia that has been attributed to intense fracturing formed during pre-Mesozoic thrusting on the OHFZ (e.g. Imber, 1998).

Table 7.5: Results for background fracturing

Locality	N (fractures)	N (spacing values)	Cv	Best fitting distribution	Geological Situation	Within OHFZ?	Transect Length (m)	Fracture Density (no./m)	Distance to major fault (m)
Dail Beag	68	67	1.08	Exponential	Banded gneiss, joint dominated	Outside OHFZ	20.64	3.29	Within 50 m of a NNW-SSE trending lineament.
Gob Thais	63	62	0.81	Exponential	Banded gneiss, joint dominated	Outside OHFZ	23.47	2.68	Approximately 25 m from a WNW-ESE trending lineament.
Hushinish	108	107	0.83	Exponential	Granitic gneiss.	Outside OHFZ	9.9	10.91	No major faulting evident. 500 m from NW-SE trending lineament.
Port Mholair	149	145	1.07	Exponential	Banded gneiss and granite, epidote bearing faulting and joints.	Outside OHFZ	33.72	4.42	No major faulting evident. ~1 km from the Minch Fault.
Tolstadh	200	199	0.95	Exponential	Heavily fractured cataclastic gneiss, cut by minor Mesozoic faults.	Within OHFZ	4.74	42.19	Probably lying within the hangingwall of a major thrust.

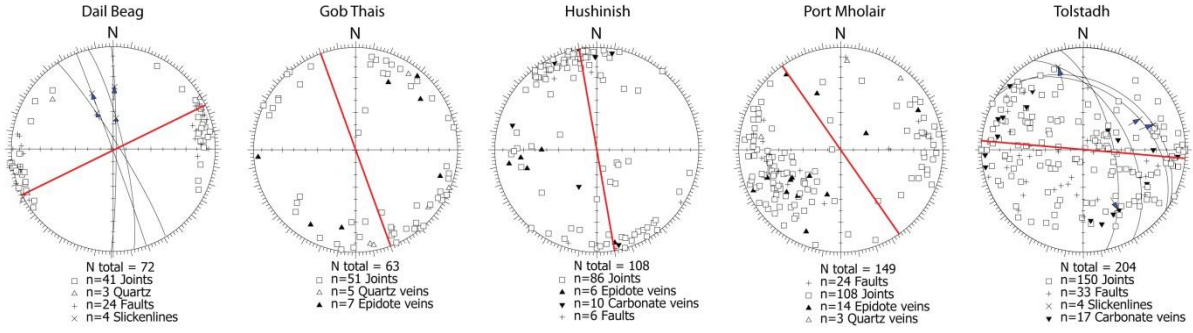

Figure 7.4: Orientation data collected from transects listed in Table 7.5.Red lines indicate transect orientation.

Exponential trend lines provide the best description of the data that was collected from these localities (Figure 7.5, Table 7.6). Steeper gradients in Figure 7.5 are representative of higher exponents, and indicate a greater relative importance of smaller fracture spacings. The distributions of spacing data from Dail Beag, Gob Thais, Port Mholair are notably similar, with relatively shallow gradients and exponents of around -3 representing low fracture densities (see Table 7.5). Hushinish and Tolstadh display steeper exponential gradients, indicating a higher fracture density. All of these transects –with the exception of Tolstadh - display relatively clustered orientation data (Figure 7.4), indicating that the transects are dominantly sampling single fracture sets. Tolstadh does not display clustering of the orientation data because the transect cuts a breccia with randomly orientated fractures.

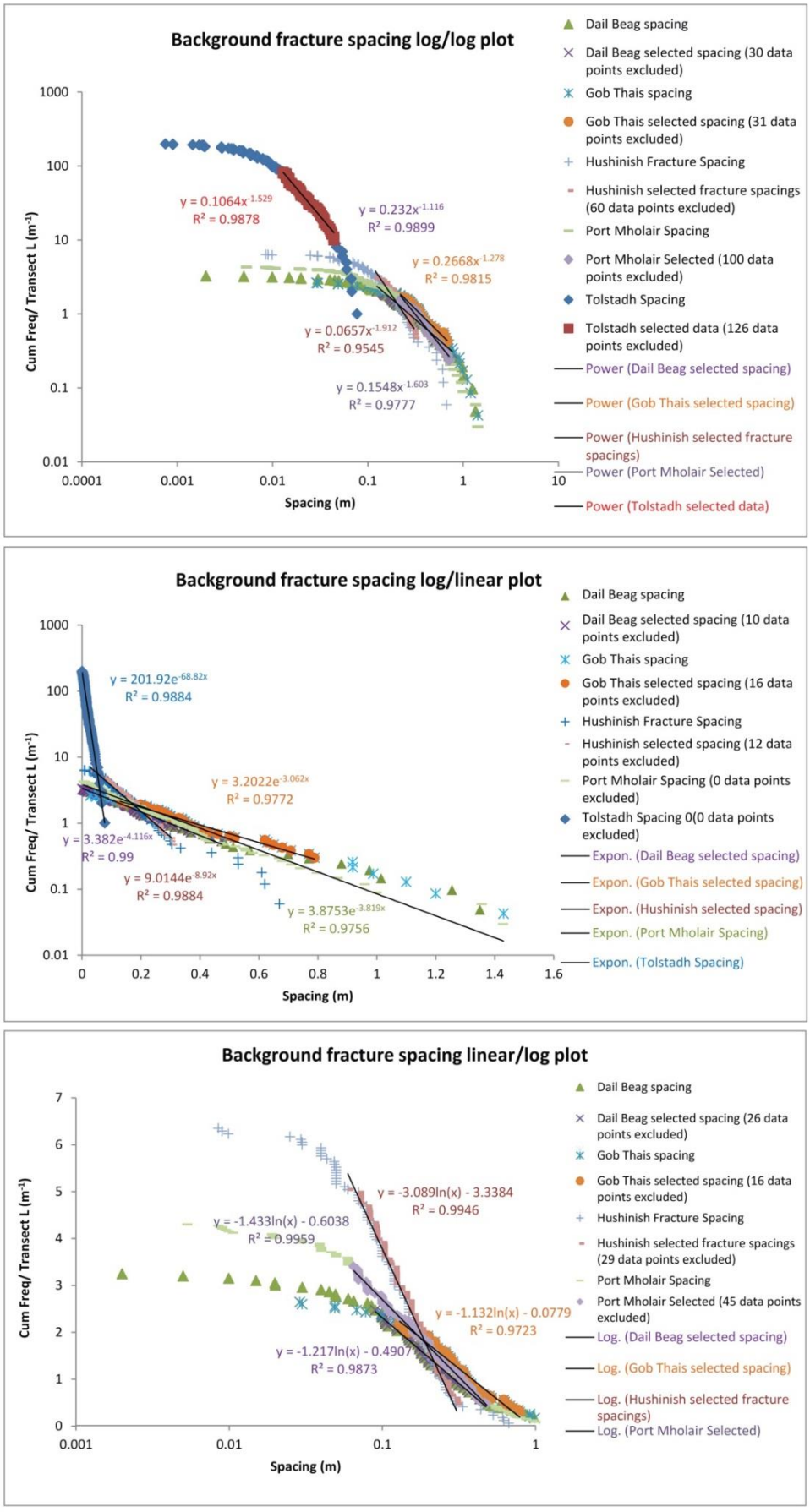

Figure 7.5: Distribution of spacing data collected from joint dominated localities. Graphs show raw and data selected for straight line portions of the distributions.

Table 7.6: Table of number of data-points excluded from each plot type (and percentage of total data).

Distribution	Dail Beag	Gob Thais	Hushinish	Port Mholair	Tolstadh
Power-law	30 (45%)	31 (50%)	60 (56%)	100 (69%)	126 (63%)
Negative exponential	10 (7%)	16 (26%)	12 (11%)	0	0
Log-normal	26 (38%)	16 (26%)	29 (27%)	45 (31%)	84 (42%)

7.3.2.1.1 Summary and discussion

Dail Beag, Gob Thais, and Port Mholair lie outside the OHFZ and are widely separated across Lewis (Figure 7.1). These transects generally cut single, well-defined fractures sets, and display very similar fracturing patterns with spacing distributions best described by negative exponential trend lines. These localities all lie within banded gneiss and are not affected by significant faulting. Higher fracture density is clearly evident at Hushinish and Tolstadh. Fracturing at Hushinish is dominated by jointing of a higher fracture density than that seen at the other joint dominated localities. The ENE-WSW strike of the fractures and association with calcite may indicate that these fractures are of Mesozoic age and related to faulting of this orientation observed in western Lewis. At Tolstadh, the very high fracture density is attributable to brecciation of the rock during cataclasis within the OHFZ, with the random nature of this illustrated by dispersed fracture orientations.

7.3.2.2 Mesozoic faulting

Faulting identified as Mesozoic was sampled in one transect at each of three localities (Garrabost, Pabail and Port Stoth), and in two transects at each of three localities: Memorial Cairn; Seaforth Fault; and Seisiadar (Figure 7.6). These localities were all selected for their proximity to large Mesozoic faults:

- The Memorial Cairn locality (Figure 3.20 and section 3.4.2.2) is close to the westerly bounding fault of the Stornoway Formation (~200 m) and dominantly samples a fault set that is sub-parallel to it and of Mesozoic age. Evidence of reactivation is observed in the form of brecciated epidote cataclasite within the fault cores. Fault-parallel and fault-

perpendicular transects were collected. The fault parallel transect is located 196 m from the bounding fault and sub-parallel to it.

- At Seaforth, the perpendicular transects 1 and 3 sample fracturing and faulting approximately perpendicular to the major Seaforth Fault (section 4.4.3), with transect 1 undertaken further from the fault (~100 m) compared to transect 3 (~50 m). The Seaforth 2 transect is fault-parallel, taken from the immediate hangingwall of the fault in a cliff face. The Seaforth transects 1 and 3 have been analysed individually and as a combined dataset in Table 7.7, to illustrate differences in the fracturing observed with increasing distance from the fault. The Seaforth fault may reactivate a pre-existing basement shear zone (section 4.4.3.2).
- Seisiadar (section 3.4.2.1.4) is the closest onshore outcrop to the Minch Fault, lying within several hundred metres to the west of it (the position of the Minch Fault is not precisely constrained). The locality displays a fault set that strikes parallel to the Minch Fault and transects were undertaken parallel and perpendicular to it.

In addition, further transects were taken cutting Mesozoic-age faults at Garrabost, Pabail and Port Stoth:

- The Garrabost transect was carried out to intersect the prominent NNW-SSE Mesozoic fault trend in the area and to analyse the attributes of fracture attributes at a larger scale. The cliffs at Garrabost are 8-10 m in height and only faults that cut the whole length of the cliffs were measured in order to investigate fracture attributes at larger scales. This was deemed appropriate as it simply shifts the scale of measurement bias (censoring and truncation) that occurs in normal line transects. Due to its long length, the transect is arcuate and hence it can only be used as an approximation for the spacing distribution at larger scales. Pre-Mesozoic, Mesozoic and younger and reactivated faults are present at Garrabost (section 3.4.2.1.1).
- The Pabail (section 3.4.2.1.3) transect was performed across minor (cm offset) normal faults associated with a large (5-6 m wide) zone of Mesozoic-age gouge and breccia dipping steeply to the ENE with dip-slip kinematics, positioned immediately adjacent to the start of the transect. Hence this dataset records dominantly Mesozoic fracturing in the hangingwall of a large Mesozoic fault.
- The Port Stoth transect was undertaken across a series of northward dipping epidote-bearing cataclasite faults, reactivated with authigenic clay bearing gouges of probable Mesozoic age (section 4.4.1.2).

The results of the transects are displayed in Figure 7.6 and Figure 7.7 (stereonets of orientation data) Figures 6 - 10 (data distribution graphs) and Table 7.7, where distances to the nearby major Mesozoic faults are given.

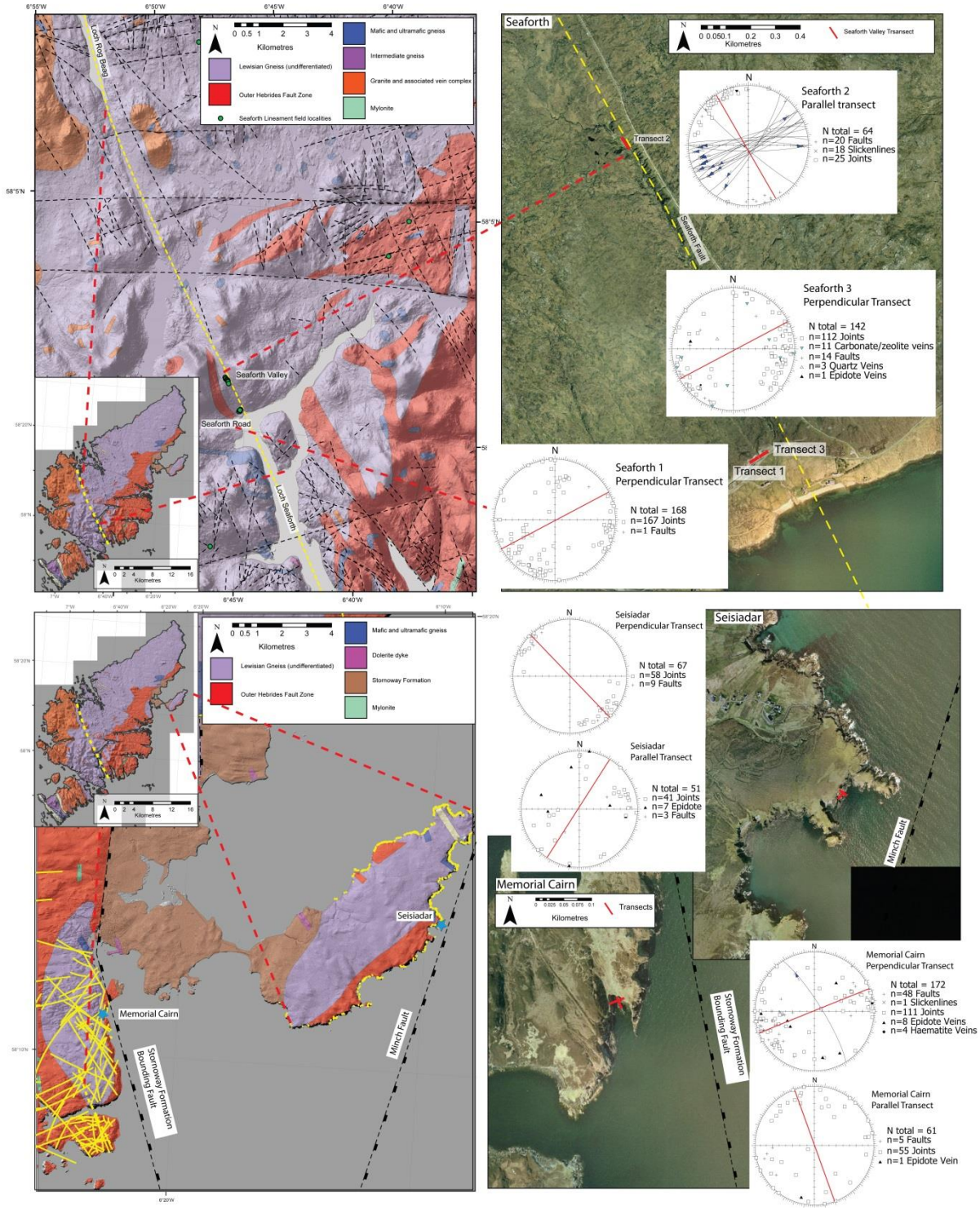

Figure 7.6: Map showing location of Seaforth (top), Memorial Cairn and Seisiadar (bottom) transects and stereonets.

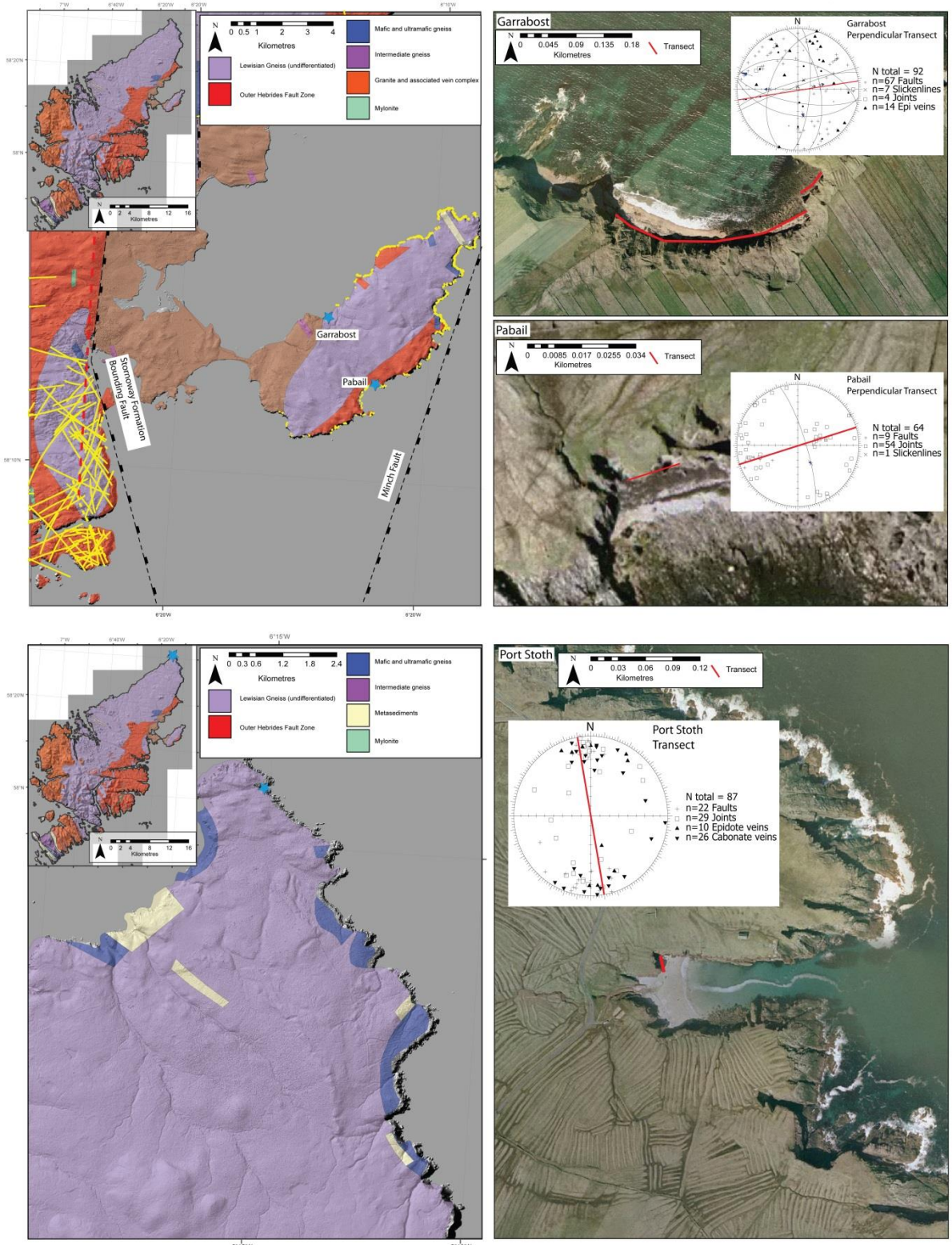

Figure 7.7: Map showing location of Garrabost, Pabail and Port Stoth transects and stereonets.

Table 7.7: Details of transects taken at localities dominated by Mesozoic age faults.

Locality	N (fracs)	N (spacing values)	Cv	D value of fitted power-law trend line	Distribution	Geological Situation	Transect Length	Fracture Density (no./m)	Distance to major fault (m)
Garrabost	85	83	1.24	1.28	Power-law/ exponential?	Cuts multiple faults, Mesozoic dominated	435.5	0.20	N/A
Pabail	63	61	0.75	1.624	Log-normal	Cuts Mesozoic faults.	10.63	5.93	Immediately adjacent to Mesozoic fault
Memorial Cairn Perpendicular	172	171	1.37	1.65	Power-law/ exponential?	Mesozoic faulting	30.22	5.69	~221 – 190.8
Memorial Cairn Parallel	61	60	0.70	N/A	Exponential	Joint dominated	12.22	4.99	~196
Port Stoth	87	86	0.82	0.888	Exponential	Epidote cataclasite bearing faults reactivated with clay gouge	8.27	10.52	N/A
Seaforth 1 (perpendicular)	168	167	1.03	1.70	Power-law/ exponential?	Joint dominated	44.54	3.77	78.9 - 120
Seaforth 3 (perpendicular)	141	138	1.34	1.03	Power-law/ exponential?	Mesozoic faulting	39.17	3.60	36.3 – 78.9
Seaforth 1 and 3 combined (perpendicular)	309	305	1.16	1.60	Power-law/ exponential?	Mesozoic faulting	83.71	3.69	36.3-120
Seaforth 2 (parallel)	46	45	0.90	N/A	Exponential	Joint and Meso/Cenozoic fault dominated	8.43	5.46	Immediately adjacent
Seisiadar Perpendicular	67	66	0.19	0.90	Power-law/ exponential?	Mesozoic faulting	13.75	4.87	~200 - 500
Seisiadar Parallel	51	50	1.10	N/A	Exponential	Join dominated	24.14	2.11	~200 - 500

Table 7.7 shows that differences in fracture spacing exist between transects taken parallel and perpendicular to Mesozoic-age structures. Parallel transects consistently display lower Cv values than their associated perpendicular counterparts, all giving values of <1 or ~1, indicating anticlustered and random spacing distributions respectively. Anticlustered data distributions are also seen in Seaforth transect 1, in the perpendicular transect taken furthest from the Seaforth Fault. There is a notable increase in the Cv value between the adjacent Seaforth transects 1 and 3 from 1.03 (random distribution) to 1.34 (clustered distribution) as the Seaforth Fault is approached. In general, with the exception of the Seaforth transect 1, perpendicular faults also display increased fracture densities and decreased mean spacing of the faults. In the field it is apparent that the parallel transects have a greater tendency to be dominated by jointing. The E-W striking faulting shown associated with the fault parallel Seaforth Transect 2 (Figure 7.6) may be attributed to late (Tertiary) E-W strike slip faults found throughout Lewis (Chapters 3 and 4).

These faults have combined with jointing to give a higher fracture density in the parallel transects compared to the perpendicular transects 1 and 3.

Data from the Memorial Cairn, Seaforth and Seisiadar are displayed graphically in Figure 7.8 and Figure 7.9, split between transects perpendicular (Figure 7.8) and parallel (Figure 7.9) to the Mesozoic fault strike at each locality. Perpendicular transects have Cv values >1 and on log-log plots the power-law trend lines extend across ~ 1 order of magnitude. Power-law exponents obtained for the perpendicular transects are 0.90 (Seisiadar), 1.60 (Seaforth) and 1.65 (Memorial Cairn). Power-law distributions along fault perpendicular transects may be expected given they directly sample a normal fault-related fracture set (e.g. Peacock, 2002). However, power-laws can only be fitted to the data if it is assumed that the curved portions of the distribution represent censoring and truncation bias. Table 7.8 shows the number of data points excluded from the straight-line portions of each plot. It can be seen that in order to fit power-law trend lines to the data, they consistently require that large numbers of points be excluded (54 – 72%, Table 7.8). The raw data distributions on the log/log plot (Figure 7.8) show convex upward slope changes around 0.1 m spacing, where spacing data is densest. Hence it seems rather unlikely that these areas of the plots are affected by censoring/truncation, and it is more likely that the upward convex nature of these data are real. For this reason, the whole datasets are better described by exponential trend lines with minimal amounts of data excluded (Figure 7.8, Table 7.8).

Fault-parallel transects are shown in Figure 7.9. As can be seen in the log/log plot, straight line portions of the distributions do not exist across an easily defined range, with >60% of data points excluded. Similarly to the fault perpendicular transects, the distributions are best fitted by exponential trend lines that discard the minimal number of data points (Table 7.8).

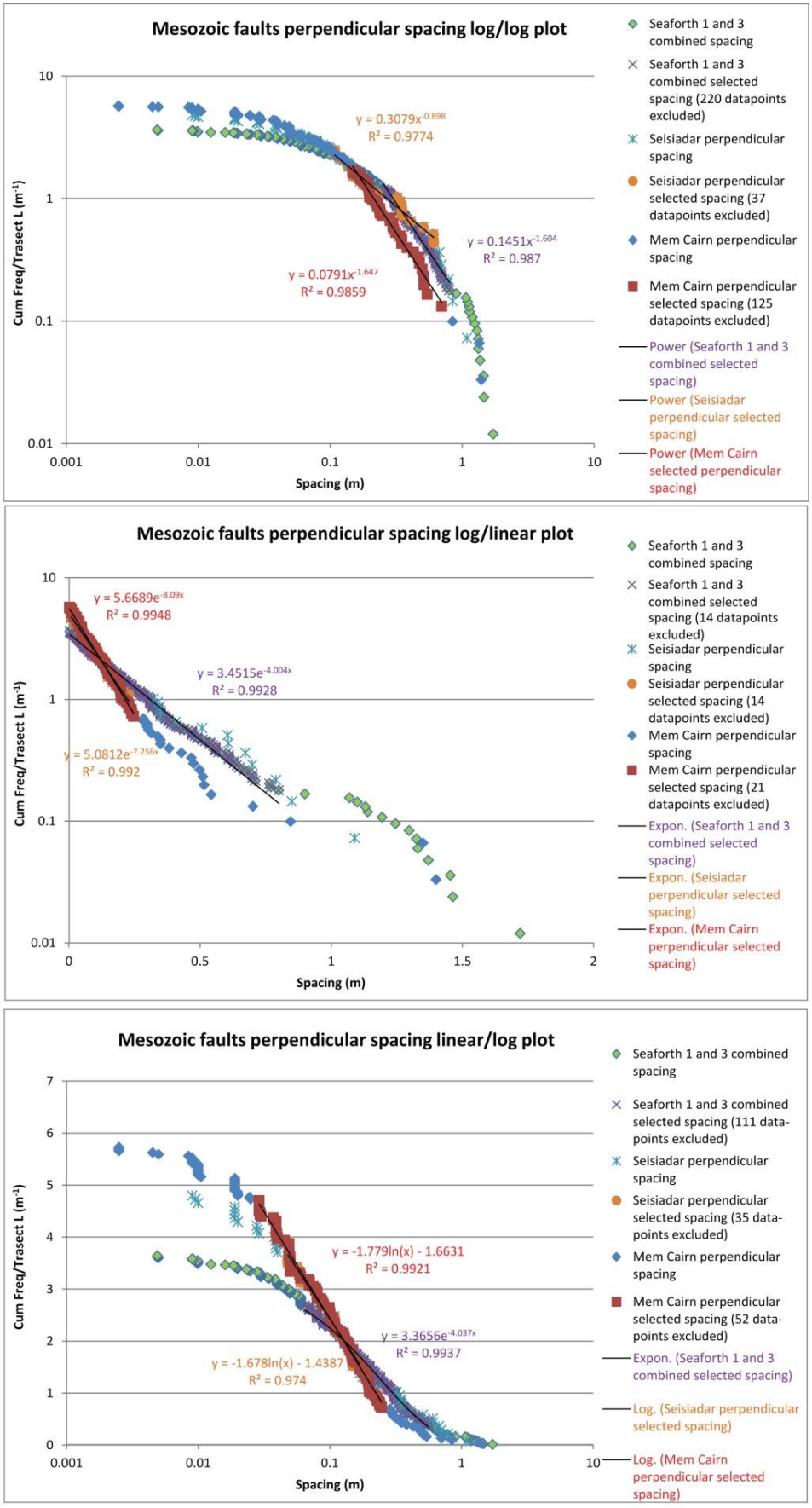

Figure 7.8: Graphs of fault perpendicular spacing data collected from transects at Mesozoic fault dominated localities. Graphs show raw and data selected for straight line portions of the distributions.

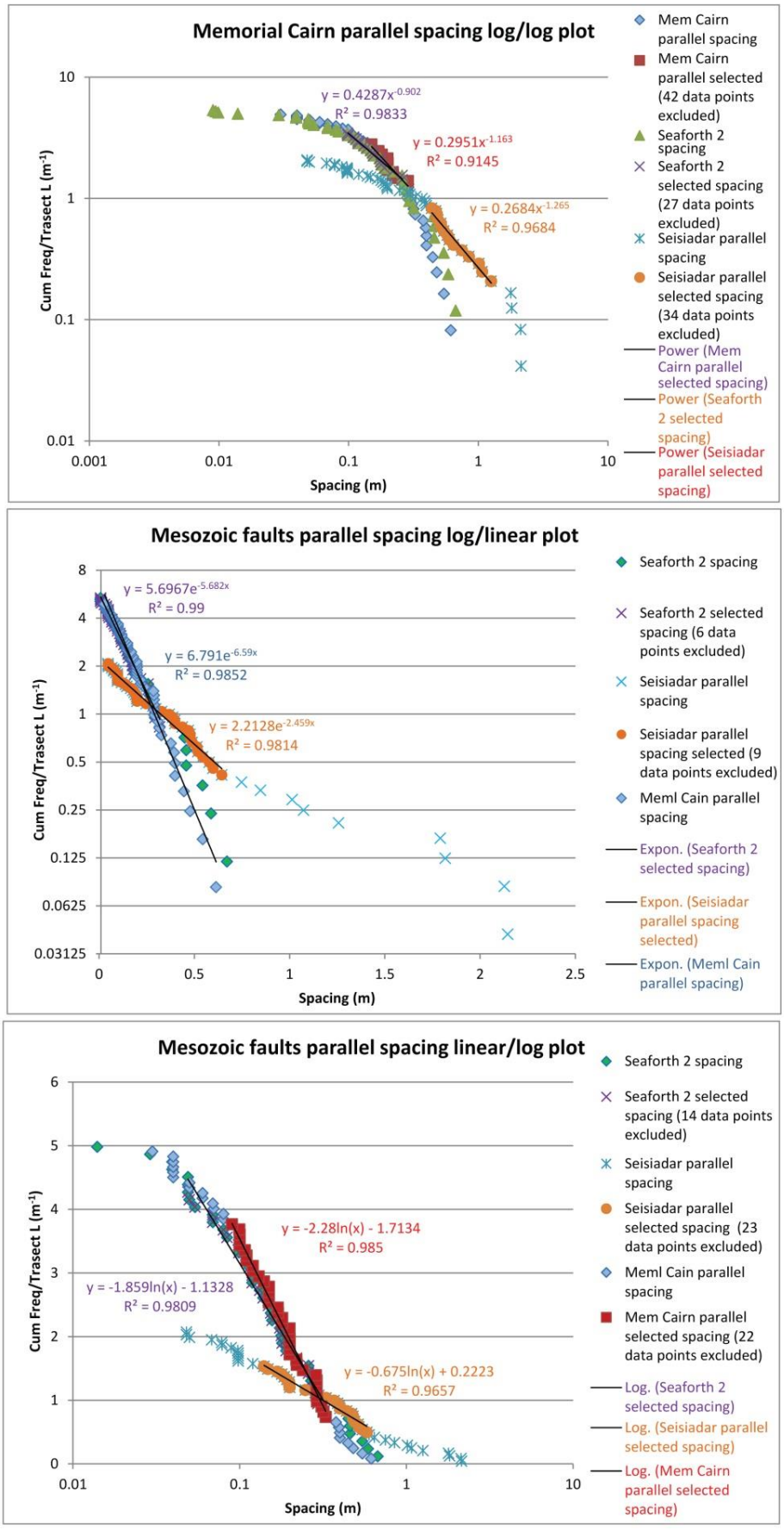

Figure 7.9: Graphs of fault parallel spacing data collected from transects at Mesozoic fault dominated localities. Graphs show raw and data selected for straight line portions of the distributions.

Table 7.8: Table of number of data-points excluded from each plot type (and percentage of total data).

Distribution	Mem Cairn parallel	Seisiadar parallel	Seaforth 2 (parallel)	Mem Cairn perp.	Seisiadar perp.	Seaforth perp.	Pabail	Port Stoth	Garrabost
Power-law	42 (70%)	34 (68%)	27 (60%)	125 (72%)	37 (54%)	220 (72%)	41 (67%)	64 (73%)	38 (45%)
Negative exponential	0	9 (18%)	6 (13%)	21 (12%)	14 (21%)	14 (5%)	12 (20%)	22 (25%)	7 (8%)
Log-normal	22 (37%)	23 (46%)	14 (31%)	52 (30%)	35 (53%)	111 (36%)	11 (18%)	29 (33%)	30 (36%)

The transect at Pabail (Figure 7.7) was undertaken dominantly across minor (cm offset) Mesozoic structures within the OHFZ. The Cv value from Pabail is 0.75, indicative of anticlustering. On a log-log plot, the graph exhibits only a very short straight line portion that can be assigned a power-law trend line, instead the data overall exhibits a convex upwards profile. Upon inspection of the plots (Figure 7.10), the best fit is achieved by a log-normal trend line with an R^2 of 0.90. However, it is not clear whether this is because of low resolution (e.g. Gillespie et al., 1993), or whether this is accurate given the effects of truncation and censoring. Results obtained from Port Stoth are similar to those from Pabail, being difficult to accurately assign a straight line trend to the data on the log/log plot (Figure 7.11). It seems likely this data is best represented by either an exponential or log-normal trend line, given the high proportion of data points that need to be removed (73%) for a power-law trend line to be fitted.

At Garrabost, (Figure 7.12), the data are very well described by a straight line on a log/linear plot, suggesting a negative exponential description may be best. As above, this does not take into account the effects of censoring and truncation. On the log/log plot, a power-law trend line may be defined across <1 order of magnitude, excluding 45% of the data. The Cv value of 1.24 indicates a degree of clustering, however it appears the data are best represented overall by an exponential distribution.

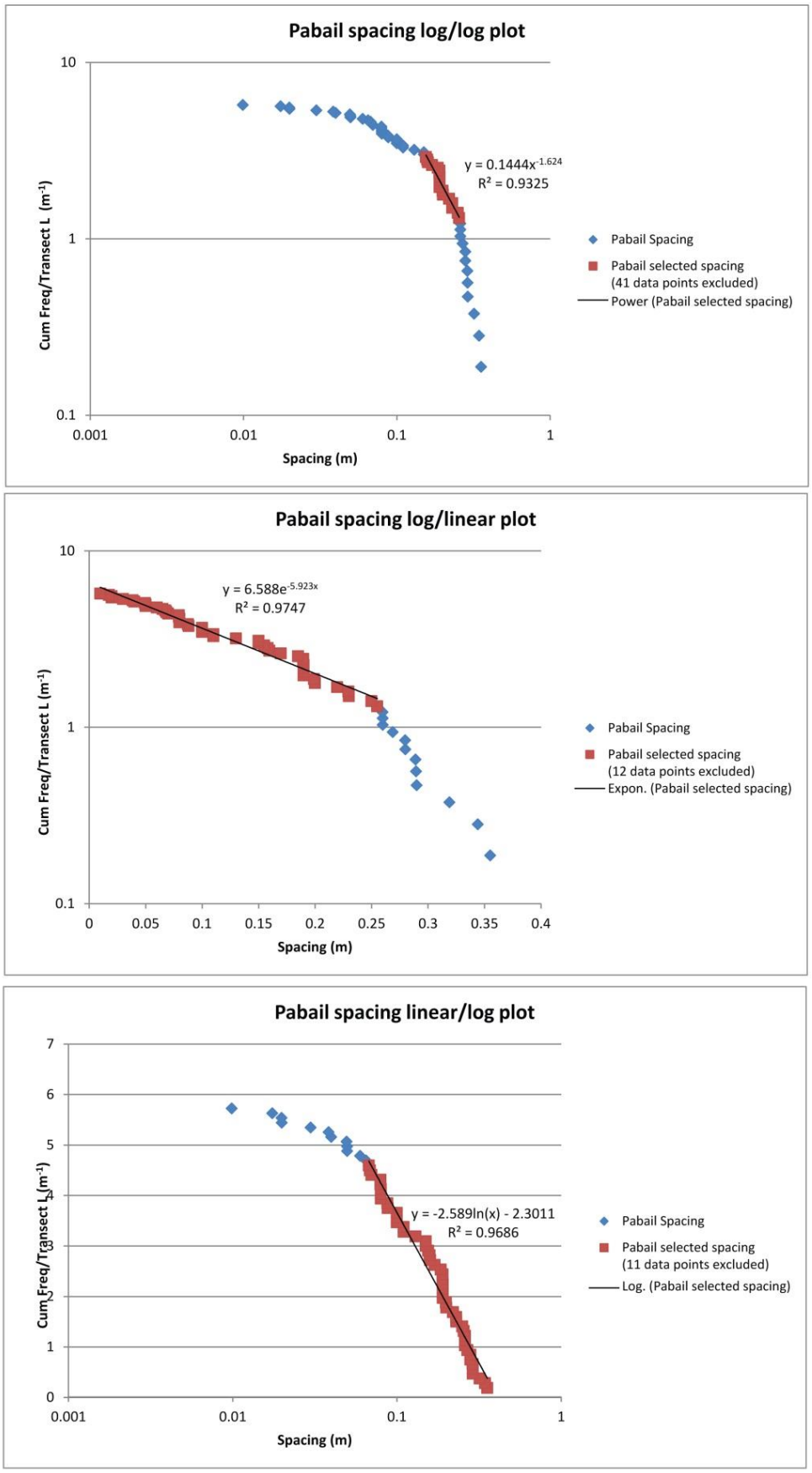

Figure 7.10: Plots of data collected at Pabail. Graphs show raw and data selected for straight line portions of the distributions.

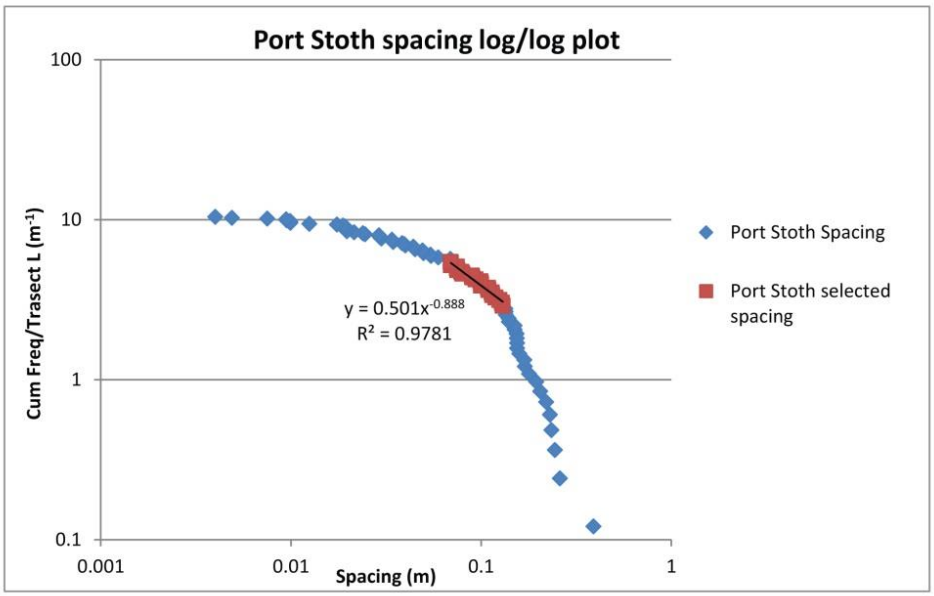

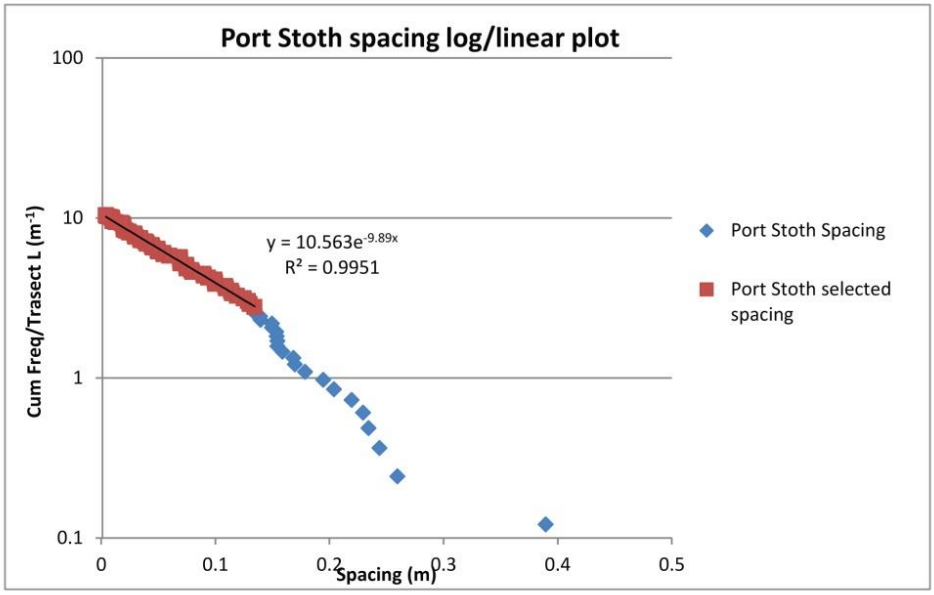

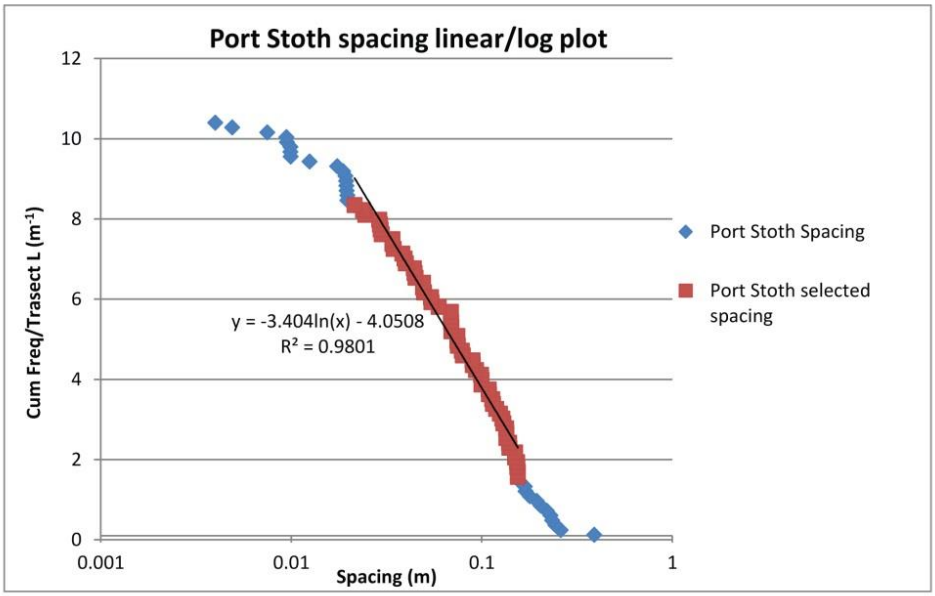

Figure 7.11: Distribution of spacing data collected from Port Stoth. Graphs show raw and data selected for straight line portions of the distributions.

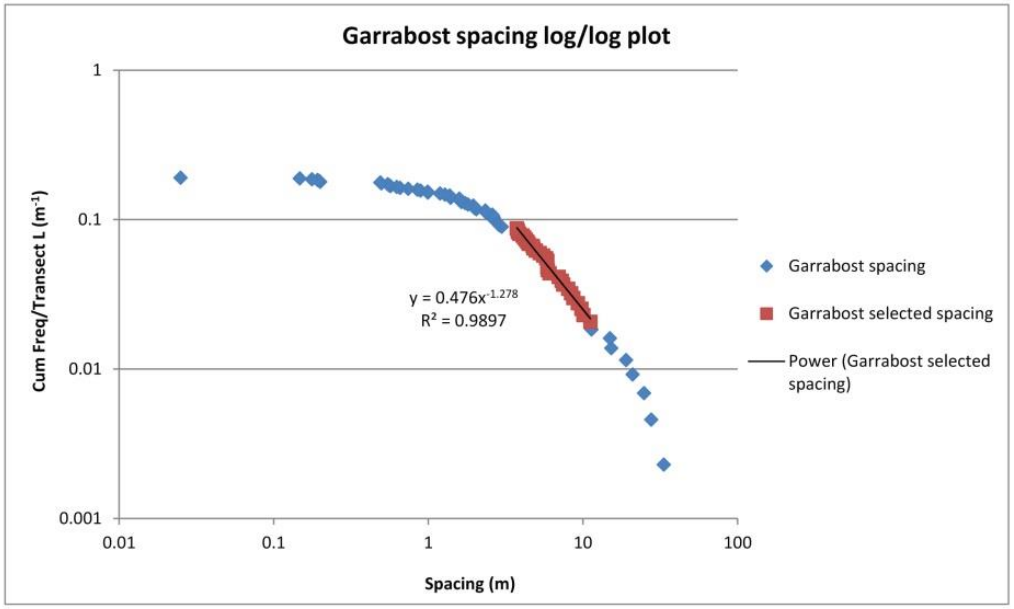

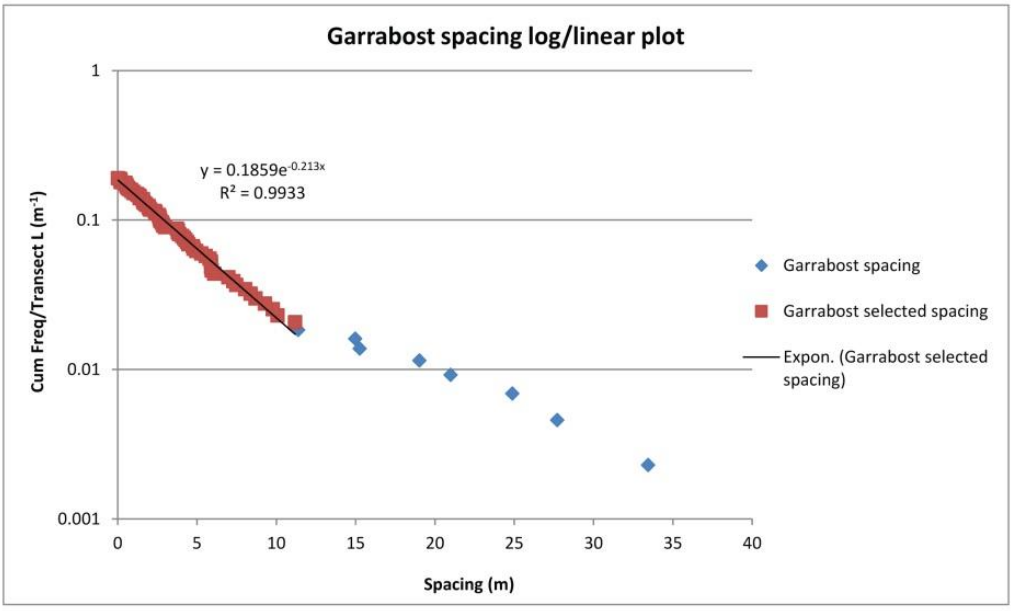

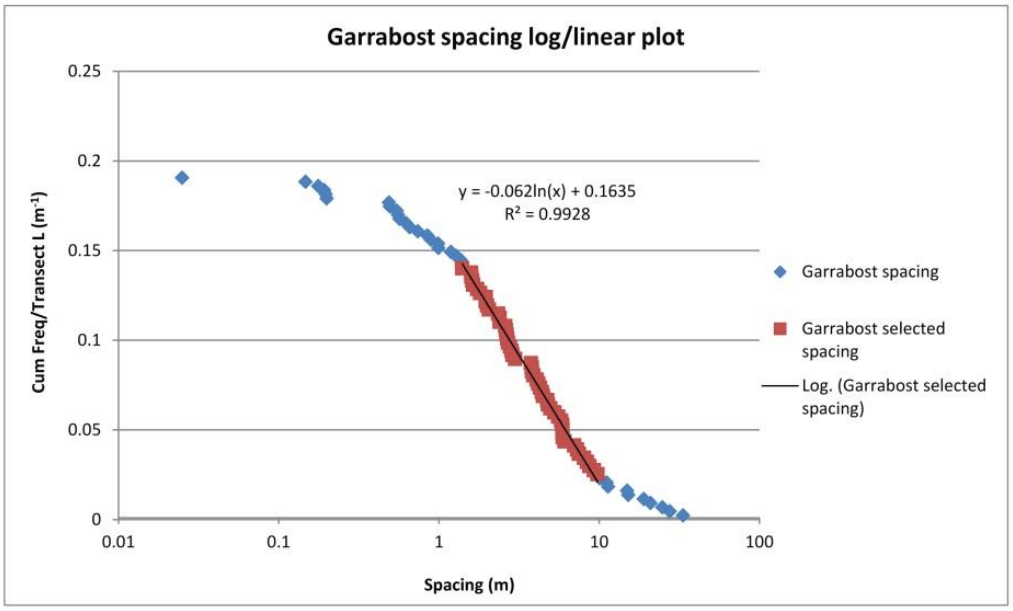

Figure 7.12: Distribution of spacing data collected from Garrabost. Graphs show raw and data selected for straight line portions of the distributions.

7.3.2.2.1 Summary and discussion

It is important at all times to bear in mind the effects of bias on the sampled data. The best-fitting model to the data may not be the best model for the population if the sample is biased (Pickering et al., 1995). The aim during statistical interpretation of these data should also be to keep the maximum number of data points and minimise their loss and/or to maintain the largest scale-range. In addition, as most of the distributions show upward-convex plots around the area of most dense data points on the plots (around 0.1 m), it seems that all data is probably best represented by exponential (random) distributions.

It is clear in Table 7.7 that a distinction between transects taken perpendicular and parallel with Mesozoic age fault sets exists. Perpendicular transects display Cv values >1, and those parallel with the faults have Cv values close to or <1. This indicates that a greater degree of fracture clustering occurs perpendicular to the faults, whilst parallel to the main fault strike minor structures are relatively more anticlustered or randomly spaced. This effect is also observed at Seaforth transects 1 and 3, where the Cv value increases towards the Seaforth fault (1.03 to 1.34), indicating a transition from a more random fracture spacing distribution to a more clustered distribution. Power-law trend lines can be fitted to straight line portions of the perpendicular transects, but cannot be easily fitted to the parallel transects, where they span a shorter scale range. These observations suggest that there is a difference in fracturing attributable to Mesozoic-age faulting that may be recognised by increased clustering of fractures within the Lewisian. However, Cv values are all relatively close to 1 (within 0.37), and all the transects are better described by exponential trend lines. This suggests that the distributions are dominated by random fractures spacings (e.g. Gillespie et al., 1993; McCaffrey and Johnston, 1996). Power-law spacing distributions show degeneration with worsening lateral resolution (i.e. length of transect) to an upwardly convex profile on log/log plots (Gillespie et al., 1993), and this may be affecting the data presented here. The lack of a break in slope in the upper parts of the exponential distribution plots may suggest that the smallest spacings in the outcrops have been adequately sampled, and the datasets may have no lower limit of resolution (Gillespie et al., 1993).

The Pabail transect predominantly samples a Mesozoic fault set with minor offsets. However, the low Cv value (0.75) indicates a degree of anti-clustering indicative of joint spacing (e.g. Beacom et al., 2001). The relatively short transect length may have led to a degree of truncation. Alternatively, the log-normal distribution of this data may be produced by anti-clustering of the small sampled faults around the large fault at the start of the transect (Ackermann and Schlische, 1997). Data from Port Stoth is similar to that at Pabail, with a low Cv (0.82) and a distribution that is poorly fitted by a power-law trend line. The data collected from Garrabost are important as they were collected at a larger scale than other transects. The power-law ascertained for the

straight line portion of the plot excludes 45% of the data points, but this is the lowest proportion excluded from a power-law trend line for all of the plots. Again however, it can be seen that the data are represented very well by exponential trend-lines. This may be expected, given that the transect crosses multiple fractures of various ages (section 3.4.2.1.1). Seaforth transect 3 was observed to be heavily dominated by zones of crackle, mosaic and chaotic breccia and fault gouges often over 1 m wide that could not be characterised due to the very large number of small fractures within zones of breccia. Consequently, although the Seaforth transect 3 still displays a high Cv value (1.34), this is a lower limit. The combined distribution of perpendicular data from Seaforth shows an easily defined straight line portion, but is again matched well by the exponential trend line.

Observations of increased fracture clustering and potential power-law spacing distributions discussed here are in agreement with those seen elsewhere across normal faults (e.g. Peacock, 2002). However, reactivation of faults can lead to a breakdown of the power-law relationships (Peacock, 2002). It is possible that the degree of reactivation, and presence of multiple fault sets of varying ages, produces the good fit displayed by the exponential trend lines.

In the studies of fracturing within the mainland Lewisian conducted by Pless (2011), power-laws can only very rarely be assigned confidently to distributions across more than one order of magnitude. Her data are similar to that presented here, with upwardly convex profiles on log/log plots. Pless (2011) has, however, interpreted these data distributions to show consistent power-law trends. Beacom et al. (2001) analysed fracture spacing along foliation parallel transects within the Lewisian and also found power-law spacing distributions of Laxfordian faults in both acid and basic gneisses. Power-law spacing distributions were not however identified within the Loch Maree Group, whose compositional heterogeneity was believed to have had significant control on fracture development (Beacom et al., 2001).

7.3.2.3 Cenozoic E-W striking faulting

Three transects were undertaken along the quarry face at Orasaigh (section 4.5.2.3, Table 7.9).

Table 7.9: Line transects undertaken at Orasaigh Quarry.

Locality	N (fractures)	N (spacing values)	Cv	Geological Situation	Within OHFZ?	Transect Length (m)	Fracture Density (no./m)
Orasaigh 1	238	220	1.26	Parallel with main ENE-WSW striking strike slip fault zone, intersecting oblique fault splays and breccia zones.	Within the OHFZ	31.48	7.56
Orasaigh 2	111	104	1.16			18.33	6.06
Orasaigh 3	57	56	2.07			7.74	7.36

The transects generally cross fault-related joints orientated WNW-ESE and NNE-SSW (Figure 7.14). The Cv value is >1, indicating a degree of clustering of the fractures. A Cv of 2.07 in the Orasaigh 3 transect is the highest value obtained along any one transect, and may be accounted for by the fact that transect 3 crosses zones of faulting and breccia, giving clustered fracture distributions. Log/log, log/linear and linear/log plots are shown in Figure 7.13, with trend lines assigned to straight line portions of the distributions on each plot. A straight line with a D value of 1.91 is a good fit to part of the log/log plot. This relatively high value indicates a predominance of small fracture spacings at this locality. However, the power-law trend line excludes the largest number of data points (62%, Table 7.10). An exponential trend line fits most of the data very well with an R^2 of 0.997 and only 4% of data points excluded. A straight line trend may also be fitted to the linear/log plot by excluding 24% of the data. Orientation data from the Orasaigh transects record two main groups of joint sets that strike N-S and E-W with near vertical dips.

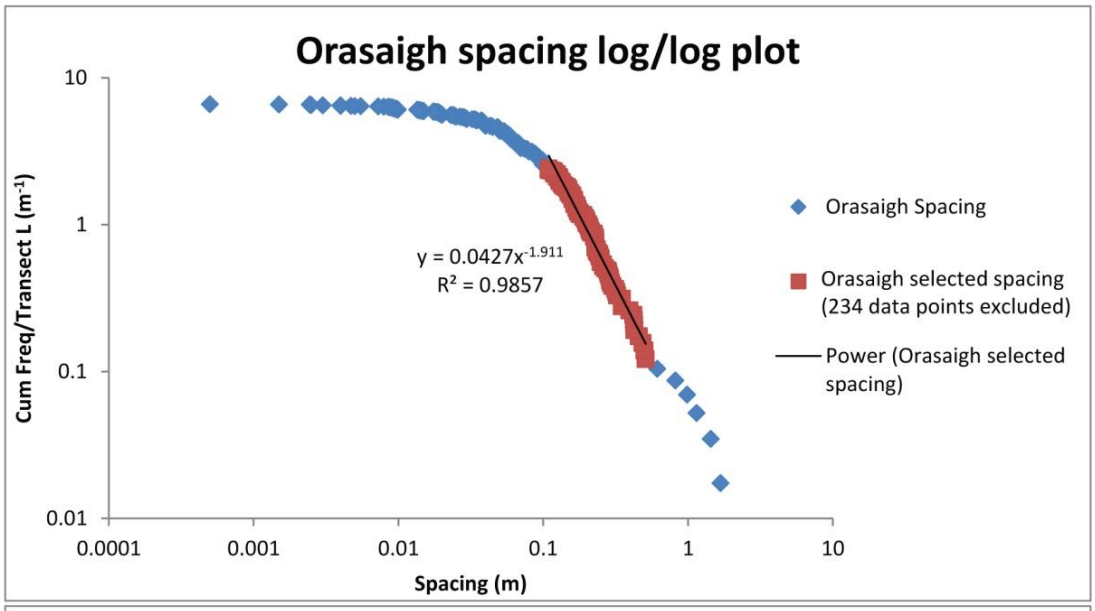

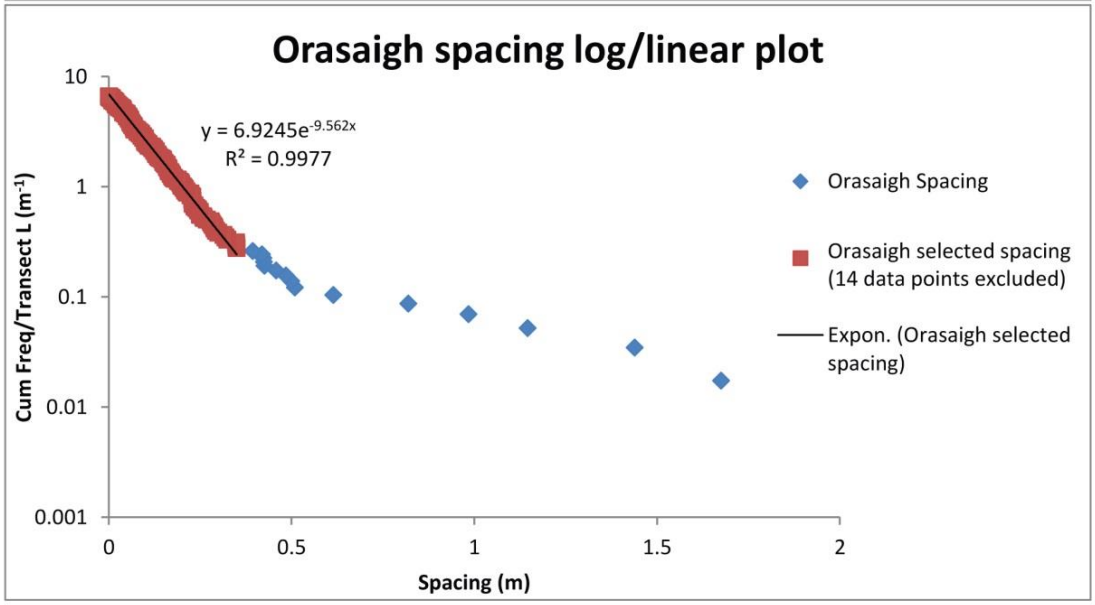

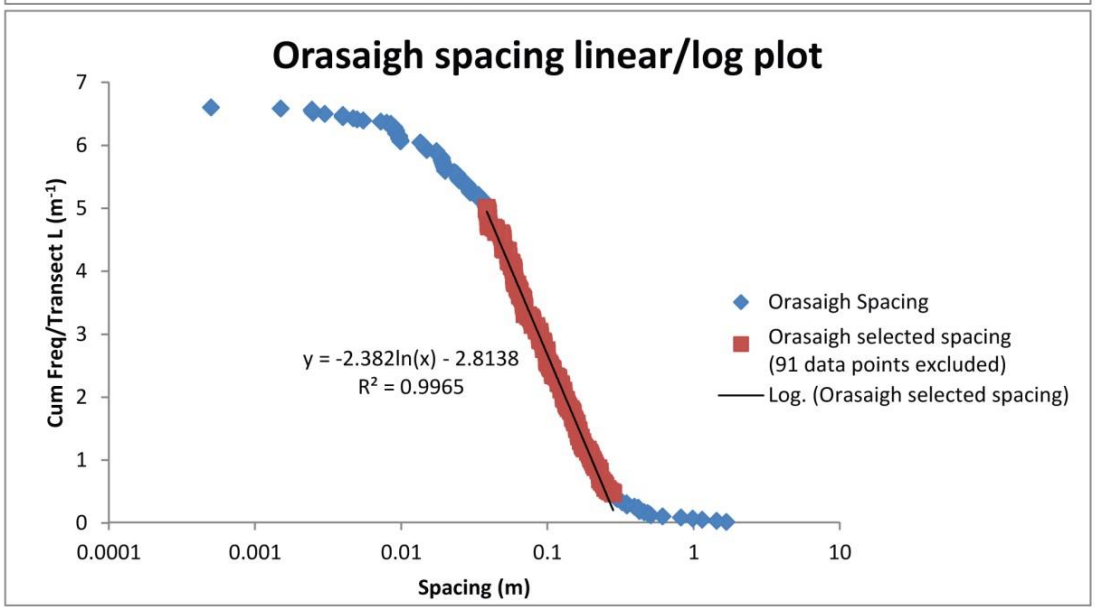

Figure 7.13: Distribution of spacing data collected from Orasaigh. Graphs show raw and selected data.

Table 7.10: Showing no of excluded data points.

Distribution	Orasaigh combined
Power-law	234 (62%)
Negative exponential	14 (4%)
Log-normal	91 (24%)

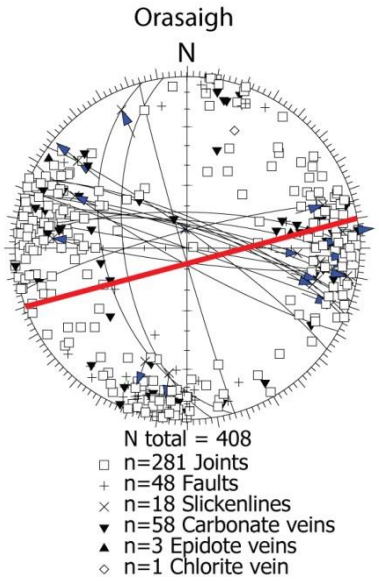

Figure 7.14: Orientation data collected from the transects at Orasaigh. Red line indicates transect orientation.

7.3.2.3.1 Summary and discussion

Although a power-law trend line can be fitted to a portion of the data, 62% of the points have to be excluded from this line. The log/log plot (Figure 7.13) shows a convex upward curve, and the exponential trend line better fits the whole distribution of data. However, the high Cv values encountered, and the straight line portion of the log/log plot of ~1 order of magnitude suggests that power-law clustering may be present. The straight line portion of the plot exists across the area of densest data (around 0.1 m), suggesting that it may be representative of the whole data set. The relatively high D value (1.911) highlights the greater relative importance of smaller fracture spacings at this locality, possibly as a result of fracturing and faulting within the OHFZ.

7.3.2.4 Lithological effects

7.3.2.4.1 Massive vs. banded gneiss

Transects were undertaken at Borve, SW Harris, within the area marked as the Harris-Uig Hills Granite Vein Complex on the BGS maps of the area (Figure 7.15). In the field the area was found to be composed of tightly banded gneiss directly juxtaposed against massive, non-foliated granite. Three transects were performed near and across the granite/banded gneiss contact to investigate any effect of lithological variation on fracturing (Figure 7.15 and Table 7.11). It seems likely that fracturing postdates the late Laxfordian emplacement of the granite when the Lewisian of Lewis and Harris was believed to have been at significant depth (Fettes et al., 1992).

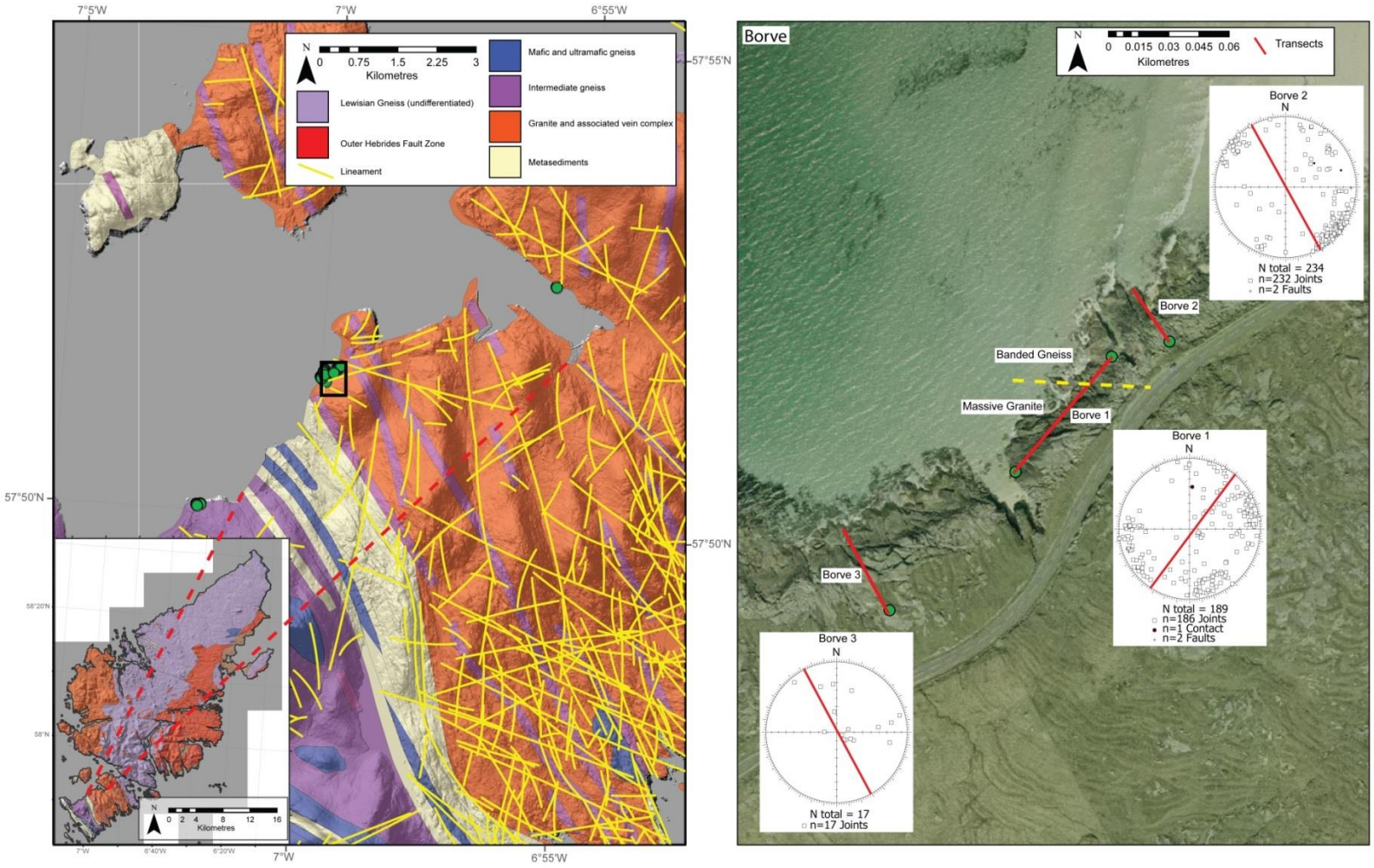

Figure 7.15: Map showing location of transects at Borve, and stereonets. Local contact between granite and banded gneiss is marked with yellow dashed line.

Table 7.11: Results from Transects undertaken at Borve.

Locality	N (fractures)	N (spacing values)	Cv	D value of fitted power-law trend line	Best fitting distribution	Geological Situation	Transect Length (m)	Fracture Density (no./m)
Borve 1 split (granite)	122	121	1.43	0.77	Power-law?	Massive granite – crosses fracture corridor	58.29	2.09
Borve 1 split (banded gneiss)	66	65	0.92	0.95	Exponential?	Banded gneiss – joint dominated	19.29	3.42
Borve 1	188	186	1.45	1.06	Power-law/log-normal	Banded gneiss and granite	77.58	2.42
Borve 2	234	233	1.58	0.94	Power-law/exponential	Banded gneiss – cuts faults and fracture corridors	33.90	6.90
Borve 3	17	16	0.99	0.44	Exponential	Massive granite – very low density fractures	61.74	0.28

Fractures at Borve are dominated by joints and fracture corridors of higher density jointing. Fracture density within the banded gneiss is higher than that in the adjacent granite (Table 7.11). In general, the banded gneiss contains at least 1 fracture per metre (Borve 1 and Borve 2, Figure 7.16). The granite displays a lower degree of fracturing, in Borve 3 fracture density is very low (0.26 fractures/m). Transect 1 cuts both granite and banded gneiss, with a fracture density of 3.42 fractures/m in the banded gneiss and 2.09 fractures/m in the granite. Rare higher density fracture corridors do also exist within the granite, and one of these is sampled between 49-53 m in Borve 1 (Figure 7.16).

Orientation data shows clustering of the fracture orientations in transects 1 and 2, but does not show any particular trend in Borve 3 (Figure 7.15). Cv values vary from 0.99 in the granite (Borve 3), representing a random spacing distribution, and 1.58 within the banded gneiss (Borve 2) representing a clustered fracture distribution. The contact between banded gneiss and granite is not fractured. When the spacing data from Borve 1 is split between the granite and banded gneiss, the granite gneiss shows clustering of fractures (Cv value >1), and the banded gneiss shows the spacing distribution is near random (Cv close to 1). This difference is discussed below.

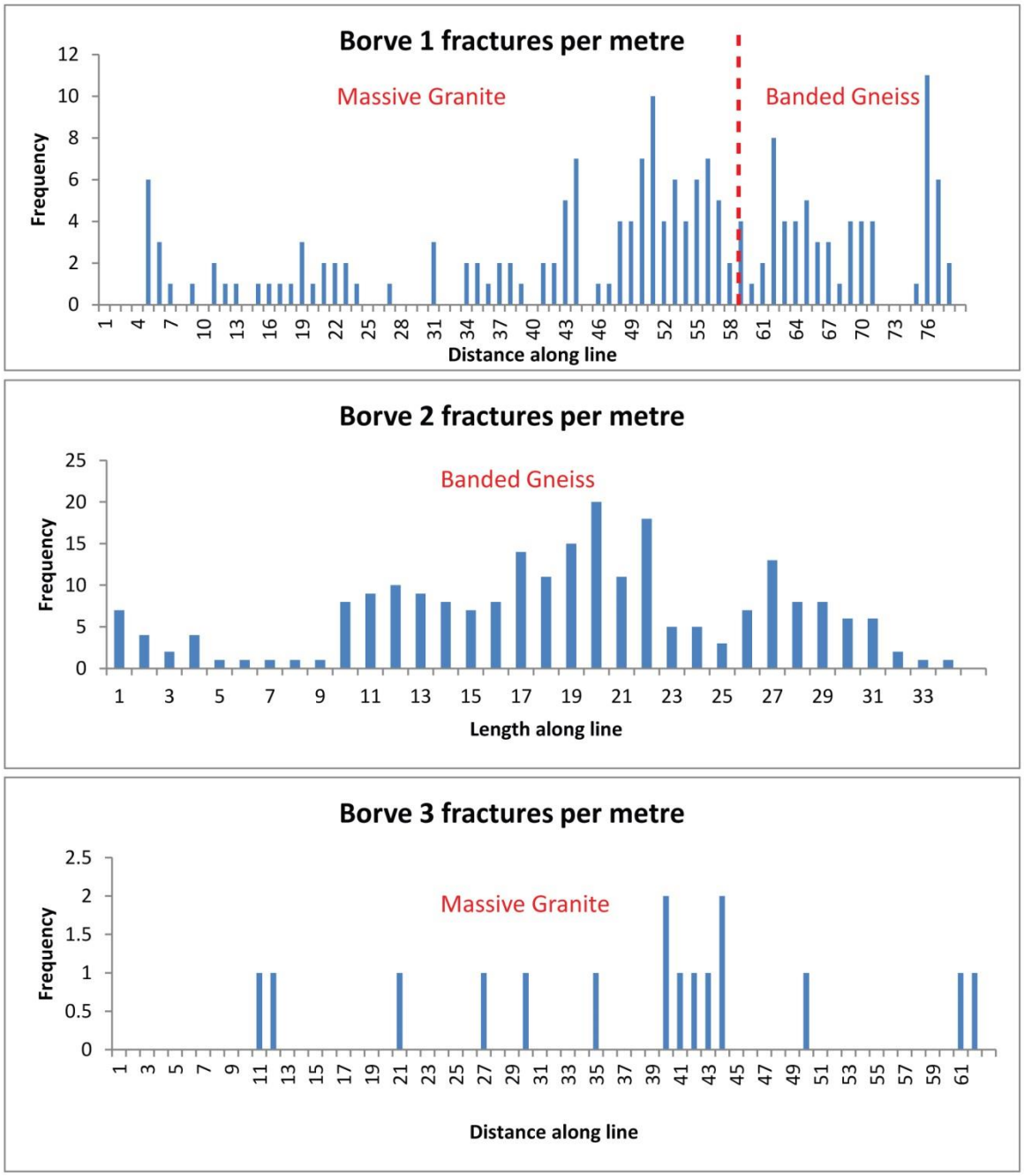

Figure 7.16: Graph of fractures per metre, showing fracture frequency along the Borve transects. The red line in Borve 1 marks the contact between banded gneiss and granite.

It is relatively difficult to assign exponential trend lines to large ranges of the data distributions at Borve. This is shown by the high proportions of data points that have to be excluded for a negative exponential trend line to describe the data well (Table 7.12). In Borve 1 overall, the exponential trend line is the poorest description of the data (Table 7.12), whereas they are better described by the power-law and log-normal trend lines with an approximately equal number of data points excluded on each plot. However, when the data are split between the two differing lithologies, the fracture spacing distribution within the banded gneiss is better described by a

negative exponential trend line (Figure 7.18). The granite from Borve 1 shows a straight line portion on the log/log plot over > 1 order of magnitude, indicating that the data are well described by a power-law trend line (Figure 7.18).

Borve 2 shows a straight line on the log/log plot across > 1 order of magnitude (Figure 7.17). Although less data is excluded from the exponential trend line on the log/linear plot, it spans only a small range of the data and is overall notably curved. The Borve 3 transect spacing data is best described by an exponential trend line (Figure 7.17). The D values for transect 1 overall and 2 are relatively similar (1.06 and 0.94), dominated by the importance of relatively small spacings. The D value for transect 3 when a power-law trend line is interpreted is substantially lower than that of the other two transects (0.44), indicating the importance of relatively larger fracture spacings within the granite. In Borve 3, the fracture spacing is markedly increased from the spacing in the granite of Borve 1, and this is due to the Borve 1 transect crossing a highly fractured zone between 49-53 m. It is difficult to assign a distribution type to Borve 3 due to the relatively low number of data points (17), however it is best described by an exponential trend line, indicating random spacing distributions. This may be expected given the very low fracture densities within the rock and lack of any apparent clustering at the scale at which the transect was carried out.

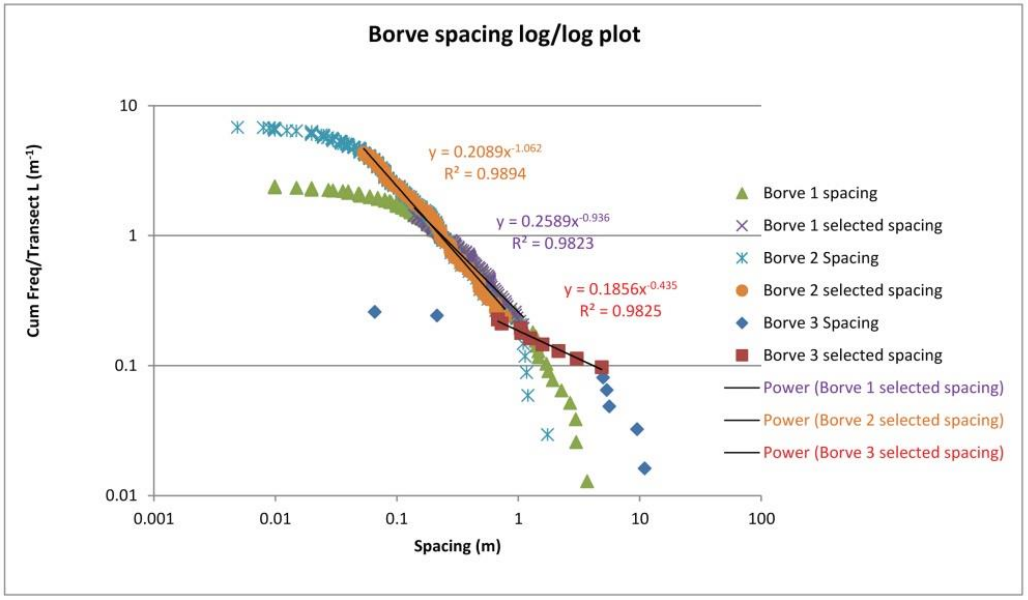

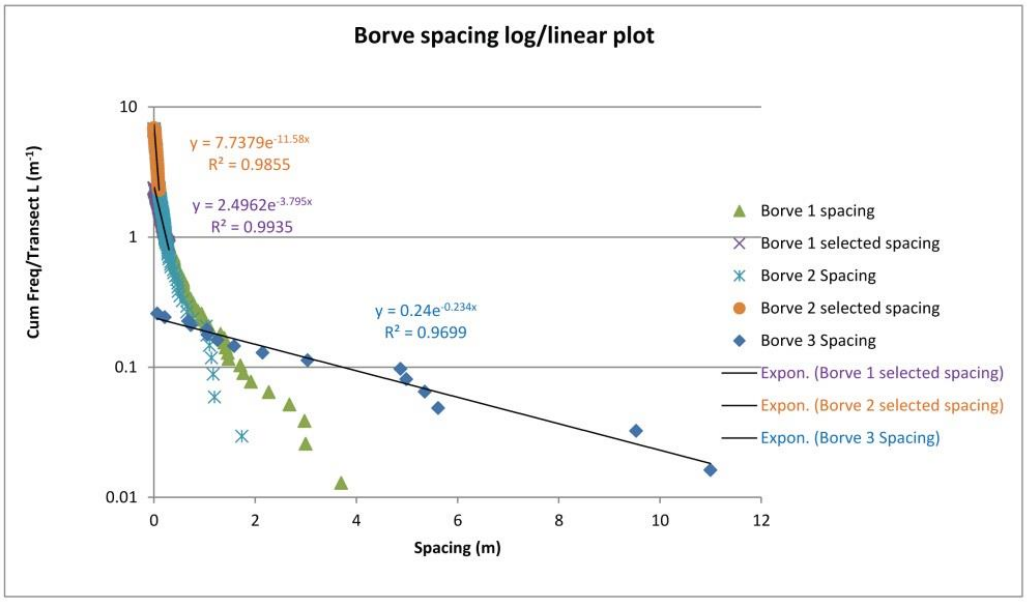

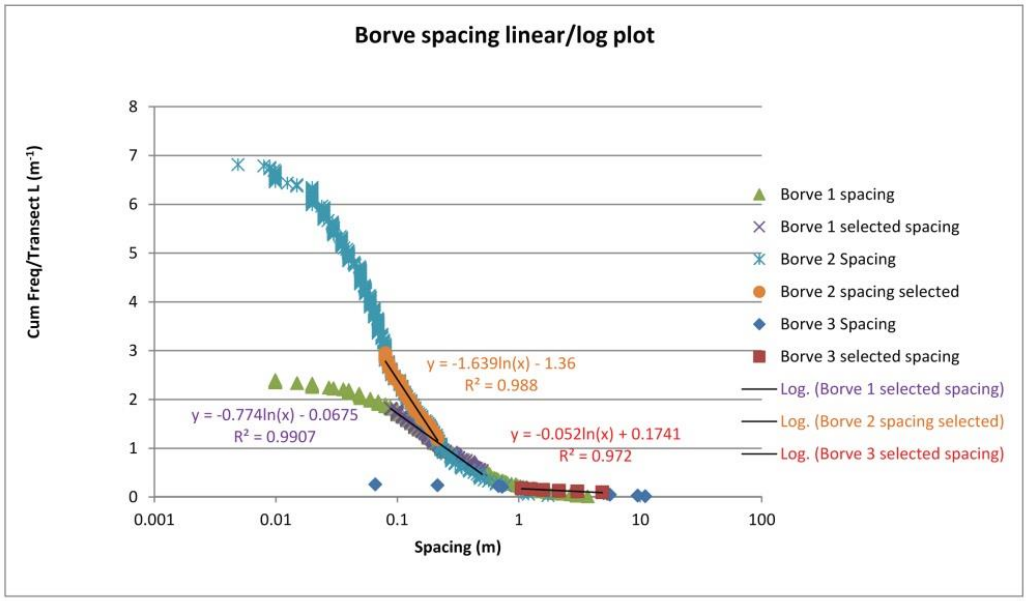

Figure 7.17: Distribution of spacing data collected from Borve. Graphs show raw and selected data.

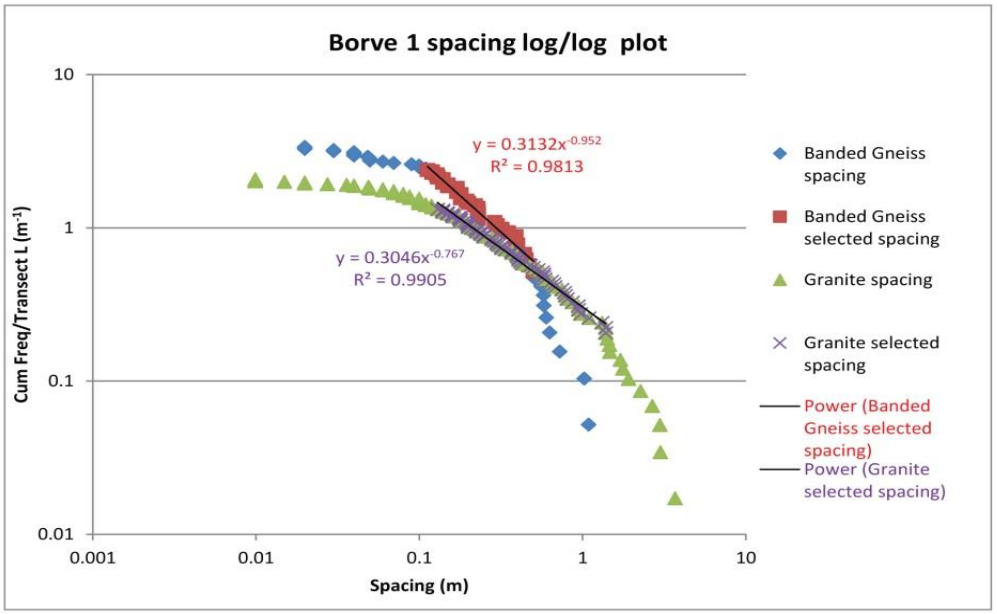

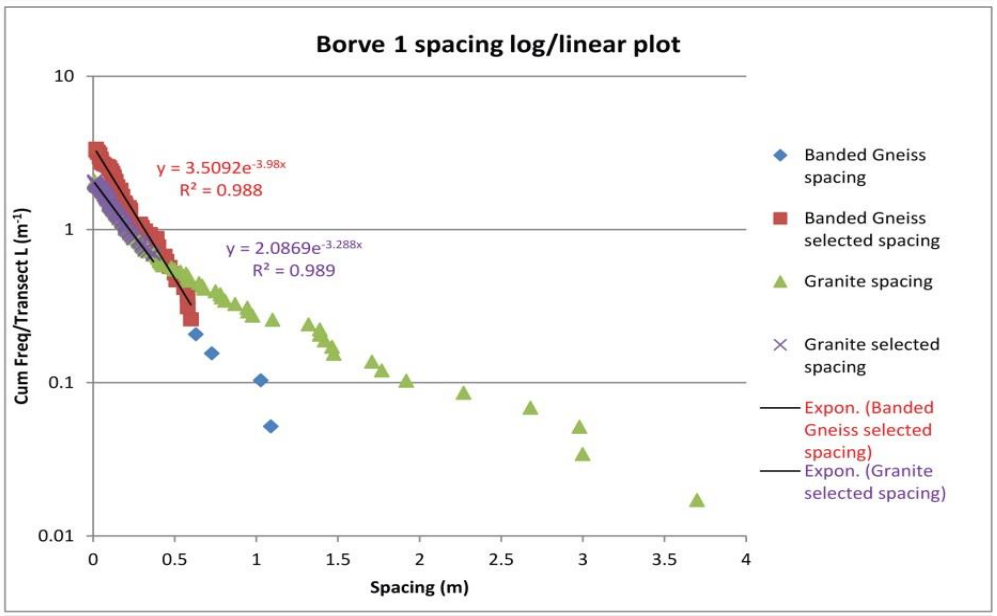

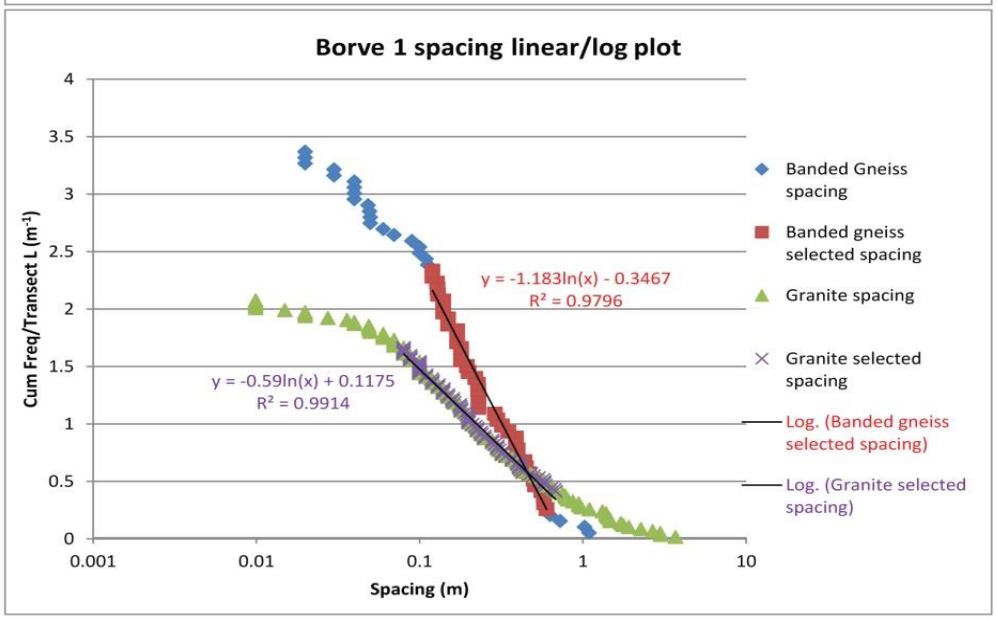

Figure 7.18: Distribution of spacing data collected from Borve 1 split between granite and banded gneiss lithologies. Graphs show raw and selected data.

Table 7.12: Table of number of data-points excluded from each plot type (and percentage of total data).

Distribution	Borve 1 banded gneiss	Borve 1 granite	Borve 1 all data	Borve 2	Borve 3
Power-law	28 (43%)	55 (45%)	89 (48%)	93 (40%)	7 (44%)
Negative exponential	4 (6%)	85 (32%)	122 (66%)	77 (33%)	0
Log-normal	24 (37%)	47 (39%)	85 (46%)	172 (89%)	10 (63%)

7.3.2.4.1.1 Summary and discussion

Although it has been found that lithological contacts within the Lewisian are often faulted, this was not the case at Borve. However, lithological differences in spacing distributions are clearly present. There is a decrease in fracture density within the granite when compared to the banded gneiss. Cv values produce conflicting results, being >1 (clustered) in the granite of Borve 1 and ~ 1 (randomly spaced) in the granite of Borve 3. This is attributable to the aforementioned fracture zone within the granite that the Borve 1 transect crosses. The fracture zone causes an increase in fracture density (as can be seen in Figure 7.16) and an increase in clustering. Fracture zones are also crossed by Borve 2, producing the clustered fracture spacing at that locality. The banded gneiss of Borve 1 does not contain a fracture corridor, and instead displays a relatively dense set of randomly spaced background fractures. The overall fracture density within the granite of Borve 1 and Borve 3 is lower than that in the banded gneiss in Borve 1 and Borve 2.

Hence, it would seem that the granite and banded gneiss both display background levels of randomly spaced fractures, with a lower density present within the granite. Where higher density fracture corridors are crossed, these contain highly clustered fractures.

Power-law trend lines can easily be assigned to the granite of Borve 1 and the banded gneiss of Borve 2 (Figure 7.18), which both cross fracture corridors and faults. An increase in the background level of fracturing is seen within the banded gneiss when compared to the granite, visible in Borve 2 and the Borve 1 granite that do not sample fracture corridors. The increase in fracture density between granite and banded gneiss may be caused by the presence of foliation within the banded gneiss. The effect of foliation may be similar to the effect of bedding in bedded sedimentary rocks, where joint spacing increases with bed thickness (Huang and Angelier, 1989).

In sedimentary rocks this produces anticlustered fracture sets, but the effect of foliation within the gneiss may be similar but may not be as marked as within sedimentary bedding.

Borve 1 banded gneiss also shows a straight line portion on the log/log plot over nearly 1 order of magnitude (Figure 7.18), but the Cv value is close to 1 (0.92). Although more data points are excluded from the power-law trend lines of Borve 1 and Borve 2 than the exponential trend lines (Table 7.12), straight lines exist within the data over more than 1 order of magnitude on the log /log plots. Borve 2 shows the longest straight line on a log/log plot of any transect studied here. This probably indicates that the spacing data is at least partly represented by a power-law distribution. These observations make a convincing case for the presence of power-law clustering of fractures across the fracture corridors, sampled in the Borve 1 granite and Borve 2 transects.

7.3.2.4.2 Fracturing within the SHSZ

Transects were taken in the Leverburgh Belt of South Harris to investigate the spacing distribution of fractures within the South Harris Shear Zone (SHSZ) (Table 7.13). Transects 1, 2 and 4 were located in the same area on a wave-cut platform. Transect 3 was undertaken in the immediate footwall of a zeolite bearing fault dipping steeply to the WNW. This fault is part of the NNE-SSW striking zeolite bearing fault set discussed in chapter 5 (section 5.4.4) that is of post-Caledonian but pre-Mesozoic age. For orientation data see Figure 7.20.

Table 7.13: Results from Transects undertaken at the SHSZ.

Locality	N (fractures)	N (spacing values)	Cv	D value of fitted power-law trend line	Best fitting distribution	Geological Situation	Transect Length (m)	Fracture Density (no./m)
SHSZ 1	179	166	1.21	1.40	Exponential	Foliation parallel, cuts faulting.	9.36	19.12
SHSZ 2	62	61	0.86	1	Exponential	Foliation perpendicular, dominantly cuts foliation parallel joints.	8.72	7.11
SHSZ 3	70	69	1.26	0.77	Exponential	Footwall of adjacent NE-SW. trending zeolite bearing fault	2.98	23.49
SHSZ 4	69	67	0.92	1.39	Exponential	Foliation oblique. Cuts several joint sets.	9	7.67

SHSZ 1 and SHSZ 3 both cut fault-related fracture sets, and the transects are sub parallel to the foliation strike. SHSZ 2 dominantly samples foliation parallel joints (not fault-related), and SHSZ 4 samples several joint sets (not fault-related). Fracture density is highest in SHSZ 1 (17.74

fractures/m) and SHSZ 3 (23.49 fractures/m), with lower values of 7 and 7.44 fractures/m obtained for SHSZ 2 and SHSZ 4, respectively. Hence it would seem fault-related fracturing clearly has a significant impact on the fracture density of the gneiss.

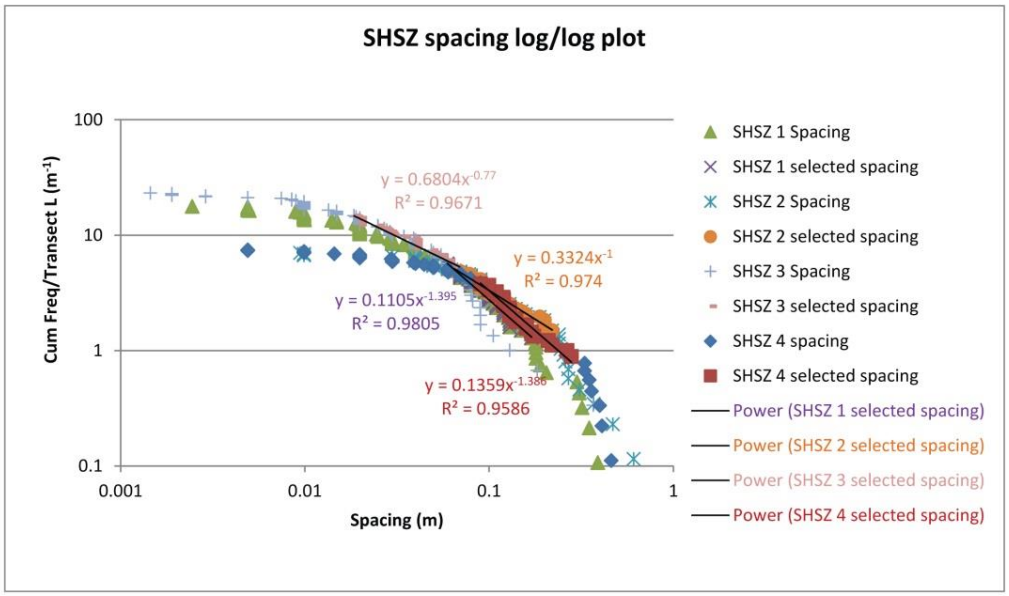

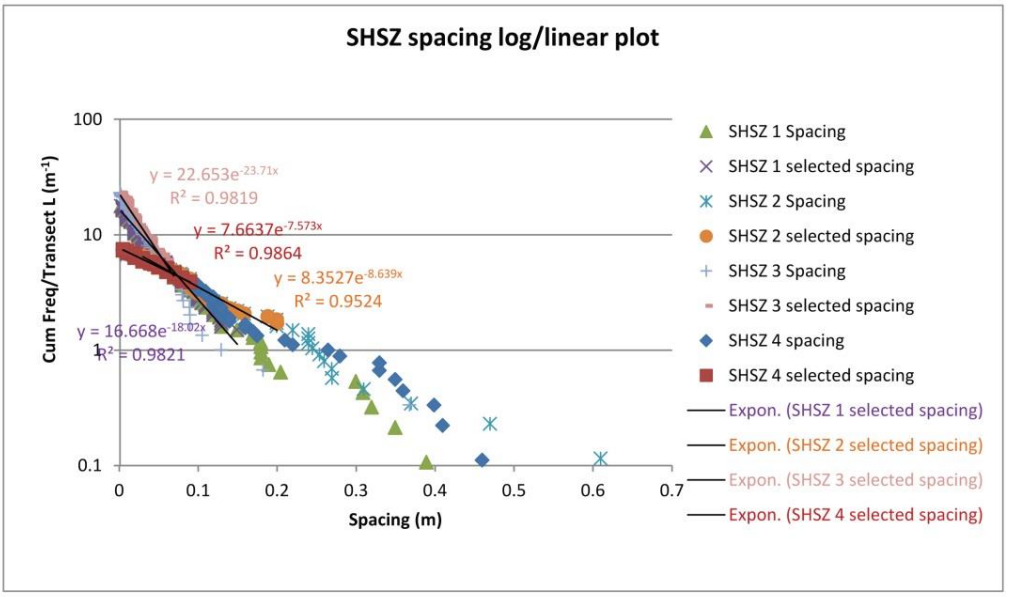

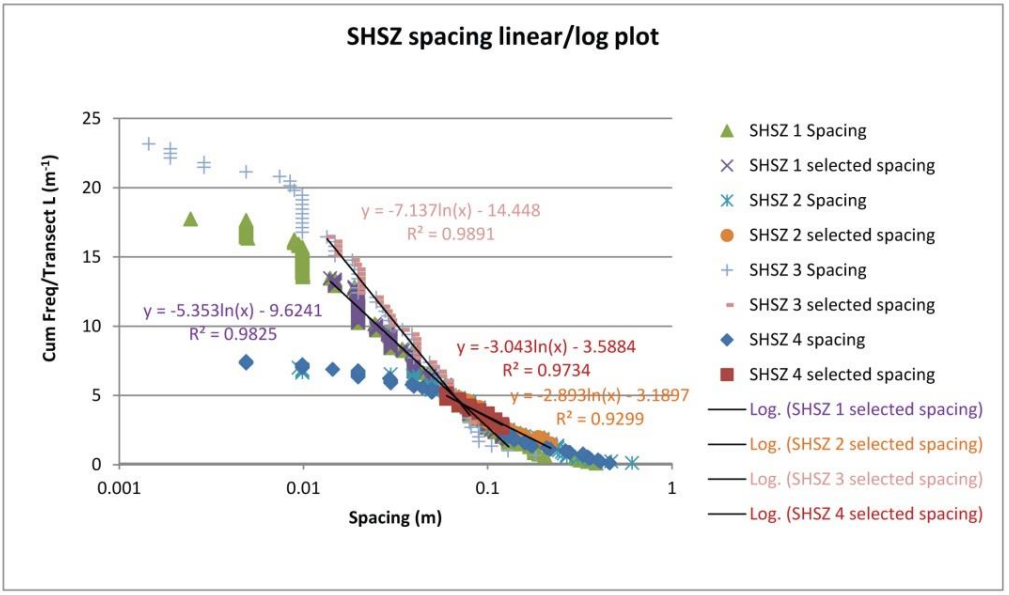

Figure 7.19: Distribution of spacing data collected from the SHSZ. Graphs show raw and selected data.

Cv values show that SHSZ 1 and SHSZ 3 are relatively clustered (Cv >1) and SHSZ 2 and SHSZ 4 are relatively anticlustered (Cv <1). When plotted on log/log axes, all of the transects plot as upwardly convex curves with only small portions (<1 order of magnitude of spacing) that can be described by a power-law trend line (Figure 7.19). The power-law D values display some variation between the transects: Transect 3, taken across the NNE-SSW striking fault-related joint set, has a low D value of 0.77. SHSZ 1 (foliation parallel) and SHSZ 4 (foliation oblique) show very similar D values of 1.40 and 1.39, respectively. SHSZ 2 (foliation perpendicular) has a D value of 1, and SHSZ 3 (foliation parallel) has a D value of 0.77.

The smallest amount of data points are removed when the data are described by exponential trend lines (Figure 7.19, Table 7.14). However, these distributions are still overall notably curved on log/linear plots and only small portions of the data range can be described by exponential trend lines. The portions of the data that can be best described by exponential trend lines lie at the tail ends affected by truncation (shallowing of the distribution curve on log/log plots at the lower end of the resolution). Similarly it is relatively difficult to fit log-normal trend lines to the distributions on the linear/log plots. However, the foliation parallel transects (SHSZ 1 and SHSZ 3), are better described by the log-normal trend lines (34% and 39% of data points excluded) compared to the foliation oblique and perpendicular transects (SHSZ 2 and 4, ≥50% data points excluded).

Table 7.14: Table of number of data-points excluded from each plot type (and percentage of total data).

Distribution	**SHSZ 1 (foliation parallel)**	**SHSZ 2 (foliation perpendicular)**	**SHSZ 3 (foliation parallel)**	**SHSZ 4 (foliation oblique)**
Power-law	124 (75%)	30 (50%)	38 (55%)	40 (78%)
Negative exponential	13 (8%)	18 (30%)	13 (19%)	34 (51%)
Log-normal	56 (34%)	30 (50%)	27 (39%)	44 (66%)

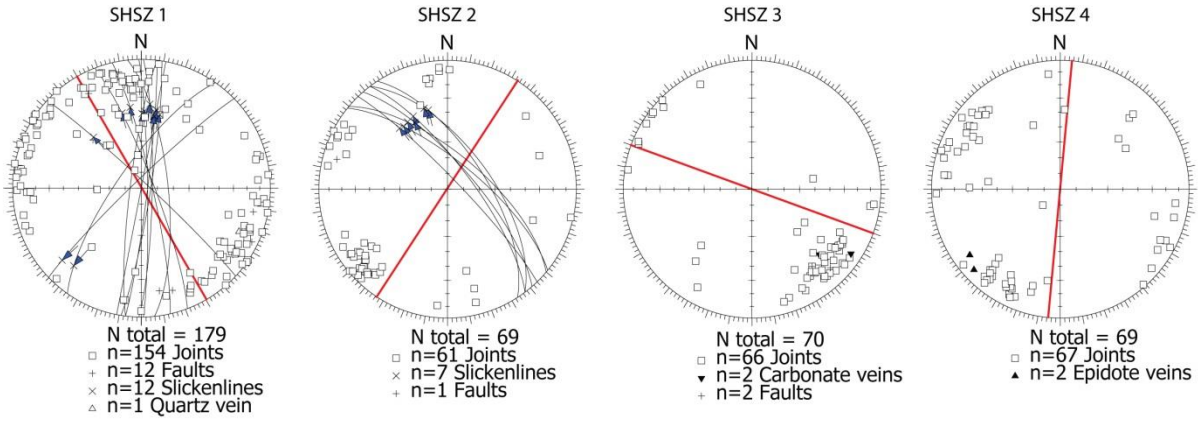

Figure 7.20: Orientation data collected from the transects on the SHSZ. Red line indicates transect orientation.

7.3.2.4.2.1 Summary and discussion

It is clear that faulting in the SHSZ leads to an increase in fracture density and an increase in the D value assigned to straight portions of the distributions on the log/log plots. Higher D values represent the increased relative importance of smaller fracture spacings in the fault-dominated transects. However, as seen elsewhere, exponential trend lines are a better fit to the data distributions, although exponential trend lines are still relatively difficult to apply, with curved distributions on log/linear plots. Log-normal trend lines are also relatively difficult to fit to the data.

The Cv from the fault-dominated foliation-parallel transects (SHSZ 1 and 3) show values that are > 1, and this is expected given that they cross fault-dominated fracture sets where clustering is observed. As Cv values >1 indicate that the data is relatively clustered, the data from SHSZ 1 and 3 may be expected to represent power-law distributions. However, power-law trend lines are difficult to fit to the data, and large proportions of the data points (> 50%) have to be excluded. It is not clear whether this is because of censoring or truncation, and it is possible that the D values obtained may not be representative. It is interesting to note that the fault-dominated transects (SHSZ 1 and 3) are more easily described by log-normal trend lines compared to SHSZ 2 and 4. This may be a reflection of the greater amount of clustering seen in these two data sets. SHSZ 2 and 4 both sample joint-dominated fracture sets and produce Cv values <1. SHSZ 2 dominantly crosses foliation-parallel jointing, and shows that these features are relatively anti-clustered.

Beacom et al. (2001) showed that intensity of the foliation on the Scottish mainland can be correlated with an increase in the clustering of fractures. Evidence of this was not observed in the South Harris Shear Zone, where foliation is highly pervasive and uniform. The data from the foliation-perpendicular transects presented by Beacom et al. (2001) have been interpreted to

display power-law distributions. Power-law distributions cannot reliably be applied to the foliation-parallel data obtained here. However, fracture density is notably very high around faults within the SHSZ.

7.3.3 Spacing data from Lewis and Harris Summary

Spacing data from Lewis and Harris is generally difficult to interpret due to the probable effects of truncation and censoring that cannot be removed from the data. These resolution effects create 'tails' on the log/log plots, preventing accurate representation of all of the data by a single trend line. Most of the spacing data is best fitted by exponential curves, with the least number of data points excluded in fitting a straight line onto the log/linear plots. However, it is important to note that the lower resolution areas of the graphs are areas affected by truncation, and exponential trend lines fit the lower end of the spacing scales of these plots very well. But, frequently the portion of the data points that can be approximated by exponential trend lines is continuous across the majority of data, and encompasses the areas where data is densest (i.e. centimetre to decimetre scale), indicating that these exponential distributions are probably real. Hence it seems that the high degree of fracturing within the Lewisian from multiple faulting and fracturing events discussed in previous chapters has essentially caused a random fracture spacing distribution at the majority of localities.

Although they may be best approximated by exponential trend lines, a higher degree of clustering is seen across (perpendicular to) the Mesozoic-age faults when compared to the fault-parallel transects. This is indicated by higher Cv values perpendicular to the main fault strikes. Lower Cv values are seen parallel with the fault strikes, and the distributions are notably more curved on log/log plots of the data. Similar portions of data points have to be excluded from the fault-perpendicular and -parallel transects to enable a power-law trend line fit (around 60% of data), however, straight line portions on the log/log plots are longer on the perpendicular transects. At Pabail, a similar number of data points are excluded in the exponential and log-normal trend lines fitted to the data. The Orasaigh (Cenozoic) transects show similar results to the Mesozoic faults, with the distribution best represented by an exponential trend line, despite relatively high Cv values.

The transects taken at Borve show differences in spacing distributions between the two lithologies encountered. Within granite, the fractures are randomly oriented and spaced except where fracture corridors exist. Fracture corridors within the granite have relatively high fracture densities with clustered spacing distributions than can be approximated with power-law trend lines.

Overall, however, the granite fracture density is low, and outside the fracture zones the spacing distribution is best approximated by an exponential trend line, representing random fracture spacing. Within the banded gneiss, the spacing data are well approximated over > 1 order of magnitude by a power-law trend line, and the gneiss shows a high fracture density. The increase in fracture density may in part be attributed to the effect of the foliation within the banded gneiss, which is absent from the granite. At the SHSZ, the foliation-perpendicular and foliation oblique transects (SHSZ 2 and 4) dominantly sample joints. The Cv values from these fracture sets show the spacing distributions to be anticlustered. Conversely, SHSZ 1 and 3 sample fault-related fracture sets and display clustered fracture spacing.

7.4 Spacing data from Clair

Transects were performed on Clair core samples to quantify fracture spacing within the Clair Group cover. Clair basement fractures have previously been extensively analysed by Pless (2011) so only one sample typical of general Clair basement fracturing is presented here (section 7.3).

7.4.1 Methods – core transects

Pless (2011) studied quantitative data collected from transects within the basement rocks at Clair, concentrating on the analysis of fracture spacing using 1D line transects. Power-law distributions were identified in all of the 10 transects undertaken in the core, with the exception of well 206/8-8 where an exponential distribution was determined. This study aims to identify the differences that exist between the basement and cover rocks through analysis of further 1D line transect data collected from the core store in Aberdeen, predominantly from the cover rocks. Gaps within the core were omitted from this study to quantify the spacing of natural fractures only (with the exception of Clair transect A). The spacing data has been analysed and plotted on log/log, log/linear and linear/log graphs, as above.

Sections of core were selected for the 1D transects to quantify fractured zones within the Clair Group for comparison with faults and fractures zones within the basement rocks discussed above and those analysed by Pless (2011).

7.4.1.1 Study sites for transect data collection

Transect localities were selected in order to collect representative data from zones of fracturing and faulting. Transects A to E were performed across zones of fracturing within the Clair Group

identified by Milodowski (1998) (Table 7.15). Transect F records fracturing and faulting within the basal conglomerate and basement rocks of well 206/8-8 for comparison.

Table 7.15: Transect localities from the Clair cores.

Name	Well	Depth range (m)	N (fractures)	Lithology	Fracture set sampled
A	206/8-8	1724 – 1729	50	Clair Group unit VI, porous oil-filled sandstone and calcite cemented sandstone.	Mostly open fractures, probably produced during core retrieval.
B	206/8-8	1747 - 1757	61	Clair Group unit VI, porous oil-filled sandstone and calcite cemented sandstone.	Calcite cemented breccia zone in calcite cemented sandstone and granulation seams within oil filled porous sandstone.
C	206/8-8	1897 - 1904	69	Clair Group Unit V	Dominantly samples granulation seams in oil filled porous sandstone.
D	206/8-8	2126 – 2129.7	38	Clair Group Unit V	Dominantly samples granulation seams in oil filled porous sandstone.
E	206/8-10z	2317 - 2320	41	Clair Group Unit V	Samples naturally open and calcite cemented fractures.
F	206/8-8	2486.4 - 2491	98	Basal conglomerate and basement	Samples epidote, quartz, adularia and calcite bearing veins in the basement.

7.4.2 Clair A to E (Clair Group) spacing results

Results are shown in Table 7.16 and the data are plotted in Figure 7.21. In all of the cores there are small areas where retrieval was not possible or samples have been removed. This results in gaps in the core that spacing cannot be calculated across. This will also tend to randomise the data, although as the gaps are relatively small the effect is expected to be similarly low. Transect A records fractures that are open and not mineralised, and are interpreted to have resulted from drilling and core retrieval – i.e. they are not natural fractures. Transects B – E sample natural fractures only that are fault related, often mineralised. Transect E was taken across a fault zone associated with natural secondary open porosity (for corresponding core observations see chapter 6).

Table 7.16: Results from transects Clair A to E.

Locality	N (fractures)	N (spacing values)	Length	Cv	D value of fitted power-law trend line	Best fitting distribution	Fracture set sampled	Fracture Density (no./m)
Clair A	48	46	4.874	0.59	1.29	Log-normal	Open non-natural fractures.	9.85
Clair B	34	29	10.409	1.82	0.43	Power-law	Calcite cemented breccia zone in calcite cemented sandstone and granulation seams within oil filled porous sandstone.	3.23
Clair C	33	30	6.098	1.88	0.35	Power-law?	Dominantly samples granulation seams in oil filled porous sandstone.	5.41
Clair D	21	19	3.694	1.69	0.47	Exponential?	Dominantly samples granulation seams in oil filled porous sandstone.	5.68
Clair E	34	33	2.854	0.96	0.88	Exponential	Samples naturally open (dissolution effects) and calcite cemented fractures.	11.91

Table 7.17: Fracture fills encountered in the Clair core transects.

Clair Transect	Granulation seam and calcite	Calcite	Granulation seam	Uncemented fault rock	Open fractures, at times with minor euhedral calcite and pyrite	Epidote, quartz and reddy-brown (adularia)
A					48 (non-natural)	
B	4	27	3			
C			33			
D	2		19			
E	2	15		3	14 (natural)	
F		38				60

Cv values vary between 0.59 (Clair A transect) and 1.88 (Clair C transect). Clair B-D all have Cv values in the range of 1.69 – 1.82. The Cv value of Clair E is very close to 1 (0.96), indicating a random spacing distribution.

The data are plotted in Figure 7.21 on log/log, log/linear and linear/log plots, with trend lines assigned to straight-line portions of the plots. The number and proportion of data points excluded by the fitted trend lines are shown in Table 7.18. The relatively steep curve of Clair A is evident within all of the plots and represents the relative importance of smaller spacings in non-natural fracture sets within the core. Natural fractures, sampled in Clair B to E (Table 7.17), show lower gradients in all plots and generally are lower than the gradients determined in all of the transects taken within the Lewisian basement rocks of Lewis and Harris, with the exception of the Borve 3 transect that displays a similar low value (0.435). Clair B to D show similar gradients of the straight line portions in all plots, confirming the similarity observed in their Cv values.

Clair A is best described by a log-normal trend line with removal of fewest data points to fit a straight line to the data (Table 7.18). Clair B is best described by a power-law trend line, and Clair C and D are also relatively well described by power-law trend lines, with Clair B and Clair C showing straight line portions on the log/log plot (Figure 7.21) of nearly two orders of magnitude. Clair D is best described by an exponential trend line, however it is likely this is not representative, given the low number of fractures sampled by this transect. On the log/log plot, the straight line portion of Clair D has a gradient close to those of Clair B and Clair C. Clair E is described best by an exponential trend line, with zero data points removed in the straight line fit to the data on the log/linear plot.

D values for the assigned power-law trend lines show variation, with the highest value of 1.29 obtained from Clair A, and the lowest value of 0.35 obtained from the Clair C transect. The D values obtained for Clair B and Clair D are similar to Clair C (0.43 and 0.47). Clair A and E show higher D values of 1.29 and 0.88, respectively, indicating the greater importance of smaller fracture spacings in these data.

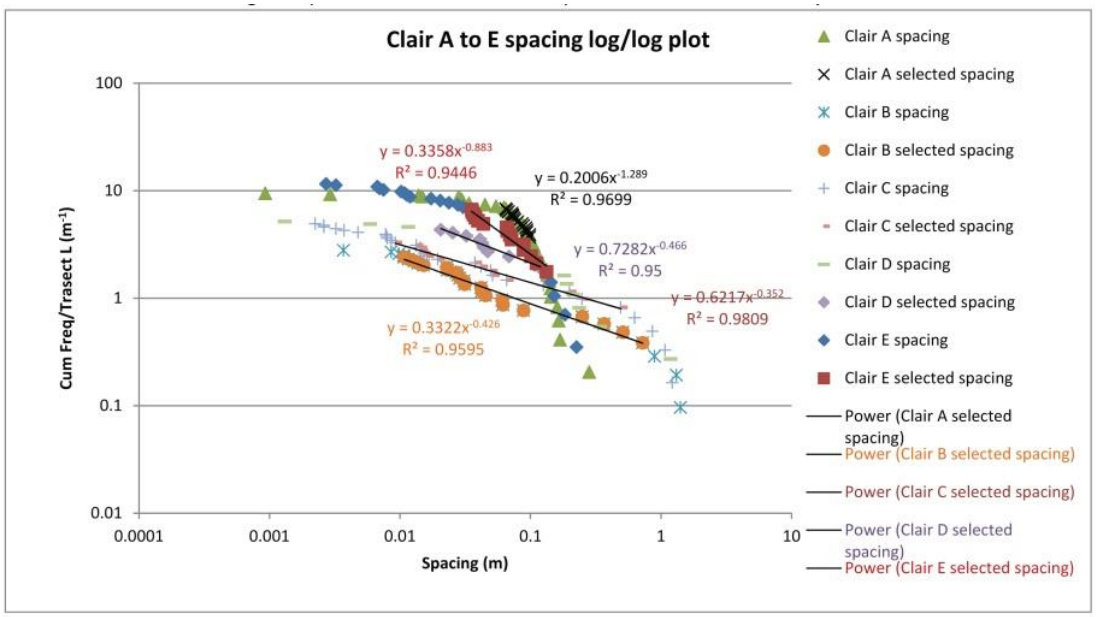

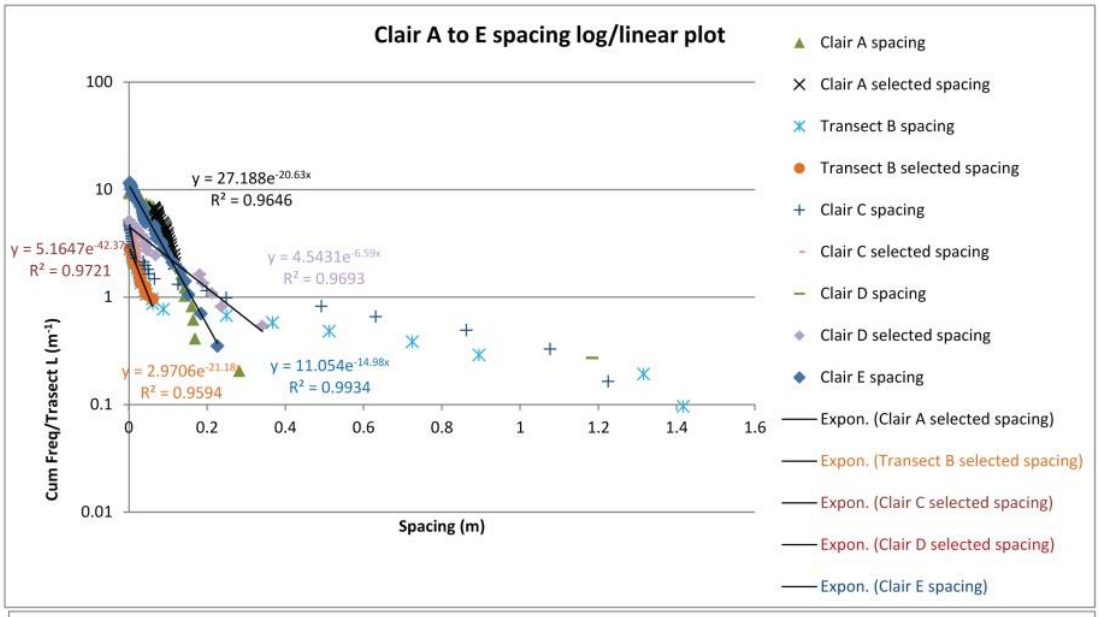

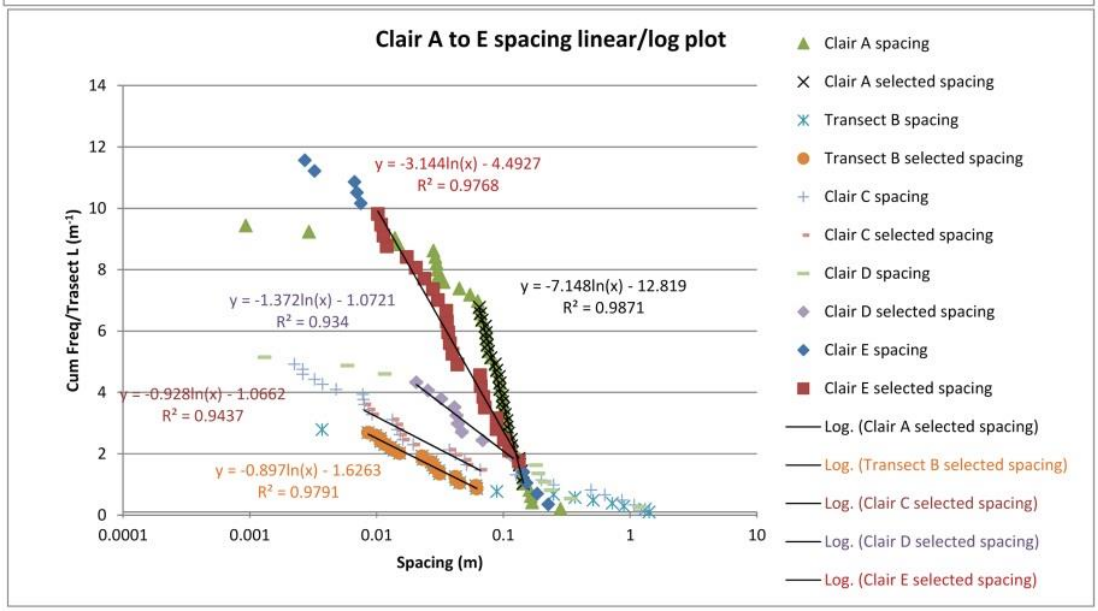

Figure 7.21: Graphs of spacing data collected from transects Clair transects A to E. Graphs show raw and selected data. Note that transect A shows data from non-natural fractures only.

Table 7.18: Table of number of data-points excluded from each plot type (and percentage of total data).

Distribution	Clair A	Clair B	Clair C	Clair D	Clair E
Power-law	30 (65%)	7 (24%)	14 (47%)	9 (47%)	18 (55%)
Negative exponential	22 (49%)	9 (31%)	13 (43%)	1 (5%)	0
Log-normal	17 (37%)	9 (31%)	16 (53%)	9 (47%)	9 (27%)

7.4.2.1 Clair A to E (Clair Group) spacing summary and discussion

Clair A – E transects comprise relatively little data when compared to transects taken on Lewis and Harris, due to the generally sparse nature of fractures in the cover sequence and the limited recovery within fault zones. However, although the number of fractures sampled in each transect is relatively low, interesting results are still present.

There are similarities between Clair B, C and D, while Clair A and E are different. As noted, the geological situations of B, C and D are relatively similar, with these transects sampling granulation seams, calcite veins and cemented breccias. It is likely that the similarities encountered here are real, given their similar geological setting. Power-law distribution may well exist across these transects and a power-law trend line is the best fitting trend line that can be assigned to Clair B.

Clair A records fracturing that has been interpreted as not natural, i.e. fracturing that was caused when the core was obtained. It is interesting to note that the low Cv value indicates a relatively anticlustered spacing distribution of these fractures, and the data are best represented by a straight line on a linear/log plot, indicating they are best described by a log-normal trend line.

Clair E records fracturing across the partially uncemented fault zone in well 206/10z that has undergone a degree of dissolution (section 6.4.1.1), with multiple natural open fractures sampled (Table 7.17). The Cv value of 0.96 obtained for Clair E is indicative of a random fracture spacing distribution that may be caused by this dissolution of the rock. A random distribution of these data is confirmed by the fact that the data lie along a very clear straight line on the log/linear plot and no data points were removed when fitting an exponential trend line.

7.4.3 Clair F (basal conglomerate and basement) spacing results

Transect F was undertaken through the basal conglomerate and basement rocks of well 206/8-8, studied in chapter 6. Results are shown in Table 7.19 and the data are plotted in Figure 7.22. Fracture types cut by the transect are shown in Table 7.17, and results are shown in Table 7.19. Within the basement rocks, fracturing is dominated by epidote bearing veins and faults and veins that are red-brown in colour and interpreted to be adularia (chapter 6). Calcite veining at times reactivates pre-existing fractures.

Table 7.19: Results from transect F.

Locality	N (fractures)	N (spacing values)	Length	Cv	D value of fitted power-law trend line	Best fitting distribution	Fracture set sampled	Fracture Density (no./m)
Clair F	98	94	4.376	1.44	0.537	Exponential	Epidote, adularia, quartz and calcite filled veins and faults	22.4

The Cv value within the basement is relatively high (1.44), indicating that the fractures are clustered. Fracture density is notably increased from the Clair Group, being at least double the values obtained across fault zones within the cover. The data are plotted in Figure 7.22 with trend lines assigned to straight-line portions of the plot. Table 7.20 shows the data points that were excluded from each of the trend lines. The power-law distribution is the poorest fit to the data, with 34% of the data excluded to produce straight line. However, the assigned straight line lies over >1 order of spacing magnitude with an R^2 of 0.99. The data is much better represented by exponential and log-normal trend lines, with 5% and 10% of data excluded (respectively) when fitting a straight line trend to the distribution.

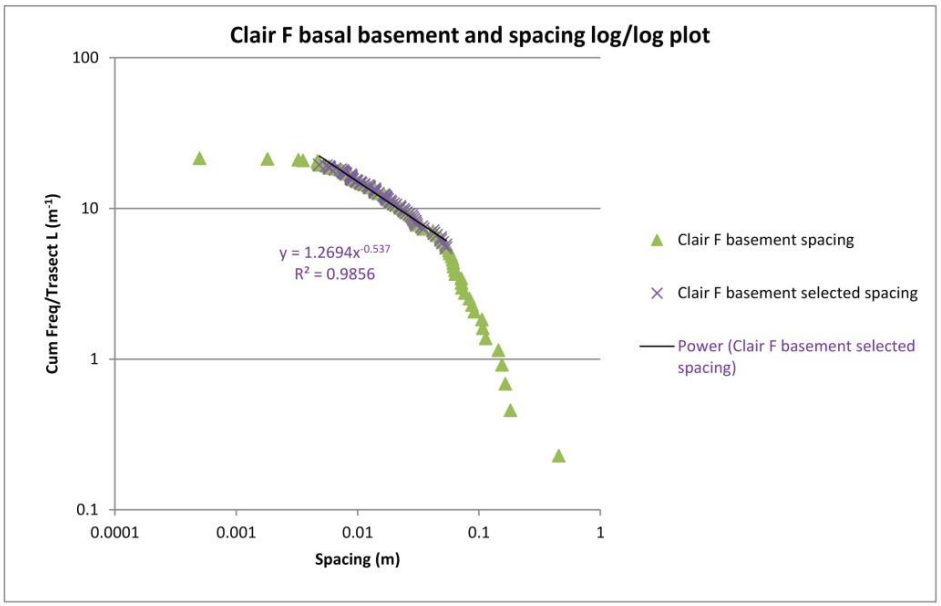

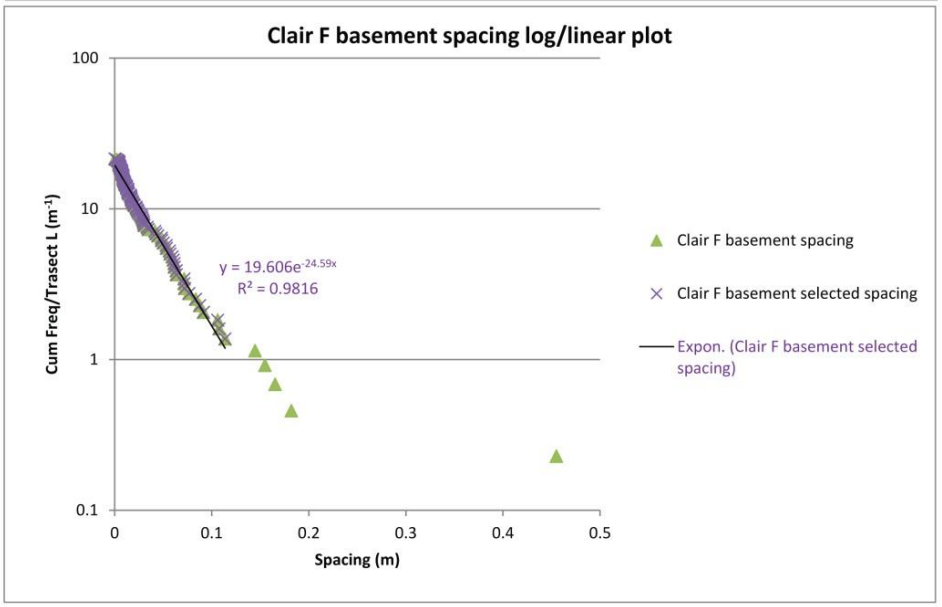

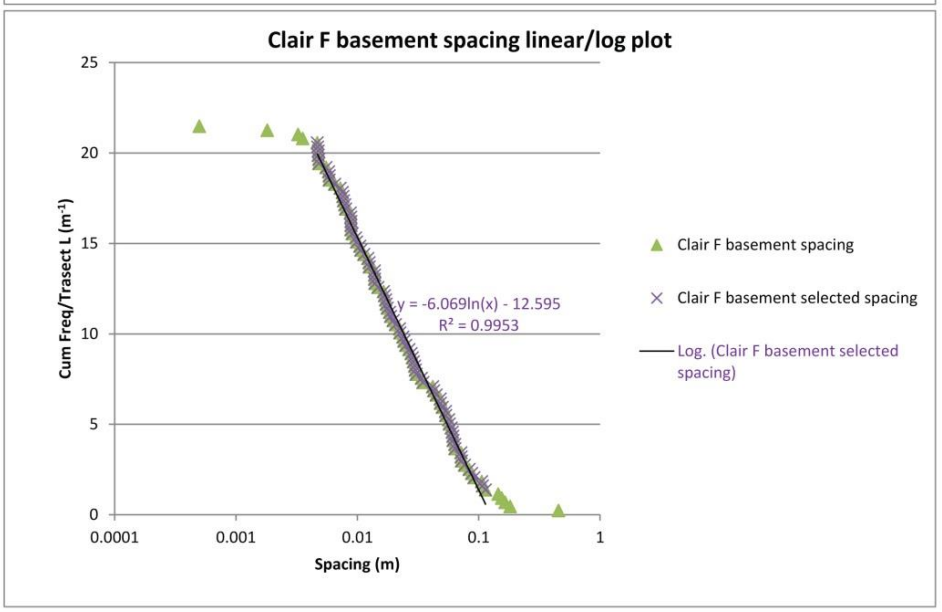

Figure 7.22: Graphs of spacing data collected from Clair transect F. Graphs show raw and selected data.

Table 7.20: Table of number of data-points excluded from each plot type (and percentage of total data).

Distribution	Clair F (basement)
Power-law	32 (34%)
Negative exponential	5 (5%)
Log-normal	9 (10%)

7.4.3.1 Clair F (basement) spacing summary and discussion

The distribution of data from Clair F is best represented by an exponential trend line that encompasses nearly all of the data (95%). However, this also includes the area of the graph affected by truncation and a portion of the graph likely affected by censoring. Log-normal trend lines similarly fit the distribution well, excluding only 10% of data points. However, a high Cv value of 1.44 indicates that the fractures are relatively clustered, and a power-law distribution can be fitted to this data excluding 34% of data points. The D value obtained for this is slightly higher than the D values obtained from transects B-D within the Clair Group that sample faulted sections of the core.

Fracture spacing within well 206/8-8 has previously been interpreted to show an exponential distribution, a Cv value of 0.868, and a fracture density of 10.54 fractures/metre (Pless, 2011). Pless (2011) notes the presence of open fractures within the 206/8-8 well that have been interpreted as natural features that were open in the sub-surface. However no evidence has been found in the section studied here to conclusively support this interpretation and no natural macroscopic open fractures were apparent in the sampled section. Interpretation of non-natural open fractures as natural features and inclusion of them into the spacing analysis will have a randomising effect. As discussed above, non-natural fractures within the Clair Group core tended to display a relatively steep gradient on all of the plot types, a low Cv value, and were best described by a log-normal trend line. Their inclusion in spacing analysis explains the low Cv value obtained by Pless (2011). The low fracture density of 10.54 fractures/metre compared to results presented here (22.4 fractures/metre) suggests a degree of selection was used in determining which fractures were included in the study of Pless (2011).

7.5 Aperture - Lewis and Harris fieldwork transect data

In addition to spacing data, aperture data were also collected from transects undertaken on the Clair core and on Lewis and Harris. Fracture apertures have previously been found to show a power-law distribution in other studies (e.g. Marrett et al., 1999; Ortega et al., 2006; Belfield, 1998). Aperture can be plotted against cumulative frequency or average spacing (inverse of cumulative frequency) to estimate the fracture density of any given scale of aperture (Ortega et al., 2006). In this study the apertures of natural fractures are examined in bulk (i.e. collectively). Because these data include all fractures measured within the Lewisian (i.e. they are natural samples), the results are therefore industrially applicable to fractures encountered when drilling in the basement at Clair.

All aperture data collected from transects on Lewis and Harris are shown in Figure 7.23, generally plotting along a straight line over ~5 orders of magnitude. On log/linear and linear/log plots the data are notably curved. Towards the lower end of resolution, several vertical trends are apparent within the data around apertures of 0.0001 and apertures of 0.001. These result from the sampling resolution where it was not possible to more accurately measure such small aperture dimensions. The power-law trend line assigned to all of the data has a D value of 0.505.

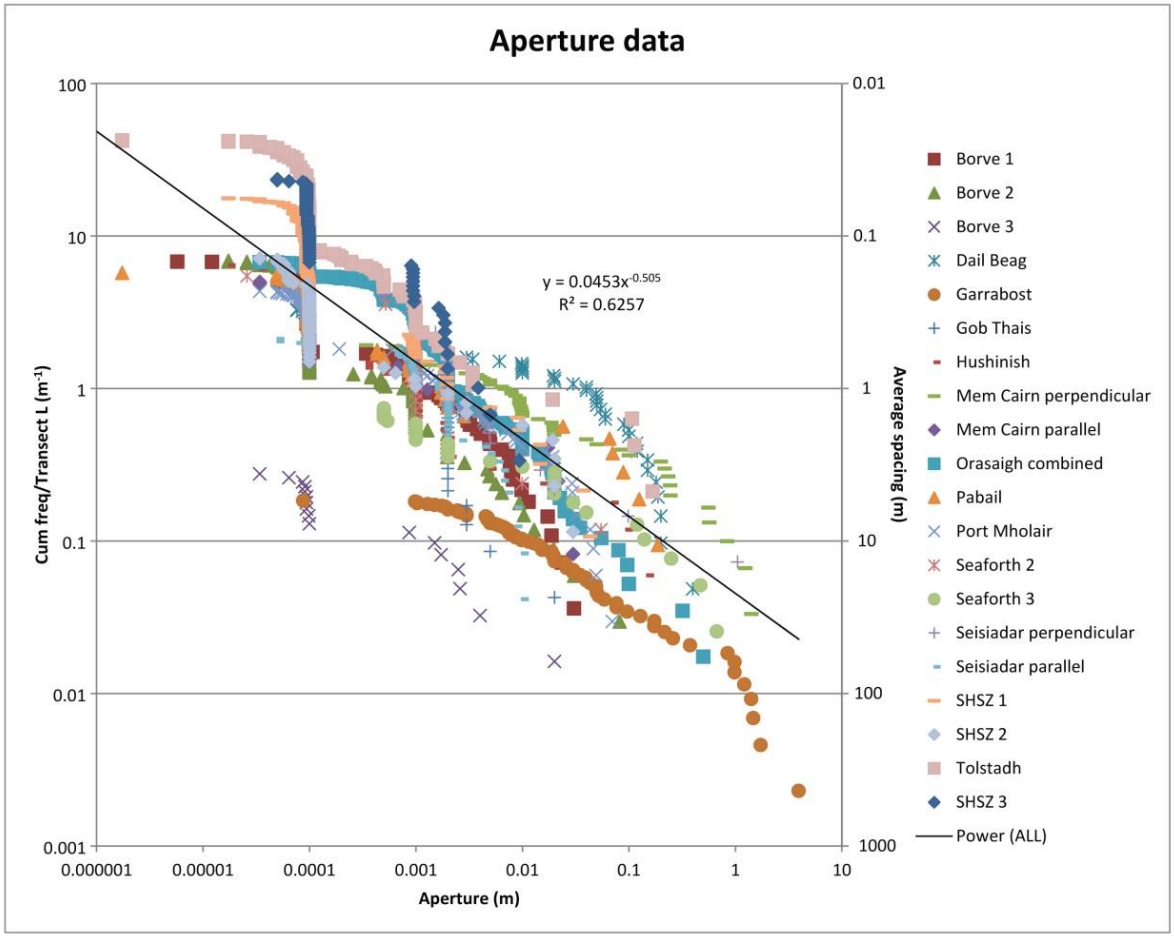

Figure 7.23: Aperture data collected from Lewis and Harris. Raw data only.

7.5.1 Preliminary aperture mechanics investigation

The fracture apertures presented above include both mode 1 and mode 2 fractures. Data from the Memorial Cairn fault-perpendicular transect (see section 7.3.2.2) are split between mode 1 and mode 2 fractures below (Figure 7.25). Both distributions can be easily described by a power law trend line. Hydrofracture (mode 1) fracture apertures are controlled by the following equation when the strike dimension on the surface (L) is less than the dip dimension (R) (see Figure 7.24) (Gudmundsson, 2011) :

$$\Delta u = \frac{2p(1 - v^2)L}{E}$$

If the strike dimension (L) is greater than the dip dimension (R), fracture aperture is given by:

$$\Delta u = \frac{4pVR}{E}$$

Where p = overpressure, Δu = fracture aperture, v = poisons ration, E = Young's Modulus.

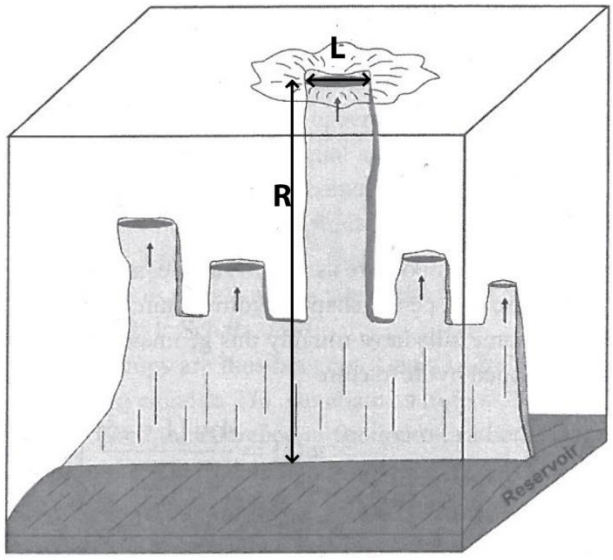

Figure 7.24: From Gudmundsson (2011), showing fracture dip dimension (R) and strike dimension (L).

Similarly for mode 2 fractures, displacement across the fracture is controlled by (Gudmundsson, 2011):

$$\Delta u = \frac{4\tau_d RV}{E}$$

As it was not possible to measure displacements in this study due to a lack of offset markers, it is not possible to properly assess this relationship.

Given that Poisson's ratio and the Young's Modulus will be relatively consistent over the metre scales measured in the line transects, it is likely that fracture aperture of mode 1 fractures is therefore dependent on the interplay between fluid pressure and fracture dimension. In mode 2 fractures, fracture displacement is dependent on the shear stress acting on the plane and fracture length.

Fracture length at the Memorial Cairn fault-perpendicular transect is shown in Figure 7.26. As can be seen, a large proportion (55% mode 1, 63.1% mode 2) of the data has to be excluded to fit power-law trend lines to the data. It is more likely that these distributions are better represented by exponential trend lines (no data excluded and 50% of data excluded, respectively), indicating a random fracture length distribution. All aperture data from the Memorial Cairn fault-perpendicular transect is plotted against corresponding fracture length data in Figure 7.27 (with 173 data points). As can be seen in the plots, there is a statistically significant correlation ($P << 0.05$) between fracture length and aperture when expotentiating the aperture value. Similarly the relationship is also statistically significant when using the untransformed (raw) aperture values (i.e. a linear relationship) and also when using a power law (a logarithmic model is discounted due to very low R^2 of 0.1289). However, the R^2 of these correlations are diminished relative to the exponential relationship (see Figure 7.27). When the outlying data point with a length of 10 is dismissed, the relationship remains statistically significant with the exponential relationship still having the largest R^2.

Given that linear, exponential and power-law models are statistically significant, the exponential model best fits the data as it has the largest R^2. It is, however, important to note that the dataset is relatively course with repeated length and aperture measurements that will have lowered the R^2 (i.e. the proportion of the variation in aperture explained by the fracture length changes). In addition, given that the exponential model describes only half the data variation ($R^2 = 0.4975$) it follows that there may be another causative agent that is affecting fracture aperture. This may be the rock strength, or pore fluid pressure, or due to length values that are not the maximum fracture dimension (as required in the equations by Gudmundsson, 2011) due to the dependence of this measurement on where the fracture is measured. In addition, the fact that the data is best fitted by an exponential relationship suggests that the linear relationship between aperture and length as suggested by Gudmundsson (2011) may not apply to this sample. This may well be due to the fact that the fractures are a natural sample of variably aged features, and it is likely that pore fluid pressure would not have remained constant through time. This could produce a non-linear distribution.

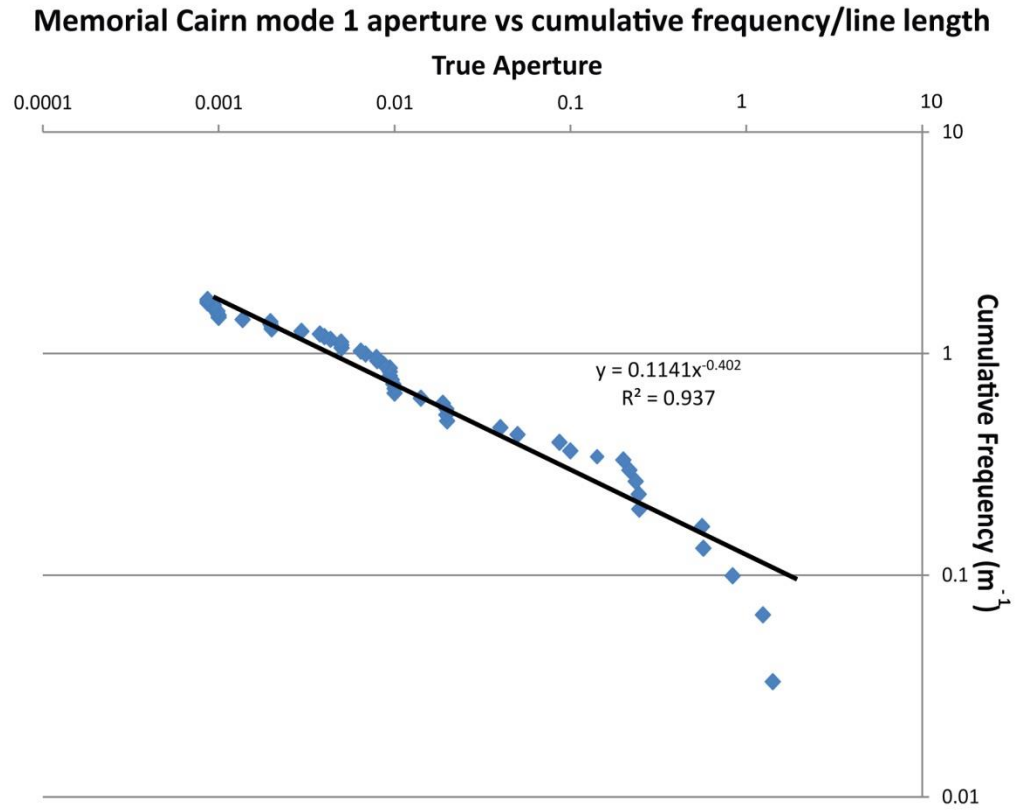

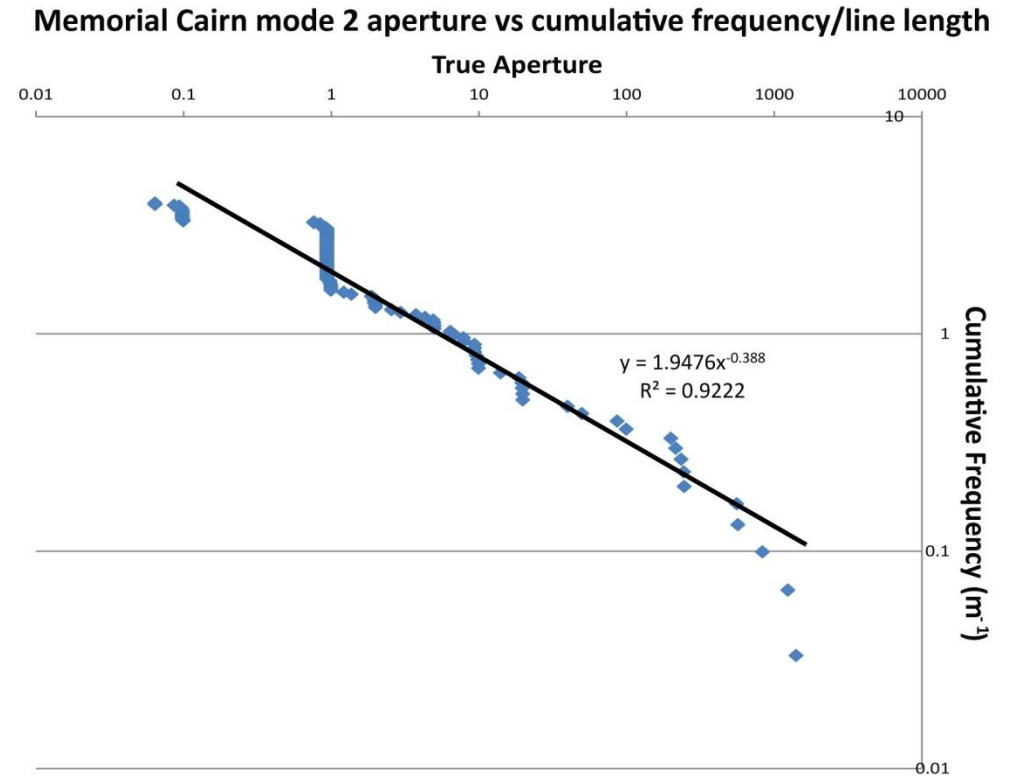

Figure 7.25: Log/log plots of aperture vs. cumulative frequency/transect length for Mode 1 and Mode 2 fracture recorded from the Memorial Cairn fault-perpendicular transect.

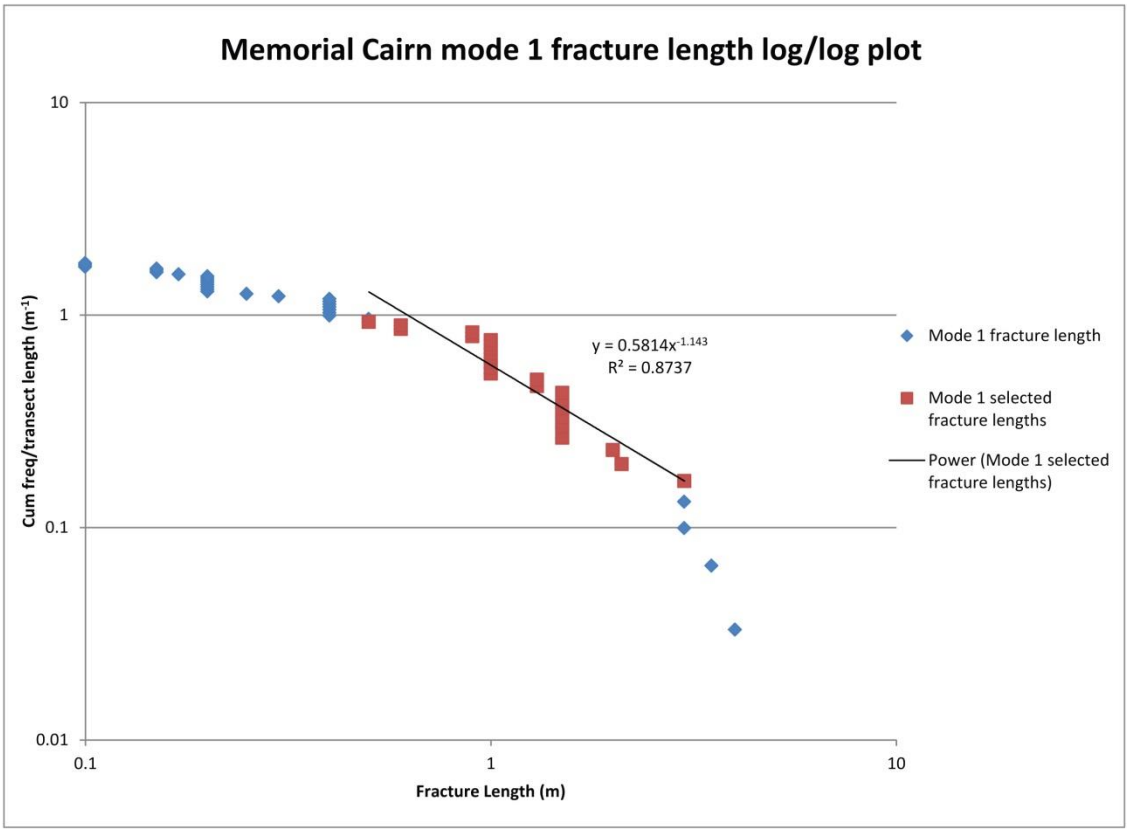

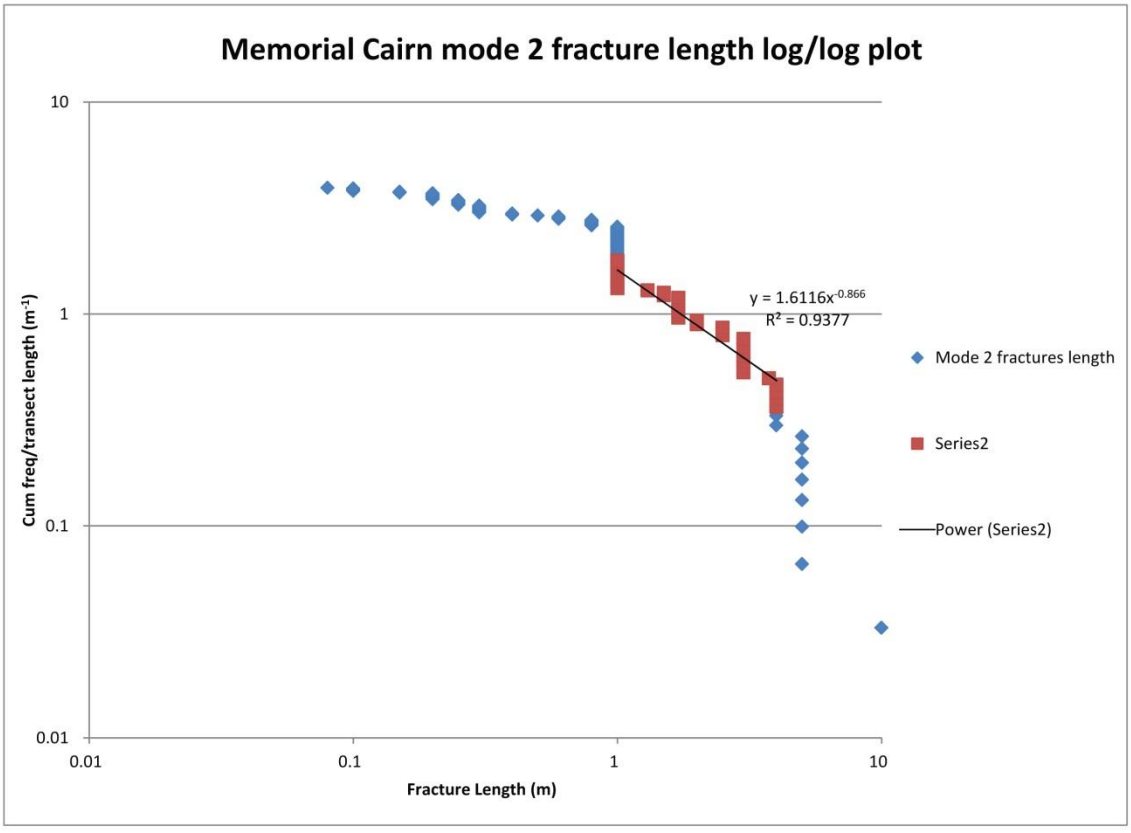

Figure 7.26: Distribution of fracture length data from the Memorial Cairn perpendicular transect locality split between mode 1 and mode 2 fractures.

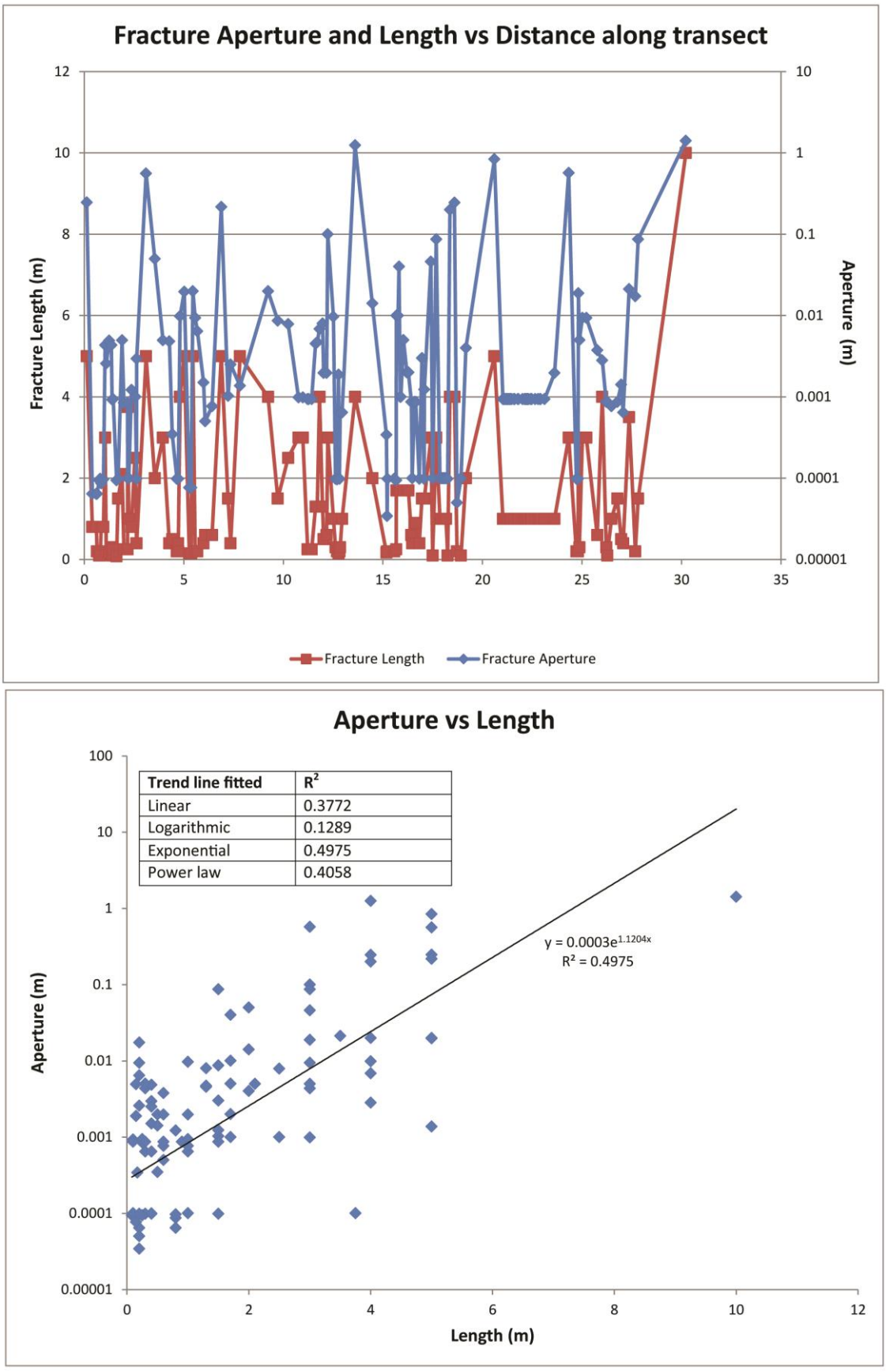

Figure 7.27: Relationship between fracture aperture and fracture length, Memorial Cairn fault-perpendicular transect.

7.6 Aperture data from Clair

7.6.1 Clair A to E aperture results

Aperture data collected from Clair transects B, C, D and E are shown in Table 7.21 and plotted on log/log, log/linear and linear/log plots in Figure 7.28.

Table 7.21: Clair A-E aperture data.

Locality	N (fractures)	D value of fitted power-law trend line	Best fitting distribution	Fracture set sampled
Clair B	34	0.451	Power-law?	Calcite cemented breccia zone in calcite cemented sandstone and granulation seams within oil filled porous sandstone.
Clair C	33	0.902	Power-law?	Dominantly samples granulation seams in oil filled porous sandstone.
Clair D	21	0.719	Power-law?	Dominantly samples granulation seams in oil filled porous sandstone.
Clair E	34	1.07	Exponential	Samples naturally open (dissolution effects) and calcite cemented fractures.

The relatively low number of data points on these plots make interpretation difficult. However, Clair B is easily defined by a power-law trend line on a log/log plot over >1 order of magnitude (Figure 7.28). The Clair B data is also well represented by a logarithmic distribution, with an equally low number of data points excluded when fitting a log-normal trend line on the linear/log plot (Table 7.22). Fewest data points were excluded from Clair transects B, C, D and E when assigning exponential trend lines to the data on the log/linear plot. However power-law trend lines can be assigned to these datasets over ≥1 order of magnitude. It therefore seems possible that Clair B, C, D, and E are best represented by power-law trend lines.

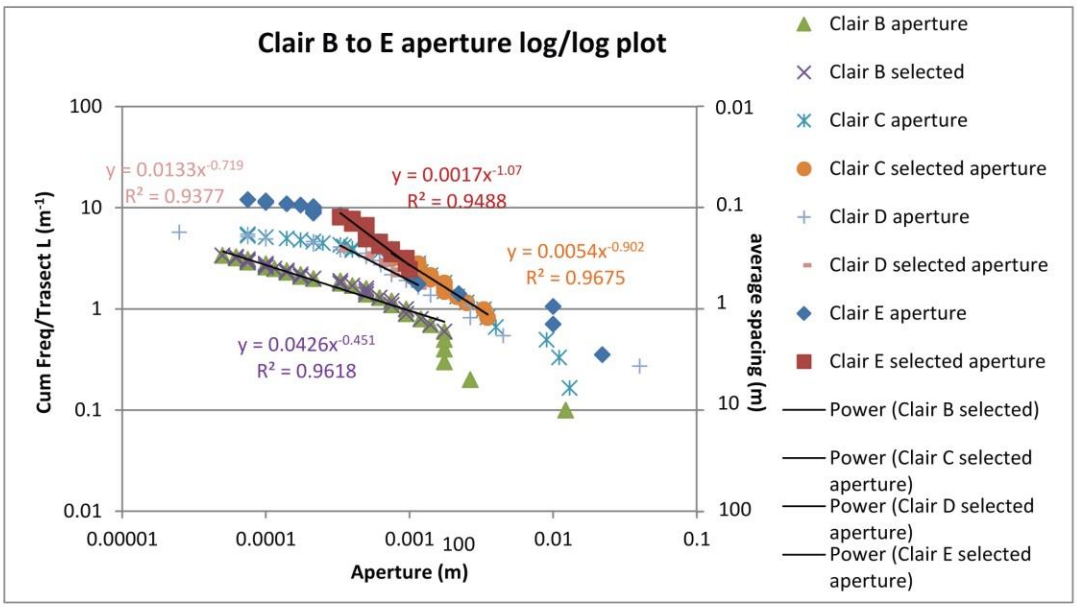

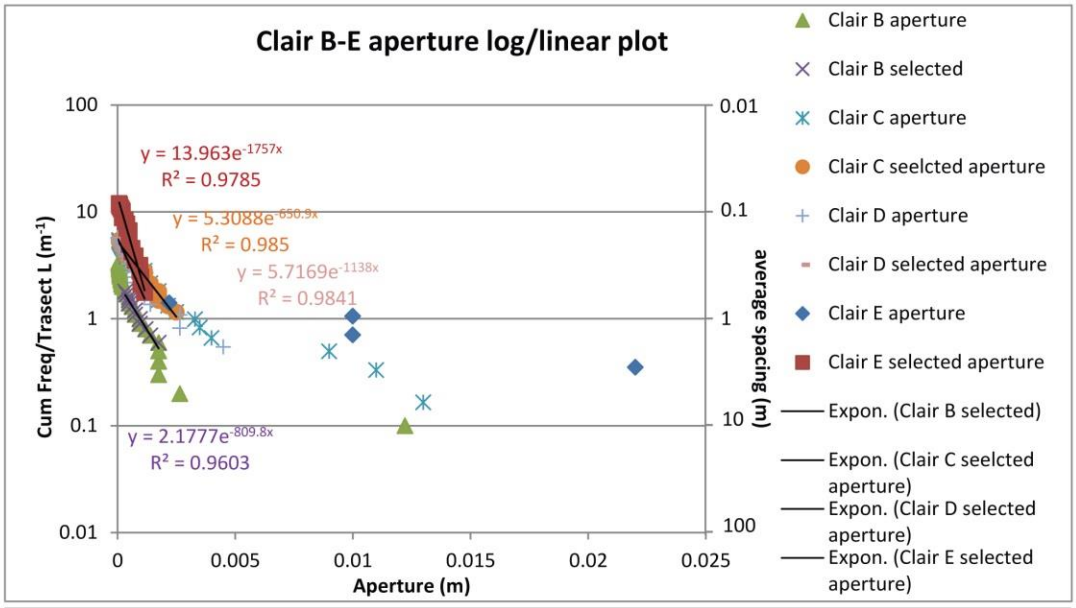

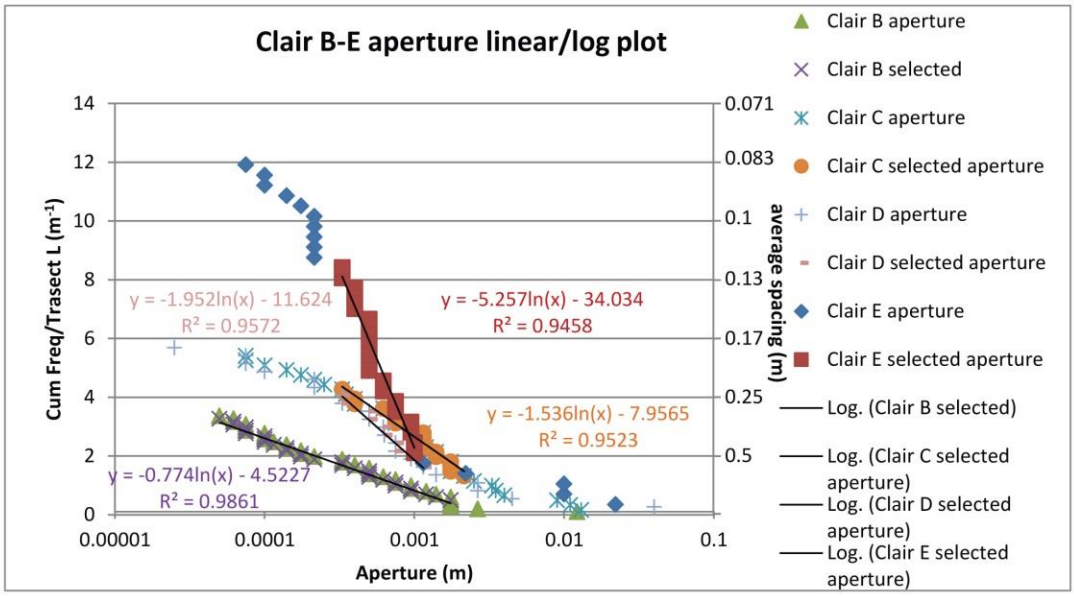

Figure 7.28: Graphs of aperture data collected from Clair transects A-E. Graphs show raw and selected data.

Table 7.22: Table of number of data-points excluded from each plot type (and percentage of total data).

Distribution	Clair B	Clair C	Clair D	Clair E
Power-law	5 (15%)	17 (52%)	11 (52%)	17 (50%)
Negative exponential	21 (62%)	6 (18%)	5 (23%)	4 (12%)
Log-normal	5 (15%)	14 (42%)	11 (52%)	5 (15%)

7.6.1.1 Clair A to E aperture summary and discussion

As the data are relatively sparse, it is relatively difficult to assign distribution types to the aperture attribute for these samples. The majority of transect B can easily be described by a power-law trend line. Transect B is however the longest transect and therefore likely to be most accurate (Gillespie et al., 1993). Transects C, D and E are more easily described by exponential trend lines, not taking into account the effects of truncation and censoring. As these transects are short, it is likely that these effects will be relatively pronounced. It is therefore possible that the fault related fracturing within the Clair Group displays a power-law distribution of apertures. Given that Clair E spacing data is well fitted by an exponential trend line due to dissolution effects, it may also be expected that aperture data would show a similar random distribution. Clair E aperture data is best described by an exponential trend line, however it is nearly as well described by the log-normal trend line. Further data is required to make a more definitive conclusion.

7.6.2 Clair F (basement) and onshore aperture results

Conductive fractures at Clair are known to be Mesozoic in age (Chapter 6), and faulting at Clair is Mesozoic-dominated. Hence, here aperture data from the basement is compared to transects undertaken across areas affected by Mesozoic faulting on Lewis and Harris (Figure 7.29, Table 7.23, Table 7.24). As the origin of joints at the surface is generally unknown and open apertures are not likely to be representative of apertures at depth, they are excluded from the aperture study presented below. Seisiadar is not included here as the transect samples a joint-dominated fracture set. The aperture data presented here includes veins and faults only.

Table 7.23: Aperture data from basement rocks.

Locality	N (fractures)	N (aperture values, excluding joints)	D value of fitted power-law trend line	Best fitting distribution	Fracture set sampled
Mem Cairn perpendicular	172	63	0.349	Power-law	Across dominant Mesozoic fault set
Seaforth 3	141	29	0.359	Power-law	Across dominant Mesozoic fault set
Garrabost	85	80	0.424	Power-law	Across Mesozoic and pre-Mesozoic fault, area dominated by major Mesozoic faults
Clair F	98	98	1.013	Power-law?	Across Mesozoic and non-Mesozoic faults, area dominated by major Mesozoic faults

Table 7.24: Fractures sampled by each transect.

Transect	Faults	Epidote veins	Haematite veins	Quartz veins	Calcite/zeolite veins	Calcite/pyrite veins	Red-brown veins ('speckled' adularia)
Mem Cairn perpendicular	51	8	4				
Seaforth 3	14	1		4	11		
Garrabost	66	9	5				
Clair F	8	47		3		36	4

As can be seen on plots of the data (Figure 7.29), the aperture data collected from the onshore transects are easily described by straight line trend lines on the log/log plot, indicating they represent power-law distributions. Exponential and logarithmic trend lines provide a poorer description of the onshore data. D values from power-laws assigned to the onshore display a relatively narrow consistent range from 0.349 to 0.424.

The offshore data collected from the basement of transect F shows a more pronounced curvature on the log/log plot (Figure 7.29), and a higher proportion of the data has to be excluded to fit the power-law distribution (Figure 7.22). However, the short transect length means that censoring is more pronounced, and hence the fractures are relatively more poorly sampled. Hence it is possible that the Clair F data does represent a power-law distribution. The D value for offshore aperture data is 1.013, representing a greater relative importance of small fracture spacings relative to large spacings.

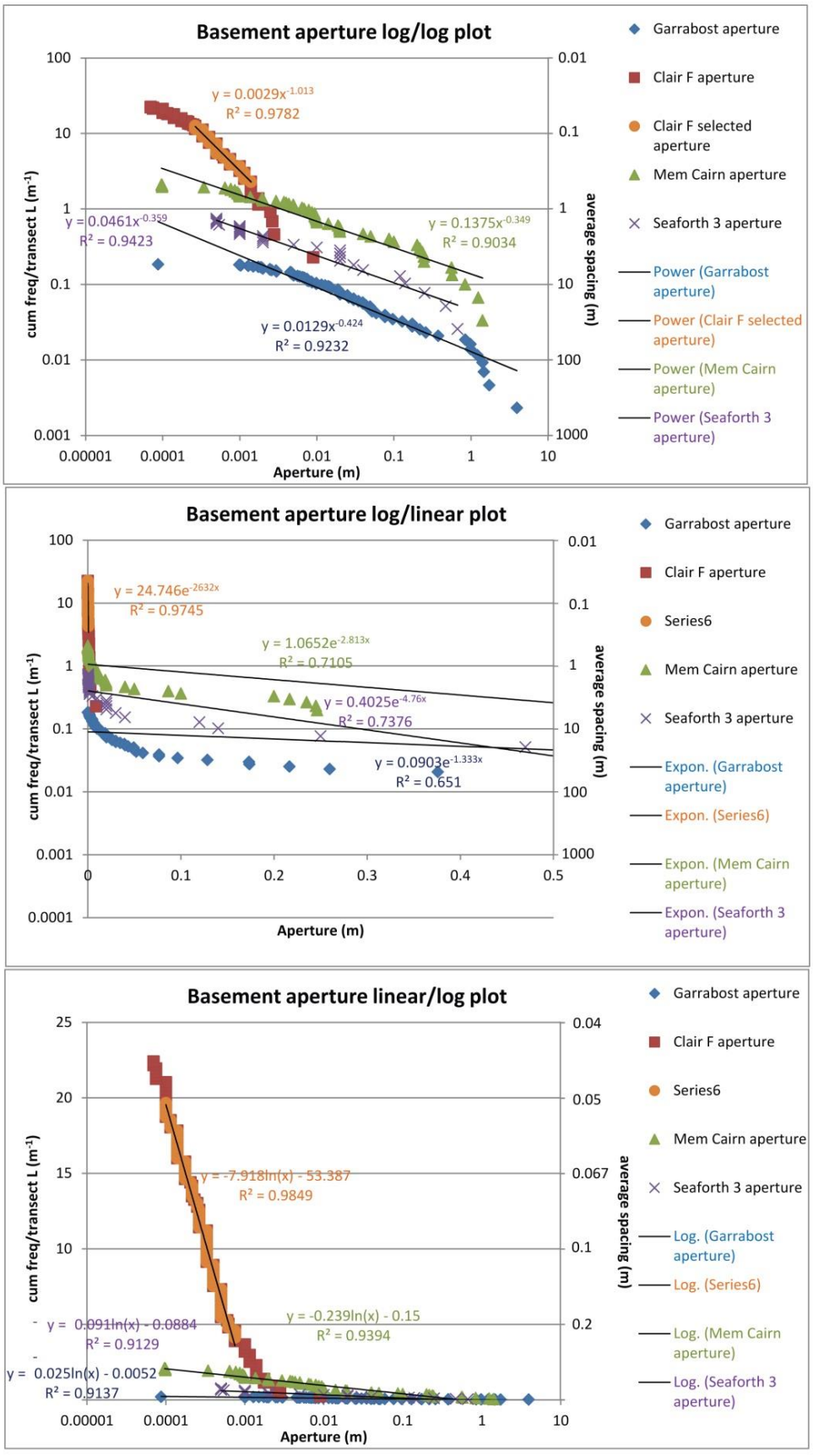

Figure 7.29: Graph of aperture vs. cumulative frequency/average spacing. Data collected from Clair transect F and transects perpendicular to Mesozoic faults on Lewis and Harris. Graphs show raw data.

Table 7.25: Table of number of data-points excluded from each plot type (and percentage of total data) for Clair F.

Distribution	Clair F
Power-law	52 (53%)
Negative exponential	18 (18%)
Log-normal	29 (30%)

7.6.2.1 Clair F (basement) and onshore aperture summary and discussion

It seems likely that basement fracture apertures, at least in regions affected by Mesozoic faulting, are best represented by power-law distributions. The Clair F transect is comprised of a short transect length and therefore bias is more pronounced, leading to a shorter straight line portion on the log/log plot. In addition, the great majority of fractures measured in the Clair F transect are veins (Table 7.24), which may have a different distribution to that present within the more fault-dominated outcrop transects. The greater density of fractures may be a result of the greater resolution available from the cores than on fieldwork. Veins may display a different distribution to the fault dominated It is also interesting to note the increase in D value between the onshore and offshore data, with onshore data displaying values around 0.4 and offshore data displaying a value around 1. Unfortunately no further data from offshore is available for comparison, however the result of power-law aperture distributions within basement rocks is an important observation.

7.7 Discussion

7.7.1 Lineament transect spacing

Spacing data from the lineament analysis display negative exponential distributions characteristic of randomly spaced fractures, confirmed by Cv values close to 1. The lineament transects are all outside the area of the OHFZ and the results may reflect the fact that fracture spacing is best represented by an exponential distribution. This would agree with the fieldwork transects undertaken (the background fracturing datasets) outside the OHFZ (section 7.3.2.1.), that also displayed exponential distributions with Cv values of close to 1. General fracturing within the Lewisian may be best represented by an exponential distribution due to the re-activation of weak pre-existing faults, or the existence of multiple overprinting fracture sets that together give a random spacing distribution. Conversely, it seems likely that the poor resolution of faults and

fractures due to peat cover, in addition to biases such as omission of any relatively low angle structures from the analysis, will have had a randomising effect on the data. As noted by Gillespie et al. (1993), degrading the resolution of fracture networks causes the power-law distribution to become upward convex on the log/log plots. It is not been possible to resolve this issue here, but groundwork has been laid for future studies on this subject.

7.7.2 Fieldwork transect spacing and aperture

As it is not possible to collect spacing data from across many scales of magnitude, it is difficult to interpret their distribution types (Bonnet et al., 2001). Power-law spacing distributions are only rarely identified within data collected on the field transects, and it is not possible to interpret these data with certainty, given the poorly defined effects of censoring and truncation on the data. It seems most likely however that transect spacing data in most geological contexts discussed in this chapter are best represented by negative exponential (i.e. random) spacing distributions. This is confirmed by Cv values that are generally quite close to 1 when compared to other studies (e.g. Beacom et al., 2001). However, a degree of increased clustering is suggested by increases in Cv values between fault-parallel and fault-perpendicular transects across Mesozoic faults, and fault-perpendicular transect data is also relatively more easily fitted by power-law trend lines than joint-dominated datasets. Spacing distributions best represented by log-normal trend lines are also encountered (e.g. at Pabail). It is possible that the different distributions here represent inherent differences in fracture system organisation, perhaps due to lithology, or differences may be attributed to the stage of fracture set development. Sleight (2001) suggests that fracture spacing develops through time, from an initial random (negative exponential) spacing distribution to a more organised distribution (i.e. clustered with log-normal or power-law distribution).

Differences in fault size (e.g. length) distributions have been found to exist between distributed (exponential) and localised (power-law) faulting in the Rift Valley in Africa (Soliva and Schultz, 2008). Different size distributions may also exist across fault systems due to anisotropy in the country rock (e.g. Wojtal, 1994), and temporal development of the fault systems (Wojtal, 1996). However these suggestions are difficult to reconcile with expected fault attribute scale invariance (Nicol et al., 1996), and the relationship between fault spacing and length is not directly known.

In the Outer Hebrides, the longevity of the Lewisian basement and the effects of multiple fracture and faulting events will likely have produced fracture spacings that are best described by exponential distributions. Exponential distributions obtained from the transect data may directly result from the sampling of multiple fracture sets within each line transect (e.g. Priest and Hudson, 1976a; Sleight, 2001). In addition, reactivation, witnessed at several of the transect localities, is more likely to produce exponential distributions (Priest and Hudson, 1976b; Sleight,

2001). Although transects were undertaken at selected localities to investigate fracturing in specific contexts, the presence of multiple fracture sets will at times have partly randomised the spacing distributions obtained. The tendency of the data presented here to be best described by exponential trend lines is confirmed by Cv values that tend to be relatively close to 1 when compared to other studies (e.g. Gillespie et al., 1999; Beacom et al., 2001; McCaffrey et al., 2003). Differences between fault-parallel and fault-perpendicular spacing was observed at Mesozoic fault localities, with enhanced clustering and probable power-law distributions of fault spacing observed perpendicular to the fault strikes. The D values of the power-laws assigned to the fault perpendicular transects are quite high (>1). It is likely that the influence of background jointing, pre-existing fractures, and reactivation of pre-existing fractures has led to relatively low Cv values, an increase in fracture density and an increase in the power-law exponent (the D value) when compared to other studies (e.g. Beacom et al., 2001).

Formation of fractures in rock is dependent on the critical thresholds of stress, postulated by several theories (Bonnet et al., 2001). Whatever the mode of fracture, the stress distribution is key in determining the geometry of the subsequent fracturing process, i.e. the stress distribution is dependent on the geometry of pre-existing fractures. In nature, the heterogeneity of rocks increases the complexity of the system, and the applied stress field is not necessarily homogeneous (Bonnet et al., 2001). In addition, fluid-rock interaction produces local variations in the stress field. A model can be postulated, whereby stress reaches the critical threshold in a zone of rock, concentrated to a particular area through local stress variations or mechanical heterogeneities in the rock. Fractures will begin to initiate within the rock, eventually leading to the formation of a dominant fracture as strain is increasingly localised to it. With fracturing, fluid influx can occur, and any increase in pore fluid pressures in the rock volume adjacent to the fracture can lead to additional failure in the surrounding rock as effective stresses are reduced. This will form a clustered fracture spacing distribution.

Reactivation of pre-existing fractures in the crust is thought to cause a breakdown in power-law fault size (e.g. Peacock, 2002). It seems likely that a similar effect may be expected with regards to fault spacing. The development of new fractures alongside existing ones, and the reactivation of pre-existing fractures will alter the spacing distribution. McCaffrey et al. (2003) determined that fracture spacing in a major basement fault system was best represented by an exponential distribution. This was partly attributed to the presence of multiple fracture sets at different orientations, i.e. repeated fracturing has caused power-law spacing distributions to break down. At the fault itself, although an increase in fracture density and clustering (as measured by the CV value) was encountered, clustering was not strong enough to produce a power law distribution (McCaffrey et al., 2003). This is very similar to results produced here, where clustering has been

observed to increase in fault perpendicular transects, but not sufficiently to warrant a power-law interpretation. It seems likely that exponential fracture spacing distributions are a common feature of basement rocks.

The effects of lithological variation were observed at Borve, where granite displays very low levels of background fracturing. Spacing data from background joints in both the banded gneiss and granite probably are best described by negative exponential spacing distributions. Where fracture corridors are intersected, power-laws can easily be assigned to long (>1 order of magnitude) straight line portions of the plots in both the granite and banded gneiss. It is highly likely that the banded gneiss displays an overall higher fracture density due to lithological differences, i.e. the presence of foliation.

Aperture data collected on fieldwork more clearly approximates a power-law distribution over approximately 5 orders of magnitude. This suggests that apertures across the basement of the Hebrides are predictable at different scales, and this can be used to predict the spacing of fractures of specified aperture size. The preliminary investigation into fracture mechanics (Section 7.5.1) suggests that the dominant control on fracture apertures within the Lewisian Gneiss rocks is fracture length, with a clear correlation between them.

7.7.3 Clair Field spacing and aperture

Spacing data obtained from the Clair core show that non-natural fractures within the cover sequence have a fracture spacing distribution that is distinct from natural fractures. Non-natural fractures (transect Clair A) are relatively anticlustered with a low Cv value, and the distribution is best described by a log-normal trend line. Natural fracture spacings within the Clair Group seem to obey a power-law, with similar results obtained from three transects across fault zones in the cover sequence. Dissolution has a tendency to randomise the spacing distribution, as shown within the Clair E transect. D values obtained from the spacing distributions of similar transects Clair B, C and D range from 0.35-0.47. This compares well with a D value of 0.537 obtained from the trend line assigned to the spacing distribution of fractures in basement rocks in transect Clair F. The slightly higher D value in the basement is attributed to a lower degree of clustering (Belfield, 1998), probably due to the influence of the multiple fracture sets and the mineralisation encountered. This is also confirmed by a decrease in the Cv value from 1.69-1.88 in transects Clair B, C and D (cover rocks) to 1.44 in transect Clair F (basement). Fracture spacing distributions within the Clair basement were sampled and interpreted by Pless (2011) to be representative of power law distributions with D values between 0.44 – 1.657 (mean of 0.892) and Cv values between 0.806 – 1.408 (mean of 1.01). Well 206/8-8 was an exception, interpreted to show an

exponential distribution with an exponent of 11.8. The exponent of the exponential relationship found for well 206/8-8 (Clair transect F) here is 24.59, substantially higher than that of Pless (2011). As discussed previously, results obtained by Pless (2011) for the 206/8-8 basement well are markedly different to those obtained here, with a much lower fracture density. This suggests that the systematic method of fracture attribute measurements undertaken in this study differs from that of Pless (2011). Hence, these results may not be comparable. The 206/8-8 well spacing distribution presented here from the Clair F (basement) transect is most easily described by an exponential distribution, and this agrees with the majority of fracture spacing distributions obtained from the Lewisian Gneiss of the Hebrides, discussed above. Observations obtained here, alongside those of Pless (2011), show a marked decrease in fracture density from the basement to the cover rocks, a decrease in fracture clustering and a decrease in assigned power-law trend line exponents from around 0.5 (0.892 in Pless, 2011) to around 0.4. However, in areas affected by dissolution in the cover sequence, the D value can be notably higher and the distribution type tends towards an exponential distribution.

Aperture data collected from the Clair Group transects C to E may be best fitted by power-law distributions. However, the short length of these transects means that they are heavily influenced by sampling bias and therefore may not be representative. Clair B, the longest transect, is likely to be the most representative sample and displays an obvious straight line portion on the log/log plot, indicating the existence of a probable power-law distribution with a D value of 0.451. Within the basement, the relatively short nature of the Clair F transect means that it is again heavily influenced by sampling bias. However, a straight line portion over ~1 order of magnitude does exist, with a D value of 1.013. This value is higher than that obtained from faulting in the Clair Group in Clair B (0.451) and for comparable data from the basement of the Hebrides (D values 0.349 - 0.424). The reasons for this are unclear, however the higher exponent in the Clair basement suggests a greater importance of smaller apertures. This may in part be due to the greater resolution of sampling clean surfaces of core as opposed to weathered outcrop surfaces.

7.8 Conclusions

- *Is Mesozoic faulting recognisable from its spacing characteristics?*

  When compared to unfaulted localities, reactivated faults, and Mesozoic fault-parallel transects, Mesozoic fault-perpendicular transects are relatively more easily described by power-law distributions with higher Cv values. Higher Cv values represent a greater degree of clustering along fault-perpendicular transects. However, Mesozoic fault-parallel

and fault-perpendicular transects are both best described by negative exponential (random) spacing distributions.

- *How does fracture spacing change between joint dominated vs. fault dominated areas?*
  Joint dominated localities are best described by exponential distributions, with Cv values around 1 and relatively low fracture densities (around the 10 cm to 1 m scale). Fracturing associated with faulting generally shows more clustered spacing distributions with Cv values >1, and distributions that can at least be partly described by power-law. However, these are also often best described by negative exponential distributions.

- *Is there any effect on fracture spacing due to lithology?*
  Lithological differences appear to have an impact on the density of fracturing observed. Granite is markedly less fractured than adjacent banded gneiss on Harris, but both lithologies show random spacing distributions away from fracture corridors. Around fracture corridors, the spacing data are well represented by power-law spacing distributions. In the SHSZ, fractures were found to localise along pervasive foliation. These foliation-parallel joints display Cv values <1 and are well fitted by exponential trend lines. Faults cutting the foliation at a high angle produce high fracture densities.

- *What are the spacing characteristics of fractures in the Clair Field and how do they compare to those from Lewis and Harris. How do these fractures vary from basement to cover?*
  Natural fractures within the Clair Group are relatively clustered and show probable power-law spacing distributions. Non-natural fractures resulting from core retrieval show markedly different characteristics, being relatively strongly anticlustered and best represented by a log-normal distribution. Dissolution and production of open fractures within Clair transect E has produced an exponential spacing distribution. In the basement of Clair, as on the Hebrides, spacing has been found in this study to be well represented by an exponential distribution trend line. Observations presented here, alongside those of Pless (2011), show a marked decrease in fracture density from the basement to the cover rocks, a decrease in fracture clustering and a decrease in assigned power-law trend line exponents.

- *What are the aperture characteristics of fractures in the Hebrides and in the Clair Field?*
  Distributions of aperture data collected from Lewis and Harris show a clear power-law relationship over ~5 orders of magnitude. In the Clair Group, it seems likely that fracture

apertures are also well represented by power-law distributions, however short transect lengths make this more uncertain. Within the basement, aperture data collected from Clair transect F shows a higher D value than those associated with mainland, however this is possibly as a result of greater sampling resolution within the Clair core.

Chapter 8: Discussion and Conclusions

8.1 Introduction

As shown in the preceding chapters, the evolution of fracturing and faulting in the Lewisian Gneiss of both the Outer Hebrides and Clair Field is complex, with multiple phases of cross-cutting faulting, fracturing and mineralisation. This work has focussed on the identification and characterisation of deformation of Mesozoic and younger ages.

8.2 Synthesis

8.2.1 Stornoway Formation and surrounding basement faulting

On Lewis, the Stornoway Formation is cut by hundreds of relatively minor faults, generally with centimetre to decimetre scale offsets. These faults are visible on aerial photography of the region. Cross-cutting relationships within the Stornoway Formation allow identification of distinct fault sets, with at least three sets of faulting being identified here (Figure 8.1). These faults tend to be in upright positions, identifiable by the presence of upright conjugate pairs, visible in the orientation data collected from the formation (section 3.3.2.2). Early conjugate NNW-SSE striking faults are common throughout the formation, with an ENE-dipping group of faults that is slightly more numerous than WSW dipping faults. These NNW-SSE striking faults were followed by quadrimodal N-S and E-W striking faults, concentrated in the west and north near the bounding faults. ENE dipping, east dipping, and south dipping faults can be directly related to the orientation of the foliation within the local basement rocks. This is proven in section 3.4.6, where a positive correlation was found between the Mesozoic faults in the surrounding Lewisian Gneiss and the gneissic foliation orientation distributions. However, it is interesting to note that N-S striking faults are also found across the Stornoway Formation in areas adjacent to gneiss with NNW-SSE striking foliation, albeit in relatively low numbers. Hence, although orientation of faults within the Stornoway Formation are generally controlled by pre-existing structures in the Lewisian Gneiss, N-S faults are still distributed across areas where the foliation does not match their orientation. It would therefore seem possible from this observation that there is a degree of detachment between faulting occurring within the cover and basement rocks.

Within the basement rocks of the OHFZ that surrounds the Stornoway Formation, fault rock characterisation has allowed identification of Mesozoic and younger faulting within the basement rocks. Mesozoic and younger faults in the Lewisian are dominated by authigenic clay-bearing gouges and cataclasites, occurring alongside calcite and zeolite/adularia mineralisation. These faults form a clear group, predominantly dipping moderately to steeply to the ENE (section 3.4.5).

The coincidence in orientation between foliation in the basement and faulting in the Stornoway Formation is probably a direct result of faulting occurring along pre-existing foliation planes in the basement. In addition, reactivation of pre-Mesozoic faults by Mesozoic and younger faulting has been recognised in the field. Within the basement it is apparent from the orientation data that there is *not* a corresponding conjugate set with opposing dip, as seen within the Stornoway Formation (Figure 8.1). Hence, conjugate faulting has developed only within the Stornoway Formation where none is present within the Lewisian. More numerous ENE dipping faults in the Stornoway Formation when compared to their conjugate WSW dipping faults is explained by a lack of full development of conjugates within the Stornoway Formation.

The onlap contact of the Stornoway Formation was observed at two localities (Dun Mor and Suardail, sections 3.5.1.2 and 3.5.1.3). At both localities, a shallowly dipping fault is observed lying within the Stornoway Formation within approximately 1 m of the actual unconformity surface. This fault is sub-parallel with the irregular, weathered unconformity surface, and must have formed after or during lithification of the rock as a result of either tectonically driven faulting or gravitationally driven slumping due to fault block rotation. Evidence of overpressure at the basement-cover interface points to the importance of high pore fluid pressure, possibly resulting from dewatering and lithification, which may have enabled faulting along these low angle structures.

At Dun Mor, sediment injection and calcite mineralisation in the basement are synchronous, and must have occurred prior or during lithification of the Stornoway Formation. Extensive calcite mineralisation is also seen at Suardail. These veins are hydrofractures recording high pore fluid pressures that may result from dewatering of the rock through lithification, or due to syn-depositional fault driven fluid movements (shown in Figure 8.1). Similarly, at Garrabost (section 3.5.1.1), although the actual contact is sheared, it is visibly not planar. Within 1 m of the unconformity surface a planar structure is present. It seems likely that these faults close to the contact are accommodating strain that cannot be accommodated along the irregular surface of the actual unconformity.

Opposing dip conjugate faults are developed throughout the Stornoway Formation, and hence it seems highly likely that they detach at or close to the basement/cover interface (Figure 8.1). As mentioned, at exposed onlap localities of the Stornoway Formation (e.g. Dun Mor, Suardail and possibly Garrabost), the unconformity-parallel detachment is typically present (Figure 8.1). Conjugate fault pairs in the cover may detach along this low angle structure. In addition, detachment at or close to the basement/cover interface would explain the existence of N-S striking faults away from areas of N-S striking foliation. Hence although the strike of faults within

the Stornoway Formation is controlled by the underlying basement, the distribution of these faults is not.

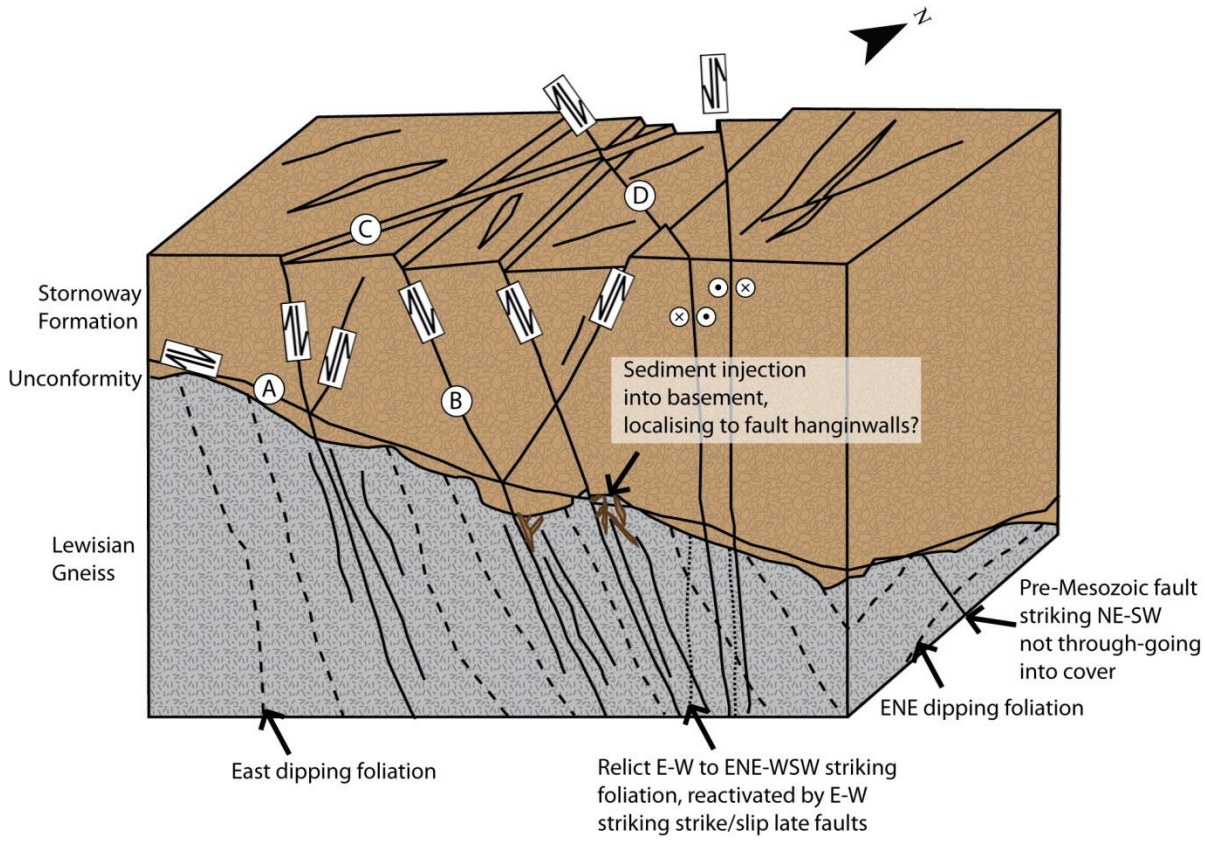

Figure 8.1: 3D block diagram of faulting in the Stornoway Formation, based on the locality at Dun Mor where the unconformity dips to the north. (**A**) Low angle fault formed from gravitational slumping during basin development. (**B**) Set 1 faults. NNW-SSE striking, with conjugates developed in the Stornoway Formation detaching against the low angle fault (fault A). (**C**) Set 2 faults. N-S striking and E-W dip-slip faulting, developed dominantly in the west, where foliation orientation dips east. Cuts Set 1 with conjugates developed in the Stornoway Formation. In the west these faults are likely to link with faults through-going into the basement (**D**) Set 3 faulting, E-W striking conjugate strike-slip faults, post-dating Tertiary dyke intrusion. May link with very early ENE-WSW to E-W striking shear zones within the Lewisian Gneiss.

Palaeostress analysis of kinematic data from the Stornoway Formation faults divided into the identified three fault sets are consistent with ENE-WSW directed Mesozoic extension, followed by E-W directed Cenozoic contraction. These fault phases are separated by Tertiary dolerite dyke intrusion. Kinematic data from the Stornoway Formation have also been back-rotated to produce horizontal bedding. Palaeostress analysis of back-rotated fault data (rotated to horizontal bedding) produces little change in the overall directions of extension for sets 1 and 2, being directed E-W and ENE-WSW, respectively. In addition the well-defined groups that are visible in the field and shown in the orientation data become obscured following back-rotation. However,

back-rotation does show that the Set 1 NNW-SSE striking faults readily identified within the Stornoway Formation are rotated into a more north-south orientation. If this is correct, it would suggest that the similarly orientated Set 2 faults may represent a continuation of the faulting distinguished as Set 1. Set 3 fault data show that E-W directed contraction post-dated the intrusion of Tertiary dykes into the Stornoway Formation.

8.2.2 Faulting on Lewis and Harris

Similarity between the trends of faults on Lewis and the trends of structures identified within the basement rocks of the Rona Ridge SW of Clair have been identified in previous work (Slightam, 2012). However this cannot be confirmed due to a lack of orientation analysis in the study by Slightam (2012). Fault trends identified in the lineament analysis and from fieldwork in this study have been found to vary from Lewis to Harris and also when compared to the mainland and Clair Field. Hence it would appear that there is significant along-strike variation of fault trends. As noted on Lewis and Harris, reactivation of older, pre-existing structures during the Mesozoic is locally common. A significant period of inactivity is central to the meaning of a reactivated structure (Holdsworth et al., 1997), and this is indicated by the development of differing fault rocks at different temperature and pressure conditions. In particular, large scale faults are susceptible to multiple phases of reactivation. Hence the presence of pre-existing structures of NNW-SSE and NW-SE orientation on Lewis and Harris may have had a significant impact on subsequent fracture formation. Near dip-slip faulting on NNW-SSE striking faults indicates that they have been near-optimally orientated during at least one phase of extension, and this Mesozoic phase of faulting (at this orientation) has not been identified in the Faroe-Shetland Basin.

In addition, there is no evidence for the existence of the Cretaceous faulting, experienced by the Clair Field region, on Lewis and Harris and no Cretaceous sediments exist in the Minch (Fyfe et al., 1993).

Lineament analysis performed across Lewis shows a strong NNW-SSE trend that can be attributed to Mesozoic faulting, followed by NNW-SSE trending Tertiary dyke intrusion and dyke margin reactivation by dip-slip faults. Dykes were often observed intruding along faults both within the Stornoway Formation and the Lewisian basement rocks across Lewis. The fault rock characterisation and identification of widespread Mesozoic faulting in the Stornoway Region has allowed identification of similar age structures with similar associated fault rocks elsewhere across the islands.

The major NNW-SSE striking Seaforth Fault has been identified as at least partly Mesozoic in age, with similar characteristics to Mesozoic faults identified in the Stornoway Region. The NW-SE striking North Harbour Fault on Scalpay is also a major structure and both structures are likely linked to movements on the Minch Fault and the fault west of Lewis and Harris. It is interesting to note that major NW-SE trending structures in the Faroe-Shetland basin have been identified as transfer faults, in addition to igneous intrusions, hydrothermal vent complexes and gas chimneys (e.g. Moy and Imber, 2009). These 'transfer zones' have often been associated with strike-slip motions (e.g. Sørensen, 2003). However, in the Faroe Islands, Palaeocene NW-SE and N-S striking faults have been identified with dip-slip normal offsets (Walker, 2010). Although faulting identified on Lewis is older than this, dip-slip motion has been identified here on NNW-SSE, N-S, and ENE-WSW striking structures, hence these structures do not appear to be simple transfer zones in the Outer Hebrides. Instead it seems more likely that the Seaforth Fault either forms a polymodal (orthorhombic) fault set with the Minch Fault and potentially the fault west of Lewis and Harris, or is an independent feature. However, the age of the Seaforth Fault that can be established from fault rock and kinematic observations suggest that the fault was active in the Mesozoic at roughly the same time as the Minch and Seaforth-bounding faults. It seems highly likely from observations of faults in the Outer Hebrides that igneous intrusions may well have also occurred along pre-existing fault zones within the Faroe-Shetland Basin.

ENE-WSW striking normal faults identified during fieldwork and also within the lineament analysis, particularly on western Lewis, are also relatively young structures. The relationship between ENE-WSW striking and NNW-SSE striking faults is not clear and they appear to be mutually cross-cutting in the lineament analysis. Both fault orientations display authigenic clay-bearing fault rocks associated with calcite, indicating a relatively young age. ENE-WSW striking faults could be attributed to late Mesozoic faulting, when the NE-SW striking faults of the Faroe-Shetland Basin were active (Dean et al., 1999). The longest lineaments on Lewis and Harris trend NNW-SSE and ENE-WSW (section 3.4.1), indicating that structures with these trends are relatively young. It is possible that NNW-SSE and ENE-WSW striking faults are part of a polymodal group, similar to that observed in the bounding faults of the Stornoway Formation.

In eastern Lewis, at Orasaigh, an en-echelon network of sinistral strike-slip faults trends ENE-WSW, cross-cutting Tertiary dykes. Late (Tertiary) strike-slip faulting is localised, and this observation has also been made in the Stornoway Region where late E-W striking strike slip faulting was highly localised to the south of the region. Evidence of post-Tertiary dyke faulting was also observed along dyke margins, with dip-slip normal motion along NNW-SSE striking faults. It seems likely that these represent a continuation of the extensional stress conditions that

existed during the emplacement of the Tertiary dyke swarm, with extension acting ENE-WSW to E-W.

South of the Seaforth Fault, the strong NNW-SSE lineament trend is replaced by a more NW-SE to WNW-ESE trend, and the foliation becomes pervasively NW-SE throughout most of Harris. NW-SE trending faults south of the Seaforth Fault commonly display soft authigenic clay gouges associated with zeolite and calcite. However different kinematics have been identified on these faults with phases of strike slip and normal motion. At Scalpay, the WNW-ESE striking North Harbour Fault has several hundreds of metres sinistral strike-slip offset that has been reported to offset Tertiary Dykes (Sibson, 1977a). If this is correct, this fault may be linked with strike-slip motion on E-W striking faults that post-date Tertiary dykes further north. Indeed, post-Tertiary dyke E-W striking strike-slip faulting has also been identified by the author in West Lewis and on North and South Uist, and hence seems widespread. Cenozoic faulting has previously been suggested in the region offshore eastern South Harris (Evans et al., 1991; O'Neill and England, 1994), where Oligocene sediments are present thickening towards the Minch Fault. This suggests that the Minch Fault was active at this time with E-W directed extension. The sinistral motion on the North Harbour Fault is not compatible with E-W directed extension on the Minch Fault, as it would suggest contraction across the fault rather than extension (Figure 8.2). It seems likely therefore that that sinistral movement on the North Harbour Fault is linked with the E-W faults seen on Lewis that post-date Tertiary dykes and are associated with E-W directed contraction.

It is interesting to note the convergence of the North Harbour Fault and the Seaforth Fault at the same point on the Minch Fault offshore western Scalpay (Figure 8.2, marked with a blue star). The Seaforth Fault also coincides with the termination of the fault west of Lewis and Harris interpreted in Fyfe et al. (1993). This suggests that strain may have been accommodated jointly on the Seaforth Fault and the fault west of Lewis if these structures are linked, possibly in an orthorhombic faulting system. Permo-Triassic sediments have been found offshore western Lewis/Harris in the Flannan Basin (Earle et al., 1989; Fyfe et al., 1993, shown in Figure 8.2). If motion on the Seaforth Fault and the fault west of Lewis/Harris is linked, it would suggest that movement on the Seaforth Fault may be at least partly Permo-Triassic in age. This agrees with observations of probable Permo-Triassic dip-slip normal faulting in the Stornoway Formation on NNW-SSE striking faults, and Permo-Triassic faulting occurring along the Minch Fault (Fyfe et al., 1993). The North Harbour Fault may similarly link with faulting along the offshore structures of post-Tertiary dyke age.

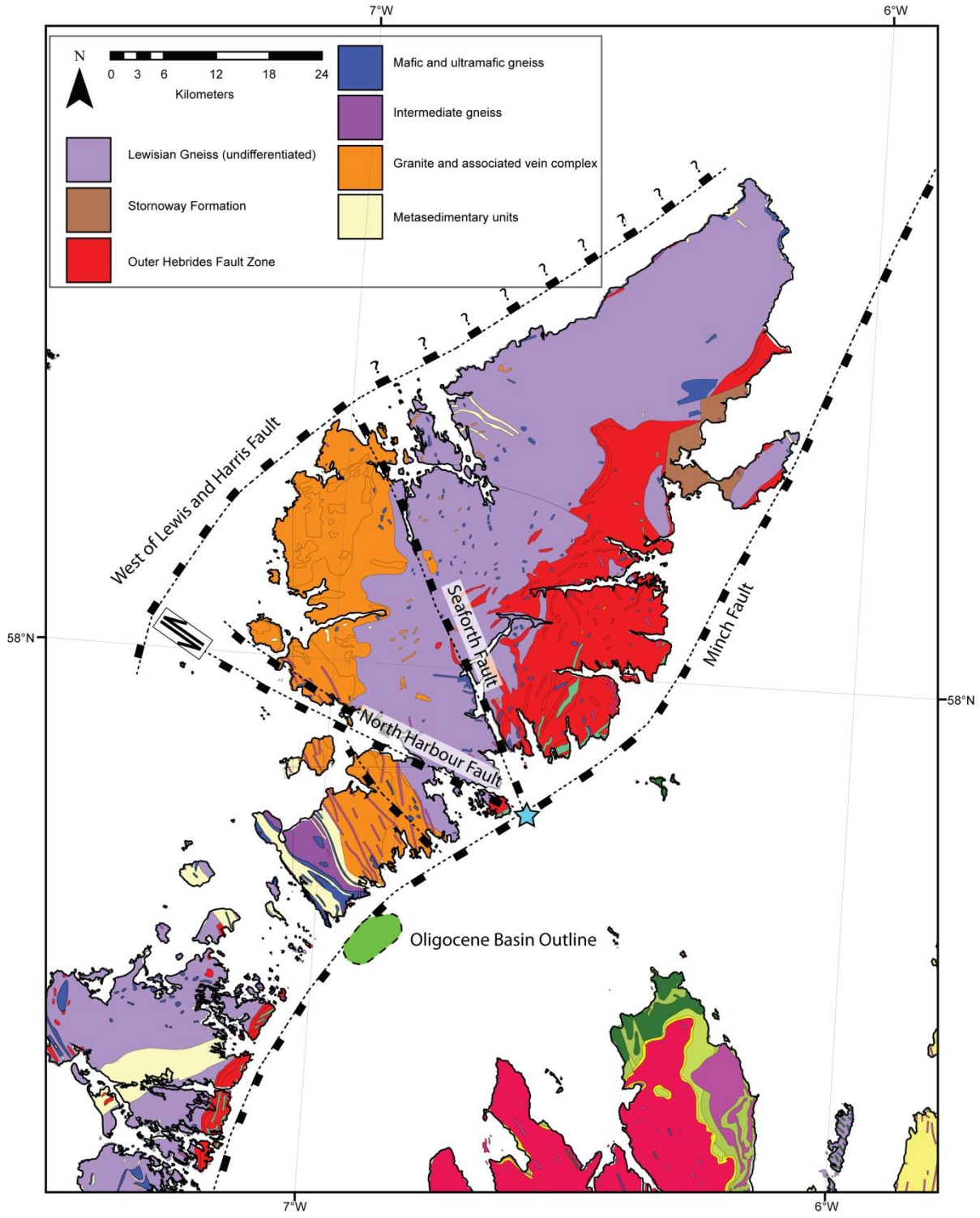

Figure 8.2: Map of Lewis and Harris showing major faults. Blue star indicates Minch/North Harbour/Seaforth Fault junction.

8.2.3 Clair Field

Faulting orientations at Clair were analysed by Pless (2011). The dominant fault trend in the Clair Group and overlying Cretaceous is NE-SW, matching the orientation of the major Ridge and Shetland Spine Faults (Pless, 2011). In the basement rocks, the dominant trend is NW-SE and

these faults have been attributed to reactivation of older ductile basement shear zones (Pless, 2011), however low resolution and scarcity of this data means that this this interpretation speculative.

Faulting style within the Clair Group is controlled by lithological variation. Where calcite cementation of the sandstones are present, faulting is dominated by breccia zones cemented with calcite. In zones of porous sandstone lacking calcite cementation, networks of granulation seams have developed, some of which show evidence of reactivation by later clay-bearing faulting. Within shalier areas, clay-bearing gouges have developed, although these are poorly recovered in the core. It has not been possible to develop a fault sequence within the Clair Group due to a lack of cross-cutting relationships. However, cross-cutting veins do exist, and this has allowed establishment of the oil influx timings relative to mineralisation within the Clair Group (e.g. Milodowski et al., 1998). The latest significant phase of diagenesis in the Clair Field occurred before or during oil influx, with the development of porosity by dissolution. This porosity is spatially associated with faulting.

The lithologies present within the Clair Field basement are similar to those of the onshore Lewisian Gneiss Complex (Pless, 2011), with the amphibolite grade gneisses of the Rhiconich terrane of the Scottish mainland found to match the lithologies at Clair most appropriately (Pless, 2011). Similarly the overall amphibolite facies grade of rocks in the Outer Hebrides also suggest it is an appropriate lithological analogue. However, no evidence was seen in the core for the development of pervasive weak foliation within the Rona Ridge, such as mylonite or phyllonite. The foliation was also not observed to be reactivated by faulting, as is common in the Stornoway Region. The lack of mylonites and phyllonites may discount the theory that the Rona Ridge is part of the OHFZ. However, evidence of multiple phases of faulting was still seen, with much epidote cataclasite development, and adularia-cemented fault rocks associated with calcite mineralisation and oil.

Within the basement rocks, several phases of calcite mineralisation are present, but they could not be readily distinguished or ordered chronologically in the manner of Milodowski (1998) due to complex cross-cutting relationships that could not be resolved. However, sparry calcite was observed to be cross-cut by micro-crystalline calcite veining, although this is the reverse of the cross cutting relationship observed between Calcite I and Calcite II-III of Milodowski (1998) in the cover sequence.

Permeability in basement rocks at Clair depends on the hydraulic conductivity of the fractures (Barton et al., 1995), and hydraulic conductivity will obviously be highly dependent on fracture fill. In this study, it has been shown that Mesozoic and younger fractures at Clair and in the Hebrides

are hydraulically conductive and have been so during oil influx during the Mesozoic due to the presence of porosity not found in earlier structures. As determined by Barton et al. (1995) the permeability of critically stressed faults is much higher than that of faults that are not optimally orientated for failure. Hence it would appear that active faults are the most important hydraulic conduits (Barton et al., 1995). In the Outer Hebrides, this seems to be confirmed by the presence of oil residing in Mesozoic and younger fault rocks in faults immediately adjacent to major regional structures (Figure 3.51).

Porosity within the basement rocks at Clair is strongly associated with uncemented fractures and fractures partly infilled with both euhedral and speckled adularia that are linked with faulting. Oil influx is synchronous with development of calcite-pyrite and speckled adularia veining within the basement at Clair, and was followed by quartz occlusion of the porosity and replacement over calcite veins. It seems likely that the two phases of adularia veining identified at Clair (euhedral and speckled, chapter 6) pre-date and post-date the deposition of the Clair Group, respectively. The euhedral adularia is locally altered to a green clay mineral, and this alteration is not seen within the speckled adularia that mutually cross-cuts the calcite-pyrite veining. Pyrite and oils associated with these veins have been shown to be Mesozoic in age (Finlay et al., 2011) and hence the speckled adularia likely postdates the deposition of the Devonian Clair Group. The green clay mineral alteration of euhedral adularia may have occurred before or around the time of exhumation of the Rona Ridge during deposition of the Clair Group sediments.

The cover-basement relationship at Clair has been observed in one core below the oil-water contact (well 206/8-8, chapter 7). Similar to the Stornoway Formation contact, the interface is associated with calcite mineralisation and calcite replacement of the matrix in the basal conglomerate – this is widespread within the Stornoway Formation. Sediment injection was also observed at Clair within a large clast of the basal conglomerate, but this was much more limited than that seen at Dun Mor. In addition, no evidence was seen at this locality for fault localisation in the vicinity of the actual unconformity surface. This is however not particularly conclusive due to the paucity of samples.

8.2.4 Comparison between the mainland, Outer Hebrides and Clair

Orientation of lineaments picked across the Lewisian Gneiss complex in this study and that of Pless (2011) are shown in Figure 8.3. It has been noted in chapters 3-5 that lineament orientations coincide with those of faults measured on fieldwork, and therefore for the purposes of discussion here lineaments are treated as faults. There are considerable differences in the trends present across the Lewisian Gneiss Complex, with those on Lewis and Harris being strongly dominated by

NNW-SSE-striking lineaments, becoming N-S on Harris. On the mainland, the main trends are NE-SE and NW-SE. It is interesting to note that the change in orientation of lineaments on Lewis and Harris occurs mostly *within* the same 'terrane' (the Tarbert Terrane) of the gneiss as determined by Kinny et al. (2005) (Figure 8.4). This would suggest the importance of regional features such as major faults and foliation in determining the orientation of faults and fractures, as opposed to uniform fault orientations within each terrane. On the mainland, orientations do not change significantly between the Assynt and Rhiconich terranes, studied by Pless (2011). Orientations of faults from Rhiconich and Assynt are similar to those obtained from the Clair Field top basement horizon (Pless, 2011), although the relative strength of the fault trends are slightly different, with the most prominent trend at Clair being NE-SW and on the mainland being NW-SE (Figure 8.3).

Although fault orientations on the Scottish mainland are similar to those of Clair, fault rock types and ages are not, with only one fault of probable Mesozoic age identified by Pless (2011) within the Rhiconich and Assynt terranes, striking NE-SW. Most fractures on the mainland have been attributed to Late Laxfordian age, striking NW-SE, and fractures of Stoer Group/Torridonian age, striking N-S to NE-SW (Pless, 2011). These early structures contain pseudotachylite, fine grained breccias and cataclasites and epidote and haematite (Pless, 2011). Similar to the Outer Hebrides, the Mesozoic fault was found to contain soft clay bearing gouges and cataclasites. The relative lack of Mesozoic and younger age structures on the Scottish Mainland indicates that fault rocks and deformation in the Outer Hebrides may be a more relevant analogue to those at Clair.

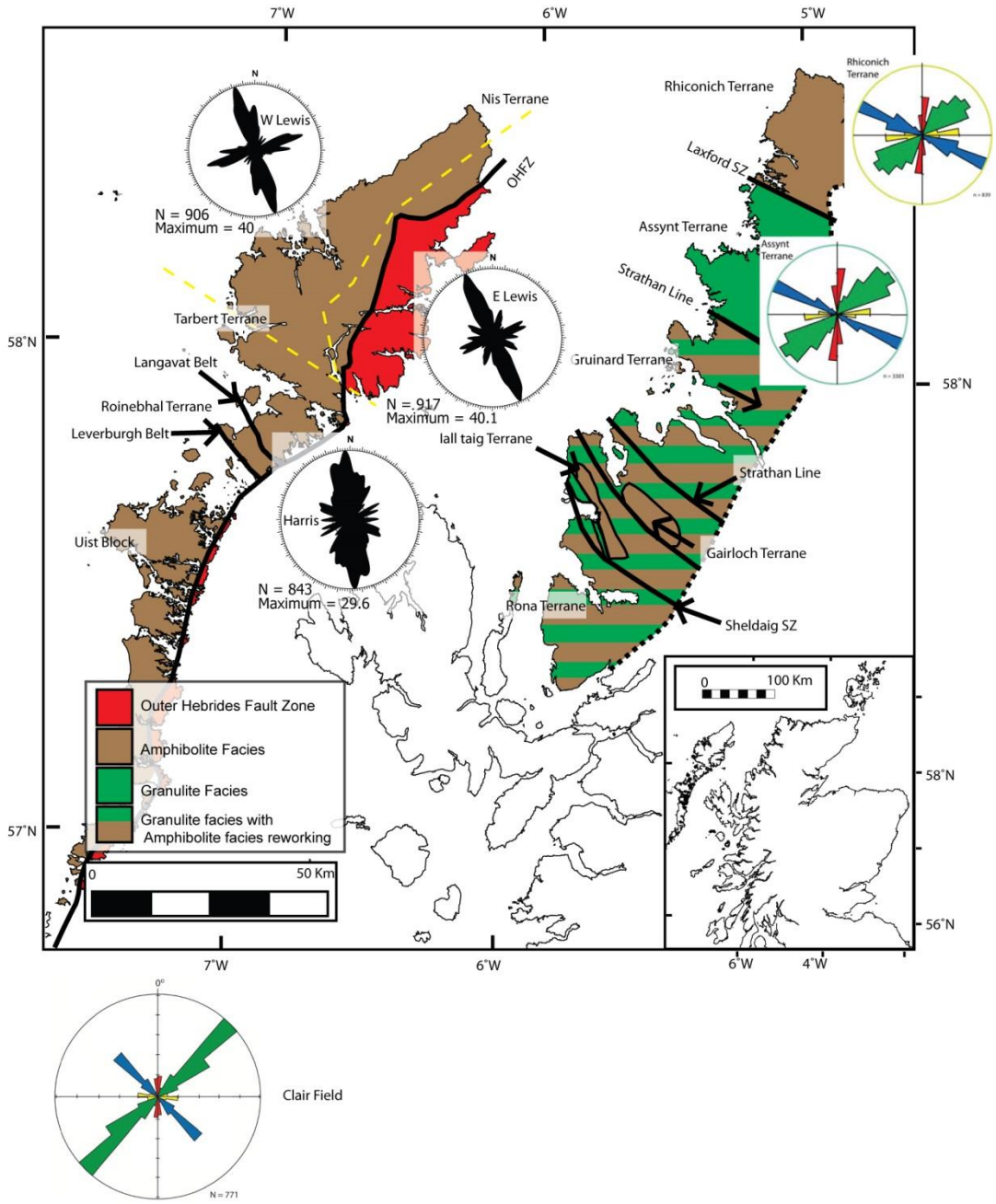

Figure 8.3: Comparison of lineament orientations across the Lewisian Gneiss Complex. Colour rose plots are from Pless (2011). Structural features within Lewisian Complex marked. Yellow dashed lines indicate division of Lewis and Harris lineament analysis data.

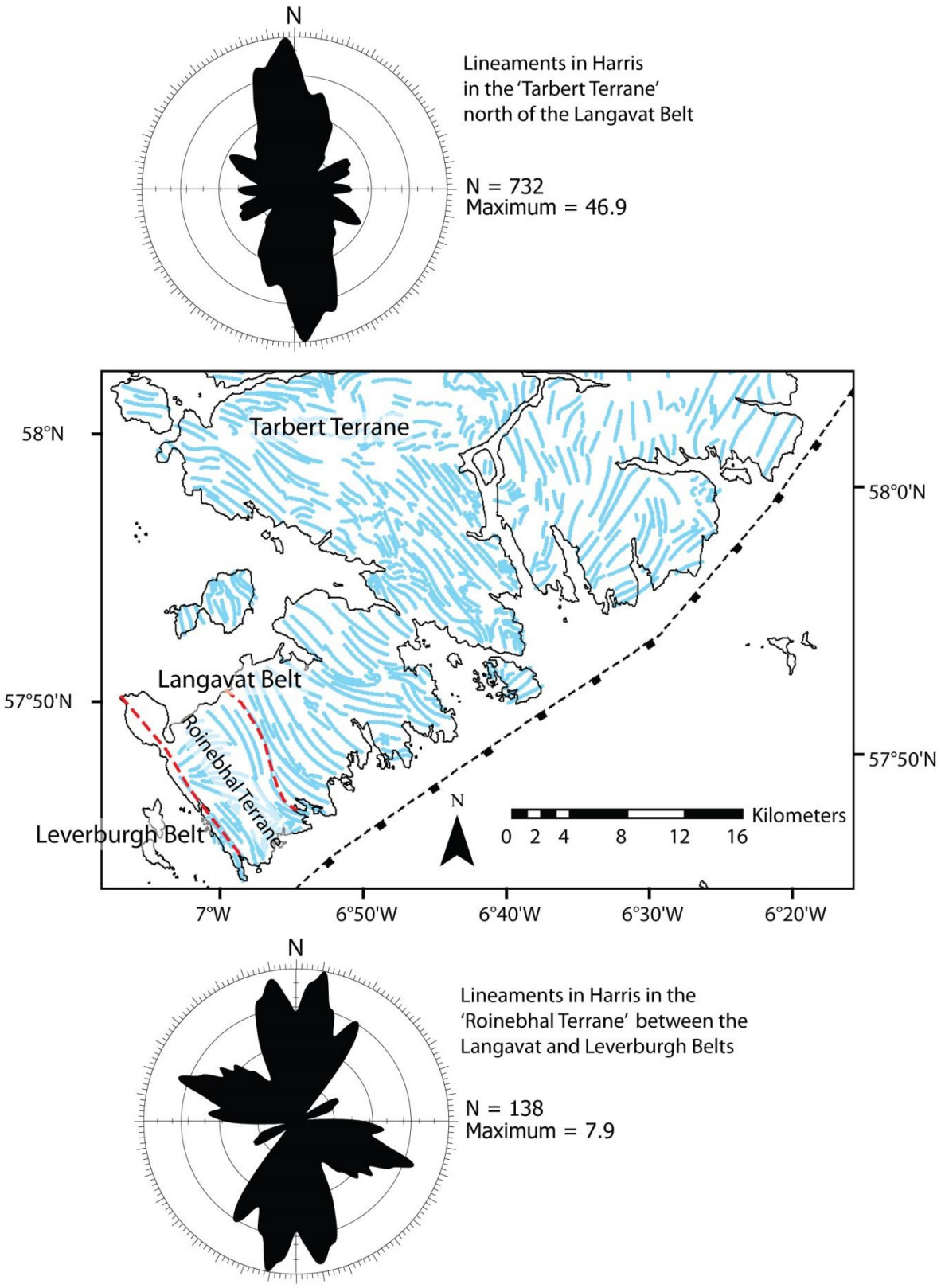

Figure 8.4: Map showing foliation trend of Harris (in blue) with South Harris Shear Zones and terrane names marked (Kinny et al., 2005). Note that lineament trends are similar in the Roinebhal terrane to those in the southern part of the Tarbert terrane (the Isle of Harris).

8.2.5 Thin section work

In faults identified as Mesozoic age within the Stornoway Region and at the northern bounding fault of the Stornoway Formation, oil has been identified alongside zeolite, surrounding brecciated gneiss clasts within the fault rocks (sections 3.4.4 and 3.5.3). Localities that have been found to contain oil are located adjacent to (or on) major structures in the Lewisian that accommodated significant displacement (tens or hundreds of metres) during normal faulting (Figure 3.51). This observation suggests that oil may well have been generated within the Minch Basin, potentially from Carboniferous coal measures or Jurassic shales (Stein, 1992). Oil is found brecciating fault rocks of the Permo-Triassic age bounding fault of the Stornoway Formation at Earabhig (chapter 3). It is not clear whether oil migration into the fault occurred during Permo-Triassic faulting or later, and hence it is not possible to determine the probable age or provenance of the oil generated. However, *active* faults are very significant conduits for fluid flow (e.g. Sibson, 1994; Barton et al., 1995), and fluid flow through the fault would have been greatest during periods of activity. If oil migration occurred during Permo-Triassic activity on the bounding fault (a set 2 fault), it seems likely that the oil seen within the faults rocks may indeed be of Carboniferous provenance.

8.2.5.1 Thin section work – cover

Within the Stornoway Formation, faults developed through the linkage of intra-clast fractures, initially increasing porosity of the rock. This was followed by development of clay minerals through incorporation from the matrix of the rock and alteration within the fault core caused by cataclasis accompanied by fluid migration. Clay alteration and cataclasis markedly reduce the porosity from up to 20% in the surrounding wall rock to zero (distinguishable in optical microscopy). Calcite within the Stornoway Formation Sets 1-3 is syntectonic, with clasts of sparry calcite incorporated in the fault rock and microcracks and porosity within the faults themselves being filled with sparry calcite. Zeolite present within the Stornoway Formation appears to be post-tectonic, often associated with dissolved calcite, producing porosity. However, zeolite is also present as clasts within fault rocks of Set 3, suggesting that these faults postdate the formation of zeolite within the Stornoway Formation. This may be expected, given that Lewis has experienced significant exhumation since the start of the Cenozoic (i.e. before/during Set 3 faulting) due to underplating (Persano et al., 2007), hence temperature and pressure conditions may have been sufficiently lowered to preclude the development of zeolite.

8.2.5.2 Thin section work – basement

In the basement rocks of the Outer Hebrides, faults of Mesozoic age are similar in mineralogy to that of the Stornoway Formation, being dominated by clays and zeolite (alongside adularia) mineralisation. These faults have been observed to be associated with porosity, particularly linked to the presence of adularia. This relationship (adularia associated with porosity) is similar to that observed in the Clair Field, where several adularia phases are associated individually with porosity in the basement rocks. Pre-Mesozoic age fault rocks do not show signs of currently open porosity.

8.2.5.3 Porosity at Clair

The origins of porosity are important to understand in order to better constrain the movement of fluids through the Clair Field. Within the basement rocks at Clair oil is found within:

- Tensile fractures partially filled with euhedral adularia, associated with faulting.
- Speckled adularia hydrofractures.
- Open fractures associated with pyrite and calcite formed synchronously with oil influx.
- Oil is also found within uncemented breccia, possibly attributable to a late phase of faulting.

At both Clair and in the Outer Hebrides, porosity is associated with adularia mineralisation, found alongside zeolite in the Outer Hebrides. At Clair, adularia forms as euhedral mineralisation partially filling open tensile fractures related to faulting, and as 'speckled' vein hydrofractures alongside clay formation that also incorporates wall rock clasts. Euhedral adularia mineralisation is probably of Devonian age, and speckled adularia vein formation likely occurred during the Mesozoic since it is associated with oil influx. Minor amounts of zeolite have been observed reactivating adularia vein margins in the Clair Field thin sections.

In the Hebrides, euhedral adularia has been found along faults associated with porosity and zeolite mineralisation. Although oil was not found alongside adularia mineralisation, oil was found along faults with zeolite mineralisation and syn-tectonic clay development in the Stornoway Region. Adularia- and zeolite- bearing faults are part of the Mesozoic age fracture set identified within the basement. Hence, similarities exist between the Clair Field and the Outer Hebrides, with relatively low temperature phases associated with porosity at both localities. However, it is interesting to note the relative lack of zeolite in the Clair Field when compared to the Hebrides, where zeolite-bearing fault rocks are common in Mesozoic faults and within the post Caledonian, Pre-Mesozoic, faults of SW Harris. This is probably explained by the different temperature and pressure conditions existing between the Clair Field and the Outer Hebrides relating to their relative depths in the crust. Adularia is associated with slightly greater temperatures and

pressures of formation than zeolite (around 200-300°C compared to <200°C, respectively). Hence the relative lack of zeolite at Clair may be due to the rocks in the Clair Field being deeper and outside of the zeolite stability zone during mineral formation. Quartz overgrowths post-dating calcite-pyrite mineralisation and oil influx observed at Clair were not seen in the Hebrides, again probably due to the greater depth of burial maintained at Clair. Quartz was observed on Lewis infilling porosity within epidote cataclasite fault rocks, indicating that quartz overgrowths and mineralisation in the Hebrides pre-dates the Mesozoic and probably post-dates the Caledonian.

8.2.5.4 Tectonic synthesis

Table 8.1 shows the history of faulting in the Outer Hebrides compared to the Clair Region. The most noticeable difference between Lewis and Harris is the change in the dominant Mesozoic fault orientation from NNW-SSE on Lewis to NW-SE on Harris, and the presence of strike slip faulting along NW-SE to WNW-ESE striking Mesozoic faults on Harris alone. These differences appear south and west of the Seaforth Fault, which clearly has significant offset and forms a major boundary on the islands. The foliation on Harris also differs from that on Lewis, with a strong NW-SE trend attributable to the main Laxfordian metamorphic deformation event (Fettes et al., 1992). The trends of the foliation do match that of the faults, but the dips are often different. This may be due to a similar model put forward by Morley (1995), where fractures initially formed parallel with the foliation are linked by through-going faults that cut the foliation (Figure 8.5).

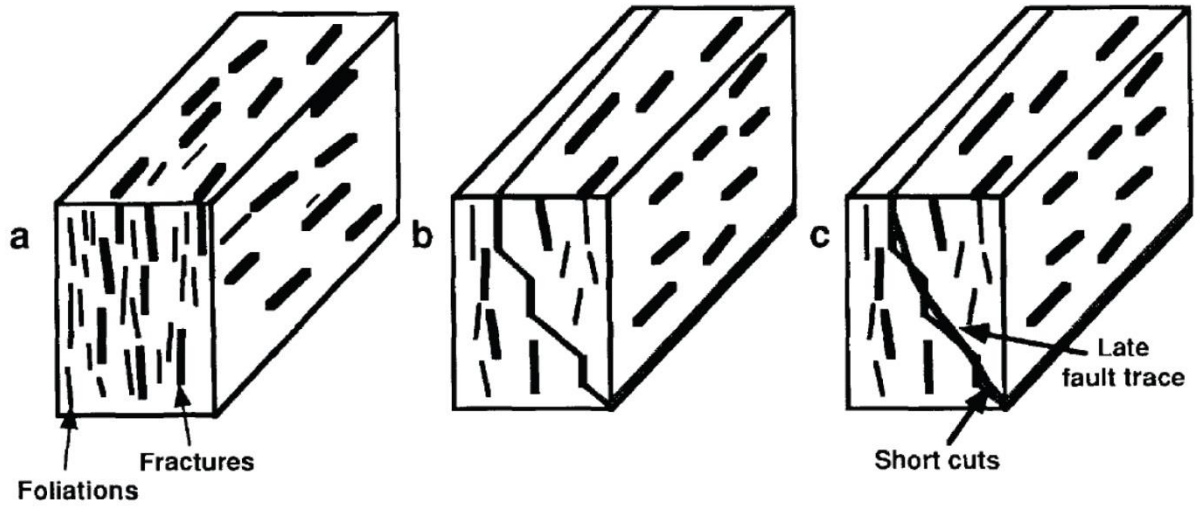

Figure 8.5: Fault development model for faults parallel with foliation strike but not dip (Morley, 1995). (**a**) Initial extensional fractures follow foliations. (**b**) Fractures are linked by faults that cut across the foliations. (**c**) As displacement increases the fault becomes smoothed.

Further heterogeneity is present in SW Harris where a set of zeolite-bearing faults predating Permo-Carboniferous dykes is present that has not been identified elsewhere. The age of these faults can be constrained by the fact that they are intruded by Permo-Carboniferous dykes and cut epidote bearing cataclasites associated with Caledonian and earlier fault movements. These observations suggest that Permo-Carboniferous faults, suggested by previous authors (e.g. Mendum, 2009) may be present. The reasons for fault localisation to SW Harris are unclear, but it is possible they may not be exposed in SE and east Harris due to greater exhumation closer to the Minch Fault associated with Mesozoic normal faults (e.g. King et al., 1988), i.e. greater exhumation and erosion closer to the Minch Fault means these faults are no longer present in east and SE Harris, at least with zeolite-bearing fault rock. The Minch fault has experienced significant offset of at least several kilometres, necessary for the deposition of significant Mesozoic sediment thicknesses in the fault hangingwall (Fyfe et al., 1993).

Dominantly sinistral offsets have been detected on the SW Harris faults, and their NNE-SSW trend is sub-parallel to the trend of the OHFZ. Within the OHFZ, sinistral strike-slip has been identified on NE-SW striking phyllonites that also postdate the Caledonian Orogeny. It is possible that these two phases of deformation may be linked, and this could be proved by further fieldwork along the south coast of Harris –transition from strike-slip within phyllonites to brittle faults deformation would be expected.

The phases of mineralisation identified point to widespread exhumation of the Lewisian Gneiss Complex of the Outer Hebrides through time, from the end of ductile deformation until the present day. Some of the most recent phases of faulting from the Mesozoic onwards have reactivated pre-existing basement faults, and, most noticeably in the Stornoway Region, foliation.

Table 8.1: Deformation, mineralisation synthesis for Lewis, Harris and Clair. ?? Denotes likely presence, although not proven in the field.

Age	Eon/Era/Period	Event	Lewis/Scalpay	Harris	Clair
OLDER	Proterozoic	Mylonite and phyllonite formation	SE dipping pervasive mylonite formation	Uplift of North Harris and Lewis across the SHSZ	
	Proterozoic	Chloritic gneiss formation	?? Cut by pseudotachylite and cataclasite		
	Silurian?	Pseudotachylite and very fine grained chlorite/epidote cataclasites.	Pseudotachylite and epidote cataclasite. Pseudotachylite development more localised, associated with top-to-the NW thrusting. 'Crush Zone' formation (Imber, 1998).	Epidote cataclasites alongside localised epidote alteration of country rock. Pseudotachylite development more localised, associated with top-to-the NW thrusting.	?? Epidote cataclasites at Clair are relatively temporally unconstrained. Predominant NW-SE trend identified in the basement by Pless (2011) may be attributable to these faults.
	Devonian?	Phyllonite formation	Within the OHFZ dipping to the east/SE. Sinistral strike-slip followed by extension (Imber et al., 2001). Generally NE-SW striking.	Within the OHFZ dipping to the east/SE. Sinistral strike-slip followed by extension (Imber et al., 2001). Generally NE-SW striking.	
	Devonian?	Type 1 detachment faulting	Parallel with and extensionally reactivating phyllonite bodies.	Parallel with and extensionally reactivating phyllonite bodies.	
	Devonian?	Adularia bearing faulting	??	??	Faulting associated with grey very fine grained cataclasite formation and euhedral adularia mineralisation. Not as common as epidote cataclasite bearing faulting and epidote veining.
	Devonian?	Widespread clay alteration			Green clay alteration of feldspar and adularia, probably during exhumation of the Clair Field.
	Devonian?	Epidote cataclasites	Associated dominantly with normal and normal oblique kinematics, trending NNW-SSE and NE-SW. NE-SW trend particularly obvious in Stornoway Region. Also E-W trend in the north. Epidote cataclasite bearing faults .	?? Epidote seen along NW-SE striking structures may be associated with similar phase on Lewis.	?? Clair Group deposition in intermontane (endorheic) basin as a result of extensional collapse (Dean et al., 1999).
	Carboniferous - Permian	Zeolite dominated faults	??	NNE-SSW striking faults localised to SW Harris only	
	Carboniferous - Permian	Camptonite - Monchiquite dykes	??	E-W striking dyke intrusion.	
	Mesozoic	Type 2 detachment faulting	Top-to-the east/SE along phyllonites in the OHFZ.	Top-to-the east, along phyllonites in the OHFZ.	
	Permo-Triassic	Authigenic clay bearing faults – with and without adularia?	Reactivate other faults, trend dominantly NNW-SSE striking, although ENE-WSW faulting also common and most evident in the west. Stornoway Formation Deposition.	NW-SE striking normal motion faulting. Likely occurred contemporaneously with faulting on Lewis.	
YOUNGER	Permo-Triassic /Jurassic?	Authigenic clay bearing faults – with and without adularia?	N-S striking normal faulting in the Stornoway Formation. May have occurred before or during the Jurassic.	??	Normal faulting along NE-SW striking faults? (Pless, 2011).

	Eon/Era/Period	Event	Lewis/Scalpay	Harris	Clair
OLDER ↓ YOUNGER	Cretaceous	Normal faulting	?? ENE-WSW and NNW-SSE striking faults active?	??	Multiple faulting phases (e.g. Dean et al., 1999). Granulation seams, calcite cemented breccias and uncemented fault zones in the cover. Calcite-pyrite and speckled adularia mineralisation in the late Cretaceous. Dissolution to produce porosity in cover and basement. NNE-SSW, N-S and E-W striking fault development.
	Palaeocene	Dolerite dyke intrusion	NNW-SSE trending dolerite dykes	NNW-SSE to NW-SE trending dolerite dykes	Sills in Clair field area (Pless, 2011).
	Palaeocene/ Oligocene?	Dyke margin reactivation	Dyke intrusion followed by: 1. NNW-SSE striking dip-slip faults formed during extension. 2. E-W to WNW-ESE striking strike-slip faults formed during compression.	Dyke intrusion followed by: 1. NNW-SSE striking dip-slip faults formed during extension. 2. E-W to WNW-ESE striking strike-slip faults formed during compression.	
	Oligocene?	Normal faulting on the Minch Fault	??	??	

8.2.6 Scalability of fractures

Line transects performed across the Lewisian of Lewis and Harris shows quantitative differences between fractures in specific geological contexts. Heavily fractured basement rocks of the Outer Hebrides are overall well represented by exponential fracture spacing distributions and power-law aperture distributions. Of particular interest to Clair, Mesozoic faults display different characteristics when compared to background jointing, fault-parallel fracture sets and reactivated faults. Fracture spacings across Mesozoic faults are more easily described by power-law trend lines and have higher Cv values, indicative of fracture clustering.

Within massive gneisses, fracturing is less developed with a much reduced fracture density, representing random fracture spacings with little organisation. However, within both the banded gneisses and the granite, background spacing outside of fracture corridors displays Cv values close to zero, indicating that randomly spaced fracturing predominates. Within fracture corridors in the banded gneiss and the granite, fracture densities are higher and the spacing distributions can be easily represented by power-law trend lines. The Leverburgh Belt, part of the SHSZ and displaying intense pervasive foliation, was found to have high fracture densities, although Cv values did not show higher clustering values than observed elsewhere. Notably, the increased fracture density was observed along foliation-parallel transects, i.e. attributable to faulting and fracturing that cuts the foliation. Foliation-parallel fractures record a more regularly spaced fracture set with lower intensity. This is due to the presence of the zeolite-bearing faults in SW Harris that occur at a high angle to the foliation. In the Stornoway Region of Lewis, the shape and intensity of the foliation distributions were found to have a positive correlation with the shape and intensity of fault distributions (section 3.4.6). This was obviously not observed in the SHSZ, and it seems highly likely that this is due to the misorientation of the foliation of the SHSZ with respect to later stress orientations, and hence the foliation was not reactivated by faulting. Where foliation is not highly misorientated, e.g. the Stornoway Region, and the Grose Bay mylonite, it has a tendency to be reactivated by faulting.

On the Scottish mainland, Pless (2011) assigned power-law distributions to all of the spacing distributions collected from fieldwork. D values from assigned power-law trend lines produce values of 0.5 - 1.99 obtained from 40 transects with an average of 47 fractures measured per transect. When all transects here are matched with a power law trend line, the mainland D value range is similar to the range presented here of 0.44 – 1.65 obtained from 25 transects with an average of 110 fractures per transect. However, it is important to note that the majority of spacing distributions could not be confidently assigned power law trend lines in the Outer Hebrides, instead most are very well represented by exponential trend lines. Cv values obtained from the mainland are also similar to those presented in this thesis, with Pless (2011) finding a

range of 0.67 - 1.27 compared to 0.7 – 2.07 found in this work. Spacing data collected from 20 transects within the Clair cores by Pless (2011) was also interpreted to display power-law trend lines, with D-values of 0.352 – 1.657, Cv values of 0.94 – 1.746, and fracture densities between 1.35 – 22.91 fractures per metre. The D-values are all within the ranges determined for fractures within the Outer Hebrides in this thesis when power-law trend lines are assigned to the data, and Cv values and fracture densities are also similar. The higher values of fracture density obtained in the 206/8-8 well in this study may be due to different sampling methods used by Pless (2011). However, all results from both studies are within an order of magnitude, suggesting that fracture spacing characteristics are broadly similar across the Lewisian Gneiss Complex. This observation and the qualitative fracture characteristics discussed in previous chapters suggest that the Outer Hebrides are a valid analogue to the Clair Field, with outcrop that is better suited to the fracture ages and structural contexts (e.g. adjacent to major Mesozoic-age faults) of the Clair Field than the mainland.

Aperture data from the Outer Hebrides show a straight line trend over ~5 orders of magnitude when all raw data are plotted together (section 7.5). Plotting aperture against fracture intensity/average spacing enables direct prediction of the density of fractures of a certain aperture (Ortega et al., 2006). Power law aperture scaling has previously been found to exist in sandstones (Hooker et al., 2011; Hooker et al., 2013). The D-values obtained by Hooker et al. (2011) in the Eriboll Formation of NW Scotland range between 0.564 – 1.1686. These results compare favourably with a range of 0.451 – 1.07 for data collected from the Clair Formation. D-values in basement rocks in the Clair Field (1.013) was found to be higher than that for data obtained from the Outer Hebrides (average of 0.505), indicating a greater importance of smaller fracture apertures. However, this difference may well be due to the greater resolution that it is possible to obtain from the Clair Field cores. Hooker et al. (2013) present spatial fracture data for fractures within sandstones in Argentina, and determine the existence of power-law, exponential and log-normal spatial distributions between different fracture sets. This result is partially used to infer that pre-existing fractures may unequally partition strain, and hence that pre-existing fractures are important in determining the spatial distribution of subsequent fracture sets.

8.3 Impact

Understanding fracture properties is becoming increasingly important in hydrocarbon/hydrogeology/geothermal production from basement rocks (e.g. Stober and Bucher, 2007; Hooker et al., 2013). This thesis has attempted a wide-ranging characterisation of basement rocks in the Outer Hebrides. This study is the first island-wide analysis of faults and fractures on the Isles of Lewis and Harris. Brittle fracturing and faulting identified here adds a geologically more recent context to the more heavily studied ductile deformation history of the OHFZ (e.g.

Sibson, 1975; Sibson, 1977b; Butler, 1995; Butler et al., 1995; Imber, 1998). The identification of fault sets within the Stornoway Formation allows further constraints to be placed on the palaeostress history of the NE Atlantic, following studies such as Dore et al. (1999). Conversely to Dore et al. (1999) It seems likely that faulting in the Minch is dominantly of Permo-Triassic age rather than Jurassic, suggested by the lack of syn-sedimentary faulting in the Minch offshore (e.g. O'Neill and England, 1994). Hence the palaeostress orientations obtained here represent Permo-Triassic stress orientations during initial rifting of the NE Atlantic. The identification of Mesozoic faults in the Stornoway Formation permits identification of Mesozoic age structures in the surrounding Lewisian Gneiss that have not previously been identified, with major structures such as the Seaforth Fault, with kilometres of offset suggesting the islands are far from a simple graben-bounded horst block. Fault orientation varies between Lewis and Harris, with fault orientation not, however, seen across the postulated Langavat terrane boundary in the SHSZ. This is an important observation as mainland results have been used to suggest a degree of detachment of faulting between the terranes.

The results obtained here also have important implications for any offshore exploration west of Lewis and Harris, if indeed onshore basement lineaments match offshore structures (e.g. Dore et al., 1999). In particular, the presence of major rift-oblique NNW-SSE striking structures such as the Seaforth Fault may be an important discovery with regards to dominant fault orientation and kinematics offshore western Lewis and Harris.

Although there is clear variation in fracture orientation between Clair and the Outer Hebrides, fracture mineralisation and fracture infills share significant similarities. The presence of adularia/zeolite partially filling open (oil-filled) fractures at Clair is mirrored by the presence of open adularia/zeolite filled fractures in the Outer Hebrides. The presence of mineralisation partially filling open fractures within the basement is likely to have a positive effect on whether the porosity remains open as pore fluid pressures are reduced (i.e. oil is extracted). It is particularly interesting to note that oil has been found at several localities on or immediately adjacent to major regional faults in the Stornoway region. This observation confirms the presence of oil residing in the Minch, potentially originating from Carboniferous coal-bearing strata, as postulated by Stein (1992). The presence of oil in or adjacent to major faults also confirms that these faults have acted as conduits for fluid flow, possibly during periods of activity in the past, and important observation that has relevance to fault-related and fault-proximal reservoirs, such as Clair.

Data obtained in this study can be used to predict and populate basement block models with fault apertures and spacings, and the relationship with length can be determined and implemented in order to better constrain basement properties. Specifically, Mesozoic faults may be directly

targeted if they can be identified as it is these structures and related fractures that are associated with open porosity. The quantitative data obtained in chapter 7 can be used to populate block models when predicting the number of fractures intersected by wells through major Mesozoic faults (e.g. Seaforth, Seisiadar, Memorial Cairn datasets). Data collected from background datasets (e.g. Borve) may be used to populate the background fracturing within block models of the Clair core.

In pre-drill modelling at the Lancaster Prospect on the Rona Ridge SW of Clair, Slightam (2012) uses observations from the Isles of Lewis and Harris as an analogue. Several areas covered in Slightam (2012) are more heavily analysed and interpreted in the present work, namely:

1. The relationship between the basement and cover, and the continuation of faults between the two is not considered by Slightam (2012).
2. The orientation and significance of Mesozoic faulting, described by Slightam (2012) as Cretaceous in age and striking NE-SW, has been found to be dominated by NNW-SSE striking faulting and probably dominantly of Permo-Triassic age.
3. Fault orientations on Lewis and Harris are described by Slightam (2012) as being comparable to the Rona Ridge (NE-SW). This result is not corroborated here.
4. Although faults are often steeply dipping within the basement, they are not typically vertical as described by Slightam (2012).
5. Fault damage zones were expected to be 30-90 m from fieldwork conducted by Slightam (2012). The results in this study suggest this is only the case for very major structures such as the Seaforth fault which is at least 40 km long. The vast majority of minor faults (tens of metres in length) lack damage zones entirely, and intermediate scale structures (hundreds of metres in length, such as the Memorial Cairn faults) typically have much smaller damage zones. The majority of faults interpreted by Slightam (2012) are intermediate scale faults of several hundred metre length, similar to lineaments interpreted on Lewis and Harris. Most of the faults interpreted in the lineament analysis typically have damage zones of < 20 m.
6. Fault orientations clearly vary between Lewis and Harris, contrary to observations by Slightam (2012) (See Figure 8.3).
7. Fracture frequency is clearly affected by lithology in rocks in the Outer Hebrides, contrary to observations by Slightam (2012). In this study, more silicic rocks, such as granitic gneisses and pegmatites have been found to display a greater degree of fracturing when compared with more mafic rocks, such as Younger and Older Basics that tend to deform more ductiley. In addition, the effect of foliation has also been found to have a clear effect on fracturing, with faulting localising parallel with the foliation. The effect of basement lithology on hydraulic conductivity has been investigated by Stober and Bucher (2007), who found that granite is

typically 2 orders of magnitude more conductive than mica-bearing gneisses, and hydraulic conductivity is heavily dependent on the local deformation history of an area. The latter result is corroborated in this study – the deformation history is clearly a major controlling feature on fracture attributes. However, although results from the Hebrides do suggest that more silicic gneisses behave in a more brittle fashion than mafic gneisses and amphibolite (also; Pless 2012), banded gneisses have been very clearly observed to be much more highly fractured than immediately adjacent massive (non-foliated) granite units, particularly around Borve in SW Harris. It is not possible to conclusively determine this disparity in observations here, however it may be that micas within the gneissic units studied by Stober and Bucher (2007) may be altering to clays that occlude developed porosity. This effect may occur more preferentially in gneissic units where fractures tend to follow the mica foliation. Further work on the basement fractures of the Clair Field and Outer Hebrides should include direct porosity and permeability tests of specific fracture sets within different lithologies in order to test this hypothesis.

8.3.1 Applications

This work has contributed to the increased understanding of porosity within the basement rocks of the Outer Hebrides and at the Clair Field. New methodology and applications from this work are:

1. Identification of major structures on the islands through a regional review (lineament analysis), followed by the characterisation of faulting at key localities enables collection of data and observations that can be applied to broad areas.
2. The identification of faults of similar ages on the basis of extensive fault rock characterisation, with relative dating of events based on cross cutting relationships with the Stornoway Formation cover sequence, has been confirmed through palaeostress analysis. This approach can be used elsewhere.
3. The nature of the basement/cover interface is of great importance globally. Results in this work suggest it is a zone of complex fracturing and faulting that may make this zone an active exploration target if present at Clair, and provides a rare insight into these interfaces.
4. The recognition of the Seaforth Fault as a major, relatively young (Mesozoic age), crustal feature with kilometre-scale offset with probable multiple phases of activation has implications for the understanding of the regional faulting patterns and accommodation of strain on the UK continental margin, particularly with implications for regional-scale polymodal faulting during Atlantic opening.

5. Detailed microscopy has revealed a complex brittle chronology in the Outer Hebrides that can be at least partially matched with deformation at Clair, with open fractures of Mesozoic age showing very similar mineralogy and characteristics that can be used to better understand the reasons for the existence of basement permeability in the Clair Field.
6. Methodology has been developed for assessing spacing and aperture characteristics that ensures minimal loss of collected data points, alongside establishment of power-law relationships and other distributions.
7. Fracture apertures measured in this study are dominantly controlled by the length of the aperture. The relationship between aperture and length can be used in future to estimate fracture apertures from fracture traces, and the aperture scaling relationships determined in this study may be used to estimate the numbers of fractures of specified aperture that could be encountered in a well. This may be of great benefit during reservoir and well modelling.

The methodology used here can be applied to any geological study of fractured basement analogues.

8.4 Conclusions

- Faulting of Mesozoic and younger age in the Outer Hebrides is distinguishable from multiple preceding fracture sets. It is associated with the development of fault rocks displaying authigenic clay, zeolite, adularia and calcite mineralisation. Oil is also seen in several fault rocks of Mesozoic age in localities close to major Mesozoic structures. In the Clair Field, fractures of Mesozoic age are associated with adularia, calcite/pyrite and zeolite mineralisation. Clay-bearing faulting is also present within the basement of the Clair Field and is Mesozoic or younger in age.

- Faults are common in the Stornoway Formation, with evidence for the existence of three fault sets formed during regimes of Mesozoic extension, followed by Cenozoic contraction. These phases are likely related to rifting associated with opening of the Atlantic. The strike of normal faults in the Stornoway Formation is likely directly controlled by faulting along the underlying basement foliation, and conjugate faults developed in the Stornoway Formation cover sequence are not present within the basement rocks.

- Reactivation of the foliation by Mesozoic faulting in the Stornoway region is confirmed by correlation between foliation and fault orientation distribution shapes and strengths. Foliation reactivation by faulting is very limited further south at the SHSZ, and it seems

this is entirely dependent on the foliation orientation. Foliation in the Clair basement is typically relatively weakly defined, but trends N-S to NNW-SSE (Pless, 2011).

- Porosity seen in faults is not present in pre-Mesozoic structures and is associated with adularia, zeolite and calcite mineralisation. Porosity development during faulting in the Stornoway Formation cover is initially increased by intra-granular fracturing and production of microfractures. Authigenic clay development subsequently reduces porosity. Dissolution of calcite associated with zeolite mineralisation in the Outer Hebrides is partly mirrored by formation of porosity by dissolution and faulting at Clair that has produced uncemented fault rock. At both Clair and on Lewis and Harris, porosity is associated with adularia mineralisation, in addition to zeolite in the Outer Hebrides. Phases of fault rock in the Clair Group (gouge, granulation seams) are strongly controlled by the lithology of the host rock.

- The complex history of the OHFZ has been expanded in this study with identification of significant Mesozoic and younger faulting. In addition, major Mesozoic island-crossing faults have been identified that have previously not been recognised, e.g. the Seaforth Fault. Mesozoic and younger faulting forms the basis for the current topography and geological exposures on Lewis and Harris.

- The basement-cover interface on Lewis is a complex zone of sediment injection, veining and gravity-driven detachment faulting. Multiple phases of sediment injection and calcite veins are probably linked to lithification and de-watering of the Stornoway Formation, and may also be linked to fault movements. At Clair, core is limited, but similar mineralisation and sediment injection is present.

- Basement rocks of the Outer Hebrides are overall well represented by exponential fracture spacing distributions. Faulting of Mesozoic age is distinguishable by its spacing characteristics in the Outer Hebrides. Mesozoic fault-perpendicular transects are more easily described by power-law spacing distributions than reactivated faults, joint-dominated localities, and fault-parallel transects. Cv values obtained across the Lewisian are generally close to 1 when compared with other studies, and the relative difficulty in assigning distribution types to the datasets is probably attributable to the great age of the rocks and presence of multiple cross-cutting and reactivated fracture sets. Dissolution in Clair Group rocks is associated with normal faulting and uncemented fault rocks, and has produced a higher fracture density and a randomly spaced fracture set. Transects across

natural fractures in the Clair Group display clustering of faulting and fractures that can be described with power-law distributions. In the basement, fracture density is higher, clustering is reduced, and the power-law exponents of power-law trend lines assigned to fracture spacing distributions are higher.

- Basement rocks of the Outer Hebrides are overall well represented by power-law fracture aperture distributions. Aperture data collected from the Outer Hebrides shows that fracture aperture is scalable across ~5 orders of magnitude. At Clair, power-law trend lines can only be assigned to ~1 order of magnitude of the aperture data from the Clair Group, probably due to short transect lengths. Fractures caused by core recovery have a notably different aperture distribution than natural fractures. Aperture distributions from transects across Mesozoic faults in the Hebrides show relatively consistent D values between 0.35-0.42. The higher D value obtained from power law trend lines assigned to the basement aperture distribution from Clair (1.01) may be due to the greater resolution it is possible to achieve from the smooth clean core surfaces from the Clair Field. Fracture aperture is proportional to fracture length, with a likely subsidiary control from fluid pressure. Hence, fracture traces can be used to estimate fracture apertures, which is turn can be used to estimate the number of fractures of a given aperture using the relationships determined in this study.

8.5 Future Work

- Lineament analysis on Lewis is limited by extensive peat cover. High resolution magnetics such as those undertaken across Northern Ireland in the TELLUS project could determine the existence of sub-peat faults and dykes, which would be particularly useful for identification of dominant features in North Lewis.

- The investigation of fracture scalability could be continued through further data collection and analysis of other attributes such as fracture length. Further work using 1D line transects should concentrate around statistical analysis and the determination of the effects of censoring and truncation to take these fully into account during interpretation.

- Lidar has been collected at the following localities:

    - Memorial Cairn – significant Mesozoic faulting in the Lewisian in cliffs within the several hundred metres of the bounding fault of the Stornoway Formation.

- Orasaigh – significant late (Cenozoic) strike-slip faulting in the Lewisian at Orasaigh Quarry.
- Seisiadar – 3D exposure of normal dip-slip faulting on a wave cut platform and cliffs, within several hundred metres of the Minch Fault.
- Suardail – headland exposure of the basement cover interface and associated faulting.

Time constraints prevented analysis of these datasets in this study. Their analysis will be particularly important in determining the 3D geometry and spatial characteristics of Mesozoic faults within crystalline basement rocks of the NE Atlantic Margin.

- Analysis of clay minerals in this study was performed using optical and scanning electron microscopy. Clay development and mineralogy within fault rocks can be further constrained by use of X-ray diffraction. This would allow better understanding of the alteration processes operating within faults and fractures in the Hebrides and at Clair, and will better constrain temperature and pressure conditions during faulting.

- Further work must include orientation analysis of open fractures encountered in the basement at Clair, in addition to further study of fracture infills and relative ages.

References

ACKERMANN, R. V. & SCHLISCHE, R. W. 1997. Anticlustering of small normal faults around larger faults. *Geology,* 25**,** 1127-1130.

ACKERMANN, R. V., SCHLISCHE, R. W. & WITHJACK, M. O. 2001. The geometric and statistical evolution of normal fault systems: an experimental study of the effects of mechanical layer thickness on scaling laws. *Journal of Structural Geology,* 23**,** 1803-1819.

ALLEN, P. A. & ALLEN, J. R. 1990. *Basin Analysis Principles and Applications,* Oxford, Blackwell Scientific Publications.

ALLEN, P. A. & MANGE-RAJETZKY, M. A. 1992. Devonian-Carboniferous sedimentary evolution of the Clair area, offshore north-western UK: impact of changing provenance. *Marine and Petroleum Geology,* 9**,** 29-52.

ANANABA, S. E. & AJAKAIYE, D. E. 1987. Evidence of tectonic control of mineralization in Nigeria from lineament density analysis A Landsat-study. *International Journal of Remote Sensing,* 8**,** 1445 - 1453.

ANDERSEN, T., AUSTRHEIM, H., BURKE, E. A. J. & ELVEVOLD, S. 1993. N2 and CO2 in deep crustal fluids: evidence from the Caledonides of Norway. *Chemical Geology,* 108**,** 113-132.

ANDERSON, E. M. 1951. *The dynamics of faulting and dyke formation with applications to Britain,* Edinburgh, Oliver & Boyd.

ANTONELLINI, M. & AYDINA, A. 1994. Effect of Faulting on Fluid Flow in Porous Sandstones: Petrophysical Properties. *AAPG Bulletin,* 78**,** 355-377.

ATTFIELD, P. 1987. The Structural History of the Canisp Shear Zone. *In:* PARK, R. G. & TARNEY, J. (eds.) *Evolution of the Lewisian and comparable Precambrian high-grade terranes.* Geological Society, London, Special Publication.

AYDIN, A. 1978. Small faults formed as deformation bands in sandstone. *Pure and Applied Geophysics,* 116**,** 913-930.

BABA, S. 2002. Tectono-metamorphic Events in the North Atlantic Region in the Palaeoproterozoic from the View Point of High-grade Metamorphic Rocks in the Lewisian Complex, South Harris, NW Scotland. *Gondwana Research,* 5**,** 757-770.

BARON, M., PARNELL, J., MARK, D., CARR, A., PRZYJALGOWSKI, M. & FEELY, M. 2008. Evolution of hydrocarbon migration style in a fractured reservoir deduced from fluid inclusion data, Clair Field, west of Shetland, UK. *Marine and Petroleum Geology,* 25**,** 153-172.

BARR, D., SAVORY, K. E., FOWLER, S. R., ARMAN, K. & MCGARRITY, J. P. 2007. Pre-development fracture modelling in the Clair field, west of Shetland. *In:* LONERGAN, L., JOLLY, R. J. H., RAWNSLEY, K. & SANDERSON, D. J. (eds.) *Fractured Reservoirs.* London: Geological Special Publication

BARTHOLOMEW, I. D., PETERS, J. M. & POWELL, C. M. 1993. *Regional structural evolution of the North Sea: oblique slip and the reactivation of basement lineaments.*, Geological Society, London.

BARTON, C. A. & ZOBACK, M. D. 1992. Self-similar distribution and properties of macroscopic fractures at depth in crystalline rock in the Cajon Pass Scientific Drill Hole. *Journal of Geophysical Research: Solid Earth,* 97**,** 5181-5200.

BARTON, C. A., ZOBACK, M. D. & MOOS, D. 1995. Fluid flow along potentially active faults in crystalline rock. *Geology,* 23**,** 683-686.

BARTON, C. C. 1995. Fractal Analysis of Scaling and Spatial Clustering of Fractures. *In:* BARTON, C. C. & LA POINTE, P. R. (eds.) *Fractals in the Earth Sciences.* New York: Plenum Press.

BAXTER, A. N. & MITCHELL, J. G. 1984. Camptonite-Monchiquite dyke swarms of Northern Scotland; Age relationships and their implications. *Scottish Journal of Geology,* 20**,** 297-308.

BEACOM, L., HOLDSWORTH, R. E., MCCAFFREY, K. J. W. & ANDERSON, T. 2001. A quantitative study of the influence of pre-existing compositional and fabric heterogenities upon fracture zone development during basement reactivation. *In:* HOLDSWORTH, R. E.,

STRACHAN, R. A., MAGLOUGHLIN, J. F. & KNIPE, R. J. (eds.) *The nature and tectonic significance of fault zone weakening.* Geological Society Special Publication.
BELFIELD, W. C. 1998. Incorporating spatial distribution into stochastic modelling of fractures: multifractals and Levy-stable statistics. *Journal of Structural Geology,* 20**,** 473-486.
BERKOWITZ, B., BOUR, O., DAVY, P. & ODLING, N. 2000. Scaling of fracture connectivity in geological formations. *Geophysical Research Letters,* 27**,** 2071-2064.
BEST, M. G. 2003. *Igneous and Metamorphic Petrology,* Oxford, Blackwell Science Ltd.
BIRD, D. K., SCHIFFMAN, P., ELDERS, W. A. & WILLIAMS, A. E. 1984. Calc-Silicate Mineralization in Active Geothermal Systems. *Economic Geology,* 79**,** 671-695.
BONNET, E., BOUR, O., ODLING, N., DAVY, P., MAIN, I., COWIE, P. & BERKOWITZ, B. 2001. Scaling of fracture systems in geological media. *Reviews of Geophysics,* 39**,** 347-384.
BOODEN, M. A. & MAUK, J. L. 2011. Host Rock Voleum Change During Alteration Promotes Self-Sealing of Hydrothermal Systems. *Society for Geology Applied to Mineral Deposits 2011 Biennial Conference.* Antofagasta, Chile.
BOUR, O., DAVY, P., DARCEL, C. & ODLING, N. 2002. A statistical scaling model for fracture network geometry, with validation on a multiscale mapping of a joint network (Hornelen Basin, Norway). *Journal of Geophysical Research: Solid Earth,* 107**,** ETG 4-1-ETG 4-12.
BREWER, J. A. & SMYTHE, D. K. 1984. MOIST and the continuity of crustal reflector geometry along the Caledonian-Appalachian orogen. *Journal of the Geological Society,* 141**,** 105-120.
BRODIE, J. & WHITE, N. 1994. Sedimentary basin inversion caused by igneous underplating: Northwest European continental shelf. *Geology,* 22**,** 147-150.
BUTLER, C. A. 1995. *Basment fault reactivation: The kinematic evolution of the Outer Hebrides Fault Zone, Scotland.* Ph.D., University of Durham.
BUTLER, C. A., HOLDSWORTH, R. E. & STRACHAN, R. A. 1995. Evidence for Caledonian sinistral strike-slip motion and associated fault zone weakening, Outer Hebrides Fault Zone, NW Scotland. *Journal of the Geological Society,* 152**,** 743-746.
BUTLER, R. W. H., HOLDSWORTH, R. E. & LLOYD, G. E. 1997. The role of basement reactivation in continental deformation. *Journal of the Geological Society,* 154**,** 69-71.
BYERLEE, J. 1978. Friction of Rocks. *In:* BYERLEE, J. & WYSS, M. (eds.) *Rock Friction and Earthquake Prediction.* Birkhäuser Basel.
CAINE, J. S., EVANS, J. P. & FORSTER, C. B. 1996. Fault zone architecture and permeability structure. *Geology,* 24**,** 1025-1028.
CHANG, O. C. & CHANG, T. W. 2000. Characteristics of Clay Minerals in Gouges of the Dongrae Fault, Southeastern Korea, and Implications for Fault Activity. *Clays and Clay Minerals,* 48**,** 204-212.
CHESTER, F. M., FRIEDMAN, M. & LOGAN, J. M. 1985. Foliated cataclasites. *Tectonophysics,* 111**,** 139-146.
CLIFF, R. A., GRAY, C. M. & HUHMA, H. 1983. A Sm-Nd isotopic study of the South Harris Igneous Complex, the Outer Hebrides. *Contributions to Mineralogy and Petrology,* 82**,** 91-98.
CLIFF, R. A. & REX, D. C. 1989. Short Paper: Evidence for a 'Grenville' event in the Lewisian of the northern Outer Hebrides. *Journal of the Geological Society,* 146**,** 921-924.
COLLETTINI, C., VITI, C., SMITH, S. A. F. & HOLDSWORTH, R. E. 2009. Development of interconnected talc networks and weakening of continental low-angle normal faults. *Geology,* 37**,** 567-570.
CONEY, D., FYFE, T. B., RETAIL, P. & SMITH, P. J. 1993. *Clair appraisal: the benefits of a co-operative approach*, Geological Society, London.
COWARD, M. P. 1972. The Eastern Gneisses of South Uist. *Scottish Journal of Geology,* 8**,** 1-12.
COWARD, M. P. 1973. Heterogeneous deformation in the development of the Laxfordian complex of South Uist, Outer Hebrides. *Journal of the Geological Society,* 129**,** 139-158.
COWARD, M. P. 1990. The Precambrian, Caledonian and Variscan framework to NW Europe. *Geological Society, London, Special Publications,* 55**,** 1-34.

COWARD, M. P., FRANCIS, P. W., GRAHAM, R. H., MYERS, J. S. & WATSON, J. 1969. Remnants of an Early Metasedimentary Assemblage in the Lewisian Complex of the Outer Hebrides. *Proceedings of the Geologists' Association,* 80**,** 387-408.

COWARD, M. P. & PARK, R. G. 1987. The role of mid-crustal shear zones in the Early Proterozoic evolution of the Lewisian. *In:* PARK, R. G. & TARNEY, J. (eds.) *Evolution of the Lewisian and comparable high-grade terranes.* Geological Society, London, Special Publication.

COX, S. F. 2007. Structural and isotopic constraints on fluid flow regimes and fluid pathways during upper crustal deformation: An example from the Taemas area of the Lachlan Orogen, SE Australia. *Journal of Geophysical Research: Solid Earth,* 112**,** B08208.

COX, S. F. & ETHERIDGE, M. A. 1983. Crack-seal fibre growth mechanisms and their significance in the development of oriented layer silicate microstructures. *Tectonophysics,* 92**,** 147-170.

DEAN, K., MCLACHLAN, K. & CHAMBERS, A. 1999. Rifting and the development of the Faeroe-Shetland Basin. *Geological Society, London, Petroleum Geology Conference series.*

DEARNLEY, R. 1962. An Outline of the Lewisian Complex of the Outer Hebrides in Relation to that of the Scottish Mainland. *Quarterly Journal of the Geological Society,* 118**,** 143-176.

DEER, W. A., HOWIE, R. A. & ZUSSMAN, J. 1992. *The Rock Forming Minerals,* Harlow, Pearson Education Limited.

DICKINSON, B. B. & WATSON, J. 1976. Variations in crustal level and geothermal gradient during the evolution of the Lewisian complex of northwest Scotland. *Precambrian Research,* 3**,** 363-374.

DORE, A. G., LUNDIN, E. R., FICHLER, C. & OLESEN, O. 1997. Patterns of basement structure and reactivation along the NE Atlantic margin. *Journal of the Geological Society,* 154**,** 85-92.

DORE, A. G., LUNDIN, E. R., JENSEN, L. N., BIRKELAND, O., ELIASSEN, P. E. & FICHLER, C. 1999. Principal tectonic events in the evolution of the northwest European Atlantic margin. *In:* FLEET, A. J. & BOLDY, S. A. R. (eds.) *Petroleum Geology of Northwest Europe: Proceedings of the 5th Conference.* London: Geological Society.

DUINDAM, P. & VAN HOORN, B. 1987. Structural Evolution of the West Shetland continental margin. *In:* BROOKS, J. & GLENNIE, K. (eds.) *Petroleum Geology of North West Europe.* London: Graham and Trotman.

EARLE, M. M., JANKOWSKI, E. J. & VANN, R. 1989. M 46: Structural and Stratigraphic Evolution of the Faeroe-Shetland Channel and Northern Rockall Trough. *Extensional Tectonics and Stratigraphy of the North Atlantic Margins.*

ENFIELD, M. A. & COWARD, M. P. 1987. The Structure of the West Orkney Basin, northern Scotland. *Journal of the Geological Society,* 144**,** 871-884.

ENGLAND, R. W. 1988. The early Tertiary stress regime in NW Britain: evidence from the patterns of volcanic activity. *Geological Society, London, Special Publications,* 39**,** 381-389.

EVANS, D., HALLSWORTH, C., JOLLEY, D. W. & MORTON, A. C. 1991. Late Oligocene terrestrial sediments from a small basin in the Little Minch. *Scottish Journal of Geology,* 27**,** 33-40.

EVANS, D., WILKINSON, G. C. & CRAIG, D. L. 1979. The Tertiary sediments of the Canna Basin, Sea of the Hebrides. *Scottish Journal of Geology,* 15**,** 329-332.

FALT, U., GUERIN, G., RETAIL, P. & EVANS, M. 1992. Clair Discovery: Evaluation of Natural Fracturation in a Horizontal Well Drilled in the Basement and Producing From Overlying Sediments. *Eurpoean Petroleum Conference* Cannes, France.

FETTES, D. J. & MENDUM, J. R. 1987. The evolution of the Lewisian complex in the Outer Hebrides. *Geological Society, London, Special Publications,* 27**,** 27-44.

FETTES, D. J., MENDUM, J. R., SMITH, D. I. & WATSON, J. V. 1992. *Geology of the Outer Hebrides,* London, HMSO.

FINLAY, A., HOLDSWORTH, H., SELBY, D., PLESS, J. & FRANKLIN, B. 2011. Rhenium-Osmium Geochronology of fracture-hosted pyrite and Bitumen from the Clair Field: Implications for absolute timing of tectonism and hydrocarbon migration – A pilot study. Durham: Durham University.

FOSSEN, H. & HESTHAMMER, J. 1998. Deformation bands and their significance in porous sandstone reservoirs. *First Break,* 16**,** 21-25.

FOSSEN, H. & HESTHAMMER, J. 2000. Possible absence of small faults in the Gullfaks Field, northern North Sea: implications for downscaling of faults in some porous sandstones. *Journal of Structural Geology,* 22**,** 851-863.

FOSSEN, H. & HURICH, C. A. 2005. The Hardangerfjord Shear Zone in SW Norway and the North Sea: a large-scale low-angle shear zone in the Caledonian crust. *Journal of the Geological Society,* 162**,** 675-687.

FREY, M. 1987. *Low Temperature Metamorphism,* Glasgow, Blackie.

FREY, M. & ROBINSON, D. 1999. *Low-Grade Metamorphism,* Cambridge, Blackwell Science Ltd.

FRIEND, FRIEND, C., KINNY & KINNY, P. 2001. A reappraisal of the Lewisian Gneiss Complex: geochronological evidence for its tectonic assembly from disparate terranes in the Proterozoic. *Contributions to Mineralogy and Petrology,* 142**,** 198-218.

FYFE, J. A., LONG, D. & EVANS, D. 1993. *The Geology of the Malin-Hebrides sea area,* London, HMSO.

FYFE, W. S. 1985. Fluids, tectonics and crustal deformation. *Tectonophysics,* 119**,** 29-36.

GABRIELSEN, R. H., BRAATHEN, A., DEHLS, J. & ROBERTS, D. 2002. Tectonic lineaments of Norway. *Norwegian Journal of Geology,* 82**,** 153-174.

GILLESPIE, P. A., HOWARD, C. B., WALSH, J. J. & WATTERSON, J. 1993. Measurement and characterisation of spatial distributions of fractures. *Tectonophysics,* 226**,** 113-141.

GILLESPIE, P. A., JOHNSTON, J. D., LORIGA, M. A., MCCAFFREY, K. J. W., WALSH, J. J. & WATTERSON, J. 1999. Influence of layering on vein systematics in line samples. *Geological Society, London, Special Publications,* 155**,** 35-56.

GILLESPIE, P. A., WALSH, J. J., WATTERSON, J., BONSON, C. G. & MANZOCCHI, T. 2001. Scaling relationships of joint and vein arrays from The Burren, Co. Clare, Ireland. *Journal of Structural Geology,* 23**,** 183-201.

GOODCHILD, M. W., HENRY, K. L., HINKLEY, R. J. & IMBUS, S. W. 1999. The Victory gas field, West of Shetland. *Geological Society, London, Petroleum Geology Conference series,* 5**,** 713-724.

GOODENOUGH, K. M., MENDUM, J. R. & KRABBENDAM, M. 2009. The Contribution of the Northern Highlands to the Understanding of Tectonic Processes. *In:* MENDUM, J. R., BARBER, A. J., BUTLER, R. W. H., FLINN, D., GOODENOUGH, K. M., KRABBENDAM, M., PARK, R. G. & STEWART, A. D. (eds.) *Lewisian, Torridonian and Moine Rocks of Scotland.* Peterborough: Joint Nature Conservation Committee.

GOODENOUGH, K. M., PARK, R. G., KRABBENDAM, M., MYERS, J. S., WHEELER, J., LOUGHLIN, S. C., CROWLEY, Q. G., FRIEND, C. R. L., BEACH, A., KINNY, P. D. & GRAHAM, R. H. 2010. The Laxford Shear Zone: an end-Archaean terrane boundary? *Geological Society, London, Special Publications,* 335**,** 103-120.

GOODWIN, J. H. 1973. Analcime and K-Feldspar in Tuffs of the Green River Formation, Wyoming. *American Mineralogist,* 58**,** 93-105.

GRAHAM, R. H. 1980. The role of shear belts in the structural evolution of the South Harris igneous complex. *Journal of Structural Geology,* 2**,** 29-37.

GUDMUNDSSON, A. 2011. *Rock Fractures in Geolgoical Processes,* Cambridge, Cambridge Univeristy Press.

HALLIDAY, A. N. & MITCHELL, J. G. 1976. Structural, KAr and40Ar39Ar age studies of adularia K-feldspars from the Lizard Complex, England. *Earth and Planetary Science Letters,* 29**,** 227-237.

HANSEN, J., JERRAM, D. A., MCCAFFREY, K. & PASSEY, S. R. 2009. The onset of the North Atlantic Igneous Province in a rifting perspective. *Geological Magazine,* 146**,** 309-325.

HARRIS, C., FRANSSEN, R. & LOOSVELD, R. 1991. Fractal analysis of fractures in rocks: the Cantor's Dust method-comment. *Tectonophysics,* 198**,** 107-111.

HAY, R. L. 1978. Geological Occurrence of Zeolites. *In:* SAND, L. B. & MUMPTON, F. A. (eds.) *Natural Zeolites; Occurence, Properties, Use.* Oxford: Pergamon.

HAY, S. J., HALL, J., SIMMONS, G. & RUSSELL, M. J. 1988. Sealed microcracks in the Lewisian of NW Scotland: a record of 2 billion years of fluid circulation. *Journal of the Geological Society,* 145**,** 819-830.

HEALY, D., JONES, R. R. & HOLDSWORTH, R. E. 2006a. New insights into the development of brittle shear fractures from a 3-D numerical model of microcrack interaction. *Earth and Planetary Science Letters,* 249**,** 14-28.

HEALY, D., JONES, R. R. & HOLDSWORTH, R. E. 2006b. Three-dimensional brittle shear fracturing by tensile crack interaction. *Nature,* 439**,** 64-67.

HESSELBO, S. P., OATES, M. J. & JENKYNS, H. C. 1998. The lower Lias Group of the Hebrides Basin. *Scottish Journal of Geology,* 34**,** 23-60.

HINZ, K., ELDHOLM, O., BLOCK, M. & SKOGSEID, J. 1993. Evolution of North Atlantic volcanic continental margins. *Geological Society, London, Petroleum Geology Conference series,* 4**,** 901-913.

HITCHEN, K. & RITCHIE, J. D. 1987. Geological review of the West Shetland area. *In:* BROOKS, J. & GLENNIE, K. (eds.) *Petroleum Geology of North West Europe.* London: Graham and Trotman.

HOLDSWORTH, R. E., BUTLER, C. A. & ROBERTS, A. M. 1997. The recognition of reactivation during continental deformation. *Journal of the Geological Society,* 154**,** 73-78.

HOOKER, J. N., LAUBACH, S. E., GOMEZ, L., MARRETT, R., EICHHUBL, P., DIAZ-TUSHMAN, K. & PINZON, E. 2011. Fracture size, frequency, and strain in the Cambrian Eriboll Formation sandstones, NW Scotland. *Scottish Journal of Geology,* 47**,** 45-56.

HOOKER, J. N., LAUBACH, S. E. & MARRETT, R. 2013. Fracture-aperture size—frequency, spatial distribution, and growth processes in strata-bounded and non-strata-bounded fractures, Cambrian Mesón Group, NW Argentina. *Journal of Structural Geology,* 54**,** 54-71.

HUANG, Q. & ANGELIER, J. 1989. Fracture spacing and its relation to bed thickness. *Geological Magazine,* 126**,** 355-362.

HUDSON, J. A. & PRIEST, S. D. 1979. Discontinuities and rock mass geometry. *International Journal of Rock Mechanics and Mining Sciences & Geomechanics Abstracts,* 16**,** 339-362.

IMBER, J. 1998. *Deformation and Fluid-Rock Interaction Along the Reatcivated Outer Hebrides Fault Zone, Scotland.* PhD, Durham University.

IMBER, J., HOLDSWORTH, R. E., BUTLER, C. A. & LLOYD, G. E. 1997. Fault-zone weakening processes along the reactivated Outer Hebrides Fault Zone, Scotland. *Journal of the Geological Society,* 154**,** 105-109.

IMBER, J., HOLDSWORTH, R. E., BUTLER, C. A. & STRACHAN, R. A. 2001. A reappraisal of the Sibson-Scholz fault zone model: The nature of the frictional to viscous (â€œbrittle-ductileâ€) transition along a long-lived, crustal-scale fault, Outer Hebrides, Scotland. *Tectonics,* 20.

IMBER, J., HOLDSWORTH, R. E., SMITH, S. A. F., JEFFERIES, S. P. & COLLETTINI, C. 2008. Frictional-viscous flow, seismicity and the geology of weak faults: a review and future directions. *Geological Society, London, Special Publications,* 299**,** 151-173.

IMBER, J., STRACHAN, R. A., HOLDSWORTH, R. E. & BUTLER, C. A. 2002. The initiation and early tectonic significance of the Outer Hebrides Fault Zone, Scotland. *Geological Magazine,* 139**,** 609-619.

JOHNSON, A. M. 1995. Orientations of faults determined by premonitory shear zones. *Tectonophysics,* 247**,** 161-238.

JOHNSTON, D., MCCAFFREY, K. & LORIGA, M. A. 1994. *A manual describing recording, analysis and prediction of vein and related fracture distributions,,* Lichfield, Mineral Industry Research Organisation.

JOLLY, R. J. H. & COSGROVE, J. W. 2003. Geological evidence of patterns of fluid flow through fracture networks: examination using random realizations and connectivity analysis. *Geological Society, London, Special Publications,* 209**,** 177-186.

JOLLY, R. J. H. & SANDERSON, D. J. 1997. A Mohr circle construction for the opening of a pre-existing fracture. *Journal of Structural Geology,* 19**,** 887-892.

JONES, C. 2012. SU-70, Introducion to FE SEM - High Resolution Imaging and Analysis. Hitachi High Technologies.

KELLEY, S. P., REDDY, S. M. & MADDOCK, R. 1994. Laser-probe 40Ar/39Ar investigation of a pseudotachylyte and its host rock from the Outer Isles thrust, Scotland. *Geology,* 22**,** 443-446.

KIM, Y.-S., ANDREWS, J. R. & SANDERSON, D. J. 2001. Reactivated strike–slip faults: examples from north Cornwall, UK. *Tectonophysics,* 340**,** 173-194.

KIM, Y.-S. & SANDERSON, D. J. 2005. The relationship between displacement and length of faults: a review. *Earth-Science Reviews,* 68**,** 317-334.

KING, G. C. P., STEIN, R. S. & RUNDLE, J. B. 1988. The Growth of Geological Structures by Repeated Earthquakes 1. Conceptual Framework. *Journal of Geophysical Research,* 93**,** 13307-13318.

KINNY, P. D. & FRIEND, C. R. L. 1997. U-Pb isotopic evidence for the accretion of different crustal blocks to form the Lewisian Complex of northwest Scotland. *Contributions to Mineralogy and Petrology,* 129**,** 326-340.

KINNY, P. D., FRIEND, C. R. L. & LOVE, G. J. 2005. Proposal for a terrane-based nomenclature for the Lewisian Gneiss Complex of NW Scotland. *Journal of the Geological Society,* 162**,** 175-186.

KLIMA, K., RIEDMULLER, G. & STATTEGGER, K. 1988. Statistical Analysis of Clay Mineral Assemblages in Fault Gouges. *Clays and Clay Minerals,* 36**,** 277-283.

KNOTT, S. D., BURCHELL, M. T., JOLLEY, E. J. & FRASER, A. J. 1993. Mesozoic to Cenozoic plate reconstructions of the North Atlantic and hydrocarbon plays of the Atlantic margins. *Geological Society, London, Petroleum Geology Conference series,* 4**,** 953-974.

KOLYUKHIN, D. & TORABI, A. 2012. Statistical analysis of the relationships between faults attributes. *Journal of Geophysical Research: Solid Earth,* 117**,** B05406.

KOOPMANS, B. N. 1986. A comparative study of lineament analysis from different remote sensing imagery over areas in the Benue Valley and Jos Plateau Nigeria. *International Journal of Remote Sensing,* 7**,** 1763 - 1771.

KRABBENDAM, M., MENDUM, J. R. & GOODENOUGH, K. M. 2009. Tectonic Setting and Evolution of the Northern Highlands. *In:* MENDUM, J. R., BARBER, A. J., BUTLER, R. W. H., FLINN, D., GOODENOUGH, K. M., KRABBENDAM, M., PARK, R. G. & STEWART, A. D. (eds.) *Lewisian, Torridonian and Moine Rocks of Scotland.* Peterborough: Joint Nature Conservation Committee.

LAILEY, M., STEIN, A. M. & RESTON, T. J. 1989. The Outer Hebrides fault: a major Proterozoic structure in NW Britain. *Journal of the Geological Society,* 146**,** 253-259.

LAMBERT, R. S. J., MYERS, J. S. & WATSON, J. 1970. An apparent age for a member of the Scourie dyke suite in Lewis, Outer Hebrides. *Scottish Journal of Geology,* 6**,** 214-220.

LIOU, J. G. Stabilities of Natural Epidotes. *In:* HOCK, V. & KOLLER, F., eds. 125 years Knappenwand, 1993 Salzburg, Austria.

LISLE, R. J. 1993. Strike-slip motion in the Minches, NW Scotland, deduced from the trends of the Scourie Dyke swarm. *Journal of the Geological Society,* 150**,** 653-656.

LOCKNER, D. A., MORROW, C., MOORE, D. & HICKMAN, S. 2011. Low strength of deep San Andreas fault gouge from SAFOD core. *Nature,* 472**,** 82-85.

MACDONALD, R. & FETTES, D. J. 2007. The Tectonomagmatic evolution of Scotland. *Transactions of the Royal Society of Edinburgh: Earth Sciences,* 97**,** 213-295.

MACINNES, E. A., ALSOP, G. I. & OLIVER, G. J. H. 2000. Contrasting modes of reactivation in the Outer Hebrides Fault Zone, northern Barra, Scotland. *Journal of the Geological Society,* 157**,** 1009-1017.

MARRETT, R., ORTEGA, O. J. & KELSEY, C. M. 1999. Extent of power-law scaling for natural fractures in rock. *Geology,* 27**,** 799-802.

MASON, A. J. & BREWER, T. S. 2004. Mafic dyke remnants in the Lewisian Complex of the Outer Hebrides, NW scotland: a geochemical record of continental break-up and re-assembly. *Precambrian Research,* 133**,** 121-141.

MASON, A. J. & BREWER, T. S. 2005. A re-evaluation of a Laxfordian terrane boundary in the Lewisian Complex of South Harris, NW Scotland. *Journal of the Geological Society,* 162**,** 401-407.

MCCAFFREY, K. & JOHNSTON, J. D. 1996. Fractal analysis of a mineralised vein deposit: Curraghinalt gold deposit, County Tyrone. *Mineralium Deposita,* 31**,** 52-58.

MCCAFFREY, K. J. W., SLEIGHT, J. M., PUGLIESE, S. & HOLDSWORTH, R. E. 2003. Fracture formation and evolution in crystalline rocks: Insights from attribute analysis. *Geological Society, London, Special Publications,* 214**,** 109-124.

MCKIE, T. & GARDEN, I. R. 1996. Hierarchical stratigraphic cycles in the non-marine Clair Group (Devonian) UKCS. *Geological Society, London, Special Publications,* 104**,** 139-157.

MENDUM, J. R. 1982. *Geology of the South-West part of South Harris*. Edinburgh: NERC.

MENDUM, J. R. 2009. Lewisian Gneiss Complex of the Outer Hebrides, Introduction. *In:* MENDUM, J. R., BARBER, A. J., BUTLER, R. W. H., FLINN, D., GOODENOUGH, K. M., KRABBENDAM, M., PARK, R. G. & STEWART, A. D. (eds.) *Lewisian, Torridonian and Moine Rocks of Scotland.* Peterborough: Joint Conservation Committee.

MENDUM, J. R., BARBER, A. J., BUTLER, R. W. H., FLINN, D., GOODENOUGH, K. M., KRABBENDAM, M., PARK, R. G. & STEWART, A. D. 2009. *Lewisian, Torridonian and Moine Rocks of Scotland,* Peterborough, Joint Nature Conservation Comittee.

MILODOWSKI, A. E., METCALFE, R., BAILEY, D. E. & NADEN, J. 1998. A pilot study of the history of fracturing and mineralisation in the Clair Field, West Shetland Basin. British Geological Survey.

MORLEY, C. K. 1995. Developments in the structural geology of rifts over the last decade and their impact on hydrocarbon exploration. *Geological Society, London, Special Publications,* 80**,** 1-32.

MORTON, A. & MILNE, A. 2012. Heavy mineral stratigraphic analysis on the Clair Field, UK, west of Shetlands: a unique real-time solution for red-bed correlation while drilling. *Petroleum Geoscience,* 18**,** 115-128.

MORTON, N. 1992. Dynamic stratigraphy of the Triassic and Jurassic of the Hebrides Basin, NW Scotland. *Geological Society, London, Special Publications,* 62**,** 97-110.

MOY, D. J. & IMBER, J. 2009. A critical analysis of the structure and tectonic significance of rift-oblique lineaments (‘transfer zones') in the Mesozoic–Cenozoic succession of the Faroe–Shetland Basin, NE Atlantic margin. *Journal of the Geological Society,* 166**,** 831-844.

MYERS, J. S. 1970. Gneiss types and their significance in the repeatedly deformed and metamorphosed Lewisian Complex of Western Harris, Outer Hebrides. *Scottish Journal of Geology,* 6**,** 186-199.

MYERS, J. S. 1987. The East Greenland Nagssugtoqidian mobile belt compared with the Lewisian Complex. *In:* PARK, R. G. & TARNEY, J. (eds.) *Evolution of the Lewisian and comparable Precambrian high-grade terranes.* Geological Society, London, Special Publication.

NEUHOFF, P. S., FRIDRIKSSON, T., ARNORSSON, S. & BIRD, D. K. 1999. Porosity evolution and mineral paragenesis during low-grade metamorphism of basaltic lavas at Teigarhorn, eastern Iceland. *American Journal of Science,* 299**,** 467-501.

NICHOLS, G. J. 2005. Sedimentary evolution of the Lower Clair Group, Devonian, West of Shetland: climate and sediment supply controls on fluvial, aeolian and lacustrine deposition. *Geological Society, London, Petroleum Geology Conference series,* 6**,** 957-967.

NICOL, A., WALSH, J. J., WATTERSON, J. & GILLESPIE, P. A. 1996. Fault size distributions -- are they really power-law? *Journal of Structural Geology,* 18**,** 191-197.

O'LEARY, D. W., FRIEDMAN, J. D. & POHN, H. A. 1976. Lineament, linear, lineation: Some proposed new standards for old terms. *Geological Society of America Bulletin,* 87**,** 1463-1469.

O'NEILL, P. S. & ENGLAND, R. W. 1994. The structure of the Sea of the Hebrides Basin: an integrated gravity and seismic model. *Scottish Journal of Geology,* 30**,** 1-9.

ODLING, N. E. 1997. Scaling and connectivity of joint systems in sandstones from western Norway. *Journal of Structural Geology,* 19**,** 1257-1271.

OLSON, J. E. 2007. Fracture aperture, length and pattern geometry development under biaxial loading: a numerical study with applications to natural, cross-jointed systems. *Geological Society, London, Special Publications,* 289**,** 123-142.

ORTEGA, O. J., MARRETT, R. A. & LAUBACH, S. E. 2006. A scale-independent approach to fracture intensity and average spacing measurement. *AAPG Bulletin,* 90**,** 193-208.

OSINSKI, G. R., ALSOP, G. I. & OLIVER, G. J. H. 2001. Extensional tectonics of the Outer Hebrides Fault Zone, South Uist, northwest Scotland. *Geological Magazine,* 138**,** 325-344.
PARK, R. G. 2005. The Lewisian terrane model: a review. *Scottish Journal of Geology,* 41**,** 105-118.
PARK, R. G. 2010. Structure and evolution of the Lewisian Gairloch shear zone: variable movement directions in a strike-slip regime. *Scottish Journal of Geology,* 46**,** 31-44.
PARK, R. G., KINNY, P. D., FRIEND, C. R. L. & LOVE, G. J. 2005. Discussion on a terrane-based nomenclature for the Lewisian Gneiss Complex of NW Scotland Journal, Vol. 162, 2005, pp. 175-186. *Journal of the Geological Society,* 162**,** 893-895.
PARSONS, A. J. & YEARLEY, R. J. 1986. An analysis of geologic lineaments seen on LANDSAT MSS imagery. *International Journal of Remote Sensing,* 7**,** 1773-1782.
PASSCHIER, C. W. & TROUW, R. A. J. 1996. *Microtectonics,* Berlin, Springer-Verlag.
PEACOCK, D. C. P. 2002. Propagation, interaction and linkage in normal fault systems. *Earth-Science Reviews,* 58**,** 121-142.
PEACOCK, D. C. P. & SANDERSON, D. J. 1992. Effects of layering and anisotropy on fault geometry. *Journal of the Geological Society,* 149**,** 793-802.
PEACOCK, D. C. P. & SANDERSON, D. J. 1994. Strain and scaling of faults in the chalk at Flamborough Head, U.K. *Journal of Structural Geology,* 16**,** 97-107.
PERSANO, C., BARFOD, D. N., STUART, F. M. & BISHOP, P. 2007. Constraints on early Cenozoic underplating-driven uplift and denudation of western Scotland from low temperature thermochronometry. *Earth and Planetary Science Letters,* 263**,** 404-419.
PESONEN, L. J., ELMING, S. Å., MERTANEN, S., PISAREVSKY, S., D'AGRELLA-FILHO, M. S., MEERT, J. G., SCHMIDT, P. W., ABRAHAMSEN, N. & BYLUND, G. 2003. Palaeomagnetic configuration of continents during the Proterozoic. *Tectonophysics,* 375**,** 289-324.
PICKERING, G., BULL, J. M. & SANDERSON, D. J. 1995. Sampling power-law distributions. *Tectonophysics,* 248**,** 1-20.
PIDGEON, R. T. & AFTALION, M. 1972. The geochronological significance of discordant U-Pb ages of oval-shaped zircons from a Lewisian Gneiss from Harris, Outer Hebrides. *Earth and Planetary Science Letters,* 17**,** 269-274.
PLESS, J. 2011. *Characterising fractured basement using the Leisian Gneiss Complex, NW Scotland: Implication for fracture systems in the Clair Field basement.* PhD, Durham University.
PRIEST, S. D. & HUDSON, J. A. 1976a. Discontinuity spacings in rock. *International Journal of Rock Mechanics and Mining Sciences & Geomechanics Abstracts,* 13**,** 135-148.
PRIEST, S. D. & HUDSON, J. A. 1976b. Discontinuity spacings in rock. *International Journal of Rock Mechanics and Mining Science & Geomechanics Abstracts,* 13**,** 135-148.
RECHES, Z. 1978. Analysis of faulting in three-dimensional strain field. *Tectonophysics,* 47**,** 109-129.
RECHES, Z. 1983. Faulting of rocks in three-dimensional strain fields II. Theoretical analysis. *Tectonophysics,* 95**,** 133-156.
REED, S. J. B. 1996. *Electron Microprobe Analysis and Scanning Electron Microscopy in Geology,* Cambridge, Cambridge University Press.
REYES, A. G. 1990. Petrology of Philippine geothermal systems and the application of alteration mineralogy to their assessment. *Journal of Volcanology and Geothermal Research,* 43**,** 279-309.
RIDD, M. F. 1981. Petroleum Geology West of the Shetlands. *In:* ILLING, L. V. & HOBSON, G. D. (eds.) *Petroleum Geology of the Continental Shelf of Northwest Europe.* London: Institute of Petroleum.
RITCHIE, J. D. & DARBYSHIRE, D. P. F. 1984. Rb-Sr dates on Precambrian rocks from marine exploration wells in and around the West Shetland Basin. *Scottish Journal of Geology,* 20**,** 31-36.
RITCHIE, J. D., HITCHEN, K. & MITCHELL, J. G. 1987. The offshore continuation of the Moine Thrust north of Shetland as deduced from basement isotopic ages. *Scottish Journal of Geology,* 23**,** 163-173.

RITCHIE, J. D., JOHNSON, H., QUINN, M. F. & GATLIFF, R. W. 2008. The effects of Cenozoic compression within the Faroe-Shetland Basin and adjacent areas. *Geological Society, London, Special Publications,* 306**,** 121-136.

ROBERTS, A. M. & HOLDSWORTH, R. E. 1999. Linking onshore and offshore structures: Mesozoic extension in the Scottish Highlands. *Journal of the Geological Society,* 156**,** 1061-1064.

ROBERTS, D. G., THOMPSON, M., MITCHENER, B., HOSSACK, J., CARMICHAEL, S. & BJORNSETH, H.-M. 1999. Palaeozoic to Tertiary rift and basin dynamics: mid-Norway to the Bay of Biscay – a new context for hydrocarbon prospectivity in the deep water frontier. *Geological Society, London, Petroleum Geology Conference series,* 5**,** 7-40.

RUTTER, E. H., HOLDSWORTH, R. E. & KNIPE, R. J. 2001. The nature and tectonic significance of fault-zone weakening: an introduction. *Geological Society, London, Special Publications,* 186**,** 1-11.

SAUNDERS, A. D., FITTON, J. G., KERR, A. C., NORRY, M. J. & KENT, R. W. 1997. Atlantic Igneous Province. *In:* MAHONEY, J. J. (ed.) *Large Igneous Provinces: Continental, Oceanic, and Planetary Flood Volcanism.* Washington D. C., USA: American Geophysical Union.

SCOTCHMAN, I. C., CARR, A. D. & PARNELL, J. Hydrocarbon generation modelling along the UK North Eastern Atlantic Margin. AAPG Hedberg Conference "Hydrocarbon Habitat of Volcanic Rifted Passive Margins", September 8-11, 2002 2002 Stavanger, Norway.

SCOTCHMAN, I. C., CARR, A. D. & PARNELL, J. 2006. Hydrocarbon generation modelling in a multiple rifted and volcanic basin: a case study in the Foinaven Sub-basin, FaroeShetland Basin, UK Atlantic margin. *Scottish Journal of Geology,* 42**,** 1-19.

SCOTCHMAN, I. C., GRIFFITH, C. E., HOLMES, A. J. & JONES, D. M. 1998. The Jurassic petroleum system north and west of Britain: a geochemical oil-source correlation study. *Organic Geochemistry,* 29**,** 671-700.

SHERLOCK, S. C., STRACHAN, R. A. & JONES, K. A. 2009. High spatial resolution 40Ar/39Ar dating of pseudotachylites: geochronological evidence for multiple phases of faulting within basement gneisses of the Outer Hebrides (UK). *Journal of the Geological Society,* 166**,** 1049-1059.

SIBSON, R. H. 1975. Generation of Pseudotachylyte by Ancient Seismic Faulting. *Geophysical Journal. Royal Astronomical Society,* 43**,** 775-794.

SIBSON, R. H. 1977a. Fault rocks and fault mechanisms. *Journal of the Geological Society,* 133**,** 191-213.

SIBSON, R. H. 1977b. *The Outer Hebrides Thrust: Its Structure, Mechanism and Deformation Environment.* PhD, Imperial College of Science and Technology.

SIBSON, R. H. 1985. A note on fault reactivation. *Journal of Structural Geology,* 7**,** 751-754.

SIBSON, R. H. 1990. Rupture nucleation on unfavorably oriented faults. *Bulletin of the Seismological Society of America,* 80**,** 1580-1604.

SIBSON, R. H. 1994. Crustal stress, faulting and fluid flow. *Geological Society, London, Special Publications,* 78**,** 69-84.

SIBSON, R. H. 2000. Fluid involvement in normal faulting. *Journal of Geodynamics,* 29**,** 469-499.

SIBSON, R. H. 2003. Thickness of the Seismic Slip Zone. *Bulletin of the Seismological Society of America,* 93**,** 1169-1178.

SLAUGHTER, M. 1970. Crystal Structure of Stilbite. *The American Mineralogist,* 55**,** 10.

SLEIGHT, J. M. 2001. *Fracture characteristics from two reactivated basement fault zones: Examples from Norway and Shetland.* Ph.D., University of Durham.

SLIGHTAM, C. 2012. Characterizing seismic-scale faults pre- and post-drilling; Lewisian Basement, West of Shetlands, UK. *Geological Society, London, Special Publications,* 374.

SMITH, P. J. & BOTT, M. H. P. 1975. Structure of the Crust Beneath the Caledonian Foreland and Caledonian Belt of the North Scottish Shelf Region. *Geophysical Journal of the Royal Astronomical Society,* 40**,** 187-205.

SMYTHE, D. K. & KENOLTY, N. 1975. Tertiary sediments in the Sea of the Hebrides. *Journal of the Geological Society,* 131**,** 227-233.

SOLIVA, R. & SCHULTZ, R. A. 2008. Distributed and localized faulting in extensional settings: Insight from the North Ethiopian Rift–Afar transition area. *Tectonics,* 27**,** TC2003.

SORENSEN, A. B. 2003. Cenozoic basin development and stratigraphy of the Faroes area. *Petroleum Geoscience,* 9**,** 189-207.
SØRENSEN, A. B. 2003. Cenozoic basin development and stratigraphy of the Faroes area. *Petroleum Geoscience,* 9**,** 189-207.
SPERNER, B., RATSCHBACHER, L. & OTT, R. 1993. Fault-striae analysis: A turbo pascal program package for graphical presentation and reduced stress tensor calculation. *Computers & Geosciences,* 19**,** 1361-1388.
SPERNER, B. & ZWEIGEL, P. 2010. A plea for more caution in fault–slip analysis. *Tectonophysics,* 482**,** 29-41.
STEEL, R. J. 1971. New Red Sandstone Movement on the Minch Fault. *Nature Physical Science,* 234**,** 158-159.
STEEL, R. J. & WILSON, A. C. 1975. Sedimentation and tectonism (?Permo-Triassic) on the margin of the North Minch Basin, Lewis. *Journal of the Geological Society,* 131**,** 183-200.
STEIN, A. M. 1988. Basement controls upon basin development in the Caledonian foreland, NW Scotland. *Basin Research,* 1**,** 107-119.
STEIN, A. M. 1992. Basin development and petroleum potential in The Minches and Sea of the Hebrides Basins. *Geological Society, London, Special Publications,* 62**,** 17-20.
STEIN, A. M. & BLUNDELL, D. J. 1990. Geological inheritance and crystal dynamics of the northwest Scottish continental shelf. *Tectonophysics,* 173**,** 455-467.
STEINER, A. 1968. Clay Minerals in Hydrothermally Altered Rocks at Wairakei, New Zealand. *Clays and Clay Minerals,* 16**,** 193-213.
STEINER, A. 1970. Genesis of hydrothermal K-feldspar (adularia) in an active geomthermal enviornment at Wairakei, New Zealand. *Mineralogical Magazine,* 37**,** 916-922.
STEVENS, A. 1914. Notes on the geology of the Stornoway district of Lewis. *Transations of the Geological Society of Glasgow,* 15**,** 51-63.
STOBER, I. & BUCHER, K. 2007. Hydraulic properties of the crystalline basement. *Hydrogeology Journal,* 15**,** 213-224.
STOKER, M. S., HITCHEN, K. & GRAHAM, C. C. 1993. The Geology of the Hebrides and West Shetland Shelves, and Adjacent Deep-water Areas. *British Geological Survey, UK Offshore Regional Report*.
STORETVEDT, K. M. & STEEL, R. J. 1977. Palaeomagnetic evidence for the age of the Stornoway Formation. *Scottish Journal of Geology,* 13**,** 265-269.
SUZEN, M. L. & TOPRAK, V. 1998. Filtering of satellite images in geological lineament analyses: an application to a fault zone in Central Turkey. *International Journal of Remote Sensing,* 19**,** 1101-1114.
SWAN, A. R. H. & SANDILANDS, M. 1995. *Introduction to Geological Data Analysis,* Oxford, Blackwell Science Ltd.
SZULC, A. G., ALSOP, G. I. & OLIVER, G. J. H. 2008. Kinematic and thermal constraints on the reactivation of the Outer Hebrides Fault Zone, NW Scotland. *Geological Magazine,* 145**,** 623-636.
TILEY, R., WHITE, N. & AL-KINDI, S. 2004. Linking Paleogene denudation and magmatic underplating beneath the British Isles. *Geological Magazine,* 141**,** 345-351.
TORABI, A. & BERG, S. S. 2011. Scaling of fault attributes: A review. *Marine and Petroleum Geology,* 28**,** 1444-1460.
TREWIN, N. H. 2004. *The Geology of Scotland,* Bath, The Geological Society.
TWISS, R. J. & MOORES, E. M. 1992. *Structural Geology,* New York, United States of America, W. H. Freeman and Company.
UNDERHILL, J. R. 1991. Implications of Mesozoic—Recent basin development in the western Inner Moray Firth, UK. *Marine and Petroleum Geology,* 8**,** 359-369.
VAN BREEMEN, O., AFTALION, M. & PIDGEON, R. T. 1971. The age of the granitic injection complex of Harris, Outer Hebrides. *Scottish Journal of Geology,* 7**,** 139-152.
VELDE, B. 1985. *Clay Minerals, A physico-Chemical Explanation of their Occurrence,* Amsterdam, Elsevier Sciences Publishers B.V.

VELDE, B., DUBOIS, J., MOORE, D. & TOUCHARD, G. 1991. Fractal patterns of fractures in granites. *Earth and Planetary Science Letters,* 104**,** 25-35.

WALKER, R. J. 2010. *The Structural Evolution of the Faroe Islands, NE Atlantic Margin.* PhD, Durham University.

WALKER, R. J., HOLDSWORTH, R. E., IMBER, J., FAULKNER, D. R. & ARMITAGE, P. J. 2013. Fault zone architecture and fluid flow in interlayered basaltic volcaniclastic-crystalline sequences. *Journal of Structural Geology*.

WARR, L. N. & COX, S. 2001. Clay mineral transformations and weakening mechanisms along the Alpine Fault, New Zealand. *Geological Society, London, Special Publications,* 186**,** 85-101.

WATSON, J. 1969. The Precambrian gneiss complex of Ness, Lewis, in relation to the effects of Laxfordian regeneration. *Scottish Journal of Geology,* 5**,** 269-285.

WATTS, L. M., HOLDSWORTH, R. E., SLEIGHT, J. A., STRACHAN, R. A. & SMITH, S. A. F. 2007. The movement history and fault rock evolution of a reactivated crustal-scale strike-slip fault: the Walls Boundary Fault Zone, Shetland. *Journal of the Geological Society,* 164**,** 1037-1058.

WEISENBERGER, T. 2009. *Zeolites in Fissures of Crystalline Basement Rocks.* PhD, Albert-Ludwigs-Universität Freiburg.

WEISENBERGER, T. & BUCHER, K. 2010. Zeolites in fissures of granites and gneisses of the Central Alps. *Journal of Metamorphic Geology,* 28**,** 825-847.

WEISENBERGER, T. & BUCHER, K. 2011. Mass transfer and porosity evolution during low temperature water–rock interaction in gneisses of the simano nappe: Arvigo, Val Calanca, Swiss Alps. *Contributions to Mineralogy and Petrology,* 162**,** 61-81.

WHEELER, J., PARK, R. G., ROLLINSON, H. R. & BEACH, A. 2010. The Lewisian Complex: insights into deep crustal evolution. *Geological Society, London, Special Publications,* 335**,** 51-79.

WHITE, S. H. 1998. Cataclasites and Mylonites. *In:* SNOKE, A. W., TULLIS, J. & TODD, V. R. (eds.) *Fault-related rocks: a photographic atlas.* Chichester, West Sussex: Princeton University Press.

WHITEHOUSE, M. J. 1990. An early-Proterozoic age for the Ness anorthosite, Lewis, Outer Hebrides. *Scottish Journal of Geology,* 26**,** 131-136.

WHITEHOUSE, M. J. 1993. Age of the Corodale Gneisses, South Uist. *Scottish Journal of Geology,* 29**,** 1-7.

WHITEHOUSE, M. J. & BRIDGWATER, D. 2001. Geochronological constraints on Paleoproterozoic crustal evolution and regional correlations of the northern Outer Hebridean Lewisian complex, Scotland. *Precambrian Research,* 105**,** 227-245.

WILKINS, S. J. & GROSS, M. R. 2002. Normal fault growth in layered rocks at Split Mountain, Utah: influence of mechanical stratigraphy on dip linkage, fault restriction and fault scaling. *Journal of Structural Geology,* 24**,** 1413-1429.

WINTSCH, R. P., CHRISTOFFERSEN, R. & KRONENBERG, A. K. 1995. Fluid-rock reaction weakening of fault zones. *Journal of Geophysical Research: Solid Earth,* 100**,** 13021-13032.

WITT, A. J., FOWLER, S. R., KJELSTADLI, R. M., DRAPER, L. F., BARR, D. & MCGARRITY, J. P. 2010. Managing the start-up of a fractured oil reservoir: development of the Clair field, West of Shetland. *Geological Society, London, Petroleum Geology Conference series,* 7**,** 299-313.

WOJTAL, S. 1994. Fault scaling laws and temporal evolution of fault systems. *Journal of Structural Geology,* 16**,** 603-612.

WOJTAL, S. F. 1996. Changes in fault displacement populations correlated to linkage between faults. *Journal of Structural Geology,* 18**,** 265-279.

WOODCOCK, N. H. & MORT, K. 2008. Classification of fault breccias and related fault rocks. *Geological Magazine,* 145**,** 435-440.

WOODCOCK, N. H. & NAYLOR, M. A. 1983. Randomness testing in three-dimensional orientation data. *Journal of Structural Geology,* 5**,** 539-548.

YAMAJI, A. 2003. *An Introduction to Tectonophysics, Theoretical Aspects of Structural Geology,* Tokyo, Terrapub.

Appendices

- EDX 1 – EDX spectra and corresponding SEM images.
- EDX 2 – EDX spectra and corresponding SEM images.
- Fieldwork measurements – 5647 measurements obtained during fieldwork. Date, locality, context, feature measured and orientation are presented.
- Lineaments_Lewis_and_Harris – 3562 lineaments picked across Lewis and Harris. Azimuth and length data.
- The Clair cores – Description of selected sections of Clair core and thin sections.
- Structural logs from Orasaigh and Seaforth Valley.